Electrochemical C–H Activations with 3d and 4d Transition Metal Catalysts

Dissertation

for the award of the degree
"Doctor rerum naturalium"
of the Georg-August-Universität Göttingen

within the doctoral program of chemistry
of the Georg-August-Universität School of Science (GAUSS)

Submitted by
Leonardo Massignan
From Desio (Italy)

Göttingen, 2021

Thesis Committee

Prof. Dr. Lutz Ackermann

Institute of Organic and Biomolecular Chemistry

Georg-August-Universität Göttingen

Prof. Dr. Alexander Breder

Institute for Organic Chemistry

Universität Regensburg

Members of the Examination Board

1st Reviewer: *Prof. Dr. Lutz Ackermann*

Institute of Organic and Biomolecular Chemistry

Georg-August-Universität Göttingen

2nd Reviewer: *Prof. Dr. Alexander Breder*

Institute for Organic Chemistry

Universität Regensburg

Further members of the Examination Board

Prof. Dr. Dr. h.c. mult. Lutz F. Tietze

Institute of Organic and Biomolecular Chemistry, Göttingen

Prof. Dr. Manuel Alcarazo

Institute of Organic and Biomolecular Chemistry, Göttingen

Dr. Michael John

Institute of Organic and Biomolecular Chemistry, Göttingen

Dr. Daniel Janßen-Müller

Institute of Organic and Biomolecular Chemistry, Göttingen

Date of the oral examination: 02.12.2021

Acknowledgements

First, I would like to express my sincere gratitude to Prof. Dr. Lutz Ackermann for giving me the opportunity of working in his excellent laboratory and for supervising me during my PhD. Your constant encouragement and insightful suggestions guided me in my studies and have shaped my scientific approach. Your devotion and strong work ethics would surely have a lasting impression on my career.

I am grateful to Prof. Alexander Breder for being my second supervisor, thank you for your valuable input in our meetings and the kind suggestions you provided. I would also like to thank Prof. Dr. Dr. h.c.mult. Lutz F. Tietze, Prof. Dr. Manuel Alcarazo, Dr. Daniel Janßen-Müller, and Dr. Michael John for agreeing to take part in my doctoral defense.

I am thankful to the Institut für Organische und Biomolekulare Chemie, Georg-August-Universität Göttingen for the workspace and the instrumental facilities, as well as the analytical departments for the punctual and precise analyses and the kind support.

I gratefully acknowledge Frau Gabriele Keil-Knepel and Frau Bianca Spitalieri for the kind assistance for the administrative works. I sincerely thank Mr. Stefan Beußhausen for taking care of all the instruments in our research group and Mr. Karsten Rauch for the kind support, help, and guidance in the use of all the glassware and in maintaining safety in the lab.

I also would like to thank the colleagues with whom I had the opportunity to collaborate: Dr. Xuefeng Tan, Dr. Cuiju Zhu, Dr. Tjark H. Meyer, Dr. Cong Tian, Dr. Rositha Kuniyil, Dr. João C. A. Oliveira, Dr. Torben Rogge, Dr Youai Qiu, Dr. Antonis M. Messinis, Maximilian Stangier, Xiaoyan Hou, Dr. Johanna Frey, and Aude Salamé. I would like to thank all the people who have proofread and helped me correcting this thesis: Alexej Scheremetjew, Nate Ang, Isaac Choi, Dr. Ramesh C. Samanta, Dr. Johanna Frey, Dr. Bartlomiej Sadowski.

I want to thank all the other members of the Ackermann group for the constant support and scientific exchange. In particular, Fabio and Antonio for the huge help in the lab, the nice chemical discussions, and the amazing times outside the lab. Moreover, I would like to thank several friends in the group for the nice time in Göttingen: Agnese, Alexej, João, Jongwoo, Max, Mélanie, Nate, Partha, Renato, Santhi, Satheesh, Tjark.
I'd like to take the chance to express my gratitude to my former supervisor Prof. Dr. Elisabetta Rossi, as well as to Dr. Valentina Pirovano.

I would like to thank all the people that enjoyed with me these last four years of my life. Grazie mille to Daniele and Giuseppe, the times all together were unforgettable. Thanks to Justin and Tomoko for the funny dinners and extraordinary cakes. Thank you, Gabriele and Nicole, for being awesome neighbors. Thanks also to Martina for the nice time together.
Most importantly I would like to thank my family. A huge thank to my parents whose support was omnipresent in the smallest and biggest challenges I had to face. Thanks Virginia, Silvio, Massimo, Emma and Adam, for being so cool and lovely. A thank also to Andrea, Mirella, Paola, and Valeria, for always creating a cozy and familiar atmosphere when together.

My utmost gratitude goes to Silvia, unique and lovely partner in my life. Your wise suggestions and tireless efforts were essential. I love to make this travel with you.
A special thank goes to Edoardo that made this last year full of love and cuteness.

Leonardo Massignan

TABLE OF CONTENTS

List of Abbreviations

A	Ampere
A	Area
Å	Ångström (s)
Ac	acetyl
acac	acetyl acetonate
Alk	alkyl
AMLA	ambiphilic metal-ligand activation
aq.	aqueous
Ar	aryl
atm	standard atmosphere
ATR	attenuated total reflectance
BDE	bond dissociation energy
BIES	base-assisted internal electrophilic substitution
Bn	benzyl
BQ	1,4-benzoquinone
br	broad
Bu	butyl
Bz	benzoyl
C	Celsius
c	concentration
calc.	calculated
cat.	catalytic
CCE	constant current electrolysis
CE	counter electrode *or* current efficiency
CMD	concerted-metalation-deprotonation
conc.	concentrated
conv.	conversion
Cp*	1,2,3,4,5-Pentamethylcyclopentadiene
CPE	constant potential electrolysis
CV	cyclic voltammetry

Cy	cyclohexyl
δ	chemical shift
d	diameter *or* doublet
DCB	2,3-dichlorobutane
DCE	1,2-dichloroethane
DCIB	1,2-dichloroisobutane
DCM	dichloromethane
dd	doublet of doublet
DFT	density functional theory
DG	directing group
DME	dimethoxyethane
DMF	*N*,*N*-dimethylformamide
DMSO	dimethyl sulfoxide
DMPU	1,3-dimethyl-3,4,5,6-tetrahydro-2(1*H*)-pyrimidinone
dppe	1,2-bis(diphenylphosphino)ethane
dt	doublet of triplet
e^-	electron
E	potential
E_p	peak potential
$E_{1/2}$	half-peak potential
e.g.	*exempli gratia*
EI	electron ionization
equiv	equivalent
ESI	electrospray ionization
Et	ethyl
EWG	electron-withdrawing group
F	Faraday-constant
Fc	ferrocene
FE	faradaic efficiency
FG	functional group
FID	flame ionization detector
G	*Gibbs* free energy
GC	gas chromatography *or* glassy carbon

GF	graphite felt
GVL	γ-valerolactone
h	hour
Hal	halogen
Het	hetero
Hept	heptyl
Hex	hexyl
HFIP	1,1,1,3,3,3-hexafluoro-propan-2-ol
HPLC	high performance liquid chromatography
HR-MS	high resolution mass spectrometry
i	*iso*
I	current *or* intensity (MS)
IES	internal electrophilic substitution
IR	infrared spectroscopy
j	current density [$mA \cdot cm^{-2}$] *or* amount of unit charge per unit time per unit area
J	coupling constant
KIE	kinetic isotope effect
L	ligand
LLHT	ligand-to-ligand hydrogen transfer
µ	micro
m	*meta*
m	multiplet *or* milli
M	molar
$[M]^+$	molecular ion peak
mA	milliampere
*m*CPBA	*meta*-chloroperoxybenzoic acid
Me	methyl
Mes	mesityl
min	minute
M. p.	melting point
MS	mass spectrometry
m/z	mass-to-charge ratio
v	scan rate

n	number of transferred electrons *or* amount of substance in mole
nd	*not detected*
NHE	Normal Hydrogen Electrode
NMP	*N*-methyl-2-pyrrolidone
NMR	nuclear magnetic resonance
o	*ortho*
OA	oxidative addition
OPV	oil pump vacuum
p	*para*
p	pentet
PAH(s)	polycyclic aromatic hydrocarbons
Ph	phenyl
PIDA	(diacetoxyiodo)benzene
PIFA	(bis(trifluoroacetoxy)iodo)benzene
Piv	pivaloyl
ppm	parts per million
Pr	propyl
PTS	Polyoxyethanyl-α-tocopheryl sebacate
py	2-pyridyl
pym	2-pyrimidinyl
PyO	2-pyridine-*N*-oxide
q	quartet
Q	8-aminoquinoline
R	rest
RDE	rotating disc electrode
RE	reference electrode
ref.	reference
r.t.	room/ambient temperature
RVC	reticulated vitreous carbon
s	singlet *or* second
sat.	saturated
SCE	saturated calomel electrode
SEM-EDS	scanning electron microscopy energy-dispersive X-ray spectroscopy

SET	single electron transfer
SPS	solvent purification system
t	*tert*
t	triplet
TAM	triazolyldimethylmethyl
*t*AmOH	*tert*-Amyl alcohol
TFA	Trifluoroacetic acid
TFAA	Trifluoroacetic anhydride
TFE	2,2,2-Trifluoroethanol
THF	tetrahydrofuran
TLC	thin layer chromatography
TM	transition metal
TMEDA	*N*,*N*,*N*',*N*'-Tetramethylethylenediamine
TOF	time-of-flight
TS	transition state
V	volt
vs.	*versus*
WE	working electrode
wt%	percentage by weight

1. Introduction

Organic synthesis went through enormous advances during the past century, opening the way to a vast number of compounds and diverse synthetic routes. These progresses allowed to ameliorate the quality of life, bringing on the prosper development of pharmaceuticals, as well as advances in other fields, such as agrochemical and material science. Even though the benefit for development and wealthiness is undoubted, chemical synthesis is still an inefficient process that requires huge amounts of resources and energy, therefore generating major amounts of undesired by-products and waste. The environmental awareness calls us to develop a more sustainable chemistry. Theoretical principles[1] and green metrics[2] want to furnish guidelines and tools for a thriving chemical sustainability. In 1998, the "12 Principles of Green Chemistry"[3] by Anastas and Warner recognized catalysis as one of the main techniques for a more environmentally benign synthesis (Scheme 1.1). The employment in catalytic amounts, the possible absence of pre-functionalizations, the robustness of syntheses, and the presence of only minor side products, outline catalysis as a very attractive strategy.

In this context, electrochemistry for transition metal-catalyzed redox reactions has recently affirmed itself as a powerful approach towards a more environmental-friendly catalysis. Indeed, with this methodology, stoichiometric redox agents are replaced by current with the use of stable and lasting electrodes.[4]

Scheme 1.1 12 Principles of Green Chemistry by Anastas and Warner.

1.1 Transition Metal-Catalyzed C–H Activation

The formation of C–C and C–Het bonds is of utmost interest in chemistry, since it opens the way for efficient and versatile syntheses. Early examples of transition metal-catalyzed cross-coupling chemistry consisted in the copper-catalyzed reactions by Glaser and Ullmann.[5] During 1970-80s, these cross-coupling approaches found large employment after the discovery of palladium-catalyzed cross-coupling chemistry, which led to the development of many named reactions, such as the Suzuki–Miyaura,[6] Negishi,[7] Mizoroki–Heck,[8] Kumada–Corriu,[9] Hiyama,[10] Stille,[11] and Sonogashira–Hagihara[12] reactions. Other landmarks for palladium-catalysis are the Tsuji–Trost reaction[13] and the Buchwald–Hartwig amination.[14] This golden age of palladium-catalysis has been recognized with the award of the Nobel Prize in Chemistry to Heck, Negishi, and Suzuki in 2010.[15]

Despite the tremendous influence of cross-coupling reactions in organic synthesis, the aim of a sustainable chemistry is still not fully met (Scheme 1.1.1,a). In fact, this approach requires pre-functionalization of the starting materials, undermining the atom-economy of the overall process.[16] For this reason, direct C–H functionalization has emerged as a powerful tool to ameliorate the step- and atom-economy (Scheme 1.1.1,b).[17] Although this approach avoids the functionalization of one substrate, it is still necessary to manipulate the coupling partner, to obtain for example an organic halide. From a step-economical viewpoint, oxidative C–H/C–H functionalizations, namely cross-dehydrogenative couplings, are most desirable (Scheme 1.1.1,c).[4b, 18] Pre-functionalizations are thus avoided and the waste formation is decreased, formally generating only H_2 as by-product, but a stoichiometric oxidant is still inconveniently required. Remarkably, the recent merger of electrochemistry and transition metal catalysis allowed for the use of electricity as cost-effective and environmental-friendly oxidant, avoiding toxic and sacrificial chemicals, thus lowering the waste production.[4]

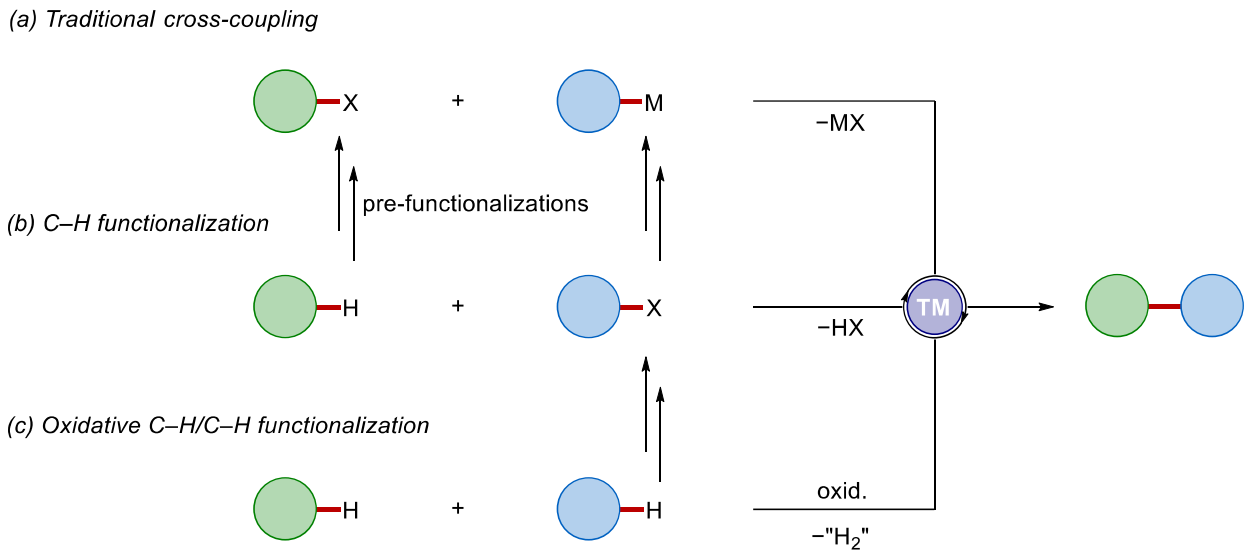

Scheme 1.1.1 Three different modes of C–H bond functionalization.

Synthetically meaningful C–H activations must face several challenges. Indeed, the bond dissociation energy (BDE) of carbon-hydrogen bonds is usually higher than the one of C–X bonds that are typically employed in the cross-coupling approach (e.g., BDE(Ph–H) ≈ 113 kcal mol^{-1} *vs.* BDE(Ph–Cl) ≈ 97 kcal mol^{-1}).[19] Moreover, the presence of numerous C–H bonds in a molecule of interest, and their similar BDEs increase the challenge for a site-selective activation.[20] Three approaches are thus used by chemists to overcome the problem and reach selectivity, as shown in Scheme 1.1.2. First, in electronically activated substrates, such as activated arenes or heterocycles, the kinetic acidity of one C–H bond is higher than the others, making it easier to selectively functionalize.[21] Second, the use of sterically demanding groups helps to shield C–H bonds and leads to the activation of the most accessible one.[22] The third approach regards the use of a directing-group (DG) to coordinate the transition metal catalyst, which can thus activate the bond in its close proximity.[23] On the one hand, the first two approaches are severely limited to the substrate's inherent features and hence the substrate scope is usually rather limited. On the other hand, directing groups (DG), despite being a very efficient mean, have the drawback of needing the incorporation of the DG itself. For this reason, the use of weakly-coordinating,[24] transient,[25] removable[26] or inherent directing groups is preferential.

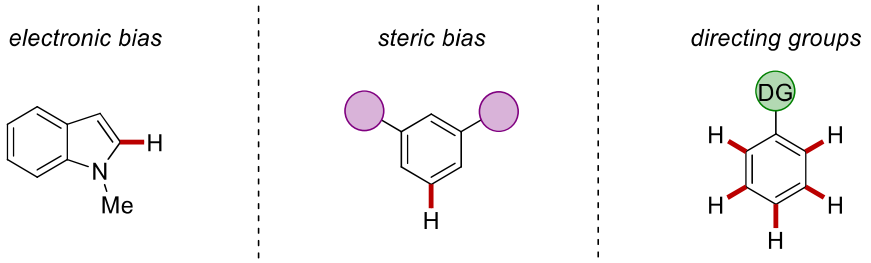

Scheme 1.1.2 Positional selectivity in C–H activation.

The crucial C–H activation step has been extensively studied, making it possible to identify five different ways to cleave the bond, which depend on the nature of the metal employed, its oxidation state, and the ligands. With the exclusion of radical-type outer-sphere mechanisms,[27] these consist in oxidative addition, electrophilic substitution, σ-bond metathesis, 1,2-addition, and base-assisted metalation (Scheme 1.1.3).[28] The oxidative additions usually take place with late and electron-rich transition metals in low oxidation states, such as palladium(0) and ruthenium(0), or iridium(I) and rhodium(I). When late transition metals are in higher oxidation states, they favor an electrophilic substitution. In contrast, early transition metals are reported to preferentially react *via* σ-bond metathesis. The 1,2-addition pathway was proposed for early transition metals with an unsaturated M=X bond. More recently, base-assisted C–H metalation, where a base facilitates the abstraction of a proton through a five- or six-membered transition state, has gained major prominence.

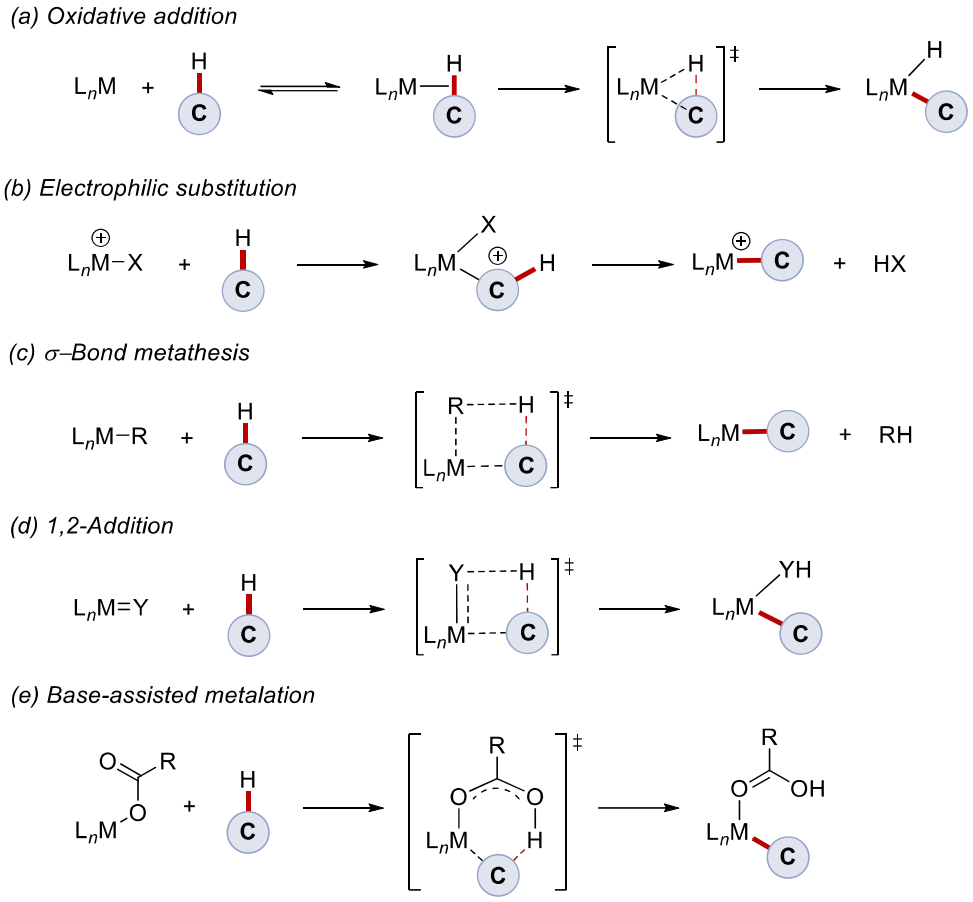

Scheme 1.1.3 Mechanistic pathways for the C–H activations.

Transition metal-catalyzed C–H activation reactions have primarily been proposed to occur generally *via* the base-assisted pathway. Extensive studies led to the proposal of different mechanisms (Scheme 1.1.4).[29] Concerted metalation-deprotonation (CMD) and ambiphilic metal-ligand activation (AMLA) have been independently proposed by Fagnou/Gorelsky[30] and MacGregor/Davies,[31] respectively, and are controlled by kinetic C–H acidity. Moreover, Ackermann introduced the base-assisted internal electrophilic-type substitution (BIES) as C–H activation pathway occurring with carboxylate support.[29, 32]

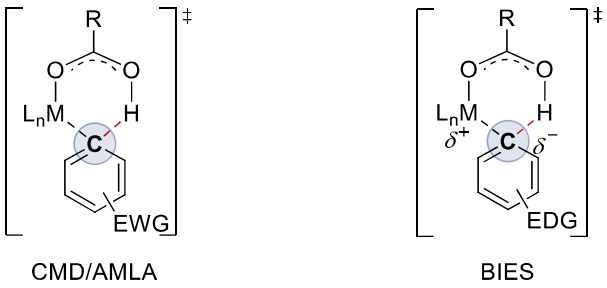

Scheme 1.1.4 Mechanistic paths for the base-assisted C–H metalation.

1.2 Organic Electrocatalysis

Since forms of energy, their consumption, and waste production are nowadays issues of high interest, chemistry is improving its way of producing molecules. An efficient synthesis should envisage a small number of steps to reach the target molecule under mild reaction conditions, together with a good selectivity and high resource-economy. This approach avoids the use of toxic reagents, reducing waste production, and adequate employment of energy. In this context, the use of electrochemistry for molecular syntheses can play a pivotal role (Scheme 1.2.1). Indeed, the replacement of chemical oxidants and reductants with electricity carries different advantages.[33] Firstly, the atom-economy and waste prevention are increased due to the absence of stoichiometric redox reagents in the reaction. It also enhances the safety, as toxic and hazardous reagents are replaced or are generated *in-situ* and possibly only in small quantities. Moreover, the tunability of the applied redox potential gives a more precise control over the desired redox event, thus allowing for milder reaction conditions and improved selectivities. Lastly, electrosynthesis is usually cost efficient, since the electrodes employed are generally inert and long-lasting.

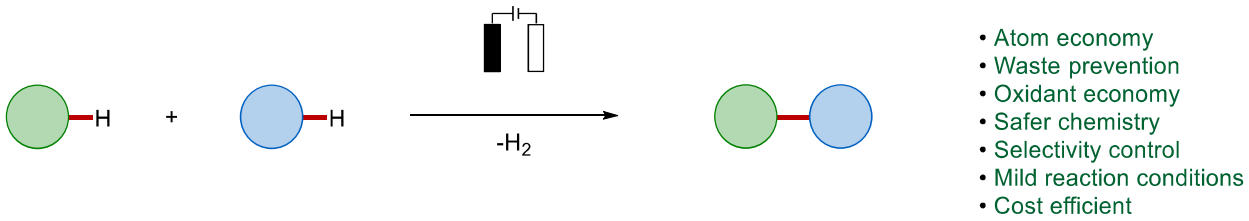

Scheme 1.2.1 Electrochemical approach for cross-dehydrogenative coupling and advantages.

The origin of electrosynthesis can be traced back to Kolbe electrolysis (Scheme 1.2.2). This first electro-organic reaction, inspired from the work of Faraday in 1834,[34] was performed by Hermann Kolbe, from Göttingen, in 1848.[35] The reaction consists of the electrochemical conversion of carboxylic acids to give CO_2 and alkanes. From this starting point, electrosynthesis made great steps with the affirmation of foreground reactions, such as the Shono oxidation,[36] as well as industrial applications, like the Simons fluorination[37] and the Monsanto process.[38]

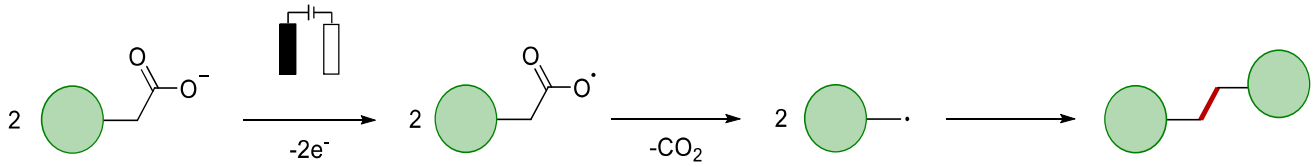

Scheme 1.2.2 The Kolbe reaction.

1.2.1 C–H Activation and Electrosynthesis

An early example of merging palladium-catalyzed C–H activation and electrosynthesis was reported by Amatore and Jutand (Scheme 1.2.3).[39] The reaction consisted of a Fujiwara-Moritani type alkenylation, where catalytic amounts of benzoquinone **3** served as indirect oxidant for the oxidation of palladium(0) species **6** formed after the reductive elimination from palladium(II) complex (Scheme 1.2.3). The benzoquinone was thus continuously re-oxidized at the carbon cloth anode. The drawbacks consisted in the need of performing the reaction in a divided cell setup to avoid the electrodeposition of palladium, and in the use of a mediator that decrease the atom-economy of the reaction, even though it is present only in catalytic amounts.

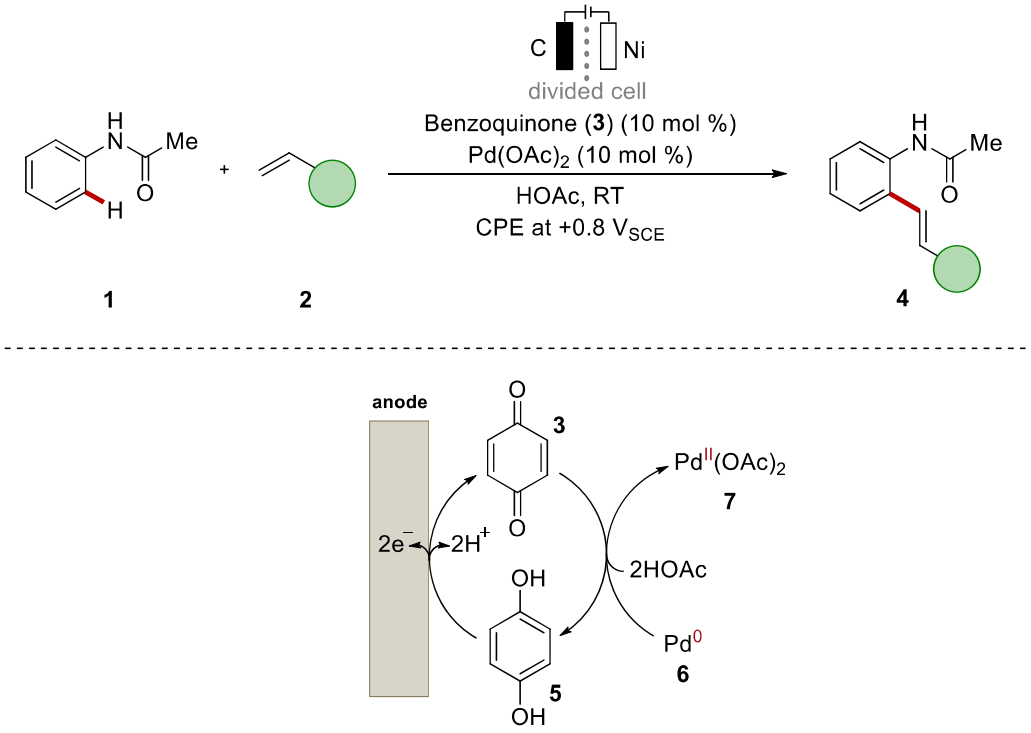

Scheme 1.2.3 Electrochemical palladium-catalyzed alkenylation by Amatore and Jutand.

In 2009, Kakiuchi disclosed electrochemical palladium-catalyzed chlorinations and brominations of 2-phenyl-pyridines (Scheme 1.2.4).[40] In this report, electricity was used to generate the halonium ion from mineral acids, thus avoiding expensive halogenation reagents. The cation was then attacked by the palladacycle, furnishing the desired product **9**. The same group extended the approach to iodinations with elemental iodine or potassium iodide.[41] More recently, Mei showed that the use of less corrosive ammonium bromides is also suitable for palladium-catalyzed electrochemical bromination.[42] These approaches were nevertheless limited to strongly coordinating pyridine directing groups.

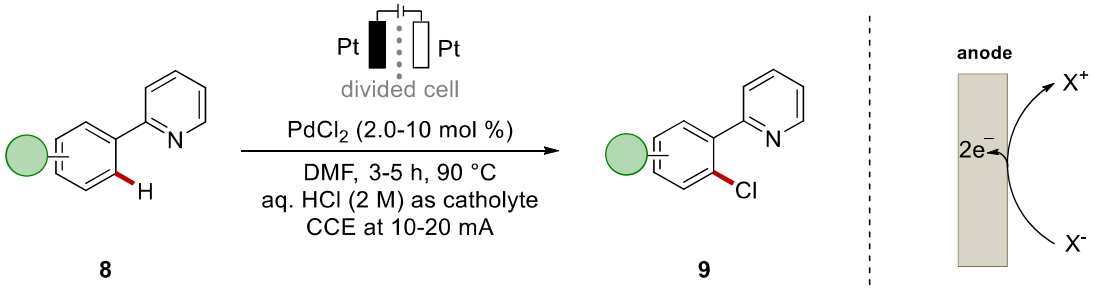

Scheme 1.2.4 Electrochemical palladium-catalyzed halogenation by Kakiuchi.

Thus far, electrochemistry was used for the regeneration of the mediator or for the formation of halonium cations, but not employed in the direct oxidation of the metal. Budnikova reported the direct oxidation of a palladacycle for the C–H perfluorocarboxylation of phenyl pyridines.[43] In 2017, Mei published the electrochemical palladium-catalyzed C(sp^3)–H oxygenation of oximes (Scheme 1.2.5).[44] The proposed catalytic cycle commences with the coordination of the oxime **10** to the palladium(II) acetate catalyst **7**. Subsequent base-assisted C–H activation delivers species **13** that is then oxidized at the anode to give a high-valent palladium(III) or palladium(IV) complex **14**. Finally, reductive elimination yields the desired product **11** and regenerates the active catalyst **7**. As supported by cyclic voltammetry studies, the palladacycle could be oxidized directly and efficiently on the platinum anode, but the reaction still required a divided cell setup to avoid electrodeposition at the cathode.

The same group performed arene C(sp^2)–H activation likewise.[45] In the following year, the group of Sanford published a similar acetoxylation of C(sp^2)–H and C(sp^3)–H bonds.[46] The electrochemical palladium catalysis was not limited to oxygenation reactions, but Mei and co-workers proved it feasible also for methylation and acylation reactions.[47]

This progress represented the state of the art at the outset of my doctoral work. Electrochemical C–H activation was limited to expensive palladium catalysis in a divided cell setup. During the past four years, the field underwent a fast growth with excellent examples from Ackermann,[4a, 48] Lei,[49] Mei,[50] and Xu,[51] among others.[52]

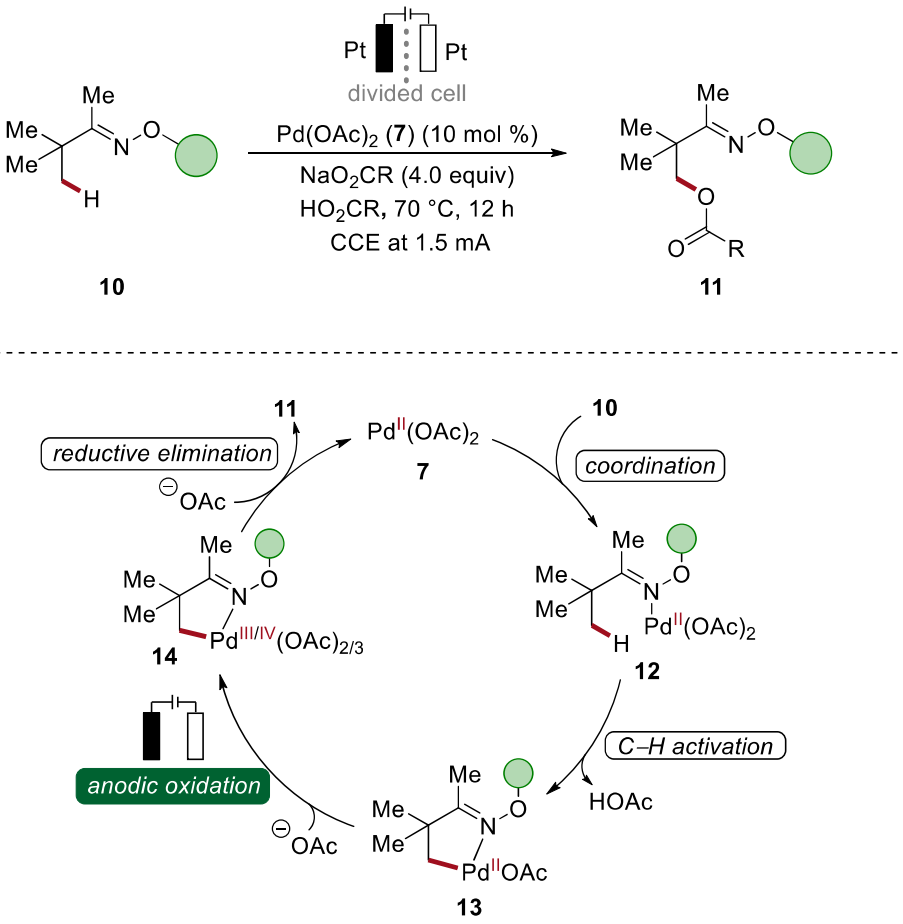

Scheme 1.2.5 Electrochemical palladium-catalyzed C(sp^3)–H oxygenation and proposed catalytic cycle.

1.3 Cobalt-Catalyzed C–H Activation

In the last twenty years, cobalt has gained particular attention among the 3d metals due to its numerous applications for C−H functionalizations. Its reduced cost in comparison to more precious transition metals of the 4d and 5d series makes its use highly desiderable. There are two reactivities that mainly describe cobalt-catalyzed C−H functionalizations, namely the low-valent and high-valent cobalt catalyses.[17]

Already in 1941, the catalytic activity of cobalt for the homocoupling of Grignard reagents was revealed by Karash and Fields.[53] Cobalt catalysis for C−H activation dates back to 1955, when a study by Murahashi showed the carbonylative cyclization of imines **15** with carbon monoxide using dicobalt octacarbonyl as catalyst (Scheme 1.3.1).[54] Even though the conditions were extremely

harsh, this pioneering work was also presenting the directing group strategy for C−H activation. In the following year, they expanded the applicability of the reaction to azobenzenes.[55]

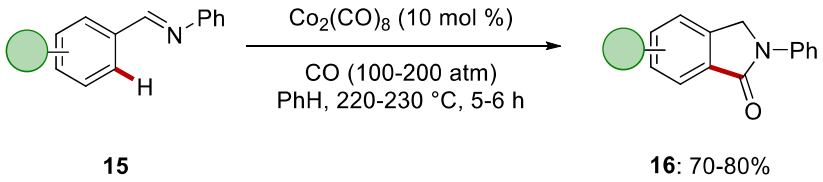

15 **16**: 70-80%

Scheme 1.3.1 Cobalt-catalyzed carbonylative cyclization by Murahashi.

After 40 years, Klein proved the ability of cobalt in performing C−H cleavage, synthesizing different cyclocobaltated complexes (Scheme 1.3.2).[56] In these studies, the employment of stoichiometric amounts of the cobalt complex [$Co(CH_3)(PMe_3)_4$] allowed to successfully synthesize 5-,[56a-d, 56f] 6-,[56d] and even the more strained 4-membered[56e] cycles, all with different Lewis-basic directing groups, including ketones, phosphines, and pyridines.

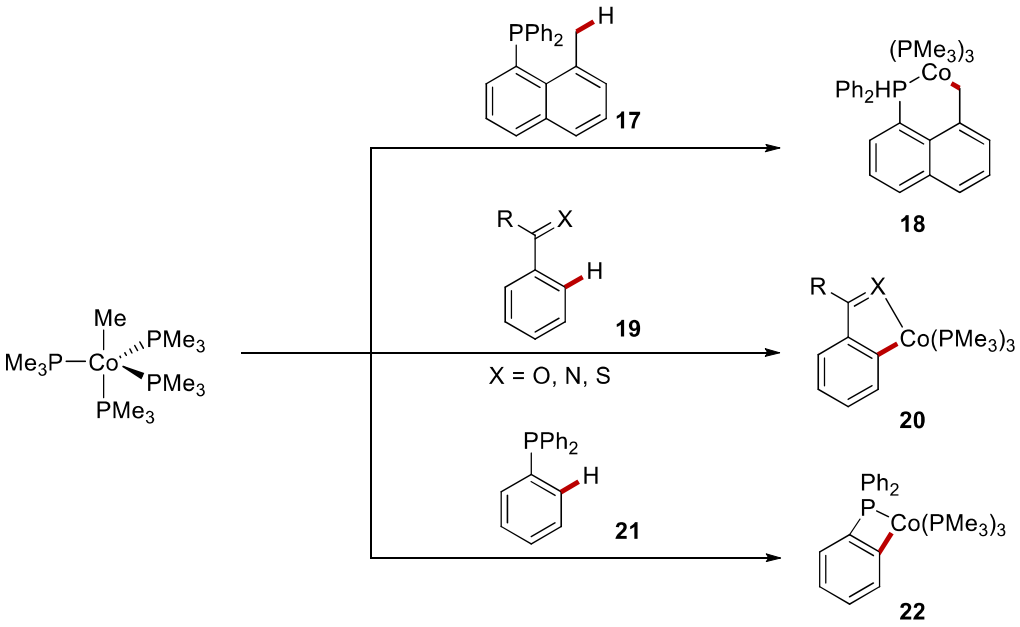

Scheme 1.3.2 Stoichiometric syntheses of cobaltacycles by Klein.

Another important milestone was the cobalt-catalyzed hydroarylation reported by Kisch and coworkers in 1994 (Scheme 1.3.3).[57] The authors employed a cobalt(I) species and azobenzenes **23** for a successful di-functionalization.

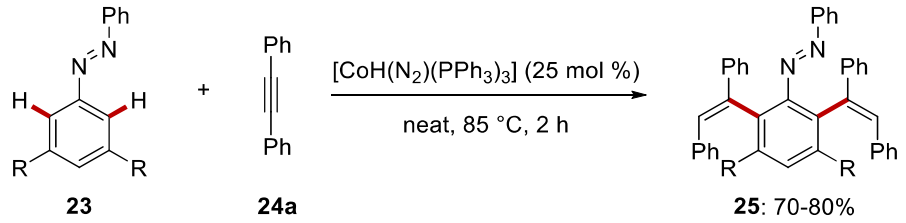

Scheme 1.3.3 Cobalt-catalyzed hydroarylation by Kisch.

1.3.1 Cobalt-Catalyzed C–H Activation with Chemical Oxidants

In 2014, Daugulis reported on the oxidative C−H/N−H annulation of benzamides **26** with alkynes **24** (Scheme 1.3.4,a).[58] 8-Aminoquinoline was employed to take advantage of a bidentate directing groups for chelation.[59] The formation of a catalytically competent high-valent cobalt(III) cycle was proven by NMR spectroscopy. Manganese(II) acetate was present in stoichiometric amounts as co-oxidant together with aerial oxygen. 2,2,2-Trifluoroethanol (TFE) was the best solvent, while carboxylates proved to be essential additives. In the same year they also expanded the reaction to alkenes **31** for C−H/N−H annulations (Scheme 1.3.4,b).[60] These reports delineated the oxidative cobalt catalysis for heterocycles synthesis as an attractive, versatile, and step-economical approach.[61]

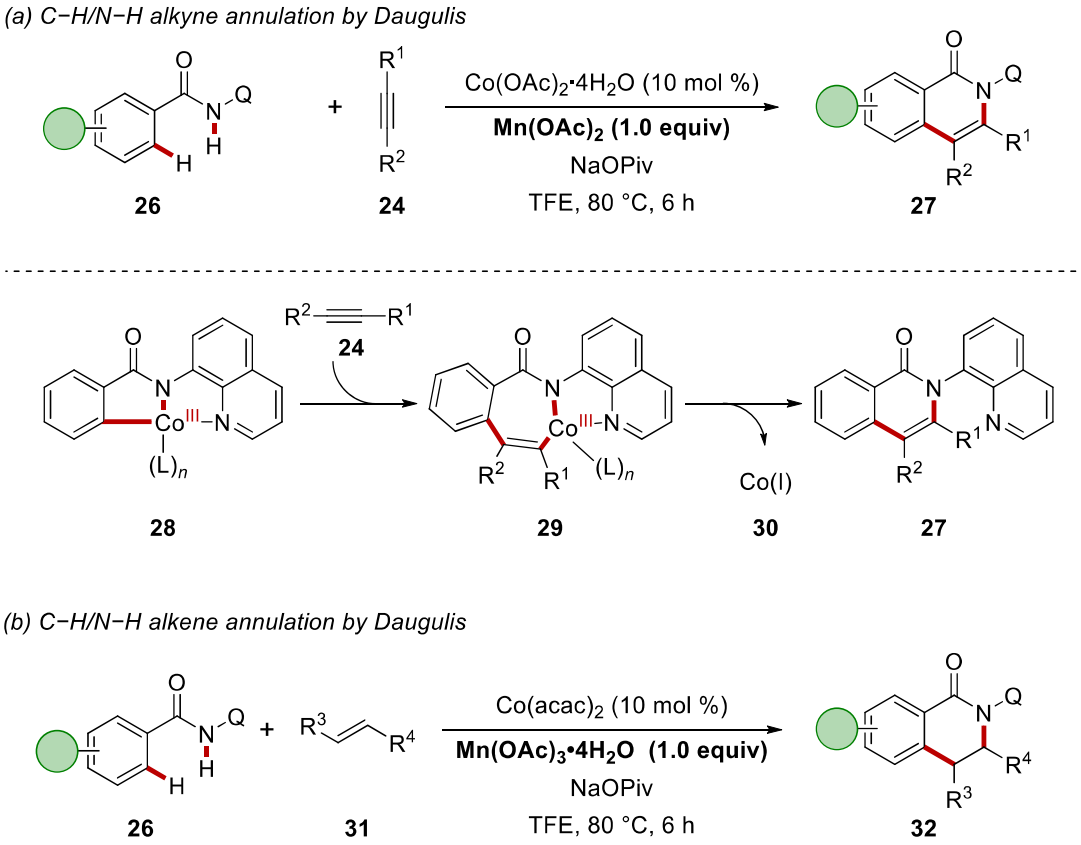

Scheme 1.3.4 Cobalt-catalyzed oxidative C−H/N−H annulations and their mechanism.

In 2016, Ackermann achieved the synthesis of isoquinolones **34** employing cobalt(II) acetate and a pyridine-*N*-oxide directing group, using for the first time molecular oxygen as the sole terminal oxidant (Scheme 1.3.5,a).[62]

Other examples of oxidative annulations using cobalt catalysts were reported with alkenes by the groups of Volla[63] and Ackermann,[64] as well as with allenes by of Volla/Maiti[65] and Cheng[66] (Scheme 1.3.5,b-e). These reports were relying on bidentate 8-aminoquinoline as directing group and manganese acetate as oxidant, besides the report by Cheng that required the presence of a silver(I) salt.

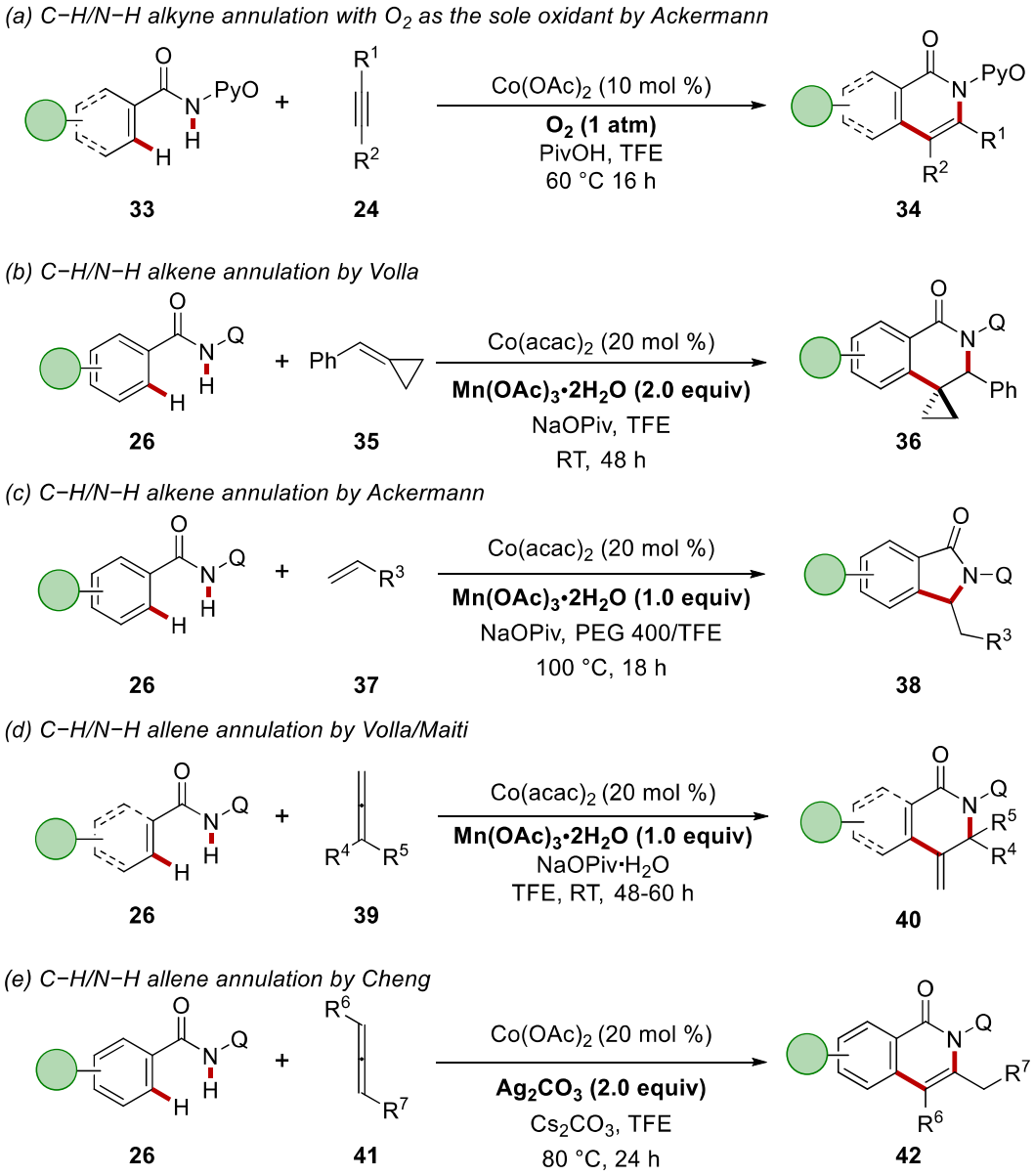

Scheme 1.3.5 Cobalt-catalyzed oxidative C−H/N−H annulations.

Besides annulation reactions, different C–C and C–Het bond formations have furthermore been studied and achieved with oxidative cobalt-catalyzed C–H activations.

First, the allylation of quinolinamides **26** was achieved with alkenes under different reaction conditions (Scheme 1.3.6).[67] The reactions benefited from DCE or chlorobenzene as the solvents, the use of silver(I) salts as chemical oxidants and cobalt acetate as the catalyst. For all the three studies the reaction showed the same selectivity, yielding the desired product **44** exclusively with allylic selectivity over the styrenyl selectivity of the conventional olefination reactions.

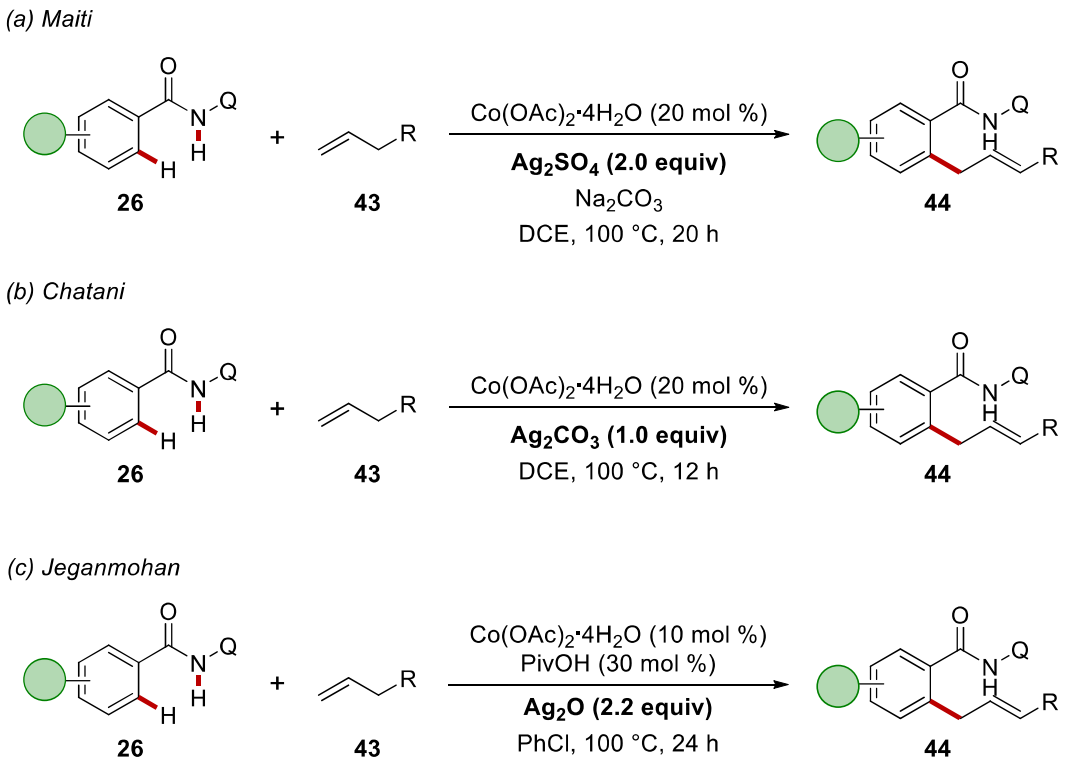

Scheme 1.3.6 Cobalt-catalyzed oxidative C–H allylations.

Moreover, Balaraman published the alkynylation in the presence of 8-aminoquinoline directing group *via* oxidative cobalt-catalyzed C–H activation (Scheme 1.3.7).[68] Cobalt(III) acetylacetonate was employed with large excess of silver carbonate as oxidant at 150 °C. The reaction mainly yielded the bis-alkynylated products **46**, unless having substituents in the *ortho*-position, bulky electron-withdrawing *meta*-substituents, or when heteroarenes were employed.

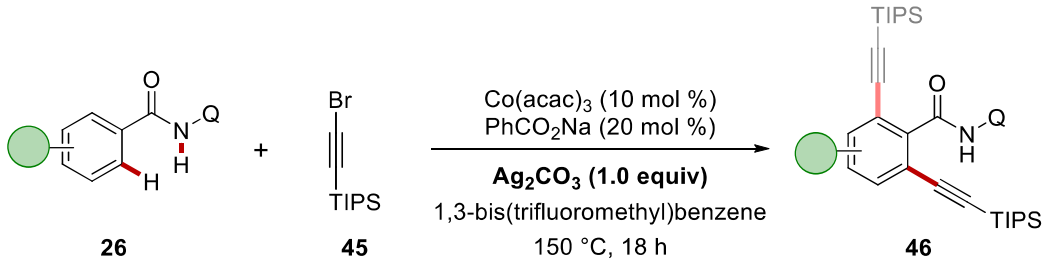

Scheme 1.3.7 Cobalt-catalyzed C–H alkynylation.

Regarding C–Het bond formations, in 2015 the oxidative cobalt-catalyzed oxygenation was reported by Niu and Song (Scheme 1.3.8,a).[69] Here, pyridine-*N*-oxide was again employed, while 1.0

equivalent of silver oxide was used as the oxidant. The access to cobalt-catalyzed C–H acyloxylation was disclosed by Zeng, who performed the reaction on arenes **49** with picolinamide as directing group (Scheme 1.3.8,b).[70] Here, carboxylic acids **50** were used as coupling partners and the reaction required 120 °C and 2.0 equivalents of silver carbonate to succeed.

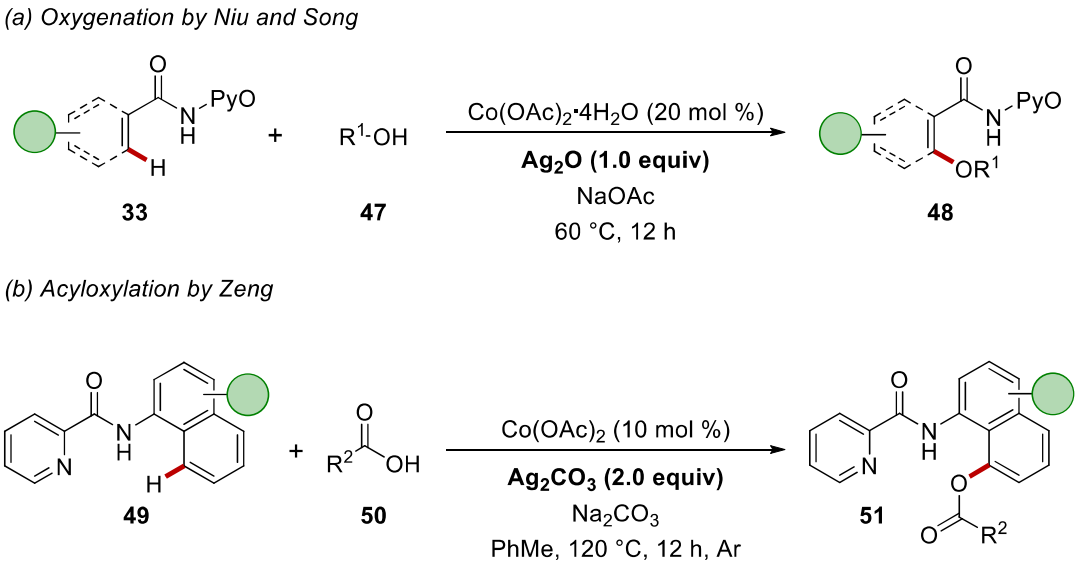

Scheme 1.3.8 Cobalt-catalyzed C–H (a) oxygenation and (b) acyloxylation.

C–H amination was likewise found to be a suitable transformation with oxidative cobalt-catalysis. Ge reported the intra- and inter-molecular amination of unactivated sp^3 C–H bond (Scheme 1.3.9,a).[71] The conditions were very harsh, performing the reaction at 150 °C with 2.5 equivalents of silver carbonate. Milder conditions were sufficient for the amination of C(sp^2)–H bonds which was reported in the following year by Niu and Song (Scheme 1.3.9,b).[72]

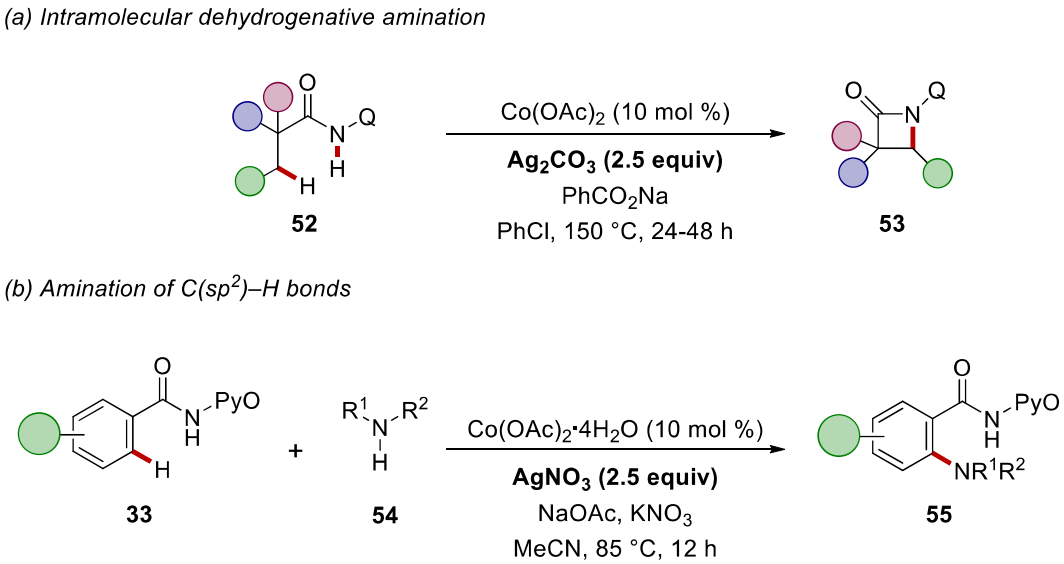

Scheme 1.3.9 Cobalt-catalyzed C−H aminations.

1.3.2 Electrochemical Cobalt-Catalyzed C–H Activation

Recently, electrochemistry has been employed as green oxidant for C–H activation. In 2017, the first example of merger electrochemistry with 3d transition metal-catalyzed C–H activation was reported by Ackermann and co-workers using cobalt-catalysis (Scheme 1.3.10).[73] Here, the use of simple cobalt acetate as catalyst and sodium pivalate as base allowed for the oxygenation of benzamides **33** with pyridine-*N*-oxide as bidentate chelating group. Different aliphatic alcohols **47** underwent the reaction in a divided cell set up with very mild reaction conditions.

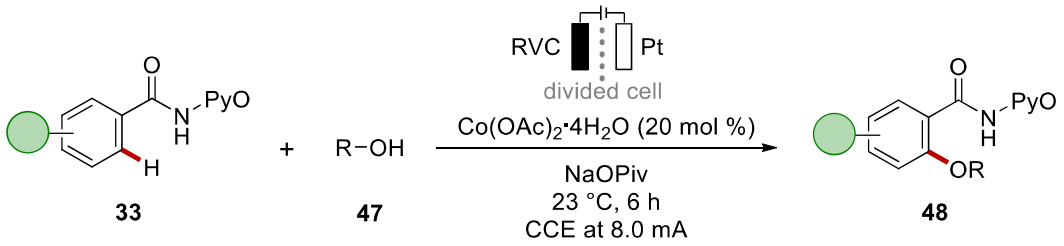

Scheme 1.3.10 Electrochemical cobalt-catalyzed C−H oxygenation.

The above-mentioned cobalt-catalyzed oxygenation from Ackermann was the only research article published prior to the publication of the project in Section 3.1 on *Angewandte Chemie*.

After the publication of the influential electrochemical cobalt-catalyzed C–H/N–H annulations of benzamides with terminal alkynes, discussed in Section 3.1, the group of Lei reported on the electrooxidative annulation with ethylene or ethyne (Scheme 1.3.11,a),[74] while the group of Ackermann further extended the applicability of the cobalt-catalyzed manifold to internal alkynes **24** on benzhydrazide **58** with an electroreductively removable directing group (Scheme 1.3.11,b).[75] Following these studies, allenes[76] **39**, as well as 1,3-diynes,[77] were also employed for the C–H/N–H cobalt-catalyzed annulation reaction by the group of Ackermann (Scheme 1.3.11,c). The group of Lei reported a similar reaction, employing sulfonamides as directing group.[78] In 2020, Ackermann published a remarkable study on the mechanism of electrochemical cobalt catalysis.[79] Herein, the authors could prove a pathway involving Co(III/IV/II) manifold for the C–H oxygenation reaction, thus through an oxidatively-induced reductive elimination. They moreover confirmed a Co(III/I) cycle for annulation reactions. Indeed, the product **60** was formed from the reaction between the isolated Co(III) intermediate and the alkyne in absence of electricity.

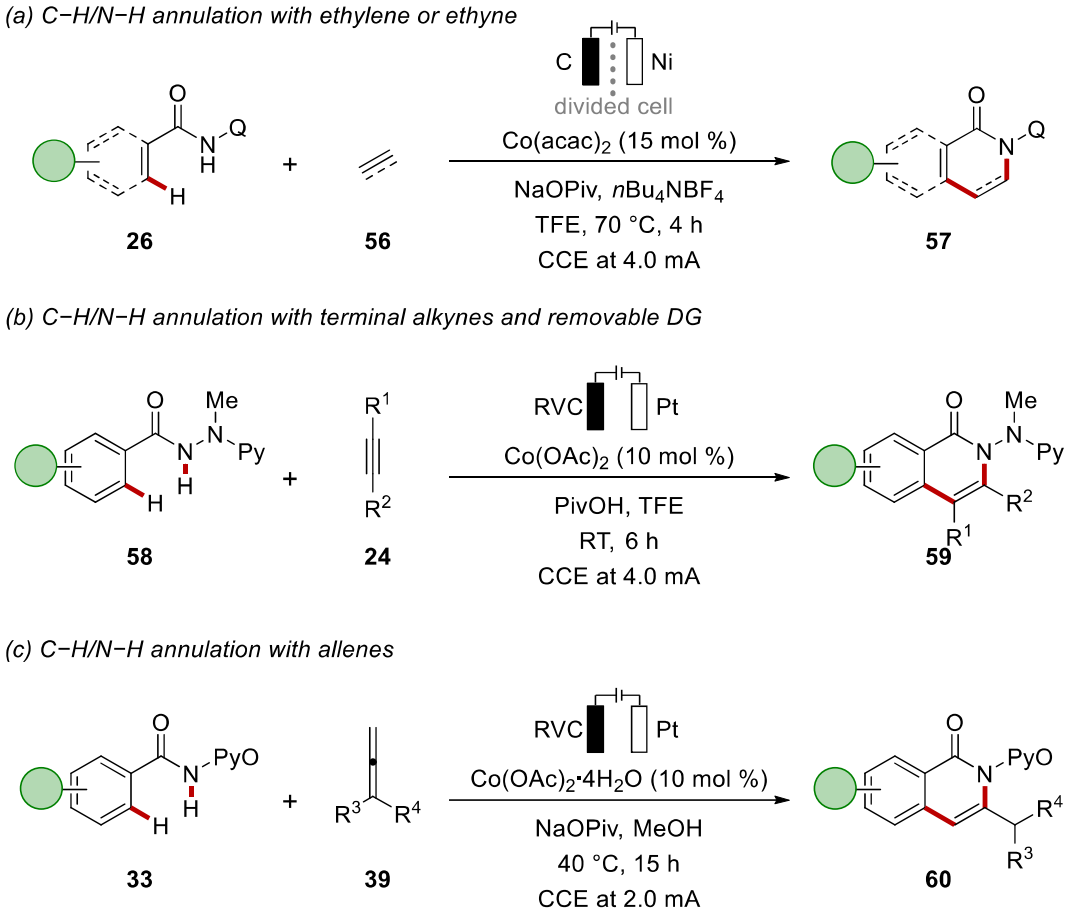

Scheme 1.3.11 Electrochemical cobalt-catalyzed C–H/N–H annulations.

In 2018, Lei reported the electrochemical cobalt-catalyzed C–H/N–H carbonylation with carbon monoxide in divided cell set up. The approach occurred in an intermolecular, as well as intramolecular fashion, to deliver amides **61** and phthalimides **62** as annulation product, respectively (Scheme 1.3.12,a).[80] Simultaneously, Ackermann published the annulation with carbon monoxide but in a user-friendly undivided cell set up (Scheme 1.3.12,b).[81] The procedure allowed for the C–H/N–H annulation also with isocyanides **64**.

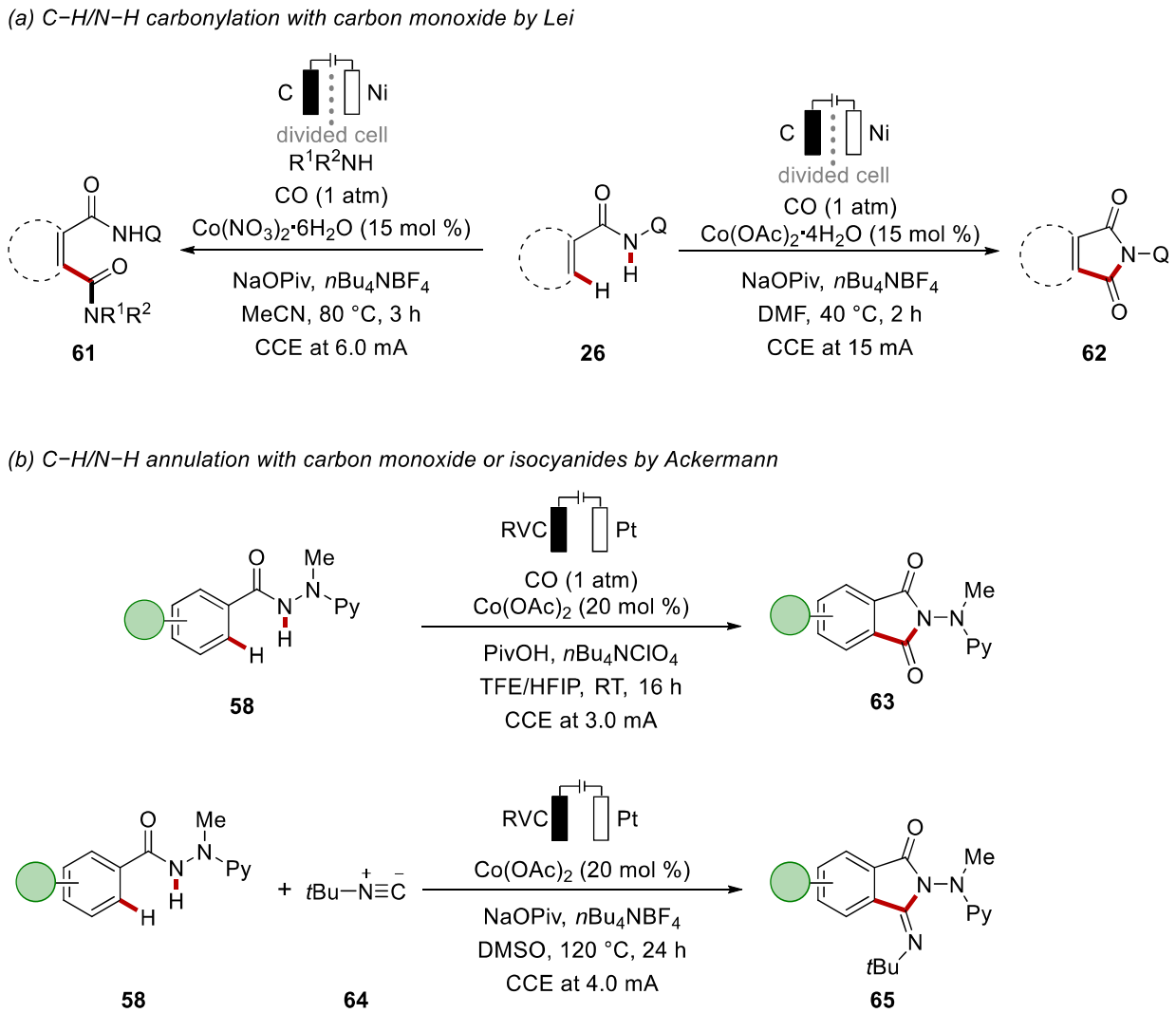

Scheme 1.3.12 Electrochemical cobalt-catalyzed C–H/N–H annulations with carbon monoxide and isocyanides **64**.

In 2020, the group of Ackermann developed the first electrochemical cobalt-catalyzed allylation reaction on benzamides **26** bearing 8-aminoquinoline as directing group (Scheme 1.3.13).[82] Here, non-electronically activated alkenes **43** could be used, with the exclusive formation of the allylated products **44** with a high chemo- and regio-selectivities.

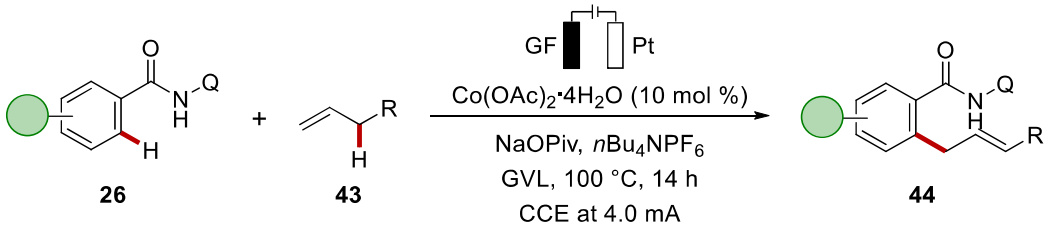

Scheme 1.3.13 Electrochemical cobalt-catalyzed C−H/N−H allylation.

Besides annulation reactions, diverse C–Het bond formation reactions were developed using cobaltaelectro-catalysis. In 2018, an amination reaction was presented by the group of Ackermann (Scheme 1.3.14,a).[83] The reaction employed electricity as oxidant in the renewable solvent γ-valerolactone (GVL) and in an undivided cell set up at 40 °C. At the same time, also Lei published an electrochemical cobalt-catalyzed C–H amination, but this approach required a divided cell and a higher temperature (Scheme 1.3.14,b).[84]

After the groundbreaking work on alkoxylation showed at the beginning of this section, another C–O bond formation was published by the Ackermann group, featuring C–H acyloxylation (Scheme 1.3.14,c).[85]

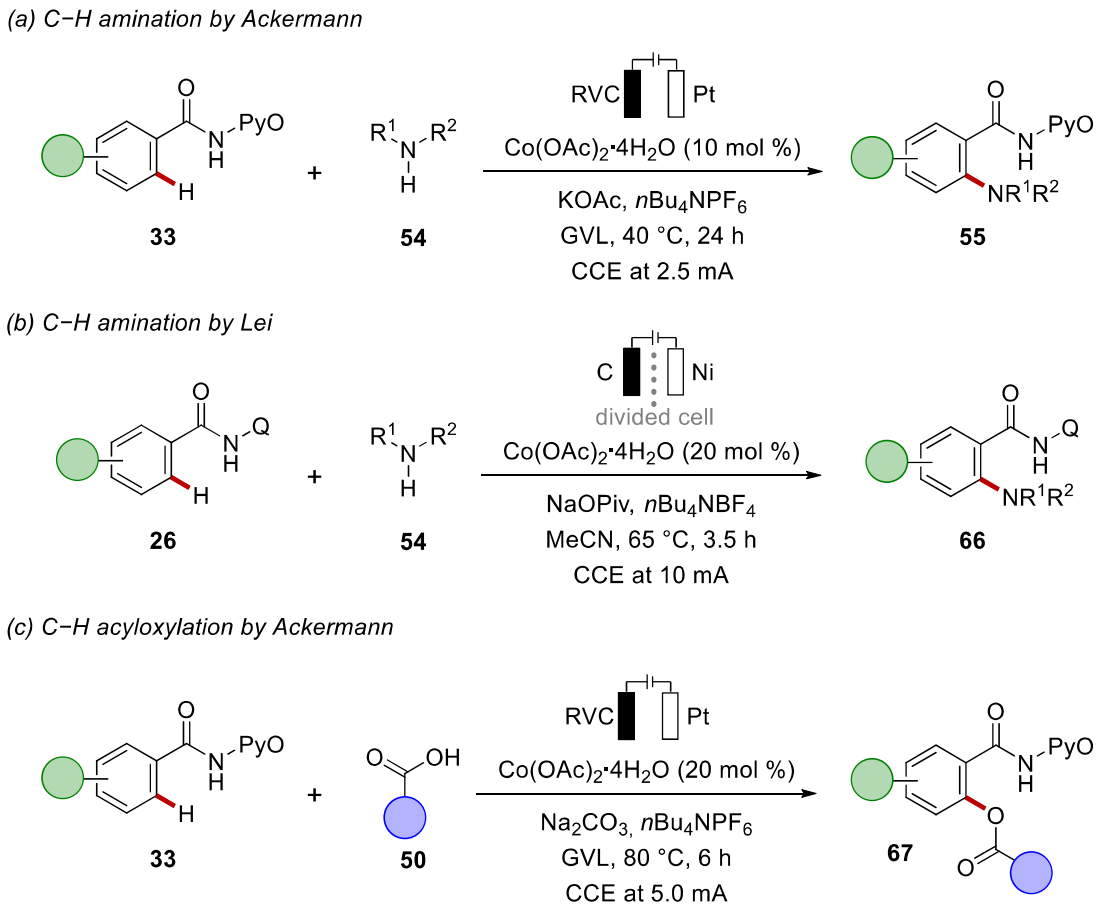

Scheme 1.3.14 Electrochemical cobalt-catalyzed C−Het formation.

1.4 Ruthenium-Catalyzed C–H Activation

While the initial developments in transition metal-catalyzed C–H functionalization have been obtained mainly with palladium and rhodium as catalysts, ruthenium has more recently gained attention due its lower price and versatility.[86] Ruthenium-catalyzed C–H activation has been mainly performed with two approaches, one *via* oxidative addition, usually with low-valent complexes, the other *via* deprotonation pathway, that requires ruthenium(II) complexes, a base and an oxidant to re-oxidize the ruthenium(0) species at the end of the catalytic cycle.[87]

The first report on ruthenium C–H activation dates back to 1965 when Chatt and Davidson could obtain the stoichiometric C–H activation of sodium naphthalene salts forming the ruthenium(0) complex **68** *via* oxidative addition (Scheme 1.4.1).[88]

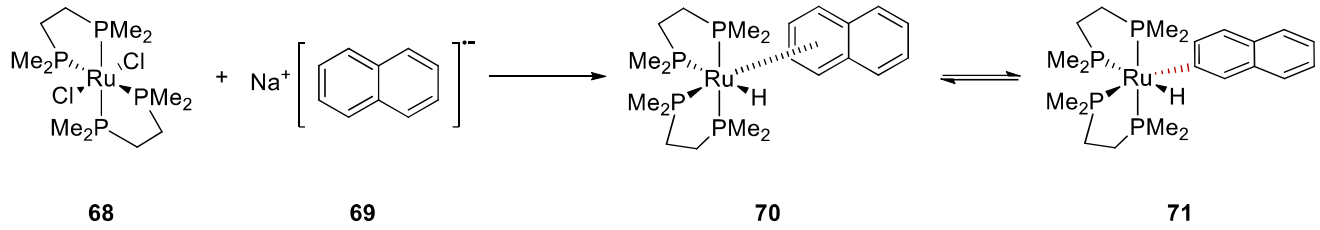

68 **69** **70** **71**

Scheme 1.4.1 First example of ruthenium-mediated C–H activation.

Only 21 years later the first catalytic ruthenium C–H activation reaction was reported, when Lewis and Smith published a study on the *ortho*-functionalization of phenols **72** with ethylene **73**, obtaining mainly the di-alkylated product **75** together with the mono-alkylated one **76** (Scheme 1.4.2).[89] The reaction required harsh conditions and benefited from the use of a transient directing group.

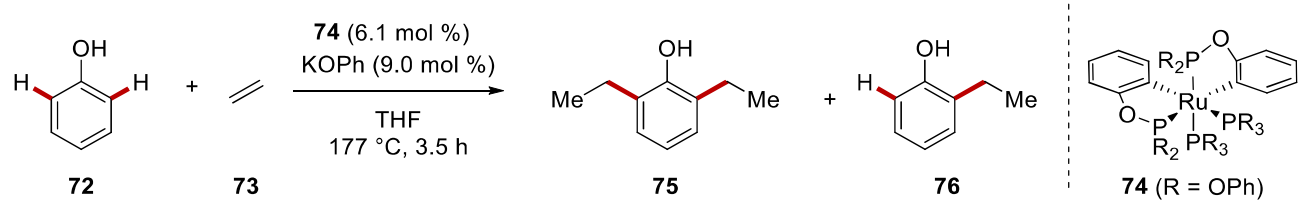

72 **73** **75** **76** **74** (R = OPh)

Scheme 1.4.2 First ruthenium-catalyzed C–H activation.

Another early example was reported by the group of Moore with the ruthenium(0)-catalyzed acylation using carbon monoxide and olefins.[90] An advance in ruthenium catalysis was achieved in 1993, when Murai published the *ortho* C–H alkylation by weak *O*-coordination[24] with the ruthenium(0) catalyst [$RuH_2(CO)(PPh_3)_3$] (Scheme 1.4.3).[91] The authors suggested that a five-membered ruthenacycle **79** was obtained *via* chelation-assisted oxidative addition. This methodology had an ample scope, showing for the first time the wide applicability of ruthenium catalyzed C–H activation.

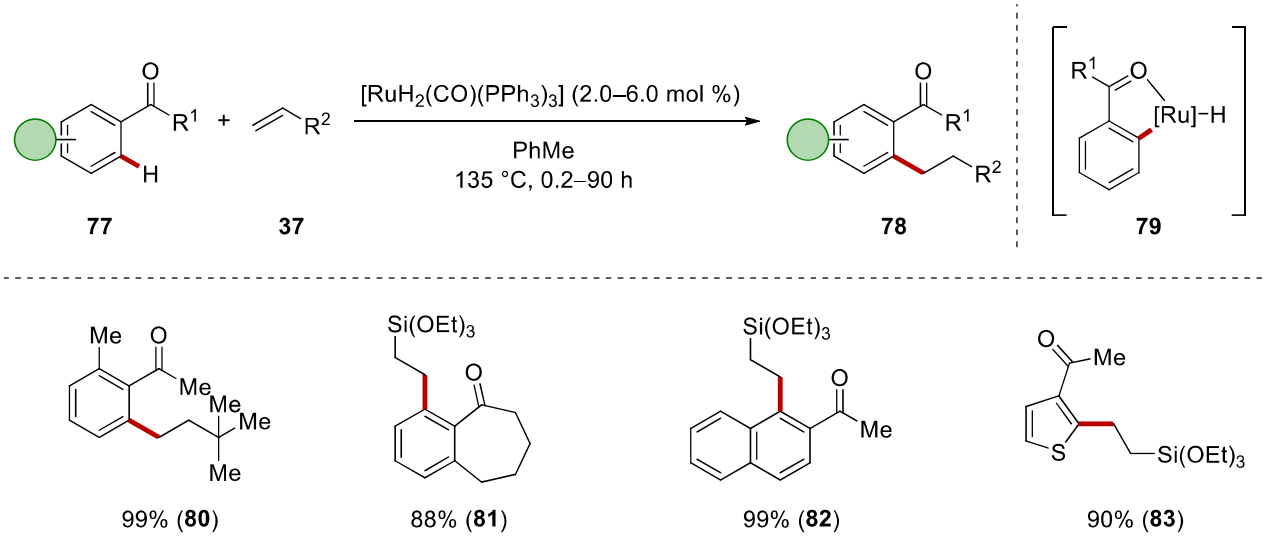

Scheme 1.4.3 Seminal report of ruthenium-catalyzed direct C–H activation.

1.4.1 Ruthenium-Catalyzed Oxidative C–H Activation with Chemical Oxidants

In 2001, the pioneering work from Milstein showed the Fujiwara–Moritani-type[92] undirected ruthenium C–H alkenylation of arenes **84** under high pressure of oxygen as terminal oxidant (Scheme 1.4.4).[93] The reaction proved feasible with different ruthenium(II) and ruthenium(III) sources.

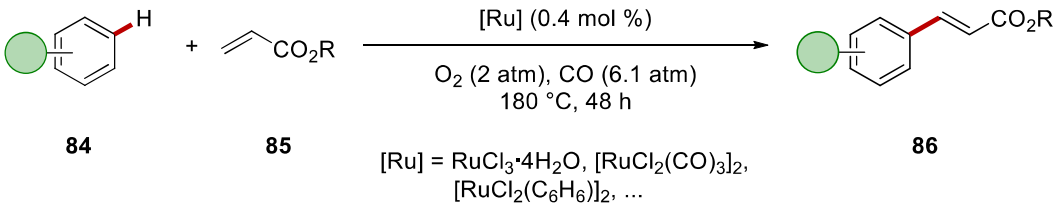

Scheme 1.4.4 First oxidative ruthenium-catalyzed C–H alkenylation.

In 2011, Ackermann achieved the synthesis of isoquinolones **88** by oxidative ruthenium catalyzed C–H/N–H annulation on benzamides **87** and alkynes **24** (Scheme 1.4.5).[94] Copper acetate was employed as oxidant and *tert*-amyl alcohol as the solvent.

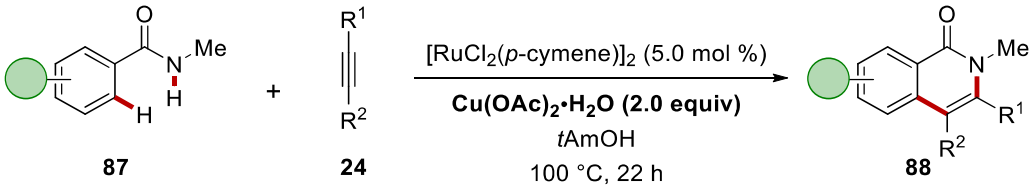

Scheme 1.4.5 Oxidative ruthenium-catalyzed C–H/N–H annulation.

In 2012, two independent reports by the groups of Ackermann[95] and Jeganmohan[96] were published regarding the oxidative ruthenium-catalyzed annulation on benzoic acids **89** to yield isocumarines **90**. The first approach used simple benzoic acids **89** and internal alkynes **24** together with copper acetate as the oxidant. Dichloro(*p*-cymene)ruthenium(II) dimer was the pre-catalyst that *in-situ* formed a cationic species **91** with the help of potassium hexafluorophosphate and copper acetate (Scheme 1.4.6). This step started the catalytic cycle proposed by the authors, followed by the carboxylate-assisted C–H ruthenation of the benzoic acid **89** to give **92**. After migratory insertion, the generated seven-membered ruthenacycle **93** underwent reductive elimination to yield the product **90** and a ruthenium(0) species that was re-oxidized by the copper.

Later, Ackermann ameliorated the procedure allowing the reaction to proceed under oxygen or air atmosphere.[97] Thus, even if convenient molecular oxygen was acting as the oxidant, the approach is of difficult scalability due to the hazard of mixing oxygen and flammable solvents. In this report, they were also able to isolate a set of the ruthenium(0) complexes and to study their behavior in the reaction conditions.

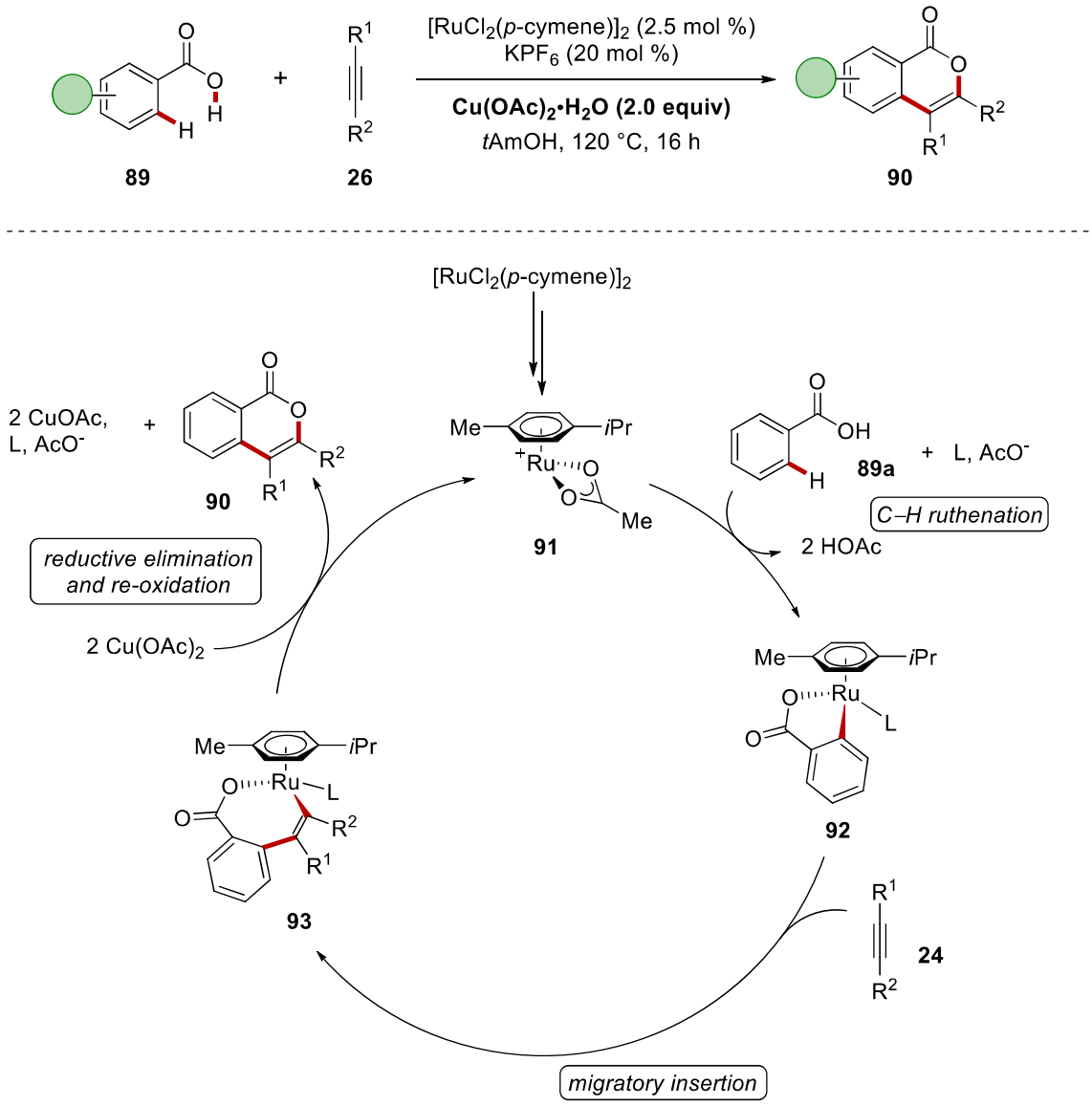

Scheme 1.4.6 Oxidative ruthenium-catalyzed C–H/N–H annulation and proposed catalytic cycle.

Another approach for the annulation reaction to give isocumarines was reported by Wang and colleagues *via* C–H alkenylation and decarboxylation of α-keto carboxylic acids **94** in presence of ruthenium(II) catalyst and copper acetate as oxidant (Scheme 1.4.7).[98]

Based on these reports, many other heterocycles have been synthesized by means of oxidative ruthenium-catalyzed C–H activation.[99]

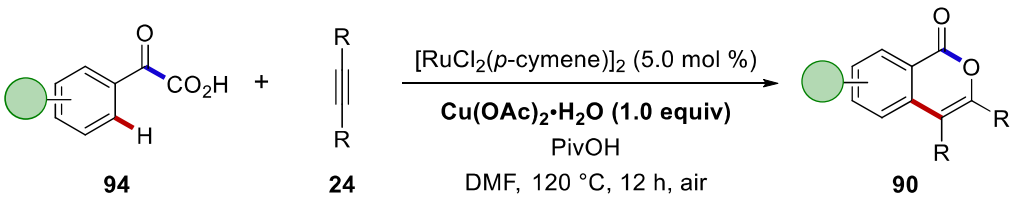

94 24 90

Scheme 1.4.7 Oxidative ruthenium-catalyzed C–H/N–H annulation through decarboxylation.

In 2011, Ackermann reported the synthesis of phtalides by alkenylation of benzoic acids **89** and activated alkenes **37**, followed by an oxa-Michael addition (Scheme 1.4.8).[100] Interestingly, the reaction could proceed in water at 80 °C. Later, the same group was able to implement O_2 as the oxidant in GVL as green solvent.[101]

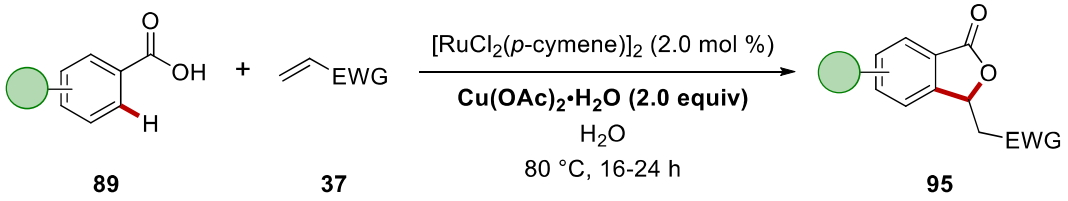

89 37 95

Scheme 1.4.8 Oxidative ruthenium-catalyzed C–H/O–H alkylation.

Ruthenium-catalyzed C–H activation can also proceed through 6-membered ring intermediates, as shown for the first time by the group of Ackermann in 2012 (Scheme 1.4.9).[102] The reports achieved C–H alkenylations with weakly-coordinating directing groups, such as anilides **1** and carbamates **97**. The following year, reports from Li and Wang[103] and from Jeganmohan[104] similarly expanded the scope regarding carbamates for this kind of approach. Another interesting ruthenium-catalyzed C–H activation occurring *via* challenging 6-membered ruthenacycle was the C7 functionalization of indoles reported by Ackermann in 2020.[105]

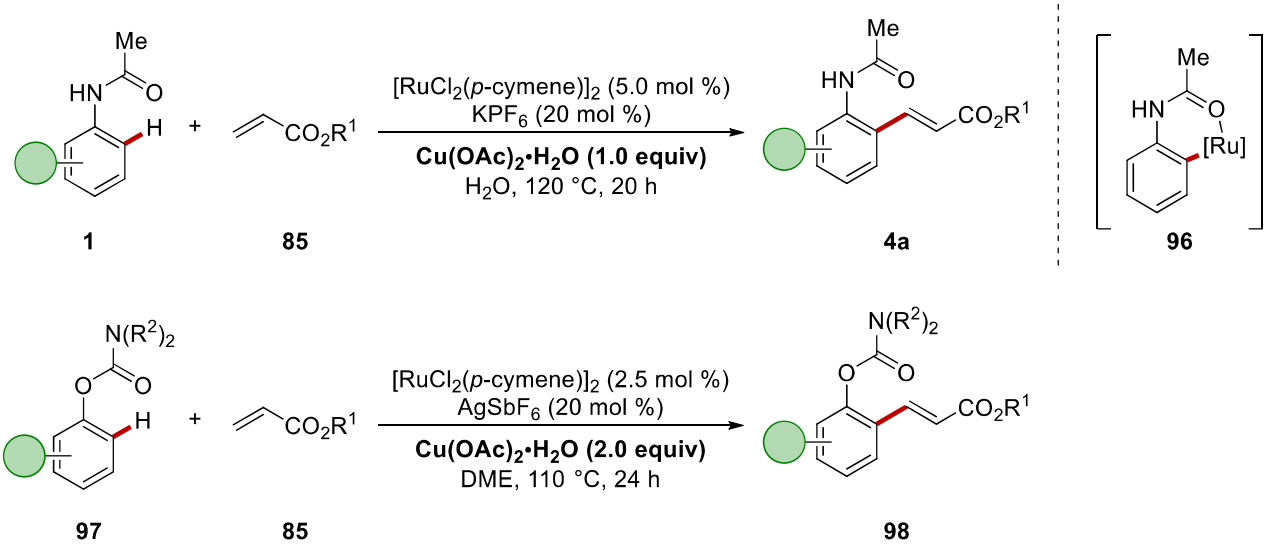

Scheme 1.4.9 Ruthenium-catalyzed C–H activation *via* 6-membered cyclometalated intermediates.

Ruthenium catalysis proved to be versatile also for C–Het bond formation. Alongside several examples of C(sp^3)–H and C(sp^2)–H amination,[106] oxygenation reactions with ruthenium catalyst had been extensively studied. Bakke and co-workers studied the RuO_4-mediated hydroxylation of sp^3 carbons.[107] More recently, Du Bois presented a more versatile methodology for C(sp^3)–H oxygenation, employing catalytic amounts of ruthenium(III) trichloride with a stoichiometric oxidant, allowing for a broader scope (Scheme 1.4.10).[108]

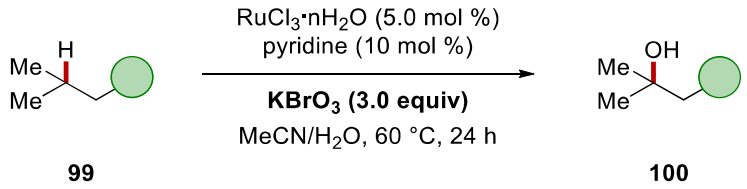

Scheme 1.4.10 Ruthenium-catalyzed C(sp^3)–H oxygenation.

The oxygenation of sp^2 carbons is more explored, with two concurrent reports from Rao[109] and Ackermann,[110] that envisaged the use of an arene-ligand-containing ruthenium(II) catalyst, TFA/TFAA as solvent mixture and a stoichiometric oxidant (Scheme 1.4.11). The approach of Rao worked on esters **101** with potassium persulfate or iodic acid as oxidant, while the one of Ackermann employed tertiary amides **103** and (diacetoxyiodo)benzene. In following reports, the scope was

shown to include ketones **105**,[111] Weinreb amides **106**,[112] carbamates **107**,[113] anilides **108**,[114] and very challenging aldehydes **109**,[115] as well as to the *para*-functionalization of anisoles **110** (Scheme 1.4.11,c).[113] The mechanistic rationale involves the formation of a ruthena(II)cycle with subsequent oxidation to ruthenium(III) or ruthenium(IV) that can thus yield the product and reform the active catalyst.

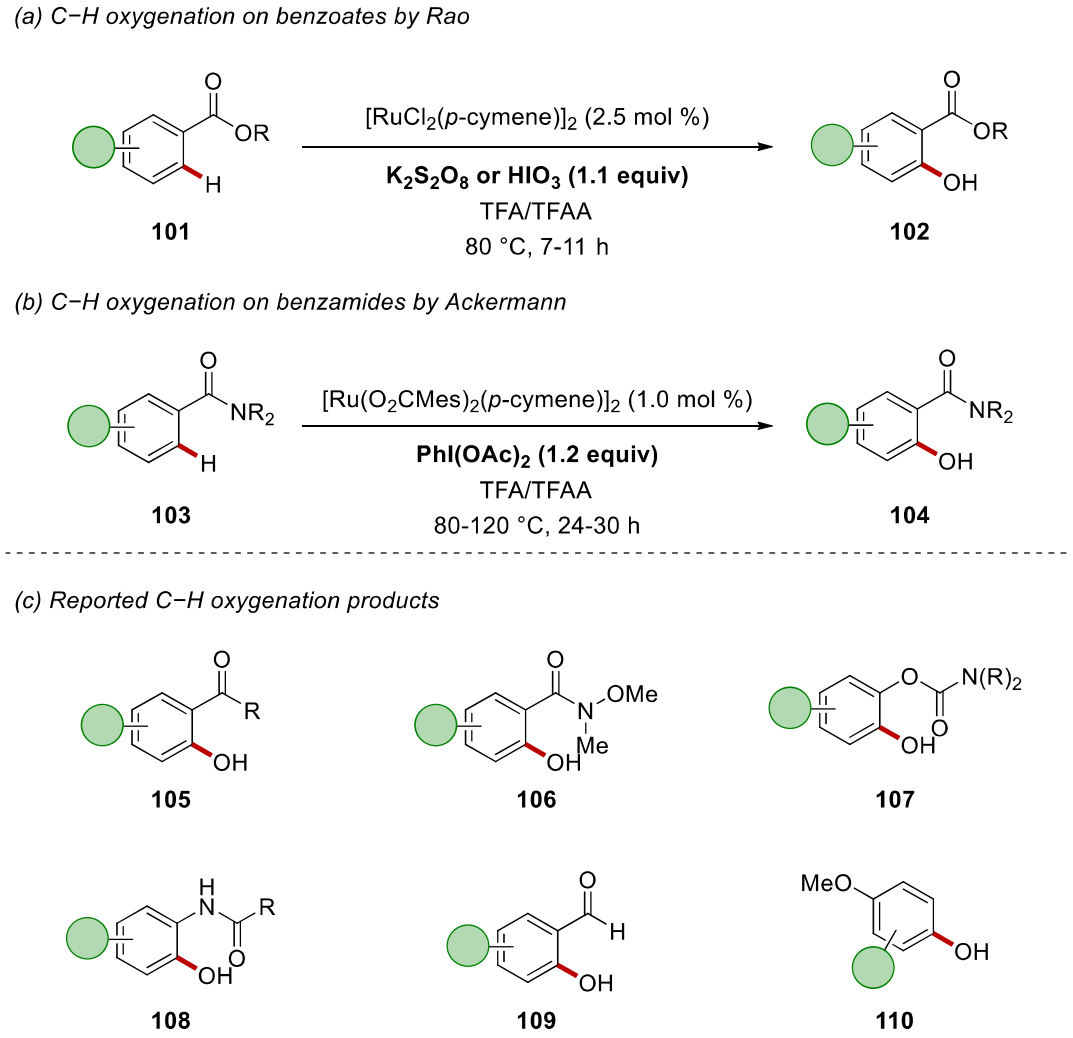

Scheme 1.4.11 Oxidative ruthenium-catalyzed C–H oxygenations.

1.5 Rhodium-Catalyzed C–H Activation

Similarly to palladium(II)/(0) processes, also rhodium(III)/(I) processes[116] have been studied for organic oxidation reactions. Indeed, analogous to the palladium-catalyzed Wacker process, the

rhodium-catalyzed Monsanto acetic acid process has been extensively investigated.[38] However, rhodium-catalysis has been underdeveloped compared to the thriving palladium catalysis.

The general mechanism for oxidative rhodium-catalyzed transformations employs a rhodium(III) active species **111** that performs C–H activation on a substrate and subsequent functionalization with a coupling partner such as alkynes **24** or alkenes **37**. Reductive elimination or β-hydride elimination led to the formation of the product **114** or **115** and a rhodium(I) species **113** that needs to be re-oxidized (Scheme 1.5.1).

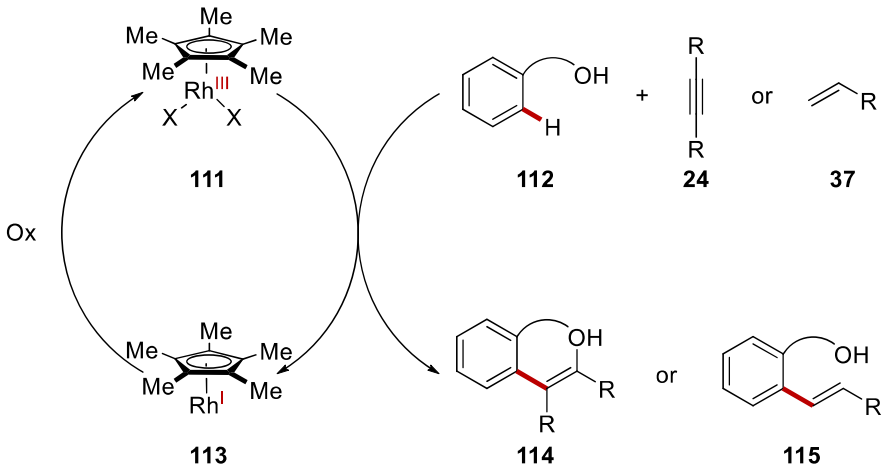

Scheme 1.5.1 Oxidative rhodium-catalyzed C–H/O–H activation.

In 1987, Maitlis and coworkers proved the ability of rhodium of forming cyclometalated complexes with benzoic acids in stoichiometric amounts,[117] opening the way to studies on rhodium catalysis.

1.5.1 Rhodium-Catalyzed Oxidative C–H Activation with Chemical Oxidant

In 2000, Matsumodo and Yoshida presented a rhodium-catalyzed oxidative coupling of benzene with ethylene in the presence of copper(II) acetate as the oxidant.[118] Inspired by the work of Maitlis, in 2007, Satoh and Miura published the annulation reaction between benzoic acids **89** and alkynes **24** or alkenes (Scheme 1.5.2).[119] In this procedure, the copper(II) acts as oxidant but it is required only in catalytic amounts since it is re-oxidized by air. This reaction was then further expanded to heteroarenes[120] and to acrylic acids[121] by the same group but with the need for stoichiometric oxidant.

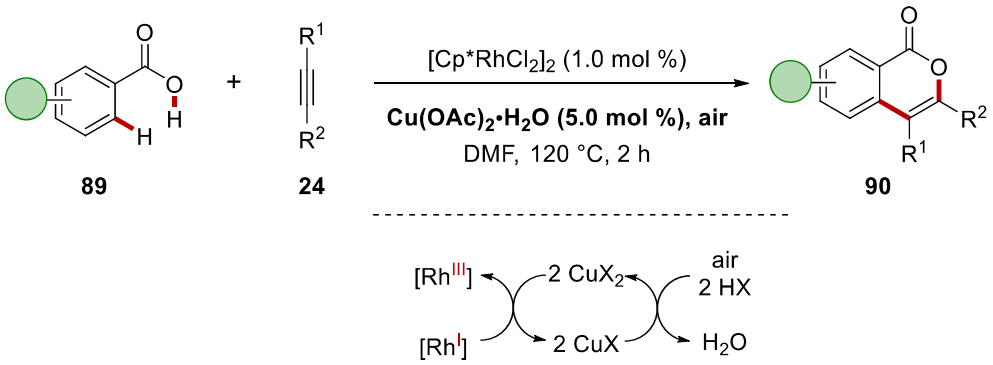

Scheme 1.5.2 Oxidative rhodium-catalyzed C–H/O–H annulation.

Moreover, salicylaldehydes **109** were found to be suitable substrates for the rhodium-catalyzed synthesis of 2,3-diarylchromones **116**. The first report was presented by Satoh and Miura in 2008, employing alkynes **24** as coupling partners (Scheme 1.5.3,a).[122] Interestingly, Li could make use of the same substrate **109** with Wilkinson's catalyst, phenylacetylene **117** as coupling partner, and 4-picoline-*N*-oxide as oxidant, to access a different pathway and furnish coumarins **118** (Scheme 1.5.3,b).[123]

(a) Rhodium-catalyzed synthesis of 2,3-diarylchromones by Satoh and Miura

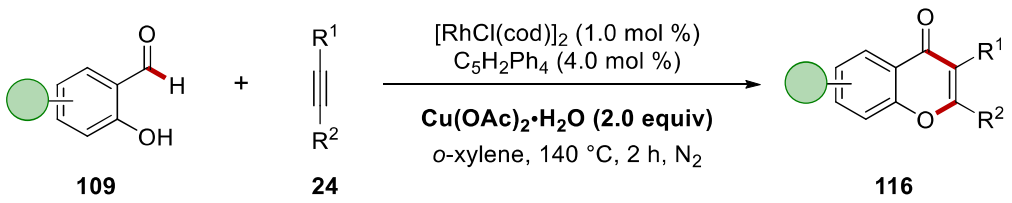

(b) Rhodium-catalyzed synthesis of Cumarines by Li

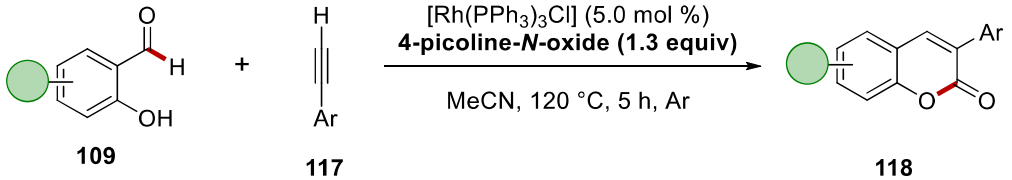

Scheme 1.5.3 Oxidative rhodium-catalyzed C–H/O–H annulation.

These examples were followed by several other rhodium-catalyzed C–H/N–H annulations,[124] including examples with amides[125] and imines.[126]

Another oxidative transformation by rhodium-catalyzed C–H activation was the hydroxylation of arenes, achieved at first in 2013 by Rao and colleagues (Scheme 1.5.4).[114a] The authors used simple $[Rh(OAc)_2]_2$ in presence of an excess of oxidant, such as potassium persulfate or (diacetoxyiodo)benzene, to yield 2-acylphenol **102**. The synthesis of phenols was also working efficiently on weakly coordinating ketones. This report demonstrated that the reaction could be performed both with ruthenium and rhodium catalysis, with the two metals being similar for selectivity and substrate scope. This is one of the rare examples of rhodium catalysis promoting oxygenation of C–H bonds.

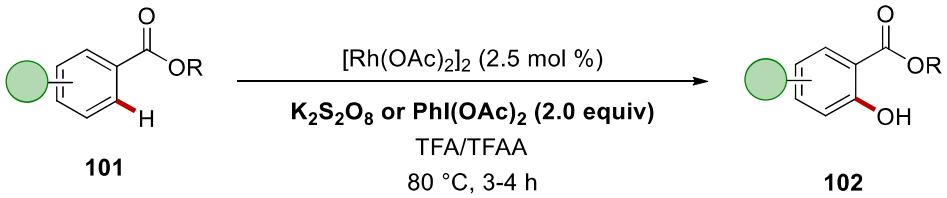

Scheme 1.5.4 Oxidative rhodium-catalyzed C–H oxygenation.

Other three reports on rhodium C–H hydroxylation were published more recently. All of them used a well-defined $[RhCp^*Cl_2]_2$ catalyst in higher loadings compared to the example by Rao. Indeed in 2017, both the groups of Kim[127] and Zhou[128] independently reported this transformation on 2-aryl pyridines **8** (Scheme 1.5.5,a-b). In the latter report, the authors were also able to obtain the acetoxylation reaction in absence of water. The following year, Wang published the C7-hydroxylation and acetoxylation of indolines **121** under mild reaction conditions (Scheme 1.5.5,c).[129]

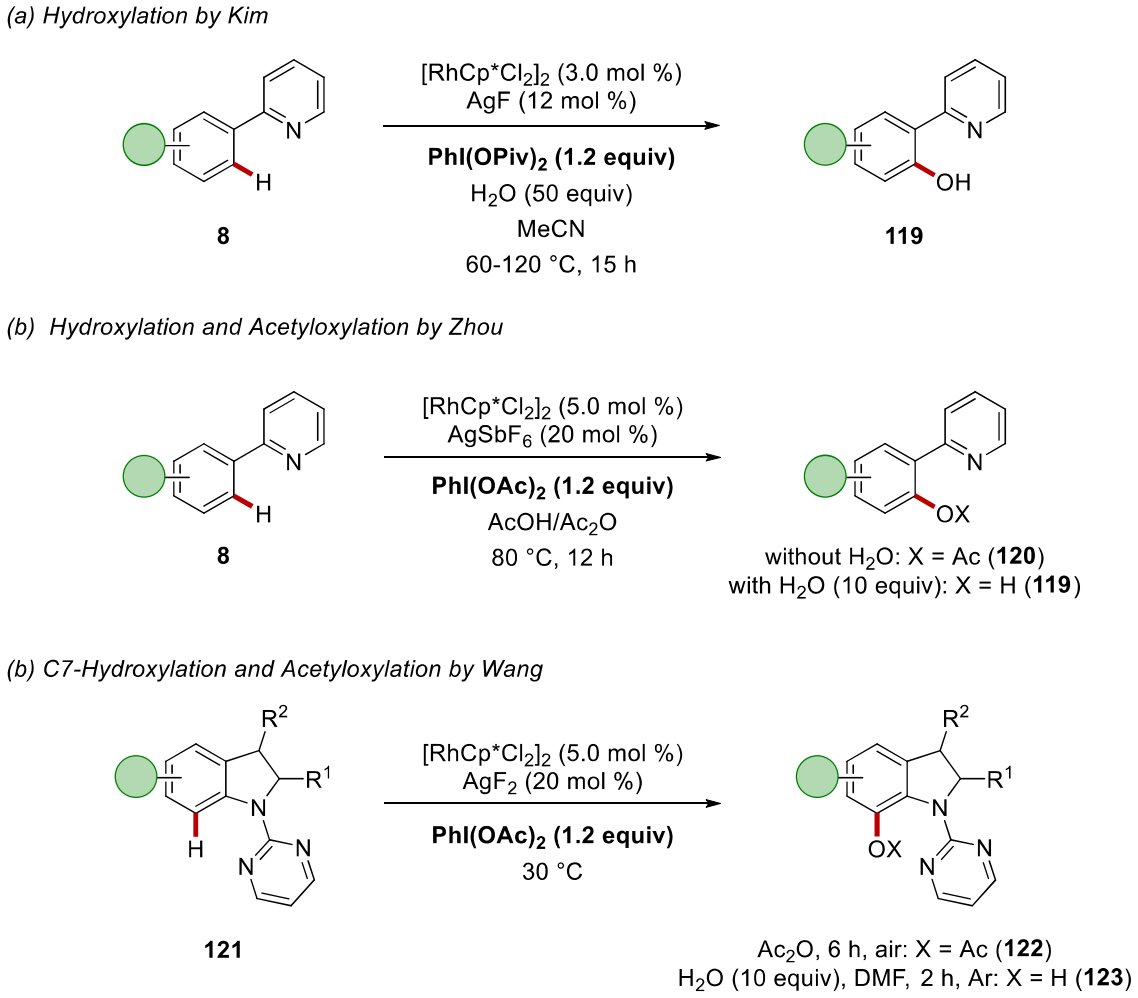

Scheme 1.5.5 Oxidative rhodium-catalyzed C–H oxygenations.

1.5.2 Electrochemical Rhodium-Catalyzed C–H Activation

Due to this expanded use of rhodium catalysis in oxidative C–H activation, it was not long before this chemistry was coupled with electricity. In Section 3.2, the first example of electrochemical rhodium C–H activation, found during the optimization of the electrochemical ruthenium annulation, is described.[130] In 2018, Ackermann reported the cross-dehydrogenative alkene annulation on weakly *O*-coordinating benzoic acids **89** in presence of $[RhCp^*Cl_2]_2$ as catalyst, potassium acetate as base, and *tert*-amyl alcohol/water as solvents in an undivided cell at 4.0 mA constant current electrolysis (Scheme 1.5.6).[131] The mechanistic rationale is very similar to the ruthenium, but here the re-oxidation at the anode takes place on a rhodium(I) to rhodium(III) species. The rhodium catalysis was not limited to α,β-unsaturated carbonyl substrates, indeed the same group also extended the reactivity to the olefination of electro-poor benzamides in a following report.[132] Electrochemical

rhodium-catalyzed C–H activation also employed alkylidenecyclopropanes (ACPs) to selectively furnish either cyclopropanes or dienes.[133]

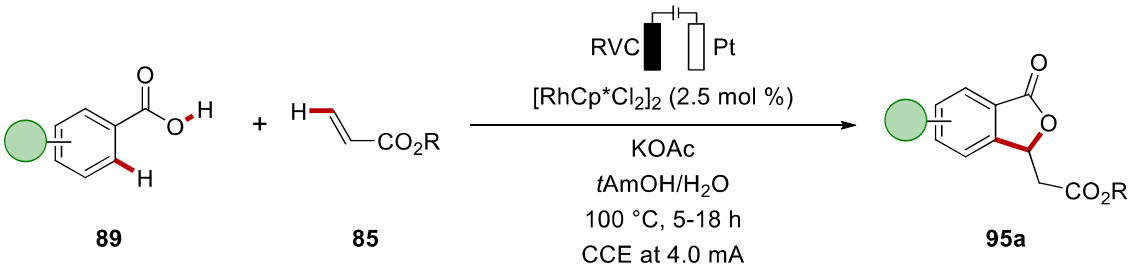

Scheme 1.5.6 Electrochemical rhodium-catalyzed C−H alkene annulation.

Moreover, the first rhodium-catalyzed electrochemical C–C activation was achieved by Ackermann in 2019 with outstanding levels of chemo- and position-selectivity (Scheme 1.5.7,a).[134] Interestingly, a competition experiment between the C–H and C–C showed the preferential activation of the latter bond, providing a way for the synthesis of 1,2,3-trisubstituted arenes (**127**), that are usually not accessible by C–H activation (Scheme 1.5.7,b).

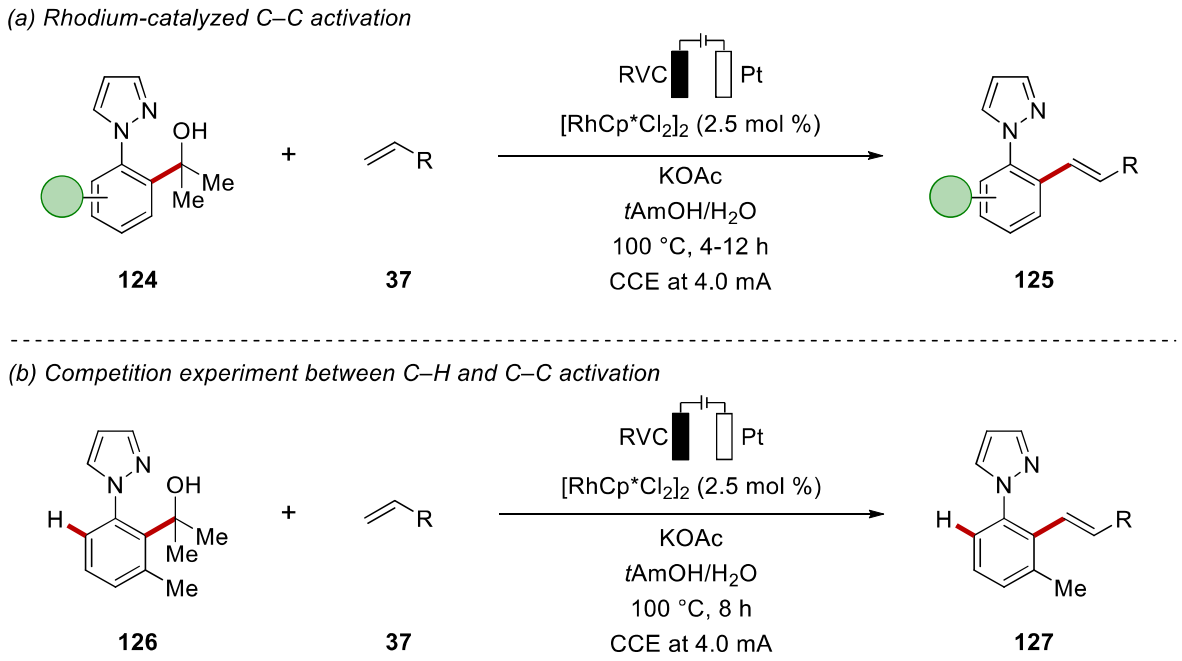

Scheme 1.5.7 (a) Electrochemical rhodium-catalyzed C−C activation and (b) competition experiment.

Besides alkenes **37** as coupling partners, alkynes **24** have also been employed in electrochemical rhodium-catalyzed C–H activation for diverse product syntheses. The first report has been published in 2019 by Ackermann and envisaged not only the [2+2+2] cycloaddition, but also the subsequent DDQ-catalyzed electrochemical cyclodehydrogenation to furnish polycyclic aromatic hydrocarbons **130** (PAHs) (Scheme 1.5.8).[135] Furthermore, the approach showed a clear advantage in comparison to classical chemical oxidants, such as AgOAc, or $Cu(OAc)_2 \cdot H_2O$, in the successful transformation of the sensitive iodo-substituted boronic acid **128a**. Similarly, the same group could also synthesize nitrogen-doped PAHs (aza-PAHs) in a following report.[136]

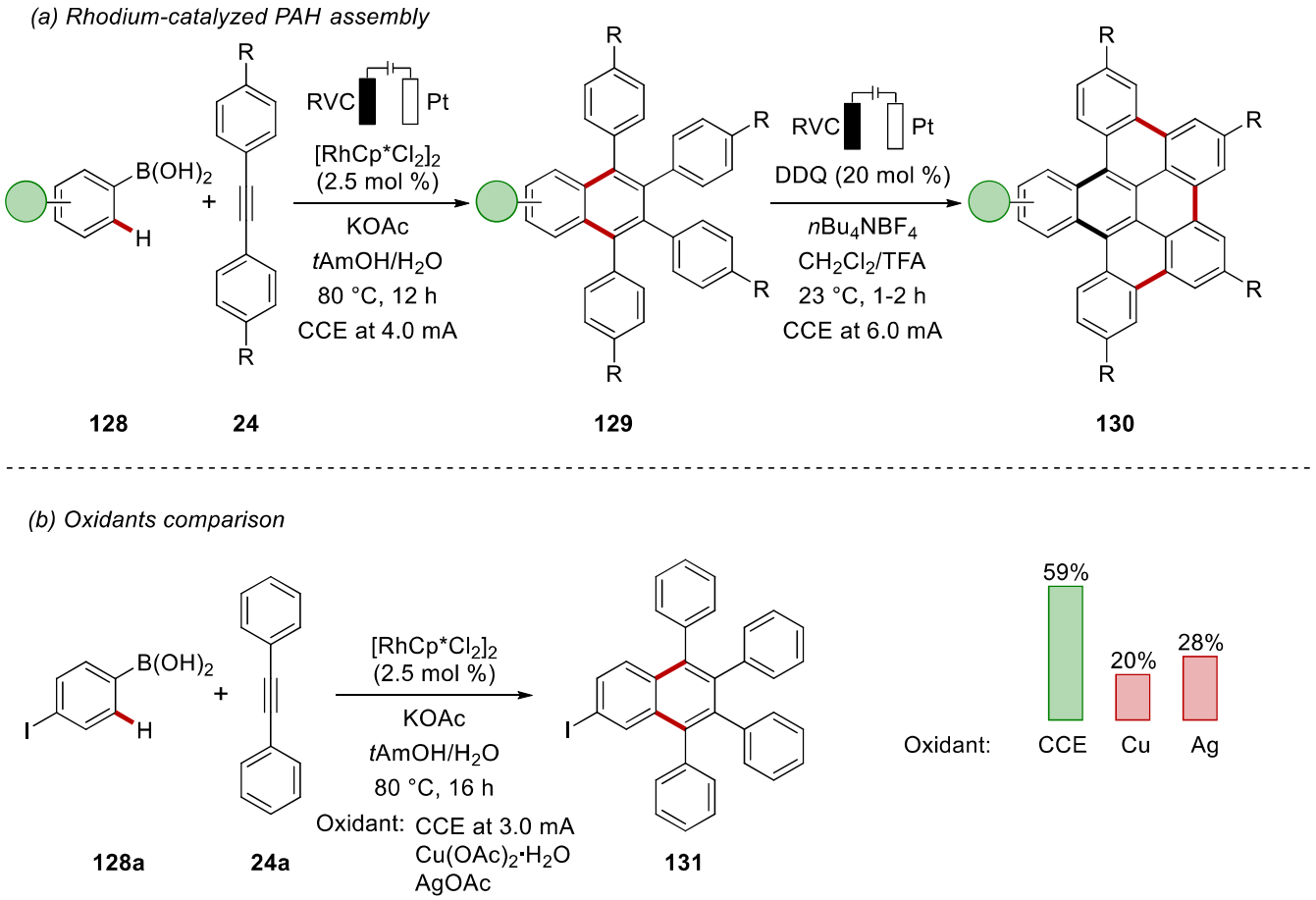

Scheme 1.5.8 (a) Electrochemical rhodium-catalyzed C–H activation and (b) comparison of the reaction with different oxidant.

Ackermann also reported the first flow-electrochemical C–H activation in 2019 (Scheme 1.5.9).[137] The studied inter- and intra-molecular alkyne annulations benefited from an efficient electron and

mass transfer. Thanks to detailed mechanistic studies and the isolation of the rhodium(III)- and rhodium(IV)-complexes, the authors were able to prove the oxidatively-induced reductive elimination,[138] with a catalytic cycle going through a rhodium(III)/(IV)/(II) regime. The rhodium(II) at the end of the catalytic cycle was re-oxidizable both electrochemically or *via* aerobic oxidation.

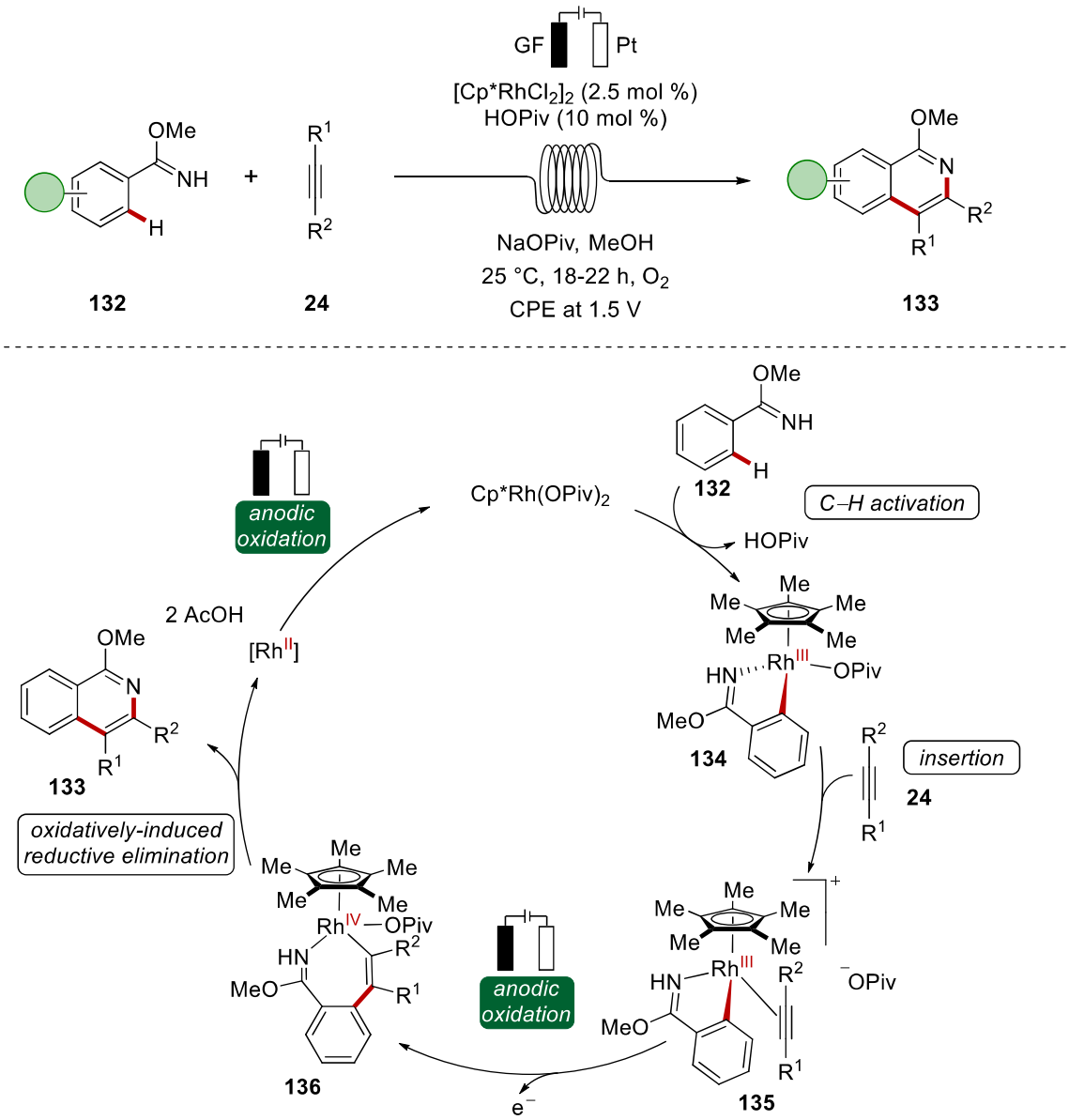

Scheme 1.5.9 Electrochemical rhodium-catalyzed C−H/N−H annulations in flow conditions.

In the context of alkyne annulations, other three reports of 2021 are worth to be cited. Ackermann reported the [5+2] rhodium-catalyzed annulation *via* C–H/O–H activations, opening the way for the electrochemical synthesis of seven-membered benzoxepines **138** (Scheme 1.5.10,a).[139] Mei

published the divergent vinylic rhodium-catalyzed C–H annulation of acrylamides **139**, allowing the synthesis of and cyclic imidates **140** and α-pyridones **141** depending on the substituent on the amides **139** (Scheme 1.5.10,b).[140] Remarkably, Ackermann developed an electrochemical rhodium-catalyzed annulation on benzaldehydes **109** to synthesize chromones **116** (Scheme 1.5.10,c).[141] The strategy also allowed the labelling of amino acids and peptides.

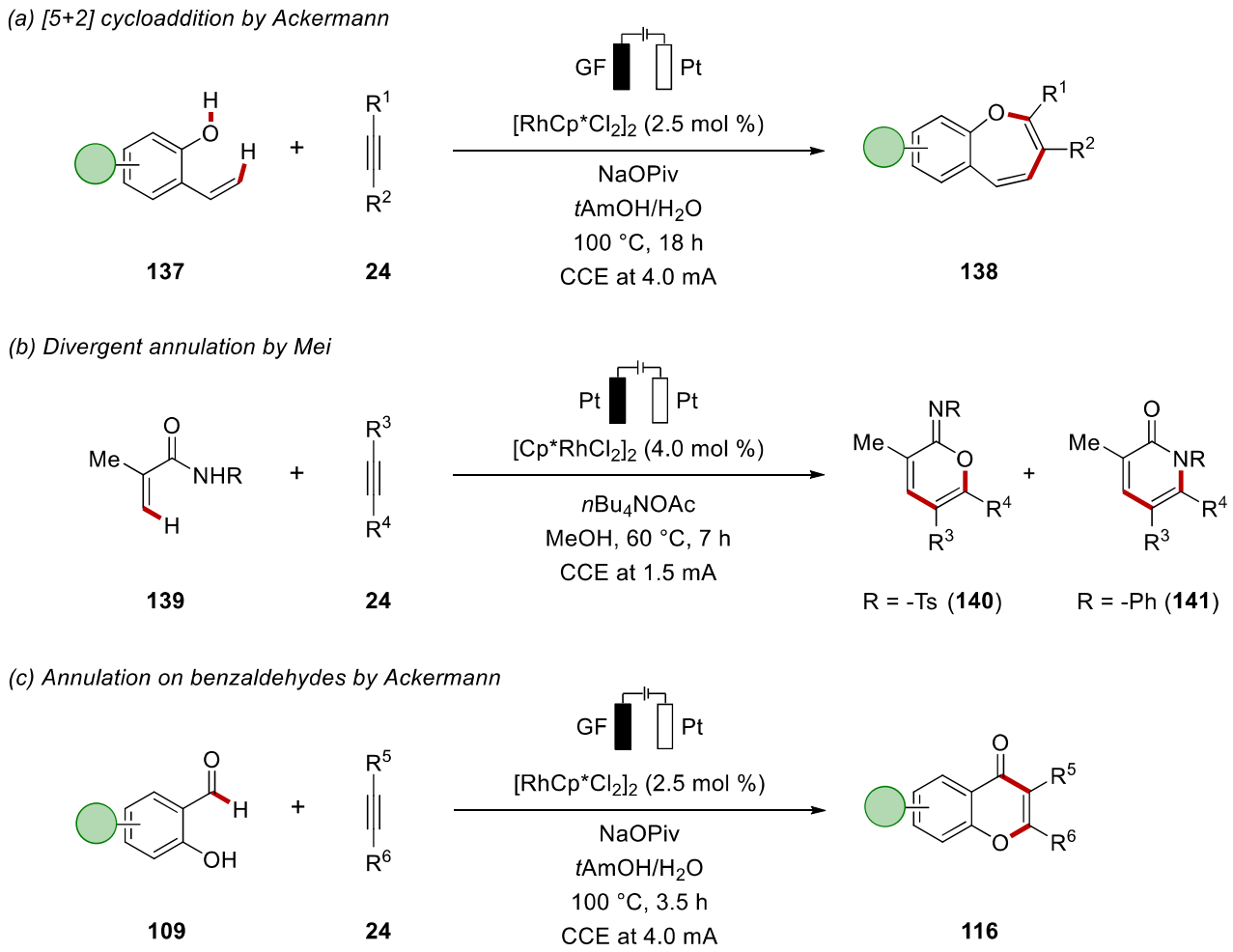

Scheme 1.5.10 Electrochemical rhodium-catalyzed C−H/N−H annulations.

Besides, C–C, C–N, and C–O bonds formation, in 2019 Xu and colleagues reported on the C–P bond formation by mean of electrochemical rhodium catalysis (Scheme 1.5.11).[51a] The robustness of the reaction was reflected by successfully performing a decagram scale that yielded 62% and 87.7 g of the product **144**, employing 1.0 mol % of the rhodium catalyst. The preparation of the rhodium(III) complex and its study suggested an oxidatively-induced reductive elimination.

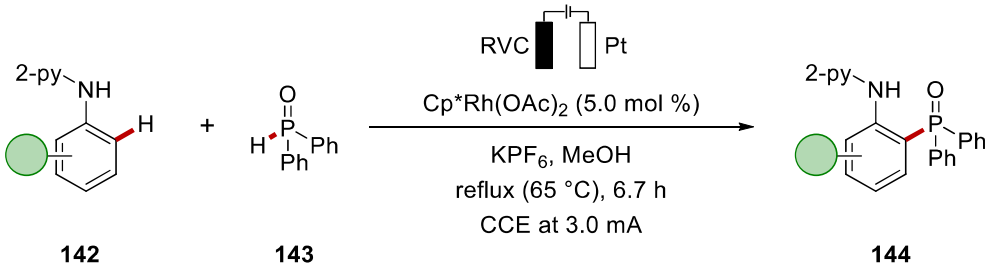

Scheme 1.5.11 Electrochemical rhodium-catalyzed C−H phosphorylation.

1.6 Manganese-Catalyzed C–H Activation

Manganese is the third most abundant transition metal and the twelfth most abundant element in the earth's crust. Because of its abundancy and thus its cost-effectiveness, manganese chemistry has become attractive in the past decade. Additionally, the range of oxidation states (-3 to +7) makes it an interesting metal for diverse catalytic systems.[17, 142] The different high- and low-spin electronic states allow for different possible coordination geometries. Moreover, its low toxicity makes it a good choice for a more environmental benign synthesis.[143]

The first example of stoichiometric C–H activation with manganese was reported in 1970 by Stone and Bruce, with the use of the manganese(I) catalyst [MnMe(CO)$_5$] **145** to yield complex **146** (Scheme 1.6.1).[144]

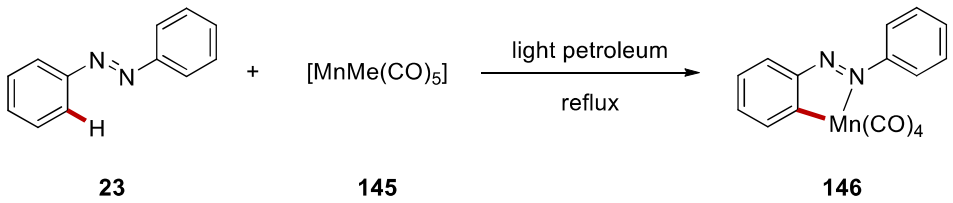

Scheme 1.6.1 First example of stoichiometric manganese(I) C−H activation.

After this report, several others well-defined manganacycles were synthesized by the groups of Nicholson/Main,[145] Woodgate,[146] and Liebeskind,[147] among others (Scheme 1.6.2).[148] These approaches utilized a [MnX(CO)$_5$] catalyst and diverse directing groups, including weakly coordinating ones.

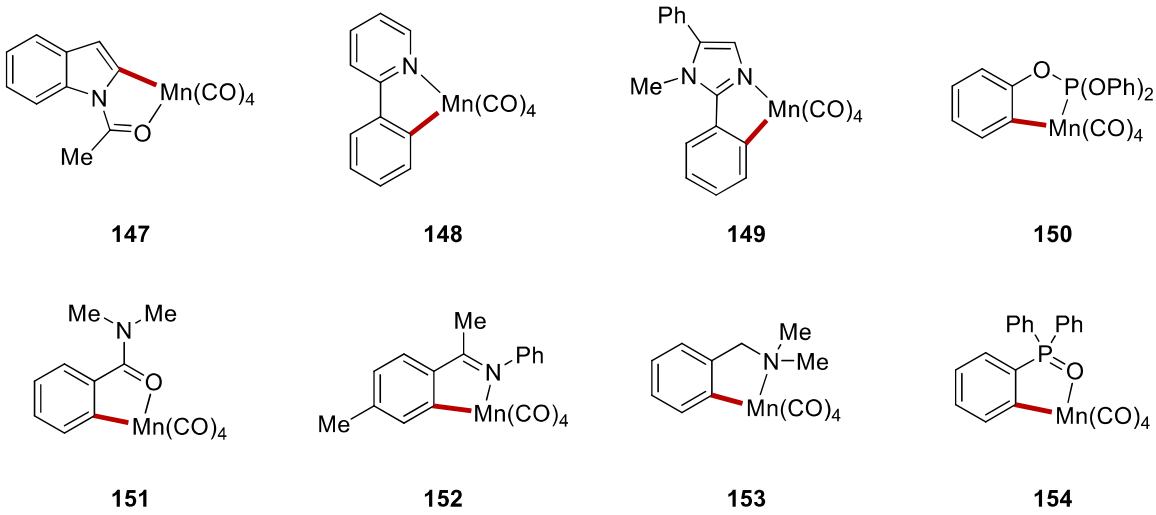

Scheme 1.6.2 Selected examples of well-defined manganacycles.

In 2007, 37 years after the report of Stone and Bruce, the first manganese-catalyzed C–H activation was reported by Kuninobu and Takai (Scheme 1.6.3).[149] They initially studied the addition of an aldehyde onto a C–H bond in the presence of stoichiometric manganese(I) salt **156**. The reaction proved to be feasible only with stoichiometric amounts of manganese, while only traces of the desired product **157** were obtained when the metal was employed in a catalytic fashion (Scheme 1.6.3,a). The addition of triethylsilane to afford the silyl ether product **159** was found to be the key to guarantee turnover, and, thus, afforded the transformation utilizing the manganese in catalytic amounts (Scheme 1.6.3,b). The authors proposed a mechanism that commences with the C–H activation *via* oxidative addition of the aromatic compound to the manganese(I), giving a Mn(III)-hydride species **160** (Scheme 1.6.3,c). Afterwards, migratory insertion occurs, and a reductive elimination takes place with the help of triethylsilane that forms the silyl-protected product **159**. This step regenerates the active catalyst **156** and gives molecular hydrogen as by-product. In 2015, the group of Wang reported the manganese-catalyzed C–H activation of aromatic rings with aldehydes and also nitriles in the absence of the silane, but stoichiometric zinc salts were required.[150] From the report of Kuninobu onwards, manganese catalysis thrived with several reports on C–H activation reactions, such as annulations, allylations, and alkylations.[17]

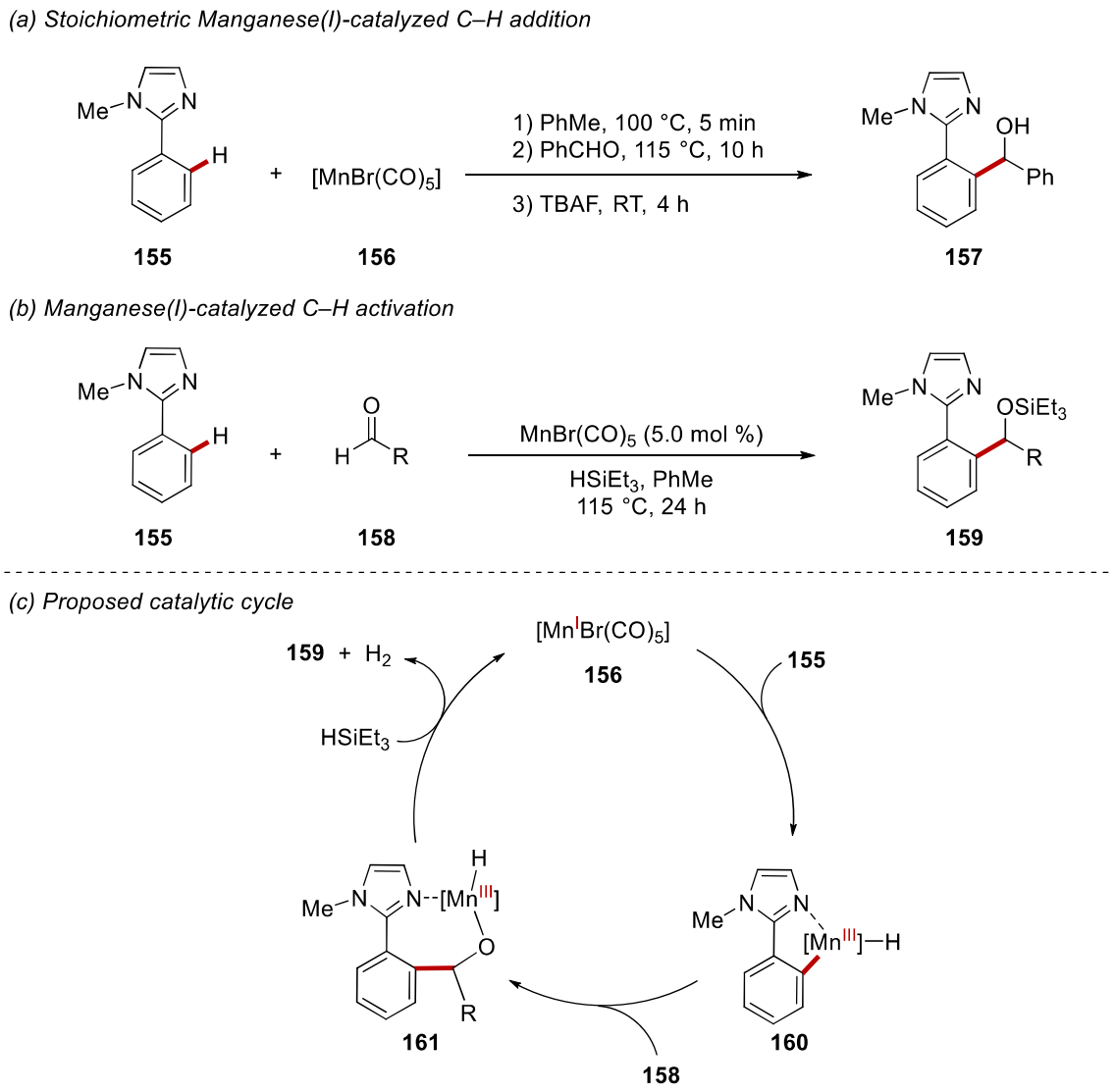

Scheme 1.6.3 Manganese-catalyzed hydroarylation of aldehydes **155**: (a) stoichiometric study, (b) catalytic reaction, and (c) proposed catalytic cycle.

1.6.1 Manganese-Catalyzed C–H Activation with Chemical Oxidants

Manganese(I) catalysis was generally limited to isohypsic addition reactions with the need of substrates containing multiple bonds.[17] To overcome this major challenge, Ackermann reported in 2017 the first low-valent manganese-catalyzed C–H alkylation with alkyl halides **163** using simple $MnCl_2$ (Scheme 1.6.4,a).[151] Interestingly, the reaction did not require any zinc salts or expensive phosphine ligand. The reaction offered a versatile approach to obtain alkylated benzamide **164** by the assistance of a removable triazolyldimethylmethyl (TAM) directing group. The authors also presented the methylation reaction, and they proposed a catalytic cycle based on their mechanistic

studies and DFT calculations (Scheme 1.6.4,b). The mechanism starts with a ligand-to-ligand hydrogen transfer (LLHT) type C–H activation to furnish complex **168**. This is then oxidized by 2,3-dichlorobutane (DCB) to give a manganese(III) intermediate **169** that undergoes the transmetalation with the alkyl reagent. After reductive elimination, the product **166** is obtained, and the catalyst is oxidized by DCB to furnish the catalytically active species.

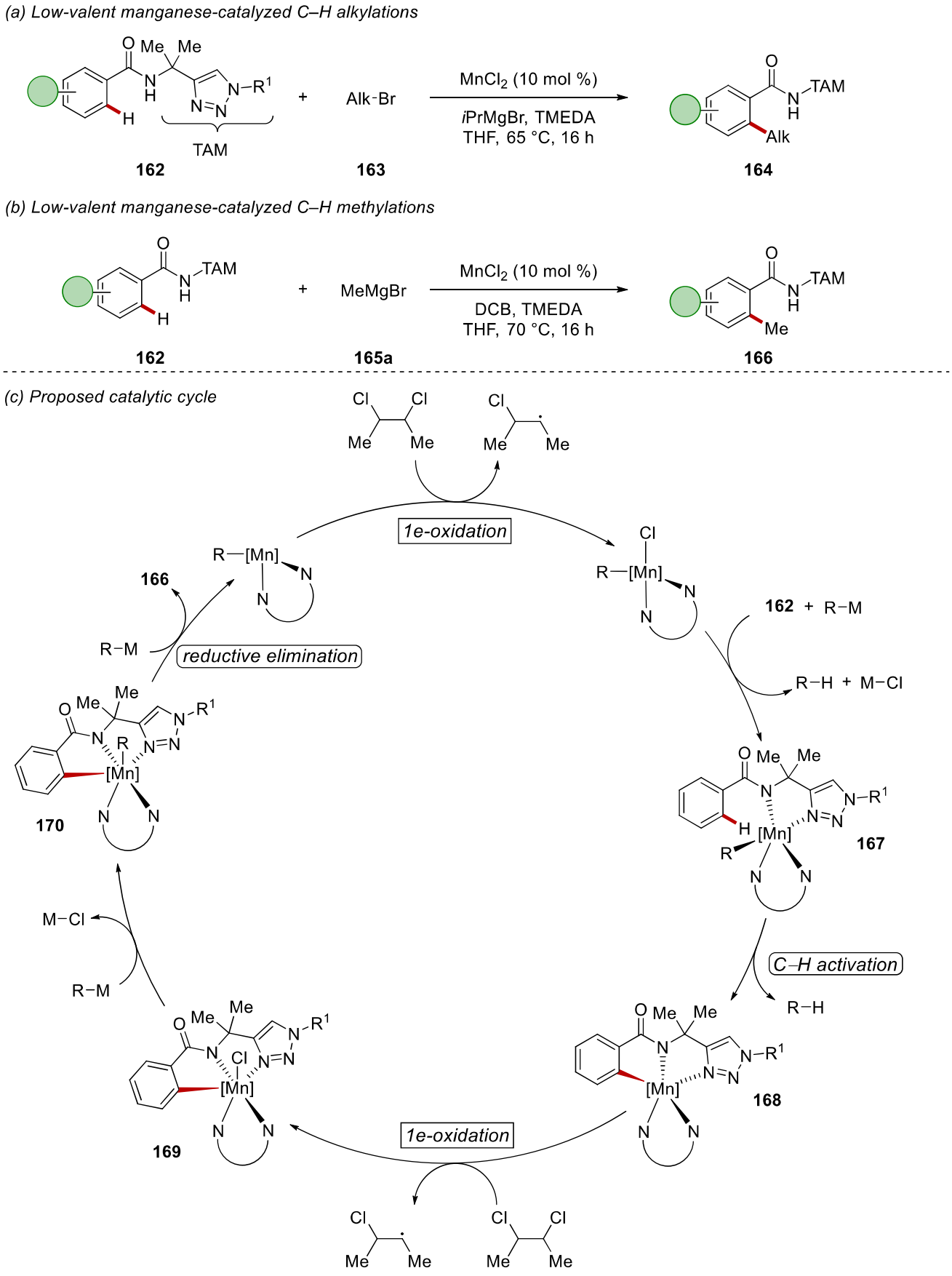

Scheme 1.6.4 First example of low-valent manganese-catalyzed C−H activation.

Inspired by this work, Nakamura and co-workers published the methylation of secondary amides **87** (Scheme 1.6.5,a), with 1-bromo-2-chloroethane acting as the oxidant.[152] In contrast, Ackermann reported the manganese-catalyzed alkylation of azines **172** with both primary as well as the more demanding secondary alkyl halides **173** (Scheme 1.6.5,b).[153] Here, examples of oxidative alkylation in the presence of Grignard as coupling partner and 1,2-dichloroisobutane (DCIB) as oxidant were also included.

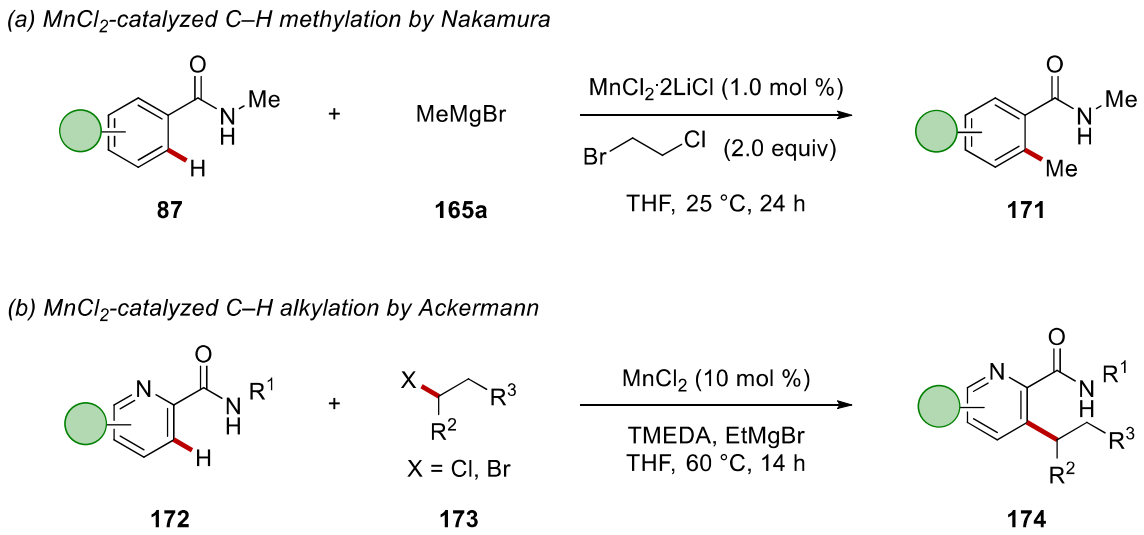

Scheme 1.6.5 Low-valent manganese C−H (a) methylation and (b) alkylations.

Lastly, in 2018 Ackermann achieved the low-valent manganese-catalyzed arylation reaction on azines **172** under flow conditions, that includes manganese(II) chloride as the catalyst and neocuproine as the ligand for a cost-efficient and environmentally benign transformation (Scheme 1.6.6).[154] The need for toxic and expensive DCIB as oxidant represented a major limitation of the approach. Recently, the same group published an approach that takes advantage of a heterogeneous manganese catalyst for this reaction.[155]

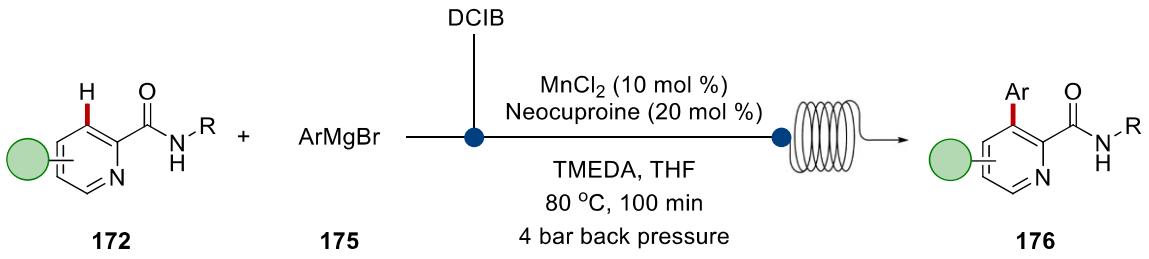

Scheme 1.6.6 Manganese-catalyzed C–H arylations using flow technique.

1.6.2 Electrochemical Manganese-Catalyzed C–H Activation

Electrochemical manganese-catalyzed C–H activation has proven elusive, in contrast to the numerous examples of its employment in electrochemical olefin difunctionalization developed by the group of Lin,[156] and in the pioneering work of Schäfer.[157] Two independent reports by Lei[158] and Ackermann[159] have highlighted the potential of manganese-catalyzed electrochemical C–H activation towards the synthesis of value added chemicals. Both the methods presented an ample scope and good selectivities for the desired azidation. These studies were based on the early reports by Hill[160] and Groves,[161] where they employed a manganese porphyrin or a Schiff-base complex and iodosylbenzene as oxidant to generate the high-valent manganese(V)-oxo intermediate. In the report of Lei, a photo-electrochemical approach was used, while Ackermann could devise a strategy with the sole electrochemistry (Scheme 1.6.7).

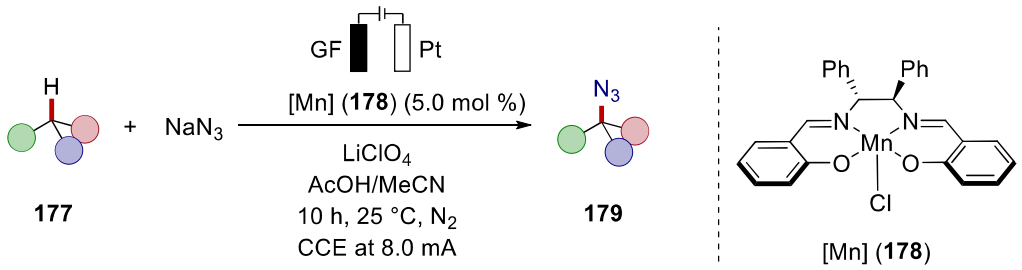

Scheme 1.6.7 Manganese-catalyzed C–H azidations enabled by electricity.

2. Objectives

The development of new approaches for selective C–C and C–Het bond formations to easily access complex molecules is highly demanded to provide chemists with diverse and efficient synthetic routes. In the last decades, enormous progresses were made in this field, first with the rise of cross-coupling chemistry, and later with step- and atom-economical C–H activation methodologies.[162] These approaches allowed for great advances in organic synthesis, but the green chemistry criteria are still far to be met. Indeed, many procedures relied on harsh conditions, hazardous or toxic chemicals, and on the use of precious metal catalysts. In this scenario, this thesis aims to address the study and development of novel and greener concepts for metal-catalyzed C–H activation, in particular focusing on the merger of transition metal catalysis and electrosynthesis as environmentally benign oxidant.[163] This approach could greatly increase the sustainable nature of oxidative transformations.

In the last two decades, cobalt catalysis thrived as a powerful and cost-effective approach for oxidative C–H activation, with elegant examples for annulation reactions.[58, 60, 164] These methodologies were nevertheless undermined by the need for stoichiometric amounts of toxic metal-based oxidants. Therefore, the investigation of an electrochemical procedure for cobalt-catalyzed C–H/N–H annulation reaction had been studied. We aimed to replace the chemical oxidant by anodic oxidation for the regeneration of the active catalyst, thus reducing the waste production (Scheme 2.1).

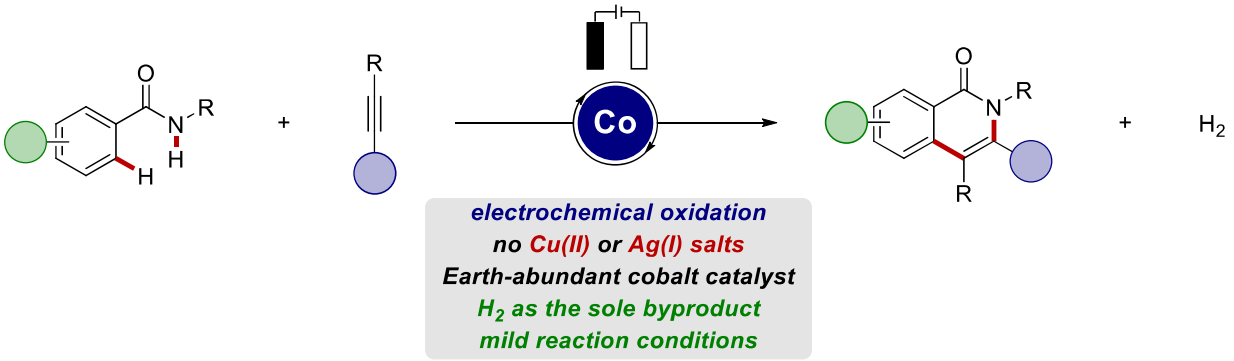

Scheme 2.1 Electrochemical cobalt-catalyzed C–H/N–H alkyne annulations.

Ruthenium-catalyzed oxidative C–H activation is a powerful tool for the synthesis of heteroarenes with weakly coordinating directing groups.[24] The use of electricity as oxidant for this approach was not reported yet at the onset of the study. We thus became interested in exploring the combination of ruthenium catalysis and electrochemistry, studying its versatility and regioselectivity in the annulation reaction between benzoic acids and unsymmetrical alkynes (Scheme 2.2). This approach would allow us to expand the precedent study on cobalt-catalyzed annulations to internal alkynes by means of ruthenium catalysis.

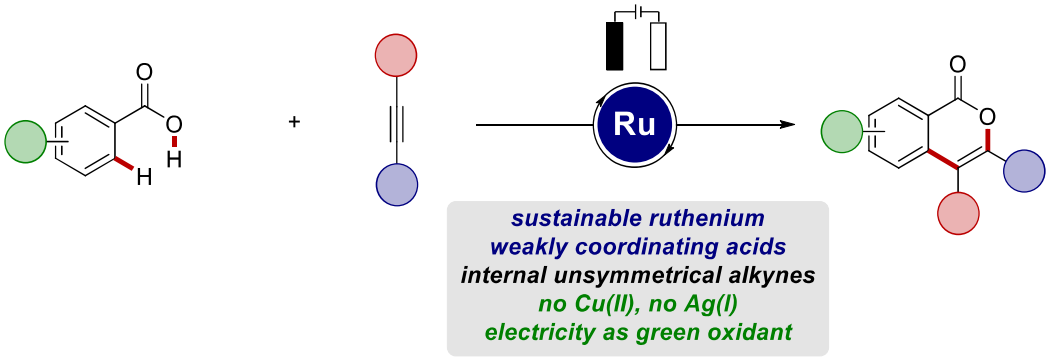

Scheme 2.2 Electrochemical ruthenium-catalyzed C–H/O–H alkyne annulations.

To harness the full potential of electrochemistry, the *in-situ* synthesis of hazardous chemicals from catalytic amounts of precursor was explored in depth. The hypervalent iodine compounds are a wide class of versatile oxidants which were reported to be electrochemically synthesizable.[165] These compounds are also viable oxidants used in stoichiometric amounts for the ruthenium-catalyzed C–H oxygenation reactions.[110-113, 115] The aim was therefore to tackle the safety and the costs of these transformations by the *in-situ* electrochemical formation of hypervalent iodine species from catalytic amounts of iodobenzene. This reactant would act as a mediator for the effective oxidation of the ruthenium catalyst, allowing the C–H oxygenation reaction to happen (Scheme 2.3). A detailed optimization study for the formation of the hypervalent iodine and the combination of this in a one-step procedure with the ruthenium-catalyzed reaction were therefore of interest. A successful application of the strategy should prove viable on an ample range of compounds. Since the ability of ruthenium catalyst of performing

remote functionalizations of substrates is well-known, this approach would also been of utmost interest for the electrochemical oxygenation reaction.

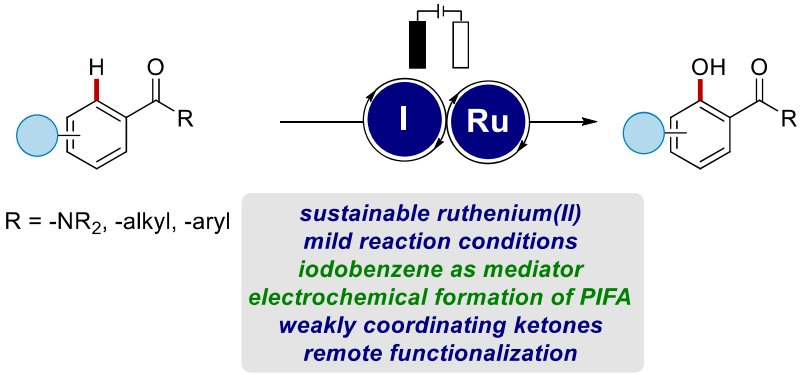

Scheme 2.3 Electrochemical hypervalent iodine formation for the ruthenium-catalyzed C–H oxygenation reaction.

The effective direct oxidation of a transition metal at the anode would avoid the use of any mediator. Thus, an even more atom-economical approach could be designed. To reach such conditions, rhodium-catalyzed C–H oxygenation was considered (Scheme 2.4). The aim was to compare the reactivity and selectivity with the ruthenium manifold, exploring possible new routes in product synthesis. Herein, a detailed study of the mechanism *via* detailed mechanistic studies, DFT calculations, and cyclic voltammetry would be highly desirable to clarify the pathway for this rhodium-catalyzed transformation, which was underreported for reactions using chemical oxidants and so far, not presented with an electrochemical approach.

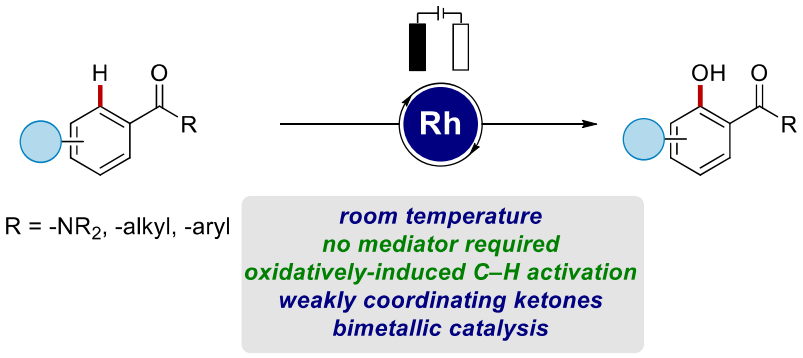

Scheme 2.4 Electrochemical rhodium-catalyzed C–H oxygenation.

C–H arylation reactions are of major interest due to the plethora of biaryl motifs in natural products.[166] After the remarkable development of electrochemical iron-catalyzed C–H arylation,[48f] the intention was to enable mono-dentate and weakly coordinating amides, while maintaining mild conditions and a broad substrate scope. Thus, the focus was directed towards manganese catalysis (Scheme 2.5). Given the unprecedented electrochemical low-valent 3d metal-catalyzed approaches, a clarification of the overall reaction path and insights in the redox events are of high interest

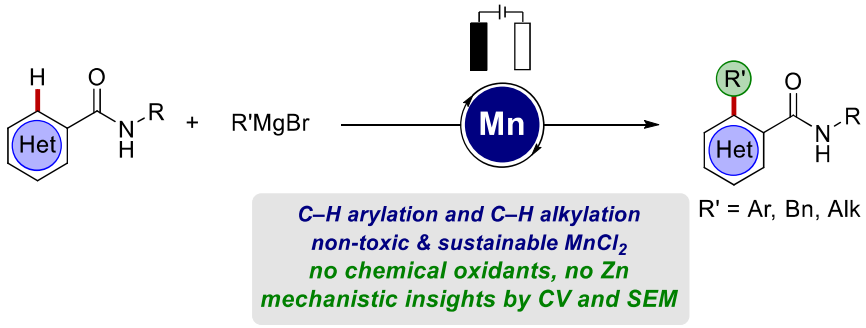

Scheme 2.5 Electrochemical manganese-catalyzed C–H arylations.

3. Results and Discussion

3.1 Electrochemical C–H/N–H Activation by Water-Tolerant Cobalt-Catalysis at Room Temperature

C–H/N–H alkyne annulations are a valuable tool for the step-economical synthesis of heterocycles. Here, cobalt catalysis has been playing an important role, but it has been strongly limited to the use of stoichiometric chemical oxidants or high reaction temperatures.[58, 60, 164] Following the groundbreaking work from Ackermann,[73] we intended to employ electricity as oxidant to enable C–H/N–H annulation reactions.

3.1.1 Optimization

The optimized reaction conditions were elaborated at first by Dr. Cong Tian (Scheme 3.1.1). The reactions were performed in an undivided cell set-up with a reticulated vitreous carbon (RVC) electrode as anode and a platinum (Pt) plate electrode as cathode, with a constant current electrolysis of 4.0 mA at room temperature. Initial results showed that H_2O or MeOH were better solvents than DMSO, with a 1:1 mixture of H_2O/MeOH giving the best performance. Moreover, sodium pivalate was found to be a better base in comparison to sodium acetate or to the absence of a base. The control experiment in the absence of electricity gave no product. Notably, the reaction was selective for the annulation product **34aa**, and no oxygenation adducts were found, even though a large excess of free alcohol was present as the co-solvent.

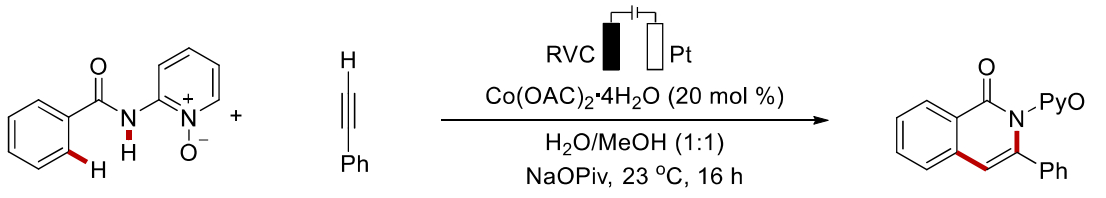

33a **117a** **34aa**

CCE at 4.0 mA: 76%
without current: ---

Scheme 3.1.1 Initial optimized conditions for the C–H/N–H alkyne annulations by Dr. C. Tian.

Further optimization studies were performed at the very beginning of my doctoral studies (Table 3.1.1). First, the reaction was tested at 60 °C, which however led to no improvement in the yield (entry 1). Performing the same reaction within a shorter time gave the same result, indicating that heating was probably increasing the rate of the reaction (entry 2). Furthermore, the influence of catalyst loading was studied (entries 3–4). Interestingly, a catalyst loading of 10 mol % gave the same result as with 20 mol % loading, while a decrease in the amount of cobalt to 1.0 mol % yielded only 8% of the annulated product **34aa**. Subsequently, the solvent system was further studied. Changing the ratio of the solvent mixture, with a 3:1 H_2O/MeOH ratio, no beneficial effect was observed (entry 5). This was probably due to the lower solubility of the reaction components. Therefore, we investigate the substitution of methanol with a surfactant.[167] Polyoxyethanyl-α-tocopheryl sebacate (PTS, 15 wt% in H_2O) was tested, resulting in 31% isolated product (entry 6). Lastly, HFIP was tested as solvent due to its facilitating effect on C–H activation and electrosynthesis,[168] but yielded only 19% of the desired product (entry 7). Additionally, the use of $Co(acac)_3$ instead of $Co(OAc)_2$ as catalyst was detrimental for the performance (entry 8). Several transition-metal catalysts were tried under the same reaction conditions. Iron, copper, palladium, iridium, ruthenium, and rhodium were found to be ineffective, underlining the unique effectiveness of the cobalt catalyst (entries 9–16).

Table 3.1.1 Further optimization of the electrochemical cobalt-catalyzed alkyne annulation.[a]

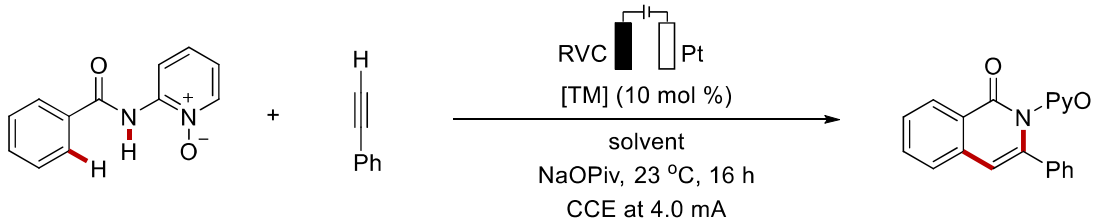

33a **117a** **34aa**

Entry	[TM]	Solvent	Yield (%)
1	$Co(OAc)_2{\cdot}4H_2O$	H_2O/MeOH (1:1)	66[b,d]
2	$Co(OAc)_2{\cdot}4H_2O$	H_2O/MeOH (1:1)	66[b,c,d]
3	**$Co(OAc)_2{\cdot}4H_2O$**	**H_2O/MeOH (1:1)**	**76**
4	$Co(OAc)_2{\cdot}4H_2O$	H_2O/MeOH (1:1)	8[e]

5	$Co(OAc)_2·4H_2O$	H_2O/MeOH (3:1)	40
6	$Co(OAc)_2·4H_2O$	PTS/H_2O	31[b]
7	$Co(OAc)_2·4H_2O$	HFIP	19[b]
8	$Co(acac)_3$	H_2O/MeOH (1:1)	-
9	$Fe(OAc)_2$	H_2O/MeOH (1:1)	-
10	$Fe(acac)_3$	H_2O/MeOH (1:1)	-
11	$Cu(OAc)_2$	H_2O/MeOH (1:1)	-
12	$Pd(OAc)_2$	H_2O/MeOH (1:1)	-
13	$[Cp^*IrCl_2]_2$	H_2O/MeOH (1:1)	-
14	$RuCl_3$	H_2O/MeOH (1:1)	-
15	Ru(*p*-cymene)$(O_2CMes)_2$	H_2O/MeOH (1:1)	-
16	$[Cp^*RhCl_2]_2$	H_2O/MeOH (1:1)	-

[a] Reaction conditions: Undivided cell, **33a** (0.50 mmol), **117a** (1.00 mmol), [TM] (10 mol %), NaOPiv (2.00 equiv), solvent (10.0 mL), 23 ºC, CCE at 4.0 mA, 16 h, RVC anode (10 mm × 15 mm × 6 mm), Pt-plate cathode (10 mm × 15 mm × 0. 125 mm), isolated yield. [b] [TM] (20 mol %). [c] 8 h. [d] 60 °C. [e] [TM] (1.0 mol %).

3.1.2 Substrate Scope

With the further optimized reaction conditions in hand, the scope of the electrochemical C–H/N–H annulation was explored by employing various amides **33** and phenylacetylene **117a** (Scheme 3.1.2). The scope was ample. The more electron-poorer or challenging substrates needed a higher catalyst loading. Differently *para*-substituted amides **33b-d** were well tolerated, either with an electron-donating (**34ba**) or an electro-withdrawing substituent (**34ca**). The valuable functional group bromo underwent the annulation without side coupling reaction (**34da**). Also, the 3,5-dimethoxy substituted amide **33e** was successfully converted, yielding the desired product **34ea**. To our delight, the reaction was not limited to arene substrates, but was working likewise on the heteroarene thiophene **33f**.

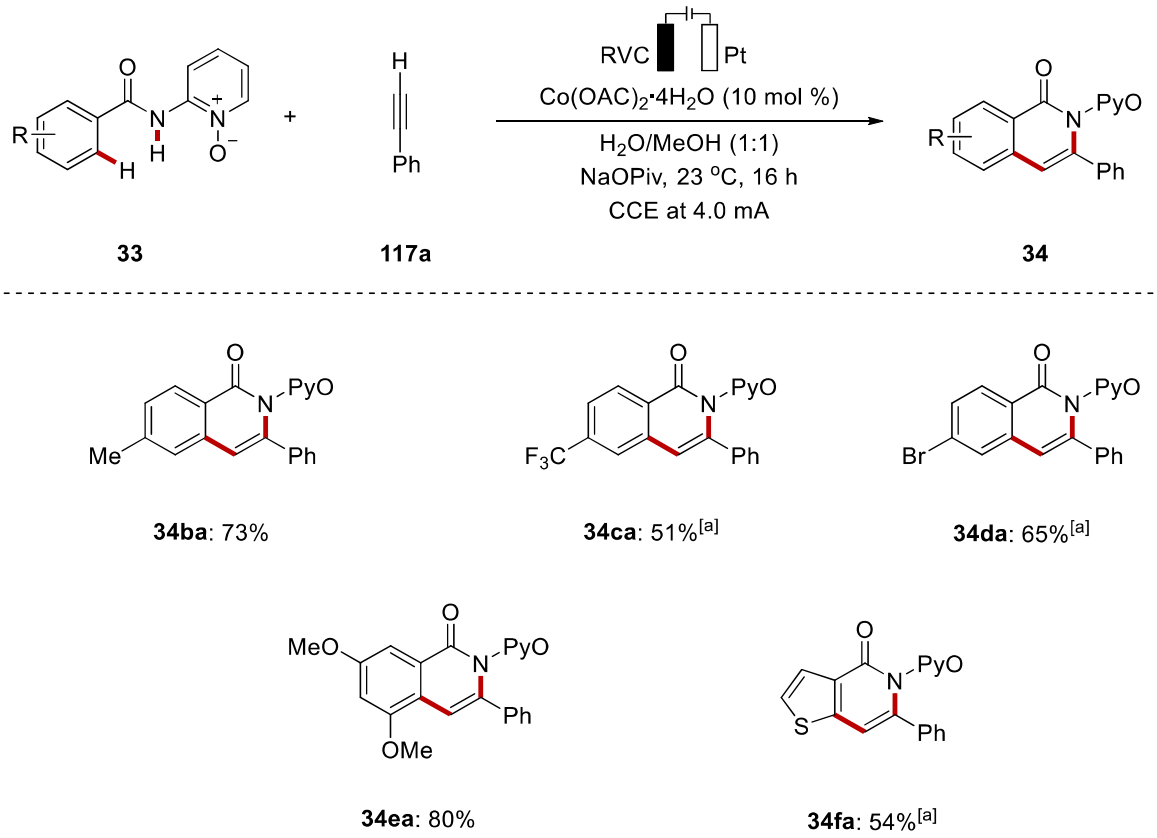

Scheme 3.1.2 Scope of the electrochemical cobalt-catalyzed C–H/N–H alkyne annulation of amides **33**. [a] $Co(OAc)_2 \cdot 4H_2O$ (20 mol %).

The robustness of the electrochemical cobalt-catalyzed C–H/N–H activation at ambient temperature was further reflected by the annulation of different alkynes **117** with the standard substrate **33a** (Scheme 3.1.3). Hence, substituents in the *para*-position of the phenylacetylenes **117** were well tolerated, especially for electron-rich groups, such as methoxy (**34ab**) and *tert*-butyl (**34ac**). Moreover, alkyl alkynes were also found to be suitable substrates for the desired reaction. Indeed, 1-heptyne (**117d**) underwent the reaction furnishing 55% of the desired product **34ad**.

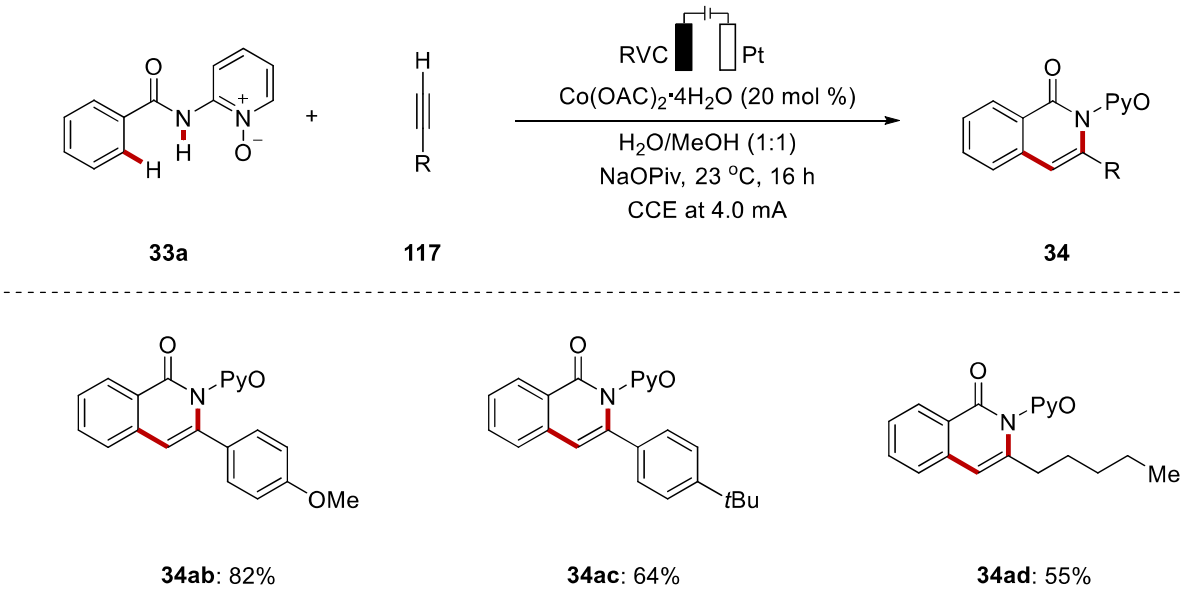

Scheme 3.1.3 Scope of the electrochemical cobalt-catalyzed annulation of alkynes **117**.

3.1.4 Mechanistic Studies

Given the new electrochemical approach for cobalt-catalyzed C–H/N–H alkyne annulation, we desired to further understand its mode of action. To this end, Dr. Cong Tian performed intermolecular competition experiments, H/D exchange evaluation in reaction conditions, and KIE studies. The higher reactivity of electron-rich substrates indicated a base-assisted internal electrophilic substitution (BIES) manifold.[29, 32] The absence of a significant deuterium incorporation suggested an irreversible, yet facile, C–H cleavage as proven by a KIE of $k_H/k_D \approx 1.1$.

Moreover, the *ortho*-alkynylated substrate **184** was independently prepared by a Sonogashira coupling of the methyl 2-iodobenzoate **180**, followed by the insertion of 2-aminopyridine-*N*-oxide **183** as the optimal directing group (Scheme 3.1.4,a). The synthesized substrate **184** was then submitted to the optimized reaction conditions and the product was not obtained (Scheme 3.1.4,b). This result suggested an organometallic alkyne annulation pathway.

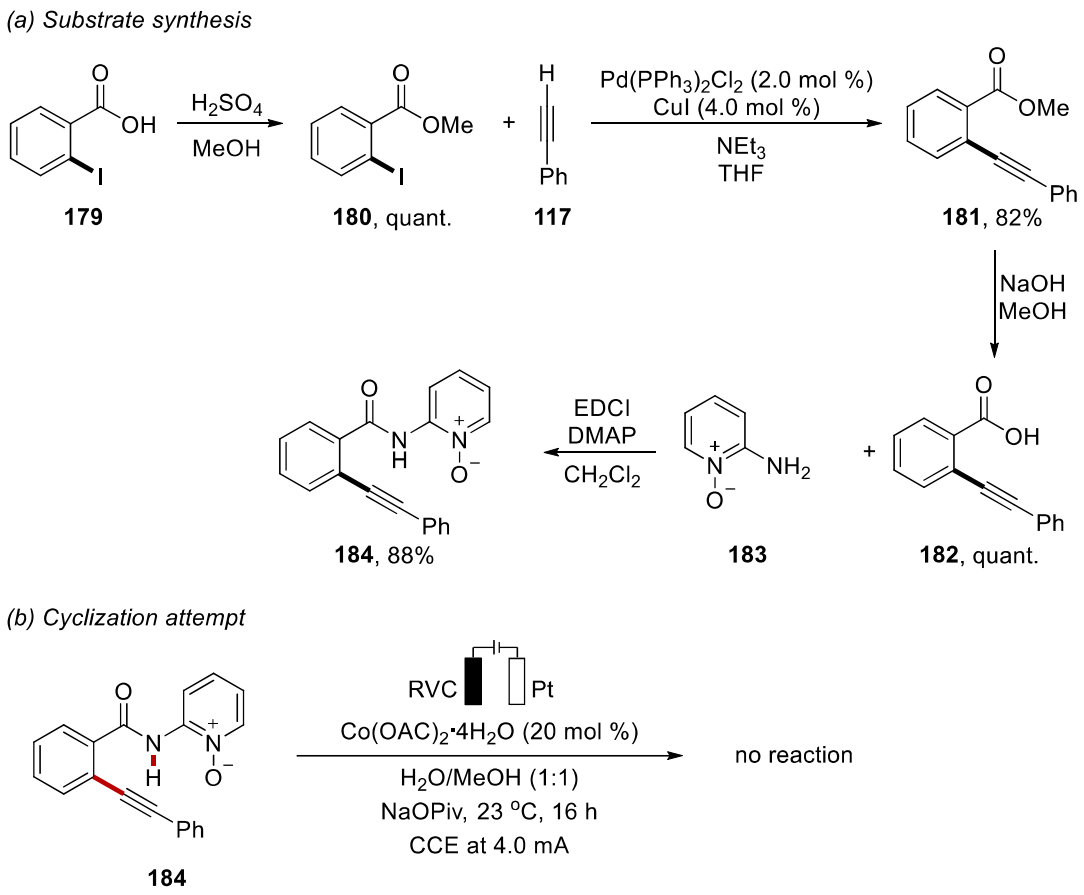

Scheme 3.1.4 Substrate **184** synthesis and attempted cyclization experiment.

To gain insights in the electrochemical event, detailed cyclic voltammetry studies were performed by Dr. T. H. Meyer (Figure 3.1.1). The amide **33a** had an oxidation potential of 1.51 V *vs.* SCE, compared to a catalyst redox event at 1.19 V *vs.* SCE. Therefore, the oxidation of the cobalt was 320 mV lower than the substrate, thus supporting a single-electron oxidation at cobalt. Phenylacetylene **117a** did not exhibit a clear oxidation event, a result that, in line with the cyclization attempt, suggested an organometallic annulation.

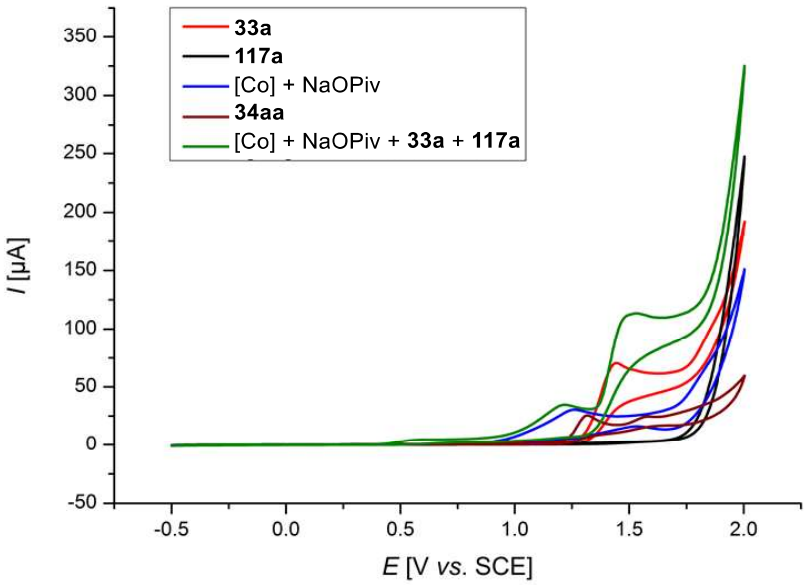

Figure 3.1.1 Cyclic voltammograms at 20 mVs^{-1}: $n$$Bu_4NPF_6$ (0.1 M in MeOH), concentration of substrates 1.0 mM (NaOPiv 4.0 mM). Performed by Dr. T. H. Meyer.

3.1.5 Proposed Catalytic Cycle

A catalytic cycle for the C–H/N–H electrochemical annulation was proposed, and it is based on the mechanistic studies presented above (Scheme 3.1.5). First, the cobalt(II) acetate catalyst undergoes oxidation to the active cobalt(III) carboxylate **185**. Second, the amide **33** gives the intermediate **186** through a facile BIES C–H cleavage. Alkyne insertion affords the cobalt complex **187** and a subsequent reductive elimination yields the desired product **34** and cobalt(I) catalyst **30a**. This is oxidized at the anode to give the active cobalt(III) catalyst **185**. While the cobalt is oxidized at the anode, the formation of H_2 takes place at the cathode.

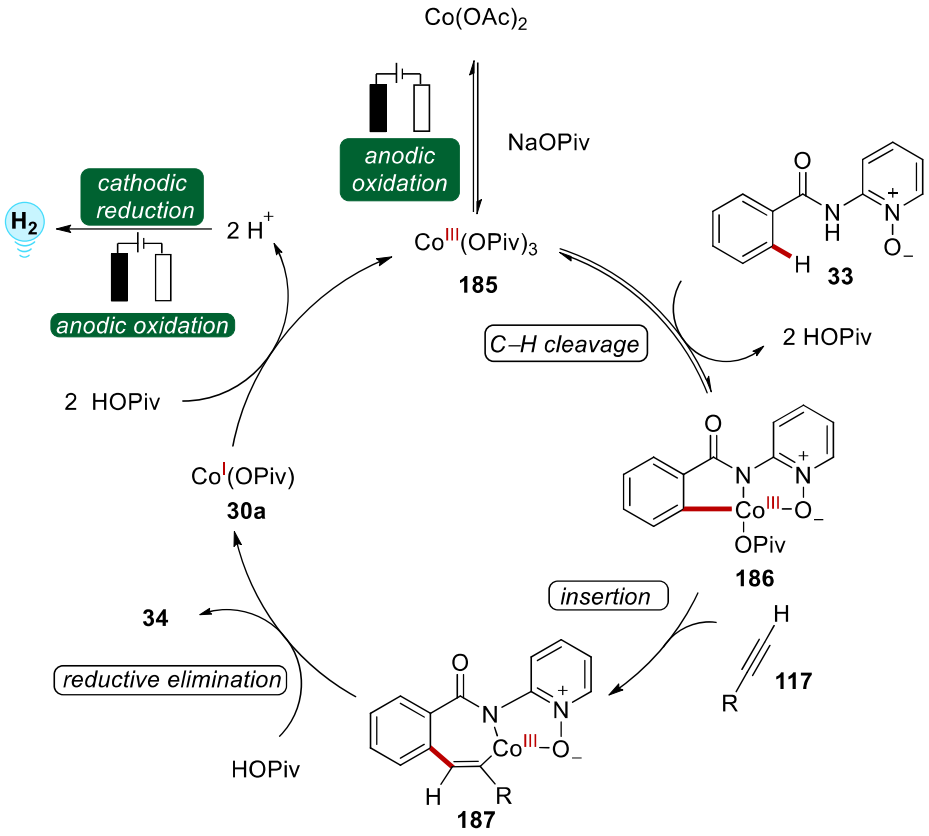

Scheme 3.1.5 Proposed catalytic cycle for the electrochemical cobalt-catalyzed C–H/N–H annulation.

3.2 Electrooxidative Ruthenium-Catalyzed C–H/O–H Annulation by Weak *O*-Coordination

Numerous oxidative reactions have been reported with ruthenium,[87] but its merger with electricity as green oxidant appeared as an important challenge. After the success of coblataelectro-catalyzed reactions, our group focused on opening the way to electrochemical ruthenium catalysis. Simultaneously, Xu reported the synthesis of indoles *via* the ruthenium-catalyzed electrochemical dehydrogenative annulation of aniline derivatives and alkynes.[51b] While Xu's report was limited to a strongly coordinating directing group, we focused on weak coordination, which led to the development of the first electrochemical ruthenium-catalyzed *O*-directed C–H activation presented in this section.

3.2.1 Optimization

At the outset of the study, we investigated the reaction between 4-methoxybenzoic acid **89b** and diphenylacetylene **24a**, with a ruthenium catalyst and potassium hexafluorophosphate in a mixture of *tert*-amyl alcohol and water, at 100 °C and a constant current electrolysis of 4.0 mA (Scheme 3.2.1). $[RuCl_2(p\text{-cymene})]_2$ and sodium pivalate as additive under a nitrogen atmosphere were employed at first and resulted in a 35% isolated yield of the desired annulated product (entry 1). By changing the catalyst to $[Ru(OAc)_2(p\text{-cymene})]$ **188a**, the product formation increased, but when the reaction was performed under air atmosphere the yield was slightly diminished (entries 2–3). The test reaction in the absence of the catalyst revealed the essential role of the ruthenium catalyst (entry 4). Analogously, the test without any applied current, but with the electrodes in the cell, showed the importance of electricity, as only 11% of the desired product was obtained (entry 5). Different solvent systems were tried. First, water was employed as the only solvent, but only 5% of product **90ba** was detected (entry 6). Then the effect of the addition of two surfactants, namely α-tocopherol (2 wt. % in H_2O) and polyoxyethanyl-α-tocopheryl sebacate (PTS, 4 wt. % in H_2O), was examined giving only very low conversions (entries 7–8). Other organic solvents were also tested, but for these attempts there was the need of adding a supporting electrolyte to increase the conductivity of the media. *γ*-

Valerolactone, and *o*-xylene were tested without success, while *tert*-amyl alcohol alone gave 12% of the desired product **90ba** (entries 9–11).

Table 3.2.1 Initial optimization of the electrochemical ruthenium-catalyzed C–H/C–O annulation.[a]

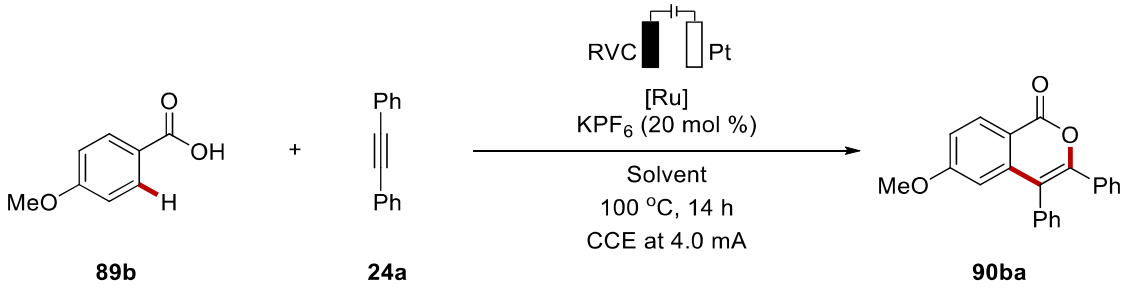

89b **24a** **90ba**

Entry	[Ru] (xx mol %)	Solvent	Notes	Yield (%)
1	$[RuCl_2(p\text{-cymene})]_2$ (2.5)	*t*AmylOH/H_2O (3:1)	N_2, NaOPiv (1.00 equiv)	35
2	$[Ru(OAc)_2(p\text{-cymene})]$ (5)	*t*AmylOH/H_2O (3:1)	N_2	47
3	$[Ru(OAc)_2(p\text{-cymene})]$ (5)	*t*AmylOH/H_2O (3:1)	--	(41)
4	--	*t*AmylOH/H_2O (3:1)	--	nr
5	$[Ru(OAc)_2(p\text{-cymene})]$ (5)	*t*AmylOH/H_2O (3:1)	No current	(11)
6	$[Ru(OAc)_2(p\text{-cymene})]$ (5)	H_2O	--	(5)
7	$[Ru(OAc)_2(p\text{-cymene})]$ (5)	H_2O/α-tocopherol	--	(8)
8	$[Ru(OAc)_2(p\text{-cymene})]$ (5)	PTS/H_2O	--	(11)
9	$[Ru(OAc)_2(p\text{-cymene})]$ (5)	GVL	$n Bu_4NBF_4$ (0.50 equiv)	nr
10	$[Ru(OAc)_2(p\text{-cymene})]$ (5)	*o*-xylene	$n Bu_4NBF_4$ (1.00 equiv)	nr
11	$[Ru(OAc)_2(p\text{-cymene})]$ (5)	*t*AmylOH	$n Bu_4NBF_4$ (2.00 equiv)	(12)

[a] Reaction conditions: Undivided cell, **89b** (1.00 mmol), **24a** (0.50 mmol), [Ru] (as specified), KPF_6 (20 mol %), solvent (10.0 mL), 100 ºC, CCE at 4.0 mA, 14 h, RVC anode (10 mm × 15 mm × 6 mm), Pt-plate cathode (10 mm × 15 mm × 0. 125 mm), isolated yield, yields in parentheses are determined by ^{1}H-NMR analysis with 1,3,5-trimethoxybenzene as internal standard.

Since Dr. Youai Qiu was also studying the same type of reaction, forces were joined, and the optimization was then carried on with *o*-toluic acid **89c** as the standard substrate (Table 3.2.2). The reaction with 5.0 mol % of $[RuCl_2(p\text{-cymene})]_2$ and *tert*-amyl alcohol/water mixture yielded the desired product **90ca** in 85% isolated yield (entry 1). Changing the base to sodium acetate was found to be detrimental for the catalytic reactivity (entry 2). The solvents had not comparable performance

to the solvent system in use. Indeed, the reactions in pure *tert*-amyl alcohol, water, 2,2,2-trifluoroethanol (TFE), or acetonitrile, were all found to deliver the products only in low to decent yields (entries 3–6). Decreasing the catalyst loading to 1.0 mol % delivered the desired product **90ca** in 31% yield, while lowering the temperature to 80 °C was found to be beneficial to the reaction, increasing the obtained isolated product to 90% (entries 7–8). Other transition metal (TM) catalysts were tested at 100 °C under the optimized conditions (entries 9–11). Interestingly, iridium and cobalt catalysts were found to be completely ineffective for the envisioned reaction, while the pentamethylcyclopentadienyl rhodium dichloride dimer yielded 82% of the annulated product **90ca**. Remarkably, this result represented the first electrochemical rhodium-catalyzed C–H activation.

Table 3.2.2 Optimization of the electrochemical ruthenium-catalyzed C–H/C–O annulation.[a]

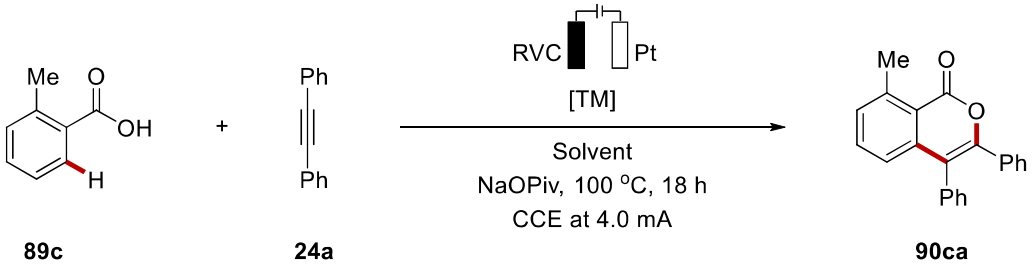

89c **24a** **90ca**

Entry	[TM]	Solvent	Yield (%)
1	$[RuCl_2(p\text{-cymene})]_2$ (5)	*t*AmylOH/H_2O (3:1)	85[b]
2	$[RuCl_2(p\text{-cymene})]_2$ (5)	*t*AmylOH/H_2O (3:1)	27[c]
3	$[RuCl_2(p\text{-cymene})]_2$ (5)	*t*AmylOH	10
4	$[RuCl_2(p\text{-cymene})]_2$ (5)	H_2O	44
5	$[RuCl_2(p\text{-cymene})]_2$ (5)	TFE	35[d]
6	$[RuCl_2(p\text{-cymene})]_2$ (5)	MeCN	17
7	$[RuCl_2(p\text{-cymene})]_2$ (1)	*t*AmylOH/H_2O (3:1)	31
8	**$[RuCl_2(p\text{-cymene})]_2$ (5)**	***t*AmylOH/H_2O (3:1)**	**90**[b,e]
9	$[Cp^*RhCl_2]_2$ (5)	*t*AmylOH/H_2O (3:1)	82
10	$[Cp^*IrCl_2]_2$ (5)	*t*AmylOH/H_2O (3:1)	-
11	$[Cp^*Co(MeCN)_3(SbF_6)_2]$ (10)	*t*AmylOH/H_2O (3:1)	-

[a] Reaction conditions: Undivided cell, **89c** (0.50 mmol), **24a** (1.00 mmol), [TM] (as specified), NaOPiv (1.00 equiv), solvent (4.0 mL), 100 °C, CCE at 4.0 mA, 18 h, RVC anode (10 mm × 15 mm

× 6 mm), Pt-plate cathode (10 mm × 15 mm × 0. 125 mm), isolated yield. [b] Performed by Dr. Youai Qiu. [c] NaOAc as additive. [d] 70 °C. [e] 80 °C.

3.2.2 Substrate Scope

We then moved on to assess the versatility of the electrochemical ruthenium-catalyzed C–H/C–O annulation. As shown in Scheme 3.2.1, *para*-methoxy benzoic acid (**89b**) was converted to the desired product **90ba** in 60% yield under the optimized conditions. The remaining substrate scope for differently decorated benzoic acids **89** was mainly performed by Dr. Youai Qiu. Interestingly, *meta*-substituted benzoic acids were selectively converted to a single regioisomer, with the functionalization occurring on the less sterically hindered position, as shown for product **90da**. Moreover, relevant electrophilic functional groups, such as bromo (**89e**) and cyano (**89f**), were well tolerated. Furthermore, heterocyclic substrates also underwent the annulation reaction in good yields. Indeed, both thiophene-3-carboxylic acid **89g** and 3-furoic acid **89h** were converted in 79% and 65% isolated yield, respectively.

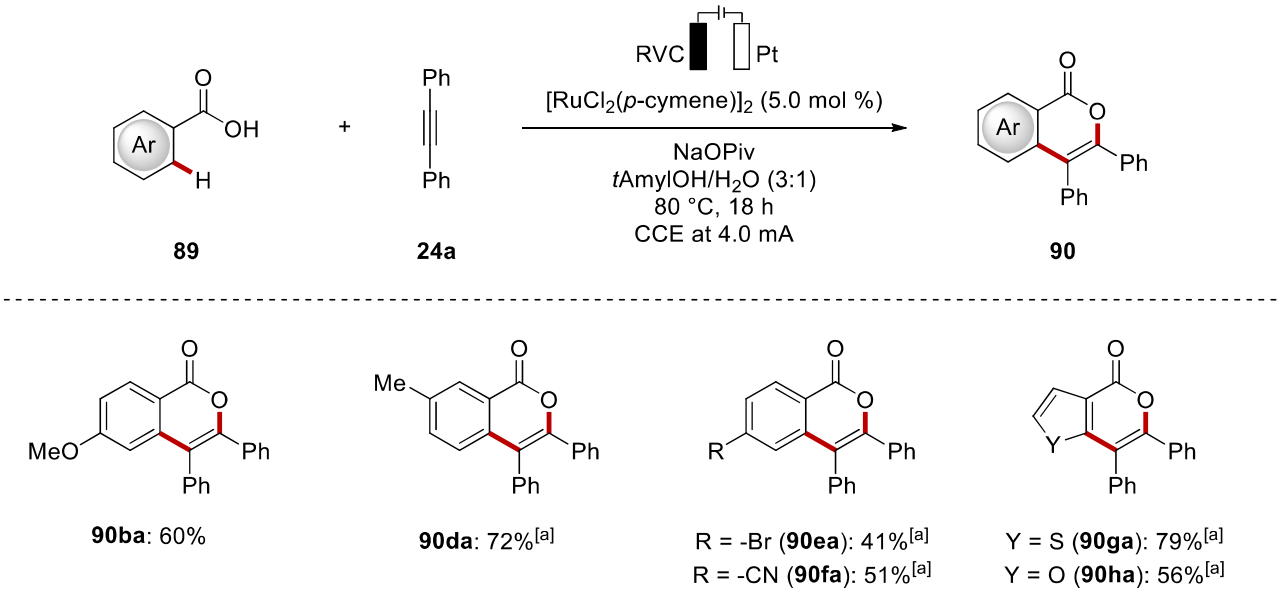

Scheme 3.2.1 Scope of the electrochemical ruthenium-catalyzed C–H/O–H alkyne annulation by weakly coordinating benzoic acids **89**. [a] Performed by Dr. Youai Qiu.

The robustness of the reaction was also tested with different alkynes **24**, with Dr. Cong Tian mainly focusing on symmetrical alkynes, which were well tolerated by the reaction.

Regarding the substrate scope that I conducted, 3-hexyne **24b** was smoothly converted into the desired product **90cb** (Scheme 3.2.2). Moreover, asymmetrical alkynes were thus tested. 1-pheny-1-butyne (**24c**) yielded 93% of product **90cc**, together with 5% of the other regioisomer **90cc'**. All the regioisomers were easily separated by column chromatography and characterized. The reaction with substrate **24d** gave 81% of **90cd** together with 6% of **90cd'**. Likewise, **24f** gave 65% of the major product **90cf** and 7% of the minor one **90cf'**, while substrate **24g** gave 88% and 7%, respectively. In the case of 1-chloro-4-(hex-1-yn-1-yl)benzene **24e** a satisfactory 78% yield was obtained. The generally accepted rationale behind this kind of selectivity is correlated to the fact that in oxidative type reactions the regio-determining step is usually the alkyne insertion into the Ru–C bond that furnishes the seven-membered ruthenacycle, showing the same selectivity in several reports.[95, 169]

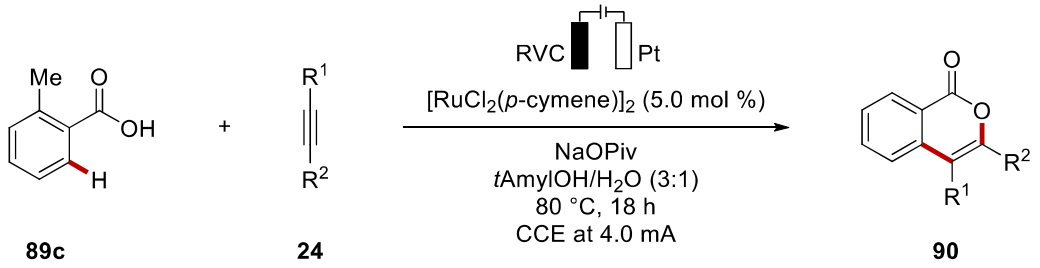

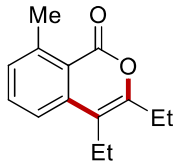

90cb: 60%

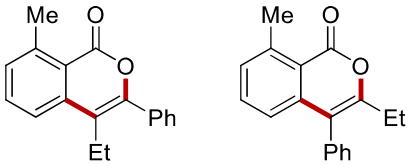

90cc: 93% + **90cc'**: 5%

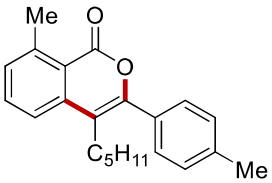

90cd: 81% +

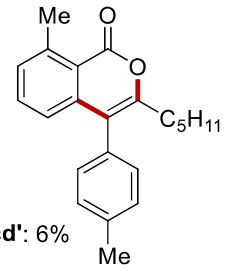

90cd': 6%

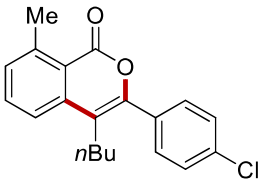

90ce: 78%

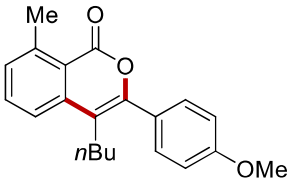

90cf: 65% +

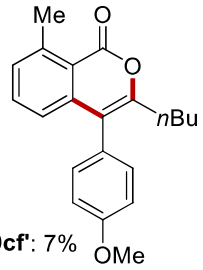

90cf': 7%

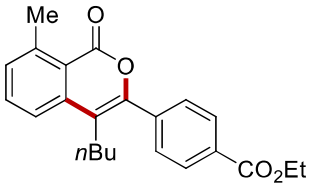

90cg: 88% +

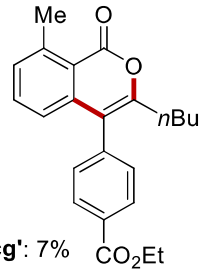

90cg': 7%

Scheme 3.2.2 Scope of the electrochemical ruthenium-catalyzed C–H/O–H annulation with alkynes **24**.

The envisioned C–H/O–H alkyne annulation was not limited to benzoic acids **89** but proved amenable to benzamides **87** likewise (Scheme 3.2.3). Thus, the reaction allowed the synthesis of isoquinolones **88** in good yields. The reaction between *N*-methylbenzamide **87a** and ethyl 4-(hex-1-yn-1-yl)benzoate **24g** provided 42% of product **88ag**, while the other regioisomer was not detected.

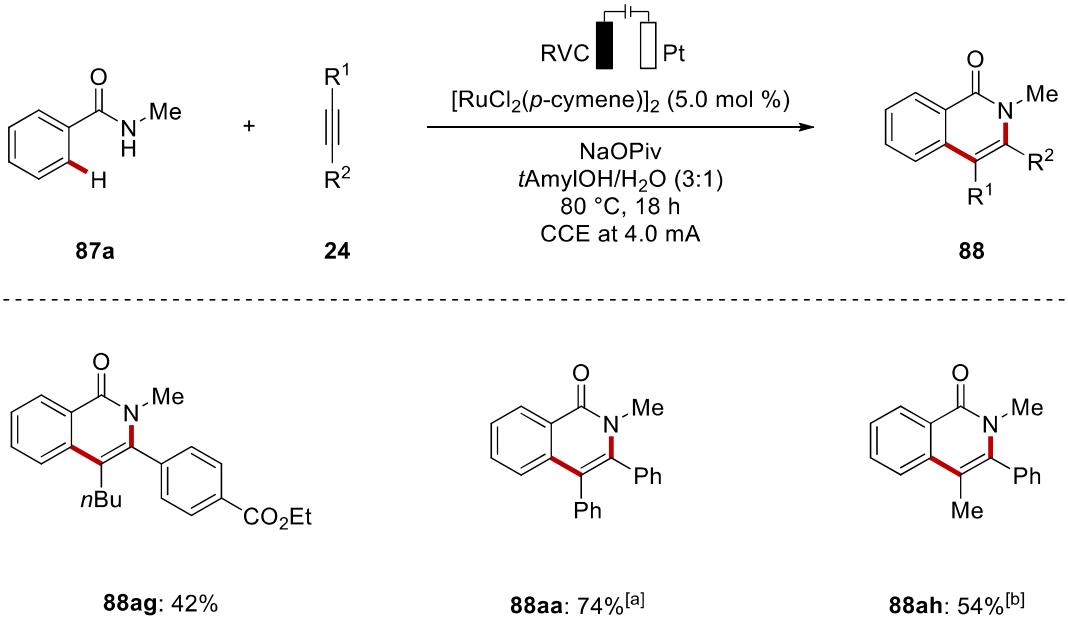

Scheme 3.2.3 Scope of the electrochemical ruthenium-catalyzed C–H/O–H alkyne annulation by benzamides **87**. [a] Performed by Dr. Youai Qiu. [b] Performed by Dr. Cong Tian.

Further, phenylacetylene (**117a**) was submitted to the optimized reaction conditions in order to test if terminal alkynes are feasible substrates (Scheme 3.2.4). Unfortunately, no desired product **189aa** was detected.

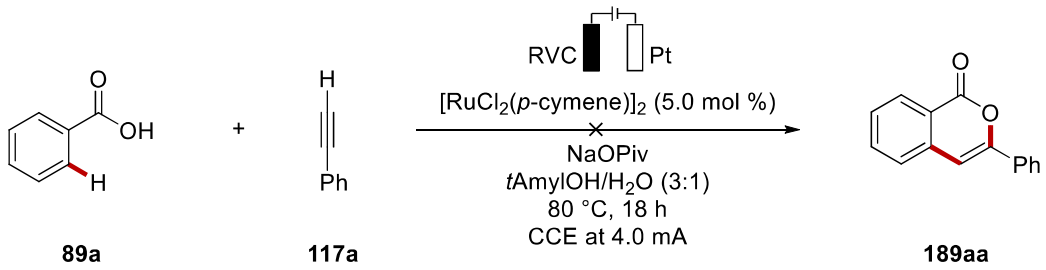

Scheme 3.2.4 Attempt for the electrochemical ruthenium-catalyzed C–H/O–H annulation of phenylacetylene **117a**.

3.2.3 Mechanistic Studies and Proposed Catalytic Cycle

The mechanistic studies were performed by Dr. Youai Qiu. The H/D exchange experiment showed the presence of deuterium incorporation in both the recovered starting material and the product. This

indicates a reversible C–H cleavage by the ruthenium catalyst. Moreover, intermolecular competition experiments showed a preferential reactivity of the electron-rich arenes and alkynes. With these insights in hand, we proposed a plausible catalytic cycle (Scheme 3.2.5) that starts from the C–H activation by the ruthenium catalyst on the arene **89**, followed by a regio-determining migratory insertion step. After reductive elimination, the ruthenium(0) intermediate **193** undergoes an anodic oxidation to yield the desired product **90** and to regenerate the active catalyst **188b**.

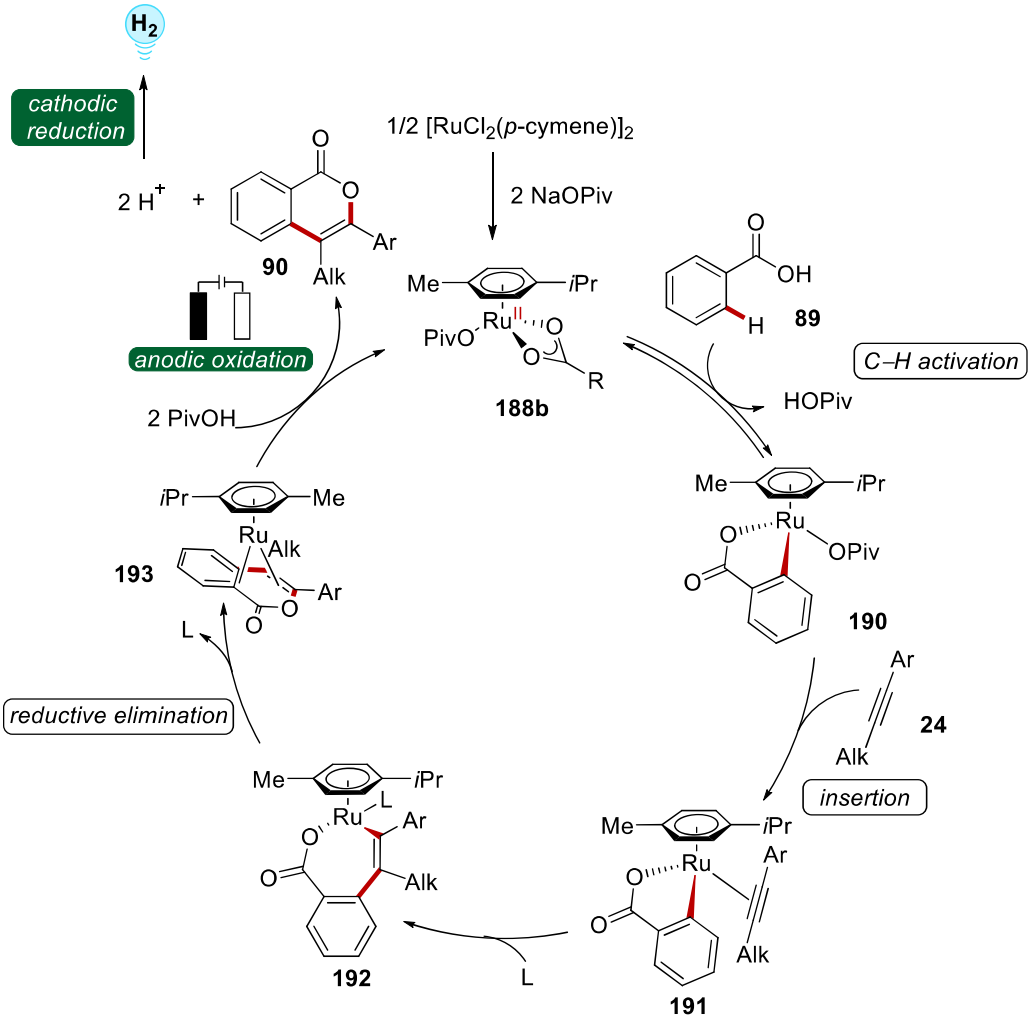

Scheme 3.2.5 Proposed catalytic cycle for the electrochemical ruthenium-catalyzed C–H/O–H alkyne annulation.

3.3 C−H Oxygenation Reactions Enabled by Dual Catalysis with Electrogenerated Hypervalent Iodine Species and Ruthenium Complexes

The electrochemical oxidation of aryl iodides was revealed to be a valuable approach for the *in-situ* synthesis of hypervalent iodine species, thus allowing for a safer chemistry that eliminates the need for hazardous and expensive chemical oxidants.[165d] The first example was published by Fuchigami and Fujita in 1994, where they could remarkably employ catalytic amounts of 4-iodoanisole for the formation of hypervalent iodobenzene difluoride to allow a *gem*-difluorination reaction.[165g] Lately, this methodology has been used for several transformation, but always with stoichiometric amounts of the aryl iodide precursor.[165a-c, 165e-f] In this context, our efforts focused on the coupling of the electrochemical generated hypervalent iodine from catalytic amounts of iodobenzene with ruthenium-catalyzed C–H oxygenation.

3.3.1 Optimization

The project started with the optimization of reaction conditions for the electrochemical formation of hypervalent iodine **195** (Table 3.3.1). The identified solvents for the formation of hypervalent iodine were acetic acid, trifluoroacetic acid, TFE, and HFIP. The reactions were initially performed with 4Å molecular sieves and under nitrogen. The yields were obtained by ^{1}H-NMR analysis of the reaction with the addition of an internal standard. The classical 1,3,5-trimethoxybenene could not be employed since it would react with the hypervalent iodine. Dibromomethane was thus used instead.

First, TFE was employed as solvent, obtaining 42% of the desired product after 2 hours, and 75% after 4 hours (entries 1–2). The use of tetrabutylammonium hexafluorophosphate as the electrolyte yielded 60% over 4 hours (entry 3), while there was no reaction in the absence of an electrolyte (entry 4). Interestingly, when HFIP was used as the solvent, the reaction was yielding trace amounts of the desired product in presence of lithium perchlorate as electrolyte, while a promising 65% yield was obtained with tetrabutylammonium hexafluorophosphate (entries 5–6). Trifluoroacetic acid was also a solvent of interest, therefore the electrochemical formation of (bis(trifluoroacetoxy)iodo)benzene **195aa** was investigated in TFA. Under the same previous conditions , 69% yield was obtained with $LiClO_4$, and 68% using nBu$_4$NPF$_6$ as the electrolytes

(entries 7–8). The removal of the molecular sieves proved beneficial, as well as performing the reaction under air, which gave 88% yield (entries 9–10). Different currents were then attempted. The reaction worked with 7.0 mA for 5 hours, but the yield decreased to 42% (entry 11). When the current was lowered to 4.0 mA for 16 hours, it resulted in an 88% yield (entry 12). Lastly, control reactions were performed and confirmed the necessity of both the electrolyte and the current (entries 13–14). The idea of substituting the electrolyte with sodium trifluoroacetate did not prove successful (entry 15).

As shown in Figure 3.3.1, the formation of the hypervalent iodine species was easily followed by ^{1}H-NMR spectroscopy, since the aromatic resonances of the product are clearly shifted towards low fields.[165e]

Table 3.3.1 Optimization for the electrochemical formation of hypervalent iodine.[a]

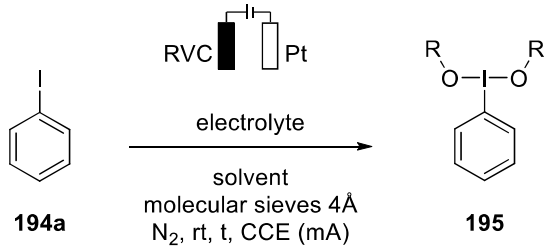

194a **195**

Entry	Solvent	Electrolyte	mA	t	notes	Yield[b]
1	TFE	$LiClO_4$	10	2 h		42%
2	TFE	$LiClO_4$	10	4 h		75%
3	TFE	nBu$_4$NPF$_6$	10	4 h		60%
4	TFE	-	10	4 h		-
5	HFIP	$LiClO_4$	10	4 h		traces
6	HFIP	nBu$_4$NPF$_6$	10	4 h		65%
7	TFA	$LiClO_4$	10	4 h		69%
8	TFA	nBu$_4$NPF$_6$	10	5 h		68%
9[c]	TFA	nBu$_4$NPF$_6$	10	5 h	Without mol. sieves	75%[c]
10[c]	TFA	nBu$_4$NPF$_6$	10	5 h	Without mol. sieves, under air	88%[c]
11[c]	TFA	nBu$_4$NPF$_6$	7	5 h		42%[c]
12[c]	TFA	nBu$_4$NPF$_6$	4	16 h		84%[c]
13[c]	TFA	-	10	5 h		-[c]

14[c]	TFA	nBu$_4$NPF$_6$	10	5 h	Without current	-[c]
15[c]	TFA	NaOTFA (2.0 equiv)	10	5 h		-[c]

[a] Reaction conditions: Undivided cell, **194a** (0.50 mmol), electrolyte (1.00 equiv), solvent (5.0 mL), 23 ºC, CCE, N_2, molecular sieves 4Å, RVC anode (10 mm × 15 mm × 6 mm), Pt-plate cathode (10 mm × 15 mm × 0. 125 mm). [b] ^{1}H-NMR yield with dibromomethane as internal standard. [c] Without molecular sieves.

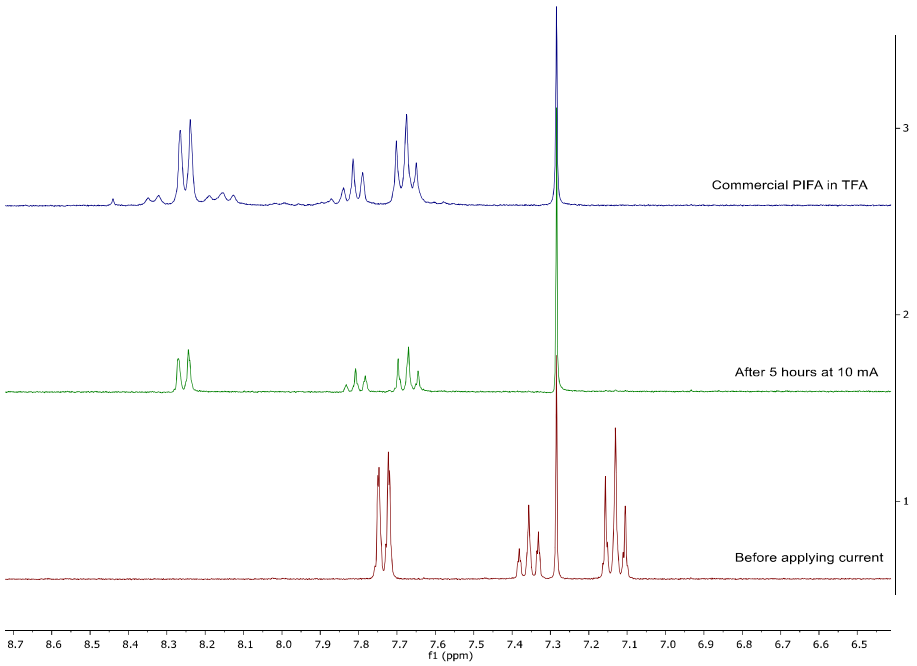

Figure 3.3.1 Analysis of *in-situ* generation of PIFA **195aa** with TFA, ^{1}H-NMR (300 MHz).

The aim of the project was to ideally couple the study on electrochemical-generated hypervalent iodine with mediated electrolysis for transition metal catalysis. Therefore, based on literature precedents from the Ackermann group,[110-113, 115] we identified Weinreb amides, carbamates, and aldehydes as suitable substrates for the desired reaction. In these reports, the solvents used were a mixture of trifluoroacetic acid and trifluoroacetic anhydride, or 1,2-dichloroethane. The first media was considered to be more easily applicable, since the hypervalent iodine species is formed in TFA. In the case of DCE, another solvent would need to be added. Hence, the ruthenium oxygenation of weakly-coordinating Weinreb amides **196** was studied in electrochemical conditions, with the *in-situ*

generation of hypervalent iodine as oxidant from catalytic amounts of iodobenzene **194a** and TFA as solvent.

The initial tests were performed with a two steps procedure, where first the hypervalent iodine **195aa** formed in TFA, and then, after the addition of substrate **196a**, catalyst, and TFAA, the C–H activation reaction occurred to yield the desired product **106a** (Table 3.3.2). When the reaction was performed under air no product could be observed, even when the iodobenzene **194a** was used in excess (entry 1). The second reaction was conducted under an inert atmosphere, but no improvement was noticed (entry 2).

Table 3.3.2 Attempts for the two-step procedure for ruthenium oxygenation with $LiClO_4$ as electrolyte.[a]

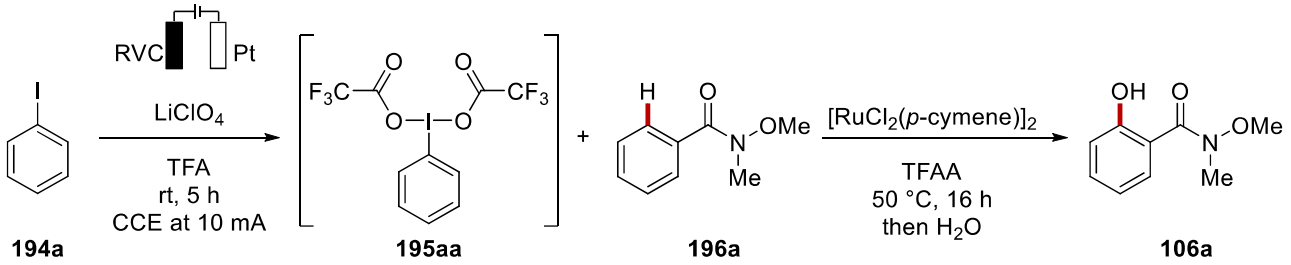

Entry	Atmosphere	Yield
1	air	-
2	N_2	-

[a] Reaction conditions: a) Undivided cell, **194a** (0.60 mmol), electrolyte (1.25 equiv), TFA (5.0 mL), 23 ºC, 5 h CCE at 10 mA, RVC anode (10 mm × 15 mm × 6 mm), Pt-plate cathode (10 mm × 15 mm × 0. 125 mm); b) **196a** (0.25 mmol), $[RuCl_2(p\text{-cymene})]_2$ (2.5 mol %), TFAA (1.0 mL), 50 °C, 16 h.

Next, the reaction was carefully analyzed. The only differences between the above shown reaction (Table 3.3.2) and the literature precedent[112] lied in the use of PIFA instead of PIDA and in the presence of the electrolyte. Consequently, the reaction with the commercial chemical oxidant was analyzed (Table 3.3.3). First, the oxygenation with PIDA was repeated, yielding 80% of the desired product **106a** (entry 1). Then, a test reaction with PIFA instead of PIDA, gave a comparable yield (entry 2). Subsequently, the reaction with the chemical oxidant and without current was tried in the

presence of the lithium perchlorate, to evaluate its effect (entry 3). Interestingly, the reactivity was completely suppressed in the presence of this electrolyte. The same reaction was also tried with tetrabutylammonium hexafluorophosphate, and - to our great delight - succeeded with 84% of the isolated desired product **106a** (entry 4).

Table 3.3.3 Effect of the electrolyte on oxygenation reaction with chemical oxidant.[a]

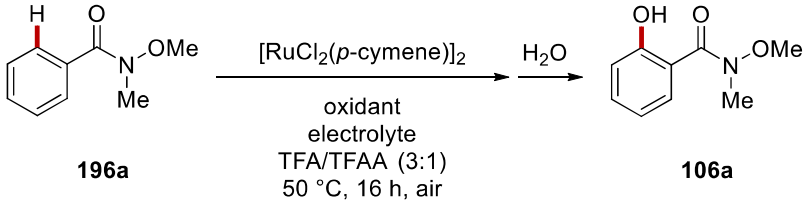

196a **106a**

Entry	Oxidant	Electrolyte	Yield
1	PIDA	-	80%[b]
2	PIFA	-	75%[b]
3	PIFA	$LiClO_4$	-
4	PIFA	$n Bu_4NPF_6$	84%

[a] Reaction conditions: Undivided cell, **196a** (0.25 mmol), $[RuCl_2(p\text{-cymene})]_2$ (2.5 mol %), oxidant (1.00 equiv), electrolyte (1.25 equiv), TFA/TFAA (3:1, 4.0 mL), 50 °C, 16 h, air. [b] ^{1}H-NMR yield with dibromomethane as internal standard.

With these insights in hand, the two-step procedure was attempted with tetrabutylammonium hexafluorophosphate as the electrolyte (Table 3.3.4). This change proved to be successful, and the oxygenated product **106a** was obtained in 75% yield under nitrogen atmosphere and in 80% under air (entries 1–2). In the same reaction conditions, the concentration of the Weinreb amide **196a** and the catalyst were increased, with a benefit for the yield of product **106a** (entry 3).

Table 3.3.4 Two-step procedure for ruthenium oxygenation with $n Bu_4NPF_6$.[a]

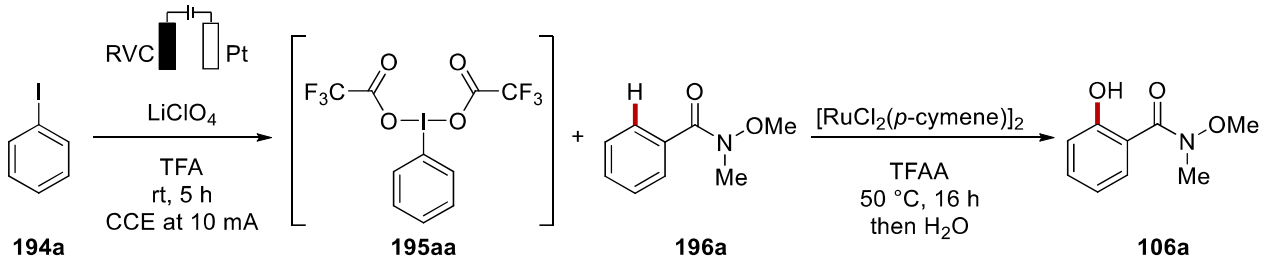

Entry	Atmosphere	note	Yield
1	N_2	-	75%
2	air	-	80%
3	air	0.50 mmol of **196a**	84%

[a] Reaction conditions: a) Undivided cell, **194a** (0.60 mmol), electrolyte (1.25 equiv), TFA (5.0 mL), 23 ºC, 5 h, CCE at 10 mA, RVC anode (10 mm × 15 mm × 6 mm), Pt-plate cathode (10 mm × 15 mm × 0. 125 mm); b) **196a** (0.25 mmol), $[RuCl_2(p\text{-cymene})]_2$ (2.5 mol %), TFAA (1.0 mL), 50 °C, 16 h.

The desired reaction would form the hypervalent iodine *in-situ* and possibly with catalytic amounts of iodobenzene **194a**. The experiments above showed that all the components of the first step are tolerated in the ruthenium-catalyzed oxygenation, so the attempt on performing the reaction in one-step was tried (Table 3.3.5). Unfortunately, both the iodobenzene **194a** in stoichiometric amounts (1.2 equiv) or in catalytic (20 mol %), provided only traces amount of the desired product **106a** (entry 1–2).

Table 3.3.5 Attempts for the *in-situ* ruthenium catalyzed oxygenation.[a]

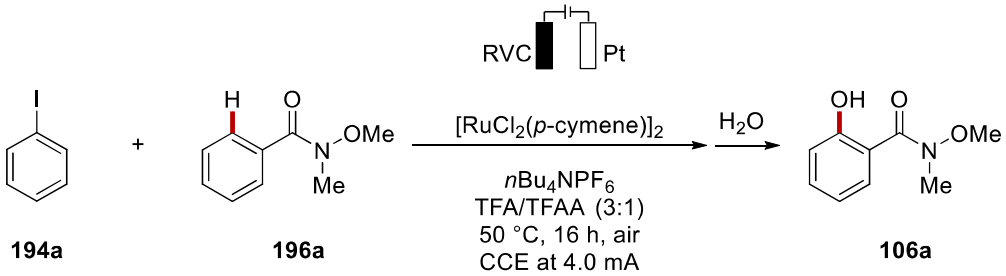

Entry	194a	Yield
1	120 mol %	traces

2	20 mol %	traces

[a] Reaction conditions: Undivided cell, **194a** (as specified), **196a** (0.5 mmol), $[RuCl_2(p\text{-cymene})]_2$ (2.5 mol %), nBu$_4$NPF$_6$ (1.25 equiv), TFA/TFAA (3:1, 4.0 mL), 50 °C, 16 h, air, CCE at 4.0 mA, RVC anode (10 mm × 15 mm × 6 mm), Pt-plate cathode (10 mm × 15 mm × 0. 125 mm).

Since the two-step reaction worked, while the one-step reaction was thus far unsuccessful, the attention was focused on the differences between the conditions for the electrochemical formation of PIFA (as in Scheme 3.3.1) and the one for the one-step reaction (as in Scheme 3.3.5). Two differences were the temperature of the reaction and the nature of the solvent mixture. These different conditions were then separately tested for the electrochemical synthesis of PIFA **195aa** (Table 3.3.6). The reaction worked well both at 50 °C as well as with a TFA/TFAA mixture (3:1) as the solvent media (entries 1–2), proving that the differences in the conditions were not prohibitive to the product formation. Another hypothesis could be related to the oxidation potentials of the components of the reactions. As shown by cyclic voltammetry (Figure 3.3.2, performed by Dr. T. H. Meyer), ruthenium **188a** was indeed having a lower oxidation potential as compared to iodobenzene **194a**. Thus, the reason for the one-pot procedure failure might lie in the preferential oxidation of the metal complex rather than the iodobenzene. In the previous project on electrochemical ruthenium-catalyzed C–H/C–O annulation,[130] it was found that the ruthenium catalysis worked with a RVC anode, but not with a platinum-plate anode. It was deductible that the direct oxidation of this metal on such an electrode is not optimal. Therefore, the formation of the hypervalent iodine **195aa** was tried with a platinum-platinum electrodes setup, giving 80% NMR conversion (entry 3).

Table 3.3.6 Further optimization for the electrochemical formation of hypervalent iodine.[a]

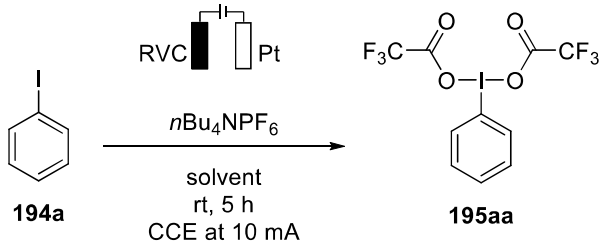

Entry	Solvent	Note	Yield[a]

1	TFA	50 °C	95%
2	TFA/TFAA (3:1)	-	99%
3	TFA	Pt-Pt electrodes	80%

[a] Reaction conditions: Undivided cell, **194a** (0.50 mmol), electrolyte (1.25 equiv), solvent (3.0 mL), 23 °C, 5 h, air, CCE at 10 mA, RVC anode (10 mm × 15 mm × 6 mm), Pt-plate cathode (10 mm × 15 mm × 0. 125 mm). [b] ^{1}H-NMR yield with CH_2Cl_2 as the internal standard.

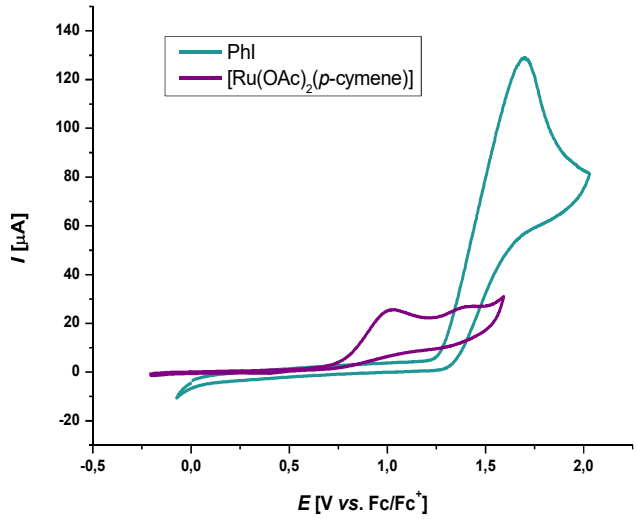

Figure 3.3.2 Selected data from the cyclic voltammograms performed by Dr. T. H. Meyer at a scan rate of 100 mVs^{-1} with TFA and nBu$_4$NPF$_6$ (0.1 M) as the electrolyte and a GC working electrode; the concentration of all substrates was 5.0 mM. (green) iodobenzene **194a**, (purple) [Ru(OAc)$_2$(*p*-cymene)] **188a**.

After detailed optimization, the reaction conditions were found to be with 20 mol % of iodobenzene **194a**, 2.5 mol % of [RuCl$_2$(*p*-cymene)]$_2$, tetrabutylammonium hexafluorophosphate as electrolyte, TFA/TFAA (3:1) as solvent mixure, 50 °C, with platinum electrodes. The desired product **106a** could thus be obtained in a one-step procedure in 70% isolated yield (Scheme 3.3.1).

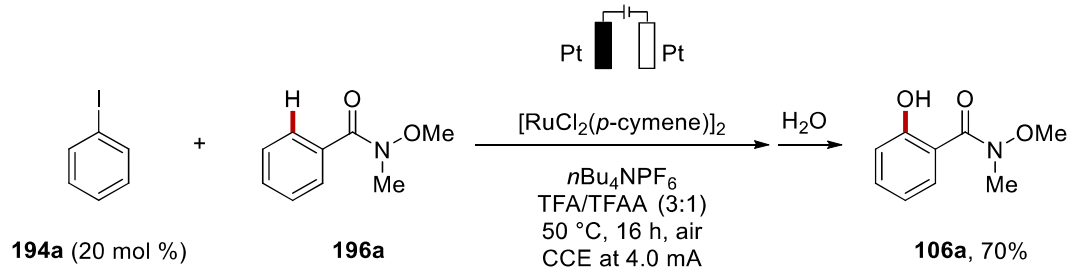

Scheme 3.3.1 Successful electrochemical ruthenium oxygenation mediated by *in-situ* formed PIFA from catalytic iodobenzene.

After this successful breakthrough, the further optimization of the reaction was started. Firstly, different ruthenium catalysts were tried for the envisioned C–H oxygenation (Table 3.3.7). [Ru(OAc)$_2$(*p*-cymene)] and [Ru(O$_2$CMes)$_2$(*p*-cymene)] were suitable catalysts, with the former being the best with 80% yield (entries 2–3). Other ruthenium sources did not prove to be viable for the desired transformation (entries 4–5). Thus, [Ru(OAc)$_2$(*p*-cymene)] (**188a**) in 5.0 mol % loading was selected as the best catalyst and further optimization studies were performed with complex **188a**.

Table 3.3.7 Optimization of the ruthenium catalyst for C–H oxygenation.[a]

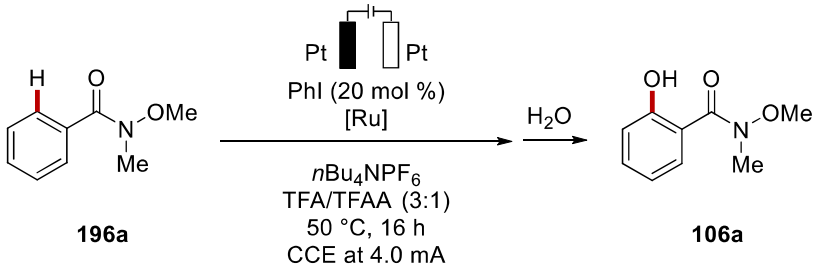

Entry	[Ru]	Yield
1	[RuCl$_2$(*p*-cymene)]$_2$ (2.5 mol %)	77%[b]
2	**[Ru(OAc)$_2$(*p*-cymene)] (5.0 mol %)**	**80%[b]**
3	[Ru(O$_2$CMes)$_2$(*p*-cymene)] (5.0 mol %)	59%
4	[Ru(NC*t*Bu)$_6$][PF$_6$]$_2$ (5.0 mol %)	-
5	RuCl$_3$ (5.0 mol %)	-

[a] Reaction conditions: Undivided cell, **196a** (0.25 mmol), PhI **194a** (20 mol %), [Ru] (as specified), nBu$_4$NPF$_6$ (1.00 equiv), TFA/TFAA (3:1, 3.0 mL), 50 °C, 16 h, air, CCE at 4.0 mA, Pt-plate electrodes (10 mm × 15 mm × 0. 125 mm).

Furthermore, the optimization was extended to gain a better understanding of the reaction (Table 3.3.8). Initially, control reactions in the absence of current, or in the absence of the ruthenium catalyst **188a** or iodobenzene **194a**, were independently checked and all the three components proved to be essential (entries 1–4). The reaction performed under an inert atmosphere of nitrogen gave a comparable result, showing that air had no influence on the reactivity (entry 5). The reaction temperature was lowered to room temperature, which gave 50% yield of the product **106a** (entry 6). Diminishing the electrolyte loading to 0.5 equivalents resulted in 52% of the desired product (entry 7). In the complete absence of the tetrabutylammonium salt the yield was 55% (entry 8). The reaction was thus clearly benefiting from a temperature of 50 °C and from the presence of the electrolyte. Moreover, 4-iodoanisole **194b** was used instead of iodobenzene to see if a lower oxidation potential of the mediator could be beneficial for the reaction but it proved to be less efficient (entry 9). Several redox mediators were added as additives instead of iodobenzene, but all of them did not furnish any desired product (entries 10–14). Chemical oxidants were employed instead of electricity to compare their efficacy, and both *meta*-chloroperoxybenzoic acid and oxone gave a poor conversion (entries 15–16). Afterwards, the focus was shifted towards the electrochemical features of the reaction. CCE was attempted at 6.0 and 2.0 mA, giving only 51% and 37% of **106a**, respectively (entries 17–18). Likewise, CPE was investigated at 2.0, 1.5, and 1.0 V *vs.* Ag/Ag$^+$, yielding 86% and 60%, respectively, for the first two reactions, while no reaction occurred with the lowest voltage applied (entries 19–21). This meant that 1.0 V *vs.* Ag/Ag$^+$ was probably too low for the efficient oxidation of iodobenzene **194a**. Even though the reaction worked very well also at 2.0 V *vs.* Ag/Ag$^+$, the scope of the reaction was performed under CCE conditions as a comparable result was obtained and the set-up is more user-friendly. Lastly, the electrodes were tested. RVC anode was again tried in the new optimized conditions and only 24% of the desired product was obtained (entry 22). A reaction with RVC anode and without iodobenzene was tried to understand if in absence of the

mediator the catalyst could efficiently be reoxidize directly on the carbon-based electrode, but it resulted in only 28% isolated yield (entry 23). The platinum electrodes were then substituted with stainless steel and nickel-plate, but in both cases the reaction failed (entry 24–25).

Table 3.3.8 General optimization for the ruthenium catalyzed C–H oxygenation.[a]

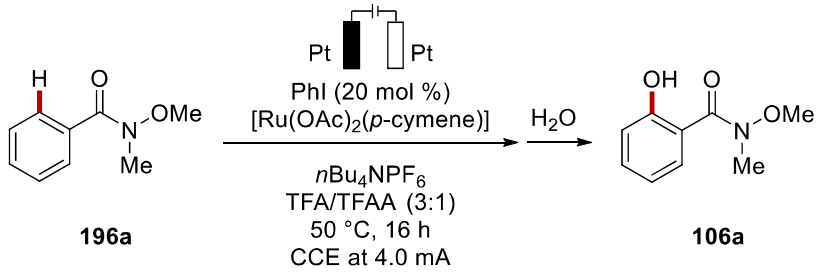

Entry	Deviation from standard conditions	Yield
1	**---**	**80%**
2	No current	-
3	Without [Ru]	-
4	Without PhI	-
5	Under N_2	70%
6	25 °C instead of 50 °C	50%
7	Electrolyte (0.50 equiv)	52%
8	Without electrolyte	55%
9	4-$MeOC_6H_4I$ instead of PhI	55%
10	PhBr instead of PhI	-
11	PhCl instead of PhI	-
12	1,4-BQ instead of PhI	-
13	PhS-SPh instead of PhI	-
14	PhSe-SePh instead of PhI	-
15	*m*CPBA (1.0 equiv) instead of electricity	15%
16	Oxone (1.0 equiv) instead of electricity	32%
17	6.0 mA	51%
18	2.0 mA	37%
19	CPE at 2.0 V *vs.* Ag/Ag^+	86%
20	CPE at 1.5 V *vs.* Ag/Ag^+	60%
21	CPE at 1.0 V *vs.* Ag/Ag^+	-

22	RVC anode instead of Pt	24%
23	RVC anode instead of Pt, without PhI	28%
24	Stainless Steel electrodes instead of Pt	-
25	Ni-plate electrodes instead of Pt	-

[a] Reaction conditions: Undivided cell, **196a** (0.25 mmol), PhI **194a** (20 mol %), [$Ru(OAc)_2$(*p*-cymene)] **188a** (5.0 mol %), *n*Bu_4NPF_6 (1.00 equiv), TFA/TFAA (3:1, 3.0 mL), 50 °C, 16 h, air, CCE at 4.0 mA, Pt-plate electrodes (10 mm × 15 mm × 0. 125 mm). Yields of the isolated products.

3.3.2 Robustness

Having the optimized reaction conditions in hand, the scope was investigated with a variety of weakly-coordinating Weinreb amides **196** in collaboration with Dr. X. Tan (Scheme 3.3.2). The reaction proved to be very robust on amides **196b-d** bearing both electron-rich and electron-deficient *para*-substituents, furnishing the desired products in good yields. 3,4-dimethyl and 3,4-dichloro arenes **196e-f** were successfully employed giving 59% and 62% yield, respectively. Electron-rich *meta*-substituents were well tolerated by the system, even though the minor regioisomer was detected in 2% yield for product **106j**. In the case of the isopropyl substituent in *meta* (**106k**), we could not detect any minor regioisomer. The same held true for electron-deficient substituents (**106l-n**), which were functionalized only in the more accessible position. Moreover, products **106o** and **106p** could also be obtained with the envisioned mediated ruthenium catalysis, underlying the compatibility of this reaction with electrophilic functional groups that are useful for subsequent late-stage modifications. As proved during the optimization, the reaction was also feasible in the absence of the electrolyte (Table 3.3.8). Some compounds were tested in these conditions also in the scope, showing that the desired products could be obtained likewise without tetrabutylammonium hexafluorophosphate with decent yields, around 20% lower than with the optimized reaction conditions.

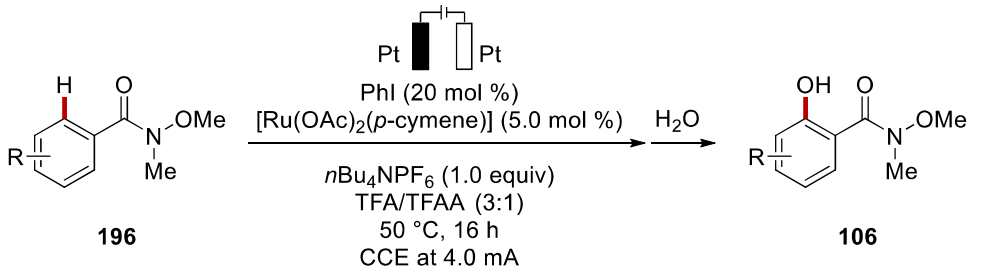

196 **106**

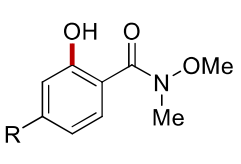

R = H (**106a**): 80%, 55%[a]
R = Me (**106b**): 73%
R = Et (**106c**): 71%, 50%[a]
R = CF_3 (**106d**): 66%[b]

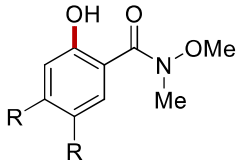

R = Me (**106e**): 59%
R = Cl (**106f**): 62%, 46%[a]

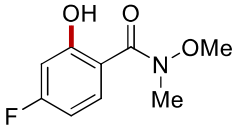

106g: 73%[b]

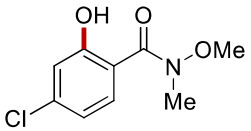

106h: 81%[b]

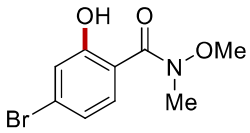

106i: 82%, 58%[a]

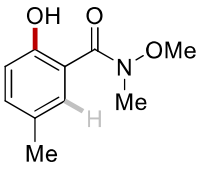

106j: 59% (2%)[b]

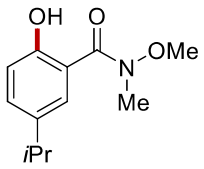

106k: 74%[b]

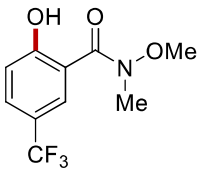

106l: 45%

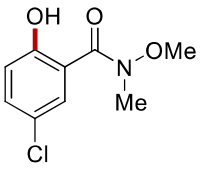

106m: 84%

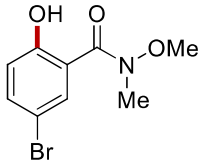

106n: 75%

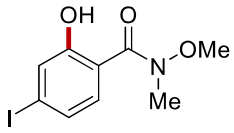

106o: 65%

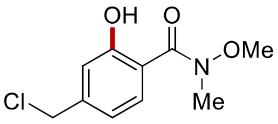

106p: 77%

Scheme 3.3.2 Scope of electrochemical ruthenium-catalyzed C–H oxygenation of Weinreb amides **196**. [a] Without nBu$_4$NPF$_6$. [b] Performed by Dr. X. Tan.

The reaction was further tested on other tertiary amides **103** (Scheme 3.3.3). The presence of a methyl group in *para* to dimethyl amide or in *meta* to diethyl amide was well tolerated, yielding product **104b** and **104c** in 84% and 64%, respectively. Further robustness studies were investigated

by Dr. X. Tan, showing that different substituted amides **103** were similarly oxygenated. Especially, product **104f** was obtained in 91% yield in the optimized conditions and in an interesting 61% yield when the electrolyte was omitted.

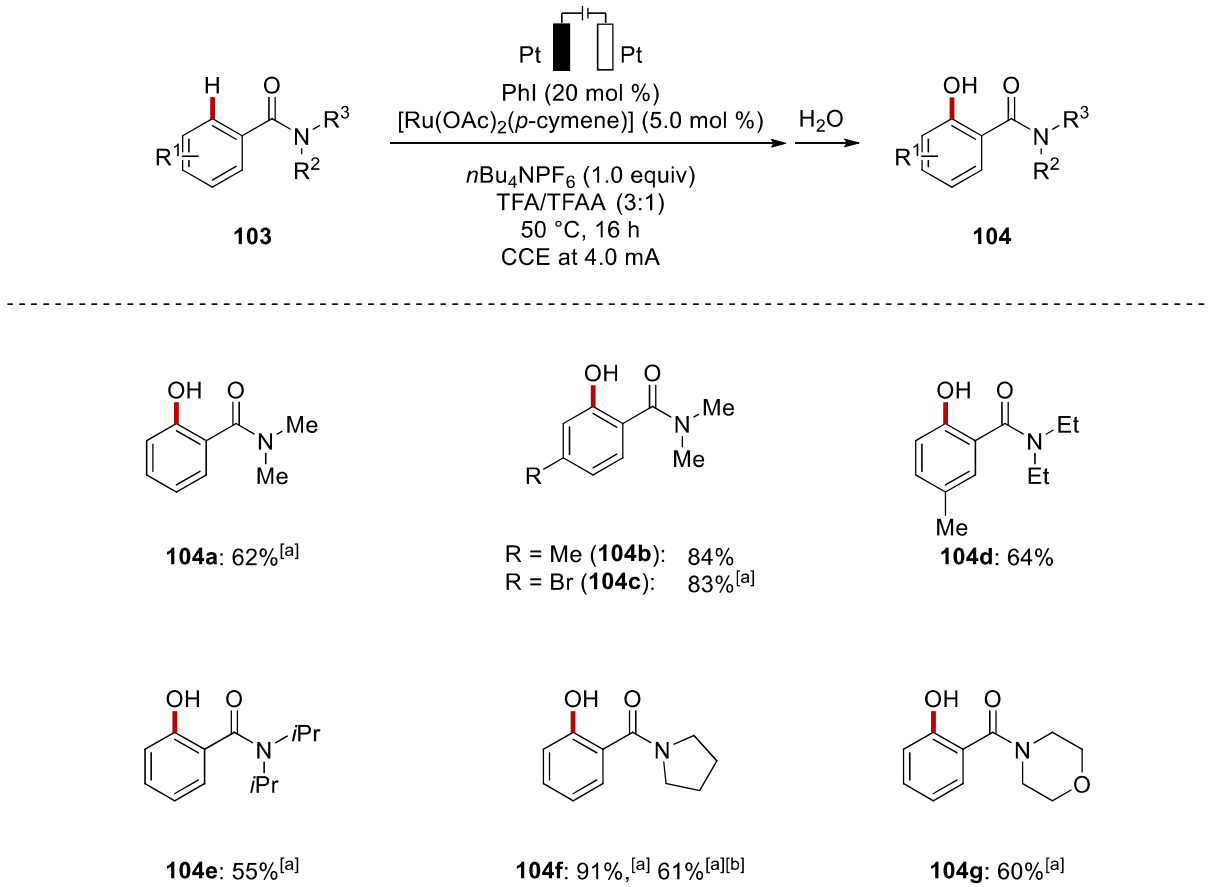

Scheme 3.3.3 Scope of electrochemical ruthenium-catalyzed C–H oxygenation of various amides **103**. [a] Performed by Dr. X. Tan. [b] Without nBu$_4$NPF$_6$.

We further aimed to extend the applicability of the reaction to more weakly coordinating directing groups. Interestingly, we found that the electrochemical mediated ruthenium oxygenation was also suitable for ketones **77** (Scheme 3.3.4). Ketones were converted slightly more efficiently by [RuCl$_2$(*p*-cymene)]$_2$, which was thus used for this part of the scope. Differently decorated ketones **77** successfully underwent the reaction, such as *tert*-butyl phenyl ketone (**77a**) and acetophenone(**77c**). Electron-rich and -poor substrates were well tolerated (**197e-h**), as well as a methyl substituent in *meta* (**197i**). Moreover, the excellent selectivity of the envisioned reaction was demonstrated on the

substrate **77k,** for which the mono-arylated product **197k** could be selectively obtained after 8 hours, while the diarylated one **197l** was selectively obtained after a 24-hour reaction. Similarly, for the unsymmetrical substrate, the electron-rich arene reacted preferentially, yielding the sole product **197m**.

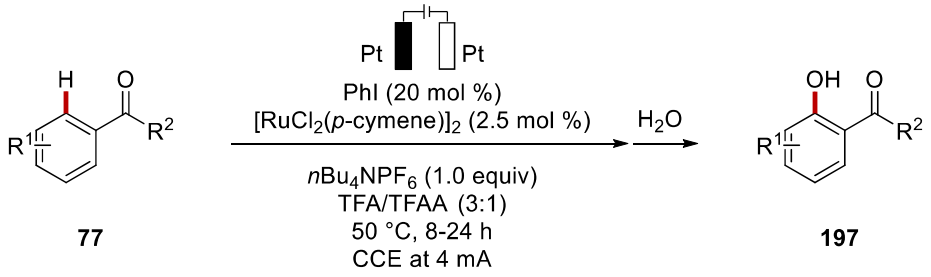

77 **197**

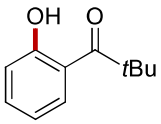

197a: 85%[a]

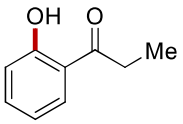

197b: 60%

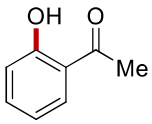

197c: 66%

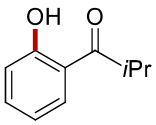

197d: 66%

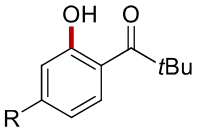

R = Me (**197e**): 51%
R = *t*Bu (**197f**): 68%[a]

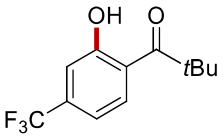

197g: 65%[a]

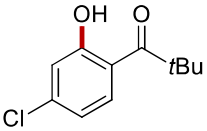

197h: 61%

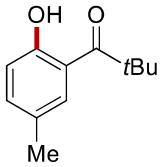

197i: 64%[a][b]

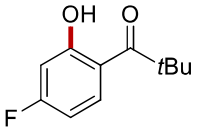

197j: 65%

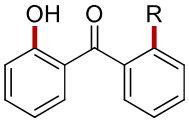

8 h: R = H (**197k**): 57%[a]
24 h: R = OH (**197l**): 59%[a]

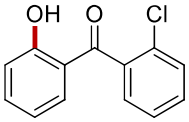

197m: 78%[a]

Scheme 3.3.4 Scope of electrochemical ruthenium-catalyzed C–H oxygenation of ketones **77**. [a] Performed by Dr. X. Tan. [b] CCE at 3.0 mA.

The power of the iodine(III)/ruthenium(II)-catalyzed C–H oxygenation was highlighted by the reactivity of more challenging substrates. After considerable experimentation, Dr. X. Tan could prove the viability of the designed reaction for pyrazole containing substrates **198** (Scheme 3.3.5).

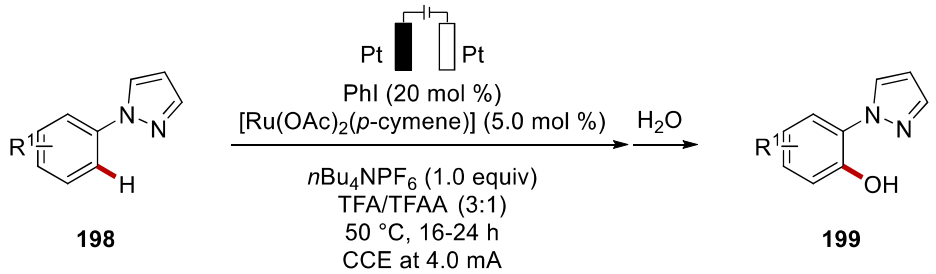

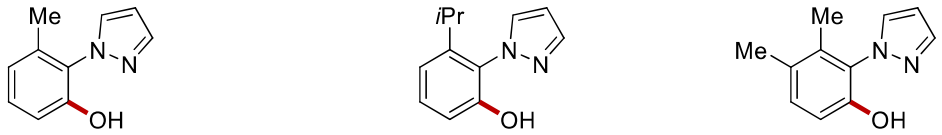

199a: 53% **199b**: 47% **199c**: 46%

Scheme 3.3.5 Scope of electrochemical ruthenium-catalyzed C–H oxygenation of pyrazole substrates **198**. Performed by Dr. X. Tan.

The challenging remote functionalization of differently substituted anisoles **200** was achieved with few modifications to the methodology (Scheme 3.3.6). This showed that the power of the presented ruthena-electrocatalysis is not restricted to chelating directing groups but is also viable on directing-group-free substrates. Due to the lower oxidation potential of anisole compared to iodobenzene,[170] the procedure has to be changed to circumvent the unfruitful oxidation of the substrate **200** on the anode. A sequential two-step/one-pot procedure was devised, where the hypervalent iodine was firstly generated in stoichiometric amounts, and then the substrate **200** and the catalyst **188a** were added into the reaction. The desired products **109** were obtained as a sole regioisomer with good

yields. In the case of the anisole **200c**, the reaction was tested also without the addition of the ruthenium catalyst, but no product was obtained.

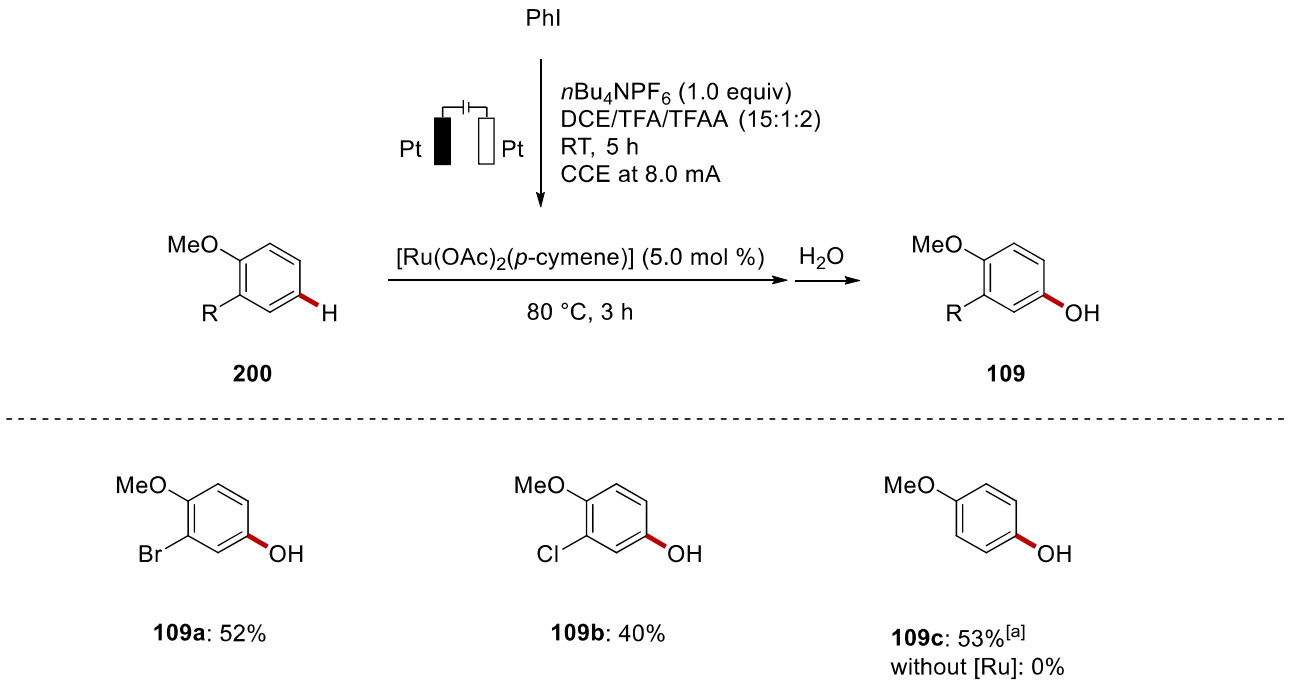

Scheme 3.3.6 Remote C–H oxygenation directing-group free. [a] Performed by Dr. X. Tan.

The robustness of the reaction was further proven by the gram-scale synthesis of the product **106a** (Scheme 3.3.7). Starting from 8.50 mmol (1.40 g), we could achieve an excellent 84% isolated yield (1.29 g), that testifies the great efficiency of the reaction also on larger scale.

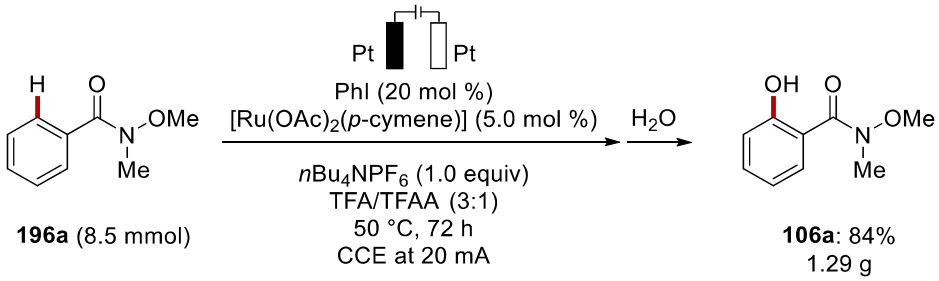

Scheme 3.3.7 Gram-scale electrochemical ruthenium-catalyzed C–H oxygenation.

3.3.3 Mechanistic Studies

To elucidate the catalytic cycle for the iodine(III)/ruthenium(II)-catalyzed C–H oxygenation, extensive mechanistic studies were carried out. First, the H/D exchange on the recovered starting material and on the obtained product was studied after 6 hours of CCE (Scheme 3.3.8,a). For substrate $[D]_n$-**196a** each *ortho*-position had 44% of deuterium incorporation, while the product $[D]_n$-**106a** had 20% of deuterium incorporation. This clearly indicated the reversibility of the C–H activation step. The same study was performed with the optimized condition for the chemical oxidant reaction (Scheme 3.3.8,b). In this case electricity was absent and commercially available PIDA was employed as oxidant. The deuterium incorporation for both the product and the starting material was detected only in traces.

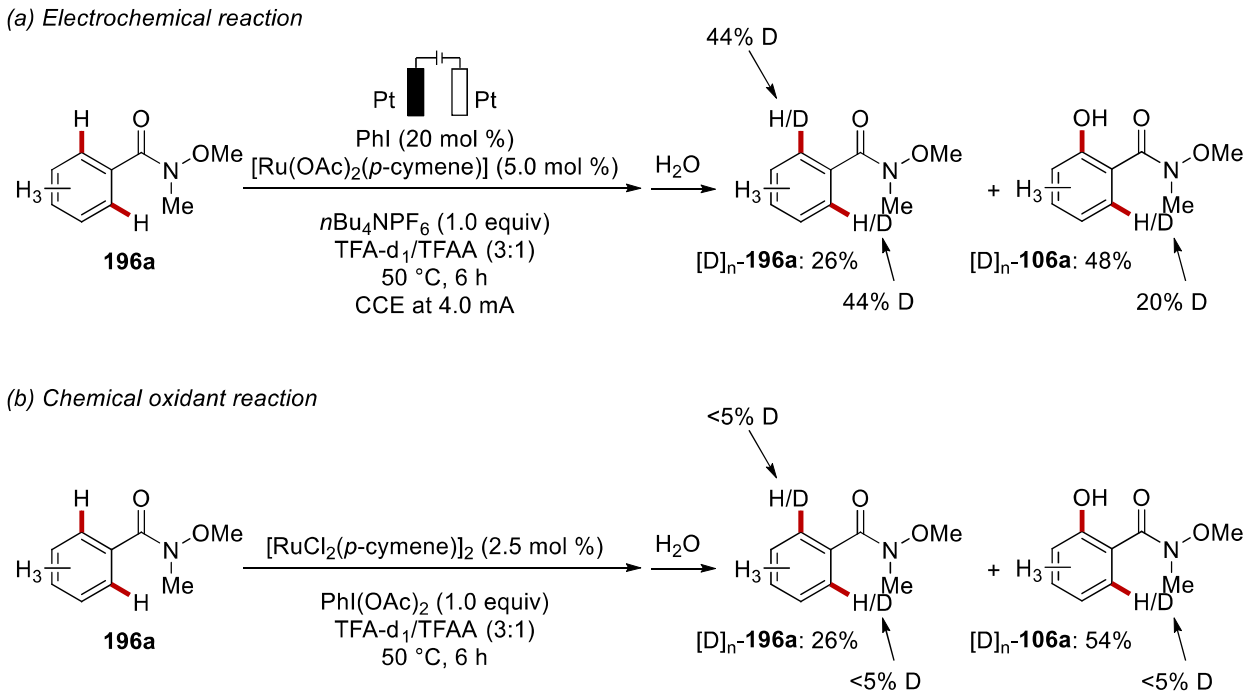

Scheme 3.3.8 H/D exchange studies for (a) the electrochemical iodine(III)/ruthenium(II)-catalyzed C–H oxygenation and (b) the ruthenium-catalyzed oxygenation with PIDA.

Afterwards, the kinetic isotope effect was evaluated (Scheme 3.3.9). The KIE was found to be $k_H/k_D \approx 1.6$, which indicated a fast C–H metalation. The comparison of this result with the KIE of $k_H/k_D \approx 3.0$ reported in the literature[112] for the chemical oxidant reaction suggests a change in the rate-

determining step between the two approaches. In the Ackermann report from 2013, the C–H activation was indeed indicated as the rate-limiting step while, in the current electrochemical study, the oxidation of the cyclometalated species seems to be the slow step. These conclusions are in good agreement with the above shown deuterium incorporation studies, delineating the electrochemical iodine(III)/ruthenium(II)-catalyzed oxygenation to have a fast and reversible C–H activation and a slow oxidation step.

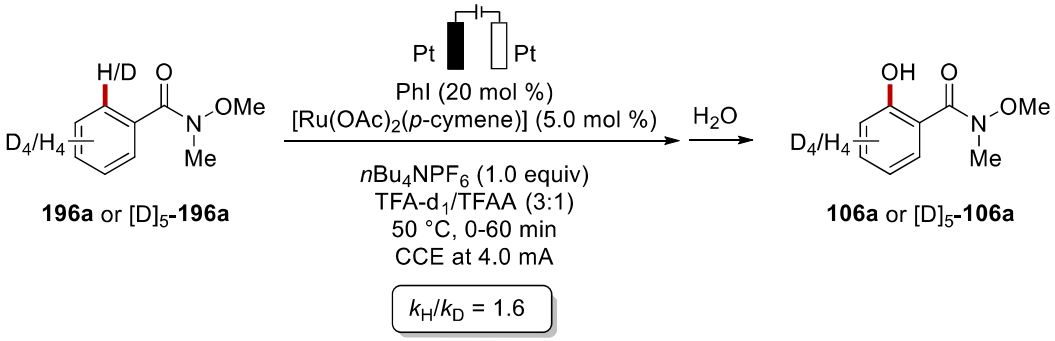

Scheme 3.3.9 KIE study for the iodine(III)/ruthenium(II)-catalyzed C–H oxygenation.

Moreover, competition experiments were performed both for Weinreb amides **196** as well as for ketones **77** (Scheme 3.3.10). In the first case, *para*-methyl and *para*-trifluoromethyl amides **196b** and **196d** were used. The product **106b** was obtained in 38% yield, while the product **106d** was only detected in traces (Scheme 3.3.10,a). As for ketones **77**, an intramolecular competition has been carried on with phenyl[4-(trifluoromethyl)phenyl]methanone (**77n**). Similarly, the more electron-rich arene was mainly functionalized (Scheme 3.3.10,b). These results are suggestive of a BIES[29, 32] for the C–H metalation.

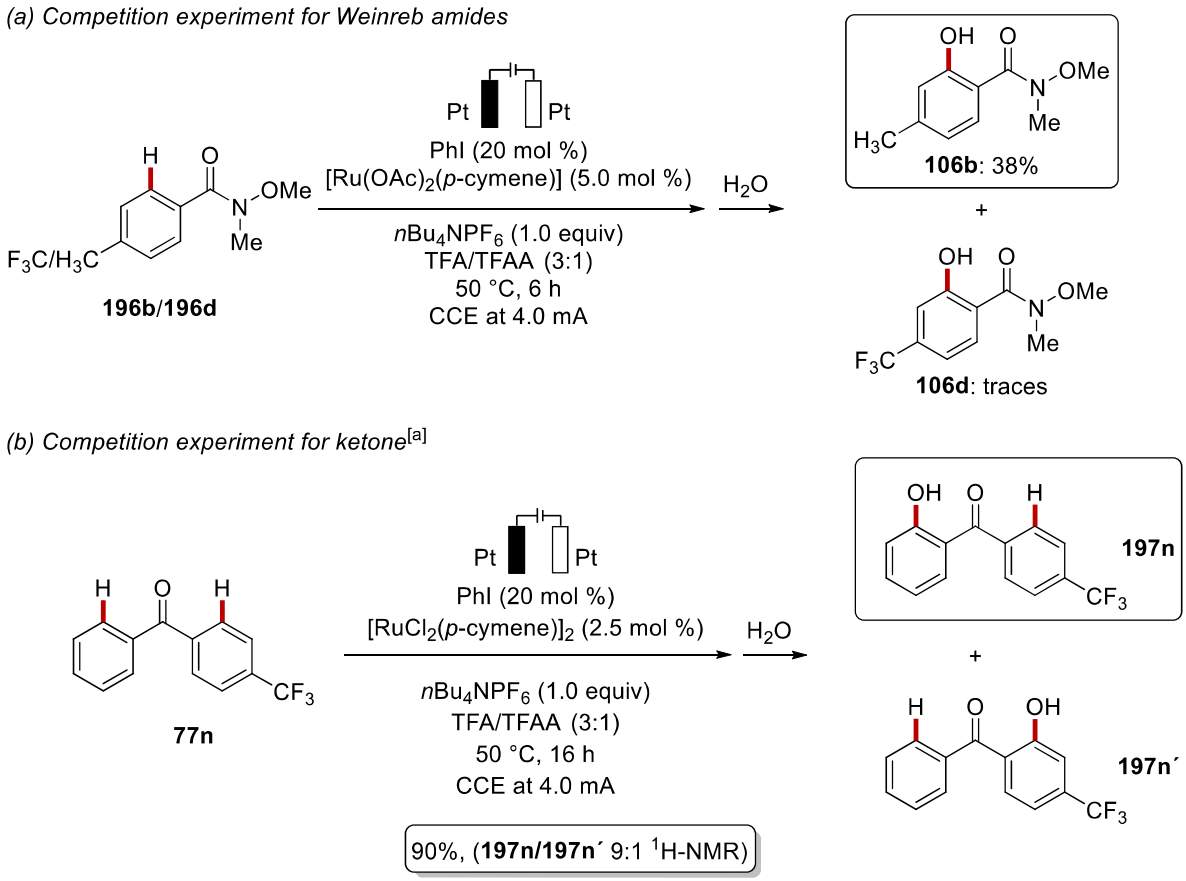

Scheme 3.3.10 Competition experiments for Weinreb amides **196** and for ketones **77**. [a] Performed by Dr. X. Tan.

An intramolecular competition between the amide and the ketone as directing groups was next designed (Scheme 3.3.11). 4-Acetyl-*N*-methoxy-*N*-methylbenzamide (**196q**) has been synthesized as the starting material. After the reaction a sole product **106q** was obtained, and it was functionalized in *ortho* to the amide group.

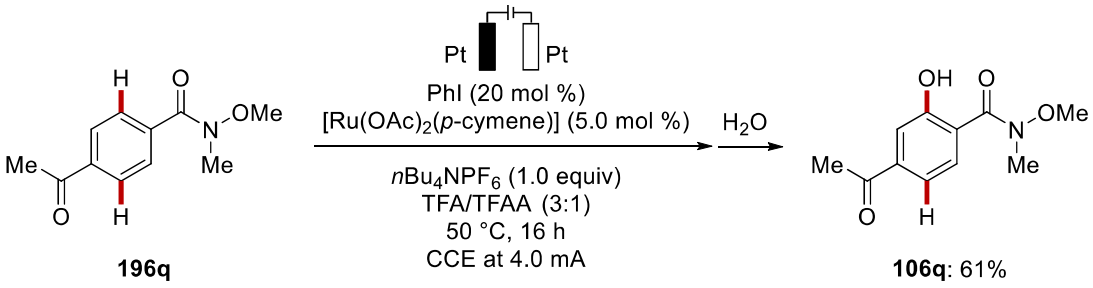

Scheme 3.3.11 Directing group comparison for the iodine(III)/ruthenium(II)-catalyzed C–H oxygenation.

In addition to these studies, we performed a gas-chromatographic headspace analysis after 16 h of reaction (Scheme 3.3.12). Herein, hydrogen gas could be detected in the Schlenk tube after completion of the electrolysis. With this insight in hand, we could assert that the other half reaction is the reduction of protons to molecular H_2.

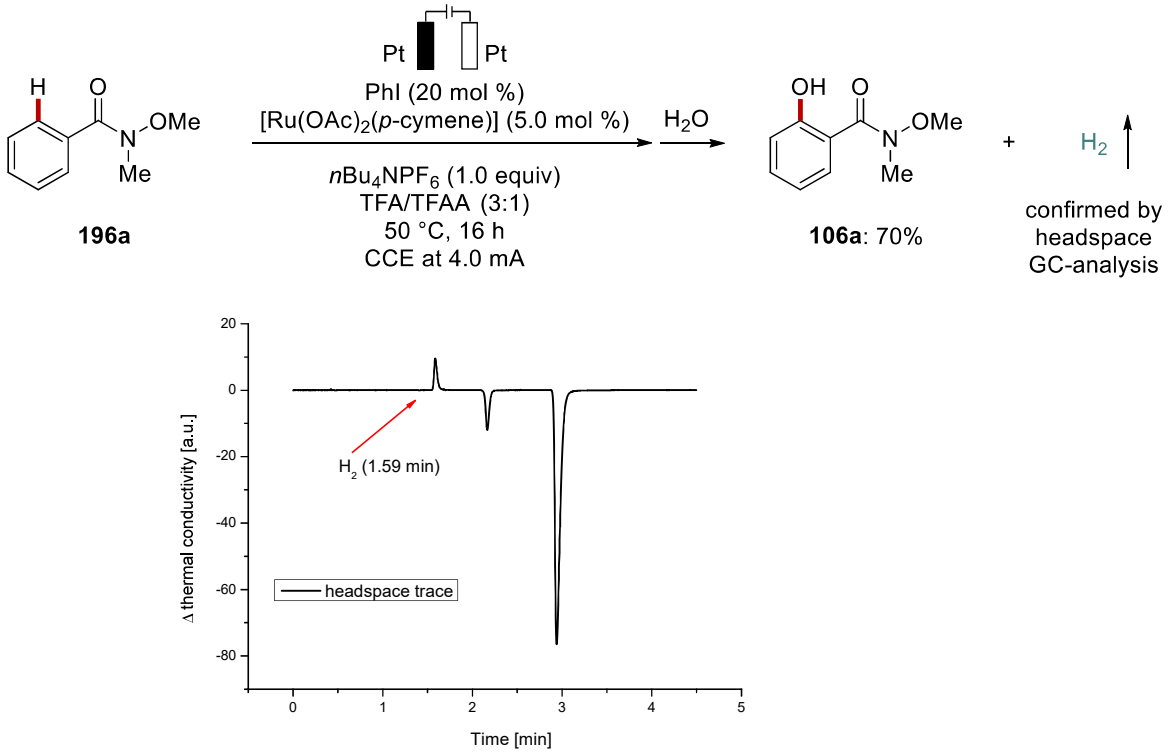

Scheme 3.3.12 Gas-chromatographic headspace analysis for the iodine(III)/ruthenium(II)-catalyzed C–H oxygenation.

Moreover, the trifluoroacetate product **201f** could be detected as intermediate in the reaction (Scheme 3.3.13, performed by Dr. X. Tan). This supported the proposed catalytic cycle (*vide infra*) where first the C–H esterification takes place and then the oxygenated product **106** is obtained *via* hydrolysis.

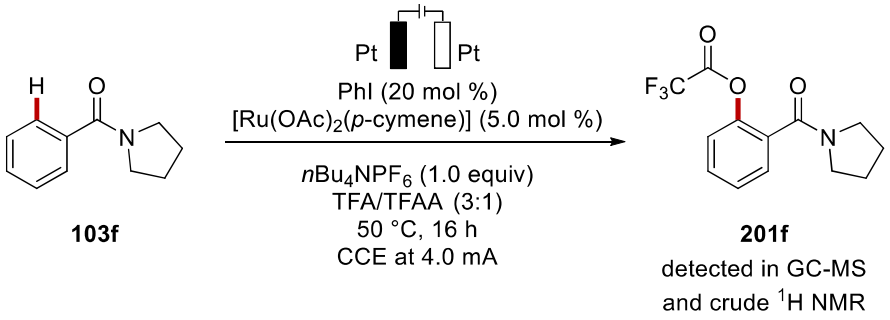

Scheme 3.3.13 Trifluoroacetate intermediate detection. Performed by Dr. X. Tan.

With the assistance of Dr. T. H. Meyer, we could obtain the kinetic profile of the reaction for the formation of the hypervalent iodine **195** *via in-operando* NMR spectroscopy (Scheme 3.3.14). By employing this approach, we could follow the formation of the rather unstable hypervalent iodine(III) species. The profile of the reaction with TFE as well as the one with the TFA/TFAA mixture used in the optimized conditions were recorded. The former profile showed almost a full conversion in only 2.5 hours at 10 mA at room temperature, while the formation of **195ca** was slightly slower under the same conditions.

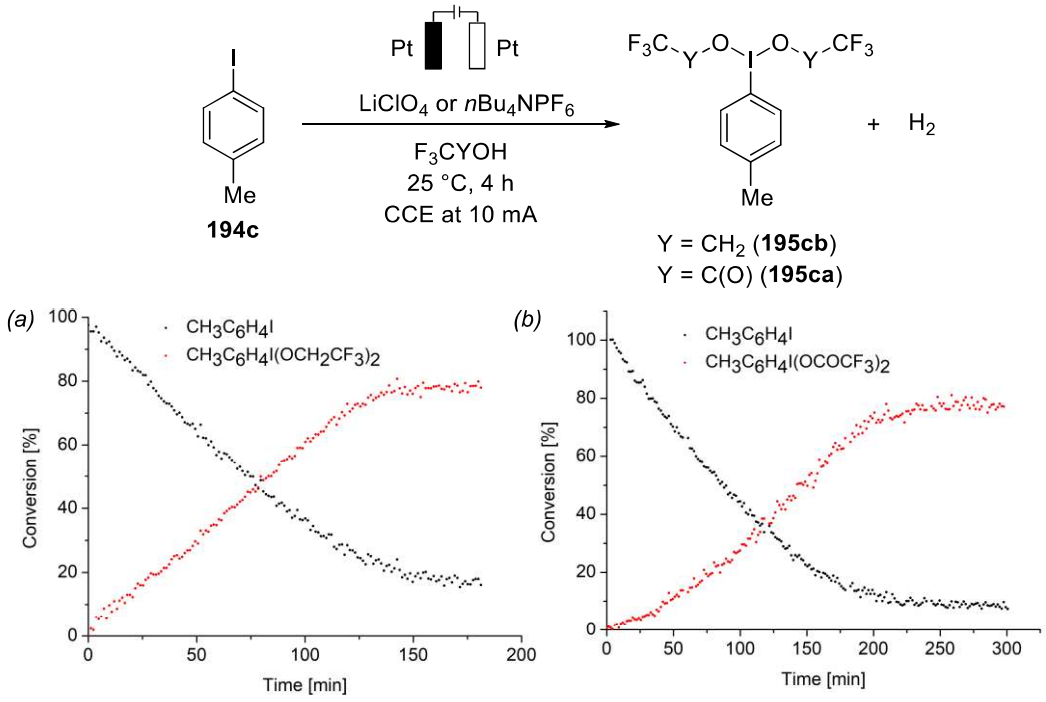

Scheme 3.3.14 *In-operando* NMR (60 MHz) studies for the formation of hypervalent iodine(III) reagents with (a) TFE or (b) TFA/TFAA (3:1). Performed with Dr. T. H. Meyer.

Dr. T. H. Meyer also performed the cyclic voltammetry studies for the envisioned reaction (Figure 3.3.15). The studies suggested that iodobenzene **194a** is oxidized before the amide **196a**. Other iodoarenes were also tested and as expected, the electron-rich 4-iodotoluene **194c** had a slightly lower oxidation potential, while methyl 4-iodobenzoate **194d** did not show a clear oxidation peak. Furthermore, DFT studies performed by Dr. R. Kuniyil, confirmed that the oxidation potential of the ruthenium(II/IV) manifold was 200 mV higher than the iodobenzene **194a**.

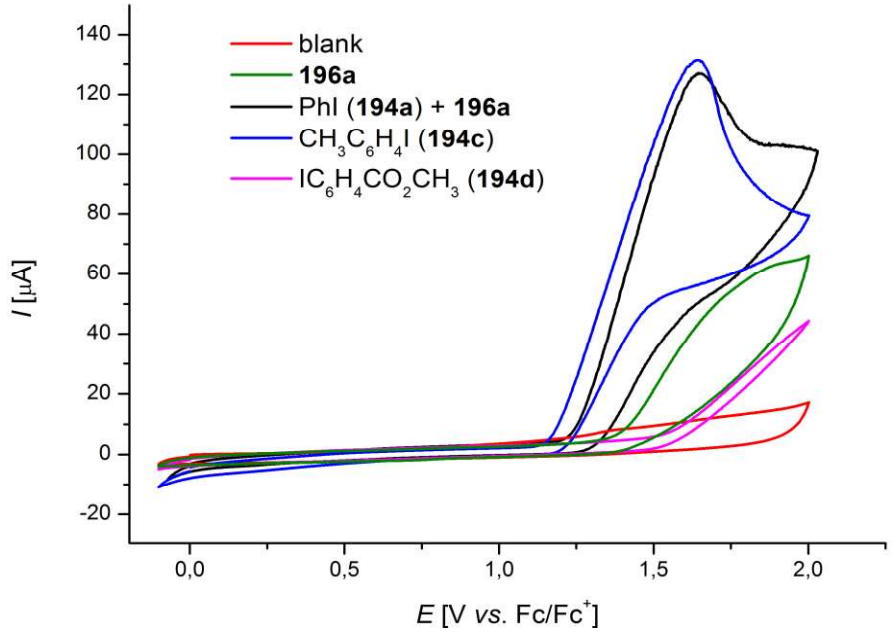

Figure 3.3.15 Selected data from the cyclic voltammograms performed by Dr. T. H. Meyer at a scan rate of 100 mVs^{-1} with TFA and nBu$_4$NPF$_6$ (0.1 M) as the electrolyte and a GC working electrode; the concentration of all substrates was 5.0 mM. (red) blank, (green) **194a**, (black) **194a** + **196a**, (blue) 4-iodotoluene **194c**, (magenta) methyl 4-iodobenzoate **194d**.

With the data from the experimental mechanistic studies, the cyclic voltammetry analysis, and the computational studies, we propose a feasible catalytic cycle (Scheme 3.3.16). The mechanism commences with the C–H activation on the amide **196** by a ruthenium(II) carboxylate species **91b**. In

the meantime, the iodobenzene **194a** is oxidize on the anode to form [bis(trifluoroacetoxy)iodo]benzene **195aa** that subsequently oxidizes the cyclometalated complex **203** to furnish a ruthenium(IV) complex **204** by group transfer. This mediated oxidation is suggested to be the rate limiting step. Subsequently, an oxidatively-induced reductive elimination yields the trifluoro ester product **201** and regenerates the active catalyst **91b**. The desired product **106** is obtained after hydrolysis. As aforementioned, the cathodic reduction forms molecular hydrogen, detectable by gas chromatography.

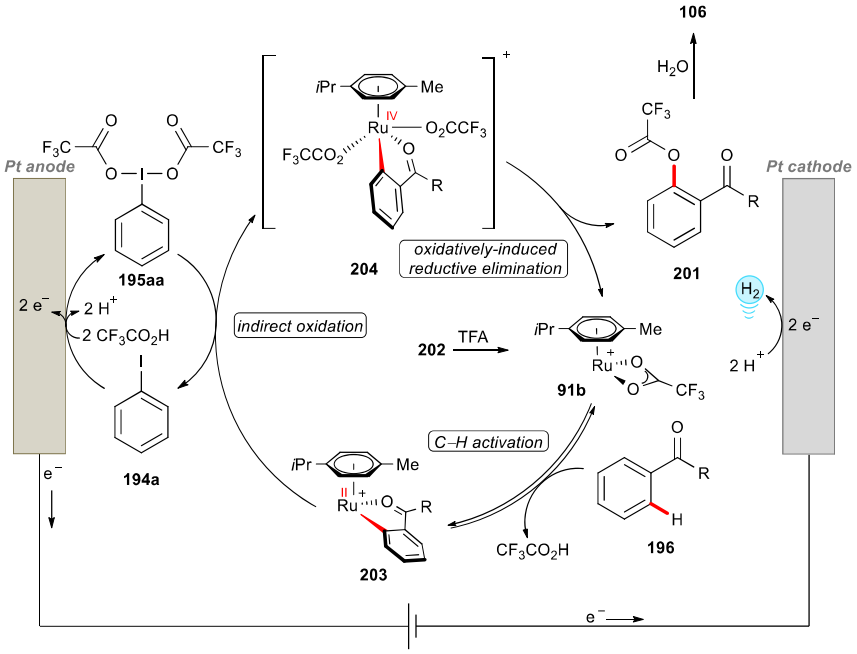

Scheme 3.3.16 Proposed catalytic cycle.

3.4 Rhoda-Electrocatalyzed Bimetallic C–H Oxygenation by Weak *O*-Coordination

Rhodium was discovered to be a suitable and versatile metal for electrochemical transformations and many reports have recently been published.[171]

3.4.1 Optimization

The optimization of the rhoda-electrocatalyzed C–H oxygenation started with the screening of typical supporting electrolytes (Table 3.4.1). Sodium trifluoroacetate did not yield the desired product **106a**, while tetrabutylammonium hexafluorophosphate gave the best result (entries 1–4). Changing the ratio of TFA/TFAA from 3:1 to 1:1 increased the yield, as well as running the reaction at room temperature did (entries 5–6). The influence of different amounts of trifluoroacetic anhydride was then explored. A 1:2 solvent mixture gave a similar result as with a 1:1 ratio, while increasing ratio to 1:3 TFA/TFAA furnished only traces of the desired product **106a** (entries 7–8). The poor solubility, hence, the poor conductivity, of the electrolyte were deemed responsible for the failure of this reaction. At this point, test reactions were performed, showing that the reaction did not work in the absence of electricity or the catalyst, while running the so-far optimized conditions under nitrogen gave the same result (entries 9–11). To resolve the solubility issue, we devised a different electrolyte. The liquid and easily available TFA·NEt_3 salt was used as electrolyte, allowing us to increase the amount of TFAA in the solvent mixture. Thus, with a 1:20 TFA/TFAA mixture and TFA·NEt_3 as the electrolyte, the highest yield was obtained with a CCE of 2.0 mA, furnishing 82% isolated yield of the desired product **106a** (entries12–13). Importantly, other catalyst did not prove more efficient (entries 14–16).

Table 3.4.1 Optimization of the electrochemical rhodium-catalyzed C–H oxygenation.[a]

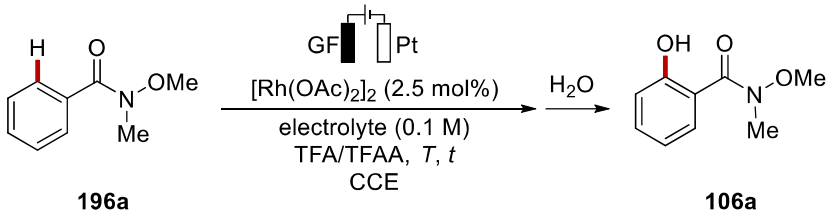

196a **106a**

Entry	Electrolyte	TFA/TFAA	I (mA)	t (h)	T (°C)	Yield (%)
1	NaO_2CCF_3	3:1	4	16	50	trace[b]
2	$LiClO_4$	3:1	4	16	50	24[b]
3	nBu$_4$NBF$_4$	3:1	4	16	50	22[b]
4	nBu$_4$NPF$_6$	3:1	4	16	50	28[b]
5	nBu$_4$NPF$_6$	1:1	4	16	50	42[b]
6	nBu$_4$NPF$_6$	1:1	4	16	RT	54[b]
7	nBu$_4$NPF$_6$	1:2	4	16	RT	52
8	nBu$_4$NPF$_6$	1:3	4	16	RT	trace[c]
9	nBu$_4$NPF$_6$	1:1	-	16	RT	ND
10	nBu$_4$NPF$_6$	1:1	4	16	RT	trace[d]
11	nBu$_4$NPF$_6$	1:1	4	16	RT	57[b,e]
12	TFA·NEt$_3$	1:20	4	8	RT	76[b,e,f]
13	**TFA·NEt$_3$**	**1:20**	**2**	**15**	**RT**	**82[b,e,f]**
14	TFA·NEt$_3$	1:20	2	15	RT	ND[f,g]
15	nBu$_4$NPF$_6$	3:1	4	16	50	28[h]
16	TFA·NEt$_3$	1:20	2	15	RT	52[f,i]

[a] Reaction conditions: **196a** (0.50 mmol), $[Rh(OAc)_2]_2$ (2.5 mol %), electrolyte (0.10 M), TFA/TFAA (3 mL), graphite felt (GF) anode (10 mm × 10 mm × 6 mm), Pt-plate cathode (10 mm × 15 mm × 0.125 mm), CCE as specified. [b] Performed by Dr. X. Tan. [c] Poor conductivity due to poor solubility of electrolyte. [d] Without $[Rh(OAc)_2]_2$. [e] Under N_2. [f] TFA·NEt$_3$ (0.33 M). [g] $[RhCp^*Cl_2]_2$ or $RhCl_3{\cdot}3H_2O$ instead of $[Rh(OAc)_2]_2$ as the catalyst. [h] $[Ru(OAc)_2(p\text{-cymene})]$ **188a** (5.0 mol %) as the catalyst. [i] $[Rh(OPiv)_2]_2$ as the catalyst. Piv = pivalate.

3.4.2 Substrate Scope

Once the system was optimized, its versatility was tested with a broad substrate range, which was performed together with Dr. X. Tan. We started the investigation with Weinreb amides **196** (Scheme 3.4.1). Electron-rich substituents in the *para*-position were nicely tolerated and also electron-poor ones gave excellent results (**106b-q**). Among these are some notable examples. The *para*-methoxy group, that was not tolerated for the mediated ruthenium electrochemical oxygenation, gave 50% isolated yield of product **106r**. Halogen substituents were very efficiently converted to the desired products (**106g-i**,**o**), and both ester (**196u**) and ketone (**196q**) moieties on the arene were feasible and

each yielded a sole product, since the amide was a better directing group. The substrates with electron-rich *meta*-substituents performed slightly less efficiently in rhodium catalysis compared to the ruthenium catalysis, giving between 3% and 7% of the minor regioisomer for products **106j**, **106v**, and **106e**. The minor product was present only for electron-rich substrates, probably due to their high reactivity (*vide infra*). However, electron-deficient groups in the *meta*-position yielded only one regioisomer at the least hindered position (**106m-n**,**f**).

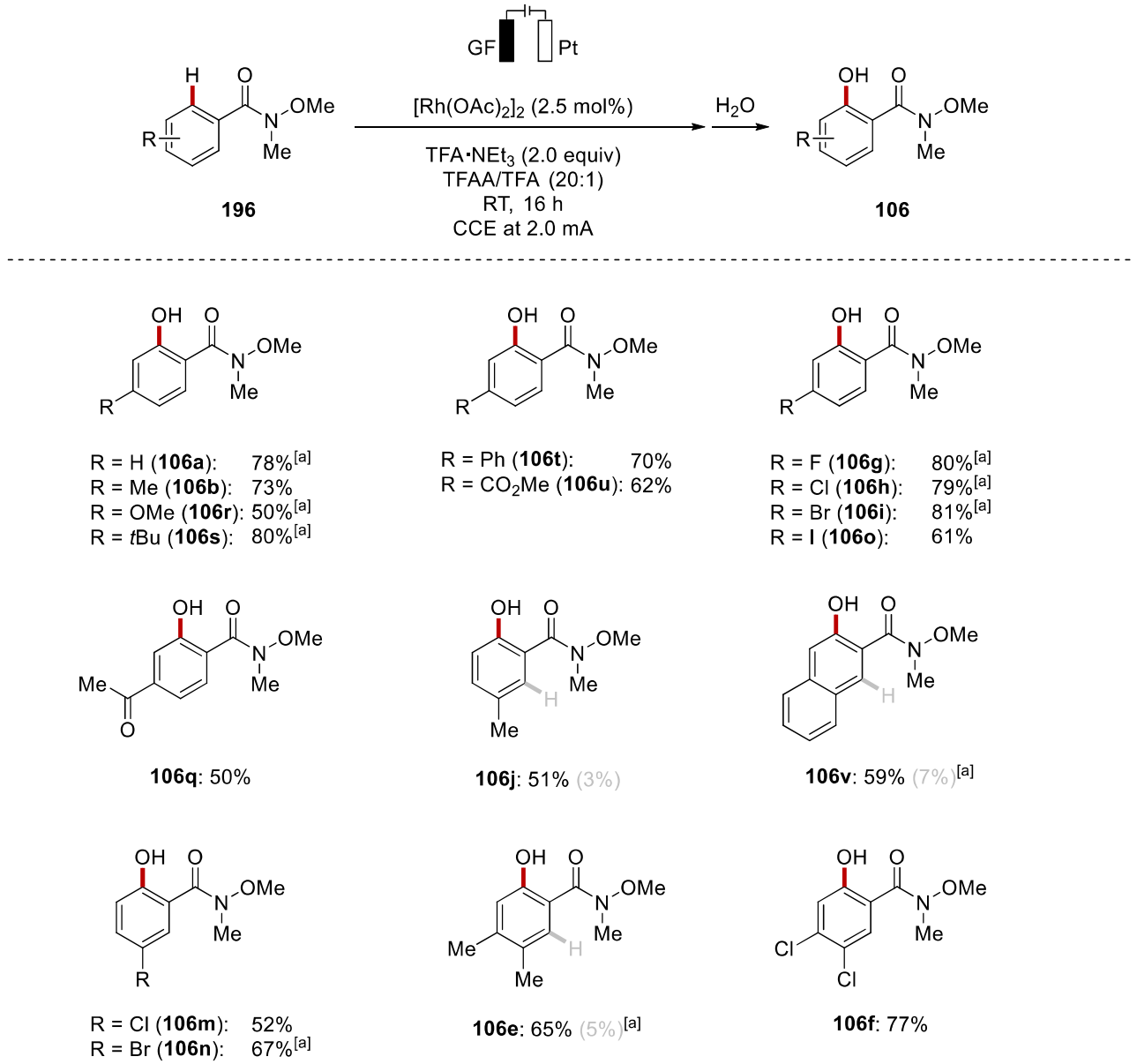

Scheme 3.4.1 Scope of electrochemical rhodium-catalyzed C–H oxygenation of Weinreb amides **196**.

[a] Performed by Dr. X. Tan.

The broad applicability of the approach enabled C–H oxygenations on tertiary amides **103** (Scheme 3.4.2). For this part of the scope and the following one, also MSc X. Hou joined the project. The reaction proved very robust on dimethyl amides. Since the *para*-methyl-substituted substrate underwent the reaction with an excellent yield, it was then tried with lower amounts of the catalyst. Product **104b** could be obtained in high yields with just 1.0 mol % or 0.5 mol % loading of the rhodium dimer. Other substituents in the *para*-position, as methoxy (**103h**), chloro (**103i**), bromo (**103c**), and trifluoromethyl (**103j**), furnished high yields of the desired products. An electron-rich substituent in the *meta*-position showed again the formation of 5% of the minor regioisomer (**104k**), while with a halogen in that position products **104l** and **104n** were obtained selectively. Other tertiary amides, like diethyl and diisopropyl amides **103m** and **103e**, were efficiently converted, as well as morpholino(phenyl)methanone (**103g**) and phenyl(pyrrolidin-1-yl)methanone (**103f**), which gave excellent results.

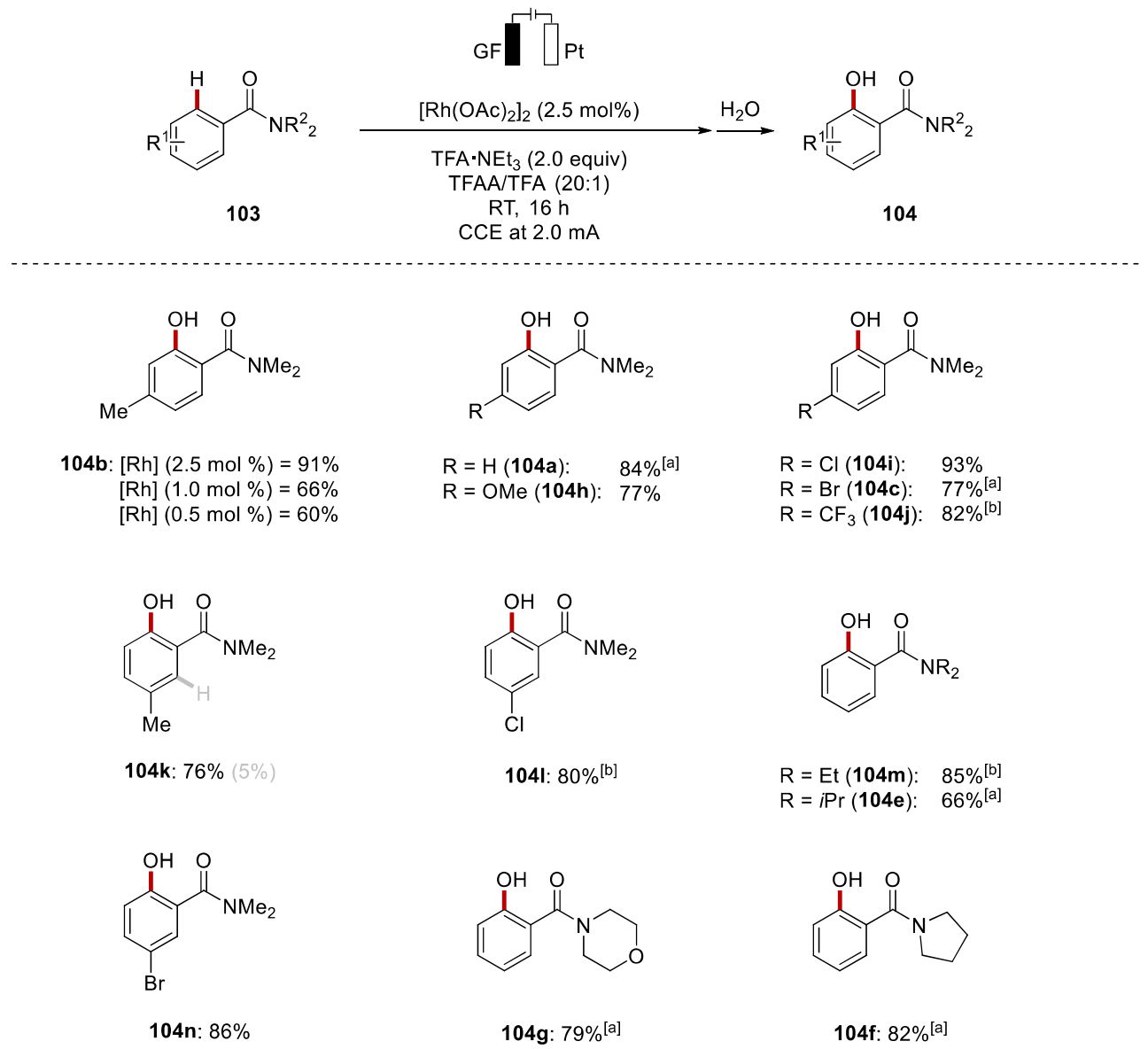

Scheme 3.4.2 Scope of the electrochemical rhodium-catalyzed C–H oxygenation of various amides **103**. [a] Performed by Dr. X. Tan. [b] Performed by MSc X. Hou.

The rhodium-catalyzed electrochemical C–H oxygenation was likewise viable on ketones **77** (Scheme 3.4.3). Acetophenone (**77c**) gave product **197c** in good yield. In the presence of 4-methyl or 4-chloro substituents the expected products **197n** and **197o** were also obtained in good yields. Propiophenone (**77b**) and phenyl *tert*-butyl ketone (**77a**) were likewise tolerated by the envisioned reaction.

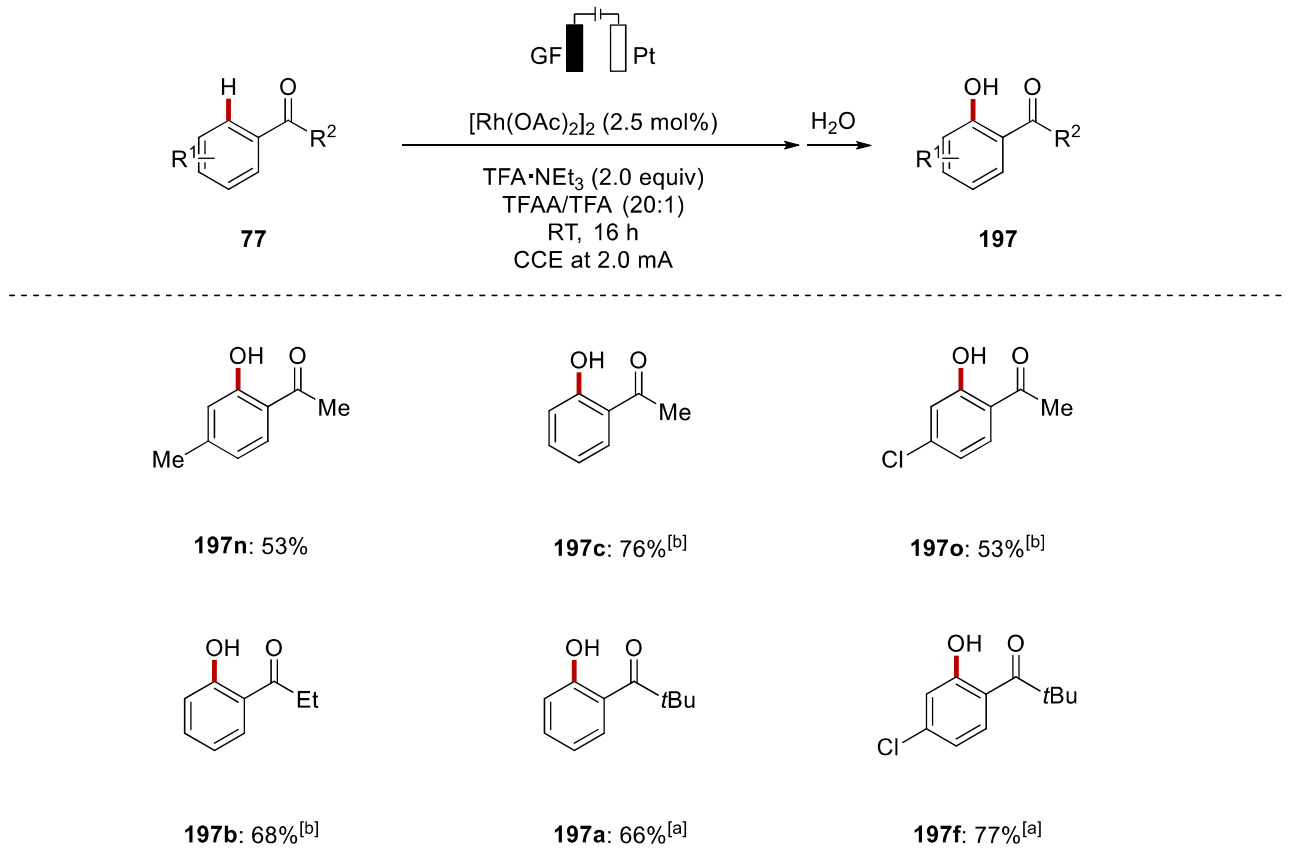

Scheme 3.4.3 Scope of the electrochemical rhodium-catalyzed C–H oxygenation of various ketones **77**. [a] Performed by Dr. X. Tan. [b] Performed by MSc X. Hou.

During the optimization studies, we sometimes encountered small amounts of *N*-demethylated product **206a** (Scheme 3.4.4). This finding was further investigated, and we proposed that the formation occurs due to a Shono-type C–H oxidation. Tuning the conditions, Dr. X. Tan could take advantage of this alternative path to access dihydrooxazinones **207**.

(a) Strategy of rhoda-electrocatalyzed cascade for the synthesis of dihydrooxazinone

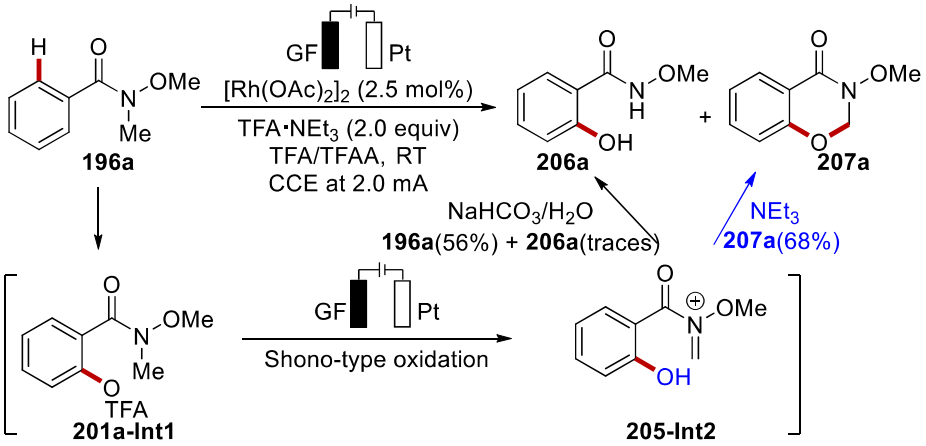

(b) Substrate scope for rhoda-electrocatalyzed double C–H functionalization

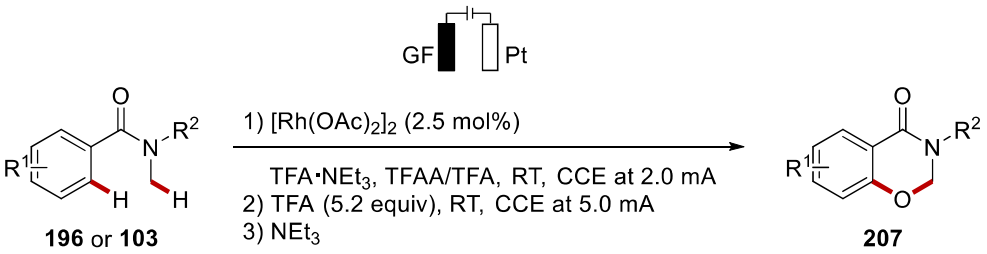

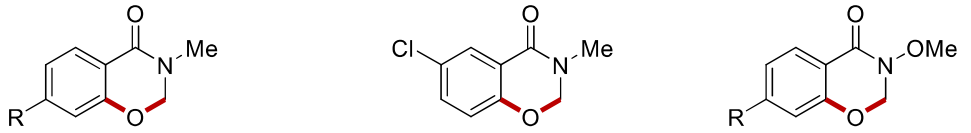

R = H (**206b**): 62%
R = OMe (**206c**): 62%

206d: 61%

R = Br (**206e**): 67%
R = *t*Bu (**206f**): 55%

Scheme 3.4.4 (a) Strategy for the cascade synthesis of dihydrooxazinone **207** and (b) selected example from the scope performed by Dr. X. Tan.

3.4.3 Mechanistic Studies

Subsequently, we focused on the mechanistic studies to better understand the process and to shine light on the possible catalytic pathway. First, a competition experiment showed a preferential reactivity of the electron-rich substrate **196b** compared to the electron-poor one **196d** (Scheme 3.4.5).

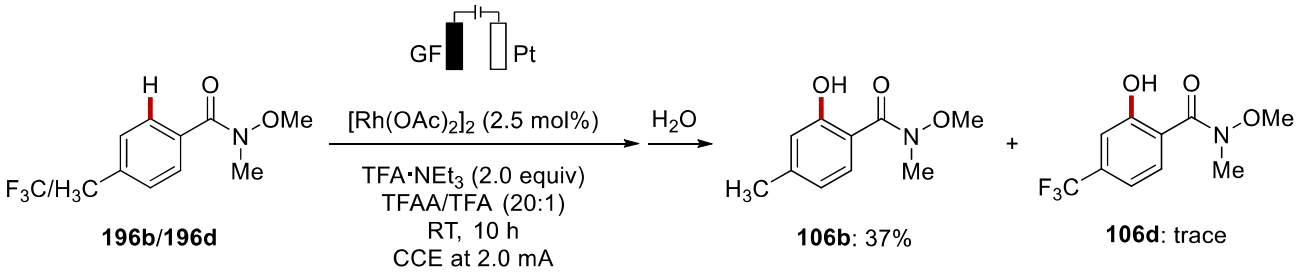

Scheme 3.4.5 Competition experiment for the electrochemical rhodium-catalyzed C–H oxygenation.

Furthermore, when the reaction was performed in the presence of deuterated trifluoroacetic acid, the deuterium incorporation was only detected in traces in both the starting material **196a** and the product **106a** (Scheme 3.4.6,a). This would suggest that the C–H metalation happens irreversibly. At the same time, the kinetic isotope effect was found to be $k_H/k_D \approx 1.1$, indicating that the C–H activation is not the rate-limiting step (Scheme 3.4.6,b). Moreover, the profile of the reaction at different constant current electrolyses showed a clear dependence of the rate of the reaction on the applied current (Scheme 3.4.6,c). The data thus implied that the oxidation is the rate-determining step, as it was for the iodo(III)/ruthenium(II) electrochemical oxygenation.

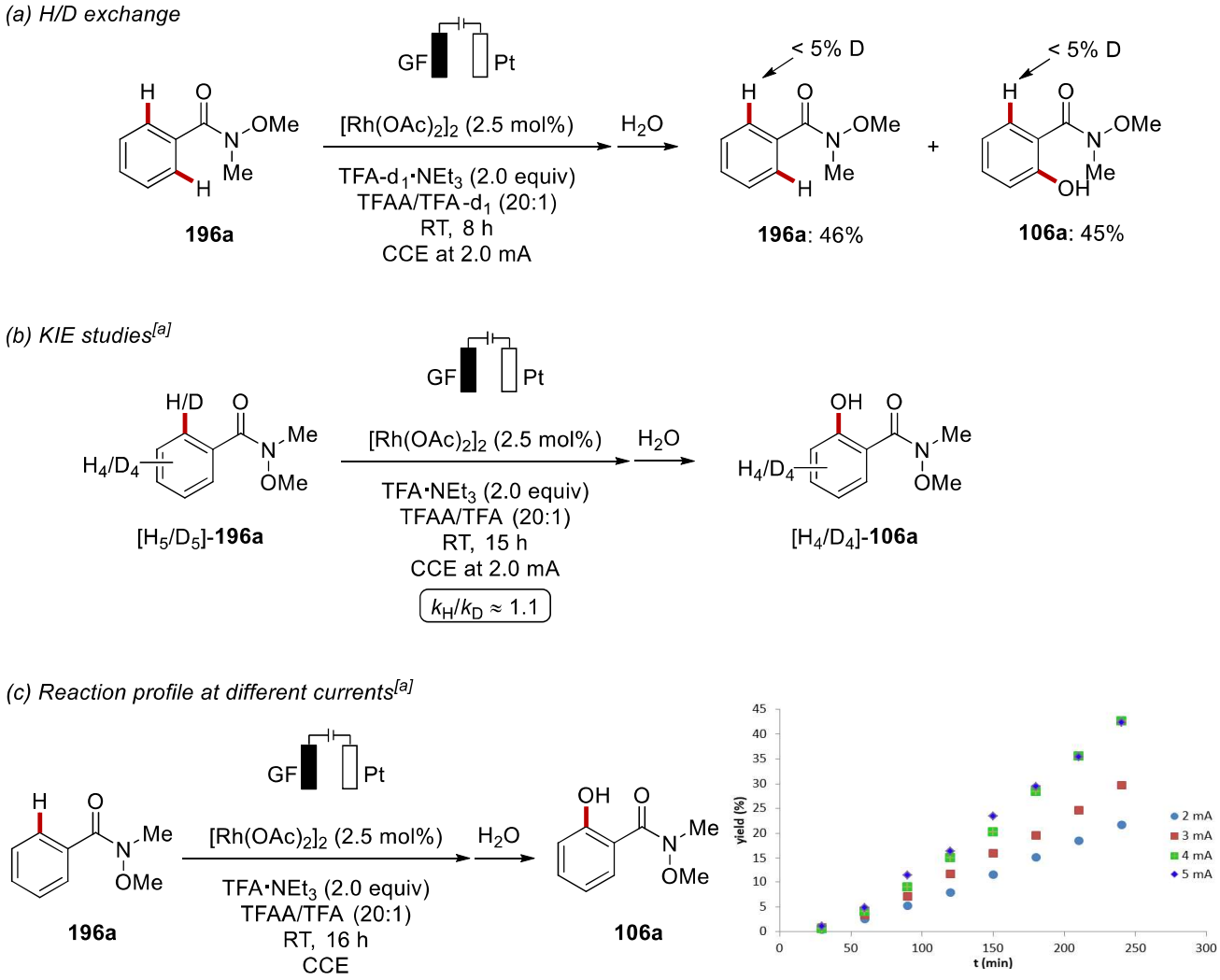

Scheme 3.4.6 (a) H/D exchange experiment, (b) KIE studies, and (c) reaction profile at different currents for the electrochemical rhodium-catalyzed C–H oxygenation. [a] Performed by Dr. X. Tan.

The reaction was studied with different catalysts to understand which kind of influence the ligands can have and, therefore, if ligand exchange with trifluoroacetic acid happens in the reaction conditions (Scheme 3.4.7,a). For this purpose, $[Rh(OTFA)_2]_2$ and $[Rh(OPiv)_2]_2$ were tested as the catalysts. The former furnished the desired product only in trace amounts, while the latter yielded 52% of **106a**. The absence of reactivity for $[Rh(OTFA)_2]_2$ could be explained by its higher oxidation potential that makes this catalyst less efficient. This has been shown by cyclic voltammetry studies conducted by M. N. Hussain, were the oxidation potential of $[Rh(OTFA)_2]_2$ was found to be 0.5 V *vs.* Ag/AgCl higher than the acetate catalyst (Figure 3.4.1). Additionally, mass spectroscopic analyses of

$[Rh(OAc)_2]_2$ in TFA/TFAA 1:1 and TFA/TFAA 1:20 solvent mixtures, conducted by Dr. X. Tan, showed a fast ligand exchange between acetate and trifluoroacetate for the catalyst in the 1:1 mixture, while a slow one was observed in the 1:20 mixture. As presented in the optimization table (Table 3.4.1, entry 6), a solvent mixture with equal parts of the trifluoroacetic acid and anhydride lowered the reaction yield. The effect of the solvent could be clearly observed also by the same cyclic voltammetry study discussed above, where the rhodium acetate dimer had a higher oxidation potential when recorded in a 1:1 mixture of TFA/TFAA. The oxidation potential also increased over time due to the increment in the ligand exchange (Figure 3.4.1). Regarding the more electron rich catalyst $[Rh(OPiv)_2]_2$, a higher reactivity than $[Rh(OAc)_2]_2$ would be expected, but instead only 52% of the desired product **106a** was obtained. This was rationalized by the fact that the catalyst is more prone to be oxidized. However, the corresponding complex could also have a lower oxidation ability to drive a fast oxidative induced C–H activation. Indeed, the reaction rate comparison between $[Rh(OAc)_2]_2$ and $[Rh(OPiv)_2]_2$ showed clearly slower kinetics for the latter (Scheme 3.4.7,b).

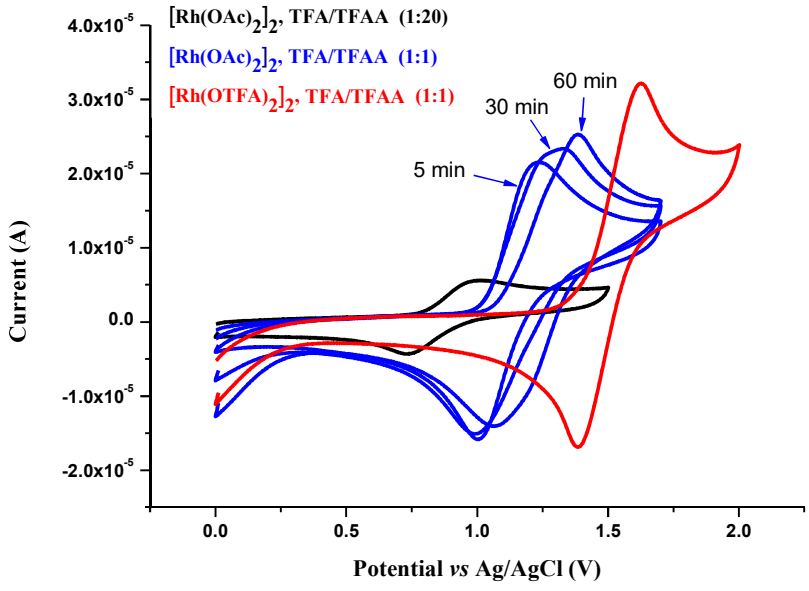

Figure 3.4.1 Cyclic voltammetry measurements with GC working electrode in TFA/TFAA with 0.15 M TFA·NEt_3 and 5.0 mM rhodium catalyst at RT with a scan rate of 100 mVs^{-1}: black, $[Rh(OAc)_2]_2$ in TFA/TFAA (1:20), stirred 10 min, poor solubility; blue, $[Rh(OAc)_2]_2$ in TFA/TFAA (1:1), measured at stirring 5, 30 and 60 min; red, $[Rh(OTFA)_2]_2$ in TFA/TFAA (1:1).

(a) Reactions with different catalysts

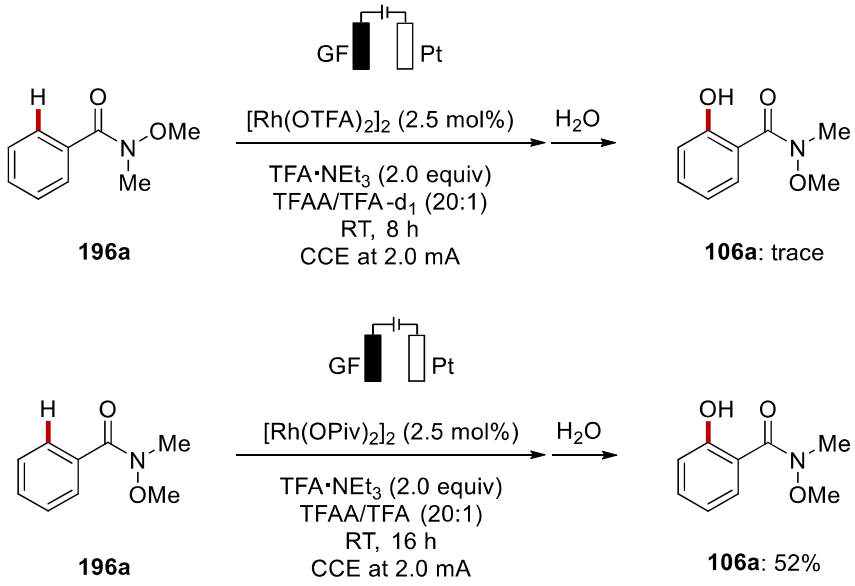

(b) Reactions profiles with different catalysts

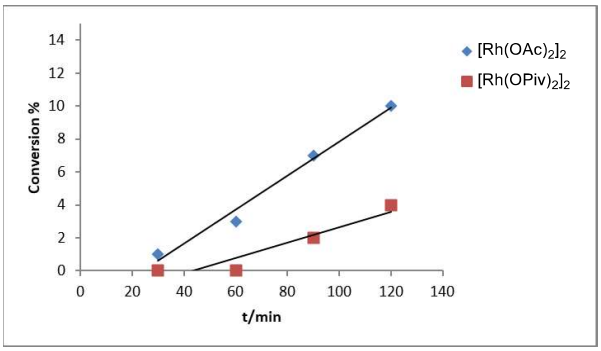

Scheme 3.4.7 (a) Reactions with $[Rh(OTFA)_2]_2$ and $[Rh(OPiv)_2]_2$ and (b) relative initial rate profile with $[Rh(OAc)_2]_2$ and $[Rh(OPiv)_2]_2$ for the electrochemical rhodium-catalyzed C–H oxygenation.

Since the peaks in the mass spectroscopy were ascribable to bimetallic complexes, we started to wonder if a bimetallic rhodium/rhodium species could be the active catalyst in the oxygenation reaction. To have some insights, Dr. X. Tan tried the reaction with stoichiometric amounts of $Rh(OAc)_3$ without electricity, and no reaction was obtained. Moreover, a mass spectrometric analysis performed after electrolysis of the sole catalyst showed that $[Rh(OAc)_2(OTFA)_2]_2$ could be a plausible intermediate. At this point, if bimetallic species were involved, the possibilities are that we are in presence of a rhodium(III)/rhodium(III) monocationic or dicationic species, or a rhodium(II)/rhodium(III) monocationic species. To clarify the situation, Dr. J. C. A. Oliveira

performed DFT calculations on the C–H activation step, which showed that the most plausible pathway was through a bimetallic rhodium Rh(III)-Rh(III) dicationic species with a barrier of 25.1 kcal mol^{-1} for the C–H activation step (Figure 3.4.2). The calculated barrier for the C–H activation elementary step for both the other bimetallic complexes in this study was significantly higher, at approximately 29 kcal mol^{-1}.

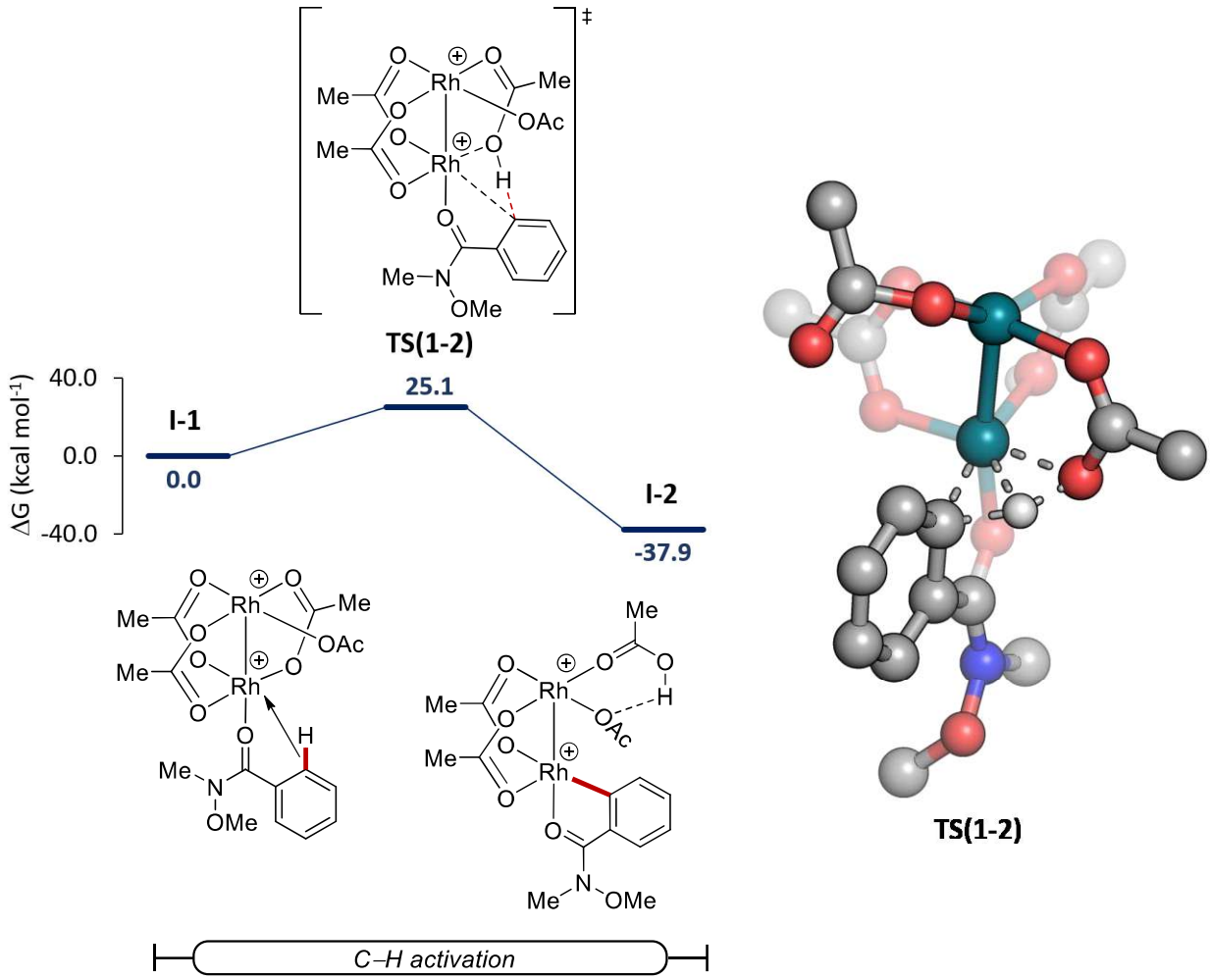

Figure 3.4.2 Calculated relative Gibbs free energies ($\Delta G_{298.15}$) in kcal mol^{-1} for the C–H activation elementary step at the B3LYP-D4/6-311++G**,Rh/SDD+SMD(DCE)//B3LYP-D3BJ/6-31G**,Rh/SDD level of theory for a dicationic Rh(III)-Rh(III) complex. In the computed transition state structure, non-relevant hydrogens are omitted for clarity. Performed by Dr. J. C. A. Oliveira.

To further prove our hypothesis, additional cyclic voltammetry studies were conducted by M. N. Hussain, showing no differences in the oxidation potential of the catalyst, neither alone nor in the

presence of the substrate **196a** (Figure 3.4.3,a). This could suggest that the catalyst did not interact with the substrate prior to its oxidation. To prove this, Dr. X. Tan performed a stepwise reaction, firstly oxidizing the catalyst and, once the current was turned off, adding the substrate to perform the C–H activation (Scheme 3.4.3,b). The product formation proved an oxidatively-induced C–H activation and oxygenation.

(a) Cyclic Voltammetry

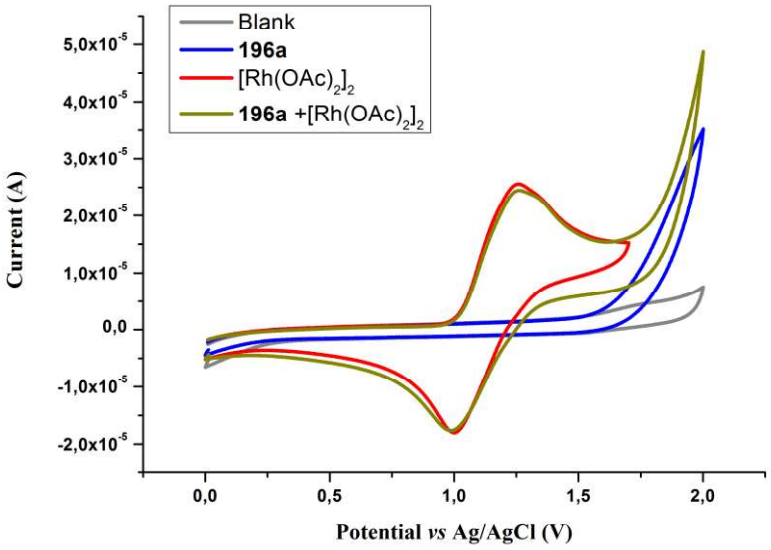

(b) Stepwise oxidation/oxygenation

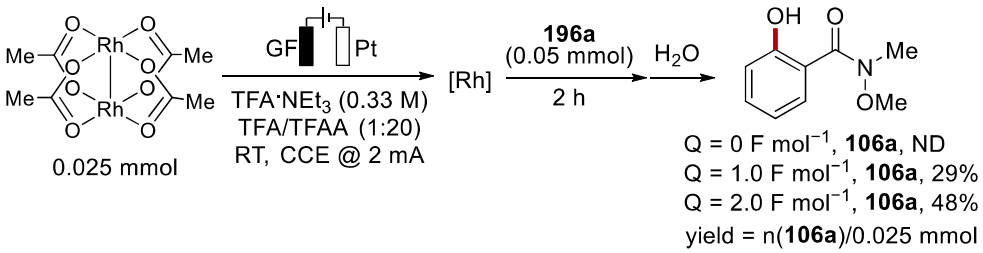

Figure 3.4.3 (a) Cyclic voltammetry measurements with GC working electrode in TFA/TFAA (1:1) with 0.15 M TFA·NEt_3 at r.t. with a scan rate of 100 mVs^{-1}; concentrations of substrates were 5.0 mM; (b) stepwise oxidation experiment.

Lastly, the trifluoroacetate ester **201** that should form prior to the hydrolysis at the end of the reaction, was detected by GC-MS for substrate **103f** (Scheme 3.4.8), as similarly performed in the previous

project (*vide supra*). The ester is very susceptible to hydrolysis, so further purification and isolation were not possible.

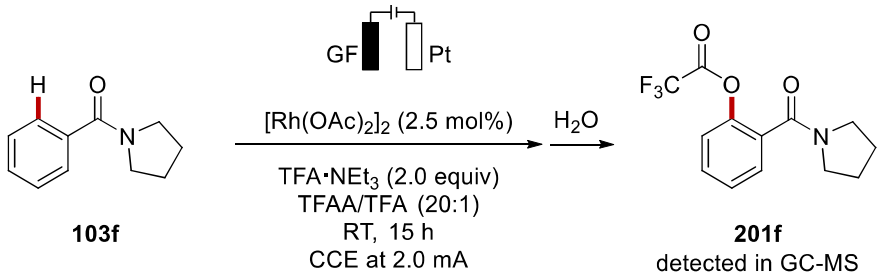

Scheme 3.4.8 Detection of the trifluoroacetate intermediate.

With the data obtained from experiments, mass spectroscopy, cyclic voltammetry, and computation, we could propose a plausible catalytic cycle for the envisioned rhodium oxygenation reaction (Scheme 3.4.9). The mechanism commences with the oxidation of the rhodium acetate dimer to generate a monocationic rhodium(III)/rhodium(II) species **208**. A subsequent oxidation drives to what the DFT calculations proposed to be the active catalyst, the dicationic rhodium(III)/rhodium(III) species **209**. Hence, after coordination of the substrate, the facile, but irreversible, C–H activation takes place. Finally, a reductive elimination yields the trifluoroacetate ester **201** of the desired product **106**, which is then obtained by aqueous workup. At the same time, anodic oxidation regenerates the catalyst **209**.

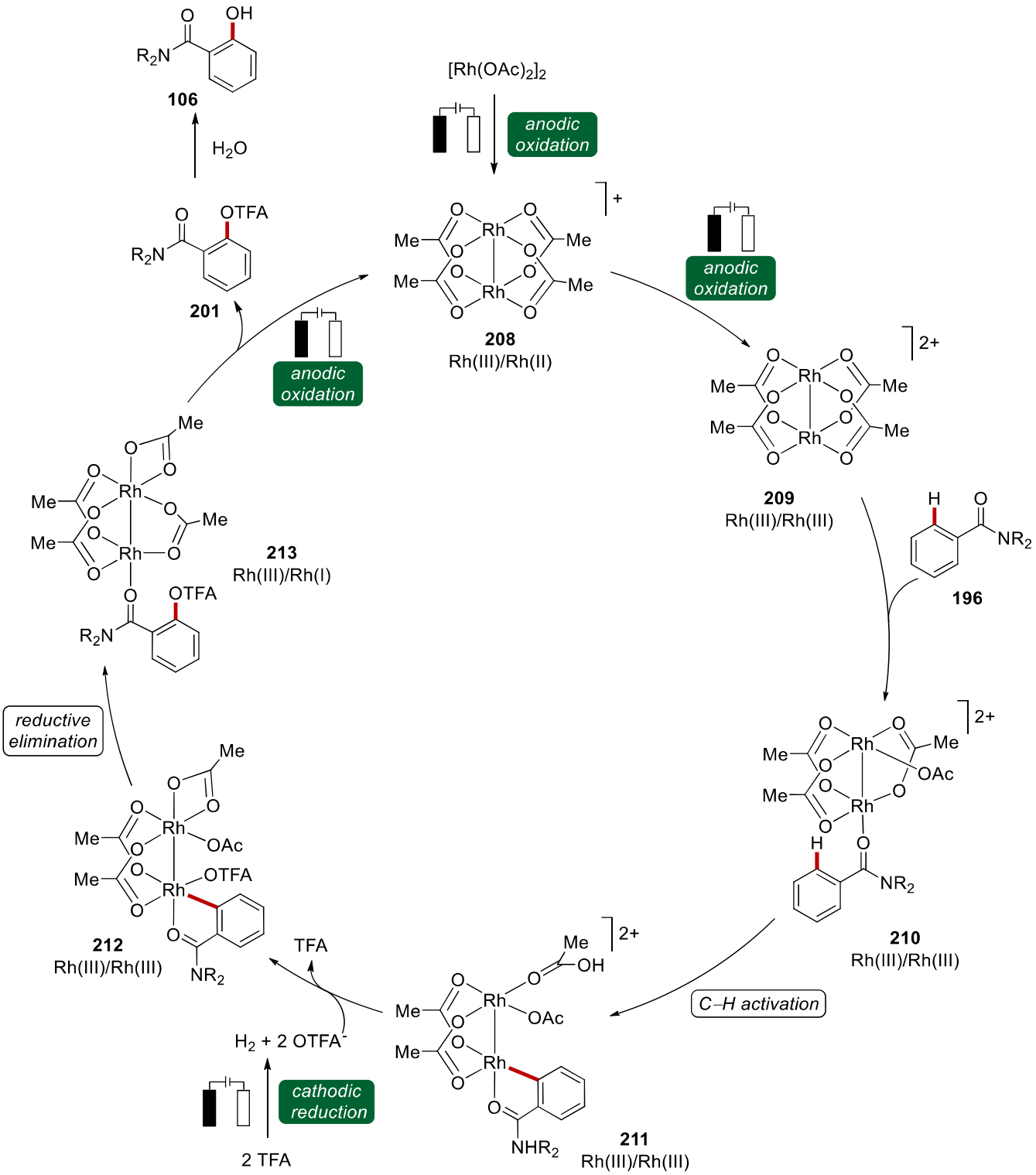

Scheme 3.4.9 Plausible catalytic cycle for the electrochemical rhodium-catalyzed C–H oxygenation.

3.5 Manganaelectro-Catalyzed Azine C–H Arylations and C–H Alkylations by Assistance of Weakly-Coordinating Amides

Electrochemical manganese-catalyzed C–H activation is underdeveloped and represented a challenge that we wanted to address. Indeed, besides the electrochemical olefin functionalizations[156-157] and azidation reactions,[158, 159] no reports on electrochemical manganese-catalyzed C–H activation were published, to the best of my knowledge. Due to our experience in low-valent manganese-catalysis[151, 153-154] and our accomplishment in electrochemical low-valent iron catalysis,[48f] we planned to develop an electrochemical approach for the low-valent mangasese catalysis.

3.5.1 Optimization

At the outset of the project, our goal was to use a weakly coordinating mono-dentate amide in order to more easily access electrochemical C–H arylations. The optimization was carried out together with Dr. C. Zhu. For this purpose, benzamide **172a** was employed under the optimized reaction conditions of an earlier former project on iron-electro-catalyzed C–H arylations of TAM-benzamides (Table 3.5.1).[48f] The first attempt was unsuccessful and a modification of the conditions with the use of different ligands, namely dppe, neocuproine, or 1,10 phenantroline, of different currents (3.0 or 5.0 mA), of $FeCl_3$ instead of $Fe(acac)_3$, or of different temperatures, did not provide any breakthrough (entries 1–7). At the same time, Dr. C. Zhu studied the reaction with different catalysts. Nickel, ruthenium, and palladium fell short in providing the desired product **176aa** (entries 8–10). Only manganese was efficiently delivering the arylated benzamide in a discrete manner and the testing of different ligands, such as 2,2'-dipyridyl, 1,10-phenantroline, and neocuproine, revealed neocuproine to be the best one, giving 70% of the isolated desired product **176aa** (entries 11–14). Manganese(I)pentacarbonyl bromide, manganese(II) acetate, and manganese(II) acetylacetonate were tested with a good outcome for each catalyst, but not as good as the inexpensive manganese(II) chloride (entries 15–17). To improve the efficiency of the electrocatalysis system, we tried supporting electrolytes, such as tetrabutylammonium hexafluorophosphate or lithium perchlorate, but these were not beneficial for the reaction (entries 18–19). Control experiments were performed to probe the essential role of the catalyst, TMEDA, and electricity, and all the components proved to be

essential for the reactivity (entries 20–22). Moreover, the reaction gave a similar result when the CCE was set at 2.5 mA (entry 23). Lastly, a 1:1 mixture of tetrahydrofuran and *N*-methyl-2-pyrrolidone, or γ-valerolactone were tested as alternative solvents, but neither provided any product (entries 24–25).

Table 3.5.1 Optimization of the electrochemical manganese-catalyzed C–H arylation.[a]

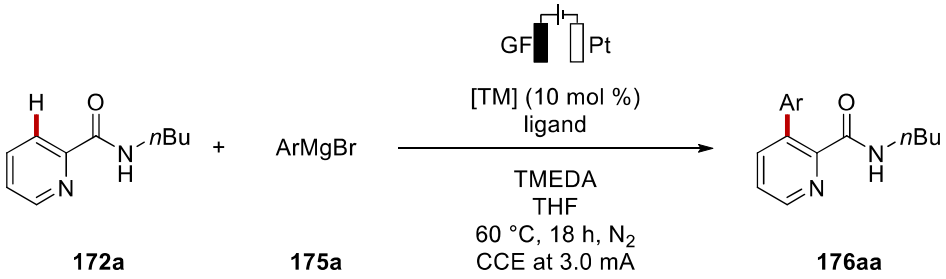

172a **175a** **176aa**

entry	[TM]	ligand	Deviation from standard conditions	yield (%)
1	$Fe(acac)_3$	dppe (10 mol %)	40 °C, 6 h, 5.0 mA	traces
2	$Fe(acac)_3$	dppe (10 mol %)	40 °C, 5.0 mA	11
3	$Fe(acac)_3$	dppe (10 mol %)	5.0 mA	traces
4	$Fe(acac)_3$	neocuproine (20 mol %)	---	---
5	$Fe(acac)_3$	neocuproine (20 mol %)	5.0 mA	---
6	$Fe(acac)_3$	1,10-phenanthroline (20 mol %)	40 °C, 5.0 mA	7
7	$FeCl_3$	dppe (10 mol %)	40 °C, 5.0 mA	10
8	$Ni(DME)Cl_2$	neocuproine (20 mol %)	---	---[b]
9	$RuCl_3 \cdot (H_2O)_n$	neocuproine (20 mol %)	---	---[b]
10	$PdCl_2$	neocuproine (20 mol %)	---	---[b]
11	$MnCl_2$	2,2'-dipyridyl (20 mol %)	---	40[b]
12	$MnCl_2$	1,10-phenanthroline (20 mol %)	---	61[b]
13	**$MnCl_2$**	**neocuproine (20 mol %)**	**---**	**70[b]**
14	$MnCl_2$	---	---	34[b]
15	$MnBr(CO)_5$	neocuproine (20 mol %)	---	47
16	$Mn(OAc)_2$	neocuproine (20 mol %)	---	50
17	$Mn(acac)_2$	neocuproine (20 mol %)	---	55
18	$MnCl_2$	neocuproine (20 mol %)	nBu_4NPF_6	---

19	$MnCl_2$	neocuproine (20 mol %)	$LiClO_4$	30[b]
20	---	neocuproine (20 mol %)	---	---[b]
21	$MnCl_2$	neocuproine (20 mol %)	without TMEDA	---[b]
22	$MnCl_2$	neocuproine (20 mol %)	without electricity	10[b]
23	$MnCl_2$	neocuproine (20 mol %)	2.5 mA	67[b]
24	$MnCl_2$	neocuproine (20 mol %)	THF/NMP	---[b]
25	$MnCl_2$	neocuproine (20 mol %)	GVL	---[b]

[a] Reaction conditions: undivided cell, **172a** (0.25 mmol), **175a** (1.00 mmol), [TM] (10 mol %), ligand (as specified), TMEDA (0.50 mmol), solvent (4.0 mL), 60 °C, 18 h, N_2, CCE at 3.0 mA, graphite felt (GF) anode (10 mm × 15 mm × 6 mm), Pt-plate cathode (10 mm × 15 mm × 0.125 mm), yield of isolated products. Ar = 4-$MeOC_6H_4$, TMEDA = N^1,N^1,N^2,N^2-*tetra*-methylethane-1,2-diamine. dppe = 1,2-bis(diphenylphosphino) ethane. [b] Performed by Dr. C. Zhu.

3.5.2 Substrate Scope

The optimized conditions were then applied to a broad range of secondary amides **172** to prove the robustness of the reaction (Scheme 3.5.1). Several groups were acceptable on the amide moiety, such as benzyl (**172b**) and *n*-hexyl substituents (**172c**). Also, *para*-substituents on the benzyl group did not alter the course of the arylation reaction, and both a methoxy (**172d**) and a fluoro (**172e**) substituents were used in that position. The bulkier *ortho*-fluoro benzyl derivative **172f** was likewise converted to product **176fa**. Moreover, 1,2,3,4-tetrahydronaphthalene or cyclohexene groups were tolerated (**176ga**, **176ha**). Regarding the pyridine moiety, the *para*-phenyl substrate **172j** was efficiently converted. Interestingly, the manganese-catalyzed electrochemical approach was also feasible for nicotinic and isonicotinic amides (**172k**-**n**). For the former, both the unsubstituted and the bulkier *meta*-methyl substrate provided the desired products **176ka** and **176la**, as well two examples **176ma** and **176na** were successfully obtained for the latter.

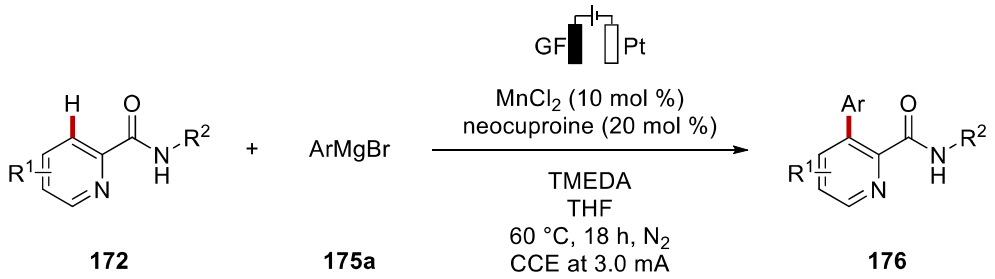

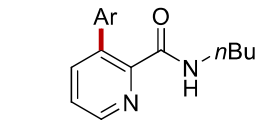

176aa: 70%[a]

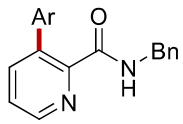

176ba: 58%

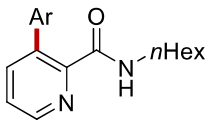

176ca: 77%[a]

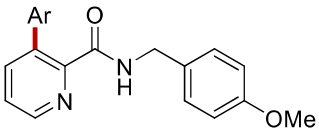

176da: 51%

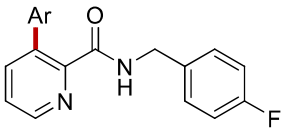

176ea: 46%

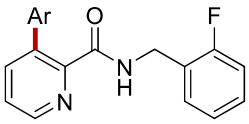

176fa: 56%

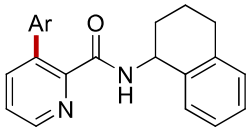

176ga: 74%

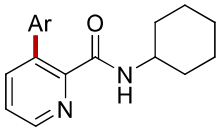

176ha: 61%

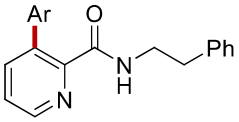

176ia: 70%[a]

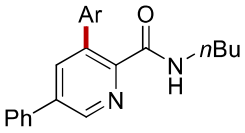

176ja: 59%[a]

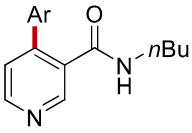

176ka: 51%[a]

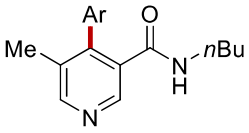

176la: 60%[a]

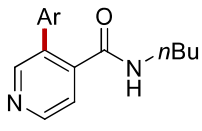

176ma: 65%[a]

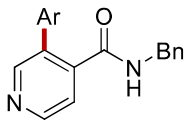

176na: 56%[a]

Scheme 3.5.1 Scope of electrochemical manganese-catalyzed C–H arylation of amides **172**. [a] Performed by Dr. C. Zhu. Ar = 4-$MeOC_6H_4$.

The scope was further extended with the probing of diverse aryl Grignard reagents **175** as the arylating agents (Scheme 3.5.2). Besides the anisole moiety (**172a**), the unsubstituted phenyl group

(**172b**) could also be easily installed. Other substrates with electron-rich groups, including methyl, *tert*-butyl, and phenyl substituents, were converted with excellent yields (**172c-e**). The 4-fluorobenzylmagnesiumbromide furnished likewise 60% of the product **172f**. Good yields were also obtained with methoxy or fluoro groups in the *meta*-position (**176ag-ah**) The challenging thiophene motif (**172i**) succeeded in the arylation reaction giving a modest yield for product **176ai**. Lastly, the naphthyl-substituted Grignard reagent **172j** also provided the arylated product **176aj** in good amounts.

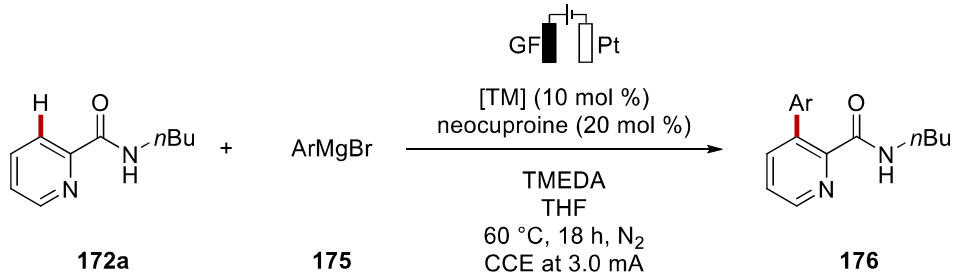

172a **175** **176**

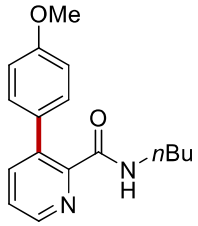

176aa: 70%[a]

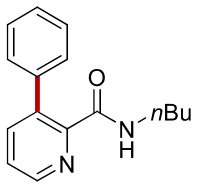

176ab: 75%

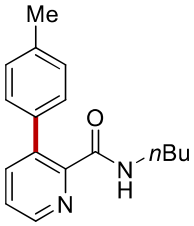

176ac: 78%

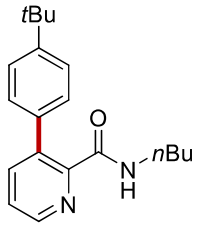

176ad: 73%

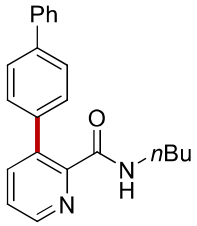

176ae: 57%[a]

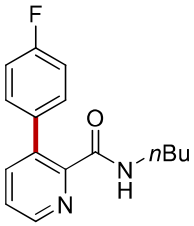

176af: 60%[a]

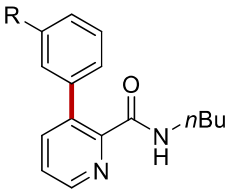

R = -OMe (**176ag**): 76%
R = -F (**176ah**): 70%

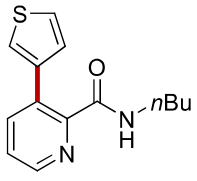

176ai: 21%[a]

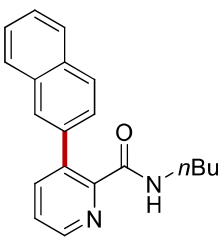

176aj: 52%[a]

Scheme 3.5.2 Scope of electrochemical manganese-catalyzed C–H arylation with different arylating agents **172**. [a] Performed by Dr. C. Zhu.

During the attempts to expand the scope, we were delighted to discover that the envisioned manganese-catalyzed methodology was also feasible for unprecedented electrochemical C–H alkylations (Scheme 3.5.3). With this approach we were able to perform the C–H methylation reaction (**214aa**), that is considered a very important reaction for pharmaceutical industries due to the so-called 'magic methyl effect', which can lead to an enhancement in bioactivity or selectivity of a drug candidate after the insertion of a sole CH_3 group.[172] The isopropyl group was also successfully introduced, yielding the desired product **214ab**. Moreover, the reaction proved amenable for benzylation likewise (**214hc**).

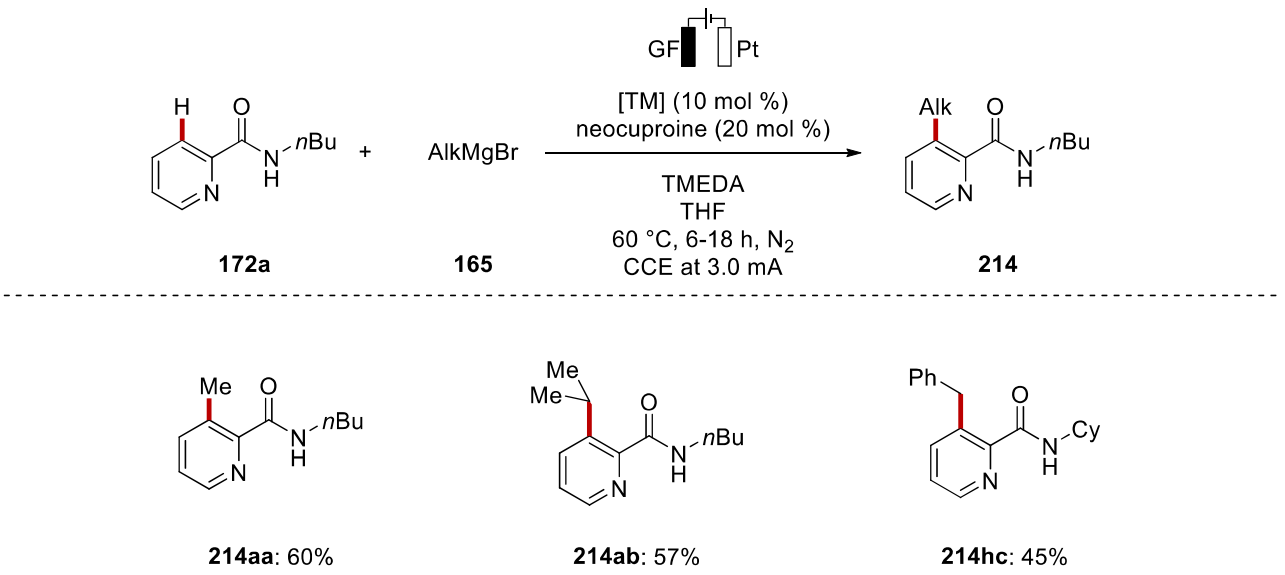

Scheme 3.5.3 Scope of electrochemical manganese-catalyzed C–H alkylation of amides **172**.

3.5.3 Mechanistic Studies

Subsequently, mechanistic studies were performed, starting with competition experiments between the Grignard reagents **175c** and **175f**. The more electron-rich Grignard **175c** reacted preferentially, with a 31% yield of product **176ac**, while the electron-poor one gave 17% of **176af** (Scheme 3.5.4,a). The preference for the electron-rich substrate **175c** is in accordance with the proposal of a ligand-to-

ligand hydrogen transfer (*vide infra*). Another competition experiment was conducted between the picolinic and nicotinic amides **172a** and **172k**, with the former reacting faster. Moreover, the kinetic isotope effect, studied on parallel reactions, was found to be $k_H/k_D \approx 1.1$, suggesting that the C–H activation is not the rate determining step (Scheme 3.5.4,b, performed by Dr. C. Zhu).

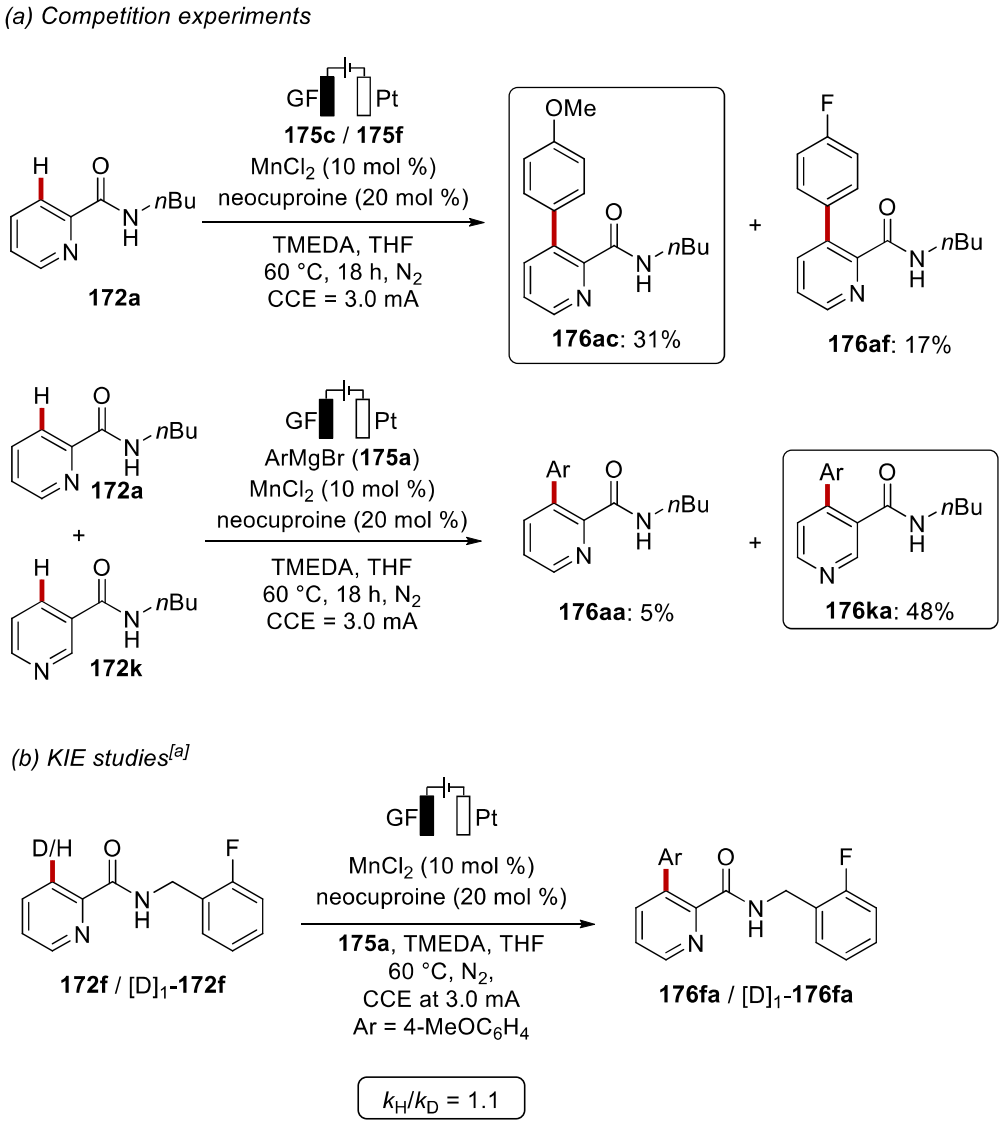

Scheme 3.5.4 Mechanistic findings for the electrochemical manganese-catalyzed C–H activation. [a] Performed by Dr. C. Zhu. Ar = 4-$MeOC_6H_4$.

Since the C–H activation did not seem to be the slow step, the dependence of the rate on the current was tested next (Figure 3.5.1). The profiles clearly showed an increasing rate with increasing currents.

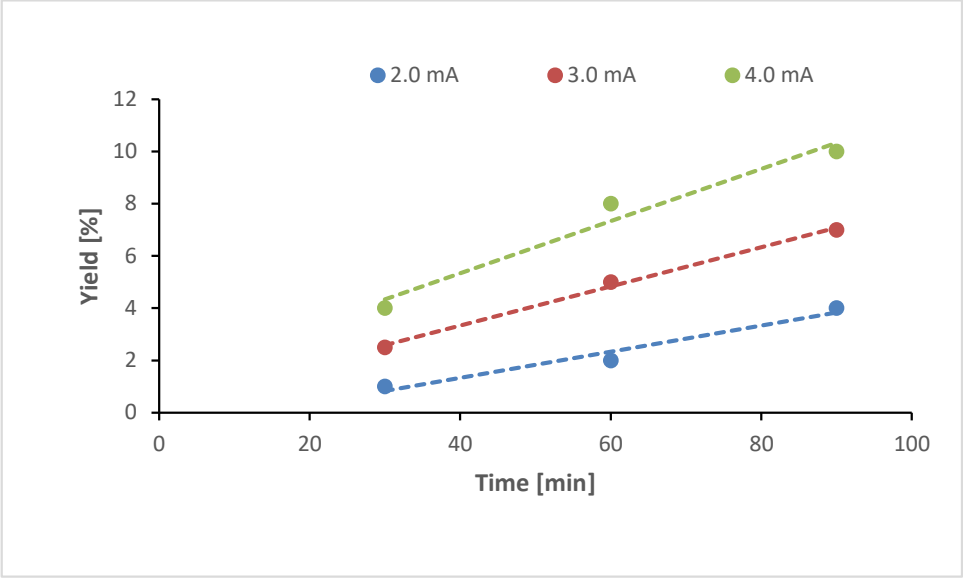

Figure 3.5.1 Profile of the manganese-catalyzed C–H activation at different currents.

Then, the well-defined manganese complex **215** was synthesized and tested under the reaction conditions (Scheme 3.5.5). The complex **215** gave a comparable yield, confirming its catalytic activity. Together with MSc A. Salamé, we analyzed the manganese-neocuproine complex by cyclic voltammetry, and it showed a reversible oxidation, supposedly manganese(II)/(III), at $E_{1/2}$ = +0.80 V *vs.* Ag/AgCl (Figure 3.5.2). The addition of the amide **172a** did not modify the oxidation event. The presence of all the reaction compounds, caused the irreversibility of the mentioned oxidation, due to plausible transmetalation.

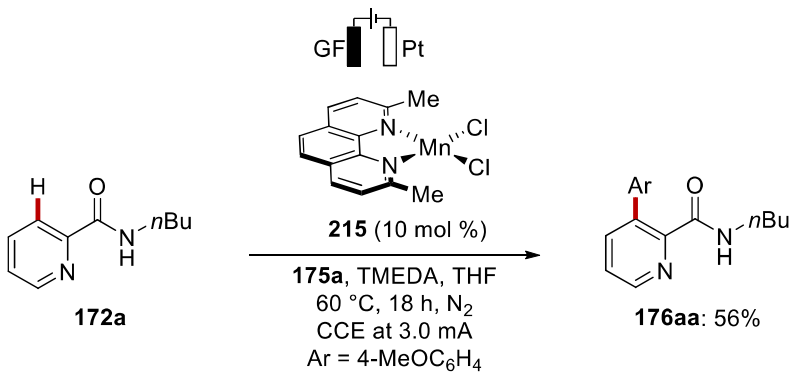

Scheme 3.5.5 Manganese complex **215** in the electrochemical manganese-catalyzed C–H activation.

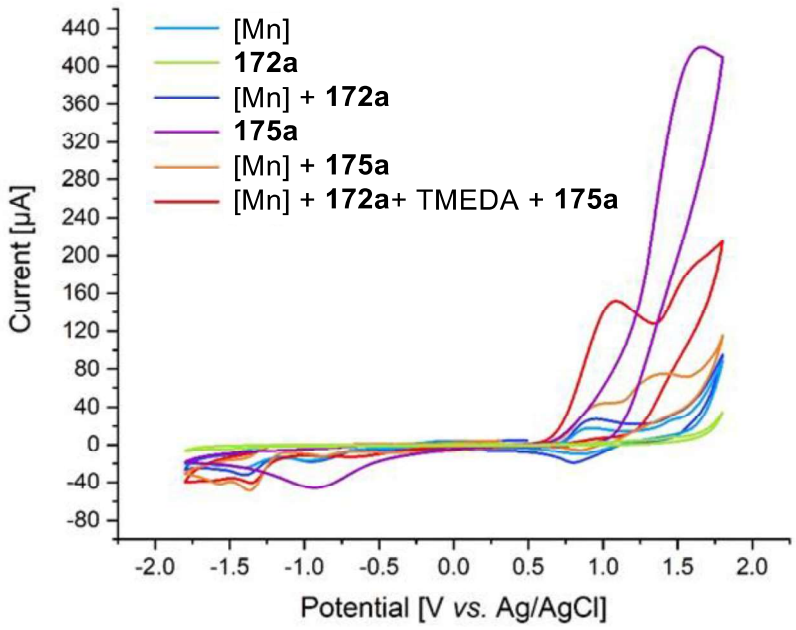

Figure 3.5.2 Cyclic voltammograms recorded with GC working electrode at 100 mVs^{-1} with nBu$_4$NBF$_4$ (0.2 mM in THF); concentration of substrates 5.0 mM (**175a** 20 mM). [173] = complex **215**. Performed with MSc A. Salamé.

Having clarified the oxidative event, the reductive event had to be investigated. Thus, Dr. P. Liu performed scanning electron microscopy energy-dispersive X-ray spectroscopy (SEM-EDS) on the platinum cathode after the electrocatalysis (Figure 3.5.3). From this analysis, magnesium was found on the surface of the cathode, suggesting that magnesium ions were directly reduced on the platinum surface. This finding underlined one of the dissimilarities with the iron-catalyzed electrochemical C–H arylation where zinc was deposit on the cathode. Indeed, in the iron-electrocatalyzed C–H activation, zinc was preferentially reduced due to its redox potential of −0.76 V *vs.* NHE that is higher than the one of magnesium of −2.36 V *vs.* NHE.[174]

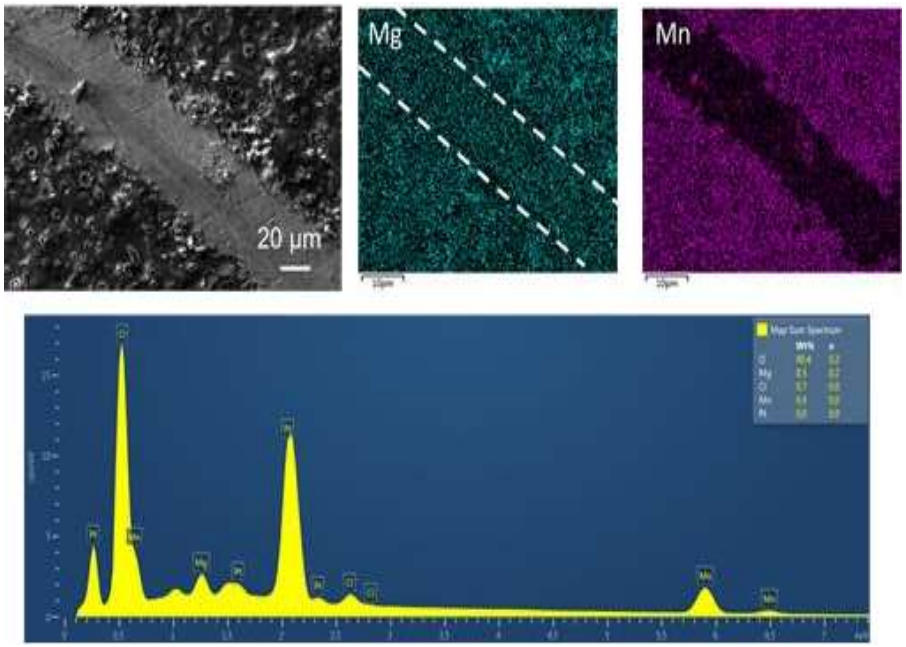

Figure 3.5.3 SEM-EDS studies on the post-catalysis cathodic material. Performed by Dr. P. Liu.

Based on our detailed mechanistic observations, a plausible catalytic cycle has been deduced (Scheme 3.5.6). Initially, the active catalyst **216** is formed upon coordination the ligand and the Grignard reagent. Subsequently, C–H activation through a ligand-to-ligand hydrogen transfer (LLHT) takes place. After a transmetalation event, an anodic oxidation induces the reductive elimination from a manganese(III) intermediate **220**. Lastly, another trasmetalation yields the product **176** and the manganese(I) complex **222**. An anodic oxidation then regenerates the active catalyst **216**.

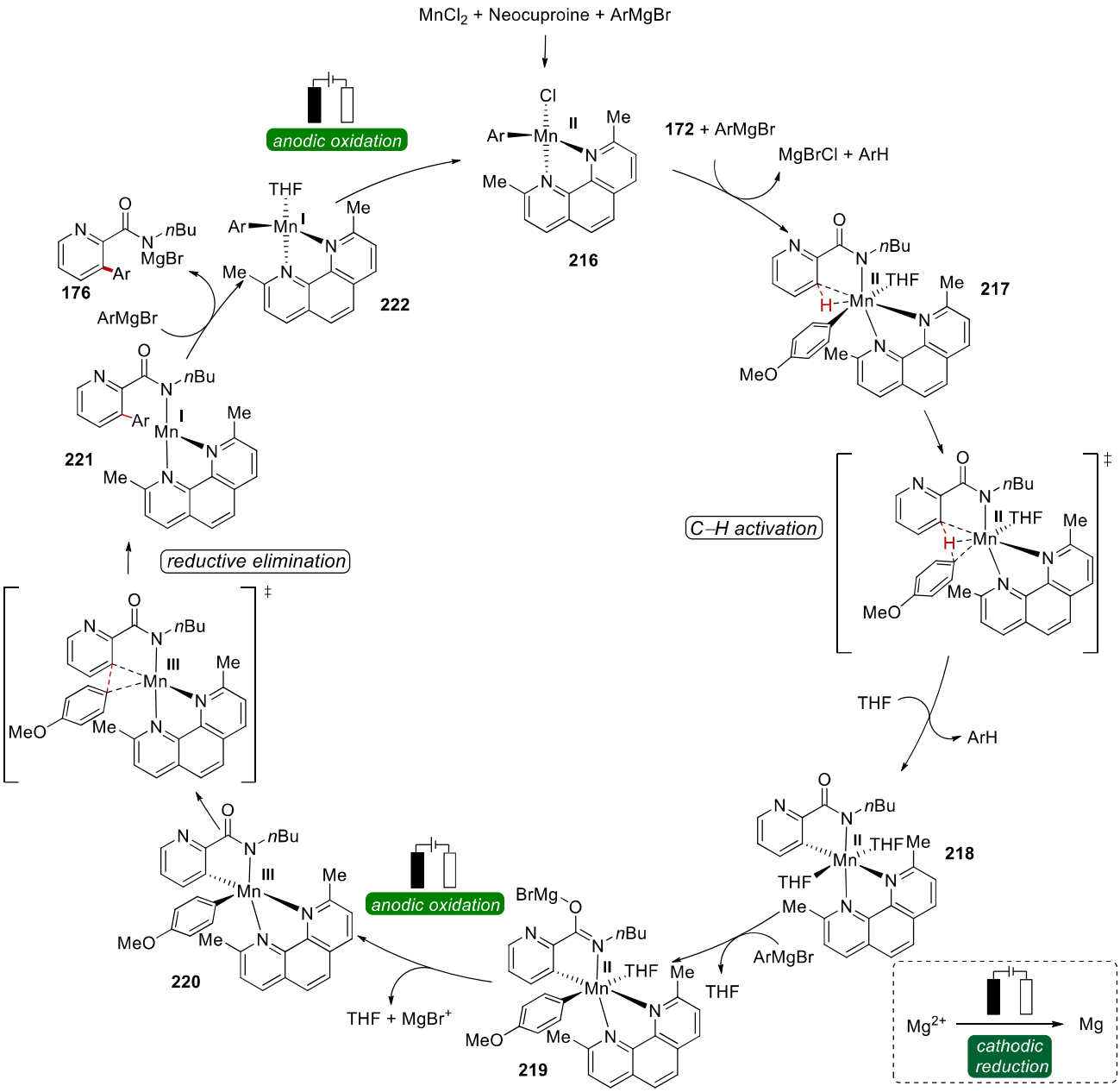

Scheme 3.5.6 Plausible catalytic cycle for the electrochemical manganese-catalyzed C–H arylation.

4 Summary and Outlook

The oxidative metal-catalyzed C–H activation of inert bonds is a powerful tool for the functionalization of complex molecules. This platform allows broadening of the organic chemists' toolbox and to improve the resource-economy of synthetic routes, avoiding prefunctionalizations of starting materials. Nevertheless, its applications were constrained by the use of stoichiometric oxidants, which limited the sustainability of this approach. In contrast, the use of electricity as environmental-friendly and versatile oxidant enhanced the sustainability of oxidative metal-catalyzed C–H activation and opened the way to the study of novel reactivities and selectivities.

In the first project, an electrochemical strategy was studied for the C–H/N–H annulation reaction with a cost-effective cobalt(II) salts as the catalyst (Scheme 4.1).[175] The approach occurred under extremely mild conditions, allowing the electrolysis to occur at room temperature with water as the cosolvent. The newly established electrochemical procedure proved to be user-friendly, with an undivided cell setup and constant current electrolysis at 4.0 mA. A variety of alkynes **117**, including heteroarenes, furnished the desired products **34** with excellent levels of positional selectivity.

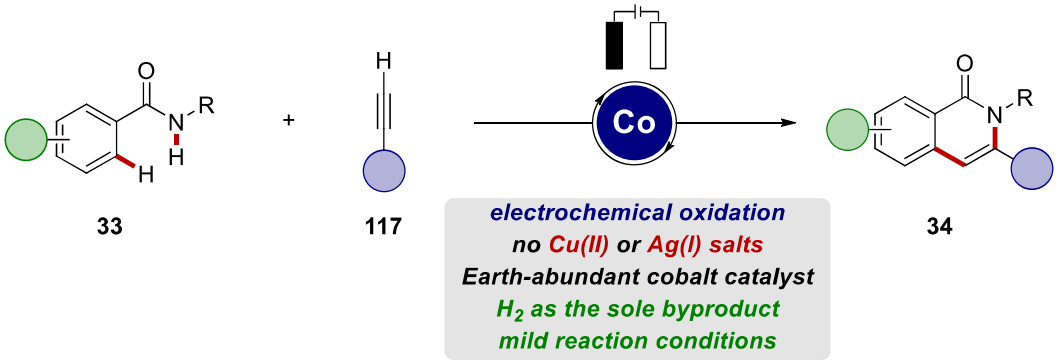

Scheme 4.1 Electrochemical cobalt-catalyzed C–H/N–H alkyne annulations.

The electrochemical oxidative metal-catalyzed annulation approach was then applied to internal unsymmetrical alkynes **24** by mean of ruthenium-catalysis (Scheme 4.2).[130] This project represented the first ruthenaelectro-catalysis with weakly *O*-coordinating directing groups. The scope proved broad with examples of diaryl-, diheteroaryl-, dialkyl-substituted, and unsymmetrical alkynes **24**.

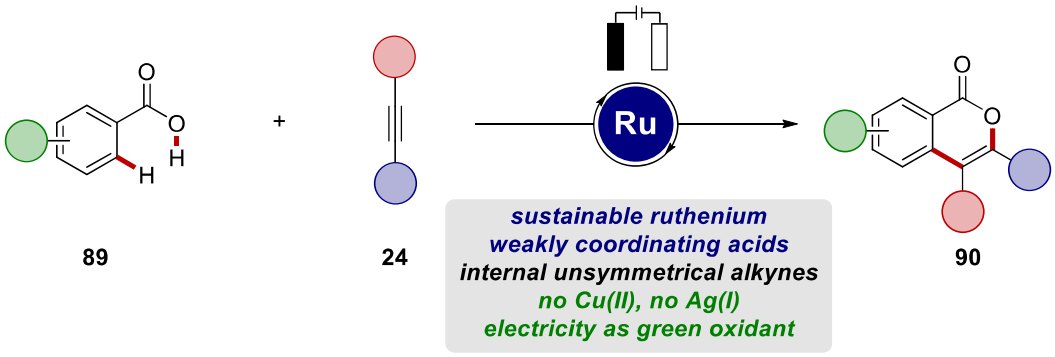

Scheme 4.2 Electrochemical ruthenium-catalyzed C–H/O–H alkyne annulations.

Having established a robust platform for electrooxidative C–H activations, we aimed to broaden its applicability. Therefore, a study on the electrosynthesis of hypervalent iodine as mediator in ruthenium-catalyzed oxygenations was carried out (Scheme 4.3).[176] The use of electricity allowed the use of catalytic amounts of iodoarenes **194a**, without the need for other stoichiometric oxidants. The environmental footprint of such approach was thus minimized, as only H_2 was generated as byproduct. The reaction featured a broad scope, selectively delivering the desired products **106**, **104**, **197**, and **199** with Weinreb amides **196**, tertiary amides **103**, ketones **77**, and even pyrazoles **198** as directing groups. The reaction was also tolerant of electron-rich as well as electron-poor arenes, and electrophilic functional groups, useful for late-stage modifications. Remarkably, the same reaction could be conducted for a two-step/one-pot remote undirected functionalization (**109**).

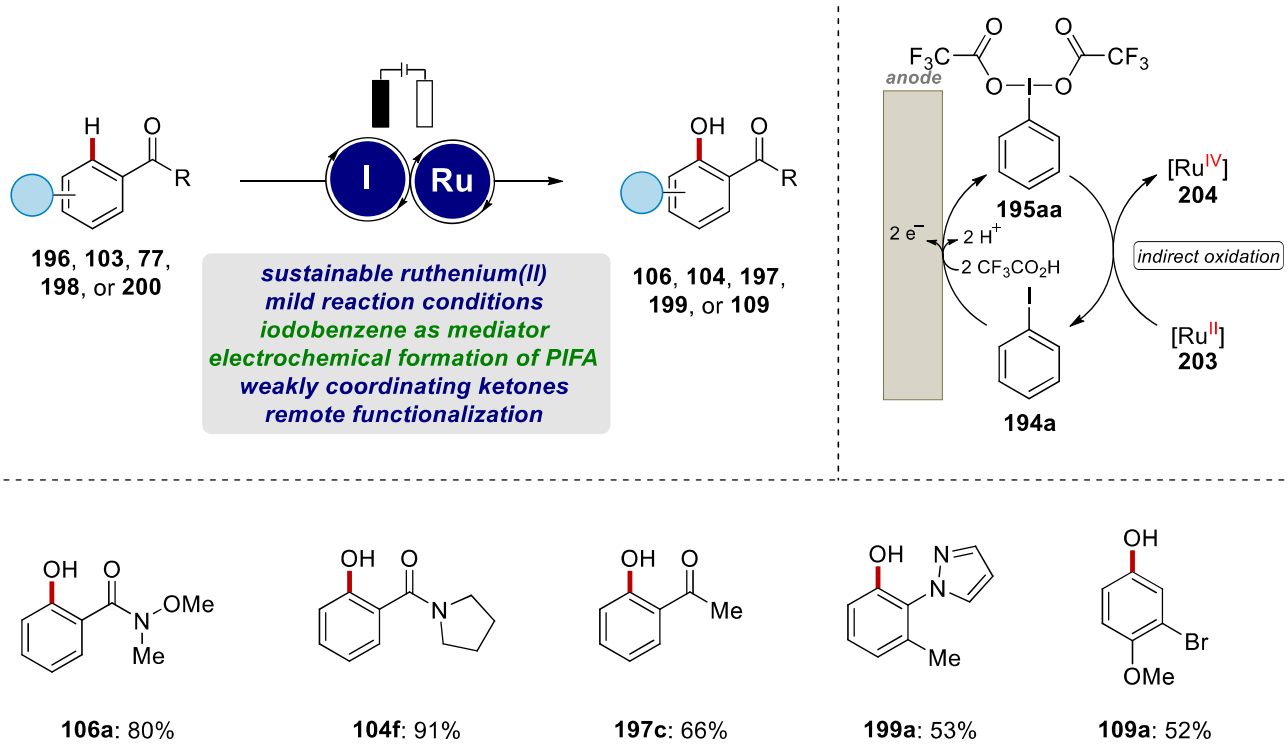

Scheme 4.3 Electrochemical hypervalent iodine formation for the ruthenium-catalyzed C–H oxygenation reaction.

Subsequently, we focused on rhodium catalysis to attain an effective oxidation of the metal catalyst directly at the anode (Scheme 4.4).[177] For this approach, the substrate scope proved similarly good to the ruthenium-catalyzed reaction. By taking advantage of the presence of electricity, it was also possible to access the cascade synthesis of dihydrooxazinone *via* a Shono oxidation. Comprehensive mechanistical studies, including CV analysis and DFT calculcations, demonstrated the bimetallic nature of the active rhodium catalyst and an oxidatively-induced C–H activation event.

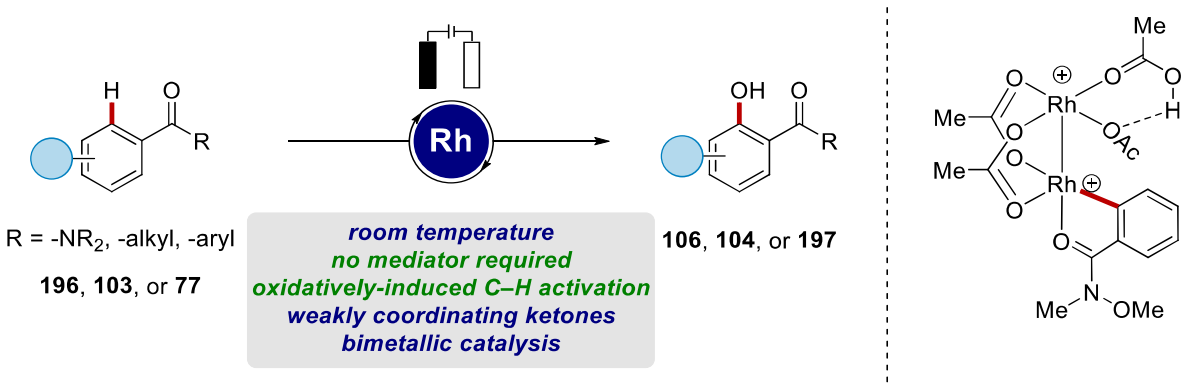

Scheme 4.4 Electrochemical rhodium-catalyzed C–H oxygenation and computed cyclometalated bimetallic intermediate.

Finally, the C–H arylation by earth-abundant manganese as catalyst and electricity as sustainable oxidant in a user-friendly undivided cell setup was developed (Scheme 4.5).[178] In contrast to an iron-electrocatalyzed C–H arylation,[48f] weakly coordinating mono-dentate azinylamides **172** could be employed. During the development of the project, it was possible to expand the approach to C–H alkylations, allowing for the introduction of the relevant methyl group (**214**).[172] Insights in the electrochemical events were accessed by means of experimental studies, CV, and SEM-EDS analysis, providing support for the proposed oxidation of the cyclometalated species and the reduction of magnesium.

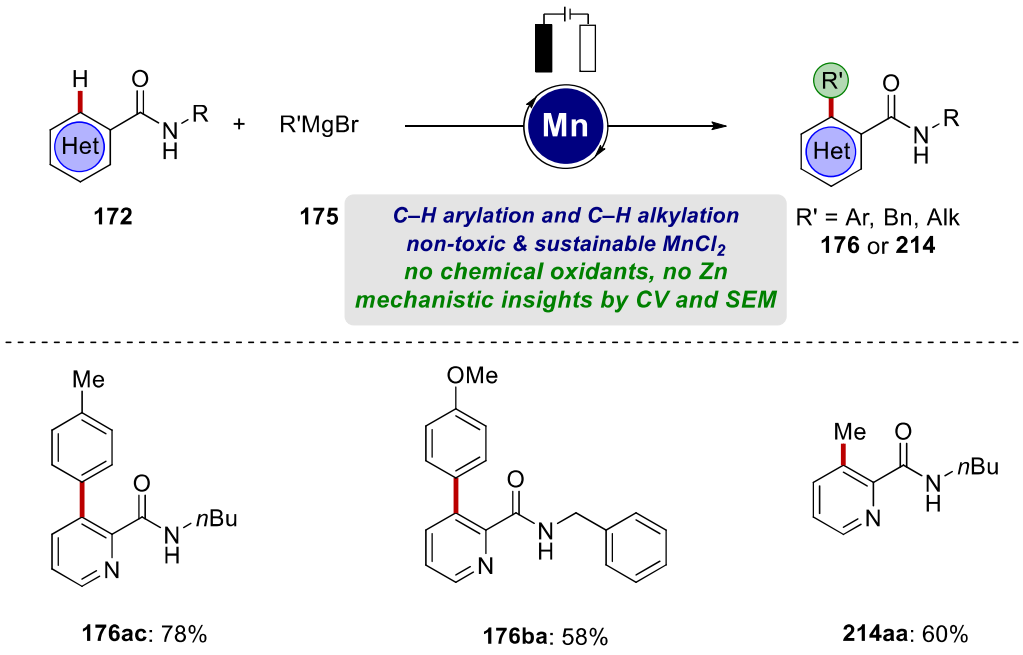

Scheme 4.5 Electrochemical manganese-catalyzed C–H arylations.

The application of electrochemistry in C–H activation was successful with diverse transition metal catalysts. Nevertheless, many challenges still need to be addressed to further develop this approach.[163a] First, electricity could be used to further enhance the sustainability of these reactions, with the replacement or the *in-situ* synthesis of different toxic or hazardous chemicals. Novel

strategies, such as paired electrolysis, can moreover improve the atom-efficiency.[179] The development of enantioselective electrochemical transformation is also of utmost importance to the scientific community.[180] Other interesting approaches can be envisioned in photoelectrocatalysis,[181] flow-electrocatalysis,[182] the design of electrode materials,[183] and by the aid from artificial intelligence.[184] Electrocatalysis is thus still a novel area of research with important challenges but a bright future ahead.

5. Experimental Data

5.1 General Remarks

Reactions involving air- or moisture-sensitive compounds were conducted under an atmosphere of nitrogen using pre-dried glassware and standard Schlenk or glovebox techniques. Liquids and solutions were transferred *via* nitrogen-flushed syringes by BRAUN, with oven-dried stainless-steel cannulas (pre-dried at 120 °C). Solids were added under counter flow of nitrogen (standard *Schlenk* technique). Solutions were concentrated under reduced pressure by rotary evaporation at 40 °C with a HEIDOLPH *Hei-VAP Core*. Non-volatile products were dried under OPV for 14 h. Air and moisture sensitive substances were stored in a MBRAUN glovebox. If not otherwise noted, yields refer to isolated compounds, estimated to be >95% pure by GC and NMR.

Vacuum

The following average pressure was measured on the used rotary vane pump *RD4* from VACUUBRAND®: 0.8×10^{-1} mbar (uncorrected value).

Melting points

Melting points were measured on a *Stuart® Melting Point Apparatus SMP3* from BARLOWORLD SCIENTIFIC and are uncorrected.

Chromatography

Analytical thin-layer chromatography (TLC) was used for reaction monitoring, analysis of column chromatography, and determination of R_f values. TLC was performed on silica gel 60 coated aluminium-sheets, with fluorescence indicator F-254 (MACHEREY NAGEL, by MERCK). The plates were either visualized by UV light (λ = 254 nm or 366 nm), if applicable, or by staining solution ($KMnO_4$ aq. solution) followed by gentle heating by heat-gun.

Chromatographic purification of crude products was accomplished by flash column chromatography using MERCK silica gel, grade 60 (40–63 µm, 70–230 mesh ASTM, *Geduran SI 60*). The crude

products were loaded in the column with the respective eluent. For acid-sensitive compounds the silica gel was neutralized with Et_3N prior to use.

Gas Chromatography

Gas chromatographic analysis (GC) was performed on an AGILENT *7890A GC System* or AGILENT *7890B GC System* equipped with an AGILENT *HP-5MS* column (30 m × 0.25 mm diameter, 0.25 µm film thickness) and a flame-ionization detector (FID) using hydrogen as the carrier gas. Gas chromatography coupled with mass spectrometry (GC-MS) was performed on the same instrument equipped with an AGILENT *5875C Triple-Axis-Detector* or AGILENT *5977B MSD*. Mass spectra were obtained with electron-ionization (EI) at 70 eV in positive ion mode. Gas-chromatogrphical analysis of the headspace after reaction was performed on a SHIMADZU *S2014 GC System* using a Thermal Conductivity Detector and a 5A MS column.

Mass Spectrometry

Electrospray-ionization (ESI) mass spectra were recorded on a quadrupole time-of-flight on a *micrOTOF* or a *maXis* from BRUKER DALTONICS or a *LTQ Orbitrab XL* from THERMO SCIENTIFIC. Electron-ionization (EI) mass spectra were recorded on a time-of flight mass spectrometer JEOL *AccuTOF* instrument at 70 eV. The ratio of mass to charge (m/z) is given, intensities I relative to the base signal ($I = 100$) are written in parentheses.

Infrared Spectroscopy (IR)

Infrared (IR) spectra of were measured on a BRUKER *Alpha-P* FT-IR spectrometer with a diamond ATR probe in the range of $\tilde{\nu}$ = 4000–400 cm^{-1}. Analysis of the spectra was performed with the software *Opus 6.5* from BRUKER. *In-situ* IR measurements were performed with a *ReactIR™ 15* from METTLER TOLEDO equipped with a diamond ATR probe and an MCT detector. Spectra were acquired using METTLER TOLEDO *iC IR* software version 7.0.297 in the range of 650–2200 cm^{-1} with a 4 cm^{-1} resolution. A Pearson's Correction was applied as baseline correction in all measurements.

Nuclear Magnetic Resonance (NMR) Spectroscopy

Nuclear magnetic resonance (NMR) spectra were recorded on BRUKER *Avance* 300, *Avance* III HD 400, *Avance Neo* 400, *Avance* III HD 500; VARIAN *Mercury VX* 300, *Inova* 500 or *Inova* 600 spectrometer at 300 MHz, 400 MHz, 500 MHz, 600 MHz (^{1}H-NMR), 75 MHz, 100 MHz, 125 MHz (^{13}C-NMR) and 282 MHz (^{19}F-NMR). Unless stated otherwise, all measurements were performed at 298 K. Chemical shifts (δ) are reported relative to tetramethylsilane and are referenced using the residual proton peak or the carbon peak of the deuterated solvent (Table 5.1.1).

Table 5.1.1 Chemical shifts of residual proton signals or carbon signals of common deuterated solvents.

Solvent	**^{1}H-NMR**	**^{13}C-NMR**
$CDCl_3$	7.26 ppm	77.16 ppm
DMSO-d_6	2.50 ppm	39.52 ppm
Acetone-d_6	2.05 ppm	206.7, 29.92 ppm
Methanol-d_4	4.78, 3.31 ppm	49.15 ppm
THF-d_8	3.58, 1.73 ppm	67.57, 25.37 ppm

The measured resonance multiplicities were reported using the following abbreviations: s (singlet), d (doublet), t (triplet), q (quartet), quint (quintet), sext (sextet), sept (septet), dd (doublet of doublets), dt (doublet of triplets), ddd (doublet of doublets of doublets), td (triplet of doublets), dddd (doublet of doublets of doublets of doublets), m (multiplet) and br (broad singlet). The coupling constants *J* are reported in Hertz (Hz). Analysis of all spectra until February 2019 was performed with *MestReNova v10.0.2* and from February onwards with *MestReNova v14.1.0* from MESTRELAB RESEARCH S.L.

^{1}H-NMR spectroscopic experiments in flow were performed on a *Magritek Spinsolve 60^{ULTRA}* from MAGRITEK GmbH, Germany. These spectra were batch-processed with the reaction monitoring wizard of the *MestReNova v12.0.3* software. Arbitrary integral values were transformed to mmol and percentage values by referencing with dibromomethane as the internal standard.

Data Analysis and Plots

Data analysis and plotting were performed using Microsoft® Excel 2016 software. CVs were analyzed and plotted using OriginLab© OriginPro 8.5G software.

Electrochemistry

Constant Current Electrolysis (CCE)

The electrocatalytic reactions were performed in undivided electrochemical cells (10 mL) using pre-dried glassware, unless stated otherwise. Platinum electrodes (10 mm × 15 mm × 0.125 mm, 99.9%, CHEMPUR Karlsruhe, Germany or 99.95%; ESG-EDELMETALL-HANDEL GMBH & CO. KG), graphite felt electrodes (10 mm × 15 mm × 6 mm, *SIGRACELL®GFA 6 EA*, SGL CARBON, Wiesbaden, Germany) and reticulated vitreous carbon (RVC) (40 mm x 5.0 mm x 6.0 mm, *Duocel® Reticulated Vitreous Carbon RVC100* (100 PPI) ERG AEROSPACE CORPORATION, Oakland, United States of America) were connected using stainless steel adapters, following the published protocol.[185] Electrolysis was conducted using an AXIOMET *AX-3003P* galvanostat in constant current mode. Divided cells, separated by a P4 glass frit, were custom-made and obtained from GLASGERÄTEBAU OCHS LABORFACHHANDEL e. K. (Bovenden, Germany). For reactions performed with the standardized electrochemistry kit, *ElectraSyn 2.0* from IKA, the commercialized electrodes and 10 mL undivided cells were used, if not stated otherwise. If reactions were performed at temperatures other than room temperature, the vial was connected *via* the IKA *ElectraSyn GOGO Module*® and mounted in a silicon oil bath.

For reactions in flow, an ISMATEC *REGLO Digital MS-2/12 (ISM 596)* peristaltic pump and a KEYSIGHT *E36104A* galvanostat was employed. The flow-electrocatalysis was performed with a commercially available IKA *ElectraSyn flow* system and the respective half-cell electrodes.

Constant Potential Reactions under Amperometric Detection

The constant potential electrolyses (CPE) were performed using a METROHM *Autolab PGSTAT204* or a METROHM *Dropsense 8000P* workstation and *Nova 2.1* or the *Dropview 8400* software, respectively. A silver wire (d = 1 mm) was used as the pseudo-reference electrode in close proximity to the working electrode. To ensure comparable constant potential conditions with the results gained by

cyclic voltammetry, calibration of the pseudo-reference electrode *versus* ferrocene was performed for each reaction system. If applicable, an aqueous Ag/AgCl reference electrode was used instead of the silver wire.

Cyclic Voltammetry

The cyclic voltammetry measurements were carried out using a METROHM *Autolab PGSTAT204* workstation, and the following data analysis was performed with *Nova 2.1* software. For the experiments, a glassy carbon (GC) disc electrode (d = 3 mm) was used as the working electrode (WE). Either a saturated calomel electrode (SCE); a 3 M aq. Ag/AgCl or a non-aqueous $Ag/AgNO_3$ (solution of MeCN with $AgNO_3$ (0.01 M) and $n$$Bu_4NClO_4$ (0.1 M)) was used as the reference electrode (RE), if not stated otherwise. If a silver-wire (d = 1 mm) was used as the pseudo-reference electrode, the voltammograms were referenced internally *versus* ferrocene. The counter electrode (CE) was a coiled platinum wire (d = 1 mm). The electrodes were purchased from ALS JAPAN Co., Ltd. Measurements were recorded at a scan rate of 100 $mV \cdot s^{-1}$, if not indicated otherwise. The working temperature was 298 K, if not indicated otherwise. All solutions were degassed *via* freeze-pump-thaw method prior to use and dry nitrogen was bubbled through the solutions for at least 5 min before the experiment was performed. During the voltammetric measurements, an overpressure of dry nitrogen was maintained. The rotating-disc electrode (RDE) experiments were performed using a METROHM *Autolab PGSTAT204* workstation and a *RRDE-3A Rotating Ring Disk Electrode Apparatus Ver.2.0* purchased from ALS JAPAN Co., Ltd. For the RDE experiments, a glassy carbon disc electrode (d = 4 mm, disc-electrode) was used as the working electrode, a coiled platinum wire (d = 1 mm) was used as the counter electrode and a non-aqueous $Ag/AgNO_3$ (solution of MeCN with $AgNO_3$ (0.01 M) and $n$$Bu_4NClO_4$ (0.1 M)) was used as the reference electrode. The operation temperature was 25 °C and dry nitrogen was bubbled through the solution for at least 5 min before the analytical experiment was performed.

Solvents

All solvents used for work-up and purification were distilled prior to use. Solvents used in reactions involving air- or moisture-sensitive compounds were dried and stored under an inert atmosphere of nitrogen or argon according to the following standard procedures: Solvents purified by solvent purification system (SPS-800) from MBRAUN: toluene, THF, diethyl ether, DCM, and DMF. Solvents dried and distilled over CaH_2: DCE, DMA, and NMP. Solvents dried over 4Å molecular sieves and degassed using multiple cycles of freeze-pump-thaw: *t*AmOH, *o*-, *m*-, *p*-xylene, 1,4-dioxane, DME, methanol, TFE, and HFIP, 2-methyltetrahydrofuran, *n*hexane, toluene-d_8, and THF-d_8. Water was degassed before its use applying repeated freeze-pump-thaw cycles.

Reagents

Reagents obtained from commercial sources with a purity >99% were used without further purification unless stated otherwise. The following compounds were synthesized according to previously reported procedures: **33**, **106**, **104**, **197**, **199**, **172**, **175**.

The following compounds were kindly synthesized and/or provided by the persons listed below:

Karsten Rauch: $[RuCl_2(p\text{-cymene})]_2$ and $[Ru(OAc)_2(p\text{-cymene})]$ **188a**

Dr. Xuefeng Tan: **103f**, **103h**, **103i**, **103n**, and **196t**.

Dr. Cuiju Zhu: **172c**, **172e**, **172f**, **172i**, **172k**, and **172l**.

Dr. Nikolaos Kaplaneris: **24d**, and **24e**.

5.2 General Procedures

5.2.1 General Procedure A: Electrochemical Cobalt-Catalyzed C–H/N–H Annulation

The electrolysis was carried out in an undivided cell, with a RVC anode (10 mm × 15 mm × 6 mm) and a platinum cathode (10 mm × 15 mm × 0.125 mm). Benzamide **33** (0.50 mmol, 1.00 equiv), alkyne **117** (1.00 mmol, 2.00 equiv), NaOPiv (124 mg, 1.00 mmol, 2.00 equiv) and $Co(OAc)_2{\cdot}4H_2O$ (12.7 mg, 10 mol %) were placed in a 20 mL cell and dissolved in 10 mL of H_2O/MeOH (1:1). The electrolysis was performed at ambient temperature with a constant current of 4.0 mA maintained for 16 h. The reaction was quenched by adding saturated aqueous $NaHCO_3$ (10 mL). The RVC anode was washed with CH_2Cl_2 (3 × 10 mL) with the aid of an ultrasonic bath. The mixture of organic phases and of the aqueous one, was separated and further extracted with CH_2Cl_2 (3 × 10 mL), then dried over Na_2SO_4. Evaporation of the solvent and subsequent column chromatography on silica gel afforded the desired products **34**.

5.2.2 General Procedure B: Electrochemical Cobalt-Catalyzed C–H/N–H Annulation

The electrolysis was carried out in an undivided cell, with a RVC anode (10 mm × 15 mm × 6 mm) and a platinum cathode (10 mm × 15 mm × 0.125 mm). Benzamide **33** (0.50 mmol, 1.00 equiv), alkyne **117** (1.00 mmol, 2.00 equiv), NaOPiv (124 mg, 1.00 mmol, 2.00 equiv) and $Co(OAc)_2{\cdot}4H_2O$ (25.7 mg, 20 mol %) were placed in a 20 mL cell and dissolved in 10 mL of H_2O/MeOH (1:1). The electrolysis was performed at ambient temperature with a constant current of 4.0 mA maintained for 16 h. The reaction was quenched by adding saturated aqueous $NaHCO_3$ (10 mL). The RVC anode was washed with CH_2Cl_2 (3 × 10 mL) with the aid of an ultrasonic bath. The mixture of organic phases and of the aqueous one, was separated and further extracted with CH_2Cl_2 (3 × 10 mL), then dried over Na_2SO_4. Evaporation of the solvent and subsequent column chromatography on silica gel afforded the desired products **34**.

5.2.3 General Procedure C: Electrochemical Ruthenium-Catalyzed C–H/Het–H Annulation

The electrolysis was carried out in an undivided cell with a RVC anode (10 mm × 15 mm × 6 mm) and a platinum cathode (10 mm × 15 mm × 0.125 mm). Benzoic acids **89** or benzamide **87** (1.0 mmol, 2.0 equiv), alkyne **24** (0.5 mmol, 1.0 equiv), NaOPiv (62 mg, 0.5 mmol, 1.0 equiv) and $[RuCl_2(p\text{-cymene})]_2$ (15.3 mg, 5.0 mol %) were dissolved in *t*AmOH/H_2O (3/1, 4.0 mL). The electrolysis was performed at 80–100 °C with a constant current of 4.0 mA maintained for 18–24 h. The RVC anode was washed with CH_2Cl_2 (3×10 mL) with the aid of an ultrasonic bath and the organic phases were combined. Evaporation of the solvent and subsequent column chromatography on silica gel afforded the corresponding products **90** or **88**.

5.2.4 General Procedure D: Electrochemical Ruthenium-Catalyzed C–H Oxygenation of Amides

The electrolysis was carried out in an undivided cell with platinum electrodes (10 mm × 15mm × 0.125 mm). The cell was charged with amide **196** or **103** (0.50 mmol, 1.0 equiv), iodobenzene **194a** (11 μL, 20.4 mg, 20 mol %), $[Ru(OAc)_2(p\text{-cymene})]$ **188a** (8.8 mg, 5.0 mol %), and $n Bu_4NPF_6$ (194 mg, 1.0 equiv) in TFA/TFAA (3:1, 3.0 mL). The electrolysis was performed at 50 °C with a constant current of 4.0 mA maintained for 16 h. After the reaction was completed, a saturated aqueous solution of $NaHCO_3$ (25 mL) was added and the reaction mixture was extracted with EtOAc (3 × 15 mL). The combined organic layers were washed with brine (25 mL), dried over Na_2SO_4, filtered, and concentrated *in vacuo*. The crude product **106** or **104** was purified by column chromatography on silica gel.

5.2.5 General Procedure E: Electrochemical Ruthenium-Catalyzed C–H Oxygenation of Ketones

The electrolysis was carried out in an undivided cell with platinum electrodes (10 mm × 15mm × 0.125 mm). The cell was charged with ketone **77** (0.50 mmol, 1.0 equiv), iodobenzene **194a** (11 μL, 20.4 mg, 20 mol %), $[RuCl_2(p\text{-cymene})]_2$ (7.7 mg, 2.5 mol %), and $n Bu_4NPF_6$ (194 mg, 1.0 equiv) in TFA/TFAA (3:1, 3.0 mL). The electrolysis was performed at 50 °C with a constant current of 4.0 mA

maintained for 16–24 h. After the reaction was completed, a saturated aqueous solution of $NaHCO_3$ (25 mL) was added and the reaction mixture was extracted with EtOAc (3 × 15 mL). The combined organic layers were washed with brine (25 mL), dried over Na_2SO_4, filtered, and concentrated *in vacuo*. The crude product **197** was purified by column chromatography on silica gel.

5.2.6 General Procedure F: Electrochemical Ruthenium-Catalyzed C–H Oxygenation in *para*-Position

The electrolysis was carried out in an undivided cell with platinum electrodes (10 mm × 15 mm × 0.125 mm). The cell was charged with iodobenzene **194a** (68 μL, 122 mg, 1.2 equiv), and nBu$_4$NPF$_6$ (194 mg, 1.0 equiv) in TFA/TFAA/DCE (1:2:15, 3.6 mL). The electrolysis was performed at room temperature with a constant current of 8.0 mA for 5 h. Subsequently, anisole **200** (0.50 mmol, 1.0 equiv) and [Ru(OAc)$_2$(*p*-cymene)] **188a** (8.8 mg, 5.0 mol %) were added and the reaction was heated at 80 °C for 3 h. After the reaction was completed, water (25 mL) was added, and the reaction mixture was extracted with EtOAc (3 × 15 mL). The combined organic layers were washed with brine (25 mL), dried over Na_2SO_4, filtered, and concentrated *in vacuo*. The crude product **109** was purified by column chromatography on silica gel.

5.2.7 General Procedure G: Electrochemical Rhodium-Catalyzed C–H Oxygenation of Amides

The electrolysis was carried out in an undivided cell (10 mL) equipped with a graphite felt (GF) anode (10 mm × 10 mm × 6 mm) and a platinum cathode (10 mm × 15 mm × 0.125 mm). [Rh(OAc)$_2$]$_2$ (5.5 mg, 0.0125 mmol, 2.5 mol %), TFA·NEt$_3$ (215 mg, 1.0 mmol), TFA (0.15 mL), amide **196** or **103** (0.50 mmol) and TFAA (3.0 mL) were successively added. The electrolysis was performed at 2.0 mA at ambient temperature for 15–17 h (2.2–2.5 F mol^{-1}). After completion, the reaction mixture was transferred into a separatory funnel and the electrodes were rinsed with EtOAc (10 mL). A saturated aqueous $NaHCO_3$ solution (50 mL) was added slowly, and the mixture was extracted with ethyl acetate (3 × 20 mL). The combined organic layers were dried over Na_2SO_4 and concentrated under vacuum. The crude reaction mixture was purified column chromatography on silica gel to yield the desired product **106** or **104**.

5.2.7 General Procedure H: Electrochemical Rhodium-Catalyzed C–H Oxygenation of Ketones

The electrolysis was carried out in an undivided cell (10 mL) equipped with a graphite felt (GF) anode (10 mm × 10 mm × 6 mm) and a platinum cathode (10 mm × 15 mm × 0.125 mm). $[Rh(OAc)_2]_2$ (5.5 mg, 0.0125 mmol, 2.5 mol %), TFA·NEt_3 (215 mg, 1.0 mmol), TFA (0.20 mL), ketone **77** (0.50 mmol) and TFAA (3.0 mL) were successively added. The electrolysis was performed at 2.0 mA at ambient temperature for 17 h (2.5 F mol^{-1}). After completion, the reaction mixture was transferred into a separatory funnel and the electrodes were rinsed with EtOAc (10 mL). A saturated aqueous $NaHCO_3$ solution (50 mL) was added slowly, and the mixture was extracted with ethyl acetate (3 × 20 mL). The combined organic layers were dried over Na_2SO_4 and concentrated under vacuum. The crude reaction mixture was purified column chromatography on silica gel to yield the desired product **197**.

5.2.8 General Procedure I: Electrochemical Manganese(II/III/I)-Catalyzed C–H Arylation

The electrolysis was carried out in an undivided cell with a graphite felt (GF) anode (10 mm × 15 mm × 6 mm) and a platinum cathode (10 mm × 15 mm × 0.125 mm). A mixture of amide **172** (0.25 mmol, 1.00 equiv), $MnCl_2$ (3.1 mg, 10 mol %), neocuproine (10.4 mg, 20 mol %), and TMEDA (74 μL, 2.0 equiv) were placed in a 10 mL cell under nitrogen atmosphere and dissolved in THF (4.0 mL). A solution of ArMgBr **175** or AlkMgBr **165** (4.0 equiv, in THF) was slowly added. Electrolysis was performed at 60 °C with a constant current of 3.0 mA maintained for 18 h. At ambient temperature, a saturated aqueous NH_4Cl solution (10 mL) was added, and the GF anode was washed with EtOAc (3 × 2.0 mL) in an ultrasonic bath. The mixture of organic phases and of the aqueous one, was separated and further extracted with EtOAc (3 × 10 mL) and then dried over Na_2SO_4. Evaporation of the solvents and purification by column chromatography on silica gel yielded the desired product **176** or **214**.

5.3 Electrochemical C–H/N–H Activation by Water-Tolerant Cobalt-Catalysis at Room Temperature

5.3.1 Characterization Data

2-[1-Oxo-3-phenylisoquinolin-2(1*H*)-yl]-pyridine-2-oxide (34aa)

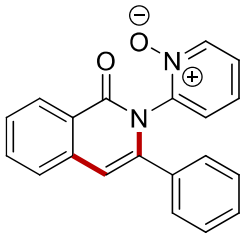

The general procedure **A** was followed using benzamide **33a** (107 mg, 0.50 mmol) and alkyne **117a** (102 mg, 1.00 mmol). Purification by column chromatography on silica gel (dichloromethane/acetone: 3/1) yielded **34aa** (119 mg, 76%) as a white solid.

M. p.: 225–226 °C.

^{1}H-NMR (300 MHz, $CDCl_3$): δ = 8.46–8.37 (m, 1H), 8.23–8.14 (m, 1H), 7.73–7.63 (m, 1H), 7.53 (dt, J = 7.2, 0.7 Hz, 1H), 7.51–7.44 (m, 1H), 7.44–7.35 (m, 2H), 7.28–7.16 (m, 3H), 7.16–7.08 (m, 2H), 7.08–7.00 (m, 1H), 6.59 (s, 1H).

^{13}C-NMR (125 MHz, $CDCl_3$): δ = 161.7 (C_q), 145.3 (C_q), 142.4 (C_q), 139.8 (CH), 136.9 (C_q), 134.7 (C_q), 133.2 (CH), 128.9 (CH), 128.2 (CH), 128.0 (CH), 127.8 (CH), 127.5 (CH), 126.9 (CH), 126.2 (CH), 125.3 (CH), 124.9 (CH), 124.8 (C_q), 107.9 (CH).

IR (ATR): 1664, 1624, 1490, 1261, 889, 843, 764, 526 cm^{-1}.

MS (ESI) *m/z* (relative intensity): 353 (5), 337 (30) $[M+Na]^+$, 315 (60) $[M+H]^+$, 221 (20).

HR-MS (ESI) *m/z* calc. for $C_{20}H_{15}N_2O_2$ $[M+H]^+$: 315.1128, found: 315.1128.

The analytical data are in accordance with those previously reported in the literature.[62]

2-[6-Methyl-1-oxo-3-phenylisoquinolin-2(1*H*)-yl]-pyridine-2-oxide (34ba)

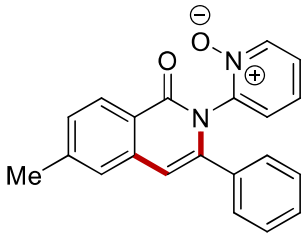

The general procedure **A** was followed using benzamide **33b** (114 mg, 0.50 mmol) and alkyne **117a** (102 mg, 1.00 mmol). Purification by column chromatography on silica gel (dichloromethane/acetone: 3/1) yielded **34ba** (121 mg, 73%) as a white solid.

M. p.: 220–221 °C.

^{1}H-NMR (300 MHz, $CDCl_3$): δ = 8.29 (d, J = 8.0 Hz, 1H), 8.21-8.10 (m, 1H), 7.43–7.36 (m, 2H), 7.34–7.27 (m, 2H), 7.25–7.17 (m, 3H), 7.17–7.10 (m, 2H), 7.06–6.97 (m, 1H), 6.52 (s, 1H), 2.48 (s, 3H).

^{13}C-NMR (125 MHz, $CDCl_3$): δ = 161.8 (C_q), 145.7 (C_q), 143.9 (C_q), 142.5 (C_q), 140.0 (CH), 137.0 (C_q), 134.8 (C_q), 128.8 (CH), 128.5 (CH), 128.2 (CH), 128.0 (CH), 127.8 (CH), 127.6 (CH), 126.0 (CH), 125.1 (CH), 125.0 (CH), 122.6 (C_q), 107.8 (CH), 21.9 (CH_3).

IR (ATR): 3059, 1664, 1626, 1486, 1260, 909, 769, 727 cm^{-1}.

MS (EI) *m/z* (relative intensity): 328 (25) $[M]^+$, 283 (15), 208 (25), 181 (100), 165 (15), 78 (65).

HR-MS (EI) *m/z* calc. for $C_{21}H_{16}N_2O_2$ $[M]^+$: 328.1212, found: 328.1213.

The analytical data are in accordance with those previously reported in the literature.[62]

2-[6-Trifluoromethyl-1-oxo-3-phenylisoquinolin-2(1*H*)-yl]-pyridine-2-oxide (34ca)

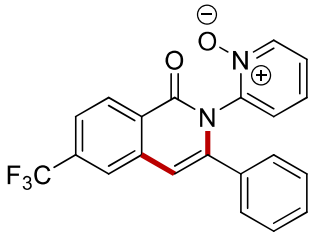

The general procedure **B** was followed using benzamide **33c** (141 mg, 0.50 mmol) and alkyne **117a** (102 mg, 1.00 mmol). Purification by column chromatography on silica gel (dichloromethane/acetone: 3/1) yielded **34ca** (97.2 mg, 51%) as a white solid.

M. p.: 190–191 °C.

^{1}H-NMR (400 MHz, $CDCl_3$): δ = 8.57–8.52 (m, 1H), 8.24 (d, J = 6.4 Hz, 1H), 7.87–7.82 (m, 1H), 7.74–7.66 (m, 1H), 7.44–7.37 (m, 2H), 7.32–7.22 (m, 3H), 7.21–7.14 (m, 2H), 7.13–7.07 (m, 1H), 6.66 (s, 1H).

^{13}C-NMR (100 MHz, $CDCl_3$): δ = 161.1 (C_q), 145.1 (C_q), 144.3 (C_q), 140.1 (CH), 137.1 (C_q), 134.9 (q, $^{2}J_{C–F}$ = 32.6 Hz, C_q), 134.3 (C_q), 129.5 (CH), 129.5 (CH), 128.4 (CH), 127.9 (CH), 127.6 (CH), 127.1 (C_q), 125.7 (CH), 125.3 (CH), 125.0 (q, $^{1}J_{C–F}$ = 273.4 Hz, C_q), 123.6 (q, $^{3}J_{C–F}$ = 3.9 Hz, CH), 123.1 (q, $^{3}J_{C–F}$ = 3.2 Hz, CH), 107.5 (CH).

^{19}F-NMR (376 MHz, $CDCl_3$) δ = –63.13 (s).

IR (ATR): 1672, 1490, 1431, 1319, 1126, 920, 729, 698 cm^{-1}.

MS (EI) *m/z* (relative intensity): 382 (30) $[M]^+$, 365 (20), 337 (20), 262 (30), 181 (100), 78 (85).

HR-MS (EI) *m/z* calc. for $C_{21}H_{13}F_3N_2O_2$ $[M]^+$: 382.0929, found: 382.0928.

The analytical data are in accordance with those previously reported in the literature.[164c]

2-[6-Bromo-1-oxo-3-phenylisoquinolin-2(1*H*)-yl]-pyridine-2-oxide (34da)

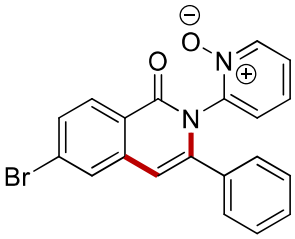

The general procedure **B** was followed using benzamide **33d** (146 mg, 0.50 mmol) and alkyne **117a** (102 mg, 1.00 mmol). Purification by column chromatography on silica gel (dichloromethane/acetone: 3/1) yielded **34da** (127 mg, 65%) as a white solid.

M. p.: 212–215 °C.

^{1}H-NMR (300 MHz, $CDCl_3$): δ = 8.24 (d, J = 8.6 Hz, 1H), 8.19 (d, J = 6.2 Hz, 1H), 7.69 (d, J = 1.9 Hz, 1H), 7.56 (dd, J = 8.6, 1.9 Hz, 1H), 7.41–7.34 (m, 2H), 7.30–7.17 (m, 3H), 7.17–7.09 (m, 2H), 7.09–7.00 (m, 1H), 6.49 (s, 1H).

^{13}C-NMR (125 MHz, $CDCl_3$): δ = 161.2 (C_q), 145.1 (C_q), 144.0 (C_q), 139.9 (CH), 138.3 (C_q), 134.3 (C_q), 130.2 (CH), 130.0 (CH), 129.2 (CH), 128.6 (CH), 128.4 (C_q), 128.1 (CH), 127.7 (CH), 127.5 (CH), 125.4 (CH), 124.9 (CH), 123.5 (C_q), 106.7 (CH).

IR (ATR): 1666, 1627, 1491, 1428, 1368, 1255, 900, 727 cm^{-1}.

MS (EI) *m/z* (relative intensity): 394 (10) [M^+] (^{81}Br), 392 (10) [M^+] (^{79}Br), 377 (15), 349 (15), 274 (10), 268 (15), 181 (100), 165 (10), 78 (55).

HR-MS (EI) *m/z* calc. for $C_{20}H_{13}{}^{79}BrN_2O_2$ [M^+] 392.0160, found 392.0160.

The analytical data are in accordance with those previously reported in the literature.[62]

2-[5,7-Dimethoxy-1-oxo-3-phenylisoquinolin-2(1*H*)-yl]-pyridine-2-oxide (34ea)

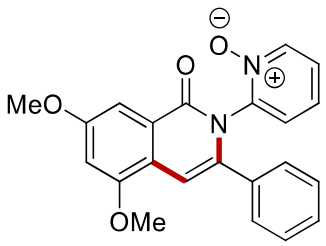

The general procedure **A** was followed using benzamide **33e** (137 mg, 0.50 mmol) and alkyne **117a** (102 mg, 1.00 mmol). Purification by column chromatography on silica gel (dichloromethane/acetone: 3/1) yielded **34ea** (150 mg, 80%) as a white solid.

M. p.: 246–247 °C.

^{1}H-NMR (300 MHz, $CDCl_3$): δ = 8.25–8.18 (m, 1H), 7.42 (d, J = 2.4 Hz, 1H), 7.40–7.34 (m, 2H), 7.23–7.15 (m, 3H), 7.15–7.06 (m, 2H), 7.06–6.99 (m, 1H), 6.92 (d, J = 0.6 Hz, 1H), 6.73 (d, J = 2.3 Hz, 1H), 3.89 (s, 3H), 3.88 (s, 3H).

^{13}C-NMR (125 MHz, $CDCl_3$): δ = 161.2 (C_q), 159.4 (C_q), 155.9 (C_q), 145.7 (C_q), 139.8 (CH), 139.4 (C_q), 135.2 (C_q), 128.6 (CH), 128.0 (CH), 127.9 (CH), 127.4 (CH), 126.4 (C_q), 125.2 (CH), 124.7 (CH), 122.6 (C_q), 103.8 (CH), 102.4 (CH), 99.6 (CH), 55.9 (CH_3), 55.6 (CH_3).

IR (ATR): 1664, 1606, 1488, 1433, 1366, 1046, 784, 753 cm^{-1}.

MS (EI) *m/z* (relative intensity): 374 (15) [$M]^+$, 330 (10), 269 (10), 254 (15), 181 (100), 78 (60).

HR-MS (EI) *m/z* calc. for $C_{22}H_{18}N_2O_4$ [$M]^+$: 374.1267, found: 374.1264.

2-[4-Oxo-6-phenylthieno[3,2-c]pyridin-5(4*H*)-yl]-pyridine-2-oxide (34fa)

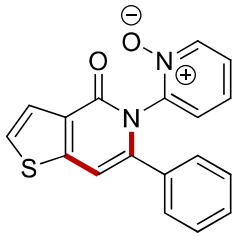

The general procedure **B** was followed using 2-(thiophene-3-carboxamido)pyridine 1-oxide **33f** (110 mg, 0.50 mmol) and alkyne **117a** (102 mg, 1.00 mmol). Purification by column chromatography on silica gel (dichloromethane/acetone: 5/1) yielded **34fa** (87.0 mg, 54%) as a white solid.

M. p.: 215–218 °C.

^{1}H-NMR (300 MHz, $CDCl_3$): δ = 8.22–8.17 (m, 1H), 7.67 (dd, J = 5.3, 0.7 Hz, 1H), 7.40–7.35 (m, 2H), 7.30 (d, J = 5.3 Hz, 1H), 7.25–7.19 (m, 3H), 7.16–7.09 (m, 2H), 7.09–7.03 (m, 1H), 6.78 (d, J = 0.6 Hz, 1H).

^{13}C-NMR (125 MHz, $CDCl_3$): δ = 158.1 (C_q), 148.5 (C_q), 145.3 (C_q), 143.5 (C_q), 140.0 (CH), 134.5 (C_q), 129.4 (C_q), 129.3 (CH), 128.3 (CH), 127.9 (CH), 127.7 (CH), 125.6 (CH), 125.5 (CH), 125.0 (CH), 124.8 (CH), 103.8 (CH).

IR (ATR): 3072, 1664, 1584, 1267, 768, 727, 522 cm^{-1}.

MS (EI) *m/z* (relative intensity): 320 (15) $[M]^+$, 275 (15), 200 (35), 181 (100), 171 (20), 78 (60).

HR-MS (EI) *m/z* calc. for $C_{18}H_{12}N_2O_2S$ $[M]^+$: 320.0619, found: 320.0616.

2-[1-Oxo-3-(4-methoxy)-isoquinolin-2(1*H*)-yl]-pyridine-2-oxide (34ab)

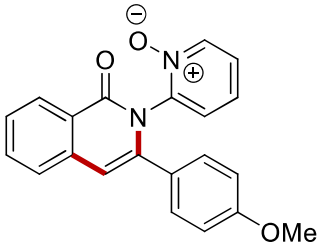

The general procedure **B** was followed using benzamide **33a** (107 mg, 0.50 mmol) and alkyne **117b** (132 mg, 1.00 mmol). Purification by column chromatography on silica gel (dichloromethane/acetone: 3/1) yielded **34ab** (141 mg, 82%) as a white solid.

M. p.: 228–230 °C.

^{1}H-NMR (300 MHz, $CDCl_3$): δ = 8.44–8.38 (m, 1H), 8.25–8.19 (m, 1H), 7.72–7.64 (m, 1H), 7.56–7.51 (m, 1H), 7.50–7.45 (m, 1H), 7.35–7.30 (m, 2H), 7.18–7.11 (m, 2H), 7.11–7.05 (m, 1H), 6.76–6.70 (m, 2H), 6.57 (s, 1H), 3.74 (s, 3H).

^{13}C-NMR (125 MHz, $CDCl_3$): δ = 162.0 (C_q), 160.0 (C_q), 145.6 (C_q), 142.4 (C_q), 140.0 (CH), 137.2 (C_q), 133.3 (CH), 129.3 (CH), 128.3 (CH), 127.7 (CH), 127.3 (C_q), 126.9 (CH), 126.2 (CH), 125.4 (CH), 125.1 (CH), 124.8 (C_q), 113.6 (CH), 107.8 (CH), 55.1 (CH_3).

IR (ATR): 2359, 2010, 1670, 1511, 1251, 1028, 762, 561 cm^{-1}.

MS (ESI) *m/z* (relative intensity): 368 (23), 367 (100) $[M+Na]^+$, 345 (30) $[M+H]^+$, 337 (5).

HR-MS (ESI) *m/z* calc. for $C_{21}H_{17}N_2O_3$ $[M+H]^+$: 345.1234, found: 345.1232.

2-[3-(4-(*tert*-Butyl)phenyl)-1-oxoisoquinolin-2(1*H*)-yl]-pyridine-2-oxide (34ac)

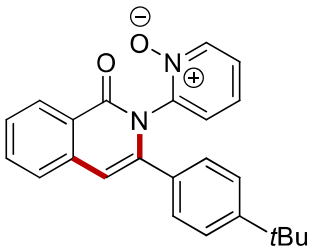

The general procedure **B** was followed using benzamide **33a** (136 mg, 0.50 mmol) and alkyne **117c** (158 mg, 1.00 mmol). Purification by column chromatography on silica gel (dichloromethane/acetone: 4/1) yielded **34ac** (119 mg, 64%) as a white solid.

M. p.: 162–165 °C.

^{1}H-NMR (400 MHz, $CDCl_3$): δ = 8.41 (ddt, J = 8.0, 1.4, 0.7 Hz, 1H), 8.21 (dd, J = 6.9, 1.5 Hz, 1H), 7.67 (ddd, J = 8.0, 7.1, 1.4 Hz, 1H), 7.53 (ddd, J = 8.3, 1.1, 0.5 Hz, 1H), 7.47 (ddd, J = 8.2, 7.1, 1.2 Hz, 1H), 7.32–7.28 (m, 2H), 7.23–7.19 (m, 2H), 7.16–7.11 (m, 2H), 7.06 (ddd, J = 8.6, 6.9, 1.5 Hz, 1H), 6.60–6.56 (m, 1H), 1.22 (s, 9H).

^{13}C-NMR (100 MHz, $CDCl_3$): δ = 162.0 (C_q), 152.2 (C_q), 145.6 (C_q), 142.7 (C_q), 140.0 (CH), 137.2 (C_q), 133.3 (CH), 132.0 (C_q), 128.4 (CH), 127.8 (CH), 127.7 (CH), 127.0 (CH), 126.2 (CH), 125.3 (CH), 125.1 (CH), 124.9 (CH), 124.9 (C_q), 108.0 (CH), 34.6 (C_q), 31.1 (CH_3).

IR (ATR): 3063, 2962, 1671, 1626, 1482, 1432, 1272, 759 cm^{-1}.

MS (EI) *m/z* (relative intensity): 370 (20) $[M]^+$, 238 (20), 237 (100), 194 (25), 78 (40), 43 (30).

HR-MS (EI) *m/z* calc. for $C_{24}H_{22}N_2O_2$ $[M]^+$: 370.1681, found: 370.1688.

2-[3-*n*-Pentyl-1-oxoisoquinolin-2(1*H*)-yl]-pyridine-2-oxide (34ad)

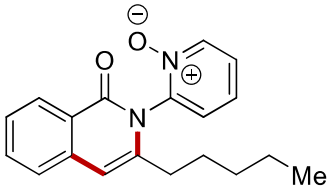

The general procedure **B** was followed using benzamide **33a** (107 mg, 0.50 mmol) and alkyne **117d** (96.2 mg, 1.00 mmol). Purification by column chromatography on silica gel (dichloromethane/acetone: 3/1) yielded **34ad** (85.2 mg, 55%) as a yellow oil.

^{1}H-NMR (400 MHz, $CDCl_3$): δ = 8.43–8.37 (m, 1H), 8.36–8.29 (m, 1H), 7.69–7.60 (m, 1H), 7.50–7.44 (m, 2H), 7.44–7.40 (m, 1H), 7.40–7.36 (m, 2H), 6.44 (s, 1H), 2.41–2.09 (m, 2H), 1.62–1.47 (m, 2H), 1.28–1.18 (m, 4H), 0.84 (t, J = 6.9 Hz, 3H).

^{13}C-NMR (100 MHz, $CDCl_3$): δ = 162.6 (C_q), 144.5 (C_q), 142.5 (C_q), 140.6 (CH), 137.5 (C_q), 133.2 (CH), 128.2 (CH), 128.0 (CH), 126.3 (CH), 126.0 (CH), 125.7 (CH), 125.3 (CH), 124.4 (C_q), 104.9 (CH), 31.9 (CH_2), 31.2 (CH_2), 27.2 (CH_2), 22.2 (CH_2), 13.8 (CH_3).

IR (ATR): 2358, 2001, 1667, 1634, 1258, 824, 773, 749 cm^{-1}.

MS (EI) *m/z* (relative intensity): 308 (45) $[M]^+$, 291 (80), 251 (60), 234 (100), 171 (35), 78 (60).

HR-MS (EI) *m/z* calc. for $C_{19}H_{20}N_2O_2$ $[M]^+$: 308.1525, found: 308.1529.

2-(2-(phenylethynyl)benzamido)pyridine 1-oxide (184)

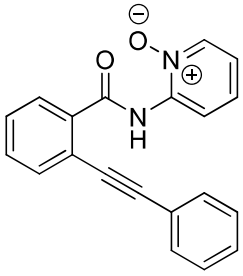

M. p.: 126–128 °C.

^{1}H-NMR (300 MHz, $CDCl_3$): δ = 11.42 (s, 1H), 8.67 (dd, J = 8.5, 1.8 Hz, 1H), 8.26 (dd, J = 6.5, 1.5 Hz, 1H), 8.09–7.94 (m, 1H), 7.71–7.62 (m, 3H), 7.57–7.39 (m, 2H), 7.36–7.29 (m, 4H), 6.98 (ddd, J = 8.0, 6.4, 2.0 Hz, 1H)

^{13}C-NMR (100 MHz, $CDCl_3$): δ = 165.5 (C_q), 144.8 (C_q), 137.2 (CH), 135.1 (C_q), 134.2 (CH), 132.0 (CH), 131.6 (CH), 129.7 (CH), 128.9 (CH), 128.6 (CH), 128.3 (CH), 127.6 (CH), 122.6 (C_q), 121.2 (C_q), 118.9 (CH), 115.4 (CH), 96.8 (C_q), 86.4 (C_q).

IR (ATR): 3055, 1672, 1503, 1426, 1265, 1208, 757, 735 cm^{-1}.

MS (EI) *m/z* (relative intensity): 651 (70) $[2M+Na]^+$, 337 (100) $[M+Na]^+$, 315 (90) $[M+H]^+$.

HR-MS (EI) *m/z* calc. for $C_{24}H_{22}N_2O_2$ $[M]^+$: 315.1128, found: 315.1121.

5.4 Electrooxidative Ruthenium-Catalyzed C–H/O–H Annulation by Weak *O*-Coordination

5.4.1 Characterization Data

8-Methyl-3,4-diphenyl-1*H*-isochromen-1-one (90ca)

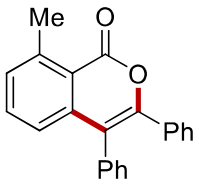

The general procedure **C** was followed using carboxylic acid **89c** (136 mg, 1.0 mmol) and **24a** (89.1 mg, 0.5 mmol) at 80 °C for 18 h. Purification by column chromatography on silica gel (*n*hexane/ethyl acetate: 20/1) yielded **90ca** (140 mg, 90%) as a white solid.

M. p.: 143–144 °C.

^{1}H-NMR (400 MHz, $CDCl_3$): δ = 7.44 (dd, J = 8.1, 7.4 Hz, 1H), 7.41–7.35 (m, 3H), 7.34–7.27 (m, 3H), 7.25–7.13 (m, 5H), 6.99 (dd, J = 8.1, 1.3 Hz, 1H), 2.90 (s, 3H).

^{13}C-NMR (100 MHz, $CDCl_3$): δ = 161.4 (C_q), 150.6 (C_q), 143.4 (C_q), 140.4 (C_q), 134.9 (C_q), 133.6 (CH), 132.9 ($_{Cq}$), 131.3 (CH), 131.0 (CH), 129.0 (CH), 129.0 (CH), 128.7 (CH), 127.9 (CH), 127.7 (CH), 123.6 (CH), 118.9 (C_q), 116.9 (C_q), 23.5 (CH_3).

IR (ATR): 1719, 1616, 1317, 1489, 1264, 732 cm^{-1}.

MS (ESI) *m/z* (relative intensity): 325 (100) $[M+Na]^+$, 313 (60) $[M+H]^+$.

HR-MS (ESI) *m/z* calc. for $C_{22}H_{17}O_2$ $[M+H]^+$: 313.1223, found: 313.1224.

The analytical data are in accordance with those previously reported in the literature.[95]

6-Methoxy-3,4-diphenyl-1*H*-isochromen-1-one (90ba)

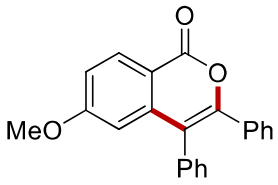

The general procedure **C** was followed using carboxylic acid **89b** (152 mg, 1.0 mmol) and **24a** (89.1 mg, 0.5 mmol) at 100 °C for 24 h. Purification by column chromatography on silica gel (*n*hexane/ethyl acetate: 10/1) yielded **90ba** (98.5 mg, 60%) as a white solid.

M. p.: 178–180 °C.

^{1}H-NMR (400 MHz, $CDCl_3$): δ = 8.28 (d, J = 8.0 Hz, 1H), 7.43–7.37 (m, 3H), 7.34–7.28 (m, 3H), 7.26–7.21 (m, 2H), 7.21–7.13 (m, 3H), 6.95 (d, J = 1.5 Hz, 1H), 2.35 (s, 3H).

^{13}C-NMR (125 MHz, $CDCl_3$): δ = 164.6 (C_q), 161.9 (C_q), 151.5 (C_q), 141.1 (C_q), 134.3 (C_q), 133.0 (C_q), 131.9 (CH), 131.1 (CH), 129.2 (CH), 129.0 (CH), 128.9 (CH), 128.1 (CH), 127.8 (CH), 116.7 (C_q), 115.6 (CH), 113.6 (C_q), 108.4 (CH), 55.4 (CH_3).

IR (ATR): 1717, 1604, 1488, 1264, 905, 728 cm^{-1}.

MS (ESI) *m/z* (relative intensity): 351 (30) $[M+Na]^+$, 329 (100) $[M+H]^+$.

HR-MS (ESI) *m/z* calc. for $C_{22}H_{17}O_3$ $[M+H]^+$: 329.1172, found: 329.1176.

The analytical data are in accordance with those previously reported in the literature.[95]

3,4-Diethyl-8-methyl-1*H*-isochromen-1-one (90cb)

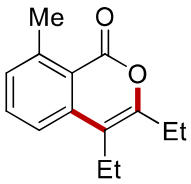

The general procedure **C** was followed using carboxylic acid **89c** (136 mg, 1.00 mmol) and alkyne **24b** (41.1 mg, 0.50 mmol). Purification by column chromatography on silica gel (*n*hexane/ethyl acetate: 20/1) yielded **90cb** (91.9 mg, 85%) as a colourless oil.

^{1}H-NMR (300 MHz, $CDCl_3$): δ = 7.51 (dd, J = 8.1, 7.4 Hz, 1H), 7.32 (d, 1H), 7.18 (dt, J = 7.4, 0.9 Hz, 1H), 2.61–2.50 (m, 4H), 1.23 (t, J = 7.5 Hz, 3H), 1.13 (t, J = 7.5 Hz, 3H).

^{13}C-NMR (125 MHz, $CDCl_3$): δ = 161.90 (C_q), 154.42 (C_q), 143.47 (C_q), 138.99 (C_q), 133.45 (CH), 129.85 (CH), 120.25 (CH), 119.19 (C_q), 112.70 (C_q), 23.94 (CH_2), 23.60 (CH_3), 19.58 (CH_2), 14.17 (CH_3), 12.47 (CH_3).

IR (ATR): 2967, 2932, 2716, 2648, 2571, 1469, 1268, 1023, 806, 707 cm^{-1}.

MS (ESI) *m/z* (relative intensity): 216 (100) $[M]^+$, 201 (90).

HR-MS (ESI) *m/z* calc. for $C_{14}H_{16}O_2$ $[M]^+$: 216.1150, found: 216.1147.

The analytical data are in accordance with those previously reported in the literature.[95]

4-Ethyl-8-methyl-3-phenyl-1*H*-isochromen-1-one (90cc)

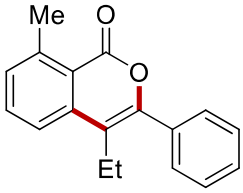

The general procedure **C** was followed using carboxylic acid **89c** (136 mg, 1.00 mmol) and alkyne **24c** (65.1 mg, 0.50 mmol). Purification by column chromatography on silica gel (*n*hexane/ethyl acetate: 20/1) yielded **90cc** (123 mg, 93%) and **90cc'** (6.6 mg, 5%) as white solids.

M. p.: 119-121 °C.

^{1}H-NMR (300 MHz, $CDCl_3$): δ = 7.69–7.61 (m, 1H), 7.61–7.55 (m, 2H), 7.55–7.51 (m, 1H), 7.51–7.42 (m, 3H), 7.37–7.32 (m, 1H), 2.90 (s, 3H), 2.79–2.64 (m, 2H), 1.28 (t, J = 7.4 Hz, 3H).

^{13}C-NMR (100 MHz, $CDCl_3$): δ = 161.65 (C_q), 151.11 (C_q), 143.89 (C_q), 139.11 (C_q), 133.81 (CH), 133.62 (C_q), 130.87 (CH), 129.26 (CH), 128.93 (CH), 128.31 (CH), 121.44 (CH), 119.82 (C_q), 115.10 (C_q), 23.74 (CH_3), 20.38 (CH_2), 14.66 (CH_3).

IR (ATR): 3058, 2967, 2930, 1717, 1467, 1094, 1031, 699 cm^{-1}.

MS (EI) *m/z* (relative intensity): 264 (100), 249 (40), 221 (90).

HR-MS (ESI) *m/z* calc. for $C_{18}H_{16}O_2$ $[M+H]^+$: 264.1150, found: 264.1161.

3-Ethyl-8-methyl-4-phenyl-1*H*-isochromen-1-one (90cc')

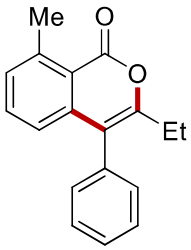

M. p.: 119-121 °C.

^{1}H-NMR (400 MHz, $CDCl_3$): δ = 7.47–7.35 (m, 4H), 7.26–7.21 (m, 3H), 6.78–6.72 (m, 1H), 2.85 (s, 3H), 2.35–2.27 (m, 2H), 1.15 (t, J = 7.6 Hz, 3H).

^{13}C-NMR (100 MHz, $CDCl_3$): δ = 162.1 (C_q), 155.8 (C_q), 143.3 (C_q), 140.4 (C_q), 135.1 (C_q), 133.6 (CH), 130.6 (CH), 130.3 (CH), 128.9 (CH), 127.9 (CH), 123.0 (CH), 118.6 (C_q), 115.7 (C_q), 24.9 (CH_2), 23.5 (CH_3), 12.4 (CH_3).

IR (ATR): 3057, 2970, 2932, 1720, 1648, 1470, 1185, 1021, 805, 704 cm^{-1}.

MS (EI) *m/z* (relative intensity): 264 (100) [M]+, 235 (80), 179 (70).

HR-MS (ESI) *m/z* calc. for $C_{18}H_{16}O_2$ $[M]^+$: 264.1150, found: 264.1147.

4-Butyl-3-(4-methylphenyl)-8-methyl-1*H*-isochromen-1-one (90cd)

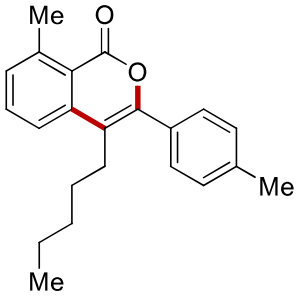

The general procedure **C** was followed using carboxylic acid **89c** (136 mg, 1.00 mmol) and alkyne **24d** (93.2 mg, 0.50 mmol). Purification by column chromatography on silica gel (*n*hexane/ethyl acetate: 20/1) yielded **90cd** (130 mg, 81%) and **90cd'** (9.6 mg, 6%) as white solids.

M. p.: 110–113 °C.

^{1}H-NMR (300 MHz, $CDCl_3$): δ = 7.64 (t, *J* = 7.8 Hz, 1H), 7.52–7.43 (m, 3H), 7.35–7.26 (m, 3H), 2.89 (s, 3H), 2.76–2.58 (m, 2H), 2.44 (s, 3H), 1.75–1.52 (m, 2H), 1.45–1.26 (m, 4H), 0.95–0.84 (m, 3H).

^{13}C-NMR (75 MHz, $CDCl_3$): δ = 161.78 (C_q), 151.45 (C_q), 143.79 (C_q), 139.49 (C_q), 139.22 (C_q), 133.70 (CH), 130.81 (C_q), 130.68 (CH), 128.94 (CH), 128.91 (CH), 121.41 (CH), 119.74 (C_q), 113.69 (C_q), 31.83 (CH_2), 29.61 (CH_2), 27.21 (CH_2), 23.74 (CH_3), 22.32 (CH_2), 21.41 (CH_3), 14.02 (CH_3).

IR (ATR): 2954, 2925, 1720, 1591, 1471, 1081, 1036, 803, 731, 499 cm^{-1}.

MS (ESI) *m/z* (relative intensity): 320 (70) [M]+, 292 (10), 263 (95), 235 (100).

HR-MS (ESI) *m/z* calc. for $C_{22}H_{24}O_2$ $[M]^+$: 320.1776, found: 320.1779.

8-Methyl-3-pentyl-4-(*p*-methylphenyl)-1*H*-isochromen-1-one (90cd')

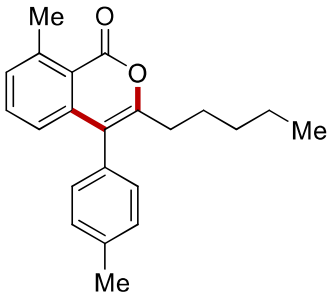

M. p.: 110–113 °C.

^{1}H-NMR (400 MHz, $CDCl_3$): δ = 7.36 (t, J = 7.8 Hz, 1H), 7.26–7.24 (m, 2H), 7.20 (d, J = 7.4 Hz, 1H), 7.11–7.08 (m, 2H), 6.76 (d, J = 8.0 Hz, 1H), 2.84 (s, 3H), 2.42 (s, 3H), 2.31–2.27 (m, 2H), 1.65–1.57 (m, 2H), 1.22–1.16 (m, 4H), 0.83–0.79 (m, 3H).

^{13}C-NMR (100 MHz, $CDCl_3$): δ = 162.2 (C_q), 154.9 (C_q), 143.3 (C_q), 140.6 (C_q), 137.6 (C_q), 133.5 (CH), 132.0 (C_q), 130.5 (CH), 130.2 (CH), 129.5 (CH), 128.9 (CH), 123.0 (CH), 118.6 (C_q), 116.1 (C_q), 31.3 (CH_2), 31.2 (CH_2), 27.3 (CH_2), 23.5 (CH_3), 22.3 (CH_2), 21.3 (CH_3), 13.9 (CH_3).

IR (ATR): 2955, 2926, 2857, 1726, 1645, 1591, 1496, 1022, 805, 520 cm^{-1}.

MS (ESI) *m/z* (relative intensity): 320 (100) $[M]^+$, 263 (20), 249 (90), 235 (30).

HR-MS (ESI) *m/z* calc. for $C_{22}H_{24}O_2$ $[M]^+$: 320.1776, found: 320.1776.

4-Butyl-3-(4-chlorophenyl)-8-methyl-1*H*-isochromen-1-one (90ce)

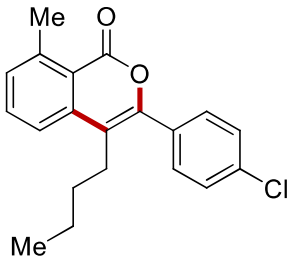

The general procedure **C** was followed using carboxylic acid **89c** (136 mg, 1.00 mmol) and alkyne **24e** (103 mg, 0.50 mmol). Purification by column chromatography on silica gel (*n*hexane/ethyl acetate: 20/1) yielded **90ce** (128 mg, 78%) as a white solid.

M. p.: 96–100 °C.

^{1}H-NMR (300 MHz, $CDCl_3$): δ = 7.60 (t, J = 8.1 Hz, 1H), 7.49–7.37 (m, 5H), 7.30 (d, J = 7.4, 1.0 Hz, 1H), 2.83 (s, 3H), 2.65–2.55 (m, 2H), 1.63–1.51 (m, 2H), 1.40–1.26 (m, 2H), 0.87 (t, J = 7.3 Hz, 3H).

^{13}C-NMR (125 MHz, $CDCl_3$): δ = 161.17 (C_q), 149.84 (C_q), 143.73 (C_q), 138.93 (C_q), 135.11 (C_q), 133.67 (CH), 131.94 (C_q), 130.92 (CH), 130.26 (CH), 128.43 (CH), 121.40 (CH), 119.66 (C_q), 114.19 (C_q), 31.98 (CH_2), 26.88 (CH_2), 23.66 (CH_3), 22.70 (CH_2), 13.76 (CH_3).

IR (ATR): 2956, 2928, 2869, 1720, 1489, 1470, 1229, 1093, 1032, 803 cm^{-1}.

MS (EI) *m/z* (relative intensity): 326 (60) $[M]^+$, 283 (50), 255 (30), 248 (100).

HR-MS (ESI) *m/z* calc. for $C_{20}H_{19}ClO_2$ $[M]^+$: 326.1074, found: 326.1069.

The analytical data are in accordance with those previously reported in the literature.[95]

4-Butyl-3-(4-methoxyphenyl)-8-methyl-1*H*-isochromen-1-one (90cf)

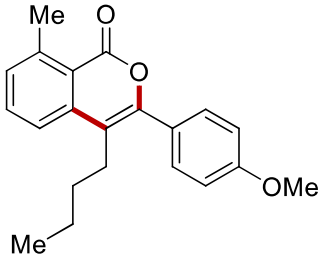

The general procedure **C** was followed using carboxylic acid **89c** (136 mg, 1.00 mmol) and alkyne **24f** (101 mg, 0.50 mmol). Purification by column chromatography on silica gel (*n*hexane/ethyl acetate: 20/1) yielded **90cf** (105 mg, 65%) and **90cf'** (11.3 mg, 7%) as white solids.

M. p.: 72–76 °C.

^{1}H-NMR (300 MHz, $CDCl_3$): δ = 7.59 (dd, J = 8.1, 7.4 Hz, 1H), 7.50–7.42 (m, 3H), 7.30–7.25 (m, 1H), 6.99–6.91 (m, 2H), 3.84 (s, 3H), 2.85 (s, 3H), 2.66–2.57 (m, 2H), 1.63–1.53 (m, 2H), 1.42–1.28 (m, 2H), 0.88 (t, J = 7.3 Hz, 3H).

^{13}C-NMR (125 MHz, $CDCl_3$): δ = 161.61 (C_q), 160.04 (C_q), 151.09 (C_q), 143.60 (C_q), 139.42 (C_q), 133.53 (CH), 130.46 (CH), 130.31 (CH), 126.02 (C_q), 121.27 (CH), 119.57 (C_q), 113.57 (CH), 113.31 (C_q), 55.32 (CH_3), 32.03 (CH_2), 27.00 (CH_2), 23.71 (CH_3), 22.75 (CH_2), 13.81 (CH_3).

IR (ATR): 2956, 2927, 1717, 1510, 1252, 1176, 1032, 842, 804, 522 cm^{-1}.

MS (ESI) *m/z* (relative intensity): 322 (40) $[M]^+$, 294 (30), 279 (35), 251 (100).

HR-MS (ESI) *m/z* calc. for $C_{21}H_{22}O_3$ $[M]^+$: 322.1569, found: 322.1566.

The analytical data are in accordance with those previously reported in the literature.[95]

3-Butyl-4-(4-methoxyphenyl)-8-methyl-1*H*-isochromen-1-one (90cf')

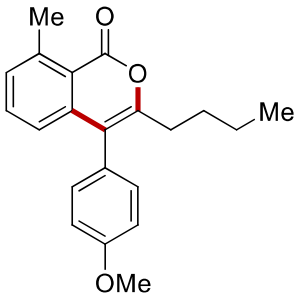

M. p.: 72–76 °C.

^{1}H-NMR (400 MHz, $CDCl_3$): δ = 7.37 (t, J = 7.8 Hz, 1H), 7.22–7.18 (m, 1H), 7.14–7.11 (m, 2H), 7.00–6.96 (m, 2H), 6.77 (ddd, J = 8.0, 1.3, 0.7 Hz, 1H), 3.86 (s, 3H), 2.84 (d, J = 0.9 Hz, 3H), 2.33–2.28 (m, 2H), 1.60–1.54 (m, 2H), 1.26–1.22 (m, 2H), 0.80 (t, J = 7.3 Hz, 3H).

^{13}C-NMR (100 MHz, $CDCl_3$): δ = 162.1 (Cq), 159.2 (C_q), 155.1 (C_q), 143.3 (C_q), 140.8 (C_q), 133.5 (CH), 131.8 (CH), 130.2 (CH), 127.1 (C_q), 123.0 (CH), 118.6 (Cq), 115.8 (Cq), 114.3 (CH), 55.3 (CH_2), 31.0 (CH_2), 29.7 (CH_3), 23.5 (CH_3), 22.6 (CH_2), 13.8 (CH_3).

IR (ATR): 2957, 2928, 2860, 1721, 1512, 1468, 1245, 1176, 1029, 842 cm^{-1}.

MS (ESI) *m/z* (relative intensity): 322 (90) $[M]^+$, 265 (100), 253 (50), 237 (70).

HR-MS (ESI) *m/z* calc. for $C_{21}H_{22}O_3$ $[M]^+$: 322.1569, found: 322.1582.

The analytical data are in accordance with those previously reported in the literature.[95]

Ethyl 4-(4-butyl-8-methyl-1-oxo-1*H*-isochromen-3-yl)benzoate (90cg)

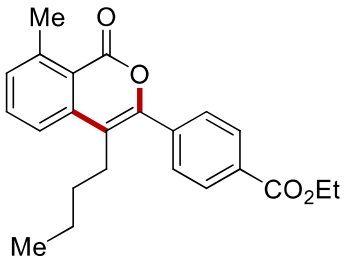

The general procedure **C** was followed using carboxylic acid **89c** (136 mg, 1.00 mmol) and alkyne **24g** (115 mg, 0.50 mmol). Purification by column chromatography on silica gel (*n*hexane/ethyl acetate: 20/1) yielded **90cg** (160 mg, 88%) and **90cg'** (12.8 mg, 7%) as white solids.

M. p.: 106–109 °C.

^{1}H-NMR (300 MHz, $CDCl_3$): δ = 8.14–8.08 (m, 2H), 7.67–7.57 (m, 3H), 7.47 (d, *J* = 8.2 Hz, 1H), 7.35–7.29 (m, 1H), 4.39 (q, *J* = 7.2 Hz, 2H), 2.85 (s, 3H), 2.65–2.58 (m, 2H), 1.63–1.53 (m, 2H), 1.40 (t, *J* = 7.1 Hz, 3H), 1.37–1.28 (m, 2H), 0.86 (t, *J* = 7.3 Hz, 3H).

^{13}C-NMR (125 MHz, $CDCl_3$): δ = 165.84 (C_q), 161.15 (C_q), 149.98 (C_q), 143.84 (C_q), 138.90 (C_q), 137.65 (C_q), 133.74 (CH), 131.11 (CH), 130.92 (C_q), 129.37 (CH), 128.95 (CH), 121.50 (CH), 119.78 (C_q), 114.69 (C_q), 61.20 (CH_2), 32.05 (CH_2), 26.89 (CH_2), 23.71 (CH_3), 22.72 (CH_2), 14.38 (CH_3), 13.78 (CH_3).

IR (ATR): 2957, 2929, 2871, 1716, 1608, 1469, 1270, 1100, 772, 705cm^{-1}.

MS (ESI) *m/z* (relative intensity): 364 (90) $[M]^+$, 321 (10), 293 (25), 249 (100).

HR-MS (ESI) *m/z* calc. for $C_{23}H_{24}O_4$ $[M]^+$: 364.1675, found: 364.1684.

Ethyl 4-(3-butyl-8-methyl-1-oxo-1*H*-isochromen-4-yl)benzoate (90cg')

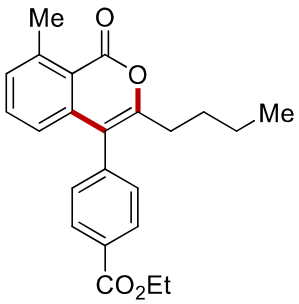

M. p.: 106–109 °C.

^{1}H-NMR (300 MHz, $CDCl_3$): δ = 8.14 (dd, *J* = 8.3, 1.9 Hz, 2H), 7.37 (t, *J* = 7.7 Hz, 1H), 7.34–7.29 (m, 2H), 7.24 (s, 1H), 6.67 (d, *J* = 8.0 Hz, 1H), 4.44–4.38 (m, 2H), 2.84 (s, 3H), 2.30–2.24 (m, 2H), 1.61–1.56 (m, 2H), 1.44–1.39 (m, 3H), 1.25–1.19 (m, 2H), 0.79 (t, *J* = 7.3 Hz, 3H).

^{13}C-NMR (100 MHz, $CDCl_3$): δ = 165.84 (C_q), 161.15 (C_q), 149.98 (C_q), 143.84 (C_q), 138.90 (C_q), 137.65 (C_q), 133.74 (CH), 131.11 (CH), 130.92 (C_q), 129.37 (CH), 128.95(CH), 121.50 (CH), 119.78 (C_q), 114.69 (C_q), 61.20 (CH_2), 32.05 (CH_2), 26.89 (CH_2), 23.71 (CH_3), 22.72 (CH_2), 14.38 (CH_3), 13.78 (CH_3).

IR (ATR): 2958, 2928, 2870, 1717, 1470, 1270, 1100, 1020, 773, 713cm^{-1}.

MS (ESI) *m/z* (relative intensity): 364 (100) $[M]^+$, 307 (20), 280 (25).

HR-MS (ESI) *m/z* calc. for $C_{23}H_{24}O_4$ $[M]^+$: 364.1675, found: 364.1670.

Ethyl 4-(4-butyl-2,8-dimethyl-1-oxo-1,2-dihydroisoquinolin-3-yl)benzoate (88ag)

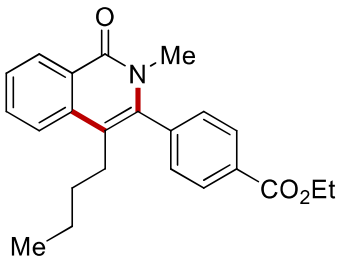

The general procedure **C** was followed using amide **87a** (136 mg, 1.00 mmol) and alkyne **24g** (115 mg, 0.50 mmol). Purification by column chromatography on silica gel (*n*hexane/ethyl acetate: 20/1) yielded **88ag** (76.3 mg, 42%) as an oil.

^{1}H-NMR (400 MHz, $CDCl_3$): δ = 8.55–8.49 (m, 1H), 8.21–8.15 (m, 2H), 7.70–7.66 (m, 2H), 7.53–7.47 (m, 1H), 7.39–7.34 (m, 2H), 4.42 (q, J = 7.1 Hz, 2H), 3.19 (s, 3H), 2.37–2.31 (m, 2H), 1.42 (t, J = 7.1 Hz, 5H), 1.21 (s, 3H), 1.20–1.13 (m, 2H), 0.75 (t, J = 7.3 Hz, 3H).

^{13}C-NMR (100 MHz, $CDCl_3$): δ = 165.97 (C_q), 162.40 (C_q), 139.98 (C_q), 139.16 (C_q), 136.12 (C_q), 132.17 (CH), 130.92 (C_q), 130.17 (C_q), 129.48 (CH), 128.43 (CH), 126.63 (CH), 125.73 (C_q), 123.28 (CH), 115.57 (C_q), 61.35 (CH_2), 34.15 (CH_3), 32.56 (CH_2), 28.16 (CH_2), 27.06 (CH_3), 22.83 (CH_2), 14.34 (CH_3), 13.71 (CH_3).

IR (ATR): 2956, 2931, 2871, 1716, 1648, 1608, 1271, 1100, 1019, 771 cm^{-1}.

MS (ESI) *m/z* (relative intensity): 363 (50) $[M]^+$, 247 (100).

HR-MS (ESI) *m/z* calc. for $C_{23}H_{25}NO_3$ $[M]^+$: 363.1834, found: 363.1843.

5.5 C−H Oxygenation Reactions Enabled by Dual Catalysis with Electrogenerated Hypervalent Iodine Species and Ruthenium Complexes

5.5.1 Characterization Data

2-Hydroxy-*N*-methoxy-*N*-methylbenzamide (106a)

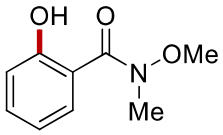

The general procedure **D** was followed using *N*-methoxy-*N*-methylbenzamide **196a** (82.5 mg, 0.50 mmol). Isolation by column chromatography (*n*hexane/ethyl acetate: 5/1→3/1) yielded **106a** (72.5 mg, 80%) as a colourless oil. The same procedure without the addition of electrolyte (nBu$_4$NPF$_6$) yielded **106a** (49.8 mg, 55%) as a colourless oil.

^{1}H-NMR (400 MHz, $CDCl_3$) δ = 10.40 (s, 1H), 7.89 (dd, J = 8.1, 1.7 Hz, 1H), 7.34 (ddd, J = 8.4, 7.2, 1.7 Hz, 1H), 6.95 (dd, J = 8.4, 1.3 Hz, 1H), 6.82 (ddd, J = 8.1, 7.2, 1.3 Hz, 1H), 3.61 (s, 3H), 3.37 (s, 3H).

^{13}C-NMR (100 MHz, $CDCl_3$) δ = 169.8 (C_q), 160.9 (C_q), 133.7 (CH), 129.4 (CH), 118.5 (CH), 117.9 (CH), 114.3 (C_q), 61.1 (CH_3), 34.0 (CH_3).

IR (ATR): 2936, 1625, 1590, 1452, 1249, 973, 754, 527 cm^{-1}.

MS (ESI) *m/z* (relative intensity): 385 (30) $[2M+Na]^+$, 204 (100) $[M+Na]^+$, 182 (100) $[M+H]^+$.

HR-MS (ESI) *m/z* calc. for $C_9H_{12}NO_3^+$ $[M+H]^+$ 182.0814, found 182.0812.

The analytical data are in accordance with those previously reported in the literature.[112]

2-Hydroxy-*N*-methoxy-*N*,4-dimethylbenzamide (106b)

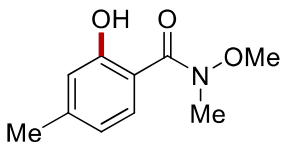

The general procedure **D** was followed using *N*-methoxy-*N*,4-dimethylbenzamide **196b** (89.6 mg, 0.50 mmol). Isolation by column chromatography (*n*hexane/ethyl acetate: 5/1→3/1) yielded **106b** (71.6 mg, 73%) as a pale yellow oil.

^{1}H-NMR (400 MHz, $CDCl_3$) δ = 11.36 (s, 1H), 7.88 (d, J = 8.3 Hz, 1H), 6.82 (d, J = 1.8 Hz, 1H), 6.67 (dd, J = 8.3, 1.8 Hz, 1H), 3.67 (s, 3H), 3.41 (s, 3H), 2.34 (s, 3H).

^{13}C-NMR (100 MHz, $CDCl_3$) δ = 170.0 (C_q), 161.2 (C_q), 144.9 (C_q), 129.3 (CH), 119.7 (CH), 118.2 (CH), 111.5 (C_q), 61.1 (CH_3), 34.0 (CH_3), 21.6 (CH_3).

IR (ATR): 2933, 1584, 1502, 1432, 1351, 1201, 949, 594 cm^{-1}.

MS (ESI) *m/z* (relative intensity): 413 (10) $[2M+Na]^+$, 218 (90) $[M+Na]^+$, 196 (100) $[M+H]^+$.

HR-MS (ESI) *m/z* calc. for $C_{10}H_{14}NO_3^+$ $[M+H]^+$ 196.0969, found 196.0968.

The analytical data are in accordance with those previously reported in the literature.[112]

4-Ethyl-2-hydroxy-*N*-methoxy-*N*-methylbenzamide (106c)

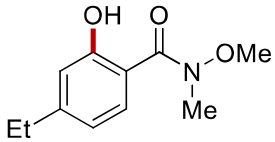

The general procedure **D** was followed using 4-ethyl-*N*-methoxy-*N*-methylbenzamide **196c** (96.6 mg, 0.50 mmol). Isolation by column chromatography (*n*hexane/ethyl acetate: 5/1→3/1) yielded **106c** (74.5 mg, 71%) as a yellow oil. The same procedure without the addition of electrolyte ($n$$Bu_4NPF_6$) yielded **106c** (52.3 mg, 50%) as yellow oil.

^{1}H-NMR (400 MHz, $CDCl_3$) δ = 11.37 (br, 1H), 7.90 (d, J = 8.4 Hz, 1H), 6.84 (d, J = 1.7 Hz, 1H), 6.70 (dd, J = 8.4, 1.7 Hz, 1H), 3.67 (s, 3H), 3.41 (s, 3H), 2.64 (q, J = 7.6 Hz, 2H), 1.25 (t, J = 7.6 Hz, 3H). **^{13}C-NMR** (100 MHz, $CDCl_3$) δ = 170.0 (C_q), 161.4 (C_q), 151.0 (C_q), 129.4 (CH), 118.5 (CH), 116.9 (CH), 111.7 (C_q), 61.1 (CH_3), 34.1 (CH_3), 28.8 (CH_2), 14.7 (CH_3).

IR (ATR): 2968, 1632, 1584, 1499, 1433, 1356, 1202, 974 cm^{-1}.

MS (ESI) *m/z* (relative intensity): 232 (100) $[M+Na]^+$, 210 (100) $[M+H]^+$.

HR-MS (ESI) *m/z* calc. for $C_{11}H_{16}NO_3^+$ $[M+H]^+$ 210.1129, found 210.1125.

The analytical data are in accordance with those previously reported in the literature.[112]

2-Hydroxy-*N*-methoxy-*N*-4,5-trimethylbenzamide (106e)

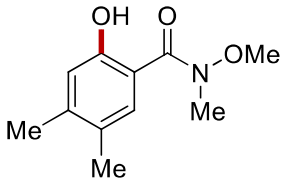

The general procedure **D** was followed using *N*-methoxy-*N*-3,4-trimethylbenzamide **196e** (96.5 mg, 0.50 mmol). Purification by column chromatography on silica gel (*n*hexane/ethyl acetate: 5/1) yielded **106e** (61.5 mg, 59%) as a white solid.

M.p.: 102–104 °C.

^{1}H-NMR (400 MHz, $CDCl_3$) δ = 10.38 (br, 1H), 7.67 (s, 1H), 6.76 (s, 1H), 3.63 (s, 3H), 3.36 (s, 3H), 2.21 (s, 3H), 2.16 (s, 3H).

^{13}C-NMR (100 MHz, $CDCl_3$) δ = 170.2 (C_q), 159.1 (C_q), 143.5 (C_q), 129.7 (CH), 126.6 (C_q), 118.6 (CH), 111.7 (C_q), 61.0 (CH_3), 34.2 (CH_3), 20.1 (CH_3), 19.0 (CH_3).

IR (ATR): 2985, 1736, 1373, 1235, 1044, 916, 730, 607 cm^{-1}.

MS (ESI) *m/z* (relative intensity): 438 (26) $[2M+Na]^+$, 232 (100) $[M+Na]^+$, 210 (90) $[M+H]^+$.

HR-MS (ESI) *m/z* calc. for $C_{11}H_{16}NO_3^+$ $[M+H]^+$ 210.1127, found 210.1125.

4,5-Dichloro-2-hydroxy-*N*-methoxy-*N*-methylbenzamide (106f)

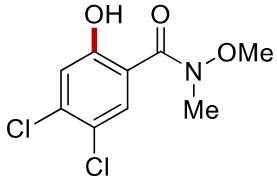

The general procedure **D** was followed using 3,4-dichloro-*N*-methoxy-*N*-methylbenzamide **196f** (117 mg, 0.50 mmol). Purification by column chromatography on silica gel (*n*hexane/ethyl acetate: 5/1) yielded **106f** (77.2 mg, 62%) as a white solid. The same procedure without the addition of electrolyte (nBu_4NPF_6) yielded **106f** (57.5 mg, 46%) as a white solid.

M.p.: 114–117 °C.

^{1}H-NMR (400 MHz, $CDCl_3$) δ = 11.51 (s, 1H), 8.17 (s, 1H), 7.14 (s, 1H), 3.70 (s, 3H), 3.42 (s, 3H).

^{13}C-NMR (100 MHz, $CDCl_3$) δ = 167.8 (C_q), 160.4 (C_q), 137.6 (C_q), 130.7 (CH), 121.9 (C_q), 119.8 (CH), 113.7 (C_q), 61.5 (CH_3), 33.7 (CH_3).

IR (ATR): 2936, 1625, 1570, 1454, 1334, 1180, 978, 649 cm^{-1}.

MS (ESI) *m/z* (relative intensity): 521 (10) $[2M+Na]^+$ (^{35}Cl), 251 (100) $[M+H]^+$ (^{35}Cl).

HR-MS (ESI) *m/z* calc. for $C_9H_{10}{}^{35}Cl_2NO_3^+$ $[M+H]^+$ 250.0030, found 250.0032.

4-Bromo-2-hydroxy-*N*-methoxy-*N*-methylbenzamide (106h)

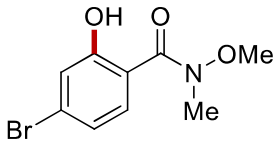

The general procedure **D** was followed using 4-bromo-*N*-methoxy-*N*-methylbenzamide **196h** (121 mg, 0.50 mmol). Purification by column chromatography on silica gel (*n*hexane/ethyl acetate: 5/1) yielded **106h** (107 mg, 82%) as a white solid. The same procedure without the addition of electrolyte (nBu$_4$NPF$_6$) yielded **106h** (74.8 mg, 58%) as a white solid.

M.p.: 92–95 °C.

^{1}H-NMR (300 MHz, $CDCl_3$) δ = 11.21 (br, 1H), 7.89 (d, J = 8.7 Hz, 1H), 7.19 (d, J = 2.0 Hz, 1H), 6.99 (dd, J = 8.7, 2.0 Hz, 1H), 3.66 (s, 3H), 3.41 (s, 3H).

^{13}C-NMR (100 MHz, $CDCl_3$) δ = 169.0 (C_q), 161.9 (C_q), 130.6 (CH), 127.8 (C_q), 121.9 (CH), 121.2 (CH), 113.0 (C_q), 61.3 (CH_3), 33.8 (CH_3).

IR (ATR): 2935, 1621, 1481, 1343, 1236, 1075, 861, 590 cm^{-1}.

MS (ESI) *m/z* (relative intensity): 543 (35) $[2M+Na]^+$ (^{81}Br), 280 (10) $[M+Na]^+$ (^{81}Br), 262 (100) $[M+H]^+$ (^{81}Br).

HR-MS (ESI) *m/z* calc. for $C_9H_{11}{}^{81}BrNO_3^+$ $[M+H]^+$ 261.9898, found 261.9897.

2-Hydroxy-*N*-methoxy-*N*-methyl-5-(trifluoromethyl)benzamide (106l)

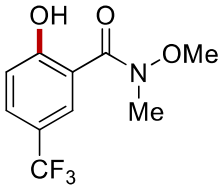

The general procedure **D** was followed using *N*-methoxy-*N*-methyl-3-(trifluoromethyl)benzamide **196l** (117 mg, 0.50 mmol). Purification by column chromatography on silica gel (*n*hexane/ethyl acetate: 5/1) yielded **106l** (56.0 mg, 45%) as a yellow oil.

^{1}H-NMR (400 MHz, $CDCl_3$) δ = 11.83 (s, 1H), 8.37 (d, J = 2.3 Hz, 1H), 7.63 (dd, J = 8.8, 2.3 Hz, 1H), 7.12–7.06 (m, 1H), 3.70 (s, 3H), 3.45 (s, 3H).

^{13}C-NMR (100 MHz, $CDCl_3$) δ = 168.5 (C_q), 163.9 (C_q), 130.5 (q, $^{3}J_{C–F}$ = 3.4 Hz, CH), 127.5 (q, $^{3}J_{C–F}$ = 3.4 Hz, CH), 124.1 (q, $^{1}J_{C–F}$ = 271.1 Hz, C_q), 120.8 (q, $^{2}J_{C–F}$ = 33.0 Hz, C_q), 118.7 (CH), 113.8 (C_q), 61.4 (CH_3), 33.8 (CH_3).

^{19}F-NMR (376 MHz, $CDCl_3$) δ = –61.74 (s).

IR (ATR): 2956, 1747, 1460, 1374, 1237, 1048, 742, 385 cm^{-1}.

MS (ESI) *m/z* (relative intensity): 271 (80) $[M+Na]^+$, 250 (100) $[M+H]^+$.

HR-MS (ESI) *m/z* calc. for $C_{10}H_{11}F_3NO_3^+$ $[M+H]^+$ 250.0684, found 250.0686.

5-Chloro-2-hydroxy-*N*-methoxy-*N*-methylbenzamide (106m)

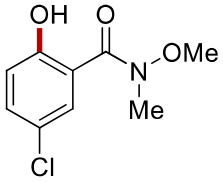

The general procedure **D** was followed using 3-chloro-*N*-methoxy-*N*-methylbenzamide **196m** (99.8 mg, 0.50 mmol). Purification by column chromatography on silica gel (*n*hexane/ethyl acetate: 5/1) yielded **106m** (90.3 mg, 84%) as a white solid.

M.p.: 74–77 °C.

^{1}H-NMR (400 MHz, $CDCl_3$) δ = 11.21 (s, 1H), 8.00 (d, J = 2.6 Hz, 1H), 7.5 (dd, J = 8.9, 2.6 Hz, 1H), 6.95 (d, J = 8.9 Hz, 1H), 3.69 (s, 3H), 3.42 (s, 3H).

^{13}C-NMR (100 MHz, $CDCl_3$) δ = 168.5 (C_q), 159.7 (C_q), 133.7 (CH), 129.0 (CH), 123.3 (C_q), 119.6 (CH), 115.1 (C_q), 61.4 (CH_3), 33.8 (CH_3).

IR (ATR): 2958, 2253, 1630, 1586, 1469, 1249, 903, 722 cm^{-1}.

MS (ESI) *m/z* (relative intensity): 453 (15) $[2M+Na]^+$ (^{35}Cl), 238 (30) $[M+Na]^+$ (^{35}Cl), 216 (100) $[M+H]^+$ (^{35}Cl).

HR-MS (ESI) *m/z* calc. for $C_9H_{11}{}^{35}ClNO_3^+$ $[M+H]^+$ 216.0415, found 216.0422.

5-Bromo-2-hydroxy-*N*-methoxy-*N*-methylbenzamide (106n)

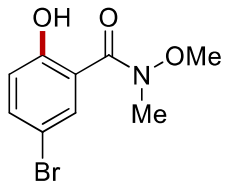

The general procedure **D** was followed using 3-bromo-*N*-methoxy-*N*-methylbenzamide **196n** (121 mg, 0.50 mmol). Purification by column chromatography on silica gel (*n*hexane/ethyl acetate: 5/1) yielded **106n** (97.4 mg, 75%) as a yellow oil.

^{1}H-NMR (400 MHz, $CDCl_3$) δ = 11.19 (s, 1H), 8.10 (d, J = 2.5 Hz, 1H), 7.43 (dd, J = 8.9, 2.5 Hz, 1H), 6.86 (d, J = 8.9 Hz, 1H), 3.65 (s, 3H), 3.38 (s, 3H).

^{13}C-NMR (100 MHz, $CDCl_3$) δ = 168.4 (C_q), 160.1 (C_q), 136.5 (CH), 131.9 (CH), 119.9 (CH), 115.7 (C_q), 110.2 (C_q), 61.4 (CH_3), 33.8 (CH_3).

IR (ATR): 2985, 1737, 1447, 1372, 1233, 1043, 847, 608 cm^{-1}.

MS (ESI) *m/z* (relative intensity): 543 (20) $[2M+Na]^+$ (^{79}Br), 260 (100) $[M+H]^+$ (^{79}Br).

HR-MS (ESI) *m/z* calc. for $C_9H_{11}{}^{79}BrNO_3^+$ $[M+H]^+$ 259.9914, found 259.9917.

4-Iodo-2-hydroxy-*N*-methoxy-*N*-methylbenzamide (106o)

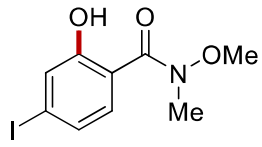

The general procedure **D** was followed using 4-iodo-*N*-methoxy-*N*-methylbenzamide **196o** (146 mg, 0.50 mmol). Purification by column chromatography on silica gel (*n*hexane/ethyl acetate: 5/1) yielded **106o** (99.7 mg, 65%) as a yellow liquid.

^{1}H-NMR (400 MHz, $CDCl_3$) δ = 10.68 (br, 1 H), 7.65 (d, J = 8.6 Hz, 1H), 7.36 (d, J = 1.8 Hz, 1H), 7.16 (dd, J = 8.6, 1.8 Hz, 1H), 3.61 (s, 3H), 3.36 (s, 3H).

^{13}C-NMR (100 MHz, $CDCl_3$) δ = 169.1 (C_q), 161.2 (C_q), 130.4 (CH), 127.8 (CH), 127.2 (CH), 113.6 (C_q), 100.3 (C_q), 61.3 (CH_3), 33.8 (CH_3).

IR (ATR): 2934, 1618, 1476, 1341, 1233, 972, 809, 586 cm^{-1}.

MS (ESI) *m/z* (relative intensity): 634 (16) $[2M+Na]^+$, 330 (16) $[M+Na]^+$, 308 (100) $[M+H]^+$.

HR-MS (ESI) *m/z* calc. for $C_9H_{11}INO_3^+$ $[M+H]^+$ 307.9780, found 307.9778.

The analytical data are in accordance with those previously reported in the literature.[112]

4-(Chloromethyl)-2-hydroxy-*N*-methoxy-*N*-methylbenzamide (106p)

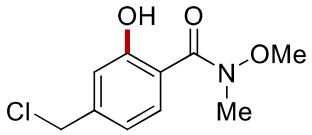

The general procedure **D** was followed using 4-(chloromethyl)-*N*-methoxy-*N*-methylbenzamide **196p** (107 mg, 0.50 mmol). Purification by column chromatography on silica gel (*n*hexane/ethyl acetate: 5/1) yielded **106p** (88.2 mg, 77%) as an orange oil.

^{1}H-NMR (400 MHz, $CDCl_3$) δ = 11.36 (s, 1H), 7.99 (d, J = 8.4 Hz, 1H), 7.02 (d, J = 1.8 Hz, 1H), 6.89 (dd, J = 8.4, 1.8 Hz, 1H), 4.54 (s, 2H), 3.67 (s, 3H), 3.42 (s, 3H).

^{13}C-NMR (100 MHz, $CDCl_3$) δ = 169.3 (C_q), 161.3 (C_q), 143.2 (C_q), 130.1 (CH), 118.5 (CH), 117.8 (CH), 114.0 (C_q), 61.3 (CH_3), 45.3 (CH_2), 33.9 (CH_3).

IR (ATR): 2985, 1636, 1589, 1265, 904, 724, 650, 534 cm^{-1}.

MS (ESI) *m/z* (relative intensity): 252 (20) $[M+Na]^+$ (^{35}Cl), 230 (100) $[M+H]^+$ (^{35}Cl).

HR-MS (ESI) *m/z* calc. for $C_{10}H_{13}{}^{35}ClNO_3^+$ $[M+H]^+$ 230.0585, found 230.0578.

The analytical data are in accordance with those previously reported in the literature.[112]

2-Hydroxy-*N*,*N*,4-trimethylbenzamide (104b)

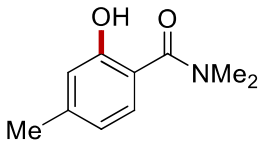

The general procedure **D** was followed using *N*,*N*,4-trimethylbenzamide **103b** (81.5 mg, 0.50 mmol). Purification by column chromatography on silica gel (*n*hexane/ethyl acetate: 5/1→3/1) yielded **104b** (75.2 mg, 84%) as a white solid.

M.p.: 118–120 °C.

^{1}H-NMR (300 MHz, $CDCl_3$) δ = 9.05 (br, 1H), 7.22 (d, J = 8.0 Hz, 1H), 6.82 (d, J = 1.6 Hz, 1H), 6.67 (dd, J = 8.0, 1.6 Hz, 1H), 3.16 (s, 6H), 2.33 (s, 3H).

^{13}C-NMR (100 MHz, $CDCl_3$) δ = 172.1 (C_q), 159.1 (C_q), 143.4 (C_q), 128.4 (CH), 119.2 (CH), 118.1 (CH), 114.2 (C_q), 38.4 (CH_3), 21.5 (CH_3).

IR (ATR): 2935, 1595, 1494, 1452, 1400, 1262, 1199, 754 cm^{-1}.

MS (ESI) *m/z* (relative intensity): 202 (100) $[M+Na]^+$, 180 (85) $[M+H]^+$.

HR-MS (ESI) *m/z* calc. for $C_{10}H_{14}NO_2^+$ $[M+H]^+$ 180.1017, found 180.1019.

The analytical data are in accordance with those previously reported in the literature.[186]

_N_,_N_-Diethyl-2-hydroxy-5-methylbenzamide (104d)

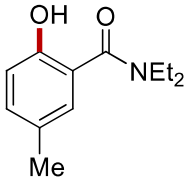

The general procedure **D** was followed using *N*,*N*-diethyl-3-methylbenzamide **103d** (95.6 mg, 0.50 mmol). Purification by column chromatography on silica gel (*n*hexane/ethyl acetate: 5/1→3/1) yielded **104d** (66.3 mg, 64%) as a white solid.

M.p.: 116–119 °C.

^{1}H-NMR (400 MHz, $CDCl_3$) δ = 9.19 (br, 1H), 7.13 (dd, J = 8.3, 2.1 Hz, 1H), 7.07 (d, J = 2.1 Hz, 1H), 6.91 (d, J = 8.3 Hz, 1H), 3.54 (q, J = 7.1 Hz, 4H), 2.30 (s, 3H), 1.29 (t, J = 7.1 Hz, 6H).

^{13}C-NMR (100 MHz, $CDCl_3$) δ = 171.5 (C_q), 156.1 (C_q), 132.9 (CH), 127.6 (C_q), 127.4 (CH), 118.2 (C_q), 117.7 (CH), 42.1 (CH_2), 20.6 (CH_3), 13.4 (CH_3).

IR (ATR): 3160, 2973, 1586, 1486, 1440, 1286, 1244, 820 cm^{-1}.

MS (ESI) *m/z* (relative intensity): 437 (10) $[M+2Na]^+$, 230 (108) $[M+Na]^+$, 208 (80) $[M+H]^+$.

HR-MS (ESI) *m/z* calc. for $C_{12}H_{18}NO_2^+$ $[M+H]^+$ 208,1337, found 208.1332.

The analytical data are in accordance with those previously reported in the literature.[187]

4-Acetyl-2-hydroxy-*N*-methoxy-*N*-methylbenzamide (106q)

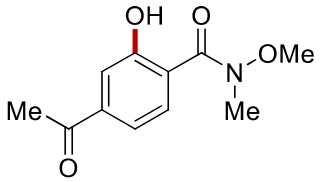

The general procedure **D** was followed using 4-acetyl-*N*-methoxy-*N*-methylbenzamide **196q** (104 mg, 0.50 mmol). Isolation by column chromatography (*n*hexane/ethyl acetate: 8/1→3/1) yielded **106q** (67.8 mg, 61%) as a colourless liquid.

^{1}H-NMR (400 MHz, $CDCl_3$) δ = 10.97 (s, 1H), 8.06–7.90 (d, J = 8.4 Hz, 1H), 7.49 (d, J = 1.8 Hz, 1H), 7.38 (dd, J = 8.4, 1.8 Hz, 1H), 3.61 (s, 3H), 3.39 (s, 3H), 2.56 (s, 3H).

^{13}C-NMR (100 MHz, $CDCl_3$) δ = 197.6 (C_q), 168.7 (C_q), 160.7 (C_q), 140.8 (C_q), 129.8 (CH), 118.0 (C_q), 117.9 (CH), 117.7 (CH), 61.4 (CH_3), 33.8 (CH_3), 26.7 (CH_3).

IR (ATR): 2937, 1684, 1630, 1582, 1415, 1298, 1205, 823 cm^{-1}.

MS (ESI) *m/z* (relative intensity): 246 (30) $[M+Na]^+$, 224 (100) $[M+H]^+$.

HR-MS (ESI) *m/z* calc. for $C_{11}H_{14}NO_4^+$ $[M+H]^+$ 224.0917, found 224.0917

1-(2-Hydroxyphenyl)propan-1-one (197b)

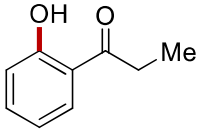

The general procedure **E** was followed using propiophenone **77b** (67.0 mg, 0.50 mmol). Purification by column chromatography on silica gel (*n*hexane/ethyl acetate: 80/1) yielded **197b** (45.1 mg, 60%) as a colorless liquid.

^{1}H-NMR (400 MHz, $CDCl_3$) δ = 12.33 (s, 1H), 7.74 (dd, J = 8.0, 1.6 Hz, 1H), 7.43 (ddd, J = 8.4, 7.2, 1.6 Hz, 1H), 6.95 (dd, J = 8.4, 1.2 Hz, 1H), 6.87 (ddd, J = 8.0, 7.2, 1.2 Hz, 1H), 3.02 (q, J = 7.3 Hz, 2H), 1.22 (t, J = 7.3 Hz, 3H).

^{13}C-NMR (100 MHz, $CDCl_3$) δ = 207.1 (C_q), 162.3 (C_q), 136.1 (CH), 129.8 (CH), 119.2 (C_q), 118.8 (CH), 118.4 (CH), 31.5 (CH_2), 8.16 (CH_3).

IR (ATR): 2984, 1641, 1488, 1265, 1206, 906, 272, 649 cm^{-1}.

MS (ESI) *m/z* (relative intensity): 323 (50) $[2M+Na]^+$, 151 (100) $[M+H]^+$.

HR-MS (ESI) *m/z* calc. for $C_9H_{11}O_2^+$ $[M+H]^+$ 151.0753, found 151.0754.

The analytical data are in accordance with those previously reported in the literature.[114a]

1-(2-Hydroxyphenyl)ethan-1-one (197c)

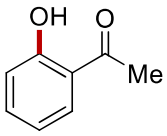

The general procedure **E** was followed using acetophenone **77c** (60.0 mg, 0.50 mmol). Purification by column chromatography on silica gel (*n*hexane/ethyl acetate: 50/1) yielded **197c** (45.0 mg, 66%) as a colorless liquid.

^{1}H-NMR (400 MHz, $CDCl_3$) δ = 12.24 (s, 1H), 7.72 (dd, J = 8.1, 1.7 Hz, 1H), 7.45 (ddd, J = 8.7, 7.2, 1.7 Hz, 1H), 6.96 (dd, J = 8.7, 1.2 Hz, 1H), 6.88 (ddd, J = 8.1, 7.2, 1.2 Hz, 1H), 2.62 (s, 3H).

^{13}C-NMR (100 MHz, $CDCl_3$) δ = 204.5 (C_q), 162.4 (C_q), 136.4 (CH), 130.7 (CH), 119.7 (C_q), 118.9 (CH), 118.4 (CH), 26.6 (CH_3).

IR (ATR): 3054, 1637, 1615, 1446, 1243, 1218, 752, 619 cm^{-1}.

MS (ESI) *m/z* (relative intensity): 283 (8), 157 (7), 135 (100) $[M-H]^-$, 121 (5).

HR-MS (ESI) *m/z* calc. for $C_8H_7O_2^-$ $[M-H]^-$ 135.0452, found 135.0443.

The analytical data are in accordance with those previously reported in the literature.[114a]

1-(2-Hydroxyphenyl)-2-methylpropan-1-one (197d)

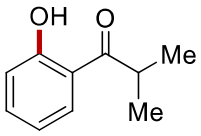

The general procedure **E** was followed using 2-methyl-1-phenylpropan-1-one **77d** (74.0 mg, 0.50 mmol). Purification by column chromatography on silica gel (*n*hexane/ethyl acetate: 100/1) yielded **197d** (54.2 mg, 66%) as a yellow oil.

^{1}H-NMR (300 MHz, $CDCl_3$) δ = 12.55 (s, 1H), 7.82 (dd, J = 8.1, 1.5 Hz, 1H), 7.56–7.43 (m, 1H), 7.02 (d, J = 8.4 Hz, 1H), 6.93 (dd, J = 8.1, 7.1 Hz, 1H), 3.63 (h, J = 6.9 Hz, 1H), 1.28 (d, J = 6.8 Hz, 6H).

^{13}C-NMR (100 MHz, $CDCl_3$) δ = 210.8 (C_q), 163.1 (C_q), 136.2 (CH), 129.8 (CH), 118.8 (CH), 118.7 (CH), 118.2 (C_q), 34.9 (CH), 19.3 (CH_3).

IR (ATR): 2975, 1636, 1446, 1273, 1208, 1151, 982, 754 cm^{-1}.

MS (ESI) *m/z* (relative intensity): 351 (50) $[2M+Na]^+$, 165 (100) $[M+H]^+$.

HR-MS (ESI) *m/z* calc. for $C_{10}H_{13}O_2^+$ $[M+H]^+$ 165.0904, found 165.0910.

The analytical data are in accordance with those previously reported in the literature.[111]

1-(2-Hydroxy-4-methylphenyl)-2,2-dimethylpropan-1-one (197e)

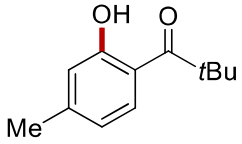

The general procedure **E** was followed using 2,2-dimethyl-1-(*p*-tolyl)propan-1-one **77e** (88.0 mg, 0.50 mmol). Purification by column chromatography on silica gel (*n*hexane/ethyl acetate: 50/1) yielded **197e** (49.2 mg, 51%) as a colorless liquid.

^{1}H-NMR (400 MHz, $CDCl_3$) δ = 12.77 (s, 1H), 7.88 (d, J = 8.4 Hz, 1H), 6.79 (d, J = 1.8 Hz, 1H), 6.64 (dd, J = 8.4, 1.8 Hz, 1H), 2.31 (s, 3H), 1.42 (s, 9H).

^{13}C-NMR (100 MHz, $CDCl_3$) δ = 211.5 (C_q), 163.9 (C_q), 146.7 (C_q), 130.7 (CH), 119.2 (CH), 119.0 (CH), 115.1 (C_q), 44.4 (C_q), 28.7 (CH_3), 21.7 (CH_3).

IR (ATR): 2978, 1632, 1301, 1190, 1136, 973, 801, 403 cm^{-1}.

MS (ESI) *m/z* (relative intensity): 407 (30) $[2M+Na]^+$, 215 (20) $[M+Na]^+$, 193 (100) $[M+H]^+$.

HR-MS (ESI) *m/z* calc. for $C_{12}H_{17}O_2^+$ $[M+H]^+$ 193.1225, found 193.1223.

The analytical data are in accordance with those previously reported in the literature.[111]

1-(4-Chloro-2-hydroxyphenyl)-2,2-dimethylpropan-1-one (197h)

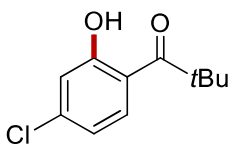

The general procedure **E** was followed using 1-(4-chlorophenyl)-2,2-dimethylpropan-1-one **77k** (98.4 mg, 0.50 mmol). Purification by column chromatography on silica gel (*n*hexane/ethyl acetate: 50/1) yielded **197k** (65.0 mg, 61%) as a colorless liquid.

^{1}H-NMR (400 MHz, $CDCl_3$) δ = 12.83 (s, 1H), 7.92 (d, J = 8.8 Hz, 1H), 6.99 (d, J = 2.2 Hz, 1H), 6.80 (dd, J = 8.8, 2.2 Hz, 1H), 1.41 (s, 9H).

^{13}C-NMR (100 MHz, $CDCl_3$) δ = 211.4 (C_q), 164.5 (C_q), 140.9 (C_q), 131.8 (CH), 119.2 (CH), 118.4 (CH), 115.9 (C_q), 44.6 (C_q), 28.6 (CH_3).

IR (ATR): 2970, 1625, 1561, 1487, 1343, 1179, 960, 799 cm^{-1}.

MS (ESI) *m/z* (relative intensity): 279 (10), 245 (8), 211 (100) $[M–H]^-$ (^{35}Cl).

HR-MS (ESI) *m/z* calc. for $C_{11}H_{12}{}^{35}ClO_2^-$ $[M–H]^-$ 211.0531, found 211.0525.

The analytical data are in accordance with those previously reported in the literature.[111]

1-(4-Fluoro-2-hydroxyphenyl)-2,2-dimethylpropan-1-one (197j)

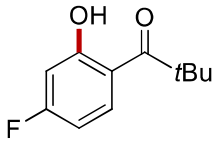

The general procedure **E** was followed using 1-(4-fluorophenyl)-2,2-dimethylpropan-1-one **77j** (90.1 mg, 0.50 mmol). Purification by column chromatography on silica gel (*n*hexane/ethyl acetate: 50/1) yielded **197j** (63.9 mg, 65%) as a colorless liquid.

^{1}H-NMR (400 MHz, $CDCl_3$) δ = 13.06 (d, J = 1.5 Hz, 1H), 8.01 (dd, J = 9.2, 6.5 Hz, 1H), 6.65 (dd, J = 10.4, 2.7 Hz, 1H), 6.54 (ddd, J = 9.2, 7.9, 2.7 Hz, 1H), 1.41 (s, 9H).

^{13}C-NMR (100 MHz, $CDCl_3$) δ = 211.0 (C_q), 166.5 (d, $^{3}J_{C–F}$ = 14.1 Hz, C_q), 166.4 (d, $^{1}J_{C–F}$ = 256.2 Hz, C_q), 133.2 (d, $^{3}J_{C–F}$ = 11.5 Hz, CH), 114.4 (d, $^{4}J_{C–F}$ = 2.6 Hz, C_q), 106.0 (d, $^{2}J_{C–F}$ = 22.5 Hz, CH), 105.5 (d, $^{2}J_{C–F}$ = 23.1 Hz, CH), 44.5 (C_q), 28.7 (CH_3).

^{19}F-NMR (376 MHz, $CDCl_3$) δ = –100.81 (ddd, J = 10.4, 7.9, 6.5 Hz).

IR (ATR): 2975, 1632, 1693, 1259, 1188, 1148, 986, 576 cm^{-1}.

MS (ESI) *m/z* (relative intensity): 195 (100) $[M–H]^-$.

HR-MS (ESI) *m/z* calc. for $C_{11}H_{12}FO_2^-$ $[M–H]^-$ 195.0827, found 195.0828.

The analytical data are in accordance with those previously reported in the literature.[186]

3-Bromo-4-methoxyphenol (109a)

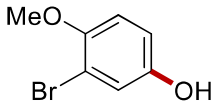

The general procedure **F** was followed using 1-bromo-2-methoxybenzene **200a** (93.0 mg, 0.50 mmol). Purification by column chromatography on silica gel (*n*hexane/ethyl acetate: 5/1) yielded **109a** (52.8 mg, 52%) as a green oil.

^{1}H-NMR (600 MHz, $CDCl_3$) δ = 7.06 (d, J = 2.8 Hz, 1H), 6.77 (d, J = 8.8 Hz, 1H), 6.74 (dd, J = 8.8, 2.8 Hz, 1H), 4.47 (s, 1H), 3.81 (s, 3H).

^{13}C-NMR (150 MHz, $CDCl_3$) δ = 150.4 (C_q), 149.8 (C_q), 120.5 (CH), 115.0 (CH), 113.2 (CH), 112.0 (C_q), 56.9 (CH_3).

IR (ATR): 3363, 2942, 2837, 1495, 1276, 1206, 1048, 744 cm^{-1}.

MS (ESI) *m/z* (relative intensity): 203 (95) $[M+H]^+$ (^{79}Br), 201 (100).

HR-MS (ESI) *m/z* calc. for $C_7H_8{}^{79}BrO_2^+$ $[M+H]^+$ 202.9537, found 202.9536.[188]

3-Chloro-4-methoxyphenol (109b)

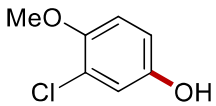

The general procedure **F** was followed using 1-chloro-2-methoxybenzene **200b** (71.0 mg, 0.50 mmol). Purification by column chromatography on silica gel (*n*hexane/ethyl acetate: 5/1) yielded **109b** (31.7 mg, 40%) as a green oil.

^{1}H-NMR (600 MHz, $CDCl_3$) δ = 6.89 (d, J = 3.0 Hz, 1H), 6.79 (d, J = 8.8 Hz, 1H), 6.68 (dd, J = 8.8, 3.0 Hz, 1H), 4.35 (s, 1H), 3.82 (s, 3H).

^{13}C-NMR (150 MHz, $CDCl_3$) δ = 149.6 (C_q), 149.4 (C_q), 123.0 (C_q), 117.6 (CH), 114.2 (CH), 113.5 (CH), 56.8 (CH_3).

IR (ATR): 3125, 2916, 1501, 1265, 1059, 908, 729, 650 cm^{-1}.

MS (ESI) *m/z* (relative intensity): 157 (100) $[M-H]^-$ (^{35}Cl), 142 (50).

HR-MS (ESI) *m/z* calc. for $C_7H_6{}^{35}ClO_2^-$ $[M-H]^-$ 157.0062, found 157.0062.

The analytical data are in accordance with those previously reported in the literature.[189]

5.5.2 Gram-Scale Synthesis of 106a

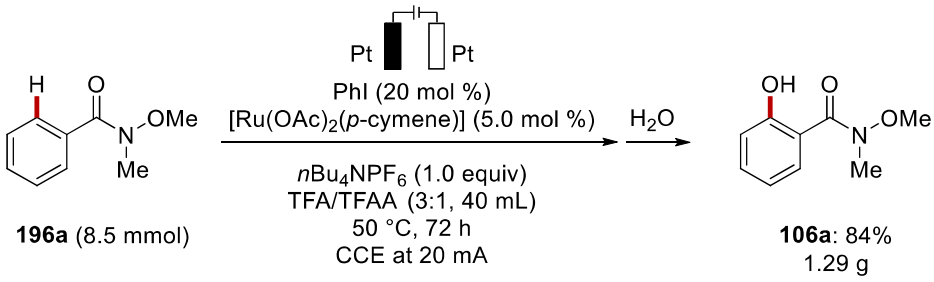

To an undivided two-necked flask (diameter: 40 mm; length: 130 mm; volume: 120 mL) equipped with a teflon-coated magnetic stirring bar and teflon cap, platinum electrodes (25 mm x 50 mm x 0.125 mm), **196a** (1.40 g, 8.5 mmol), PhI **194a** (347 mg, 1.7 mmol), [Ru(OAc)$_2$(*p*-cymene)] **188a** (150 mg, 0.43 mmol), *n*Bu$_4$NPF$_6$ (3.29 g, 8.4 mmol) were added in TFA/TFAA (3:1, 40 mL). Electrocatalysis was performed at 50 °C with a constant current of 20 mA maintained for 72 h. Thereafter, saturated aqueous NaHCO$_3$ (200 mL) was added and the reaction mixture was extracted with EtOAc (3 × 50 mL). The combined organic layers were washed with brine (100 mL), dried over Na$_2$SO$_4$, filtered, and concentrated *in vacuo*. The crude product was purified by column chromatography on silica gel (*n*hexane/ethyl acetate: 6/1) and yielded **106a** (1.29 g, 84%) as a colorless oil.

5.5.3 H/D Exchange Experiment

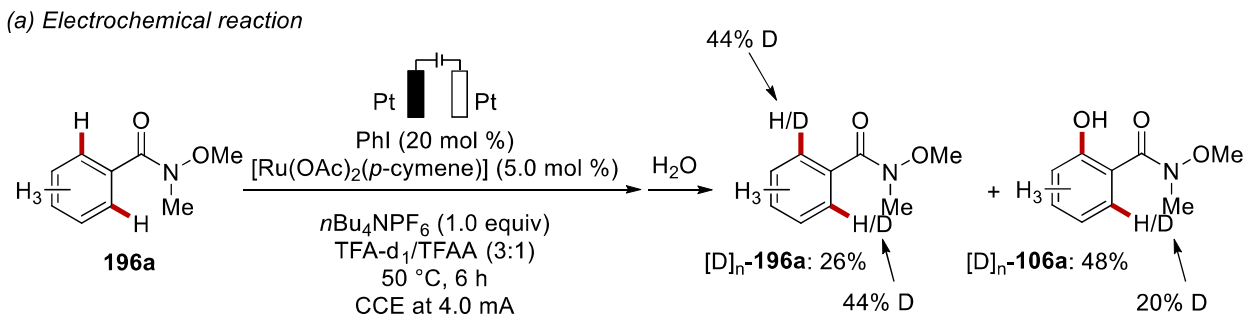

to an undivided cell equipped with Pt electrodes (10 mm x 15 mm x 0.125 mm), **196a** (82.5 mg, 0.50 mmol), PhI **194a** (20.4 mg, 20 mol %), [Ru(OAc)$_2$(*p*-cymene)] **188a** (8.8 mg, 5.0 mol %), *n*Bu$_4$NPF$_6$ (194 mg, 1.0 equiv), and TFA-d$_1$/TFAA (3:1, 3.0 mL) were added. Electrocatalysis was performed at 50 °C with a constant current of 4.0 mA maintained for 6 h. Thereafter, saturated aqueous NaHCO$_3$ (25 mL) was added, and the reaction mixture was extracted with EtOAc (3 × 15 mL). The combined organic layers were washed with brine (25 mL), dried over Na$_2$SO$_4$, filtered, and concentrated *in vacuo*. Column chromatography (*n*hexane/ethyl acetate: 5/1) yielded [D]$_n$-**196a** (21.5 mg, 26%) as a colourless oil and [D]$_n$-**106a** (43.4 mg, 48%) as a colorless oil. The D-incorporation was determined by ^{1}H-NMR spectroscopy (Figures 5.5.1-2).

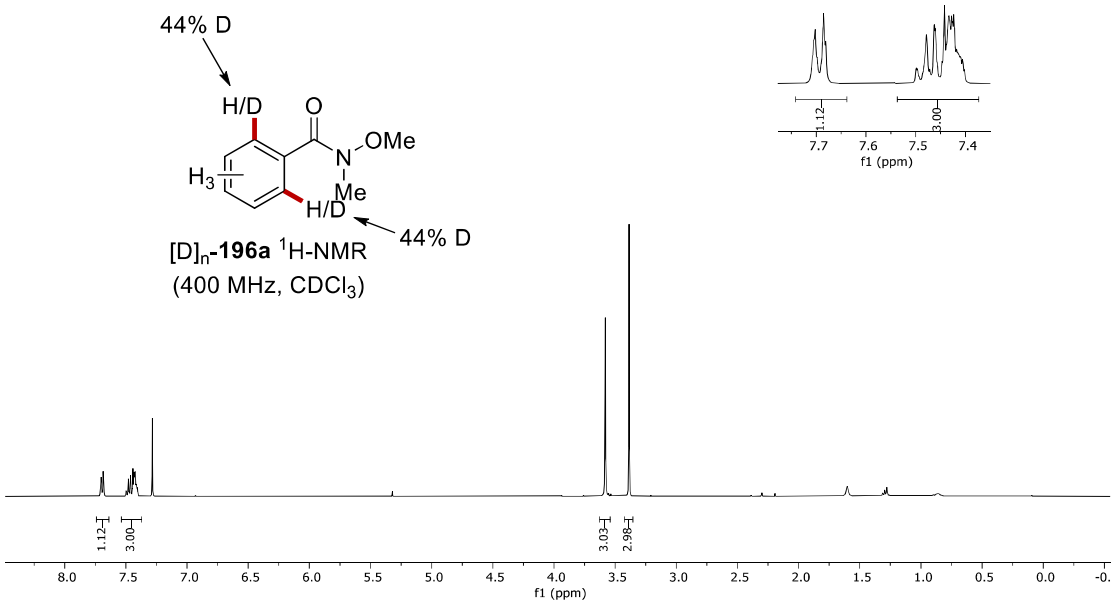

Figure 5.5.1 ^{1}H-NMR of [D]$_n$-**196a** from the deuteration study with electricity.

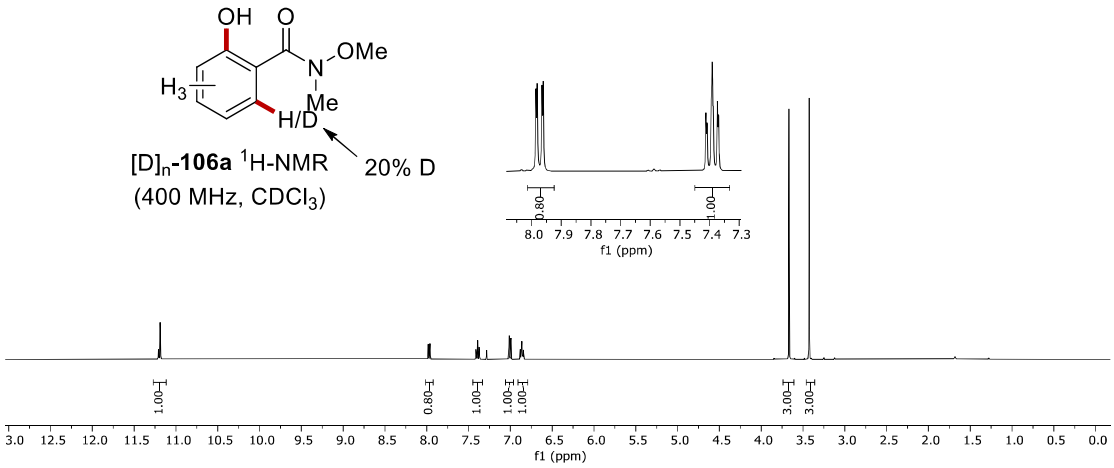

Figure 5.5.2 ^{1}H-NMR of [D]$_n$-**106a** from the deuteration study with electricity.

.

(b) Chemical oxidant reaction

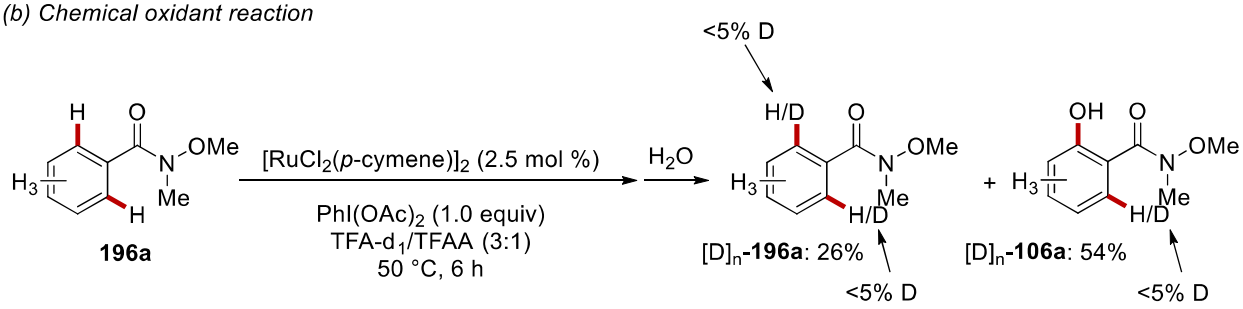

To an undivided cell, **196a** (82.5 mg, 0.50 mmol), PhI **194a** (20.4 mg, 20 mol %), [$RuCl_2$(*p*-cymene)] (8.8 mg, 5.0 mol %), $PhI(OAc)_2$ (161 mg, 1.0 equiv) *n*Bu_4NPF_6 (194 mg, 1.0 equiv), and TFA-d_1/TFAA (3:1, 3.0 mL) were added. The reaction was performed at 50 °C for 6 h. Thereafter, saturated aqueous $NaHCO_3$ (25 mL) was added and the reaction mixture was extracted with EtOAc (3 × 15 mL). The combined organic layers were washed with brine (25 mL), dried over Na_2SO_4, filtered, and concentrated *in vacuo*. Column chromatography (*n*hexane/ethyl acetate: 5/1) yielded [D]$_n$-**196a** (21.5 mg, 26%) as a colourless oil and [D]$_n$-**106a** (48.9 mg, 54%) as a colorless oil. The D-incorporation was determined by ^{1}H-NMR spectroscopy (Figures 5.5.3-4).

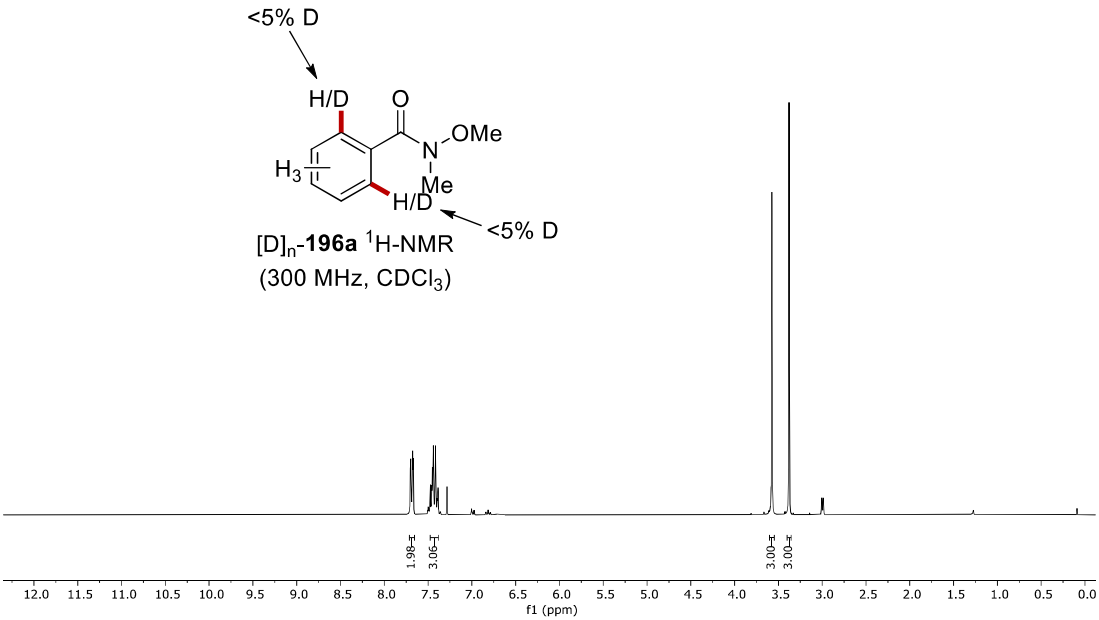

Figure 5.5.3 ^{1}H-NMR of $[D]_n$-**196a** from the deuteration study with chemical oxidant.

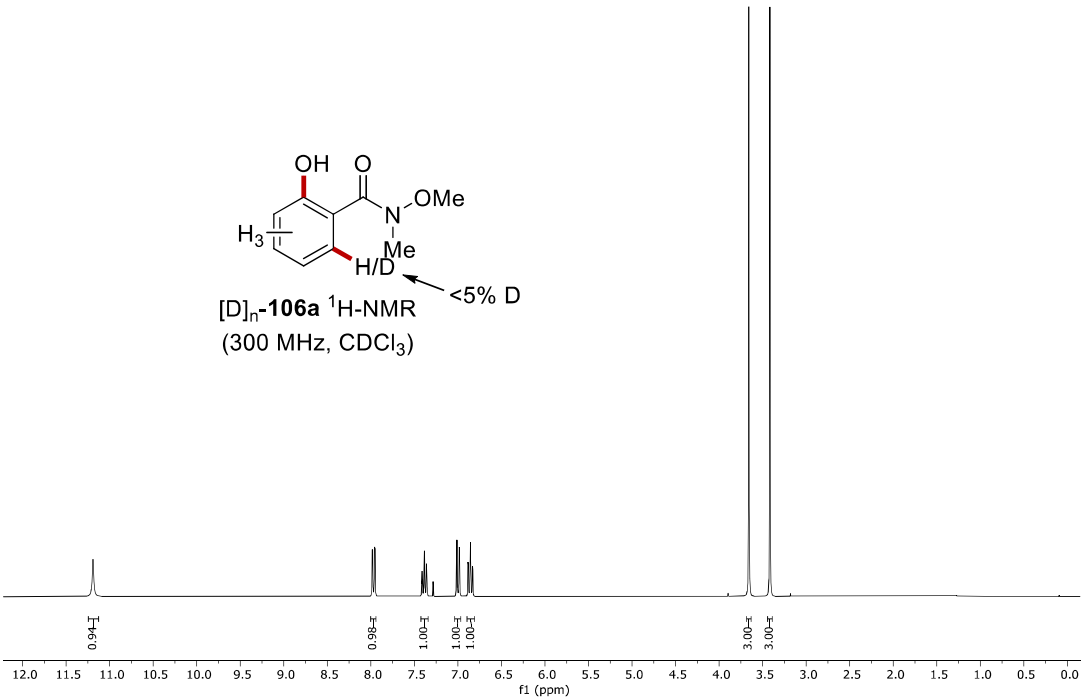

Figure 5.5.4 ^{1}H-NMR of $[D]_n$-**106a** from the deuteration study with chemical oxidant.

5.5.4 Kinetic Isotope Effect (KIE)

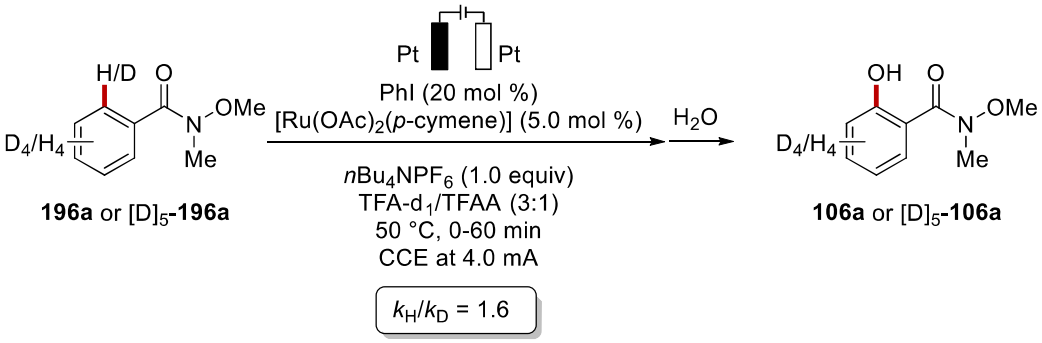

Two parallel reactions using substrates **196a** and [D]$_5$**–196a** (0.50 mmol each) were carried out to determine the KIE by comparison of the initial rates. To undivided cells equipped with Pt electrodes (10 mm x 15 mm x 0.125 mm), **196a** (82.5 mg, 0.50 mmol) or [D]$_5$**–196a** (85.1 mg, 0.50 mmol) respectevely, PhI **194a** (20.4 mg, 20 mol %), [Ru(OAc)$_2$(*p*-cymene)] **188a** (8.8 mg, 5.0 mol %) *n*Bu$_4$NPF$_6$ (194 mg, 1.0 equiv), and TFA/TFAA (3:1, 4.0 mL) were added. Electrocatalysis was performed at 50 °C with a constant current of 4.0 mA. After 20, 40 and 60 minutes, aliquots of 0.2 mL were collected from the cell. Each aliquot was then treated with saturated aqueous $NaHCO_3$ (2.0 mL) and extracted with CH_2Cl_2 (3 x 1.0 mL). After evaporation of the solvents, the crude mixture was analyzed by ^{1}H-NMR spectroscopy using CH_2Br_2 as the internal standard. The measured yields of **106a** and [D]$_5$**–106a** were plotted and a linear fit revealed a KIE of $k_H/k_D \approx 1.6$ (Figure 5.5.5).

***t*/ min**	**20**	**40**	**60**
106a / %	1	3	6
[D]$_n$-106a / %	0	1.6	3

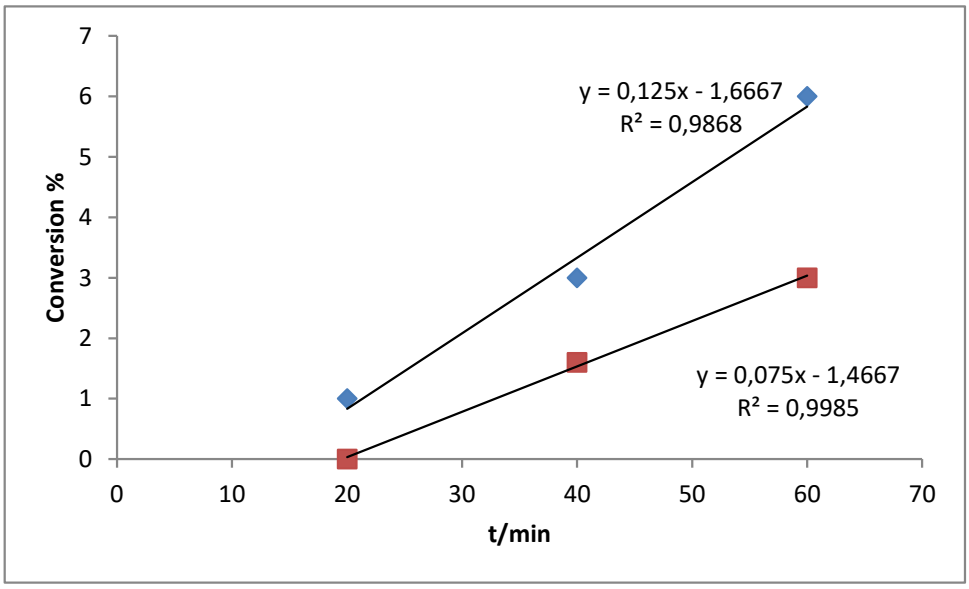

Figure 5.5.5 Linear fit for the reaction rates of **196a** and [D]$_5$–**196a**.

5.5.5 Competition Experiment

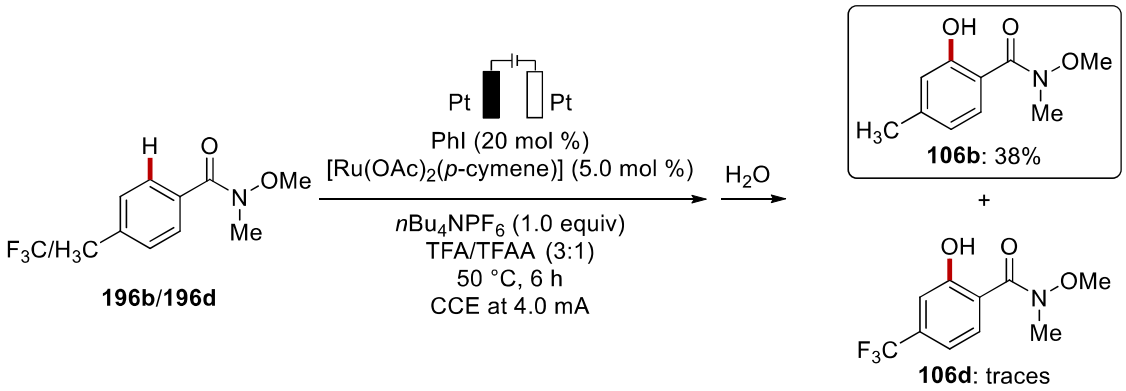

To an undivided cell equipped with Pt electrodes (10 mm x 15 mm x 0.125 mm), **196b** (44.8 mg, 0.25 mmol), **196d** (58.5 mg, 0.25 mmol), PhI **194a** (20.4 mg, 20 mol %), [Ru(OAc)$_2$(*p*-cymene)] **188a** (8.8 mg, 5.0 mol %) *n*Bu$_4$NPF$_6$ (194 mg, 1.0 equiv), and TFA/TFAA (3:1, 3.0 mL) were added. Electrocatalysis was performed at 50 °C with a constant current of 4.0 mA maintained for 6 h. Thereafter, saturated aqueous NaHCO$_3$ (25 mL) was added, and the reaction mixture was extracted with EtOAc (3 × 15 mL). The combined organic layers were washed with brine (25 mL), dried over Na$_2$SO$_4$, filtered, and concentrated *in vacuo*. Purification by column chromatography on silica gel

(*n*hexane/ethyl acetate: 10/1→5/1) yielded **106b** (31.8 mg, 38%) as a colourless solid. **106d** was obtained only in trace amount.

5.5.6 Directing Group Competition

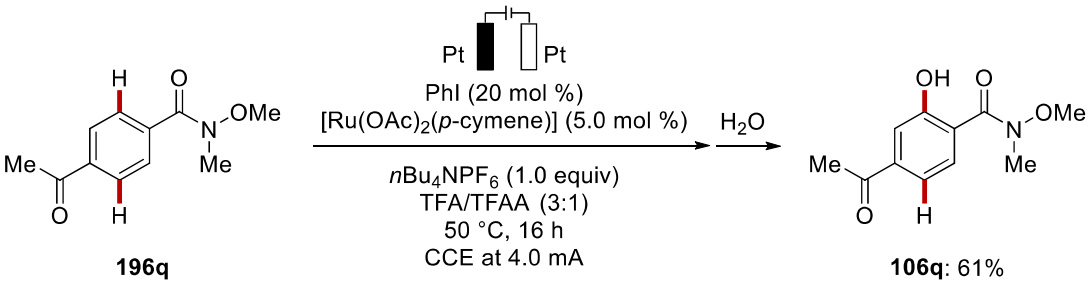

The general procedure **D** was followed using 4-acetyl-*N*-methoxy-*N*-methylbenzamide **196q** (104 mg, 0.50 mmol) to evaluate the competition in directing the C–H activation between the two directing groups. Isolation by column chromatography (*n*hexane/ethyl acetate: 8/1→3/1) yielded **106q** (67.8 mg, 61%) as a colourless liquid.

5.5.7 Gas-Chromatographical Analysis of Headspace

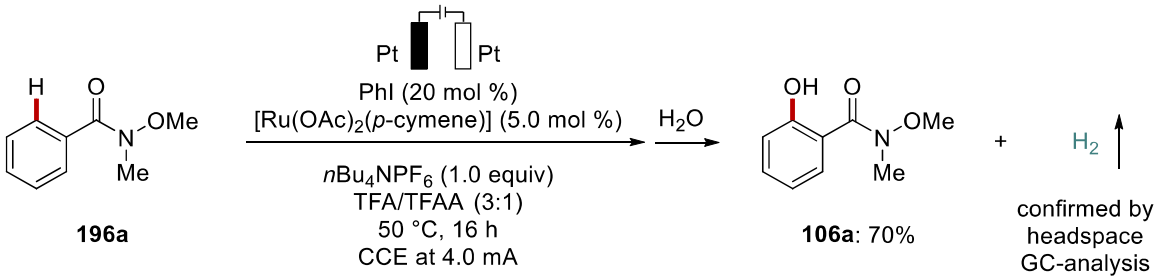

To a Schlenk tube equipped with platinum electrodes (10 mm x 15 mm x 0.125 mm), **196a** (82.5 mg, 0.50 mmol), PhI **194a** (20.4 mg, 20 mol %), [Ru(OAc)$_2$(*p*-cymene)] **188a** (8.8 mg, 5.0 mol %) *n*Bu$_4$NPF$_6$ (194 mg, 1.0 equiv), and degassed TFA/TFAA (3:1, 3.0 mL) were added under nitrogen atmosphere. Electrocatalysis was performed at 50 °C with a constant current of 4.0 mA maintained for 16 h. After cooling to ambient temperature, 1.0 mL of the gas-phase above the reaction mixture

was analyzed by GC (Figure 5.5.6). Next, a saturated aqueous $NaHCO_3$ (25 mL) was added, and the reaction mixture was extracted with EtOAc (3 × 15 mL). The combined organic layers were washed with brine (25 mL), dried over Na_2SO_4, filtered, and concentrated *in vacuo*. The crude product was purified by column chromatography on silica gel (*n*hexane/ethyl acetate: 5/1) yielding **106a** (63.4 mg, 70%) as yellow oil.

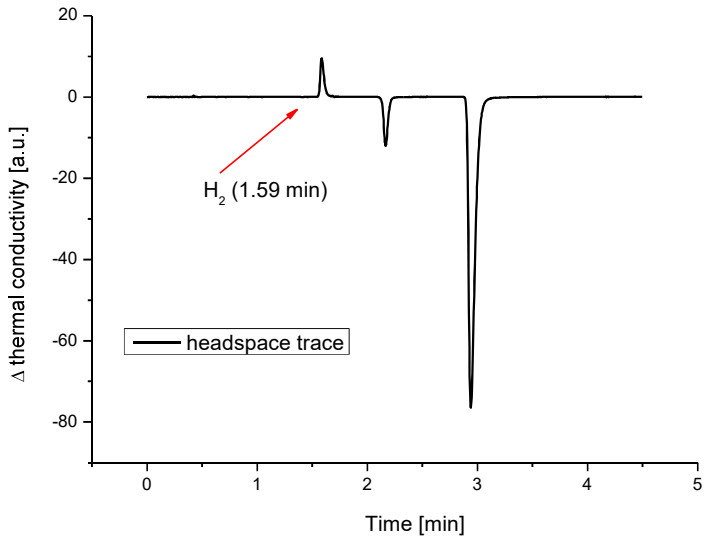

Figure 5.5.6 Gas chromatographic analysis.

5.6 Rhoda-Electrocatalyzed Bimetallic C–H Oxygenation by Weak *O*-Coordination

5.6.1 Characterization Data

2-Hydroxy-*N*-methoxy-*N*,4-dimethylbenzamide (106b)

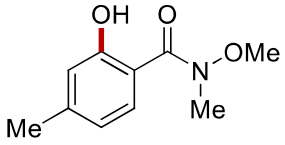

The general procedure **G** (15 h) was followed using *N*-methoxy-*N*,4-dimethylbenzamide **196b** (89.6 mg, 0.50 mmol). Purification by column chromatography (*n*hexane/ethyl acetate: 5/1→3/1) yielded **106b** (71.3 mg, 73%) as a yellow oil.

^{1}H-NMR (300 MHz, $CDCl_3$) δ = 11.38 (s, 1H), 7.88 (d, J = 8.3 Hz, 1H), 6.86–6.79 (m, 1H), 6.67 (dd, J = 8.3, 1.8 Hz, 1H), 3.67 (s, 3H), 3.41 (s, 3H), 2.34 (s, 3H).

^{13}C-NMR (100 MHz, $CDCl_3$) δ = 170.0 (C_q), 161.3 (C_q), 144.9 (C_q), 129.4 (CH), 119.7 (CH), 118.2 (CH), 111.5 (C_q), 61.1 (CH_3), 34.1 (CH_3), 21.6 (CH_3).

IR (ATR): 3069, 1634, 1586, 1350, 1265, 949, 735, 533 cm^{-1}.

MS (ESI) *m/z* (relative intensity): 413 (20) $[2M+Na]^+$, 218 (30) $[M+H]^+$, 196 (100) $[M+H]^+$.

HR-MS (ESI) *m/z* calc. for $C_{10}H_{14}NO_3^+$ $[M+H]^+$ 196.0968, found 196.0974.

The analytical data are in accordance with those previously reported in the literature.[176]

3-Hydroxy-*N*-methoxy-*N*-methyl-[1,1'-biphenyl]-4-carboxamide (106t)

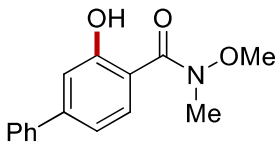

The general procedure **G** (15 h) was followed using *N*-methoxy-*N*-methyl-[1,1'-biphenyl]-4-carboxamide **196t** (121 mg, 0.50 mmol). Purification by column chromatography on silica gel (*n*hexane/ethyl acetate: 5/1) yielded **106t** (90.1 mg, 70%) as a light viscous liquid.

^{1}H-NMR (300 MHz, $CDCl_3$) δ = 11.49 (s, 1H), 8.08 (d, J = 8.4 Hz, 1H), 7.68–7.62 (m, 2H), 7.51–7.38 (m, 3H), 7.26 (d, J = 1.8 Hz, 1H), 7.12 (dt, J = 8.4, 1.3 Hz, 1H), 3.72 (s, 3H), 3.46 (s, 3H).

^{13}C-NMR (100 MHz, $CDCl_3$) δ = 169.8 (C_q), 161.6 (C_q), 146.5 (C_q), 139.7 (C_q), 130.0 (CH), 128.9 (CH), 128.3 (CH), 127.1 (CH), 117.5 (CH), 116.2 (CH), 113.0 (C_q), 61.3 (CH_3), 34.1 (CH_3).

IR (ATR): 2935, 1632, 1579, 1353, 1210, 972, 755, 696 cm^{-1}.

MS (ESI) *m/z* (relative intensity): 537 (30) $[2M+Na]^+$, 280 (30) $[M+H]^+$, 258 (100) $[M+H]^+$.

HR-MS (ESI) *m/z* calc. for $C_{15}H_{16}NO_3^+$ $[M+H]^+$ 258.1125, found 258.1126.

Methyl 3-hydroxy-4-[methoxy(methyl)carbamoyl]benzoate (106u)

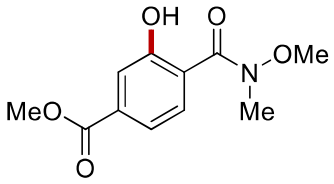

The general procedure **G** (15 h) was followed using methyl 4-[methoxy(methyl)carbamoyl]benzoate **196u** (112 mg, 0.50 mmol). Purification by column chromatography on silica gel (*n*hexane/ethyl acetate: 5/1) yielded **106u** (74.2 mg, 62%) as white solid.

M.p.: 108–110 °C.

^{1}H-NMR (300 MHz, $CDCl_3$) δ = 11.01 (s, 1H), 8.02 (d, J = 8.4 Hz, 1H), 7.64 (d, J = 1.8 Hz, 1H), 7.50 (dd, J = 8.4, 1.8 Hz, 1H), 3.93 (s, 3H), 3.65 (s, 3H), 3.42 (s, 3H).

^{13}C-NMR (100 MHz, $CDCl_3$) δ = 168.8 (C_q), 166.2 (C_q), 160.5 (C_q), 134.5 (C_q), 129.6 (CH), 119.3 (CH), 119.1 (CH), 118.1 (C_q), 61.4 (CH_3), 52.4 (CH_3), 33.8 (CH_3).

IR (ATR): 3055, 2987, 1722, 1594, 1264, 1098, 990, 732 cm^{-1}.

MS (ESI) *m/z* (relative intensity): 501 (30) $[2M+Na]^+$, 262 (30) $[M+H]^+$, 240 (100) $[M+H]^+$.

HR-MS (ESI) *m/z* calc. for $C_{11}H_{14}NO_5^+$ $[M+H]^+$ 240.0866, found 240.0868.

2-Hydroxy-4-iodo-*N*-methoxy-*N*-methylbenzamide (106o)

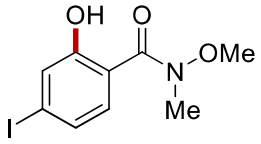

The general procedure **G** (15 h) was followed using 4-iodo-*N*-methoxy-*N*-methylbenzamide **196o** (146 mg, 0.50 mmol). Purification by column chromatography on silica gel (*n*hexane/ethyl acetate: 5/1) yielded **106o** (93.7 mg, 61%) as a yellow oil.

^{1}H-NMR (300 MHz, $CDCl_3$) δ = 11.42 (s, 1H), 7.71 (d, J = 8.6 Hz, 1H), 7.42 (d, J = 1.8 Hz, 1H), 7.21 (dd, J = 8.6, 1.8 Hz, 1H), 3.66 (s, 3H), 3.41 (s, 3H).

^{13}C-NMR (100 MHz, $CDCl_3$) δ = 169.2 (C_q), 161.4 (C_q), 130.4 (CH), 127.8 (CH), 127.3 (CH), 113.6 (C_q), 100.3 (C_q), 61.3 (CH_3), 33.8 (CH_3).

IR (ATR): 3203, 2933, 1631, 1477, 1303, 1007, 877, 751 cm^{-1}.

MS (ESI) *m/z* (relative intensity): 307 (20) $[M+H]^+$, 278 (100).

HR-MS (ESI) *m/z* calc. for $C_9H_{11}INO_3^+$ $[M+H]^+$ 307.9778, found 307.9784.

The analytical data are in accordance with those previously reported in the literature.[176]

4-Acetyl-2-hydroxy-*N*-methoxy-*N*-methylbenzamide (106q)

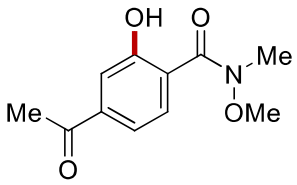

The general procedure **G** (15 h) was followed using 4-acetyl-*N*-methoxy-*N*-methylbenzamide **196q** (104 mg, 0.50 mmol). Purification by column chromatography on silica gel (*n*hexane/ethyl acetate: 5/1) yielded **106q** (55.8 mg, 50%) as a colourless liquid.

^{1}H-NMR (300 MHz, $CDCl_3$) δ = 11.08 (s, 1H), 8.04 (d, J = 8.4 Hz, 1H), 7.53 (d, J = 1.8 Hz, 1H), 7.42 (dd, J = 8.4, 1.8 Hz, 1H), 3.65 (s, 3H), 3.43 (s, 3H), 2.60 (s, 3H).

^{13}C-NMR (100 MHz, $CDCl_3$) δ = 197.5 (C_q), 168.7 (C_q), 160.8 (C_q), 140.8 (C_q), 129.8 (CH), 118.0 (C_q), 117.9 (CH), 117.7 (CH), 61.4 (CH_3), 33.8 (CH_3), 26.8 (CH_3).

IR (ATR): 3204, 2939, 1690, 1518, 1266, 1043, 884, 747 cm^{-1}.

MS (ESI) *m/z* (relative intensity): 224 (30) $[M+H]^+$, 194 (100).

HR-MS (ESI) *m/z* calc. for $C_{11}H_{14}NO_4^+$ $[M+H]^+$ 224.0917, found 224.0914.

The analytical data are in accordance with those previously reported in the literature.[176]

2-Hydroxy-*N*-methoxy-*N*,5-dimethylbenzamide (106j)

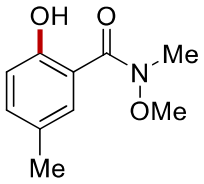

The general procedure **G** (15 h) was followed using *N*-methoxy-*N*,3-dimethylbenzamide **196j** (89.5 mg, 0.50 mmol). Purification by column chromatography on silica gel (*n*hexane/ethyl acetate: 5/1) yielded **106j** (52.0 mg, 53%) and **106j'** (2.9 mg, 3%) as colorless liquids.

^{1}H-NMR (400 MHz, $CDCl_3$) δ = 10.76 (s, 1H), 7.69 (d, J = 2.3 Hz, 1H), 7.16 (dd, J = 8.4 Hz, 2.3 Hz, 1H), 6.86 (d, J = 8.4 Hz, 1H), 3.62 (s, 3H), 3.37 (s, 3H), 2.25 (s, 3H).

^{13}C-NMR (100 MHz, $CDCl_3$) δ = 170.0 (C_q), 158.4 (C_q), 134.5 (CH), 129.3 (CH), 127.5 (C_q), 117.6 (CH), 114.2 (C_q), 61.1 (CH_3), 34.1 (CH_3), 20.6 (CH_3).

IR (ATR): 2937, 1633, 1572, 1486, 1423, 1348, 1246, 1179, 974, 822 cm^{-1}.

MS (ESI) *m/z* (relative intensity): 413 (20) $[2M+Na]^+$, 218 (40) $[M+Na]^+$, 196 (100) $[M+H]^+$.

HR-MS (ESI) *m/z* calc. for $C_{10}H_{14}NO_3^+$ $[M+H]^+$ 196.0968, found 196.0969.

The analytical data are in accordance with those previously reported in the literature.[176]

2-Hydroxy-*N*-methoxy-*N*,3-dimethylbenzamide (106j')

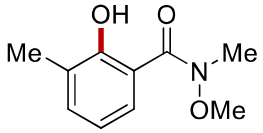

^{1}H-NMR (400 MHz, $CDCl_3$) δ = 11.28 (s, 1H), 7.75 (dd, J = 8.2, 1.7 Hz, 1H), 7.22 (dd, J = 7.3, 1.7 Hz, 1H), 6.73 (dd, J = 8.2, 7.3 Hz, 1H), 3.62 (s, 3H), 3.39 (s, 3H), 2.25 (s, 3H).

^{13}C-NMR (100 MHz, $CDCl_3$) δ = 170.4 (C_q), 159.2 (C_q), 134.6 (CH), 127.0 (CH), 126.8 (C_q), 117.8 (CH), 113.6 (C_q), 61.2 (CH_3), 34.3 (CH_3), 16.0 (CH_3).

IR (ATR): 2962, 1587, 1474, 1401, 1292, 1193, 1052, 747 cm^{-1}.

MS (ESI) *m/z* (relative intensity): 218 (100) $[M+Na]^+$, 196 (90) $[M+H]^+$.

HR-MS (ESI) *m/z* calc. for $C_{10}H_{14}NO_3^+$ $[M+H]^+$ 196.0968, found 196.0968.

The analytical data are in accordance with those previously reported in the literature.[176]

5-Chloro-2-hydroxy-*N*-methoxy-*N*-methylbenzamide (106m)

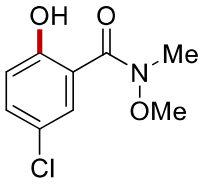

The general procedure **G** (15 h) was followed using 3-chloro-*N*-methoxy-*N*-methylbenzamide **196m** (99.8 mg, 0.50 mmol). Purification by column chromatography (*n*hexane/ethyl acetate: 5/1) yielded **106m** (56.1 mg, 52%) as as yellow solid.

M.p.: 97–99 °C.

^{1}H-NMR (400 MHz, $CDCl_3$) δ = 11.22 (s, 1H), 8.00 (d, J = 3.2 Hz, 1H), 7.34 (dd, J = 9.0, 3.2 Hz, 1H), 6.95 (d, J = 9.0 Hz, 1H), 3.69 (s, 3H), 3.42 (s, 3H).

^{13}C-NMR (100 MHz, $CDCl_3$) δ = 168.5 (C_q), 159.7 (C_q), 133.7 (CH), 129.0 (CH), 123.2 (C_q), 119.5 (CH), 115.1 (C_q), 61.4 (CH_3), 33.8 (CH_3).

IR (ATR): 2937, 1587, 1468, 1250, 1182, 974, 735, 651 cm^{-1}.

MS (ESI) *m/z* (relative intensity): 238 (30) $[M+Na]^+$, 216 (100) $[M+H]^+$.

HR-MS (ESI) *m/z* calc. for $C_9H_{11}{}^{35}ClNO_3^+$ $[M+H]^+$ 216.0422, found 216.0423.

The analytical data are in accordance with those previously reported in the literature.[176]

4,5-Dichloro-2-hydroxy-*N*-methoxy-*N*-methylbenzamide (106f)

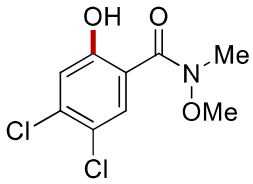

The general procedure **G** (15 h) was followed using 3,4-dichloro-*N*-methoxy-*N*-methylbenzamide **196f** (117 mg, 0.50 mmol). Purification by column chromatography (*n*hexane/ethyl acetate: 5/1) yielded **106f** (96.3 mg, 77%) as a white solid.

M.p.: 100–102 °C.

^{1}H-NMR (300 MHz, $CDCl_3$) δ = 11.51 (s, 1H), 8.16 (s, 1H), 7.13 (s, 1H), 3.70 (s, 3H), 3.42 (s, 3H).

^{13}C-NMR (100 MHz, $CDCl_3$) δ = 167.8 (C_q), 160.4 (C_q), 137.6 (C_q), 130.7 (CH), 121.9 (C_q), 119.8 (CH), 113.7 (C_q), 61.5 (CH_3), 33.7 (CH_3).

IR (ATR): 2937, 1628, 1457, 1339, 1181, 978, 649, 447 cm^{-1}.

MS (ESI) *m/z* (relative intensity): 521 (10) $[2M+Na]^+$, 272 (10) $[M+Na]^+$, 250 (100) $[M+H]^+$.

HR-MS (ESI) *m/z* calc. for $C_9H_9{}^{35}Cl_2NO_3^+$ $[M+H]^+$ 250.0032, found 250.0037.

The analytical data are in accordance with those previously reported in the literature.[176]

2-Hydroxy-*N*,*N*,4-trimethylbenzamide (104b)

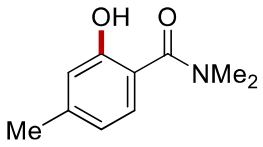

The general procedure **G** (15 h) was followed using *N*,*N*,4-trimethylbenzamide **103b** (81.6 mg, 0.50 mmol). Purification by column chromatography (*n*hexane/ethyl acetate: 3/1) yielded **104b** (81.6 mg, 91%) as a yellow oil.

The general procedure **G** (15 h) was followed using *N*,*N*,4-trimethylbenzamide **103b** (81.6 mg, 0.50 mmol) with $[Rh(OAc)_2]_2$ (2.2 mg, 0.005 mmol, 1.0 mol %). Purification by column chromatography (*n*hexane/EtOAc: 3/1) yielded **104b** (59.2 mg, 66%) as a yellow oil.

The general procedure **G** (15 h) was followed using *N*,*N*,4-trimethylbenzamide **103b** (81.6 mg, 0.50 mmol) with $[Rh(OAc)_2]_2$ (1.1 mg, 0.0025 mmol, 0.5 mol %). Purification by column chromatography (*n*hexane/EtOAc: 3/1) yielded **104b** (53.8 mg, 60%) as a yellow oil.

^{1}H-NMR (300 MHz, $CDCl_3$) δ = 9.96 (s, 1H), 7.22 (d, J = 8.0 Hz, 1H), 6.8 (s, 1H), 6.67 (d, J = 8.0 Hz, 1H), 3.16 (s, 6H), 2.33 (s, 3H).

^{13}C-NMR (100 MHz, $CDCl_3$) δ = 172.1 (C_q), 159.5 (C_q), 143.5 (C_q), 128.5 (CH), 119.2 (CH), 118.2 (CH), 114.1 (C_q), 38.5 (CH_3), 21.6 (CH_3).

IR (ATR): 3156, 2930, 1621, 1398, 1265, 1127, 954, 812 cm^{-1}.

MS (ESI) *m/z* (relative intensity): 381 (10) $[2M+Na]^+$, 202 (20) $[M+Na]^+$, 180 (100) $[M+H]^+$.

HR-MS (ESI) *m/z* calc. for $C_{10}H_{14}NO_2^+$ $[M+H]^+$ 180.1019, found 180.1026.

The analytical data are in accordance with those previously reported in the literature.[176]

2-Hydroxy-4-methoxy-*N*,*N*-dimethylbenzamide (104h)

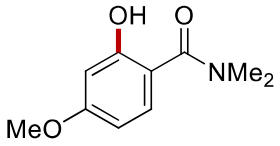

The general procedure **G** (15 h) was followed using 4-methoxy-*N*,*N*-dimethylbenzamide **103h** (89.6 mg, 0.50 mmol). Purification by column chromatography (*n*hexane/ethyl acetate: 3/1) yielded **104h** (75.2 mg, 77%) as a yellow oil.

^{1}H-NMR (400 MHz, $CDCl_3$) δ = 9.51 (br, 1H), 7.26 (d, J = 8.8 Hz, 1H), 6.50 (s, 1H), 6.40 (d, J = 8.8 Hz, 1H), 3.80 (s, 3H), 3.15 (s, 6H).

^{13}C-NMR (100 MHz, $CDCl_3$) δ = 172.3 (C_q), 163.1 (C_q), 162.0 (C_q), 130.1 (CH), 109.3 (C_q), 105.6 (CH), 101.8 (CH), 55.3 (CH_3), 38.6 (CH_3).

IR (ATR): 3022, 2925, 1626, 1390, 1268, 1078, 743, 642 cm^{-1}.

MS (ESI) *m/z* (relative intensity): 413 (10) $[2M+Na]^+$, 218 (30) $[M+Na]^+$, 196 (100) $[M+H]^+$.

HR-MS (ESI) *m/z* calc. for $C_{10}H_{14}NO_3^+$ $[M+H]^+$ 196.0974, found 196.0979.

The analytical data are in accordance with those previously reported in the literature.[190]

4-Chloro-2-hydroxy-*N*,*N*-dimethylbenzamide (104i)

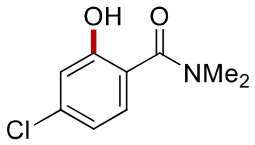

The general procedure **G** (15 h) was followed using 4-chloro-*N*,*N*-dimethylbenzamide **103i** (91.8 mg, 0.50 mmol). Purification by column chromatography (*n*hexane/ethyl acetate: 3/1) yielded **104i** (92.8 mg, 93%) as a yellow oil.

^{1}H-NMR (400 MHz, $CDCl_3$) δ = 7.26 (d, J = 8.5 Hz, 1H), 7.02 (s, 1H), 6.85 (d, J = 8.5 Hz, 1H), 3.17 (s, 6H).

^{13}C-NMR (100 MHz, $CDCl_3$) δ = 171.2 (C_q), 160.2 (C_q), 138.1 (C_q), 129.5 (CH), 118.7 (CH), 118.2 (CH), 115.5 (C_q), 38.4 (CH_3).

IR (ATR): 3093, 2936, 1580, 1398, 1254, 1094, 926, 734 cm^{-1}.

MS (ESI) *m/z* (relative intensity): 421 (10) $[2M+Na]^+$, 222 (40) $[M+Na]^+$, 200 (100) $[M+H]^+$.

HR-MS (ESI) *m/z* calc. for $C_9H_{11}{}^{35}ClNO_2^+$ $[M+H]^+$ 200.0473, found 200.0475.

2-Hydroxy-*N*,*N*,5-trimethylbenzamide (104k)

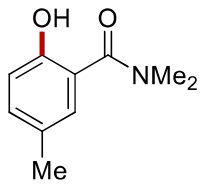

The general procedure **G** (15 h) was followed using *N*,*N*,3-trimethylbenzamide **103k** (81.6 mg, 0.50 mmol). Purification by column chromatography (*n*hexane/ethyl acetate: 3/1) yielded **104k** (68.1 mg, 76%) and **104k'** (4.5 mg, 5%) as yellow liquids.

^{1}H-NMR (300 MHz, $CDCl_3$) δ = 9.50 (br, 1H), 7.17–7.06 (m, 2H), 6.89 (d, J = 8.2 Hz, 1H), 3.16 (s, 6H), 2.28 (s, 3H).

^{13}C-NMR (100 MHz, $CDCl_3$) δ = 171.9 (C_q), 156.6 (C_q), 133.2 (CH), 128.6 (CH), 127.5 (C_q), 117.6 (CH), 117.2 (C_q), 38.3 (CH_3), 20.5 (CH_3).

IR (ATR): 3161, 2925, 1589, 1492, 1399, 1265, 1172, 734 cm^{-1}.

MS (ESI) *m/z* (relative intensity): 381 (30) $[2M+Na]^+$, 202 (50) $[M+Na]^+$, 180 (100) $[M+H]^+$.

HR-MS (ESI) *m/z* calc. for $C_{10}H_{14}NO_2^+$ $[M+H]^+$ 180.1019, found 180.1023.

2-Hydroxy-*N*,*N*,3-trimethylbenzamide (104k')

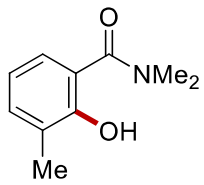

^{1}H-NMR (300 MHz, $CDCl_3$) δ = 10.13 (s, 1H), 7.25–7.13 (m, 2H), 6.77 (t, J = 7.6 Hz, 1H), 3.18 (s, 6H), 2.29 (s, 3H).

^{13}C-NMR (100 MHz, $CDCl_3$) δ = 172.5 (C_q), 157.6 (C_q), 133.5 (CH), 127.0 (C_q), 126.2 (CH), 117.6 (CH), 116.2 (C_q), 16.0 (CH_3).

IR (ATR): 2929, 1602, 1502, 1410, 1253, 1115, 759, 691 cm^{-1}.

MS (ESI) *m/z* (relative intensity): 381 (20) $[2M+Na]^+$, 202 (50) $[M+Na]^+$, 180 (100) $[M+H]^+$.

HR-MS (ESI) *m/z* calc. for $C_{10}H_{14}NO_2^+$ $[M+H]^+$ 180.1019, found 180.1019.

The analytical data are in accordance with those previously reported in the literature.[191]

5-Bromo-*N*,*N*-diethyl-2-hydroxybenzamide (104n)

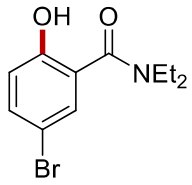

The general procedure **G** (16 h) was followed using 3-bromo-*N*,*N*-diethylbenzamide **103n** (128 mg, 0.50 mmol). Purification by column chromatography on silica gel (*n*hexane/ethyl acetate: 3/1→2/1) yielded **104n** (117 mg, 66%) as a white solid.

M.p.: 151–153 °C.

^{1}H-NMR (400 MHz, $CDCl_3$) δ = 9.59 (s, 1H), 7.38–7.31 (m, 2H), 6.83 (d, J = 8.3 Hz, 1H), 3.47 (q, J = 7.1 Hz, 4H), 1.24 (t, J = 7.1 Hz, 6H).

^{13}C-NMR (100 MHz, $CDCl_3$) δ = 169.9 (C_q), 157.2 (C_q), 134.7 (CH), 129.7 (CH), 120.3 (C_q), 119.8 (CH), 110.3 (C_q), 42.2 (CH_2), 13.3 (CH_3).

IR (ATR): 2984, 2935, 1583, 1444, 1404, 1357, 1280, 1234, 1096, 822 cm^{-1}.

MS (ESI) *m/z* (relative intensity): 567 (50) $[2M+Na]^+$, 294 (80) $[M+Na]^+$, 272 (100) $[M+H]^+$.

HR-MS (ESI) *m/z* calc. for $C_{11}H_{15}BrNO_2^+$ $[M+H]^+$ 272.0281, found 272.0285.

1-(2-Hydroxy-4-methylphenyl)ethan-1-one (197n)

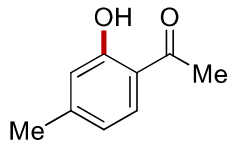

The general procedure **H** was followed using 4'-methyl-acetophenone **77n** (67.1 mg, 0.50 mmol). Purification by column chromatography (*n*hexane/ethyl acetate: 200/1) yielded **197n** (39.8 mg, 53%) as a colourless liquid.

^{1}H-NMR (300 MHz, $CDCl_3$) δ = 12.30 (s, 1H), 7.63 (d, J = 8.1 Hz, 1H), 6.80 (s, 1H), 6.73 (d, J = 8.1 Hz, 1H), 2.61 (s, 3H), 2.37 (s, 3H).

^{13}C-NMR (100 MHz, $CDCl_3$) δ = 203.9 (C_q), 162.5 (C_q), 148.1 (C_q), 130.6 (CH), 120.2 (CH), 118.4 (CH), 117.6 (C_q), 265 (CH_3), 22.0 (CH_3).

IR (ATR): 2923, 1635, 1366, 1224, 1149, 977, 792, 561 cm^{-1}.

MS (ESI) *m/z* (relative intensity): 173 (10) $[M+Na]^+$, 151 (100) $[M+H]^+$.

HR-MS (ESI) *m/z* calc. for $C_9H_{11}O_2^+$ $[M+H]^+$ 151.0754, found 151.0756.

The analytical data are in accordance with those previously reported in the literature.[192]

5.6.2 Competition Experiment

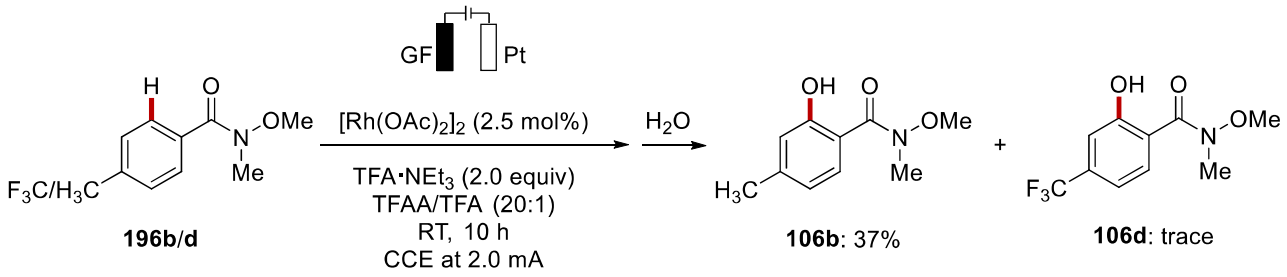

To an undivided cell equipped with graphite felt anode (10 mm × 10 mm × 6 mm) and platinum cathode (10 mm × 15 mm × 0.125 mm), **196b** (44.8 mg, 0.25 mmol), **196d** (58.5 mg, 0.25 mmol), $[Rh(OAc)_2]_2$ (5.5 mg, 0.0125 mmol, 2.5 mol %), TFA·NEt_3 (215 mg, 1.0 mmol), TFA (0.15 mL), and TFAA (3.0 mL) were added. The electrolysis was performed at 2.0 mA at ambient temperature for 10 h. After completion, the reaction mixture was transferred into a separatory funnel and the electrodes were rinsed with EtOAc (10 mL). A saturated aqueous $NaHCO_3$ solution (50 mL) was added slowly, and the mixture was extracted with ethyl acetate (20 mL × 3). The combined organic layers were dried over Na_2SO_4, filtered, and concentrated under vacuum. The crude reaction mixture was purified by silica gel column chromatography (*n*hexane/ethyl acetate: 10/1→5/1) yielding **106b** (31.0 mg, 37%) as a colourless solid. **106d** was obtained only in trace amounts.

5.6.3 H/D Exchange Experiment

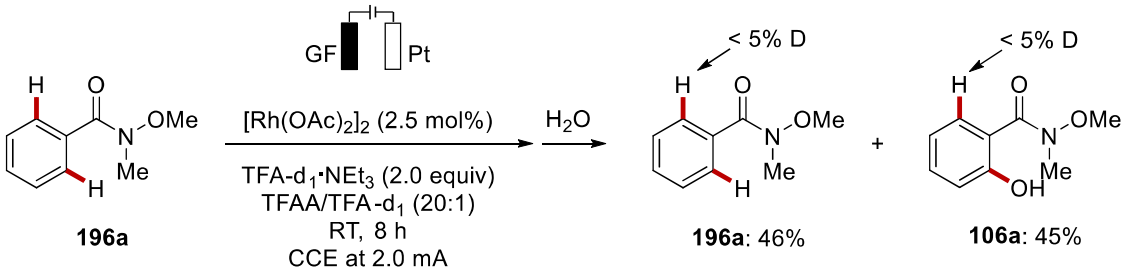

The electrolysis was carried out in an undivided cell (10 mL) equipped with a graphite felt anode (10 mm × 10 mm × 6 mm) and a platinum cathode (10 mm × 15 mm × 0.125 mm). $[Rh(OAc)_2]_2$ (5.5 mg, 0.0125 mmol, 2.5 mol %), $[D]_1$-TFA·NEt_3 (215 mg, 1.0 mmol), $[D]_1$-TFA (0.15 mL), Weinreb amide **196a** (82.5 mg, 0.50 mmol) and TFAA (3.0 mL) were successively added. The electrolysis was performed at 2.0 mA at ambient temperature for 8 h (2.2–2.5 F mol^{-1}). After completion, the reaction mixture was transferred into a separatory funnel and the electrodes were rinsed with EtOAc (10 mL). A saturated aqueous $NaHCO_3$ solution (50 mL) was added slowly, and the mixture was extracted with ethyl acetate (20 mL × 3). The combined organic layers were dried over Na_2SO_4 and concentrated. The crude reaction mixture was purified by silica gel column chromatography (*n*hexane/ethyl acetate: 5/1→4/1) yielded **196a** (38.0 mg, 46%) and **106a** (41.0 mg, 45%) without obvious H/D exchange (Figure 5.6.1-2).

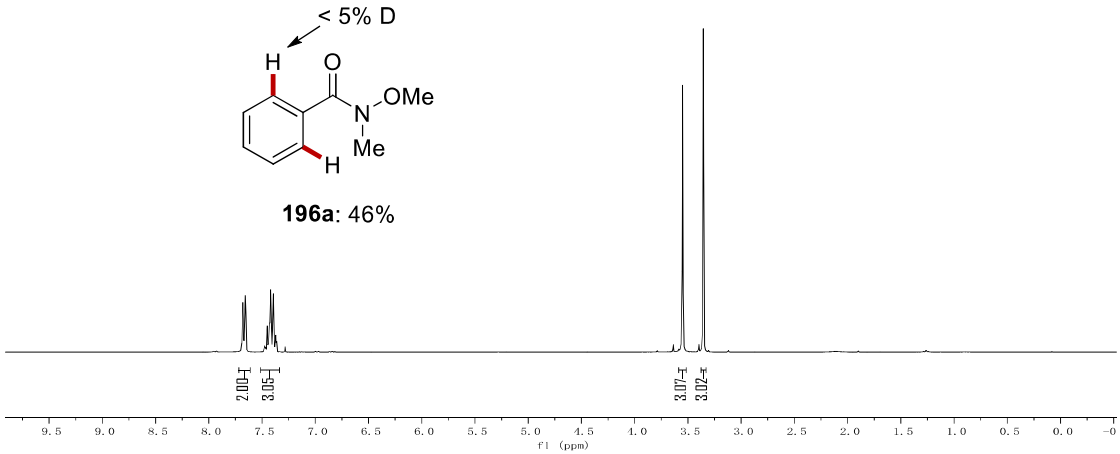

Figure 5.6.1 ^{1}H-NMR of $[D]_n$-**196a** from the deuteration study.

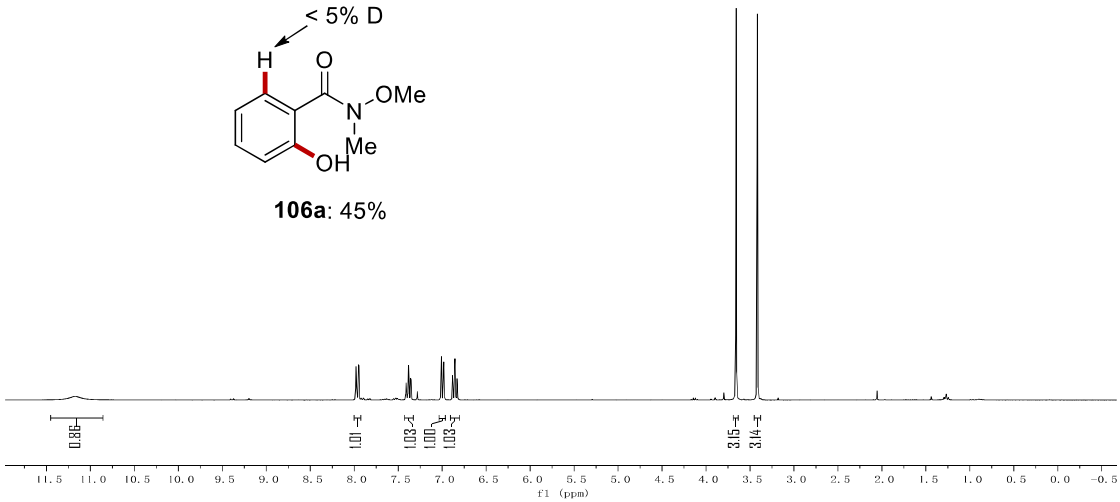

Figure 5.6.2 ^{1}H-NMR of $[D]_n$-**106a** from the deuteration study.

5.6.4 Reactions with Different Catalysts

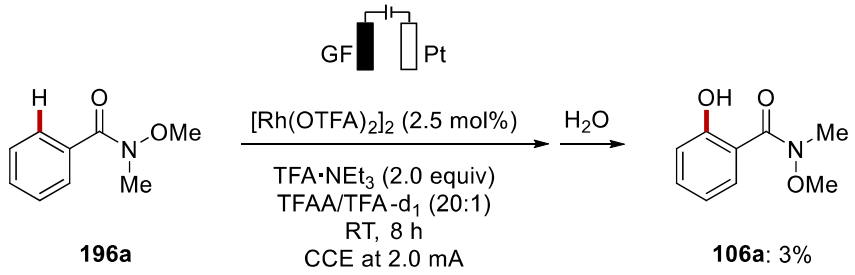

The electrolysis was carried out in an undivided cell (10 mL) equipped with a graphite felt anode (10 mm × 10 mm × 6 mm) and a platinum cathode (10 mm × 15 mm × 0.125 mm). $[Rh(OTFA)_2]_2$ (8.2 mg, 0.0125 mmol, 2.5 mol %), $TFA{\cdot}NEt_3$ (215 mg, 1.0 mmol), TFA (0.15 mL), Weinreb amide **196a** (82.5 mg, 0.50 mmol) and TFAA (3.0 mL) were successively added. The electrolysis was performed at 2.0 mA at ambient temperature for 16 h. After completion, the reaction mixture was transferred into a separatory funnel and the electrodes were rinsed with EtOAc (10 mL). A saturated aqueous $NaHCO_3$ solution (50 mL) was added slowly, and the mixture was extracted with ethyl acetate (20 mL × 3). The combined organic layers were dried over Na_2SO_4, filtered, and concentrated. The crude reaction mixture was purified by silica gel column chromatography (*n*hexane/ethyl acetate: 5/1→4/1) yielding **106a** (2.6 mg, 3%) as a colourless oil.

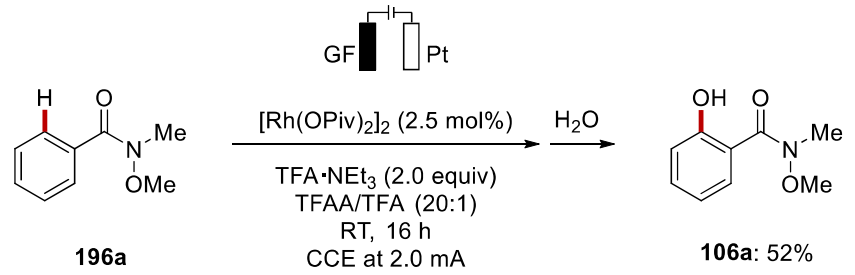

The electrolysis was carried out in an undivided cell (10 mL) equipped with a graphite felt anode (10 mm × 10 mm × 6 mm) and a platinum cathode (10 mm × 15 mm × 0.125 mm). $[Rh(OPiv)_2]_2$ (7.6 mg, 0.0125 mmol, 2.5 mol %), $TFA{\cdot}NEt_3$ (215 mg, 1.0 mmol), TFA (0.15 mL), Weinreb amide **196a** (82.5 mg, 0.50 mmol) and TFAA (3.0 mL) were successively added. The electrolysis was performed

at 2.0 mA at ambient temperature for 16 h. After completion, the reaction mixture was transferred into a separatory funnel and the electrodes were rinsed with EtOAc (10 mL). A saturated aqueous $NaHCO_3$ solution (50 mL) was added slowly, and the mixture was extracted with ethyl acetate (20 mL × 3). The combined organic layers were dried over Na_2SO_4, filtered, and concentrated. The crude reaction mixture was purified by silica gel column chromatography (*n*hexane/ethyl acetate: 5/1→4/1) yielding **106a** (47.1 mg, 52%) as a colourless oil.

5.6.5 Initial Rate Comparison between $[Rh(OAc)_2]_2$ and $[Rh(OPiv)_2]_2$

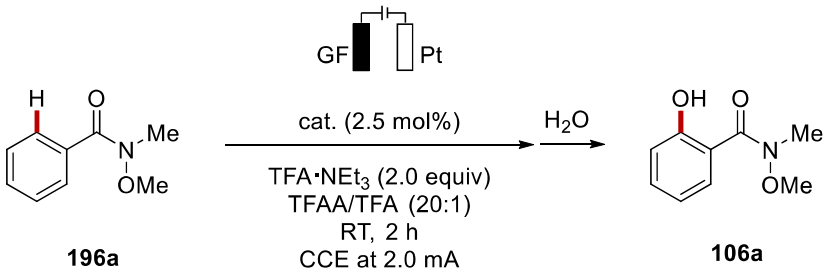

Two parallel electrolyses were carried out in undivided cells (10 mL), each equipped with graphite felt anode (10 mm × 10 mm × 6 mm) and platinum cathode (10 mm × 15 mm × 0.125 mm). $[Rh(OAc)_2]_2$ (5.5 mg, 0.0125 mmol, 2.5 mol %) or $[Rh(OPiv)_2]_2$ (7.6 mg, 0.0125 mmol, 2.5 mol %) respectevely, TFA·NEt_3 (215 mg, 1.0 mmol), TFA (0.15 mL), Weinreb amide **196a** (82.5 mg, 0.50 mmol), and TFAA (4.0 mL) were successively added. The electrolysis was performed at 2.0 mA at ambient temperature. In the time range of 30–120 min, aliquots of 0.1 mL were taken from each reaction mixture every 30 min. To each aliquot was added 0.1 mL of an internal standard solution (0.5 mmol of CH_2Br_2 in 4.0 mL of TFAA), then treated with a saturated aqueous $NaHCO_3$ (2.0mL) and extracted with CH_2Cl_2 (3 x 1.0 mL). After evaporation of the solvents, the crude mixture was analyzed by ^{1}H-NMR spectroscopy. The determined yields of **106a** were plotted in Figure 5.6.3.

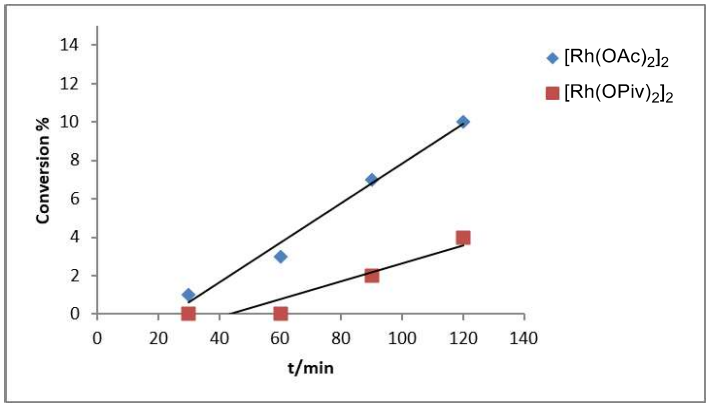

Figure 5.6.3 Reaction profiles of **106a** with different catalysts.

5.6.6 Identification of the Trifluoroacetate Product after C–H Acyloxylation

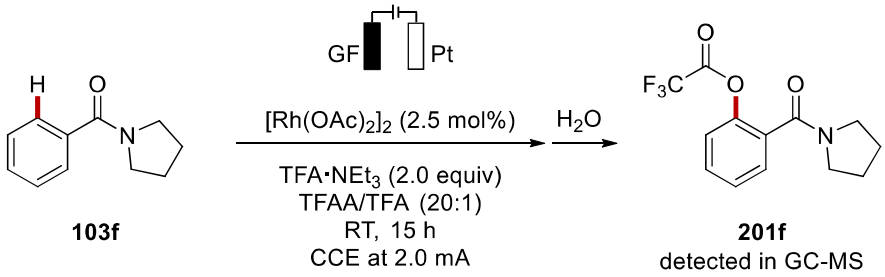

The electrolysis was carried out in an undivided cell (10 mL) equipped with a graphite felt anode (10 mm × 10 mm × 6 mm) and a platinum cathode (10 mm × 15 mm × 0.125 mm). $[Rh(OAc)_2]_2$ (5.5 mg, 0.0125 mmol, 2.5 mol %), TFA·NEt_3 (215 mg, 1.0 mmol), TFA (0.15 mL), phenyl(pyrrolidin-1-yl)methanone **103f** (87.6 mg, 0.50 mmol) and TFAA (3.0 mL) were successively added. The electrolysis was performed at 2.0 mA at ambient temperature for 16 h. The crude reaction mixture was analyzed by GC-MS. As expected, the desired trifluoroacetate ester **201f** was detected as the only product after the rhodaelectro-catalyzed C–H acyloxylation (Figure 5.6.4). However, attempts to isolate the pure form of the acyloxylated product failed due to the sensitibility to moisture.

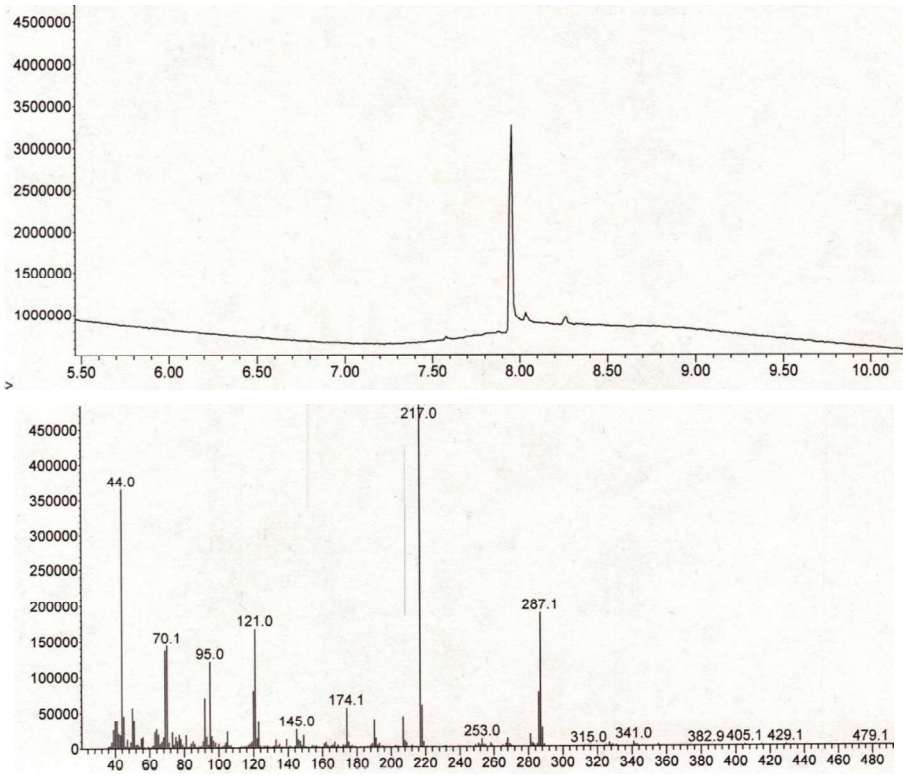

Figure 5.6.4 GC-MS data of the reaction mixture.

5.7 Manganaelectro-Catalyzed Azine C–H Arylations and C–H Alkylations by Assistance of Weakly Coordinating Amides

5.7.1 Characterization Data

N-*n*-Butyl-3-(4-methoxyphenyl)picolinamide (176aa)

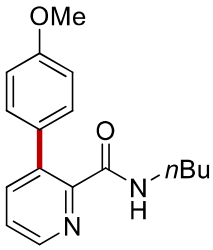

The general procedure was followed using **172a** (44.5 mg, 0.25 mmol) and **175a** (0.40 mL, 1.0 mmol, 2.5 M in THF). Isolation by column chromatography (*n*hexane/ethyl acetate: 2/1→1/1) yielded **176aa** (49.8 mg, 70%) as a white solid.

M. p.: 96–97 °C.

^{1}H-NMR (300 MHz, $CDCl_3$) δ = 8.54 (dd, *J* = 4.6, 1.7 Hz, 1H), 7.69 (dd, *J* = 7.8, 1.7 Hz, 2H), 7.43 (dd, *J* = 7.8, 4.6 Hz, 1H), 7.28 (m, 2H), 7.01–6.93 (m, 2H), 3.86 (s, 3H), 3.38 (td, *J* = 7.1, 6.0 Hz, 2H), 1.64–1.50 (m, 2H), 1.45–1.32 (m, 2H), 0.94 (t, *J* = 7.1 Hz, 3H).

^{13}C-NMR (125 MHz, $CDCl_3$) δ = 165.2 (C_q), 159.0 (C_q), 148.2 (C_q), 146.4 (CH), 139.9 (CH), 137.7 (C_q), 131.6 (C_q), 129.5 (CH), 124.9 (CH), 113.4 (CH), 55.2 (CH_3), 39.2 (CH_2), 31.7 (CH_2), 20.2 (CH_2), 13.8 (CH_3).

IR (ATR): 3200, 2957, 1648, 1511,1247, 1178, 1035, 804 cm^{-1}.

MS (ESI) *m/z* (relative intensity): 591 (100) $[2M+Na]^+$, 307 (90) $[M+Na]^+$, 285 (90) $[M+H]^+$.

HR-MS (ESI) *m/z* calc. for $C_{17}H_{21}N_2O_2$ $[M+H]^+$ 285.1598, found 285.1600.

The analytical data are in accordance with those previously reported in the literature.[154]

N-Benzyl-3-(4-methoxyphenyl)picolinamide (176ba)

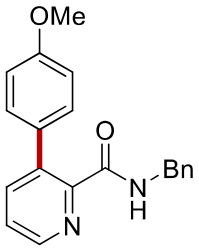

The general procedure **I** was followed using *N*-benzylpicolinamide **176b** (53.1 mg, 0.25 mmol) and **175a** (0.40 mL, 1.0 mmol, 2.5 M in THF). Isolation by column chromatography (*n*hexane/ethyl acetate: 2/1→1/1) yielded **176ba** (46.2 mg, 58%) as a white solid.

M. p.: 133–135 °C.

^{1}H-NMR (300 MHz, $CDCl_3$) δ = 8.53 (dd, J = 4.6, 1.6 Hz, 1H), 8.04 (s, 1H), 7.71 (dd, J = 7.8, 1.6 Hz, 1H), 7.45 (dd, J = 7.8, 4.6 Hz, 1H), 7.37–7.27 (m, 7H), 7.02–6.94 (m, 2H), 4.59 (d, J = 6.0 Hz, 2H), 3.88 (s, 3H).

^{13}C-NMR (100 MHz, $CDCl_3$) δ = 165.2 (C_q), 159.2 (C_q), 148.0 (C_q), 146.7 (CH), 140.2 (CH), 138.4 (C_q), 138.1 (C_q), 131.6 (C_q), 129.7 (CH), 128.6 (CH), 127.9 (CH), 127.4 (CH), 125.2 (CH), 113.5 (CH), 55.3 (CH_3), 43.5 (CH_2).

IR (ATR): 3055, 1711, 1673, 1512, 1361, 1222, 737, 531 cm^{-1}.

MS (EI) *m/z* (relative intensity): 659 (80) $[2M+Na]^+$, 341 (70) $[M+Na]^+$, 319 (100) $[M+H]^+$.

HR-MS (ESI) *m/z* calc. for $C_{20}H_{19}N_2O_2$ $[M+H]^+$ 319.1441, found 319.1441.

The analytical data are in accordance with those previously reported in the literature.[154]

_N_-(4-Methoxybenzyl)-3-(4-methoxyphenyl)picolinamide (176da)

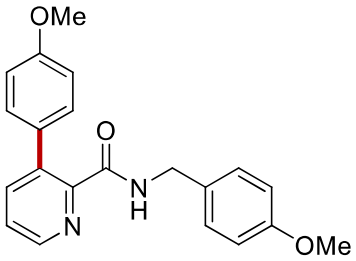

The general procedure **I** was followed using *N*-(4-methoxybenzyl)picolinamide **172d** (60.6 mg, 0.25 mmol) and **175a** (0.40 mL, 1.0 mmol, 2.5 M in THF). Isolation by column chromatography (*n*hexane/ethyl acetate: 2/1→1/1) yielded **176da** (44.4 mg, 51%) as a white solid.

M. p.: 97–98 °C.

^{1}H-NMR (300 MHz, $CDCl_3$) δ = 8.47 (dd, J = 4.6, 1.7 Hz, 1H), 7.89 (s, 1H), 7.65 (dd, J = 7.8, 1.7 Hz, 1H), 7.39 (dd, J = 7.8, 4.6 Hz, 1H), 7.28–7.20 (m, 4H), 6.97–6.91 (m, 2H), 6.86–6.81 (m, 2H), 4.47 (d, J = 5.9 Hz, 2H), 3.83 (s, 3H), 3.77 (s, 3H).

^{13}C-NMR (125 MHz, $CDCl_3$) δ = 165.3 (C_q), 159.3 (C_q), 159.0 (C_q), 148.1 (C_q), 146.7 (CH), 140.2 (CH), 138.1 (C_q), 131.7 (C_q), 130.6 (C_q), 129.8 (CH), 129.4 (CH), 125.3 (CH), 114.1 (CH), 113.6 (CH), 55.4 (CH_3), 55.4 (CH_3), 43.0 (CH_2).

IR (ATR): 3056, 1712, 1674, 1513, 1361, 1222, 737, 531 cm^{-1}.

MS (EI) *m/z* (relative intensity): 719 (60) $[2M+Na]^+$, 371 (70) $[M+Na]^+$, 349 (100) $[M+H]^+$.

HR-MS (EI) *m/z* calc. for $C_{21}H_{21}N_2O_3$ $[M]^+$ 349.1547, found 349.1548.

The analytical data are in accordance with those previously reported in the literature.[154]

_N_-(4-Fluorobenzyl)-3-(4-methoxyphenyl)picolinamide (176ea)

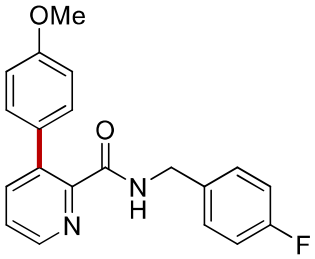

The general procedure **I** was followed using *N*-(4-fluorobenzyl)picolinamide **172e** (57.6 mg, 0.25 mmol) and **175a** (0.40 mL, 1.0 mmol, 2.5 M in THF). Isolation by column chromatography (*n*hexane/ethyl acetate: 2/1→1/1) yielded **176ea** (38.7 mg, 46%) as a white solid.

M. p.: 127–130 °C.

^{1}H-NMR (300 MHz, $CDCl_3$) δ = 8.53 (dd, J = 4.6, 1.6 Hz, 1H), 8.04 (s, 1H), 7.71 (dd, J = 7.8, 1.6 Hz, 1H), 7.45 (dd, J = 7.8, 4.6 Hz, 1H), 7.33–7.26 (m, 4H), 7.07–6.95 (m, 4H), 4.55 (d, J = 6.1 Hz, 2H), 3.88 (s, 3H).

^{13}C-NMR (100 MHz, $CDCl_3$) δ = 165.2 (C_q), 163.4 (d, $^{1}J_{C–F}$ = 245.4 Hz, C_q), 161.0 (d, $^{1}J_{C–F}$ = 245.4 Hz, C_q), 159.2 (C_q), 147.8 (C_q), 146.7 (CH), 140.2 (CH), 138.1 (C_q), 134.3 (d, $^{4}J_{C–F}$ = 3.1 Hz, C_q), 131.5 (C_q), 129.7 (CH), 129.5 (d, $^{3}J_{C–F}$ = 8.1 Hz, CH), 125.3 (CH), 115.5 (d, $^{2}J_{C–F}$ = 21.6 Hz, CH), 113.5 (CH), 55.3 (CH_3), 42.7 (CH_2).

^{19}F-NMR (282 MHz, $CDCl_3$) δ = –115.4 (tt, J = 9.0, 5.3 Hz).

IR (ATR): 2984, 2906, 1734, 1373, 1241, 1045, 913, 736 cm^{-1}.

MS (ESI) *m/z* (relative intensity): 695 (70) $[2M+Na]^+$, 359 (100) $[M+Na]^+$, 337 (90) $[M+H]^+$.

HR MS (ESI) *m/z* calc. for $C_{20}H_{18}FN_2O_2$ $[M+H]^+$ 337.1347, found 337.1349.

The analytical data are in accordance with those previously reported in the literature.[154]

N-(2-Fluorobenzyl)-3-(4-methoxyphenyl)picolinamide (176fa)

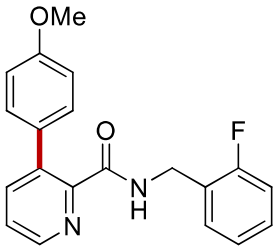

The general procedure was followed using *N*-(2-fluorobenzyl)picolinamide **172f** (57.6 mg, 0.25 mmol) and **175a** (0.40 mL, 1.0 mmol, 2.5 M in THF). Isolation by column chromatography (*n*hexane/ethyl acetate: 2/1→1/1) yielded **176fa** (47.1 mg, 56%) as a white solid.

M. p.: 114–116 °C.

^{1}H-NMR (300 MHz, $CDCl_3$) δ = 8.54 (dd, *J* = 4.7, 1.6 Hz, 1H), 8.06 (s, 1H), 7.70 (dd, *J* = 7.8, 1.6 Hz, 1H), 7.45 (dd, *J* = 7.8, 4.7 Hz, 1H), 7.41–7.34 (m, 1H), 7.30–7.27 (m, 3H), 7.16–7.01 (m, 2H), 7.00–6.90 (m, 2H), 4.71–4.57 (m, 2H), 3.87 (s, 3H).

^{13}C-NMR (125 MHz, $CDCl_3$) $_\delta$ = 165.1 (C_q), 160.9 (d, $^1J_{C–F}$ = 246.2 Hz, C_q), 159.0 (C_q), 147.8 (C_q), 146.5 (CH), 140.0 (CH), 137.9 (C_q), 131.4 (C_q), 130.1 (d, $^3J_{C–F}$ = 4.5 Hz, CH), 129.6 (CH), 129.0 (d, $^3J_{C–F}$ = 8.1 Hz, CH), 125.3 (d, $^2J_{C–F}$ = 15.0 Hz, C_q), 125.1 (CH), 124.1 (d, $^4J_{C–F}$ = 3.6 Hz, CH), 115.2 (d, $^2J_{C–F}$ = 21.4 Hz, CH), 113.4 (CH), 55.2 (CH_2), 37.3 (d, $^3J_{C–F}$ = 4.1 Hz, CH_2).

^{19}F-NMR (282 MHz, $CDCl_3$) δ = –118.8 (ddd, *J* = 10.2, 7.6, 5.6 Hz).

IR (ATR): 3057, 2984, 1733, 1373, 1242, 1046, 736, 608 cm^{-1}.

MS (ESI) *m/z* (relative intensity): 695 (40) $[2M+Na]^+$, 359 (60) $[M+Na]^+$, 337 (100) $[M+H]^+$.

HR-MS (ESI) *m/z* calc. for $C_{20}H_{18}FN_2O_2$ $[M+H]^+$ 337.1347, found 337.1349.

The analytical data are in accordance with those previously reported in the literature.[154]

3-(4-Methoxyphenyl)-*N*-(1,2,3,4-tetrahydronaphthalen-1-yl)picolinamide (176ga)

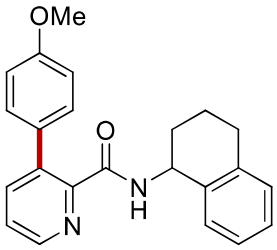

The general procedure was followed using *N*-(1,2,3,4-tetrahydronaphthalen-1-yl)picolinamide **172g** (63.1 mg, 0.25 mmol) and **175a** (0.40 mL, 1.0 mmol, 2.5 M in THF). Isolation by column chromatography (*n*hexane/ethyl acetate: 2/1→1/1) yielded **176ga** (66.4 mg, 74%) as a white solid.

M. p.: 125–126 °C.

^{1}H-NMR (400 MHz, $CDCl_3$) δ = 8.50 (dd, *J* = 4.7, 1.7 Hz, 1H), 7.86 (d, *J* = 8.9 Hz, 1H), 7.70 (dd, *J* = 7.9, 1.7 Hz, 1H), 7.43 (dd, *J* = 7.9, 4.7 Hz, 1H), 7.34 (d, *J* = 8.9 Hz, 2H), 7.28–7.24 (m, 1H), 7.21–7.10 (m, 3H), 7.01 (d, *J* = 8.9 Hz, 2H), 5.28 (dt, *J* = 9.9, 5.6 Hz, 1H), 3.89 (s, 3H), 2.90–2.74 (m, 2H), 2.16–2.04 (m, 1H), 1.94–1.79 (m, 3H).

^{13}C-NMR (100 MHz, $CDCl_3$) δ = 164.8 (C_q), 159.3 (C_q), 148.4 (C_q), 146.8 (CH), 140.0 (CH), 137.8 (C_q), 137.6 (C_q), 136.8 (C_q), 131.6 (C_q), 129.8 (CH), 129.1 (CH), 128.9 (CH), 127.2 (CH), 126.2 (CH), 125.1 (CH), 113.6 (CH), 55.3 (CH_3), 47.4 (CH), 30.1 (CH_2), 29.3 (CH_2), 20.1 (CH_2).

IR (ATR): 2984, 2905, 1734, 1373, 1241, 1046, 737, 608 cm^{-1}.

MS (EI) *m/z* (relative intensity): 739 (100) $[2M+Na]^+$, 381 (70) $[M+Na]^+$, 359 (80) $[M+H]^+$.

HR-MS (EI) *m/z* calc. for $C_{23}H_{23}N_2O_2$ $[M+H]^+$ 359.1754, found 359.1756.

The analytical data are in accordance with those previously reported in the literature.[154]

N-Cyclohexyl-3-(4-methoxyphenyl)picolinamide (176ha)

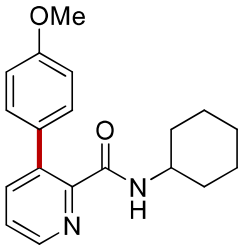

The general procedure was followed using *N*-cyclohexylpicolinamide **172h** (51.1 mg, 0.25 mmol) and **175a** (0.40 mL, 1.0 mmol, 2.5 M in THF). Isolation by column chromatography (*n*hexane/ethyl acetate: 2/1→1/1) yielded **176ha** (47.3 mg, 61%) as a white solid.

M. p.: 95–96 °C.

^{1}H-NMR (300 MHz, $CDCl_3$) δ = 8.49 (dd, J = 4.6, 1.7 Hz, 1H), 7.63 (dd, J = 7.8, 1.7 Hz, 1H), 7.57–7.47 (m, 1H), 7.38 (dd, J = 7.8, 4.7 Hz, 1H), 7.24 (d, J = 8.8 Hz, 2H), 6.92 (d, J = 8.8 Hz, 2H), 3.82 (s, 3H), 1.97–1.88 (m, 2H), 1.71–1.69 (m, 2H), 1.62–1.55 (m, 1H), 1.38–1.15 (m, 5H).

^{13}C-NMR (125 MHz, $CDCl_3$) δ = 164.3 (C_q), 159.0 (C_q), 148.4 (C_q), 146.4 (CH), 139.9 (CH), 137.7 (C_q), 131.7 (C_q), 129.5 (CH), 124.8 (CH), 113.4 (CH), 55.2 (CH_3), 48.1 (CH), 33.0 (CH_2), 25.7 (CH_2), 25.0 (CH_2).

IR (ATR): 3059, 2984, 1735, 1373, 1240, 1046, 737, 608 cm^{-1}.

MS (EI) *m/z* (relative intensity): 643 (80) $[2M+Na]^+$, 333 (90) $[M+Na]^+$, 311 (100) $[M+H]^+$.

HR-MS (EI) *m/z* calc. for $C_{19}H_{23}N_2O_2$ $[M+H]^+$ 311.1754, found 310.1755.

The analytical data are in accordance with those previously reported in the literature.[154]

***N*-*n*-Butyl-3-phenylpicolinamide (176ab)**

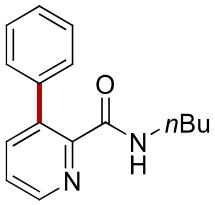

The general procedure was followed using **172a** (44.5 mg, 0.25 mmol) and phenylmagnesium bromide **175b** (0.38 mL, 1.0 mmol, 2.6 M in THF). Isolation by column chromatography (*n*hexane/ethyl acetate: 2/1→1/1) yielded **176ab** (47.7 mg, 75%) as a white solid.

M. p.: 59–61 °C.

^{1}H-NMR (400 MHz, $CDCl_3$) δ = 8.54 (dd, J = 4.7, 1.7 Hz, 1H), 7.72 (s, 1H), 7.67 (dd, J = 7.8, 1.7 Hz, 1H), 7.45–7.35 (m, 4H), 7.34–7.31 (m, 2H), 3.35 (td, J = 7.2, 6.0 Hz, 2H), 1.59–1.50 (m, 2H), 1.42–1.31 (m, 2H), 0.92 (t, J = 7.3 Hz, 3H).

^{13}C-NMR (100 MHz, $CDCl_3$) δ = 165.0 (C_q), 148.2 (C_q), 146.8 (CH), 140.0 (CH), 139.5 (C_q), 138.1 (C_q), 128.3 (CH), 127.8 (CH), 127.4 (CH), 125.0 (CH), 39.1 (CH_2), 31.6 (CH_2), 20.1 (CH_2), 13.7 (CH_3).

IR (ATR): 3250, 3060, 2957, 1649, 1510, 1313, 757, 698 cm^{-1}.

MS (ESI) *m/z* (relative intensity): 531 (100) $[2M+Na]^+$, 277 (90) $[M+Na]^+$, 255 (100) $[M+H]^+$.

HR-MS (ESI) *m/z* calc. for $C_{16}H_{19}N_2O$ $[M+H]^+$ 255.1492, found 255.1494.

The analytical data are in accordance with those previously reported in the literature.[154]

N-*n*-Butyl-3-(*p*-tolyl)picolinamide (176ac)

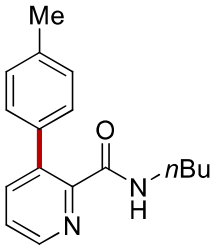

The general procedure was followed using **172a** (44.5 mg, 0.25 mmol) and *p*-tolylmagnesium bromide **xx175cx** (0.42 mL, 1.0 mmol, 2.4 M in THF). Isolation by column chromatography (*n*hexane/ethyl acetate: 2/1→1/1) yielded **176ac** (52.3 mg, 78%) as a white solid.

M. p.: 110–111 °C.

^{1}H-NMR (400 MHz, $CDCl_3$) δ = 8.52 (dd, J = 4.6, 1.6 Hz, 1H), 7.66 (dd, J = 7.8, 1.6 Hz, 2H), 7.41 (dd, J = 7.8, 4.6 Hz, 1H), 7.22 (m, 4H), 3.36 (td, J = 7.2, 6.0 Hz, 2H), 2.39 (s, 3H), 1.62–1.48 (m, 2H), 1.41–1.30 (m, 2H), 0.92 (t, J = 7.2 Hz, 3H).

^{13}C-NMR (100 MHz, $CDCl_3$) δ = 165.2 (C_q), 148.3 (C_q), 146.7 (CH), 140.0 (CH), 138.1 (C_q), 137.2 (C_q), 136.5 (C_q), 128.7 (CH), 128.2 (CH), 125.0 (CH), 39.1 (CH_2), 31.6 (CH_2), 21.3 (CH_3), 20.1 (CH_2), 13.8 (CH_3).

IR (ATR): 3250, 2958, 2920, 1665, 1550, 1315, 803, 696 cm^{-1}.

MS (EI) *m/z* (relative intensity): 268 (100) $[M]^+$, 211 (40), 168 (70).

HR-MS (ESI) *m/z* calc. for $C_{17}H_{21}N_2O$ $[M+H]^+$ 269.1648, found 269.1647.

The analytical data are in accordance with those previously reported in the literature.[154]

N-*n*-Butyl-3-[4-(*tert*-butyl)phenyl]picolinamide (176ad)

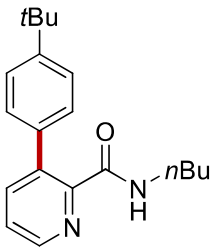

The general procedure was followed using **172a** (44.5 mg, 0.25 mmol) and (4-(*tert*-butyl)phenyl)magnesium bromide **175d** (0.40 mL, 1.0 mmol, 2.5 M in THF). Isolation by column chromatography (*n*hexane/ethyl acetate: 2/1→1/1) yielded **176ad** (56.6 mg, 73%) as a white solid.

M. p.: 106–109 °C.

^{1}H-NMR (400 MHz, $CDCl_3$) δ = 8.52 (dd, J = 4.6, 1.6 Hz, 1H), 7.67 (dd, J = 7.8, 1.6 Hz, 2H), 7.45–7.38 (m, 3H), 7.32–7.26 (m, 2H), 3.36 (td, J = 7.2, 6.0 Hz, 2H), 1.58–1.50 (m, 2H), 1.39–1.32 (m, 11H), 0.92 (t, J = 7.2 Hz, 3H).

^{13}C-NMR (100 MHz, $CDCl_3$) δ = 165.2 (C_q), 150.1 (C_q), 148.2 (C_q), 146.6 (CH), 140.1 (CH), 137.9 (C_q), 136.3 (C_q), 128.1 (CH), 124.9 (CH), 124.8 (CH), 39.1 (CH_2), 34.5 (C_q), 31.5 (CH_2), 31.3 (CH_3), 20.1 (CH_2), 13.7 (CH_3).

IR (ATR): 3280, 2961, 2871, 1649, 1510, 1002, 804, 584 cm^{-1}.

MS (ESI) *m/z* (relative intensity): 643 (70) $[2M+Na]^+$, 621 (10) $[2M+H]^+$, 333 (40) $[M+Na]^+$, 311 (100) $[M+H]^+$.

HR-MS (ESI) *m/z* calc. for $C_{20}H_{27}N_2O$ $[M+H]^+$ 311.2118, found 311.2117.

The analytical data are in accordance with those previously reported in the literature.[154]

***N*-*n*-Butyl-3-(3-methoxyphenyl)picolinamide (176ag)**

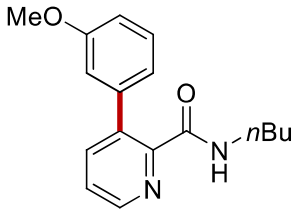

The general procedure was followed using **172a** (44.5 mg, 0.25 mmol) and (3-methoxyphenyl)magnesium bromide **175g** (0.40 mL, 1.0 mmol, 2.5 M in THF). Isolation by column chromatography (*n*hexane/ethyl acetate: 2/1→1/1) yielded **176ag** (54.0 mg, 76%) as a white solid.

M. p.: 100–102 °C.

^{1}H-NMR (400 MHz, $CDCl_3$) δ = 8.52 (dd, J = 4.7, 1.7 Hz, 1H), 7.66 (dd, J = 7.8, 1.7 Hz, 1H), 7.60 (s, 1H), 7.40 (dd, J = 7.8, 4.7 Hz, 1H), 7.34–7.26 (m, 1H), 6.92–6.83 (m, 3H), 3.80 (s, 3H), 3.34 (td, J = 7.1, 6.0 Hz, 2H), 1.57–1.48 (m, 2H), 1.39–1.29 (m, 2H), 0.90 (t, J = 7.1 Hz, 3H).

^{13}C-NMR (100 MHz, $CDCl_3$) δ = 165.2 (C_q), 159.2 (C_q), 148.6 (C_q), 147.1 (CH), 140.9 (C_q), 139.9 (CH), 137.9 (C_q), 129.0 (CH), 125.0 (CH), 121.1 (CH), 114.3 (CH), 113.0 (CH), 55.3 (CH_3), 39.3 (CH_2), 31.7 (CH_2), 20.2 (CH_2), 13.9 (CH_3).

IR (ATR): 3300, 2957, 2872, 1649, 1511, 1227, 779, 697 cm^{-1}.

MS (ESI) *m/z* (relative intensity): 591 (100) $[2M+Na]^+$, 307 (60) $[M+Na]^+$, 285 (90) $[M+H]^+$.

HR-MS (ESI) *m/z* calc. for $C_{17}H_{21}N_2O_2$ $[M+H]^+$ 285.1598, found 285.1602.

The analytical data are in accordance with those previously reported in the literature.[154]

***N*-*n*-Butyl-3-(3-fluorophenyl)picolinamide (176ah)**

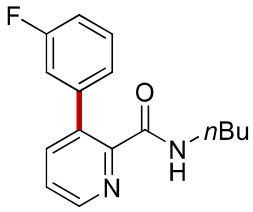

The general procedure was followed using **172a** (44.5 mg, 0.25 mmol) and (3-fluorophenyl)magnesium bromide **175h** (0.44 mL, 1.0 mmol, 2.3 M in THF). Isolation by column chromatography (*n*hexane/ethyl acetate: 2/1→1/1) yielded **176ah** (47.7 mg, 70%) as a white solid.

M. p.: 80–82 °C.

^{1}H-NMR (400 MHz, $CDCl_3$) δ = 8.56 (d, J = 4.6 Hz, 1H), 7.82 (s, 1H), 7.64 (dd, J = 7.8, 1.2 Hz, 1H), 7.44 (dd, J = 7.8, 4.6 Hz, 1H), 7.38–7.32 (m, 1H), 7.11–7.00 (m, 3H), 3.35 (td, J = 7.3, 6.3 Hz, 2H) 1.61–1.50 (m, 2H), 1.44–1.32 (m, 2H), 0.92 (t, J = 7.3 Hz, 3H).

^{13}C-NMR (100 MHz, $CDCl_3$) δ = 164.6 (C_q), 162.2 (d, $^{1}J_{C-F}$ = 245.6 Hz, C_q), 147.8 (C_q), 147.2 (CH), 141.8 (d, $^{3}J_{C-F}$ = 8.1 Hz, C_q), 139.8 (CH), 137.0 (C_q), 129.3 (d, $^{3}J_{C-F}$ = 8.4 Hz, CH), 125.0 (CH), 124.2 (d, $^{4}J_{C-F}$ = 3.0 Hz, CH), 115.4 (d, $^{2}J_{C-F}$ = 22.4 Hz, CH), 114.2 (d, $^{2}J_{C-F}$ = 21.1 Hz, CH), 39.1 (CH_2), 31.6 (CH_2), 20.1 (CH_2), 13.7 (CH_3).

^{19}F-NMR (282 MHz, $CDCl_3$) δ = –113.7.

IR (ATR): 3330, 3058, 2958, 2873, 1649, 1518, 783, 694 cm^{-1}.

MS (ESI) *m/z* (relative intensity): 567 (100) $[2M+Na]^+$, 295 (70) $[M+Na]^+$, 273 (80) $[M+H]^+$.

HR-MS (ESI) *m/z* calc. for $C_{16}H_{18}N_2OF$ $[M+H]^+$ 273.1398, found 273.1398.

The analytical data are in accordance with those previously reported in the literature.[154]

_N_-butyl-3-methylpicolinamide (214aa)

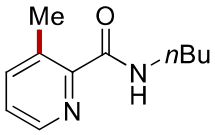

The general procedure was followed for 6 h using **172a** (44.5 mg, 0.25 mmol) and methylmagnesium bromide **165a** (0.33 mL, 1.0 mmol, 3.0 M in diethyl ether). Isolation by column chromatography (*n*hexane/ethyl acetate: 2/1→1/1) yielded **214aa** (28.8 mg, 60%) as a colourless liquid.

^{1}H-NMR (400 MHz, $CDCl_3$) δ = 8.39 (d, J = 4.6 Hz, 1H), 8.14 (s, 1H), 7.59 (d, J = 7.7 Hz, 1H), 7.33–7.27 (m, 1H), 3.45 (q, J = 6.8 Hz, 2H), 2.76 (s, 3H), 1.67–1.60 (m, 2H), 1.49–1.40 (m, 2H), 0.98 (t, J = 7.6 Hz 3H).

^{13}C-NMR (100 MHz, $CDCl_3$) δ = 166.0 (C_q), 147.5 (C_q), 145.4 (CH), 140.8 (CH), 135.3 (C_q), 125.5 (CH), 39.0 (CH_2), 31. 8 (CH_2), 20.6 (CH_3), 20.3 (CH_2), 13.8 (CH_3).

IR (ATR): 3390, 3054, 2959, 1670, 1517, 1448, 734, 468 cm^{-1}.

MS (ESI) *m/z* (relative intensity): 215 (70) $[M+Na]^+$, 193 (100) $[M+H]^+$.

HR-MS (ESI) *m/z* calc. for $C_{11}H_{17}N_2O$ $[M+H]^+$ 193.1335, found 193.1336.

The analytical data are in accordance with those previously reported in the literature.[193]

_N_-butyl-3-isopropylpicolinamide (214ab)

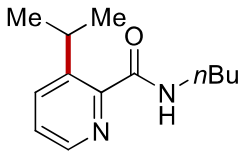

The general procedure was followed using **172a** (44.5 mg, 0.25 mmol) and isopropylmagnesium chloride **165b** (0.50 mL, 1.0 mmol, 2.0 M in THF). Isolation by column chromatography (*n*hexane/ethyl acetate: 2/1→1/1) yielded **214ab** (31.3 mg, 57%) as a yellow liquid.

^{1}H-NMR (400 MHz, $CDCl_3$) δ = 8.37 (dd, J = 4.5, 1.6 Hz, 1H), 7.97 (s, 1H), 7.80 (dd, J = 8.1, 1.7 Hz, 1H), 7.37 (dd, J = 8.0, 4.5 Hz, 1H), 4.45 (hept, J = 6.9 Hz, 1H), 3.45 (td, J = 7.1, 6.4 Hz, 2H), 1.67–1.59 (m, 2H), 1.49–1.41 (m, 2H), 1.28 (d, J = 6.9 Hz, 6H), 0.98 (t, J = 7.3 Hz, 3H).

^{13}C-NMR (100 MHz, $CDCl_3$) δ = 166.3 (C_q), 147.2 (C_q), 145.7 (C_q), 145.1 (CH), 135.5 (CH), 125.7 (CH), 39.1 (CH_2), 31.7 (CH_2), 27.6 (CH), 23.7 (CH_3), 20.3 (CH_2), 13.8 (CH_3).

IR (ATR): 3386, 3051, 2963, 1667, 1518, 1428, 735, 656 cm^{-1}.

MS (ESI) *m/z* (relative intensity): 463 (5) $[2M+Na]^+$, 243 (50) $[M+Na]^+$, 221 (100) $[M+H]^+$.

HR-MS (ESI) *m/z* calc. for $C_{13}H_{21}N_2O$ $[M+H]^+$ 221.1648, found 221.1652.

The analytical data are in accordance with those previously reported in the literature.[153]

3-benzyl-*N*-cyclohexylpicolinamide (214hc)

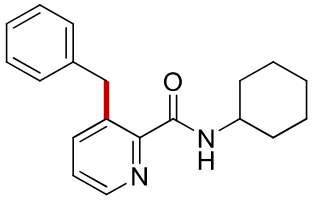

The general procedure was followed using *N*-cyclohexylpicolinamide **172h** (51.1 mg, 0.25 mmol) and benzylmagnesium chloride **165c** (0.70 mL, 1.0 mmol, 1.4 M in THF). Isolation by column chromatography (*n*hexane/ethyl acetate: 2/1→1/1) yielded **214hc** (33.1 mg, 45%) as a white solid.

M. p.: 98–100 °C.

^{1}H-NMR (400 MHz, $CDCl_3$) δ = 8.43 (d, J = 5.0 Hz, 1H), 8.10 (d, J = 1.8 Hz, 1H), 7.96 (d, J = 8.6 Hz, 1H), 7.36–7.25 (m, 3H), 7.24–7.17 (m, 3H), 4.05 (s, 2H), 4.02–3.93 (m, 1H), 2.02 (dt, J = 12.0, 4.1 Hz, 2H), 1.84–1.74 (m, 2H), 1.67 (dt, J = 12.9, 4.1 Hz, 1H), 1.50–1.22 (m, 5H).

^{13}C-NMR (100 MHz, $CDCl_3$) δ = 163.4 (C_q), 151.8 (C_q), 150.4 (C_q), 148.1 (CH), 138.6 (C_q), 129.0 (CH), 128.8 (CH), 126.8 (CH), 126.3 (CH), 122.7 (CH), 48.1 (CH), 41.4 (CH_2), 33.1 (CH_2), 25.6 (CH_2), 24.9 (CH_2).

IR (ATR): 3377, 3051, 2932, 1669, 1521, 1414, 734, 460 cm^{-1}.

MS (ESI) *m/z* (relative intensity): 611 (15) $[2M+Na]^+$, 317 (20) $[M+Na]^+$, 295 (100) $[M+H]^+$.

HR-MS (ESI) *m/z* calc. for $C_{19}H_{23}N_2O$ $[M+H]^+$ 295.1805, found 295.1806.

5.7.2 Competition Experiment

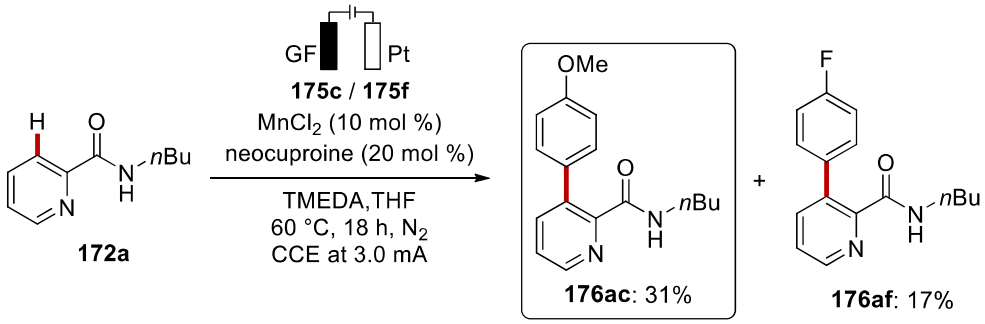

A solution of **172a** (44.5 mg, 0.25 mmol), $MnCl_2$ (3.1 mg, 10 mol %), neocuproine (10.4 mg, 20 mol %), and TMEDA (74 µL, 0.5 mmol) in THF (4.0 mL) was place in a 10 mL cell. **175c** (0.40 mL, 1.0 mmol, 2.5 M in THF) and **175f** (0.38 mL, 1.0 mmol, 2.6 M in THF) were added dropwise. The electrolysis was performed at 60 °C with a constant current of 3.0 mA for 18 h. After that, a saturated aqueous NH_4Cl solution (10 mL) was added, and the GF anode was washed with EtOAc (3 × 2 mL) in an ultrasonic bath. The reaction mixture was extracted with EtOAc (3 × 15 mL). The combined organic layers were dried over Na_2SO_4, filtered, and concentrated *in vacuo*. The crude product was purified by column chromatography (*n*hexane/ethyl acetate: 2/1→1/1) to yield **176ac** (22.0 mg, 31%) and **176af** (11.6 mg, 17%).

5.7.3 Well-defined Manganese Complex 215 as Catalyst

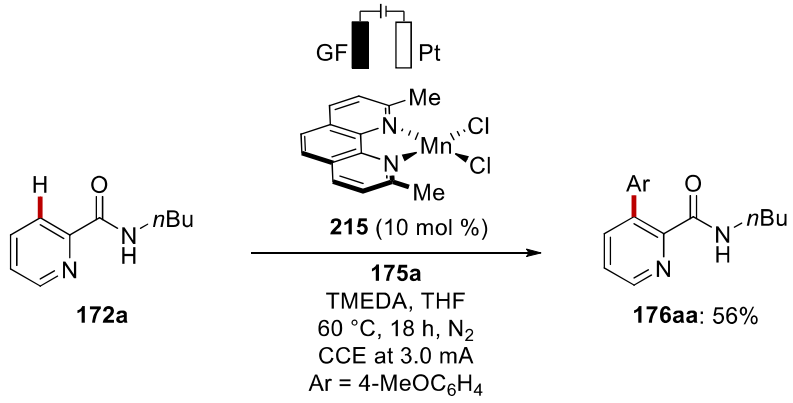

A solution of **172a** (44.5 mg, 0.25 mmol), manganese complex **215** (8.3 mg, 10 mol %), and TMEDA (74 µL, 0.5 mmol) in THF (4.0 mL) was place in a 10 mL cell. **175a** (0.40 mL, 1.0 mmol,

2.5 M in THF) was added dropwise. The electrolysis was performed at 60 °C with a constant current of 3.0 mA. for 18 h. After that, a saturated aqueous NH_4Cl solution (10 mL) was added, and the GF anode was washed with EtOAc (3 × 2 mL) in an ultrasonic bath. The reaction mixture was extracted with EtOAc (3 × 15 mL). The combined organic layers were dried over Na_2SO_4, filtered, and concentrated in vacuo. The crude product was purified by column chromatography (*n*hexane/ethyl acetate: 2/1→1/1) to yield **176aa** (39.8 mg, 56%).

5.7.4 Dependence on the Current

Three parallel electrolyses were carried out in undivided cells (10 mL), each equipped with graphite felt anode (10 mm × 10 mm × 6 mm) and platinum cathode (10 mm × 15 mm × 0.125 mm). Substrate **172a** (44.5 mg, 0.25 mmol), $MnCl_2$ (3.1 mg, 10 mol %), neocuproine (10.4 mg, 20 mol %), TMEDA (74 µL, 0.5 mmol), and THF (4.0 mL) were successively added. **175a** (0.40 mL, 1.0 mmol, 2.5 M in THF). The electrolysis was performed at 60 °C. In the time range of 30–90 min, aliquots of 0.1 mL were taken from each reaction mixture every 30 min. To each aliquot was added 0.1 mL of an internal standard solution (0.5 mmol of 1,3,5-trimethoxybenzene in 4.0 mL of THF), then treated with saturated aqueous NH_4Cl (2.0mL) and extracted with EtOAc (3 x 1.0 mL). The combined organic layers were dried over Na_2SO_4, filtered, and concentrated in vacuo. After evaporation of the solvents, the crude mixture was analyzed by ^{1}H-NMR spectroscopy. The determined yields of **176aa** were plotted in Figure 5.7.1.

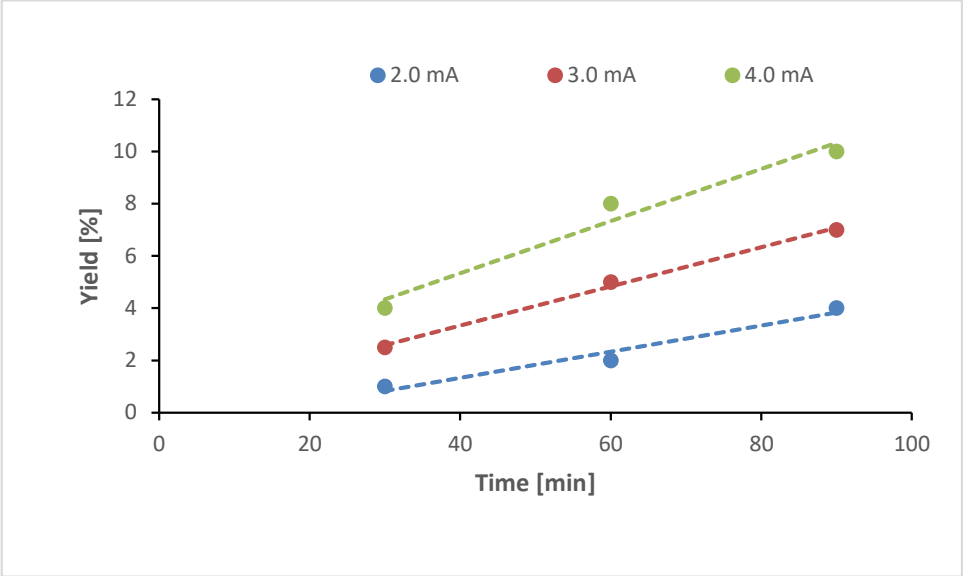

Figure 5.7.1 Manganaelectro-catalyzed C–H arylation at different currents, 1,3,5-trimethoxybenzene as internal standard.

5.7.5 Cyclic Voltammetry Studies

The cyclic voltammetry (Figure 5.7.2) was carried out with MSc Aude Salamé using a METROHM *Autolab PGSTAT204* workstation and the following analysis was performed with *Nova 2.0* software. A glassy-carbon (GC) electrode (3 mm diameter, disc-electrode) was used as the working electrode, a Pt wire was employed as the counter electrode and an Ag/Ag^+ electrode was used as a *quasi*-reference electrode with ferrocene as an internal standard. The measurements were carried out at a scan rate of 100 mVs^{-1}. The operation temperature was 298 K. All solutions were degassed via freeze-pump-thaw method prior to use and nitrogen was bubbled through the solutions for at least 5 min before the experiment was performed. The experiments were performed under inert conditions (constant flow of dry nitrogen).

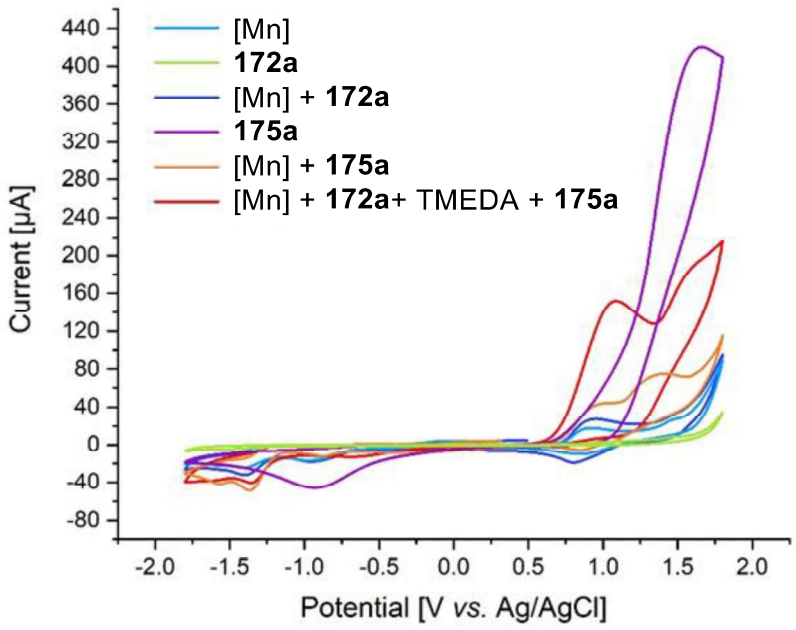

Figure 5.7.2 Cyclic voltammograms of reactants at 100 mVs^{-1} with nBu$_4$NPF$_6$ (0.2 mM in THF); concentrations of substrates 5 mM (Grignard **175a** 20 mM). [173] (light blue), **172a** (green), [173] + **172a** (blue), **175a** (purple), [173] + **175a** (orange), [173] + **172a** + TMEDA + **175a** (red). [173] = complex **215**.

6. References

[1] a) P. T. Anastas, M. M. Kirchhoff, *Acc. Chem. Res.* **2002**, *35*, 686-694; b) B. Trost, *Science* **1991**, *254*, 1471-1477.

[2] a) C. Jimenez-Gonzalez, C. S. Ponder, Q. B. Broxterman, J. B. Manley, *Org. Process Res. Dev.* **2011**, *15*, 912-917; b) D. J. C. Constable, A. D. Curzons, V. L. Cunningham, *Green Chem.* **2002**, *4*, 521-527.

[3] J. C. W. P. T. Anastas, Green Chemistry: Theory and Practice, Oxford University Press, New York, 1998.

[4] a) P. Gandeepan, L. H. Finger, T. H. Meyer, L. Ackermann, *Chem. Soc. Rev.* **2020**, *49*, 4254-4272; b) T. H. Meyer, L. H. Finger, P. Gandeepan, L. Ackermann, *Trends Chem.* **2019**, *1*, 63-76.

[5] a) F. Ullmann, J. Bielecki, *Ber. Dtsch. Chem. Ges.* **1901**, *34*, 2174-2185; b) C. Glaser, *Ber. Dtsch. Chem. Ges.* **1869**, *2*, 422-424.

[6] a) N. Miyaura, A. Suzuki, *Chem. Rev.* **1995**, *95*, 2457-2483; b) A. Suzuki, *Acc. Chem. Res.* **1982**, *15*, 178-184; c) N. Miyaura, A. Suzuki, *J. Chem. Soc., Chem. Commun.* **1979**, 866-867; d) N. Miyaura, K. Yamada, A. Suzuki, *Tetrahedron Lett.* **1979**, *20*, 3437-3440.

[7] a) E.-i. Negishi, T. Takahashi, S. Baba, D. E. Van Horn, N. Okukado, *J. Am. Chem. Soc.* **1987**, *109*, 2393-2401; b) E.-i. Negishi, *Acc. Chem. Res.* **1982**, *15*, 340-348; c) A. O. King, N. Okukado, E.-i. Negishi, *J. Chem. Soc., Chem. Commun.* **1977**, 683-684; d) E.-i. Negishi, A. O. King, N. Okukado, *J. Org. Chem.* **1977**, *42*, 1821-1823.

[8] a) H. A. Dieck, R. F. Heck, *J. Org. Chem.* **1975**, *40*, 1083-1090; b) H. A. Dieck, R. F. Heck, *J. Am. Chem. Soc.* **1974**, *96*, 1133-1136; c) R. F. Heck, J. P. Nolley, *J. Org. Chem.* **1972**, *37*, 2320-2322; d) T. Mizoroki, K. Mori, A. Ozaki, *Bull. Chem. Soc. Jpn.* **1971**, *44*, 581-581.

[9] a) R. J. P. Corriu, J. P. Masse, *J. Chem. Soc., Chem. Commun.* **1972**, 144a-144a; b) K. Tamao, K. Sumitani, M. Kumada, *J. Am. Chem. Soc.* **1972**, *94*, 4374-4376.

[10] a) T. Hiyama, *J. Organomet. Chem.* **2002**, *653*, 58-61; b) Y. Hatanaka, T. Hiyama, *J. Org. Chem.* **1988**, *53*, 918-920.

[11] a) J. K. Stille, *Angew. Chem. Int. Ed.* **1986**, *25*, 508-524; b) D. Milstein, J. K. Stille, *J. Am. Chem. Soc.* **1979**, *101*, 4992-4998; c) D. Milstein, J. K. Stille, *J. Am. Chem. Soc.* **1978**, *100*, 3636-3638; d) K. Masanori, S. Kazuo, S. Yutaka, M. Toshihiko, *Chem. Lett.* **1977**, *6*, 301-302; e) K. Masanori, S. Yutaka, M. Toshihiko, *Chem. Lett.* **1977**, *6*, 1423-1424.

[12] a) K. Sonogashira, *J. Organomet. Chem.* **2002**, *653*, 46-49; b) L. Cassar, *J. Organomet. Chem.* **1975**, *93*, 253-257; c) H. A. Dieck, F. R. Heck, *J. Organomet. Chem.* **1975**, *93*, 259-263; d) K. Sonogashira, Y. Tohda, N. Hagihara, *Tetrahedron Lett.* **1975**, *16*, 4467-4470.

[13] a) J. Tsuji, *Tetrahedron* **1986**, *42*, 4361-4401; b) B. M. Trost, *Acc. Chem. Res.* **1980**, *13*, 385-393; c) B. M. Trost, T. J. Fullerton, *J. Am. Chem. Soc.* **1973**, *95*, 292-294; d) J. Tsuji, H. Takahashi, M. Morikawa, *Tetrahedron Lett.* **1965**, *6*, 4387-4388.

[14] a) A. S. Guram, S. L. Buchwald, *J. Am. Chem. Soc.* **1994**, *116*, 7901-7902; b) F. Paul, J. Patt, J. F. Hartwig, *J. Am. Chem. Soc.* **1994**, *116*, 5969-5970.

[15] Nobel Prize Home Page: https://www.nobelprize.org/prizes/chemistry/2010/summary/ (accessed on 13.Sep.2021).

[16] P. A. Wender, V. A. Verma, T. J. Paxton, T. H. Pillow, *Acc. Chem. Res.* **2008**, *41*, 40-49.

[17] P. Gandeepan, T. Müller, D. Zell, G. Cera, S. Warratz, L. Ackermann, *Chem. Rev.* **2019**, *119*, 2192-2452.

[18] a) C.-Y. Huang, H. Kang, J. Li, C.-J. Li, *J. Org. Chem.* **2019**, *84*, 12705-12721; b) Y. Yang, J. Lan, J. You, *Chem. Rev.* **2017**, *117*, 8787-8863; c) S. H. Cho, J. Y. Kim, J. Kwak, S. Chang, *Chem. Soc. Rev.* **2011**, *40*, 5068-5083; d) C. S. Yeung, V. M. Dong, *Chem. Rev.* **2011**, *111*, 1215-1292; e) C.-J. Li, *Acc. Chem. Res.* **2009**, *42*, 335-344.

[19] S. J. Blanksby, G. B. Ellison, *Acc. Chem. Res.* **2003**, *36*, 255-263.

[20] a) Z. Huang, G. Dong, *Acc. Chem. Res.* **2017**, *50*, 465-471; b) L. Ackermann, in *Directed Metallation* (Ed.: N. Chatani), Springer Berlin Heidelberg, Berlin, Heidelberg, **2007**, pp. 35-60.

[21] E. M. Beck, M. J. Gaunt, in *C–H Activation* (Eds.: J.-Q. Yu, Z. Shi), Springer Berlin Heidelberg, **2010**, pp. 85-121.

[22] T. P. Pabst, P. J. Chirik, *Organometallics* **2021**, *40*, 813-831.

[23] a) U. Dhawa, N. Kaplaneris, L. Ackermann, *Org. Chem. Front.* **2021**, *8*, 4886-4913; b) M. Zhang, Y. Zhang, X. Jie, H. Zhao, G. Li, W. Su, *Org. Chem. Front.* **2014**, *1*, 843-895.

[24] S. De Sarkar, W. Liu, S. I. Kozhushkov, L. Ackermann, *Adv. Synth. Catal.* **2014**, *356*, 1461-1479.

[25] P. Gandeepan, L. Ackermann, *Chem* **2018**, *4*, 199-222.

[26] W. Ma, P. Gandeepan, J. Li, L. Ackermann, *Org. Chem. Front.* **2017**, *4*, 1435-1467.

[27] a) H. Yi, G. Zhang, H. Wang, Z. Huang, J. Wang, A. K. Singh, A. Lei, *Chem. Rev.* **2017**, *117*, 9016-9085; b) J.-T. Yu, C. Pan, *Chem. Commun.* **2016**, *52*, 2220-2236.

[28] a) L. Ackermann, *Chem. Rev.* **2011**, *111*, 1315-1345; b) D. Balcells, E. Clot, O. Eisenstein, *Chem. Rev.* **2010**, *110*, 749-823.

[29] T. Rogge, J. C. A. Oliveira, R. Kuniyil, L. Hu, L. Ackermann, *ACS Catal.* **2020**, *10*, 10551-10558.

[30] a) D. Lapointe, K. Fagnou, *Chem. Lett.* **2010**, *39*, 1118-1126; b) S. I. Gorelsky, D. Lapointe, K. Fagnou, *J. Am. Chem. Soc.* **2008**, *130*, 10848-10849; c) L.-C. Campeau, M. Parisien, A. Jean, K. Fagnou, *J. Am. Chem. Soc.* **2006**, *128*, 581-590.

[31] a) Y. Boutadla, D. L. Davies, S. A. Macgregor, A. I. Poblador-Bahamonde, *Dalton Trans.* **2009**, 5887-5893; b) D. L. Davies, S. M. A. Donald, S. A. Macgregor, *J. Am. Chem. Soc.* **2005**, *127*, 13754-13755.

[32] a) D. Zell, M. Bursch, V. Müller, S. Grimme, L. Ackermann, *Angew. Chem. Int. Ed.* **2017**, *56*, 10378-10382; b) D. Santrač, S. Cella, W. Wang, L. Ackermann, *Eur. J. Org. Chem.* **2016**, 5429-5436; c) H. Wang, M. Moselage, M. J. González, L. Ackermann, *ACS Catal.* **2016**, *6*, 2705-2709; d) W. Ma, R. Mei, G. Tenti, L. Ackermann, *Chem. Eur. J.* **2014**, *20*, 15248-15251.

[33] a) H. J. Schäfer, *C. R. Chimie* **2011**, *14*, 745-765; b) B. A. Frontana-Uribe, R. D. Little, J. G. Ibanez, A. Palma, R. Vasquez-Medrano, *Green Chem.* **2010**, *12*, 2099.

[34] M. Faraday, *Ann. Phys.* **1834**, *109*, 481-520.

[35] H. Kolbe, *Justus Liebigs Ann. Chem.* **1849**, *69*, 257-294.

[36] T. Shono, *Tetrahedron* **1984**, *40*, 811-850.

[37] J. H. Simons, *J. Electrochem. Soc.* **1949**, *95*, 47-52.

[38] a) A. K. Fazlur-Rahman, J.-C. Tsai, K. M. Nicholas, *J. Chem. Soc., Chem. Commun.* **1992**, 1334-1335; b) M. Bressan, A. Morvillo, *Inorg. Chim. Acta* **1989**, *166*, 177-179; c) H. Mimoun, *Angew. Chem. Int. Ed.* **1982**, *21*, 734-750; d) H. Mimoun, M. M. Perez Machirant, I. Seree de Roch, *J. Am. Chem. Soc.* **1978**, *100*, 5437-5444; e) M. M. Baizer, *J. Electrochem. Soc.* **1964**, *111*, 215.

[39] C. Amatore, C. Cammoun, A. Jutand, *Adv. Synth. Catal.* **2007**, *349*, 292-296.

[40] F. Kakiuchi, T. Kochi, H. Mutsutani, N. Kobayashi, S. Urano, M. Sato, S. Nishiyama, T. Tanabe, *J. Am. Chem. Soc.* **2009**, *131*, 11310-11311.

[41] H. Aiso, T. Kochi, H. Mutsutani, T. Tanabe, S. Nishiyama, F. Kakiuchi, *J. Org. Chem.* **2012**, *77*, 7718-7724.

[42] Q.-L. Yang, X.-Y. Wang, T.-L. Wang, X. Yang, D. Liu, X. Tong, X.-Y. Wu, T.-S. Mei, *Org. Lett.* **2019**, *21*, 2645-2649.

[43] Y. B. Dudkina, D. Y. Mikhaylov, T. V. Gryaznova, A. I. Tufatullin, O. N. Kataeva, D. A. Vicic, Y. H. Budnikova, *Organometallics* **2013**, *32*, 4785-4792.

[44] Q.-L. Yang, Y.-Q. Li, C. Ma, P. Fang, X.-J. Zhang, T.-S. Mei, *J. Am. Chem. Soc.* **2017**, *139*, 3293-3298.

[45] Y.-Q. Li, Q.-L. Yang, P. Fang, T.-S. Mei, D. Zhang, *Org. Lett.* **2017**, *19*, 2905-2908.

[46] A. Shrestha, M. Lee, A. L. Dunn, M. S. Sanford, *Org. Lett.* **2018**, *20*, 204-207.

[47] C. Ma, C.-Q. Zhao, Y.-Q. Li, L.-P. Zhang, X.-T. Xu, K. Zhang, T.-S. Mei, *Chem. Commun.* **2017**, *53*, 12189-12192.

[48] a) L. Ackermann, *Acc. Chem. Res.* **2020**, *53*, 84-104; b) R. Mei, U. Dhawa, R. C. Samanta, W. Ma, J. Wencel-Delord, L. Ackermann, *ChemSusChem* **2020**, *13*, 3306-3356; c) R. C. Samanta, T. H. Meyer, I. Siewert, L. Ackermann, *Chem. Sci.* **2020**, *11*, 8657-8670; d) S.-K. Zhang, R. C. Samanta, A. Del Vecchio, L. Ackermann, *Chem. Eur. J.* **2020**, *26*, 10936-10947; e) Y. Qiu, J. Struwe, L. Ackermann, *Synlett* **2019**, *30*, 1164-1173; f) C. Zhu, M. Stangier, J. C. A. Oliveira, L. Massignan, L. Ackermann, *Chem. Eur. J.* **2019**, *25*, 16382-16389; g) N. Sauermann, T. H. Meyer, L. Ackermann, *Chem. Eur. J.* **2018**, *24*, 16209-16217; h) N. Sauermann, T. H. Meyer, Y. Qiu, L. Ackermann, *ACS Catal.* **2018**, *8*, 7086-7103.

[49] a) P. Wang, X. Gao, P. Huang, A. Lei, *ChemCatChem* **2020**, *12*, 27-40; b) H. Wang, X. Gao, Z. Lv, T. Abdelilah, A. Lei, *Chem. Rev.* **2019**, *119*, 6769-6787; c) Y. Yuan, A. Lei, *Acc. Chem. Res.* **2019**, *52*, 3309-3324; d) S. Tang, L. Zeng, A. Lei, *J. Am. Chem. Soc.* **2018**, *140*, 13128-13135.

[50] a) K.-J. Jiao, Y.-K. Xing, Q.-L. Yang, H. Qiu, T.-S. Mei, *Acc. Chem. Res.* **2020**, *53*, 300-310; b) Q.-L. Yang, C.-Z. Li, L.-W. Zhang, Y.-Y. Li, X. Tong, X.-Y. Wu, T.-S. Mei, *Organometallics* **2019**, *38*, 1208-1212; c) C. Ma, P. Fang, T.-S. Mei, *ACS Catal.* **2018**, *8*, 7179-7189; d) Q.-L. Yang, P. Fang, T.-S. Mei, *Chin. J. Chem .* **2018**, *36*, 338-352; e) K.-J. Jiao, C.-Q. Zhao, P. Fang, T.-S. Mei, *Tetrahedron Lett.* **2017**, *58*, 797-802.

[51] a) Z.-J. Wu, F. Su, W. Lin, J. Song, T.-B. Wen, H.-J. Zhang, H.-C. Xu, *Angew. Chem. Int. Ed.* **2019**, *58*, 16770-16774; b) F. Xu, Y.-J. Li, C. Huang, H.-C. Xu, *ACS Catal.* **2018**, *8*, 3820-3824.

[52] a) Y. H. Budnikova, *Chem. Rec.* **2021**, *21*, 2148-2163; b) X. Ye, C. Wang, S. Zhang, J. Wei, C. Shan, L. Wojtas, Y. Xie, X. Shi, *ACS Catal.* **2020**, *10*, 11693-11699; c) S. Kathiravan, S. Suriyanarayanan, I. A. Nicholls, *Org. Lett.* **2019**, *21*, 1968-1972; d) M.-J. Luo, M. Hu, R.-J. Song, D.-L. He, J.-H. Li, *Chem. Commun.* **2019**, *55*, 1124-1127; e) M.-J. Luo, T.-T. Zhang, F.-J. Cai, J.-H. Li, D.-L. He, *Chem. Commun.* **2019**, *55*, 7251-7254; f) Z.-Q. Wang, C. Hou, Y.-F. Zhong, Y.-X. Lu, Z.-Y. Mo, Y.-M. Pan, H.-T. Tang, *Org. Lett.* **2019**, *21*, 9841-9845.

[53] M. S. Kharasch, E. K. Fields, *J. Am. Chem. Soc.* **1941**, *63*, 2316-2320.

[54] S. Murahashi, *J. Am. Chem. Soc.* **1955**, *77*, 6403-6404.

[55] S. Murahashi, S. Horiie, *J. Am. Chem. Soc.* **1956**, *78*, 4816-4817.

[56] a) R. Beck, H. Sun, X. Li, S. Camadanli, H.-F. Klein, *Eur. J. Inorg. Chem.* **2008**, 3253-3257; b) S. Camadanli, R. Beck, U. Flörke, H.-F. Klein, *Dalton Trans.* **2008**, 5701-5704; c) H.-F. Klein, S. Camadanli, R. Beck, D. Leukel, U. Flörke, *Angew. Chem. Int. Ed.* **2005**, *44*, 975-977; d) H.-F. Klein, R. Beck, U. Flörke, H.-J. Haupt, *Eur. J. Inorg. Chem.* **2003**, 1380-1387; e) H.-F. Klein, S. Schneider, M. He, U. Floerke, H.-J. Haupt, *Eur. J. Inorg. Chem.* **2000**, 2295-2301; f) H.-F. Klein, M. Helwig, U. Koch, U. Flörke, H.-J. Haupt, *Z. Naturforsch. B* **1993**, *48*, 778-784.

[57] G. Halbritter, F. Knoch, A. Wolski, H. Kisch, *Angew. Chem. Int. Ed.* **1994**, *33*, 1603-1605.

[58] L. Grigorjeva, O. Daugulis, *Angew. Chem. Int. Ed.* **2014**, *53*, 10209-10212.

[59] S. Rej, Y. Ano, N. Chatani, *Chem. Rev.* **2020**, *120*, 1788-1887.

[60] L. Grigorjeva, O. Daugulis, *Org. Lett.* **2014**, *16*, 4684-4687.

[61] a) T. T. Nguyen, L. Grigorjeva, O. Daugulis, *Angew. Chem. Int. Ed.* **2018**, *57*, 1688-1691; b) S. Zhai, S. Qiu, X. Chen, J. Wu, H. Zhao, C. Tao, Y. Li, B. Cheng, H. Wang, H. Zhai, *Chem. Commun.* **2018**, *54*, 98-101; c) Á. M. Martínez, N. Rodríguez, R. Gómez-Arrayás, J. C. Carretero, *Chem. Eur. J.* **2017**, *23*, 11669-11676.

[62] R. Mei, H. Wang, S. Warratz, S. A. Macgregor, L. Ackermann, *Chem. Eur. J.* **2016**, *22*, 6759-6763.

[63] A. Dey, N. Thrimurtulu, C. M. R. Volla, *Org. Lett.* **2019**, *21*, 3871-3875.

[64] W. Ma, L. Ackermann, *ACS Catal.* **2015**, *5*, 2822-2825.

[65] N. Thrimurtulu, A. Dey, D. Maiti, C. M. R. Volla, *Angew. Chem. Int. Ed.* **2016**, *55*, 12361-12365.

[66] R. Boobalan, R. Kuppusamy, R. Santhoshkumar, P. Gandeepan, C.-H. Cheng, *ChemCatChem* **2017**, *9*, 273-277.

[67] a) S. Maity, R. Kancherla, U. Dhawa, E. Hoque, S. Pimparkar, D. Maiti, *ACS Catal.* **2016**, *6*, 5493-5499; b) R. Manoharan, G. Sivakumar, M. Jeganmohan, *Chem. Commun.* **2016**, *52*, 10533-10536; c) T. Yamaguchi, Y. Kommagalla, Y. Aihara, N. Chatani, *Chem. Commun.* **2016**, *52*, 10129-10132.

[68] V. G. Landge, G. Jaiswal, E. Balaraman, *Org. Lett.* **2016**, *18*, 812-815.

[69] L.-B. Zhang, X.-Q. Hao, S.-K. Zhang, Z.-J. Liu, X.-X. Zheng, J.-F. Gong, J.-L. Niu, M.-P. Song, *Angew. Chem. Int. Ed.* **2015**, *54*, 272-275.

[70] J. Lan, H. Xie, X. Lu, Y. Deng, H. Jiang, W. Zeng, *Org. Lett.* **2017**, *19*, 4279-4282.

[71] X. Wu, K. Yang, Y. Zhao, H. Sun, G. Li, H. Ge, *Nat. Commun.* **2015**, *6*, 6462.

[72] L.-B. Zhang, S.-K. Zhang, D. Wei, X. Zhu, X.-Q. Hao, J.-H. Su, J.-L. Niu, M.-P. Song, *Org. Lett.* **2016**, *18*, 1318-1321.

[73] N. Sauermann, T. H. Meyer, C. Tian, L. Ackermann, *J. Am. Chem. Soc.* **2017**, *139*, 18452-18455.

[74] S. Tang, D. Wang, Y. Liu, L. Zeng, A. Lei, *Nat. Commun.* **2018**, *9*, 798.

[75] R. Mei, N. Sauermann, J. C. A. Oliveira, L. Ackermann, *J. Am. Chem. Soc.* **2018**, *140*, 7913-7921.

[76] T. H. Meyer, J. C. A. Oliveira, S. C. Sau, N. W. J. Ang, L. Ackermann, *ACS Catal.* **2018**, *8*, 9140-9147.

[77] R. Mei, W. Ma, Y. Zhang, X. Guo, L. Ackermann, *Org. Lett.* **2019**, *21*, 6534-6538.

[78] Y. Cao, Y. Yuan, Y. Lin, X. Jiang, Y. Weng, T. Wang, F. Bu, L. Zeng, A. Lei, *Green Chem.* **2020**, *22*, 1548-1552.

[79] T. H. Meyer, J. C. A. Oliveira, D. Ghorai, L. Ackermann, *Angew. Chem. Int. Ed.* **2020**, *59*, 10955-10960.

[80] L. Zeng, H. Li, S. Tang, X. Gao, Y. Deng, G. Zhang, C.-W. Pao, J.-L. Chen, J.-F. Lee, A. Lei, *ACS Catal.* **2018**, *8*, 5448-5453.

[81] S. C. Sau, R. Mei, J. Struwe, L. Ackermann, *ChemSusChem* **2019**, *12*, 3023-3027.

[82] U. Dhawa, C. Tian, W. Li, L. Ackermann, *ACS Catal.* **2020**, *10*, 6457-6462.

[83] N. Sauermann, R. Mei, L. Ackermann, *Angew. Chem. Int. Ed.* **2018**, *57*, 5090-5094.

[84] X. Gao, P. Wang, L. Zeng, S. Tang, A. Lei, *J. Am. Chem. Soc.* **2018**, *140*, 4195-4199.

[85] C. Tian, U. Dhawa, J. Struwe, L. Ackermann, *Chin. J. Chem .* **2019**, *37*, 552-556.

[86] a) A. Fürstner, *J. Am. Chem. Soc.* **2019**, *141*, 11-24; b) O. M. Ogba, N. C. Warner, D. J. O'Leary, R. H. Grubbs, *Chem. Soc. Rev.* **2018**, *47*, 4510-4544; c) P. Nareddy, F. Jordan, M. Szostak, *ACS Catal.* **2017**, *7*, 5721-5745; d) L. Ackermann, *Acc. Chem. Res.* **2014**, *47*, 281-295; e) P. B. Arockiam, C. Bruneau, P. H. Dixneuf, *Chem. Rev.* **2012**, *112*, 5879-5918; f) L. Ackermann, R. Vicente, *Top. Curr. Chem.* **2010**, *292*, 211-229; g) B. M. Trost, F. D. Toste, A. B. Pinkerton, *Chem. Rev.* **2001**, *101*, 2067-2096.

[87] a) K. S. Singh, *Catalysts* **2019**, *9*, 173; b) R. Manikandan, M. Jeganmohan, *Chem. Commun.* **2017**, *53*, 8931-8947; c) R. Manikandan, M. Jeganmohan, *Org. Biomol. Chem.* **2015**, *13*, 10420-10436.

[88] J. Chatt, J. M. Davidson, *J. Chem. Soc.* **1965**, 843-855.

[89] L. N. Lewis, J. F. Smith, *J. Am. Chem. Soc.* **1986**, *108*, 2728-2735.

[90] E. J. Moore, W. R. Pretzer, T. J. O'Connell, J. Harris, L. LaBounty, L. Chou, S. S. Grimmer, *J. Am. Chem. Soc.* **1992**, *114*, 5888-5890.

[91] S. Murai, F. Kakiuchi, S. Sekine, Y. Tanaka, A. Kamatani, M. Sonoda, N. Chatani, *Nature* **1993**, *366*, 529-531.

[92] a) C. Jia, T. Kitamura, Y. Fujiwara, *Acc. Chem. Res.* **2001**, *34*, 633-639; b) Y. Fujiwara, I. Moritani, S. Danno, R. Asano, S. Teranishi, *J. Am. Chem. Soc.* **1969**, *91*, 7166-7169; c) I. Moritani, Y. Fujiwara, *Tetrahedron Lett.* **1967**, *8*, 1119-1122.

[93] H. Weissman, X. Song, D. Milstein, *J. Am. Chem. Soc.* **2001**, *123*, 337-338.

[94] L. Ackermann, A. V. Lygin, N. Hofmann, *Angew. Chem. Int. Ed.* **2011**, *50*, 6379-6382.

[95] L. Ackermann, J. Pospech, K. Graczyk, K. Rauch, *Org. Lett.* **2012**, *14*, 930-933.

[96] R. K. Chinnagolla, M. Jeganmohan, *Chem. Commun.* **2012**, *48*, 2030-2032.

[97] S. Warratz, C. Kornhaaß, A. Cajaraville, B. Niepötter, D. Stalke, L. Ackermann, *Angew. Chem. Int. Ed.* **2015**, *54*, 5513-5517.

[98] H. Tan, H. Li, J. Wang, L. Wang, *Chem. Eur. J.* **2015**, *21*, 1904-1907.

[99] a) S. Rajkumar, S. Antony Savarimuthu, R. Senthil Kumaran, C. M. Nagaraja, T. Gandhi, *Chem. Commun.* **2016**, *52*, 2509-2512; b) K. S. Singh, S. G. Sawant, P. H. Dixneuf, *ChemCatChem* **2016**, *8*, 1046-1050; c) Y. Zhao, Z. He, S. Li, J. Tang, G. Gao, J. Lan, J. You, *Chem. Commun.* **2016**, *52*, 4613-4616; d) A. Banerjee, S. K. Santra, P. R. Mohanta, B. K. Patel, *Org. Lett.* **2015**, *17*, 5678-5681; e) R. Li, Y. Hu, R. Liu, R. Hu, B. Li, B. Wang, *Adv. Synth. Catal.* **2015**, *357*, 3885-3892; f) R. Manoharan, M. Jeganmohan, *Chem. Commun.* **2015**, *51*, 2929-2932; g) R. Prakash, K. Shekarrao, S. Gogoi, *Org. Lett.* **2015**, *17*, 5264-5267; h) Y. Zheng, W.-B. Song, S.-W. Zhang, L.-J. Xuan, *Org. Biomol. Chem.* **2015**, *13*, 6474-6478; i) Z. Zuo, X. Yang, J. Liu, J. Nan, L. Bai, Y. Wang, X. Luan, *J. Org. Chem.* **2015**, *80*, 3349-3356; j) R. K. Arigela, R. Kumar, T. Joshi, R. Mahar, B. Kundu, *RSC Adv.* **2014**, *4*, 57749-57753; k) C.-H. Hung, P. Gandeepan, C.-H. Cheng, *ChemCatChem* **2014**, *6*, 2692-2697; l) S. Nakanowatari, L. Ackermann, *Chem. Eur. J.* **2014**, *20*, 5409-5413; m) J. D. Dooley, S. Reddy Chidipudi, H. W. Lam, *J. Am. Chem. Soc.* **2013**, *135*, 10829-10836.

[100] L. Ackermann, J. Pospech, *Org. Lett.* **2011**, *13*, 4153-4155.

[101] A. Bechtoldt, M. E. Baumert, L. Vaccaro, L. Ackermann, *Green Chem.* **2018**, *20*, 398-402.

[102] a) L. Ackermann, L. Wang, R. Wolfram, A. V. Lygin, *Org. Lett.* **2012**, *14*, 728-731; b) J. Li, C. Kornhaaß, L. Ackermann, *Chem. Commun.* **2012**, *48*, 11343-11345.

[103] B. Li, J. Ma, Y. Liang, N. Wang, S. Xu, H. Song, B. Wang, *Eur. J. Org. Chem.* **2013**, 1950-1962.

[104] M. C. Reddy, M. Jeganmohan, *Eur. J. Org. Chem.* **2013**, 1150-1157.

[105] I. Choi, A. M. Messinis, L. Ackermann, *Angew. Chem. Int. Ed.* **2020**, *59*, 12534-12540.

[106] V. S. Thirunavukkarasu, S. I. Kozhushkov, L. Ackermann, *Chem. Commun.* **2014**, *50*, 29-39.

[107] a) M. Drees, T. Strassner, *J. Org. Chem.* **2006**, *71*, 1755-1760; b) J. M. Bakke, A. E. Frøhaug, *J. Phys. Org. Chem.* **1996**, *9*, 310-318.

[108] a) E. McNeill, J. Du Bois, *Chem. Sci.* **2012**, *3*, 1810-1813; b) E. McNeill, J. Du Bois, *J. Am. Chem. Soc.* **2010**, *132*, 10202-10204.

[109] Y. Yang, Y. Lin, Y. Rao, *Org. Lett.* **2012**, *14*, 2874-2877.

[110] V. S. Thirunavukkarasu, J. Hubrich, L. Ackermann, *Org. Lett.* **2012**, *14*, 4210-4213.

[111] V. S. Thirunavukkarasu, L. Ackermann, *Org. Lett.* **2012**, *14*, 6206-6209.

[112] F. Yang, L. Ackermann, *Org. Lett.* **2013**, *15*, 718-720.

[113] W. Liu, L. Ackermann, *Org. Lett.* **2013**, *15*, 3484-3486.

[114] a) G. Shan, X. Han, Y. Lin, S. Yu, Y. Rao, *Org. Biomol. Chem.* **2013**, *11*, 2318-2322; b) X. Yang, G. Shan, Y. Rao, *Org. Lett.* **2013**, *15*, 2334-2337.

[115] F. Yang, K. Rauch, K. Kettelhoit, L. Ackermann, *Angew. Chem. Int. Ed.* **2014**, *53*, 11285-11288.

[116] a) D. A. Colby, R. G. Bergman, J. A. Ellman, *Chem. Rev.* **2010**, *110*, 624-655; b) B. de Bruin, P. H. M. Budzelaar, A. W. Gal, *Angew. Chem. Int. Ed.* **2004**, *43*, 4142-4157.

[117] J. M. Kisenyi, G. J. Sunley, J. A. Cabeza, A. J. Smith, H. Adams, N. J. Salt, P. M. Maitlis, *J. Chem. Soc., Dalton Trans.* **1987**, 2459-2466.

[118] a) T. Matsumoto, R. A. Periana, D. J. Taube, H. Yoshida, *J. Catal.* **2002**, *206*, 272-280; b) T. Matsumoto, H. Yoshida, *Chem. Lett.* **2000**, *29*, 1064-1065.

[119] a) K. Ueura, T. Satoh, M. Miura, *Org. Lett.* **2007**, *9*, 1407-1409; b) K. Ueura, T. Satoh, M. Miura, *J. Org. Chem.* **2007**, *72*, 5362-5367.

[120] M. Shimizu, K. Hirano, T. Satoh, M. Miura, *J. Org. Chem.* **2009**, *74*, 3478-3483.

[121] S. Mochida, K. Hirano, T. Satoh, M. Miura, *J. Org. Chem.* **2009**, *74*, 6295-6298.

[122] M. Shimizu, H. Tsurugi, T. Satoh, M. Miura, *Chem. Asian J.* **2008**, *3*, 881-886.

[123] H. Zeng, C.-J. Li, *Angew. Chem. Int. Ed.* **2014**, *53*, 13862-13865.

[124] a) L. Cai, X. Zhu, J. Chen, A. Lin, H. Yao, *Org. Chem. Front.* **2019**, *6*, 3688-3692; b) P. Sun, S. Gao, C. Yang, S. Guo, A. Lin, H. Yao, *Org. Lett.* **2016**, *18*, 6464-6467; c) S. Mochida, M. Shimizu, K. Hirano, T. Satoh, M. Miura, *Chem. Asian J.* **2010**, *5*, 847-851; d) T. Uto, M. Shimizu, K. Ueura, H. Tsurugi, T. Satoh, M. Miura, *J. Org. Chem.* **2008**, *73*, 298-300.

[125] D. R. Stuart, M. Bertrand-Laperle, K. M. N. Burgess, K. Fagnou, *J. Am. Chem. Soc.* **2008**, *130*, 16474-16475.

[126] T. Fukutani, N. Umeda, K. Hirano, T. Satoh, M. Miura, *Chem. Commun.* **2009**, 5141-5143.

[127] K. Kim, J. Hyun, J. Kim, H. Kim, *Asian J. Org. Chem.* **2017**, *6*, 907-912.

[128] Y. Wu, B. Zhou, *Org. Lett.* **2017**, *19*, 3532-3535.

[129] W. Zhai, B. Li, B. Wang, *ChemistrySelect* **2018**, *3*, 8035-8039.

[130] Y. Qiu, C. Tian, L. Massignan, T. Rogge, L. Ackermann, *Angew. Chem. Int. Ed.* **2018**, *57*, 5818-5822.

[131] Y. Qiu, W.-J. Kong, J. Struwe, N. Sauermann, T. Rogge, A. Scheremetjew, L. Ackermann, *Angew. Chem. Int. Ed.* **2018**, *57*, 5828-5832.

[132] Y. Zhang, J. Struwe, L. Ackermann, *Angew. Chem. Int. Ed.* **2020**, *59*, 15076-15080.

[133] Z. Shen, I. Maksso, R. Kuniyil, T. Rogge, L. Ackermann, *Chem. Commun.* **2021**, *57*, 3668-3671.

[134] Y. Qiu, A. Scheremetjew, L. Ackermann, *J. Am. Chem. Soc.* **2019**, *141*, 2731-2738.

[135] W.-J. Kong, L. H. Finger, J. C. A. Oliveira, L. Ackermann, *Angew. Chem. Int. Ed.* **2019**, *58*, 6342-6346.

[136] W.-J. Kong, Z. Shen, L. H. Finger, L. Ackermann, *Angew. Chem. Int. Ed.* **2020**, *59*, 5551-5556.

[137] W.-J. Kong, L. H. Finger, A. M. Messinis, R. Kuniyil, J. C. A. Oliveira, L. Ackermann, *J. Am. Chem. Soc.* **2019**, *141*, 17198-17206.

[138] J. Kim, K. Shin, S. Jin, D. Kim, S. Chang, *J. Am. Chem. Soc.* **2019**, *141*, 4137-4146.

[139] Y. Wang, J. C. A. Oliveira, Z. Lin, L. Ackermann, *Angew. Chem. Int. Ed.* **2021**, *60*, 6419-6424.

[140] Y.-K. Xing, X.-R. Chen, Q.-L. Yang, S.-Q. Zhang, H.-M. Guo, X. Hong, T.-S. Mei, *Nat. Commun.* **2021**, *12*, 930.

[141] M. Stangier, A. M. Messinis, J. C. A. Oliveira, H. Yu, L. Ackermann, *Nat. Commun.* **2021**, *12*, 4736.

[142] W. Liu, L. Ackermann, *ACS Catal.* **2016**, *6*, 3743-3752.

[143] a) P. B. Tchounwou, C. G. Yedjou, A. K. Patlolla, D. J. Sutton, in *Molecular, Clinical and Environmental Toxicology: Volume 3: Environmental Toxicology* (Ed.: A. Luch), Springer Basel, **2012**, pp. 133-164; b) S. H. Gilani, Y. Alibhai, *J. Toxicol. Environ. Health* **1990**, *30*, 23-31.

[144] M. I. Bruce, M. Z. Iqbal, F. G. A. Stone, *J. Chem. Soc. A* **1970**, 3204-3209.

[145] a) G. J. Depree, L. Main, B. K. Nicholson, *J. Organomet. Chem.* **1998**, *551*, 281-291; b) W. Tully, L. Main, B. K. Nicholson, *J. Organomet. Chem.* **1995**, *503*, 75-92; c) N. P. Robinson, L. Main, B. K. Nicholson, *J. Organomet. Chem.* **1988**, *349*, 209-218; d) L. H. P. Gommans, L. Main, B. K. Nicholson, *J. Chem. Soc., Chem. Commun.* **1987**, 761-762.

[146] a) R. C. Cambie, L. C. Mui Mui, P. S. Rutledge, P. D. Woodgate, *J. Organomet. Chem.* **1994**, *464*, 171-182; b) R. C. Cambie, M. R. Metzler, P. S. Rutledge, P. D. Woodgate, *J. Organomet. Chem.* **1992**, *429*, 41-57; c) R. C. Cambie, M. R. Metzler, P. S. Rutledge, P. D. Woodgate, *J. Organomet. Chem.* **1990**, *381*, C26-C30; d) R. C. Cambie, M. R. Metzler, P. S. Rutledge, P. D. Woodgate, *J. Organomet. Chem.* **1990**, *398*, C22-C24.

[147] L. S. Liebeskind, J. R. Gasdaska, J. S. McCallum, S. J. Tremont, *J. Org. Chem.* **1989**, *54*, 669-677.

[148] a) G. J. Depree, L. Main, B. K. Nicholson, N. P. Robinson, G. B. Jameson, *J. Organomet. Chem.* **2006**, *691*, 667-679; b) J. Albert, J. M. Cadena, J. Granell, X. Solans, M. Font-Bardia, *J. Organomet. Chem.* **2004**, *689*, 4889-4896; c) D. Lafrance, J. L. Davis, R. Dhawan, B. A. Arndtsen, *Organometallics* **2001**, *20*, 1128-1136; d) M. A. Leeson, B. K. Nicholson, M. R. Olsen, *J. Organomet. Chem.* **1999**, *579*, 243-251; e) G. J. Depree, N. D. Childerhouse, B. K. Nicholson, *J. Organomet. Chem.* **1997**, *533*, 143-151; f) J.-P. Djukic, A. Maisse, M. Pfeffer, A. de Cian, J. Fischer, *Organometallics* **1997**, *16*, 657-667; g) C. Morton, D. J. Duncalf, J. P. Rourke, *J. Organomet. Chem.* **1997**, *530*, 19-25; h) J. M. Cooney, L. H. P. Gommans, L. Main, B. K. Nicholson, *J. Organomet. Chem.* **1988**, *349*, 197-207; i) J. M. Ressner, P. C. Wernett, C. S. Kraihanzel, A. L. Rheingold, *Organometallics* **1988**, *7*, 1661-1663; j) A. Suárez, J. Manuel Vila, M. Teresa Pereira, E. Gayoso, M. Gayoso, *J. Organomet. Chem.* **1987**, *335*, 359-363; k) M. I. Bruce, B. L. Goodall, M. Z. Iqbal, F. G. A. Stone, R. J. Doedens, R. G. Little, *J. Chem. Soc. D* **1971**, 1595-1596.

[149] Y. Kuninobu, Y. Nishina, T. Takeuchi, K. Takai, *Angew. Chem. Int. Ed.* **2007**, *46*, 6518-6520.

[150] B. Zhou, Y. Hu, C. Wang, *Angew. Chem. Int. Ed.* **2015**, *54*, 13659-13663.

[151] W. Liu, G. Cera, J. C. A. Oliveira, Z. Shen, L. Ackermann, *Chem. Eur. J.* **2017**, *23*, 11524-11528.

[152] T. Sato, T. Yoshida, H. H. Al Mamari, L. Ilies, E. Nakamura, *Org. Lett.* **2017**, *19*, 5458-5461.

[153] Z. Shen, H. Huang, C. Zhu, S. Warratz, L. Ackermann, *Org. Lett.* **2019**, *21*, 571-574.

[154] C. Zhu, J. C. A. Oliveira, Z. Shen, H. Huang, L. Ackermann, *ACS Catal.* **2018**, *8*, 4402-4407.

[155] I. Choi, Z. Shen, E. Ronge, V. Karius, C. Jooss, L. Ackermann, *Chem. Eur. J.* **2021**, *27*, 12737-12741.

[156] a) L. F. T. Novaes, S. Lin, *Trends Chem.* **2020**, *2*, 84-85; b) J. C. Siu, N. Fu, S. Lin, *Acc Chem Res* **2020**, *53*, 547-560; c) N. Fu, Y. Shen, A. R. Allen, L. Song, A. Ozaki, S. Lin, *ACS Catal.* **2019**, *9*, 746-754; d) L. Lu, N. Fu, S. Lin, *Synlett* **2019**, *30*, 1199-1203; e) J. B. Parry, N. Fu, S. Lin, *Synlett* **2018**, *29*, 257-265; f) K.-Y. Ye, G. Pombar, N. Fu, G. S. Sauer, I. Keresztes, S. Lin, *J. Am. Chem. Soc.* **2018**, *140*, 2438-2441; g) N. Fu, G. S. Sauer, S. Lin, *J. Am. Chem. Soc.* **2017**, *139*, 15548-15553; h) N. Fu, G. S. Sauer, A. Saha, A. Loo, S. Lin, *Science* **2017**, *357*, 575-579.

[157] H. Schäfer, *Angew. Chem. Int. Ed.* **1970**, *9*, 158-159.

[158] L. Niu, C. Jiang, Y. Liang, D. Liu, F. Bu, R. Shi, H. Chen, A. D. Chowdhury, A. Lei, *J. Am. Chem. Soc.* **2020**, *142*, 17693-17702.

[159] T. H. Meyer, R. C. Samanta, A. Del Vecchio, L. Ackermann, *Chem. Sci.* **2021**, *12*, 2890-2897.

[160] a) C. L. Hill, J. A. Smegal, T. J. Henly, *J. Org. Chem.* **1983**, *48*, 3277-3281; b) C. L. Hill, B. C. Schardt, *J. Am. Chem. Soc.* **1980**, *102*, 6374-6375.

[161] X. Huang, T. M. Bergsten, J. T. Groves, *J. Am. Chem. Soc.* **2015**, *137*, 5300-5303.

[162] T. Rogge, N. Kaplaneris, N. Chatani, J. Kim, S. Chang, B. Punji, L. L. Schafer, D. G. Musaev, J. Wencel-Delord, C. A. Roberts, R. Sarpong, Z. E. Wilson, M. A. Brimble, M. J. Johansson, L. Ackermann, *Nat. Rev. Methods Primers* **2021**, *1*, 43.

[163] a) C. Zhu, N. W. J. Ang, T. H. Meyer, Y. Qiu, L. Ackermann, *ACS Cent. Sci.* **2021**, *7*, 415-431; b) T. H. Meyer, I. Choi, C. Tian, L. Ackermann, *Chem* **2020**, *6*, 2484-2496.

[164] a) T. T. Nguyen, L. Grigorjeva, O. Daugulis, *Chem. Commun.* **2017**, *53*, 5136-5138; b) O. Planas, S. Roldán-Gómez, V. Martin-Diaconescu, T. Parella, J. M. Luis, A. Company, X. Ribas, *J. Am. Chem. Soc.* **2017**, *139*, 14649-14655; c) X.-Q. Hao, C. Du, X. Zhu, P.-X. Li, J.-H. Zhang, J.-L. Niu, M.-P. Song, *Org. Lett.* **2016**, *18*, 3610-3613; d) T. T. Nguyen, L. Grigorjeva, O. Daugulis, *ACS Catal.* **2016**, *6*, 551-554; e) O. Planas, C. J. Whiteoak, V. Martin-Diaconescu, I. Gamba, J. M. Luis, T. Parella, A. Company, X. Ribas, *J. Am. Chem. Soc.* **2016**, *138*, 14388-14397; f) O. Daugulis, J. Roane, L. D. Tran, *Acc. Chem. Res.* **2015**, *48*, 1053-1064; g) O. Planas, C. J. Whiteoak, A. Company, X. Ribas, *Adv. Synth. Catal.* **2015**, *357*, 4003-4012; h) B. Sun, T. Yoshino, M. Kanai, S. Matsunaga, *Angew. Chem. Int. Ed.* **2015**, *54*, 12968-12972; i) L.-B. Zhang, X.-Q. Hao, Z.-J. Liu, X.-X. Zheng, S.-K. Zhang, J.-L. Niu, M.-P. Song, *Angew. Chem.*

Int. Ed. **2015**, *54*, 10012-10015; j) H. Ikemoto, T. Yoshino, K. Sakata, S. Matsunaga, M. Kanai, *J. Am. Chem. Soc.* **2014**, *136*, 5424-5431.

[165] a) S. Doobary, A. T. Sedikides, H. P. Caldora, D. L. Poole, A. J. J. Lennox, *Angew. Chem. Int. Ed.* **2020**, *59*, 1155-1160; b) W.-C. Gao, Z.-Y. Xiong, S. Pirhaghani, T. Wirth, *Synthesis* **2019**, *51*, 276-284; c) J. D. Herszman, M. Berger, S. R. Waldvogel, *Org. Lett.* **2019**, *21*, 7893-7896; d) M. Elsherbini, T. Wirth, *Chem. Eur. J.* **2018**, *24*, 13399-13407; e) T. Broese, R. Francke, *Org. Lett.* **2016**, *18*, 5896-5899; f) S. Nishiyama, Y. Amano, *Heterocycles* **2008**, *75*, 1997; g) T. Fuchigami, T. Fujita, *J. Org. Chem.* **1994**, *59*, 7190-7192.

[166] G. P. McGlacken, L. M. Bateman, *Chem. Soc. Rev.* **2009**, *38*, 2447-2464.

[167] a) S. R. Yetra, T. Rogge, S. Warratz, J. Struwe, W. Peng, P. Vana, L. Ackermann, *Angew. Chem. Int. Ed.* **2019**, *58*, 7490-7494; b) S. Handa, J. D. Smith, M. S. Hageman, M. Gonzalez, B. H. Lipshutz, *ACS Catal.* **2016**, *6*, 8179-8183; c) S. Handa, E. D. Slack, B. H. Lipshutz, *Angew. Chem. Int. Ed.* **2015**, *54*, 11994-11998; d) S. Handa, Y. Wang, F. Gallou, B. H. Lipshutz, *Science* **2015**, *349*, 1087-1091; e) T. Nishikata, A. R. Abela, S. Huang, B. H. Lipshutz, *J. Am. Chem. Soc.* **2010**, *132*, 4978-4979.

[168] a) J. M. Ramos-Villaseñor, E. Rodríguez-Cárdenas, C. E. Barrera Díaz, B. A. Frontana-Uribe, *J. Electrochem. Soc.* **2020**, *167*, 155509; b) L. Schulz, S. R. Waldvogel, *Synlett* **2019**, *30*, 275-286; c) S. K. Sinha, T. Bhattacharya, D. Maiti, *React. Chem. Eng.* **2019**, *4*, 244-253; d) O. Hollóczki, A. Berkessel, J. Mars, M. Mezger, A. Wiebe, S. R. Waldvogel, B. Kirchner, *ACS Catal.* **2017**, *7*, 1846-1852.

[169] a) M. Deponti, S. I. Kozhushkov, D. S. Yufit, L. Ackermann, *Org. Biomol. Chem.* **2013**, *11*, 142-148; b) L. Ackermann, A. V. Lygin, *Org. Lett.* **2012**, *14*, 764-767; c) L. Ackermann, L. Wang, A. V. Lygin, *Chem. Sci.* **2012**, *3*, 177-180; d) K. Parthasarathy, N. Senthilkumar, J. Jayakumar, C.-H. Cheng, *Org. Lett.* **2012**, *14*, 3478-3481; e) V. S. Thirunavukkarasu, M. Donati, L. Ackermann, *Org. Lett.* **2012**, *14*, 3416-3419.

[170] D. Nicewicz, H. Roth, N. Romero, *Synlett* **2016**, *27*, 714-723.

[171] Y. Qiu, C. Zhu, M. Stangier, J. Struwe, L. Ackermann, *CCS Chem.* **2021**, *3*, 1529-1552.

[172] a) D. Aynetdinova, M. C. Callens, H. B. Hicks, C. Y. X. Poh, B. D. A. Shennan, A. M. Boyd, Z. H. Lim, J. A. Leitch, D. J. Dixon, *Chem. Soc. Rev.* **2021**, *50*, 5517-5563; b) K. Feng, R. E. Quevedo, J. T. Kohrt, M. S. Oderinde, U. Reilly, M. C. White, *Nature* **2020**, *580*, 621-627; c) S. D. Friis, M. J. Johansson, L. Ackermann, *Nat. Chem.* **2020**, *12*, 511-519; d) H. Schönherr, T. Cernak, *Angew. Chem. Int. Ed.* **2013**, *52*, 12256-12267.

[173] A. F. B. Räder, M. Weinmüller, F. Reichart, A. Schumacher-Klinger, S. Merzbach, C. Gilon, A. Hoffman, H. Kessler, *Angew. Chem. Int. Ed.* **2018**, *57*, 14414-14438.

[174] L. R. F. A. J. Bard, *Electrochemical Methods - Fundamentals and Applications, 2nd Ed.*, John Wiley & Sons, US, **2001**.

[175] C. Tian, L. Massignan, T. H. Meyer, L. Ackermann, *Angew. Chem. Int. Ed.* **2018**, *57*, 2383-2387.

[176] L. Massignan, X. Tan, T. H. Meyer, R. Kuniyil, A. M. Messinis, L. Ackermann, *Angew. Chem. Int. Ed.* **2020**, *59*, 3184-3189.

[177] X. Tan, L. Massignan, X. Hou, J. Frey, J. C. A. Oliveira, M. N. Hussain, L. Ackermann, *Angew. Chem. Int. Ed.* **2021**, *60*, 13264-13270.

[178] L. Massignan, C. Zhu, X. Hou, J. C. A. Oliveira, A. Salamé, L. Ackermann, *ACS Catal.* **2021**, *11*, 11639-11649.

[179] a) W. Zhang, N. Hong, L. Song, N. Fu, *Chem Rec.* **2021**, *21*, 2574-2584; b) N. P. Martínez, M. Isaacs, K. K. Nanda, *New J. Chem.* **2020**, *44*, 5617-5637; c) R. S. Sherbo, R. S. Delima, V. A. Chiykowski, B. P. MacLeod, C. P. Berlinguette, *Nat. Catal.* **2018**, *1*, 501-507.

[180] a) X. Chang, Q. Zhang, C. Guo, *Angew. Chem. Int. Ed.* **2020**, *59*, 12612-12622; b) A. M. F. Phillips, A. J. L. Pombeiro, *Org. Biomol. Chem.* **2020**, *18*, 7026-7055; c) Q. Lin, L. Li, S. Luo, *Chem. Eur. J.* **2019**, *25*, 10033-10044.

[181] a) Y. Qiu, A. Scheremetjew, L. H. Finger, L. Ackermann, *Chem. Eur. J.* **2020**, *26*, 3241-3246; b) H. Yan, Z.-W. Hou, H.-C. Xu, *Angew. Chem. Int. Ed.* **2019**, *58*, 4592-4595.

[182] a) D. Pletcher, R. A. Green, R. C. D. Brown, *Chem. Rev.* **2018**, *118*, 4573-4591; b) A. A. Folgueiras-Amador, T. Wirth, *J. Flow Chem.* **2017**, *7*, 94-95.

[183] a) D. M. Heard, A. J. J. Lennox, *Angew. Chem. Int. Ed.* **2020**, *59*, 18866-18884; b) A. Das, S. S. Stahl, *Angew. Chem.* **2017**, *129*, 9018-9023; c) D. Bélanger, J. Pinson, *Chem. Soc. Rev.* **2011**, *40*, 3995-4048.

[184] M. Zhong, K. Tran, Y. Min, C. Wang, Z. Wang, C.-T. Dinh, P. De Luna, Z. Yu, A. S. Rasouli, P. Brodersen, S. Sun, O. Voznyy, C.-S. Tan, M. Askerka, F. Che, M. Liu, A. Seifitokaldani, Y. Pang, S.-C. Lo, A. Ip, Z. Ulissi, E. H. Sargent, *Nature* **2020**, *581*, 178-183.

[185] C. Tian, T. H. Meyer, M. Stangier, U. Dhawa, K. Rauch, L. H. Finger, L. Ackermann, *Nat. Protoc.* **2020**, *15*, 1760-1774.

[186] K. C. Nicolaou, J. Becker, Y. H. Lim, A. Lemire, T. Neubauer, A. Montero, *J. Am. Chem. Soc.* **2009**, *131*, 14812-14826.

[187] Y. Zhao, V. Snieckus, *J. Am. Chem. Soc.* **2014**, *136*, 11224-11227.

[188] D. R. Henton, K. Anderson, M. J. Manning, J. S. Swenton, *J. Org. Chem.* **1980**, *45*, 3422-3433.

[189] K. V. Chuang, R. Navarro, S. E. Reisman, *Chem. Sci.* **2011**, *2*, 1086-1089.

[190] S. Mavel, N. Meheux, D. Guilloteau, P. Emond, *Bioorg. Med. Chem.* **2010**, *18*, 236-241.

[191] M. A. J. Miah, M. P. Sibi, S. Chattopadhyay, O. B. Familoni, V. Snieckus, *Eur. J. Org. Chem.* **2018**, *2018*, 440-446.

[192] G. Shan, X. Yang, L. Ma, Y. Rao, *Angew. Chem. Int. Ed.* **2012**, *51*, 13070-13074.

[193] H. Xie, Z. Ye, Z. Ke, J. Lan, H. Jiang, W. Zeng, *Chem. Sci.* **2018**, *9*, 985-989.

7. Appendix: NMR Spectra

7.1 Electrochemical C–H/N–H Activation by Water-Tolerant Cobalt-Catalysis at Room Temperature

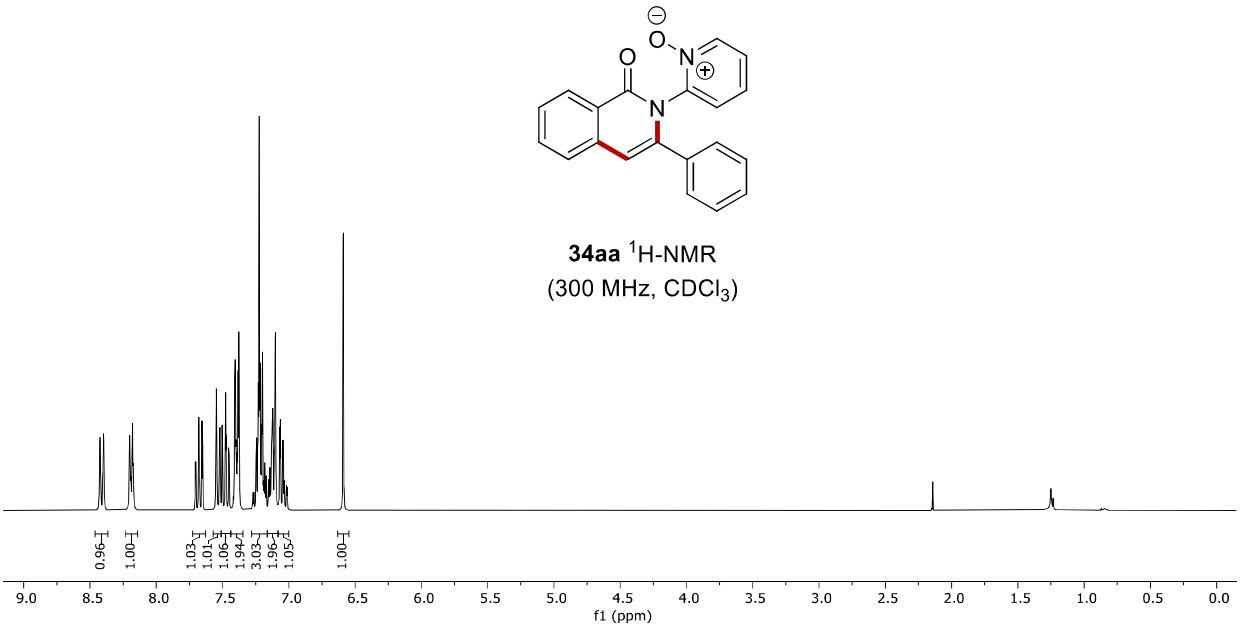

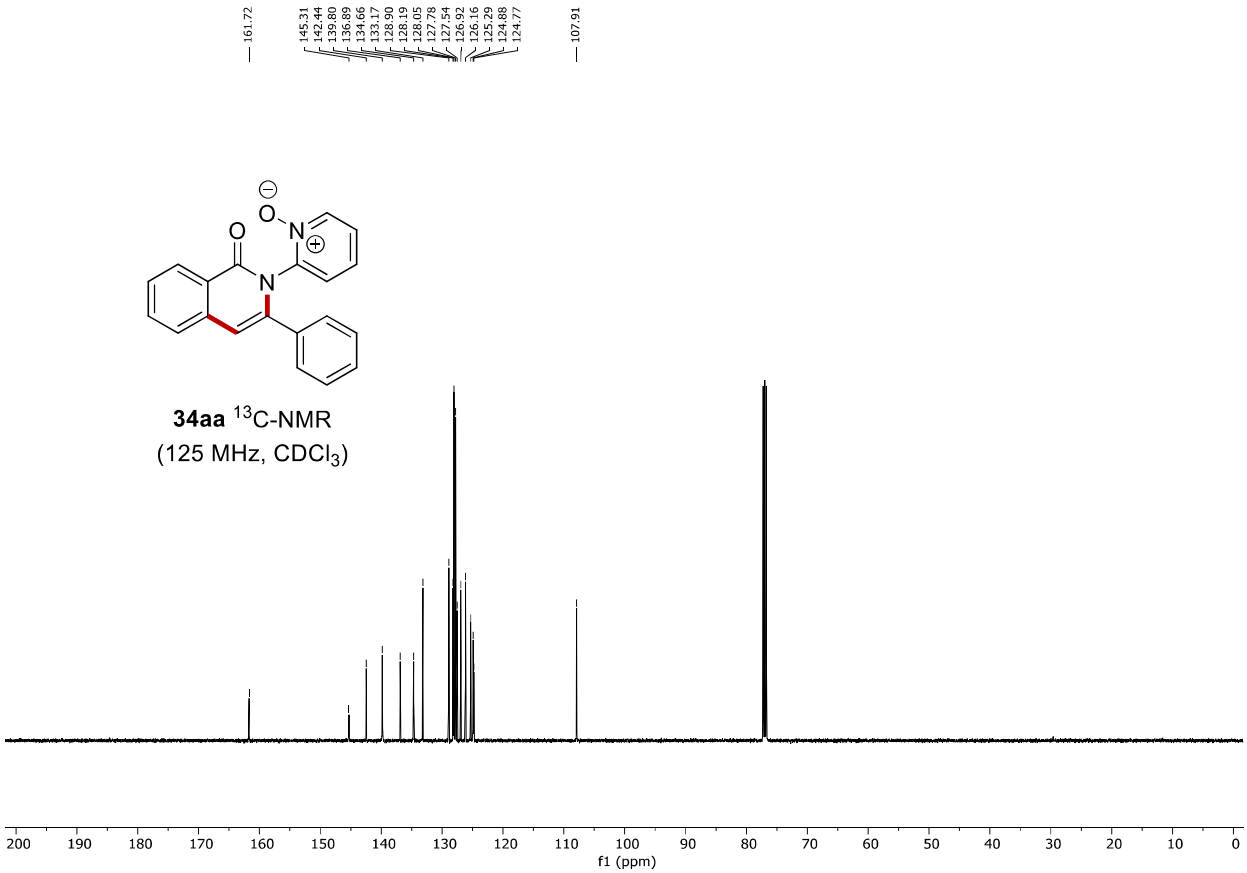

34aa ^{13}C-NMR
(125 MHz, $CDCl_3$)

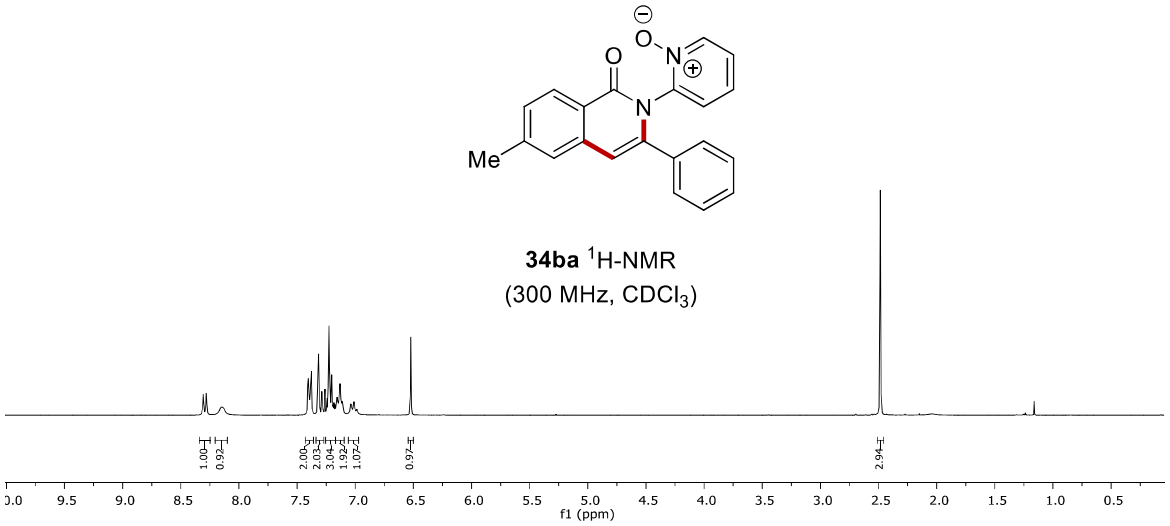

34ba ^{1}H-NMR
(300 MHz, $CDCl_3$)

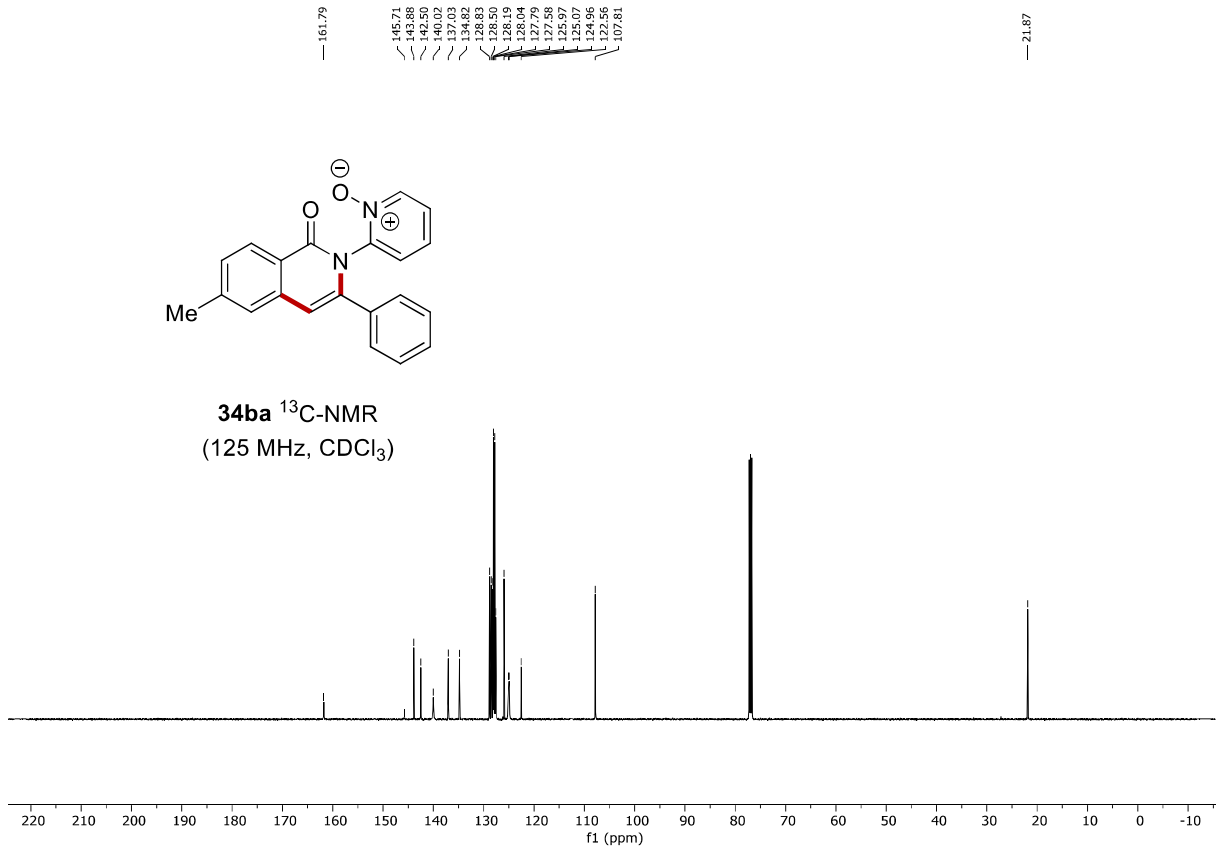

34ba ^{13}C-NMR
(125 MHz, $CDCl_3$)

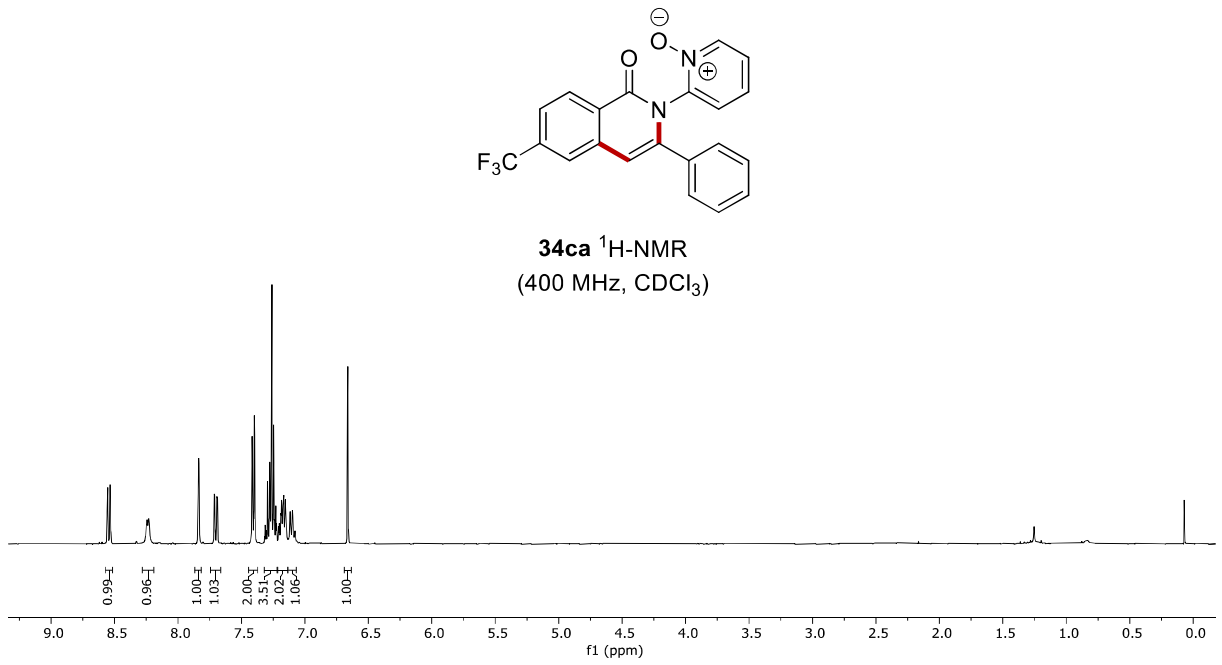

34ca ^{1}H-NMR
(400 MHz, $CDCl_3$)

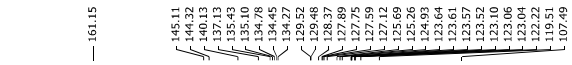

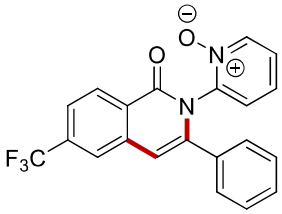

34ca ^{13}C-NMR
(100 MHz, $CDCl_3$)

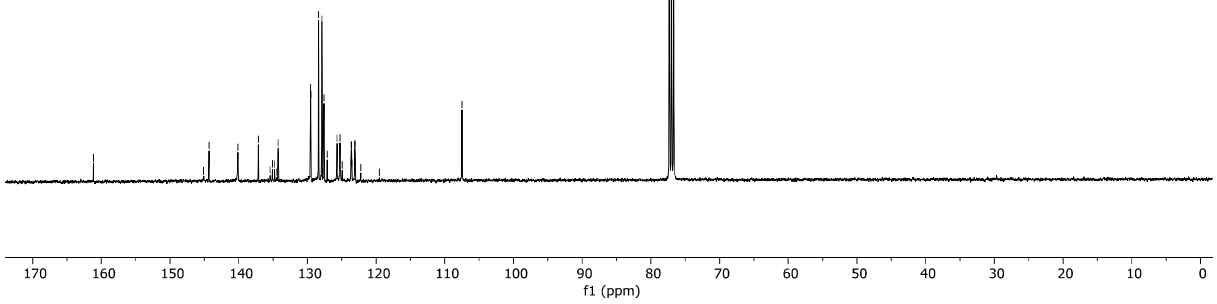

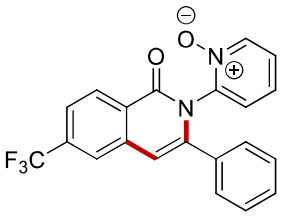

34ca ^{19}F-NMR
(376 MHz, $CDCl_3$)

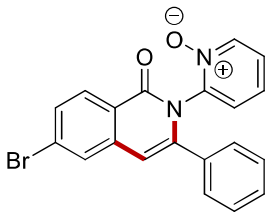

34da ^{1}H-NMR
(300 MHz, $CDCl_3$)

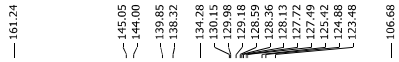

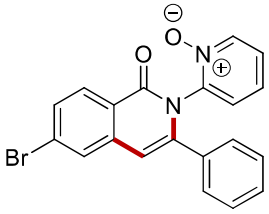

34da ^{13}C-NMR
(125 MHz, $CDCl_3$)

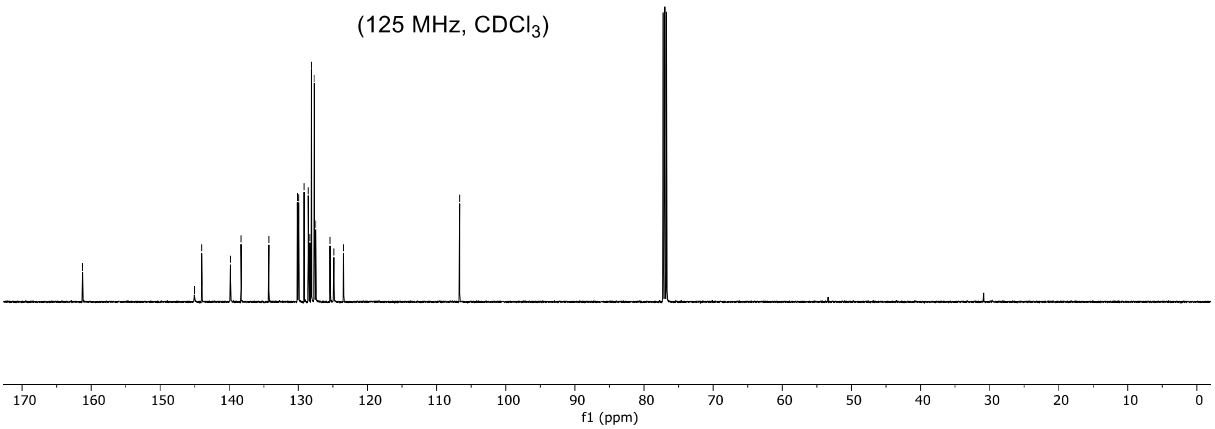

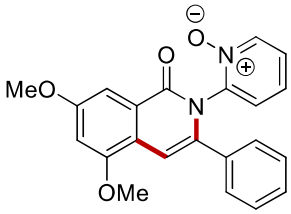

34ea ^{1}H-NMR
(300 MHz, $CDCl_3$)

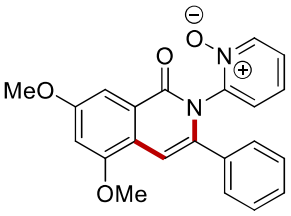

34ea ^{13}C-NMR
(125 MHz, $CDCl_3$)

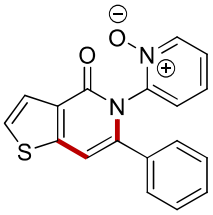

34fa ^{1}H-NMR
(300 MHz, $CDCl_3$)

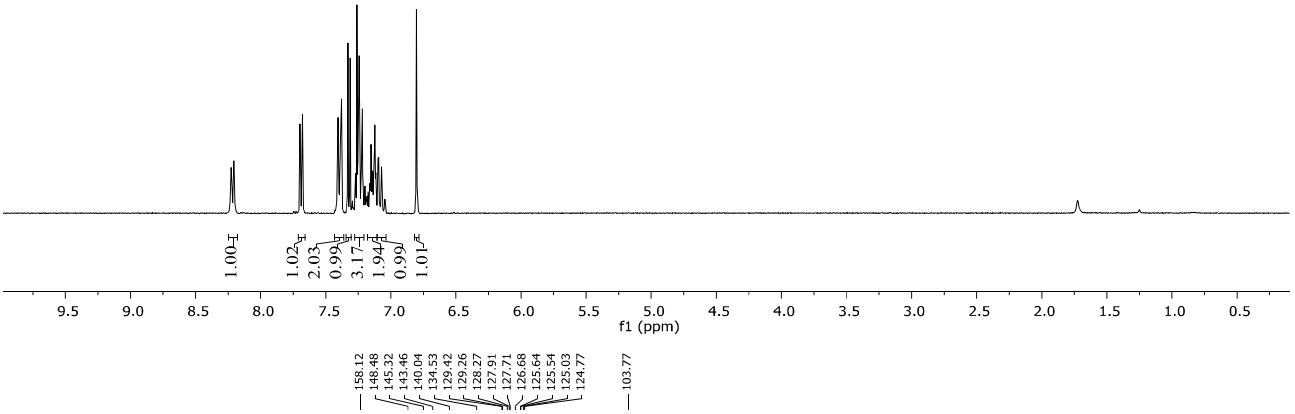

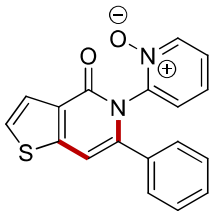

34fa ^{13}C-NMR
(125 MHz, $CDCl_3$)

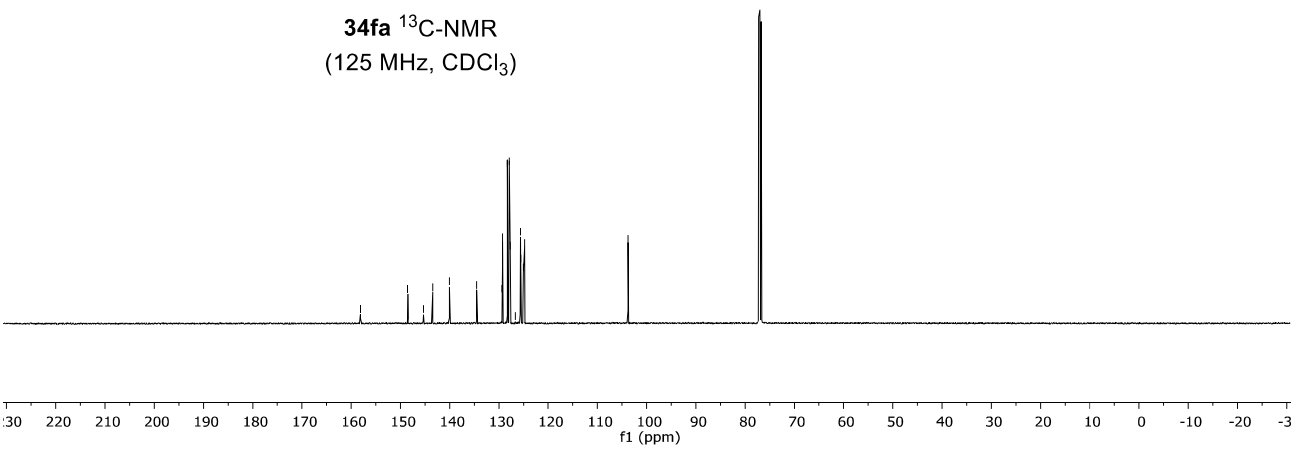

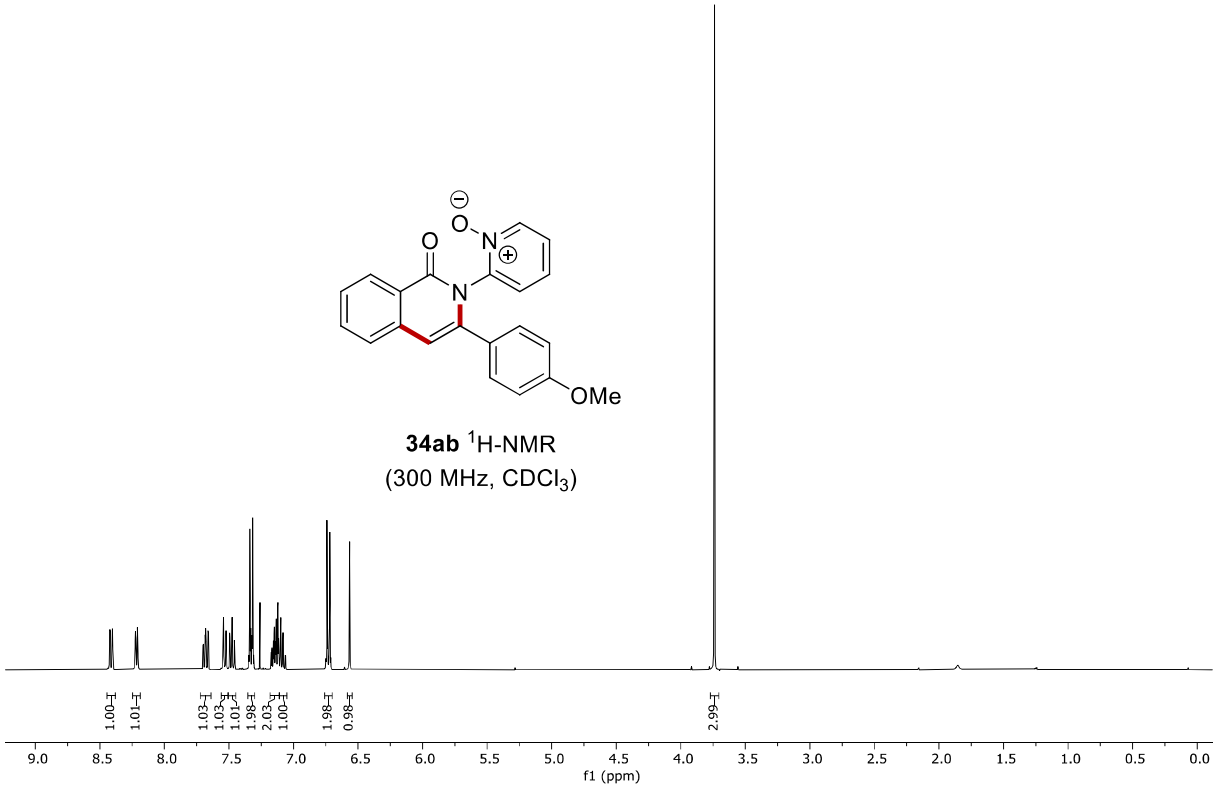
OMe
34ab 1H-NMR
(300 MHz, CDCl3)
1.00
1.01
1.03
1.03
1.01
1.98
2.03
1.00
1.98
0.98
2.99
f1 (ppm)

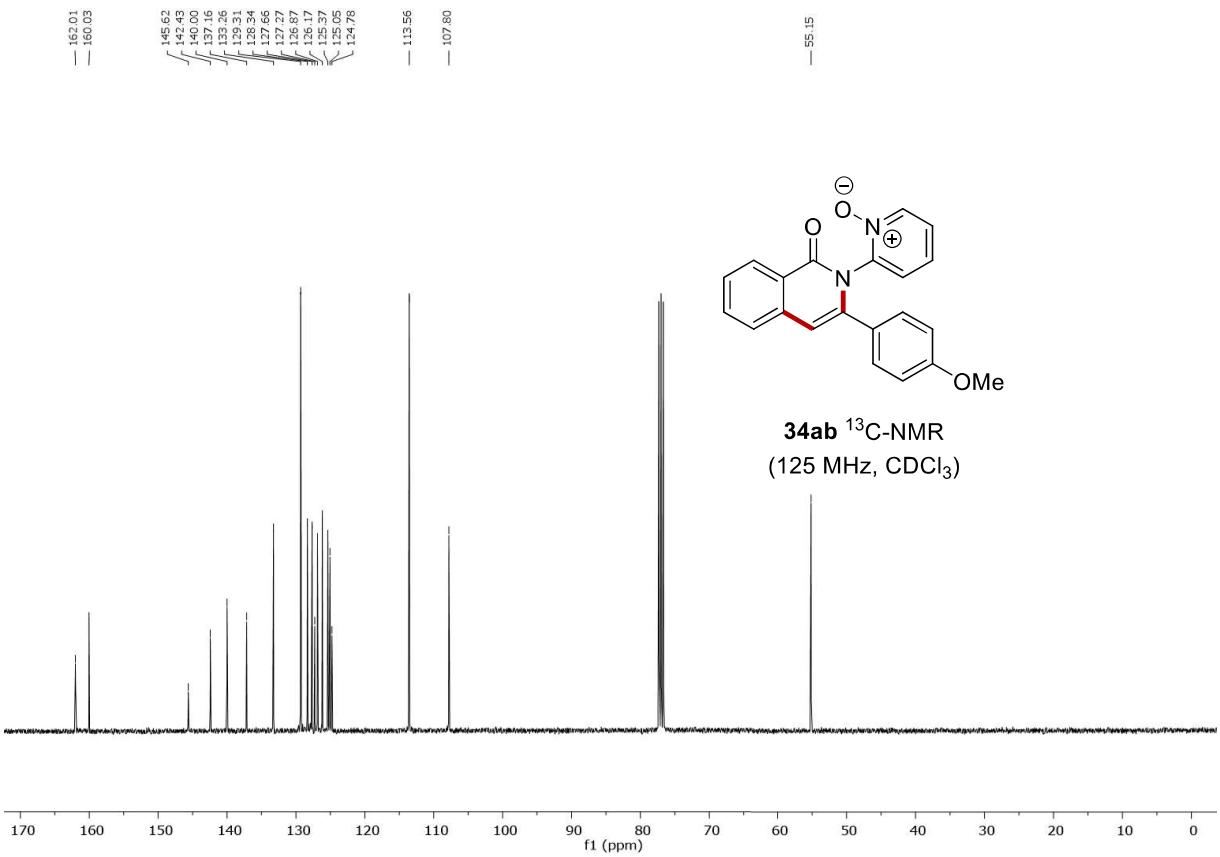
OMe
34ab 13C-NMR
(125 MHz, CDCl3)
162.01
160.03
145.62
142.43
140.00
137.16
133.26
129.31
128.34
127.66
127.27
126.87
126.17
125.37
125.05
124.78
113.56
107.80
55.15
f1 (ppm)

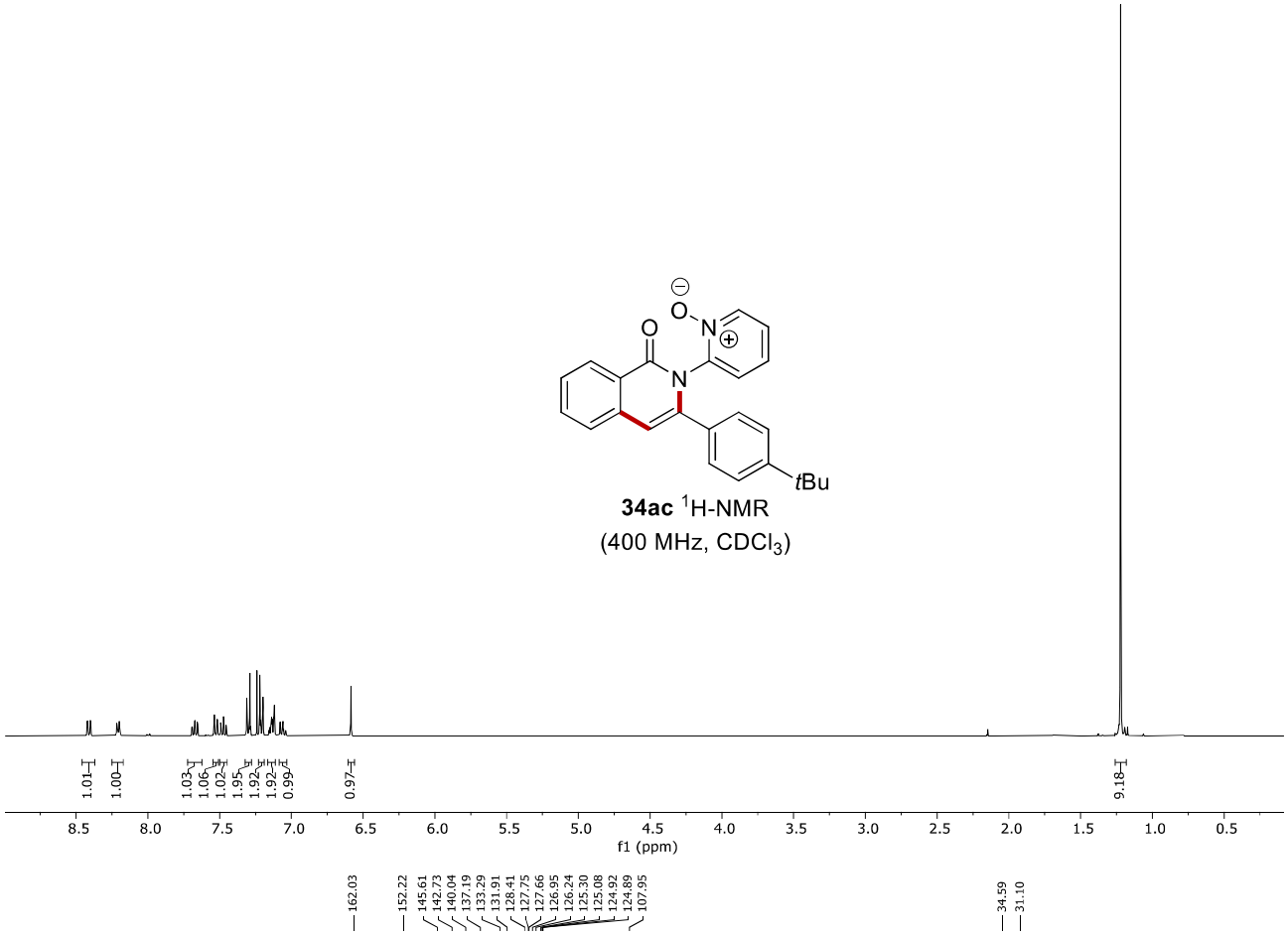

34ac ^{1}H-NMR
(400 MHz, $CDCl_3$)

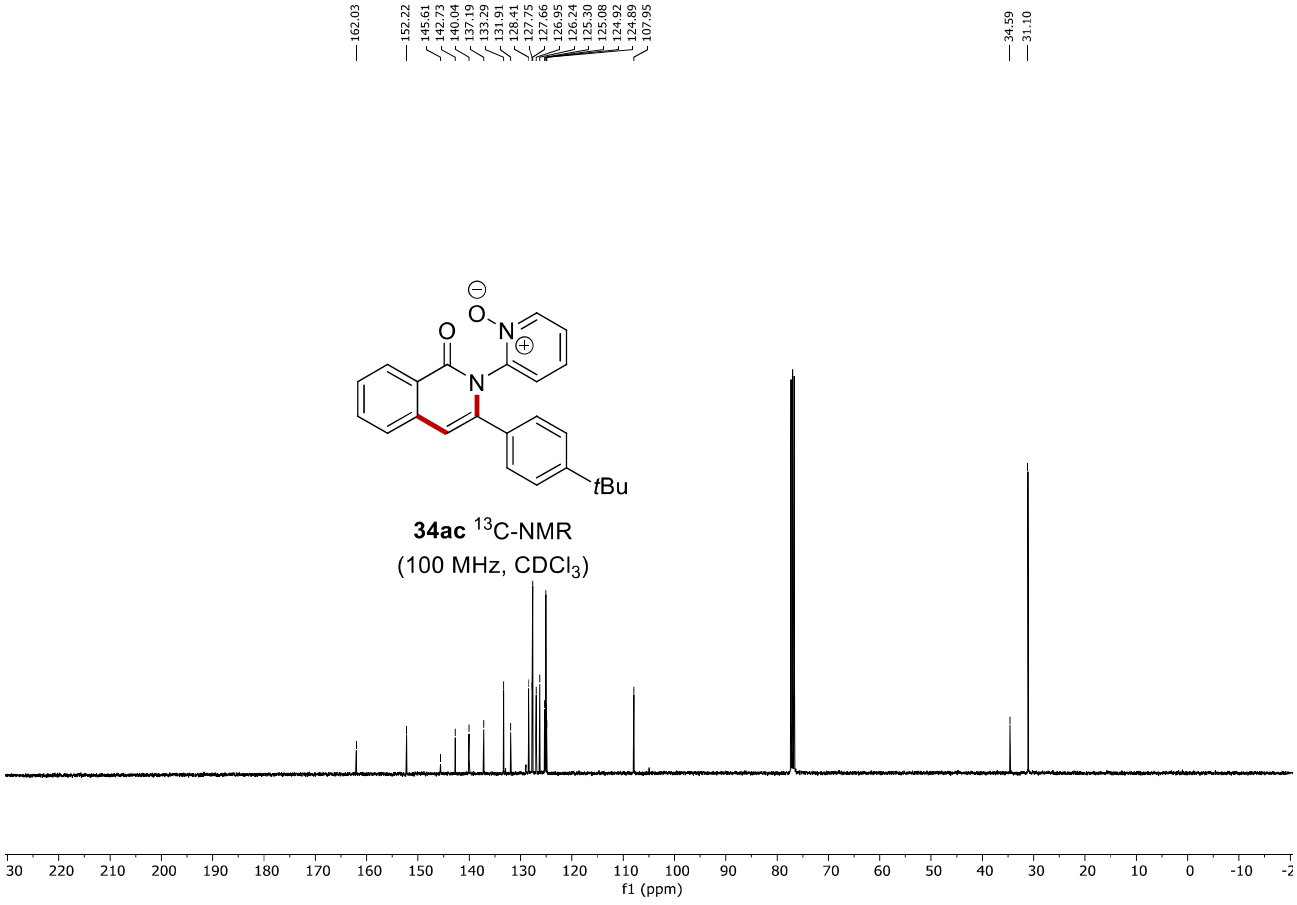

34ac ^{13}C-NMR
(100 MHz, $CDCl_3$)

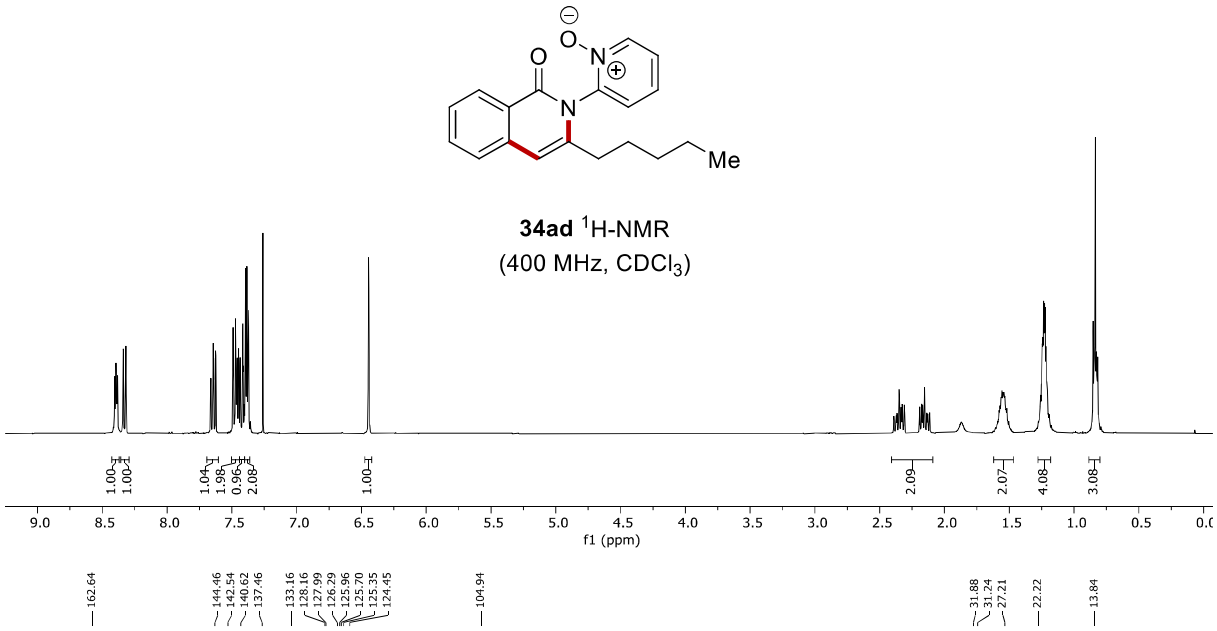
Me
34ad 1H-NMR
(400 MHz, CDCl3)
f1 (ppm)

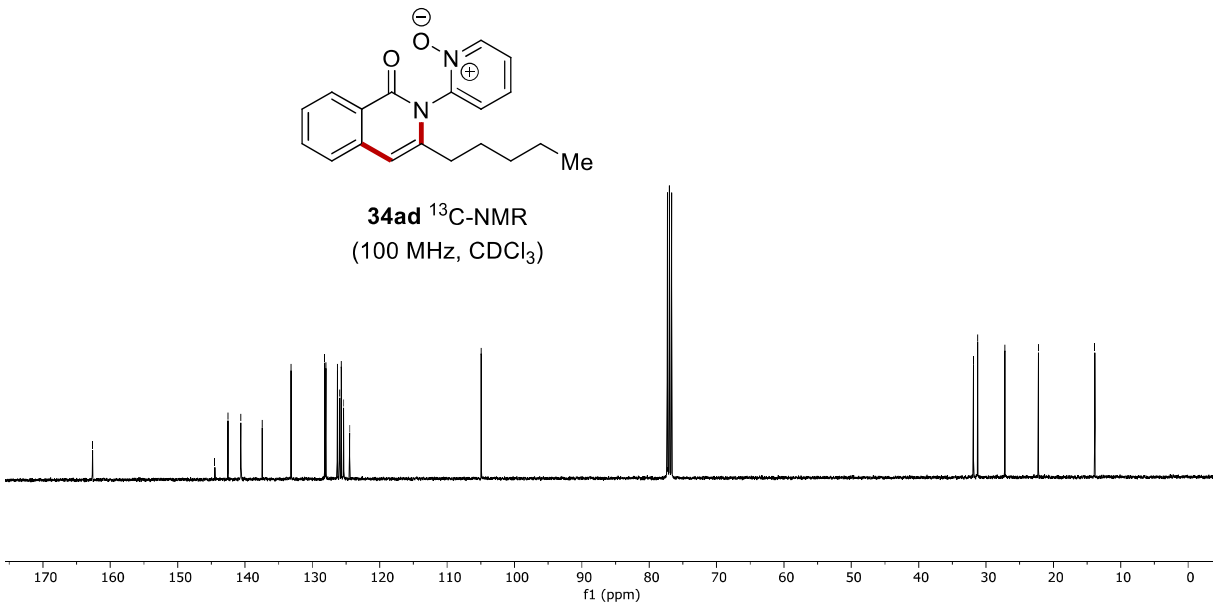
Me
34ad 13C-NMR
(100 MHz, CDCl3)
f1 (ppm)

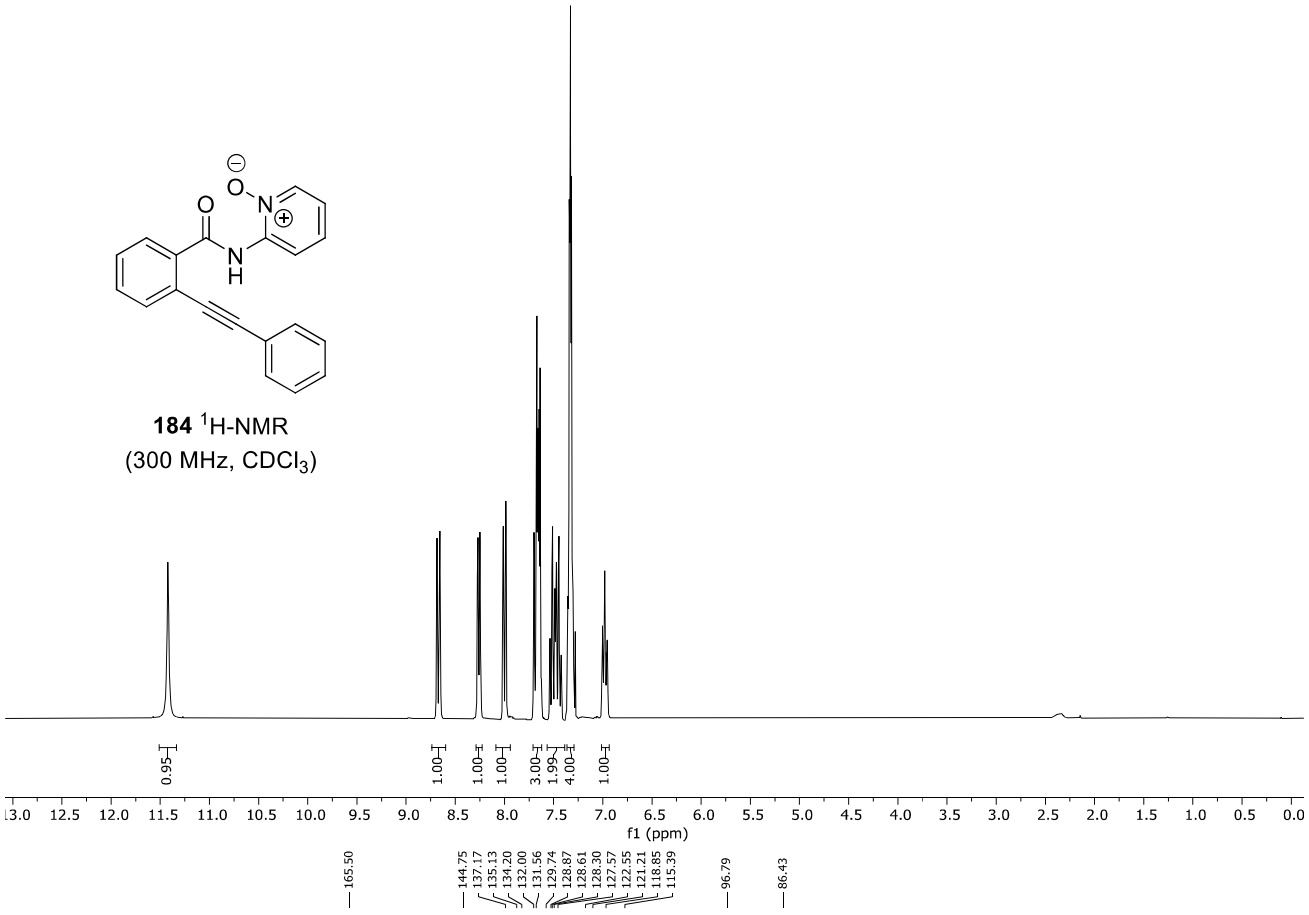
184 ^{1}H-NMR
(300 MHz, $CDCl_3$)
0.95
1.00
1.00
1.00
3.00
1.99
4.00
1.00
f1 (ppm)

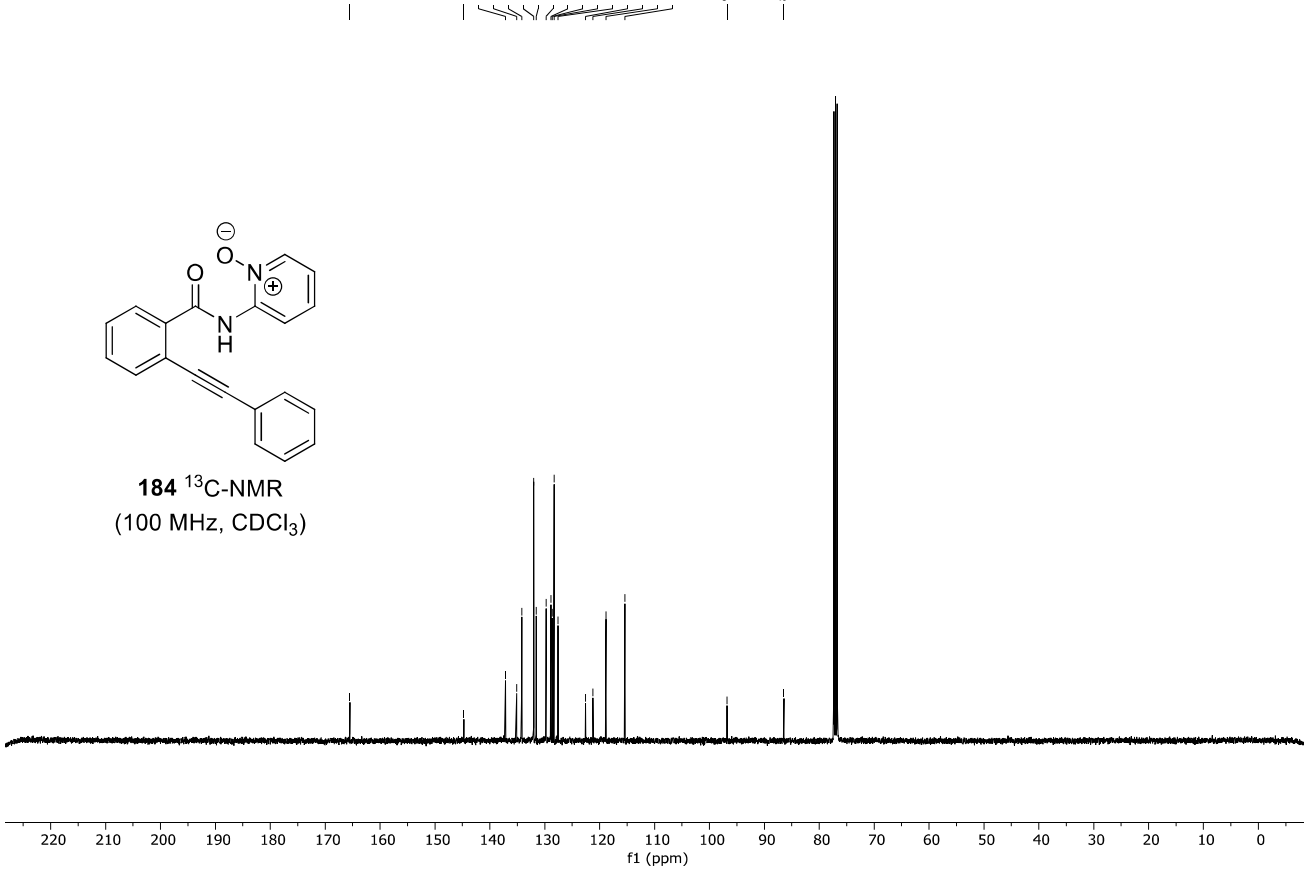
184 ^{13}C-NMR
(100 MHz, $CDCl_3$)
165.50
144.75
137.17
135.13
134.20
132.00
131.56
129.74
128.87
128.61
128.30
127.57
122.55
121.21
118.85
115.39
96.79
86.43
f1 (ppm)

7.2 Electrooxidative Ruthenium-Catalyzed C–H/O–H Annulation by Weak *O*-Coordination

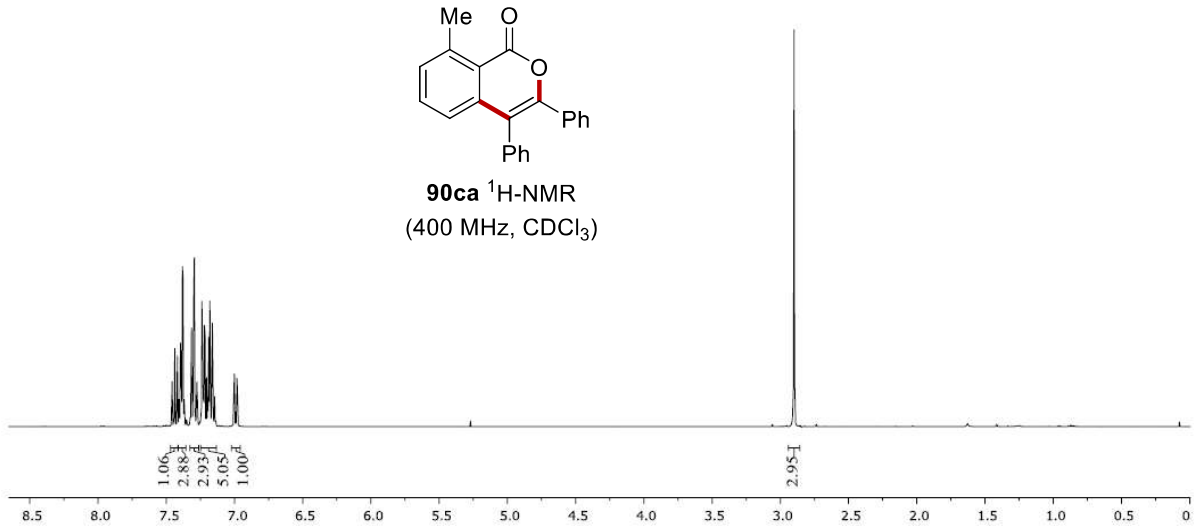

90ca ^{1}H-NMR
(400 MHz, $CDCl_3$)

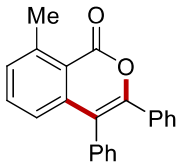

90ca ^{13}C-NMR
(100 MHz, $CDCl_3$)

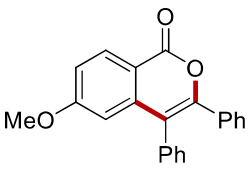

90ba ^{1}H-NMR
(400 MHz, $CDCl_3$)

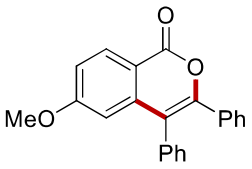

90ba ^{13}C-NMR
(125 MHz, $CDCl_3$)

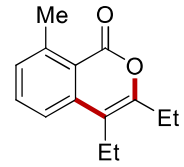

90cb ^{1}H-NMR
(300 MHz, $CDCl_3$)

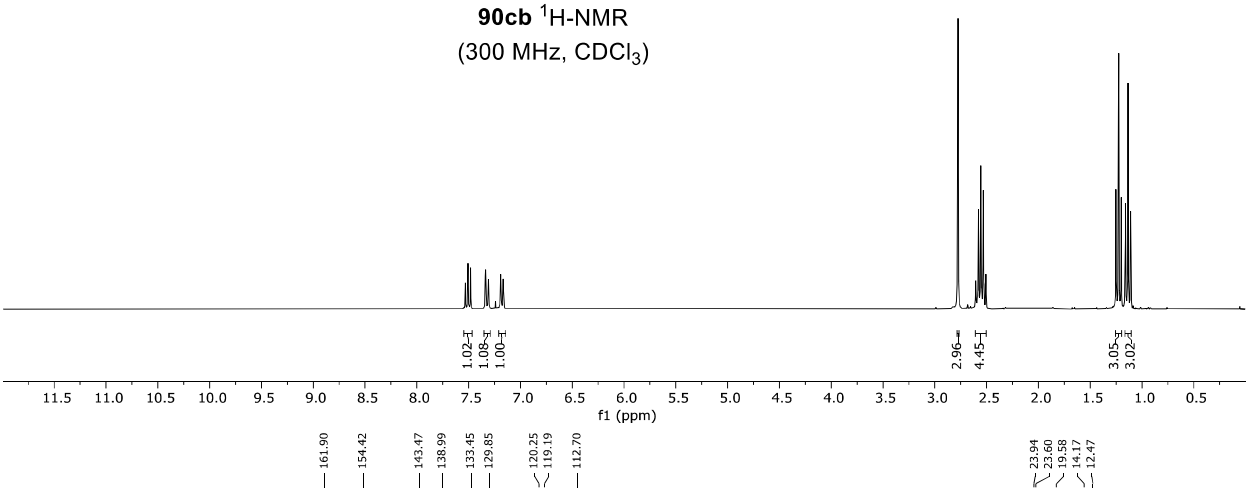

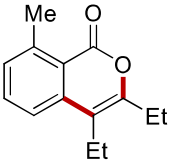

90cb ^{13}C-NMR
(125 MHz, $CDCl_3$)

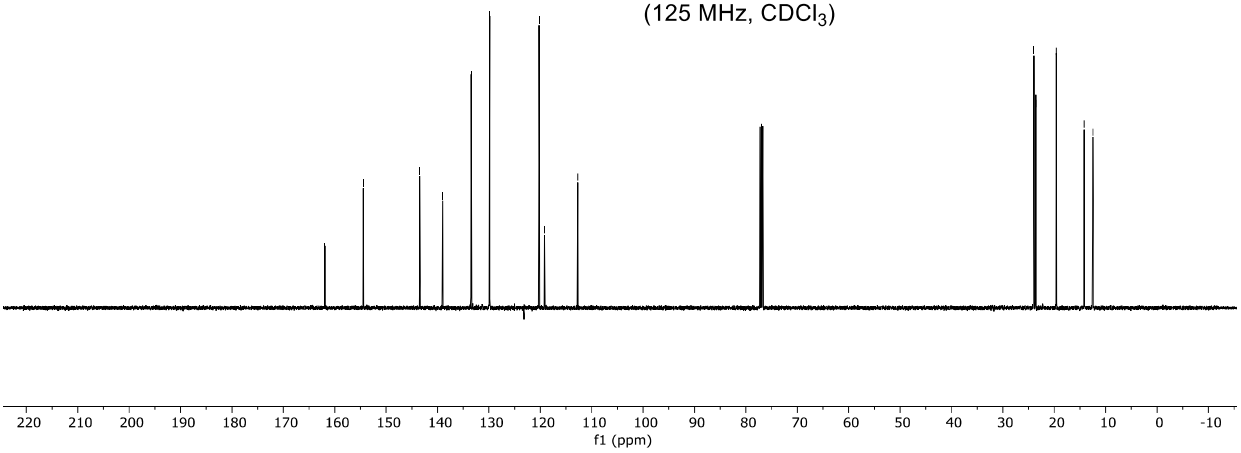

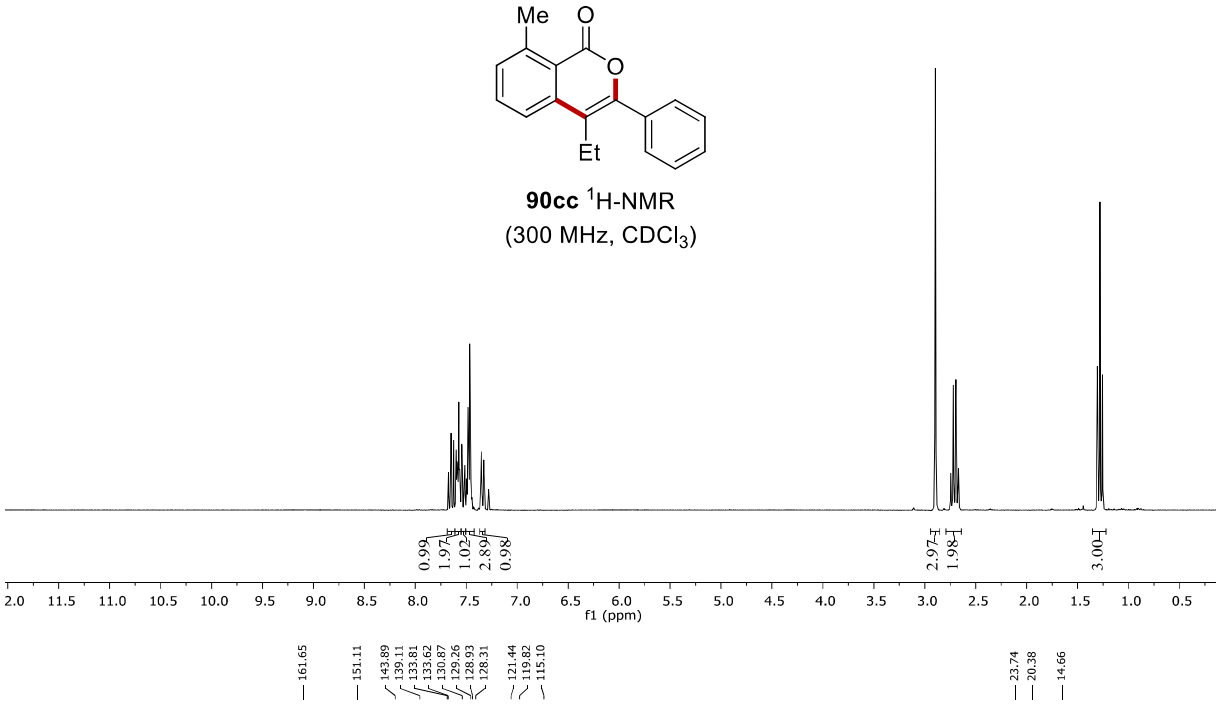

90cc ^{1}H-NMR
(300 MHz, $CDCl_3$)

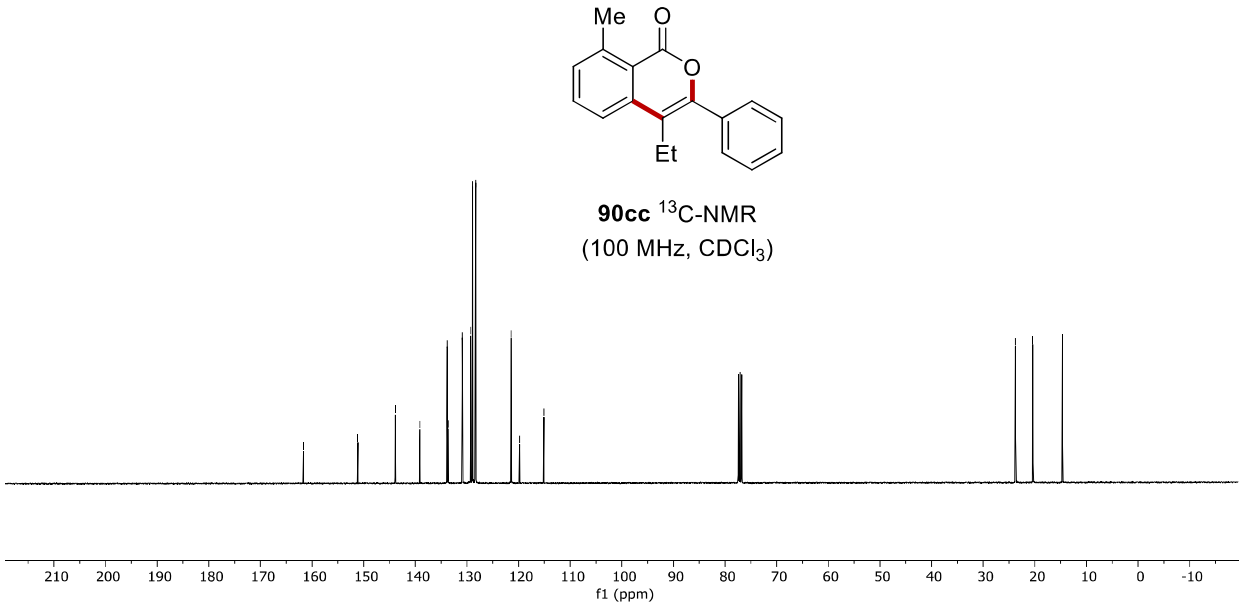

90cc ^{13}C-NMR
(100 MHz, $CDCl_3$)

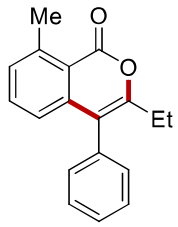

90cc' ^{1}H-NMR
(400 MHz, $CDCl_3$)

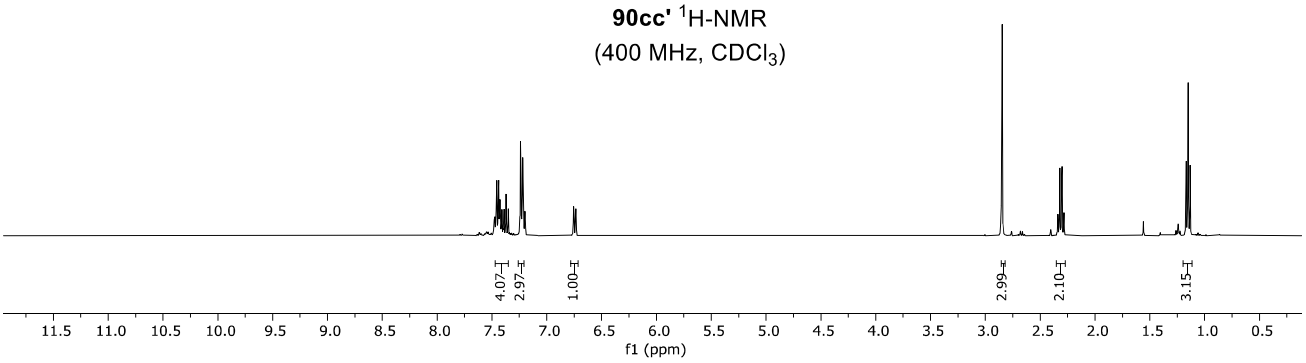

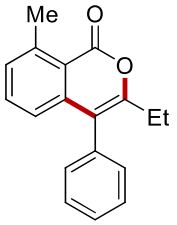

90cc' ^{13}C-NMR
(100 MHz, $CDCl_3$)

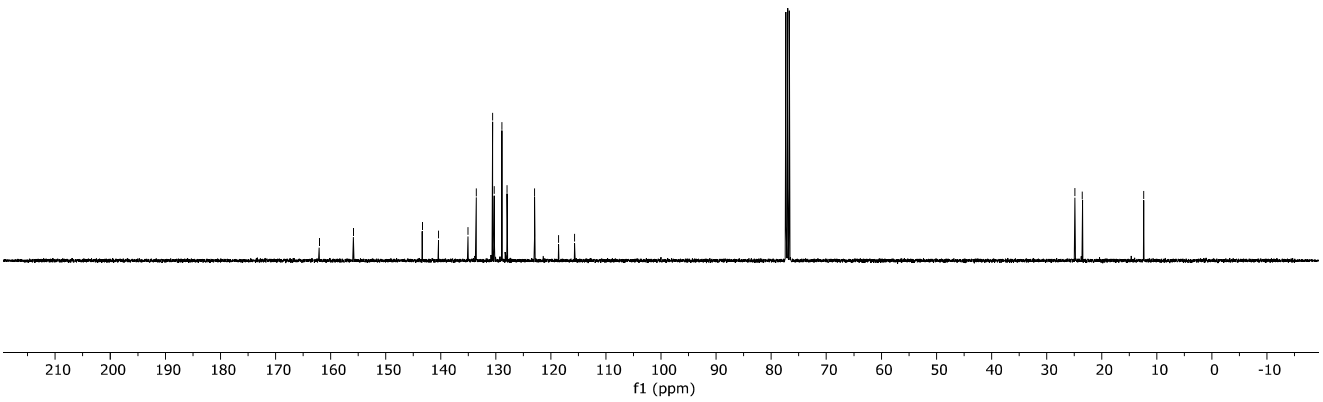

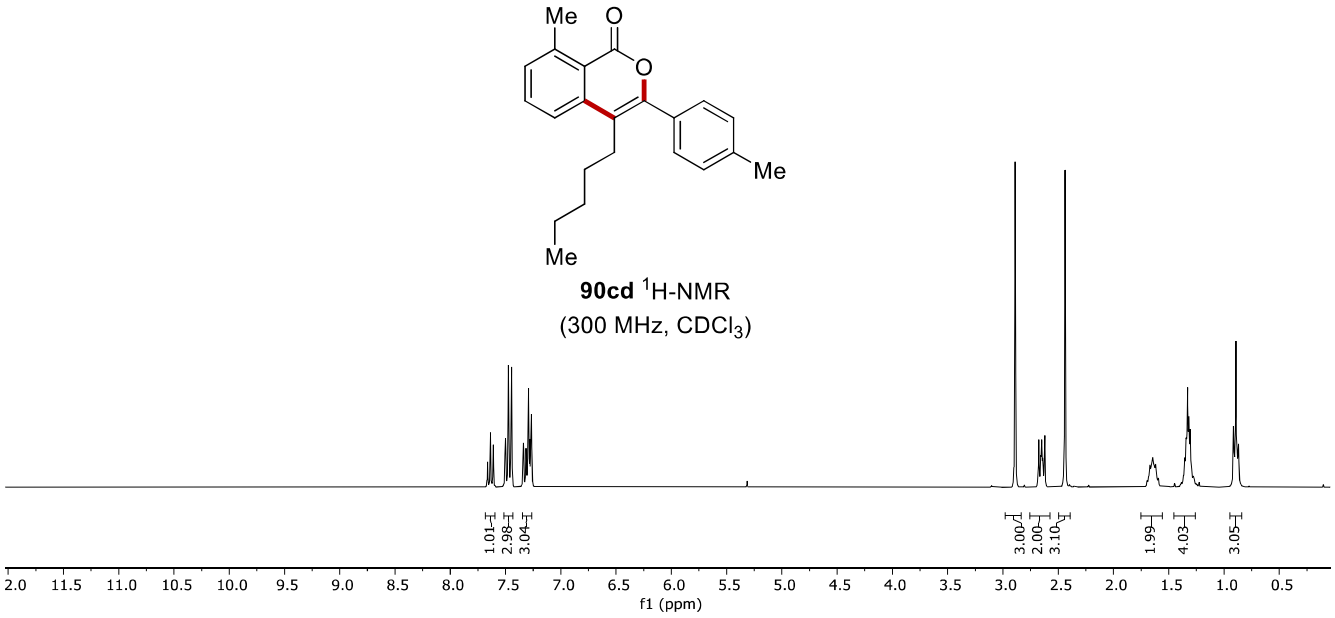

90cd ^{1}H-NMR
(300 MHz, $CDCl_3$)

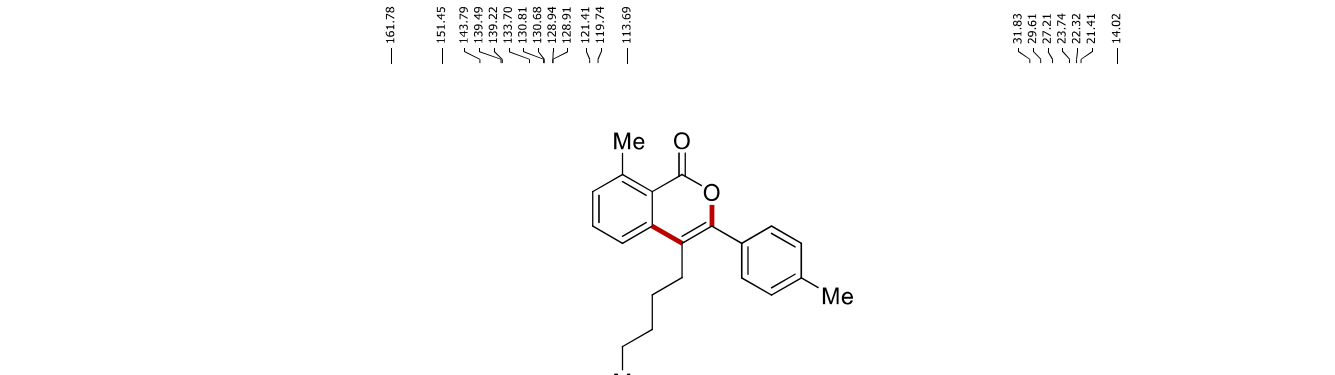

90cd ^{13}C-NMR
(75 MHz, $CDCl_3$)

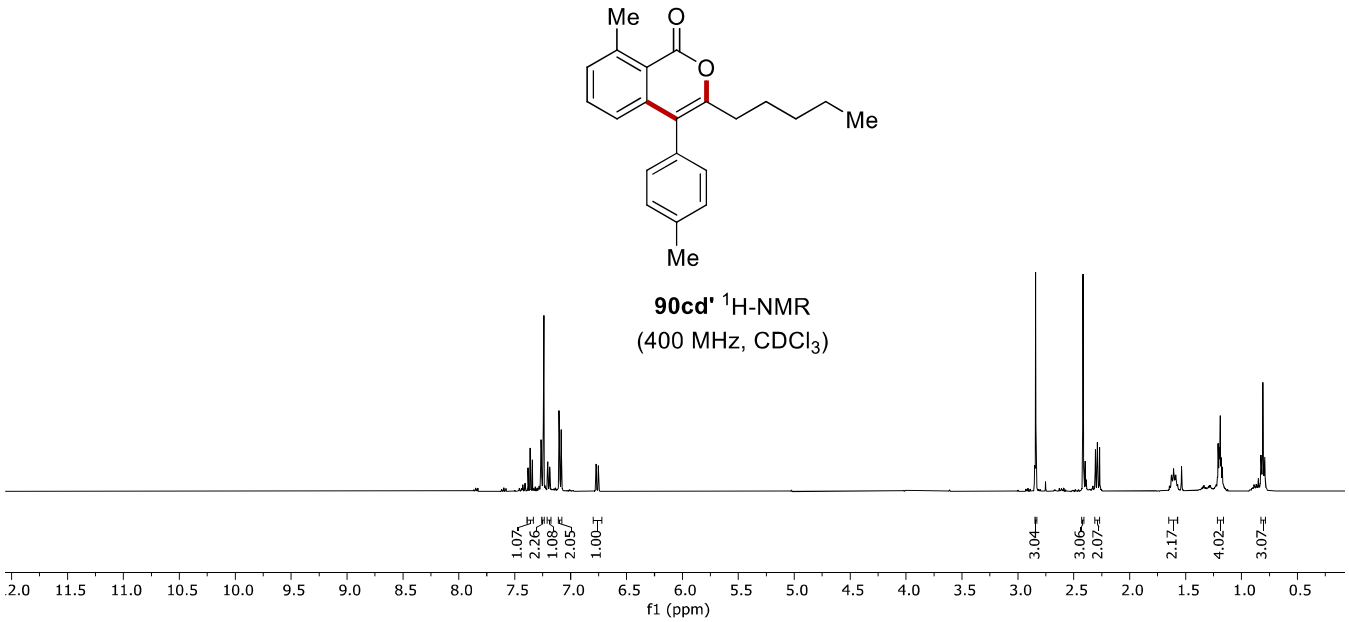
Me
O
O
Me
Me
90cd' 1H-NMR
(400 MHz, CDCl3)
1.07
2.26
1.08
2.05
1.00
3.04
3.06
2.07
2.17
4.02
3.07
f1 (ppm)

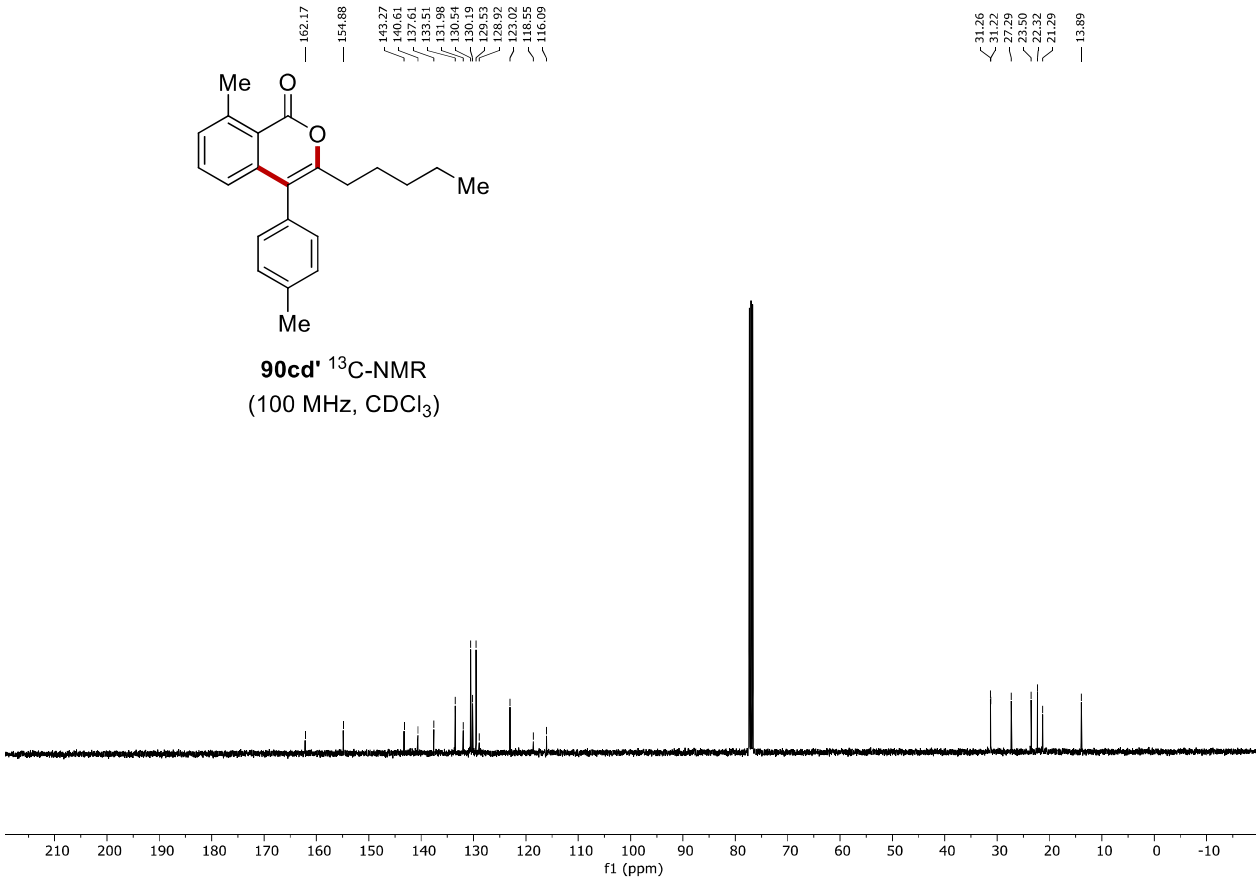
162.17
154.88
143.27
140.61
137.61
133.51
131.98
130.54
130.19
129.53
128.92
123.02
118.55
116.09
31.26
31.22
27.29
23.50
22.32
21.29
13.89
Me
O
O
Me
Me
90cd' 13C-NMR
(100 MHz, CDCl3)
f1 (ppm)

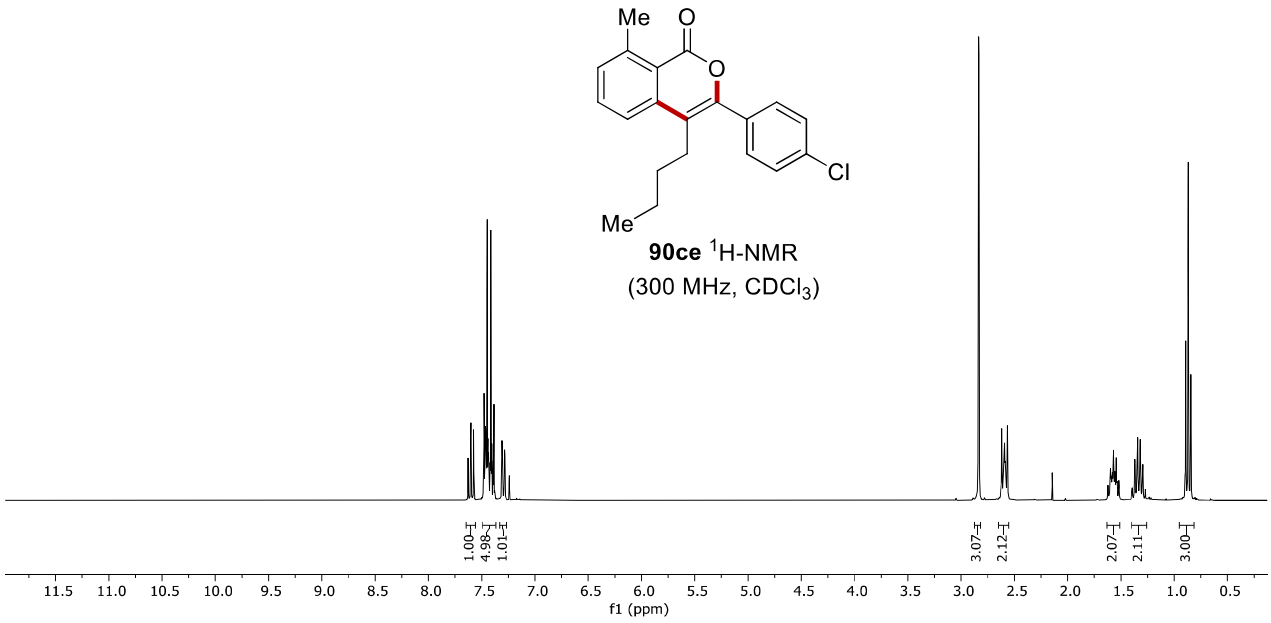

90ce ^{1}H-NMR
(300 MHz, $CDCl_3$)

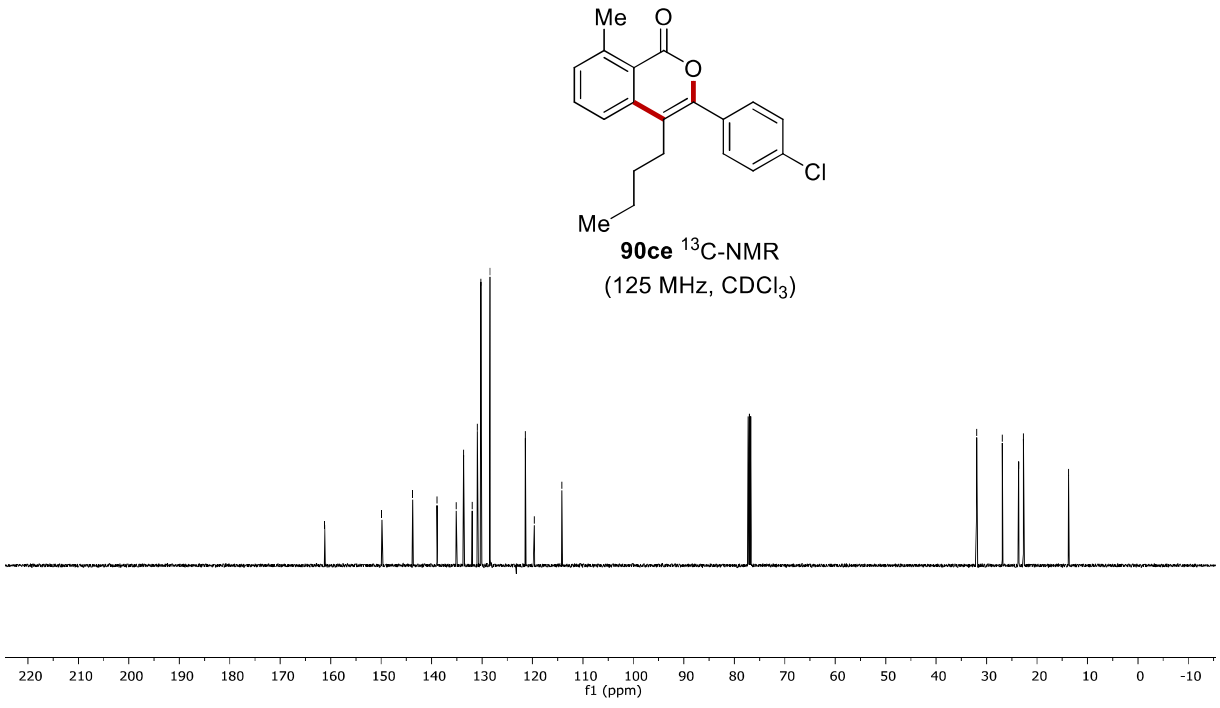

90ce ^{13}C-NMR
(125 MHz, $CDCl_3$)

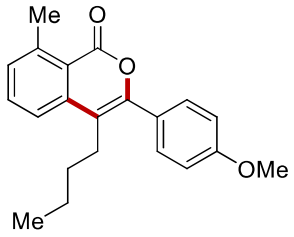

90cf ^{1}H-NMR
(300 MHz, $CDCl_3$)

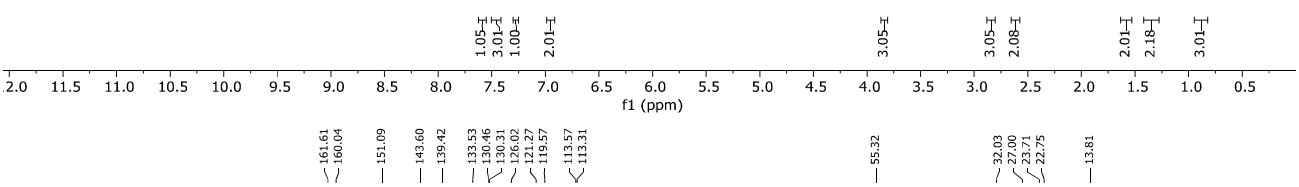

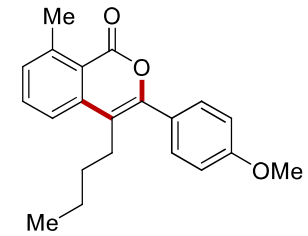

90cf ^{13}C-NMR
(125 MHz, $CDCl_3$)

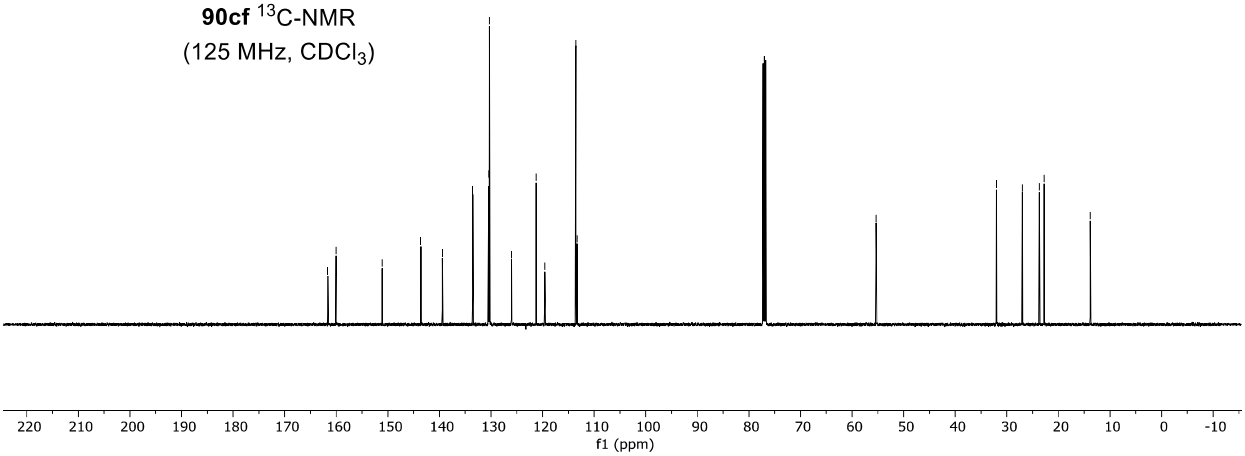

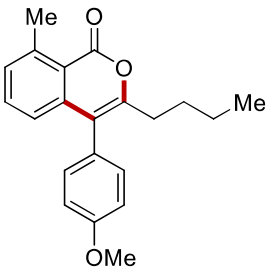

90cf' ^{1}H-NMR
(400 MHz, $CDCl_3$)

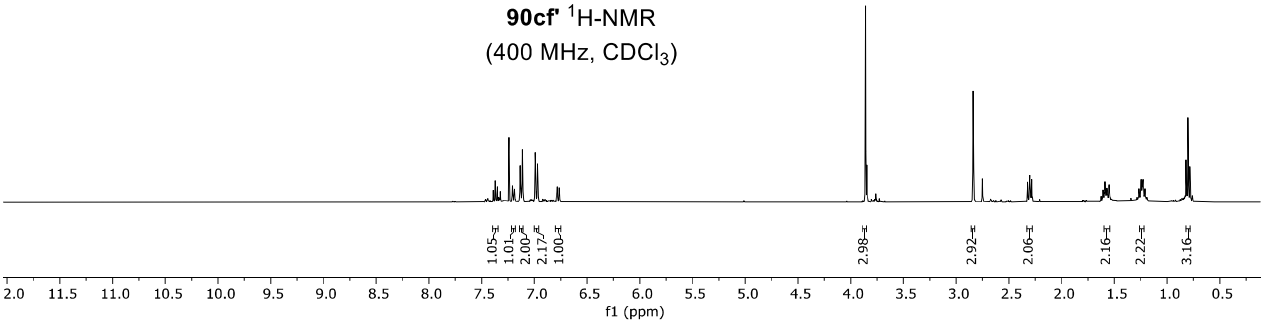

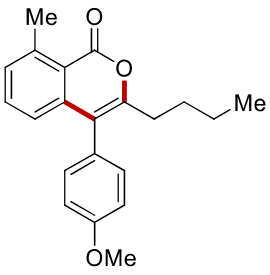

90cf' ^{13}C-NMR
(100 MHz, $CDCl_3$)

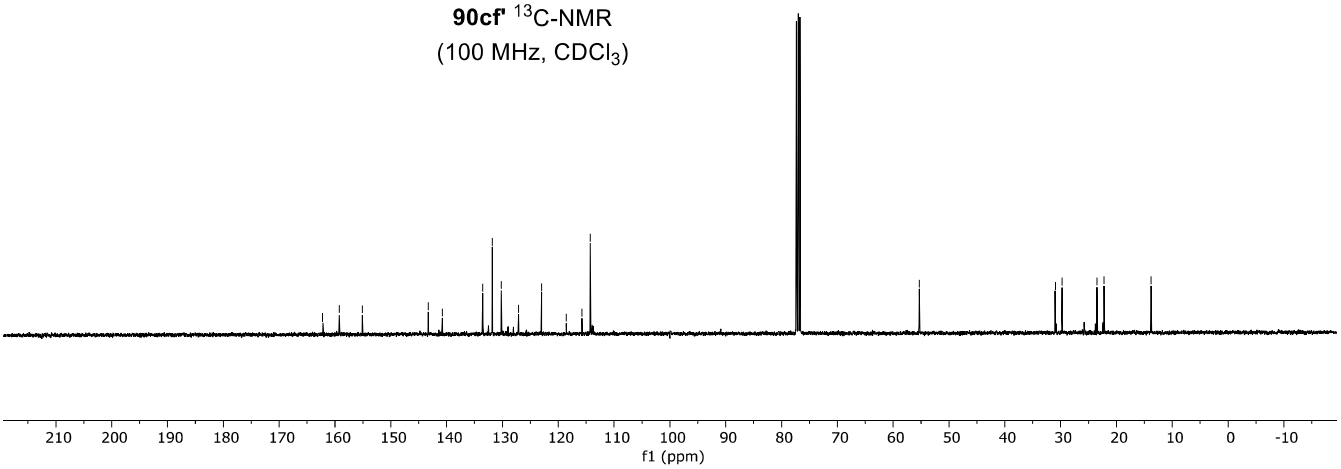

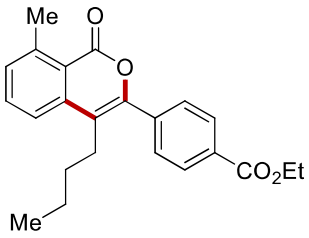

90cg ^{1}H-NMR
(300 MHz, $CDCl_3$)

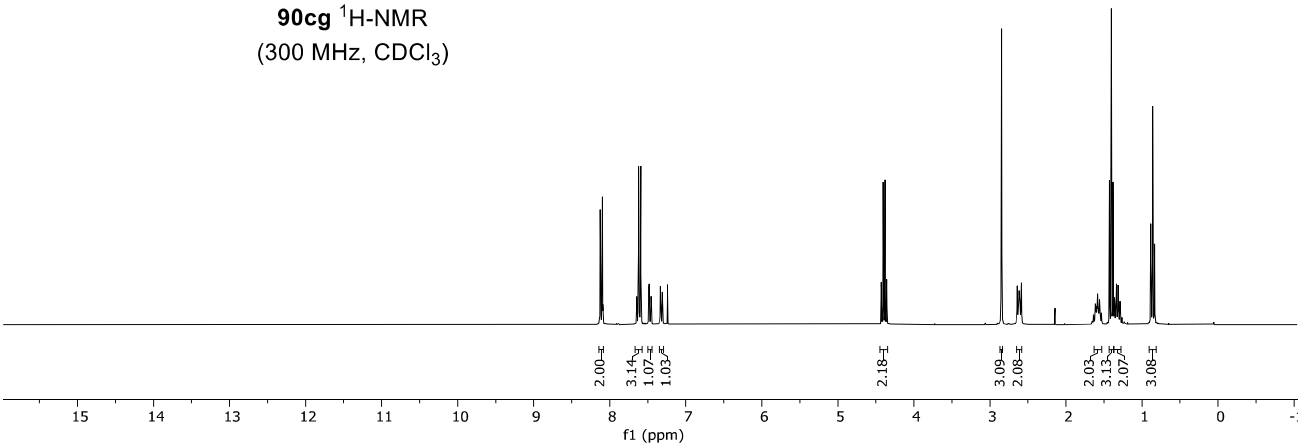

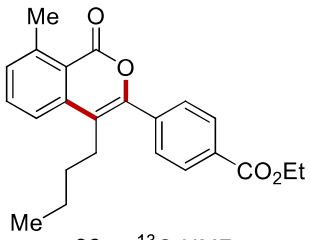

90cg ^{13}C-NMR
(125 MHz, $CDCl_3$)

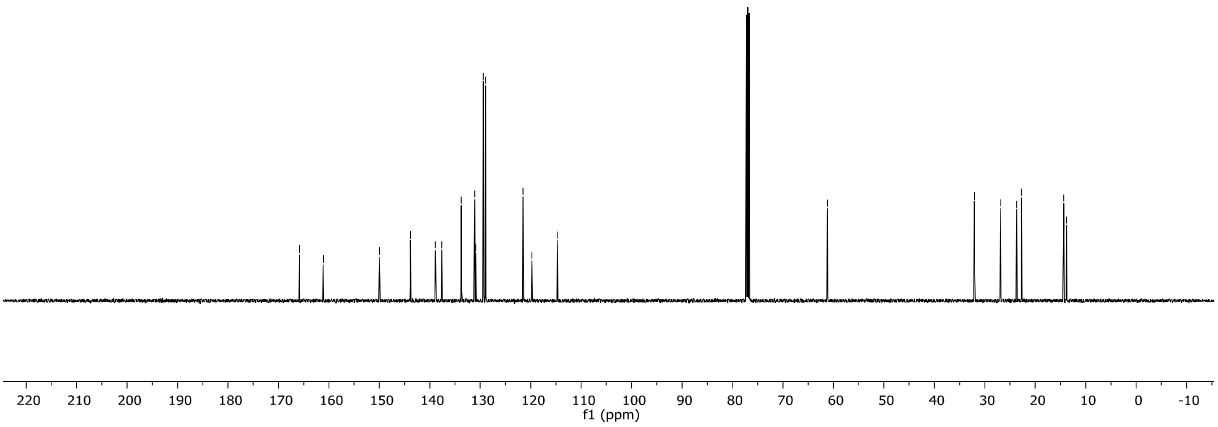

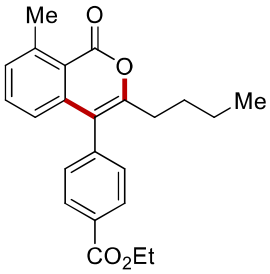

90cg' ^{1}H-NMR
(300 MHz, $CDCl_3$)

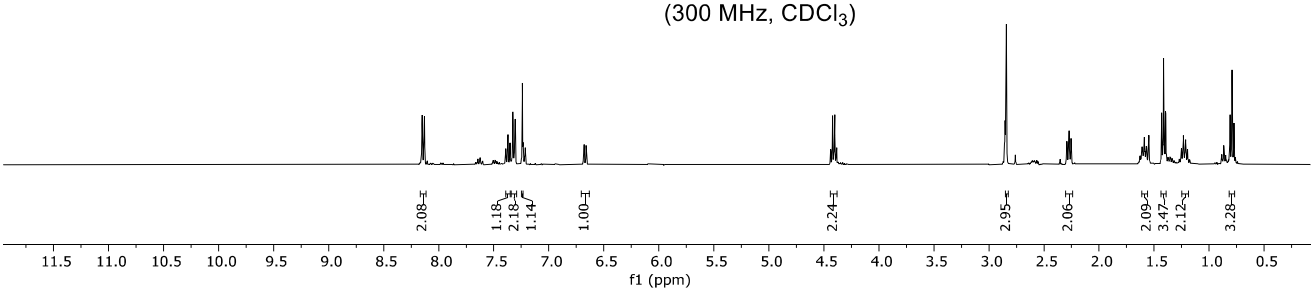

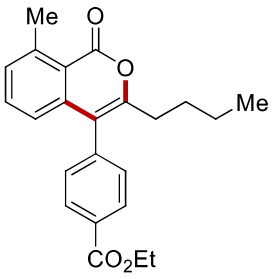

90cg' ^{13}C-NMR
(100 MHz, $CDCl_3$)

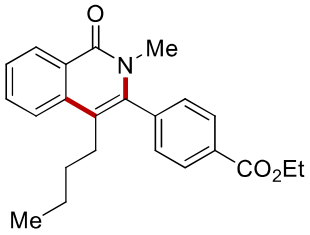

88ag ^{1}H-NMR
(400 MHz, $CDCl_3$)

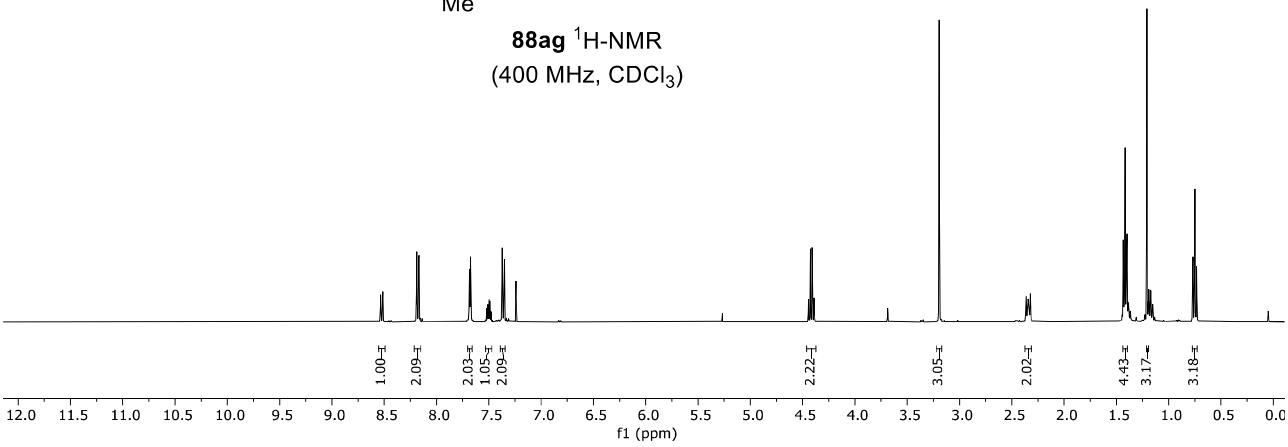

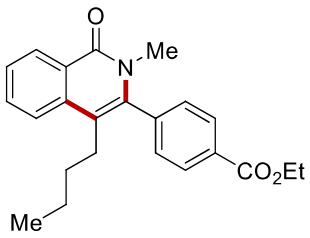

88ag ^{13}C-NMR
(100 MHz, $CDCl_3$)

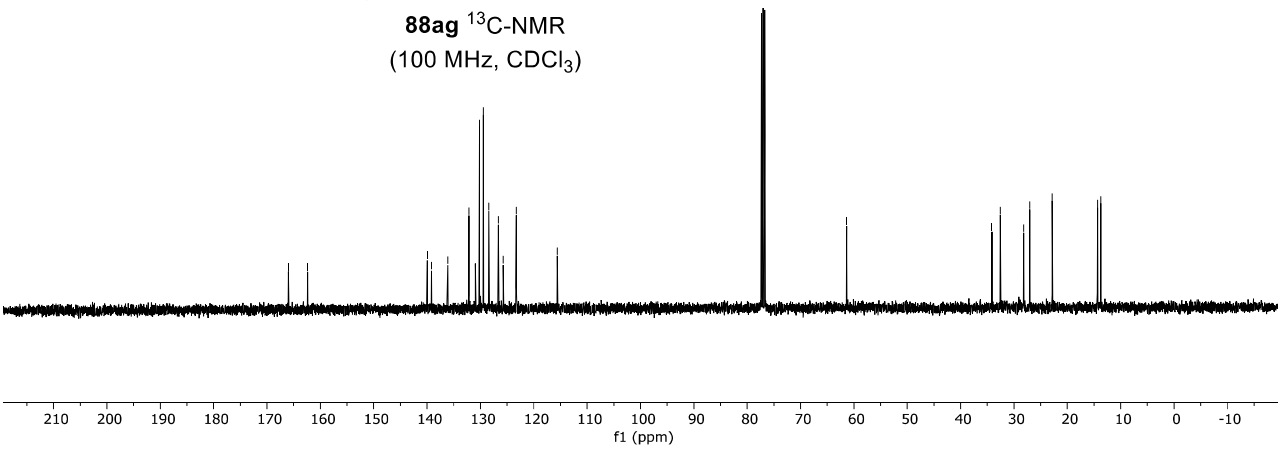

7.3 C−H Oxygenation Reactions Enabled by Dual Catalysis with Electrogenerated Hypervalent Iodine Species and Ruthenium Complexes

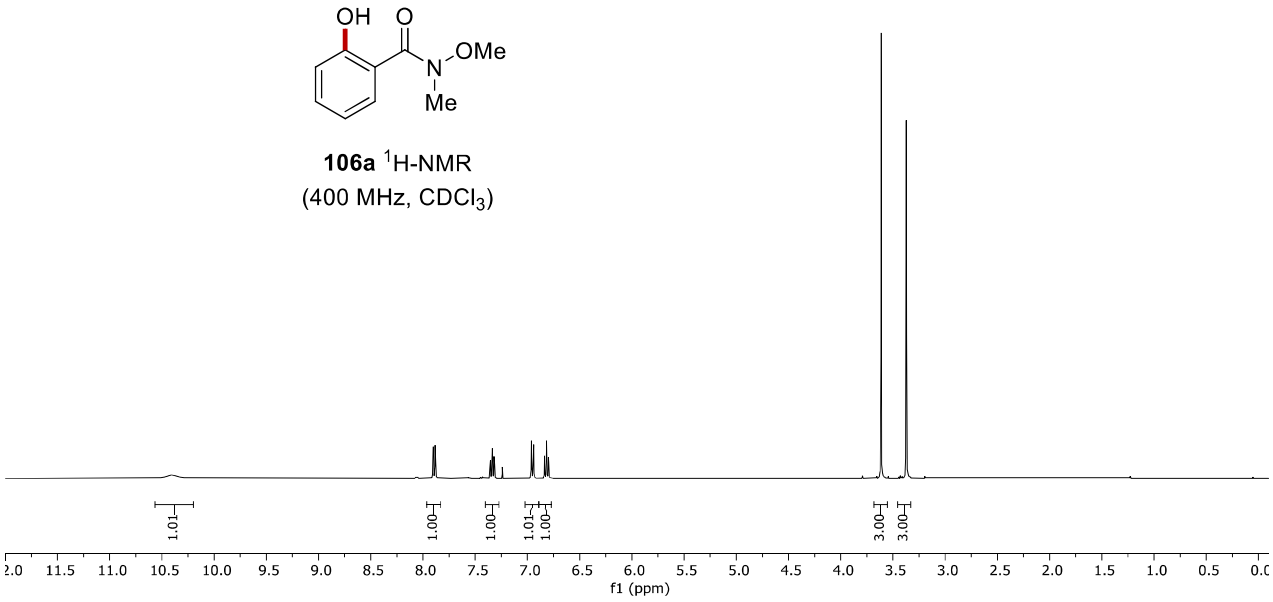

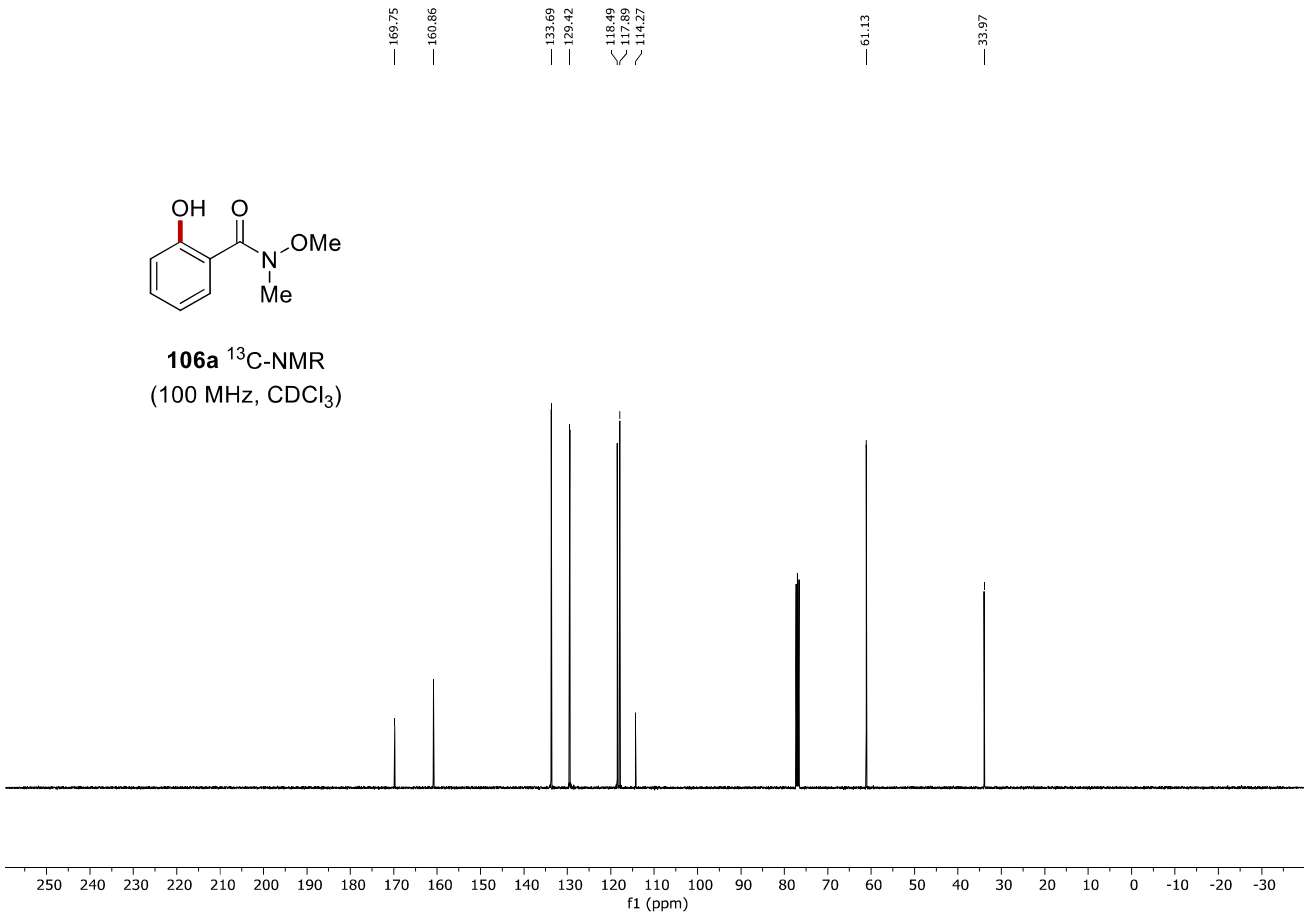

106a ^{13}C-NMR
(100 MHz, $CDCl_3$)

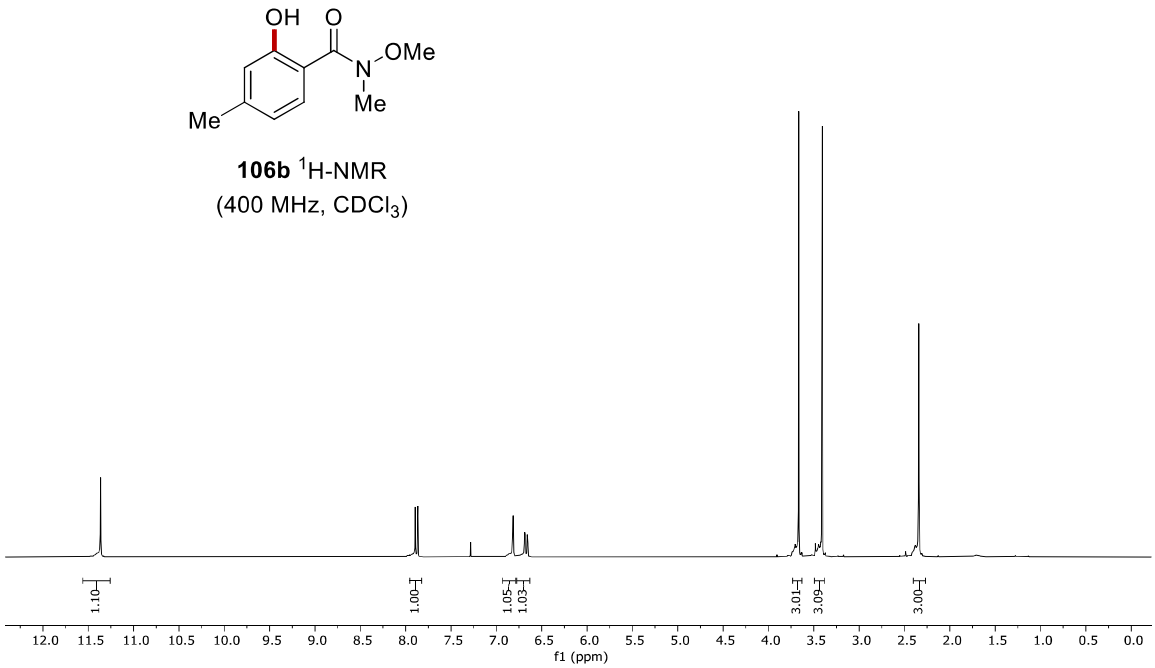

106b ^{1}H-NMR
(400 MHz, $CDCl_3$)

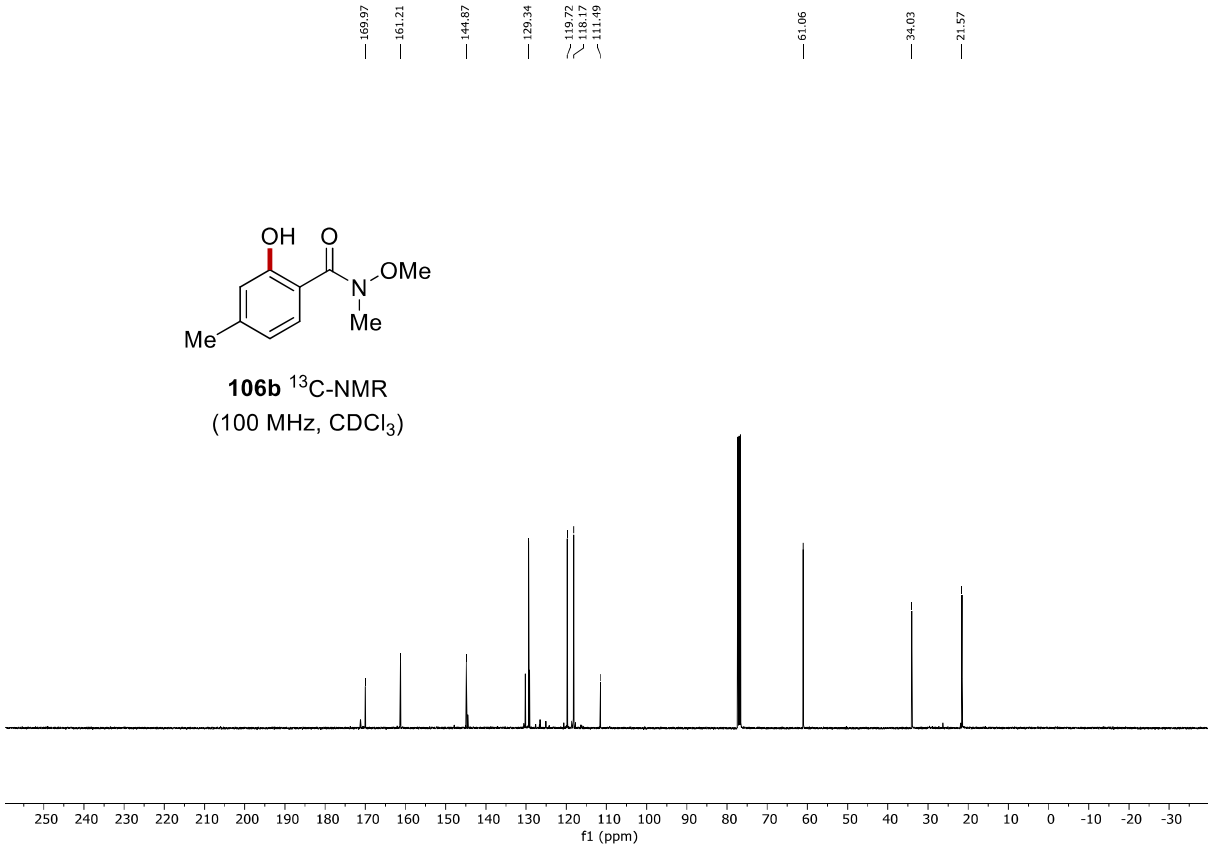
169.97
161.21
144.87
129.34
119.72
118.17
111.49
61.06
34.03
21.57
OH
O
N
OMe
Me
Me
106b 13C-NMR
(100 MHz, CDCl3)
250 240 230 220 210 200 190 180 170 160 150 140 130 120 110 100 90 80 70 60 50 40 30 20 10 0 -10 -20 -30
f1 (ppm)

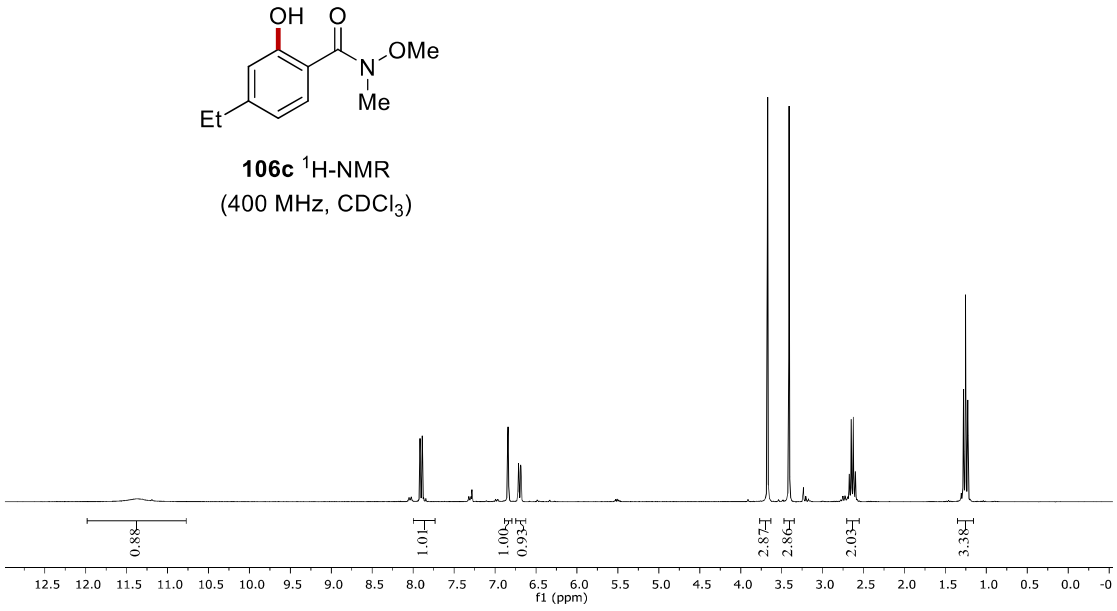
OH
O
N
OMe
Me
Et
106c 1H-NMR
(400 MHz, CDCl3)
0.88
1.01
1.00
0.93
2.87
2.86
2.03
3.38
12.5 12.0 11.5 11.0 10.5 10.0 9.5 9.0 8.5 8.0 7.5 7.0 6.5 6.0 5.5 5.0 4.5 4.0 3.5 3.0 2.5 2.0 1.5 1.0 0.5 0.0 -0
f1 (ppm)

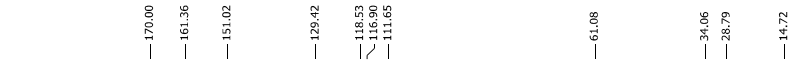

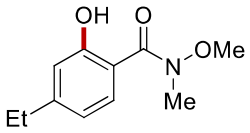

106c ^{13}C-NMR
(100 MHz, $CDCl_3$)

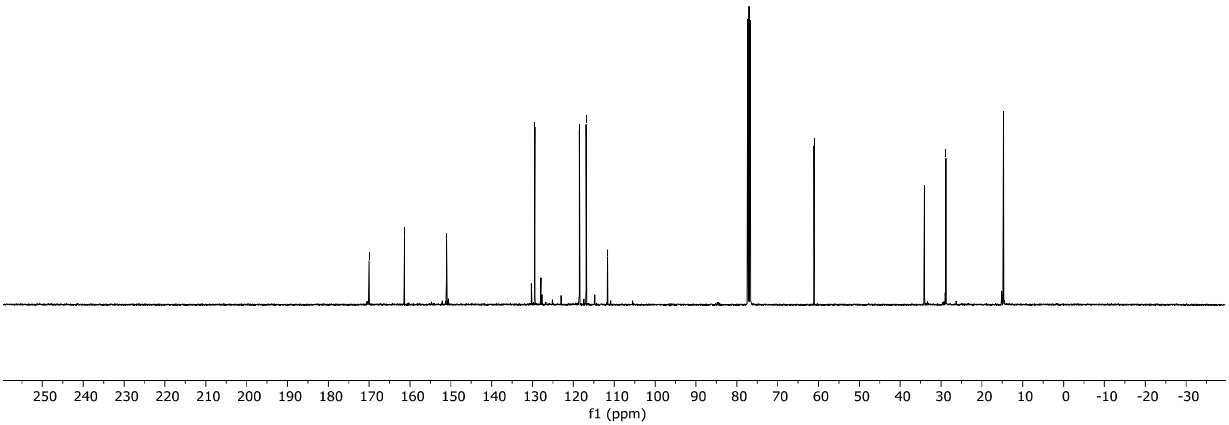

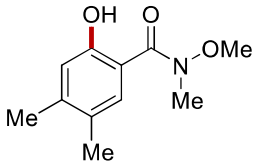

106e ^{1}H-NMR
(400 MHz, $CDCl_3$)

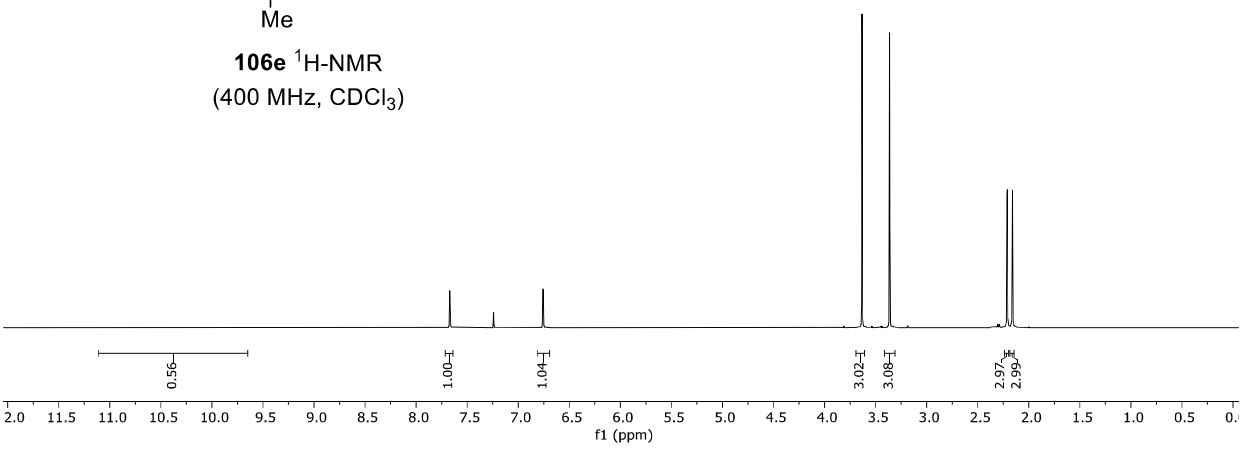

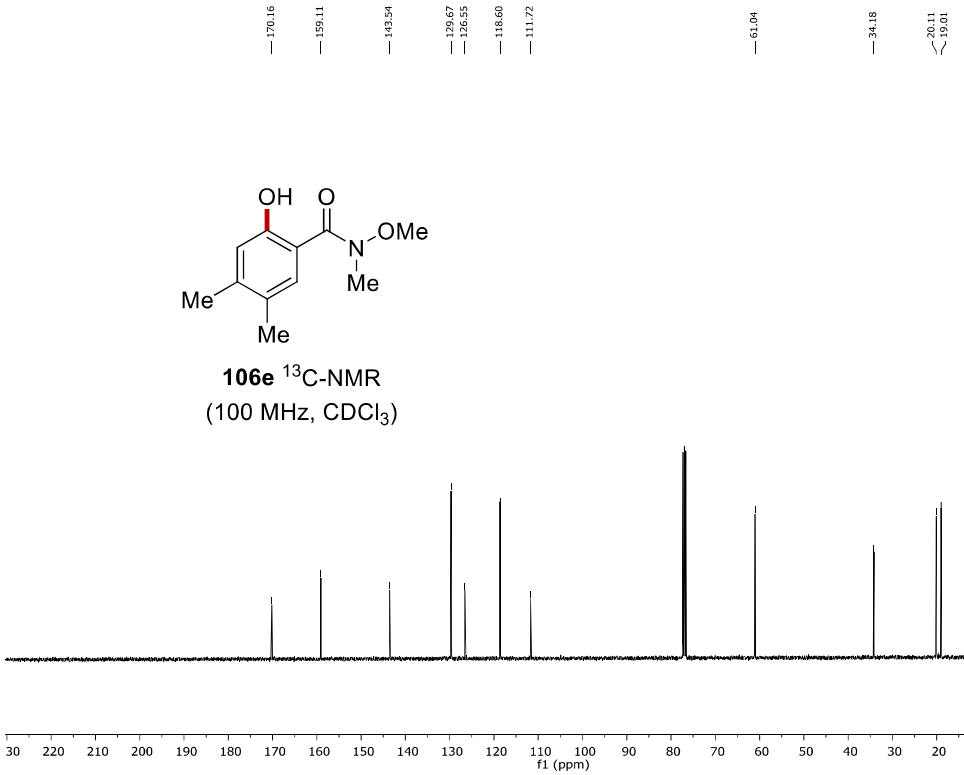

106e ^{13}C-NMR
(100 MHz, $CDCl_3$)

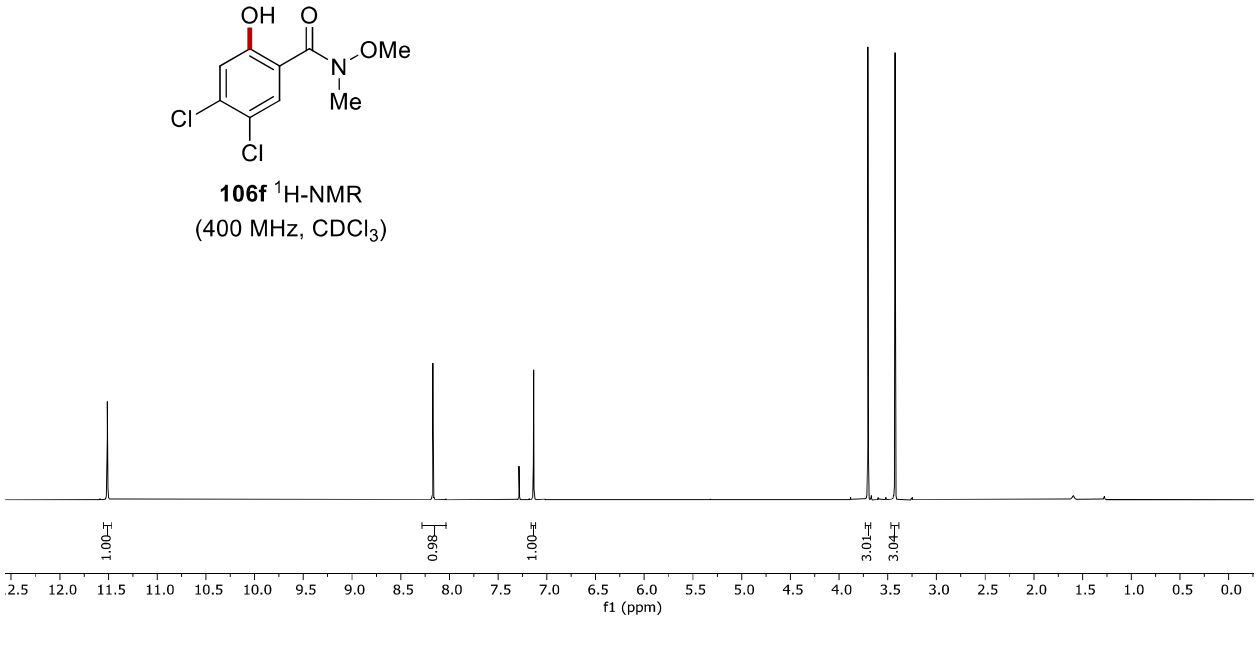

106f ^{1}H-NMR
(400 MHz, $CDCl_3$)

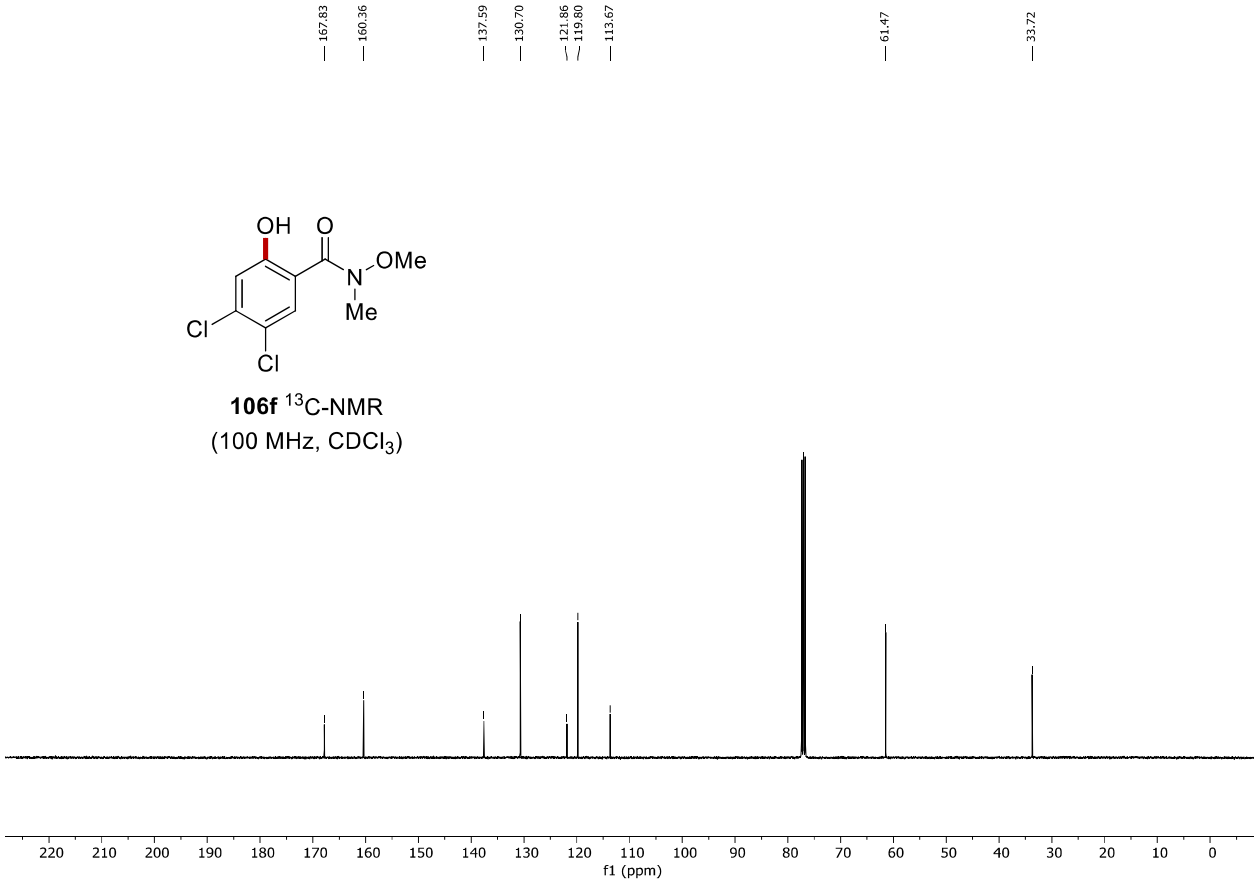

106f ^{13}C-NMR
(100 MHz, $CDCl_3$)

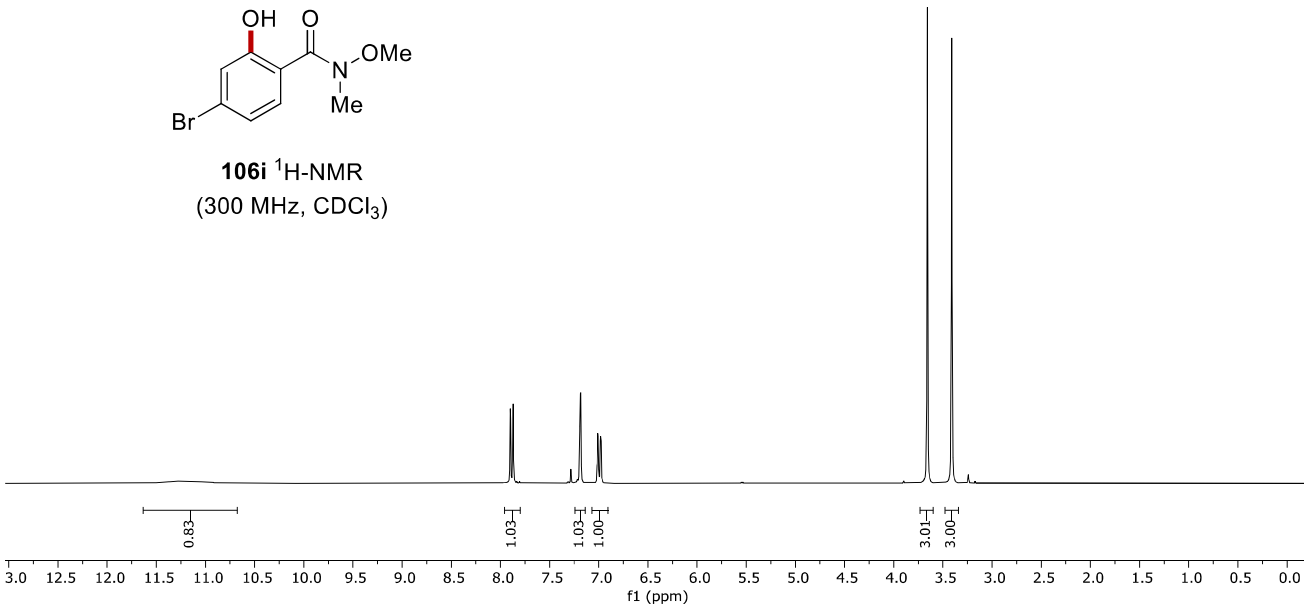

106i ^{1}H-NMR
(300 MHz, $CDCl_3$)

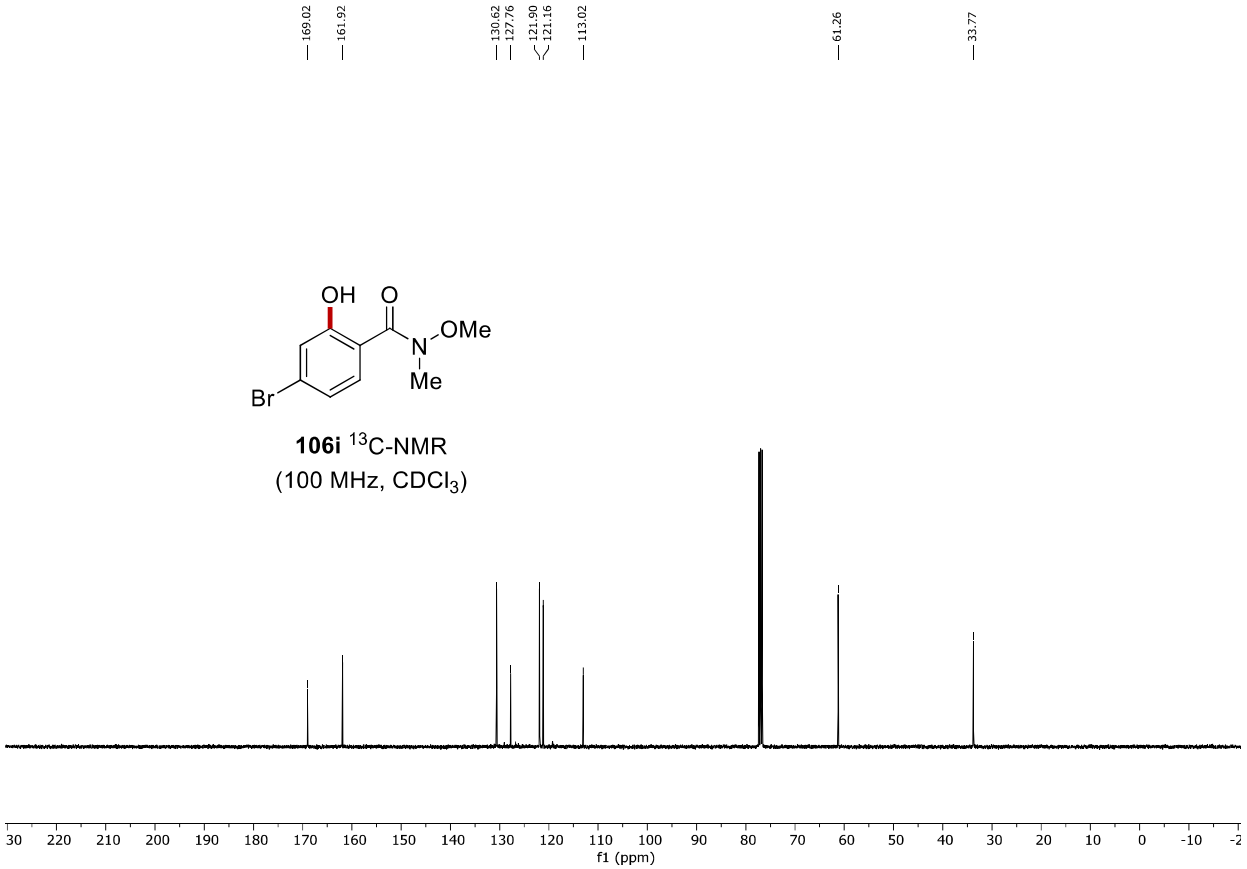

106i ^{13}C-NMR
(100 MHz, $CDCl_3$)

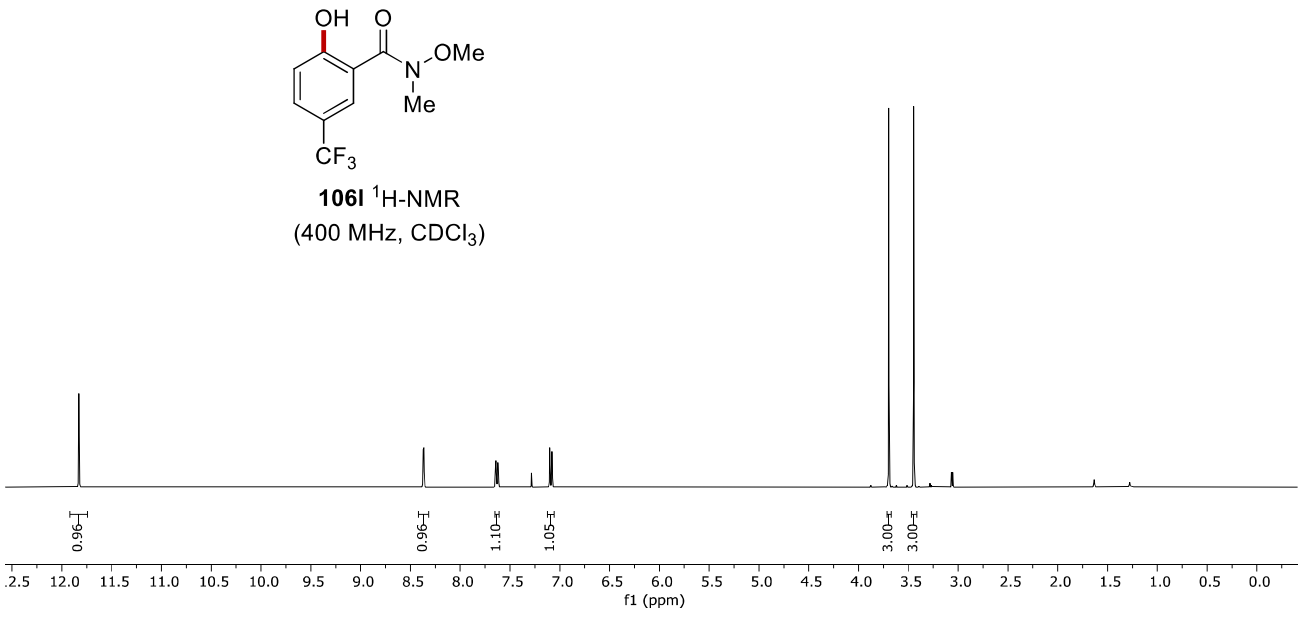

106l ^{1}H-NMR
(400 MHz, $CDCl_3$)

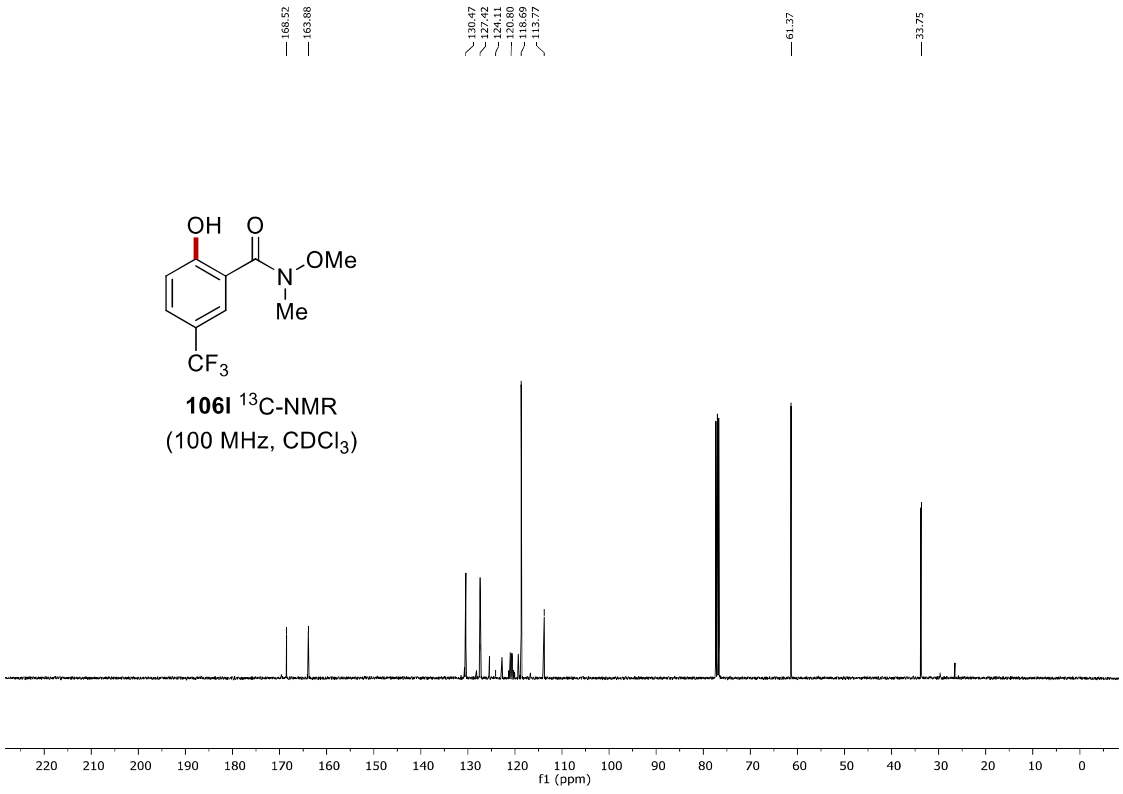

106l ^{13}C-NMR
(100 MHz, $CDCl_3$)

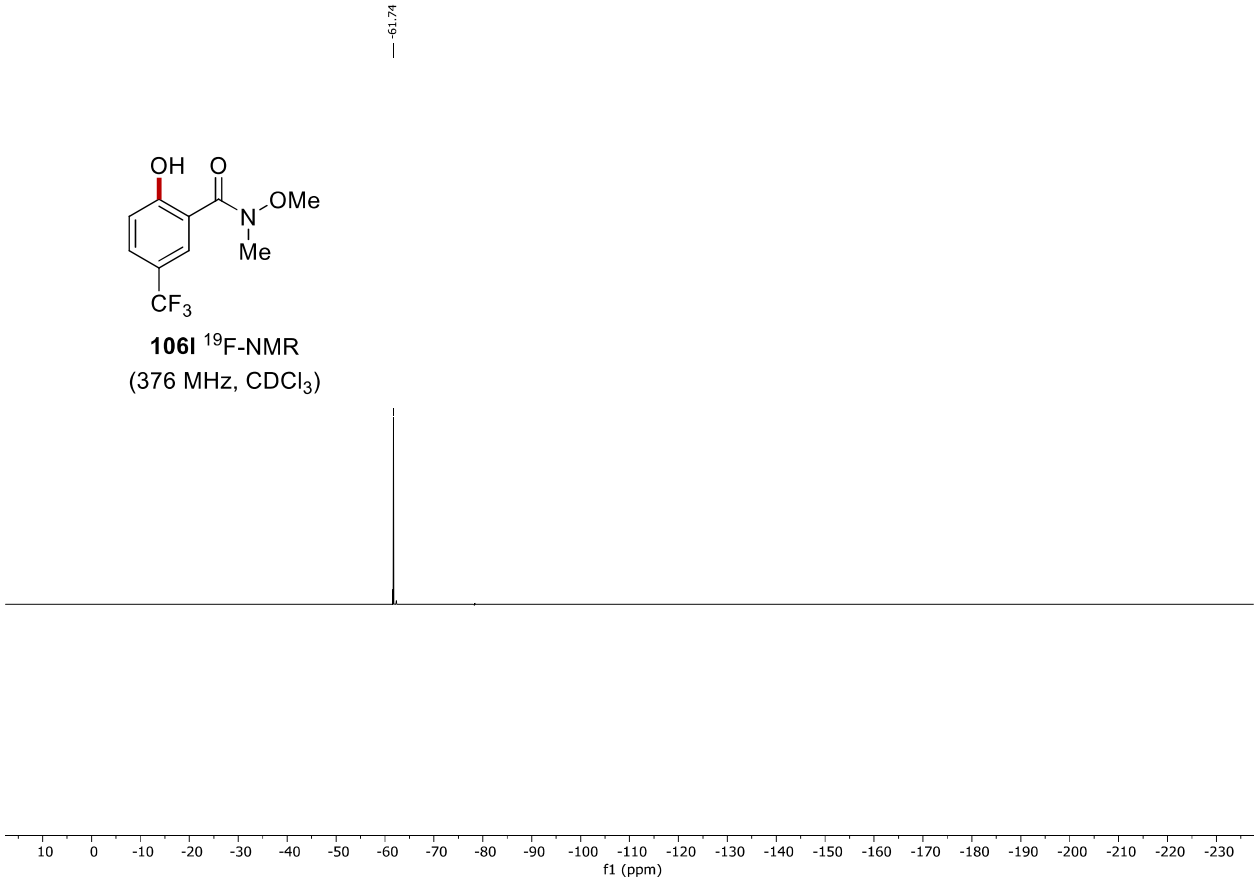

106l ^{19}F-NMR
(376 MHz, $CDCl_3$)

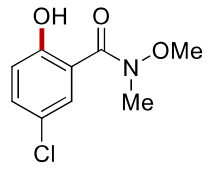

106m ^{1}H-NMR
(400 MHz, $CDCl_3$)

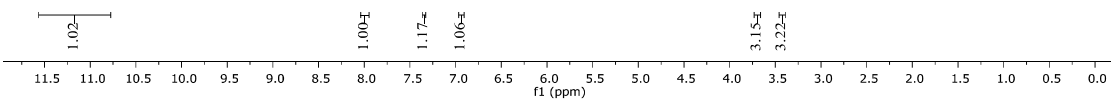

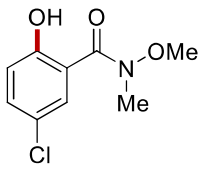

106m ^{13}C-NMR
(100 MHz, $CDCl_3$)

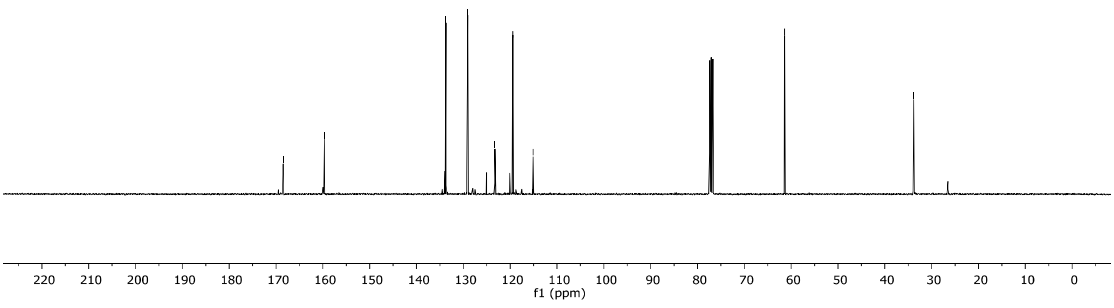

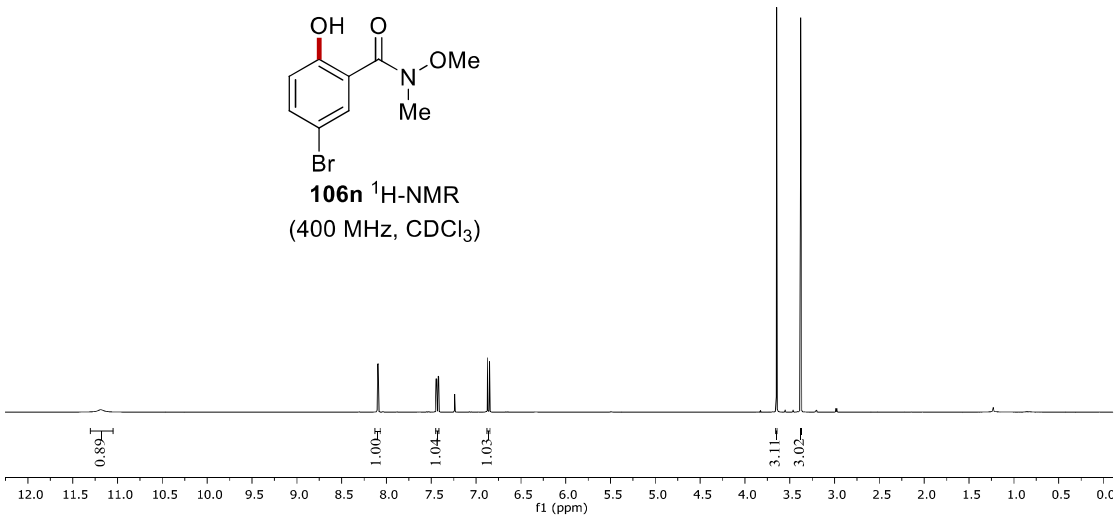

106n ^{1}H-NMR
(400 MHz, $CDCl_3$)

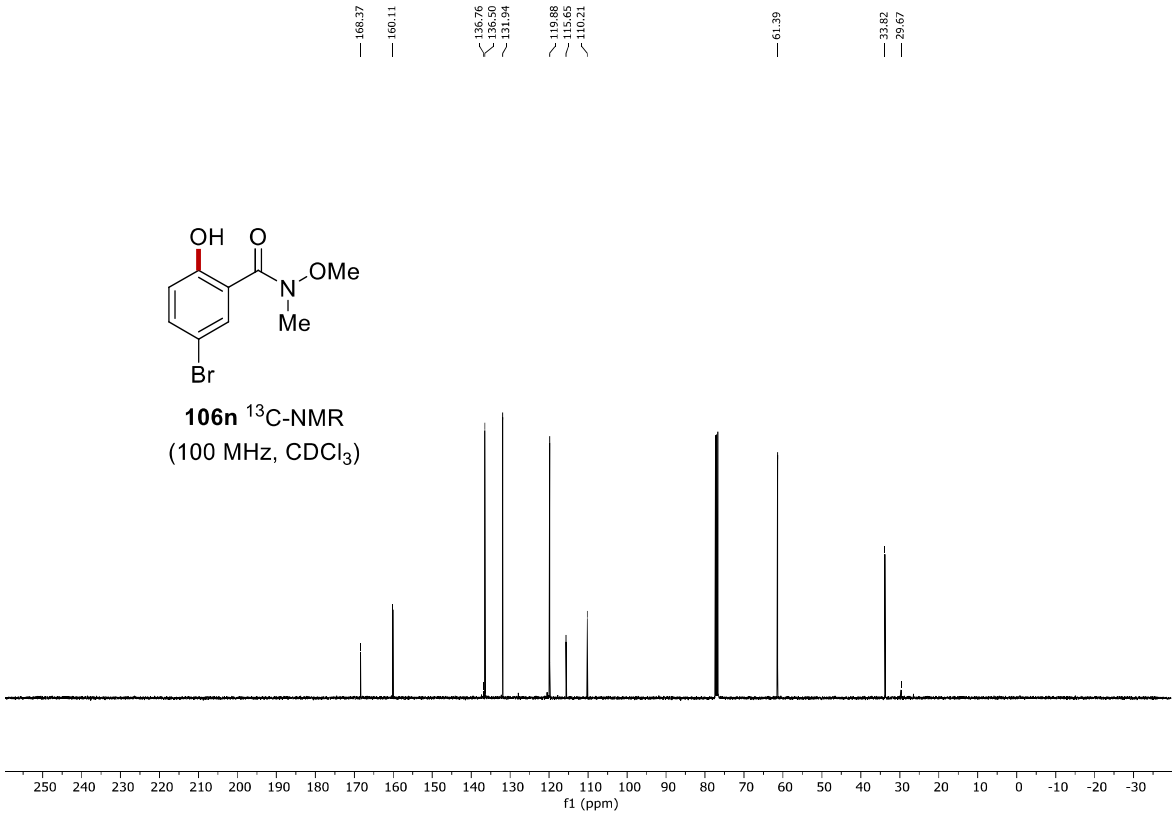

106n ^{13}C-NMR
(100 MHz, $CDCl_3$)

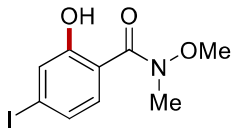

106o ^{1}H-NMR
(400 MHz, $CDCl_3$)

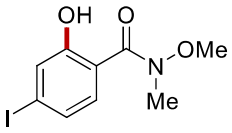

106o ^{13}C-NMR
(100 MHz, $CDCl_3$)

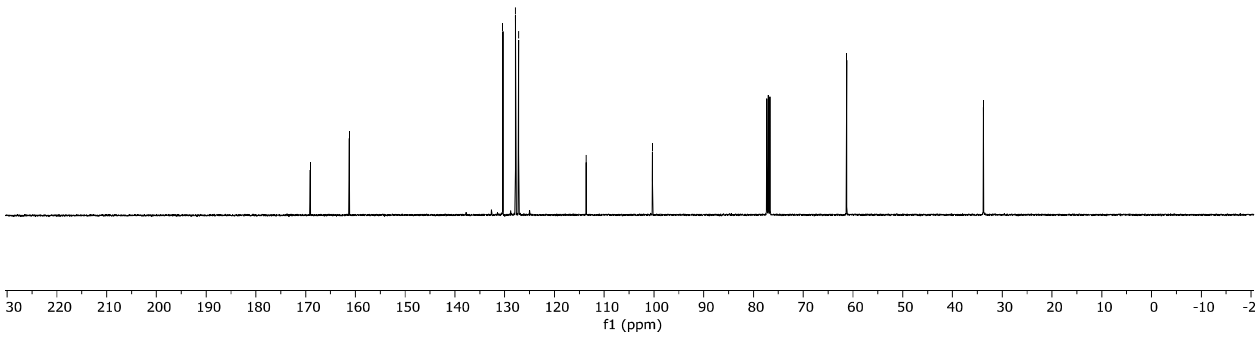

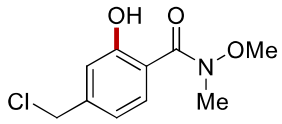

106p ^{1}H-NMR
(400 MHz, $CDCl_3$)

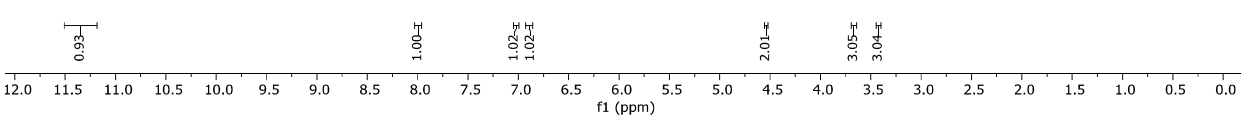

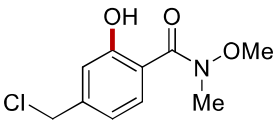

106p ^{13}C-NMR
(100 MHz, $CDCl_3$)

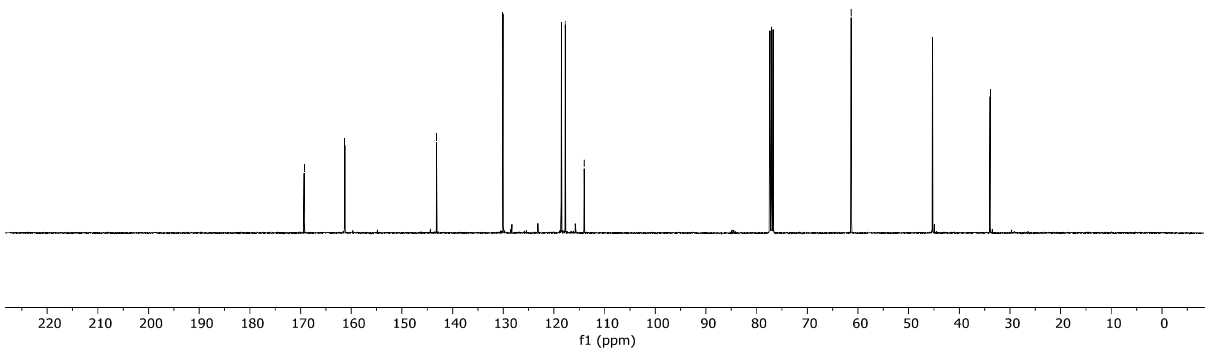

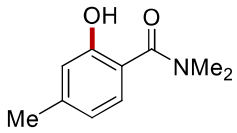

104b ^{1}H-NMR
(300 MHz, $CDCl_3$)

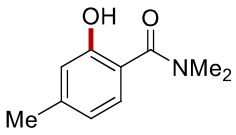

104b ^{13}C-NMR
(100 MHz, $CDCl_3$)

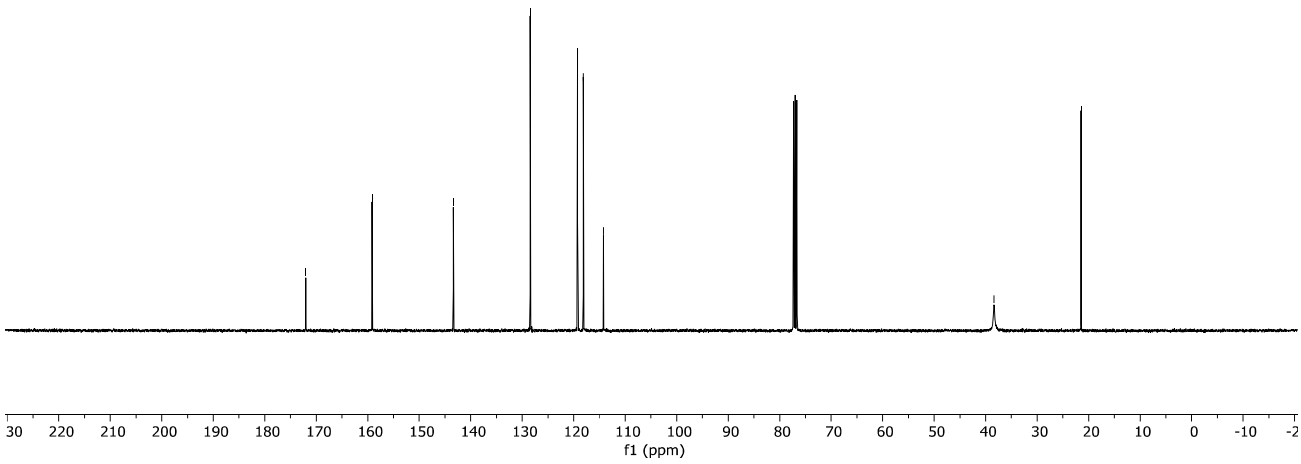

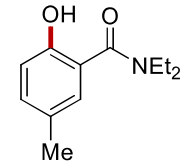

104d ^{1}H-NMR
(400 MHz, $CDCl_3$)

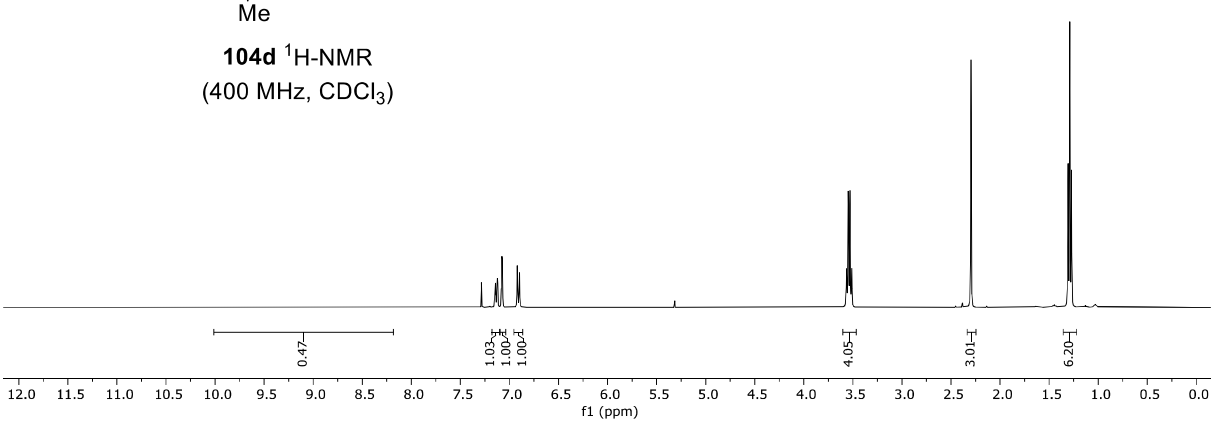

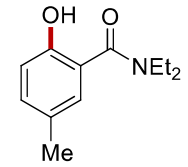

104d ^{13}C-NMR
(100 MHz, $CDCl_3$)

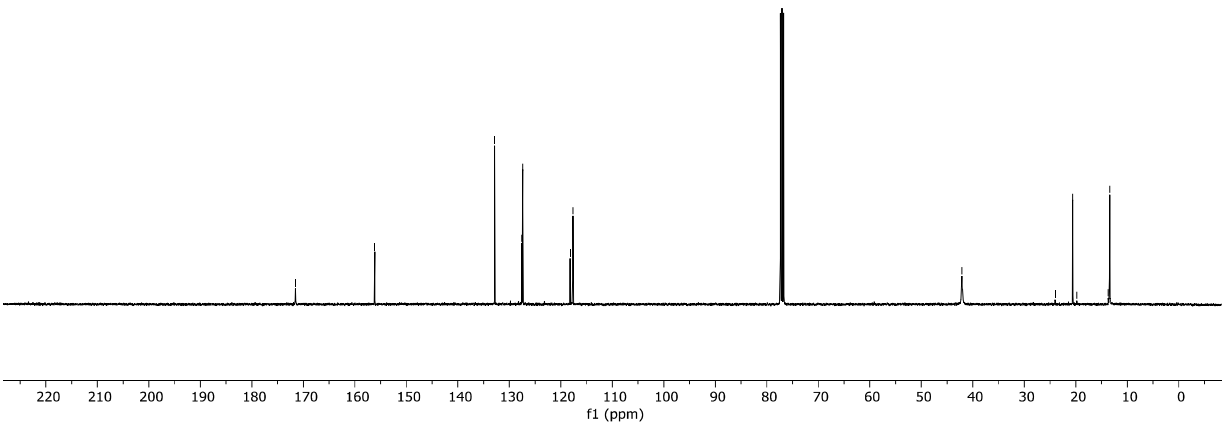

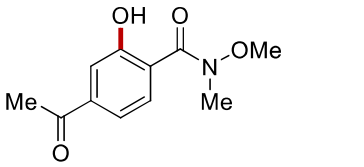

106q ^{1}H-NMR
(400 MHz, $CDCl_3$)

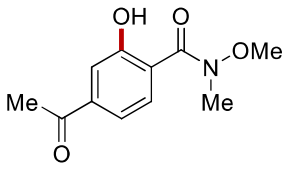

106q ^{13}C-NMR
(100 MHz, $CDCl_3$)

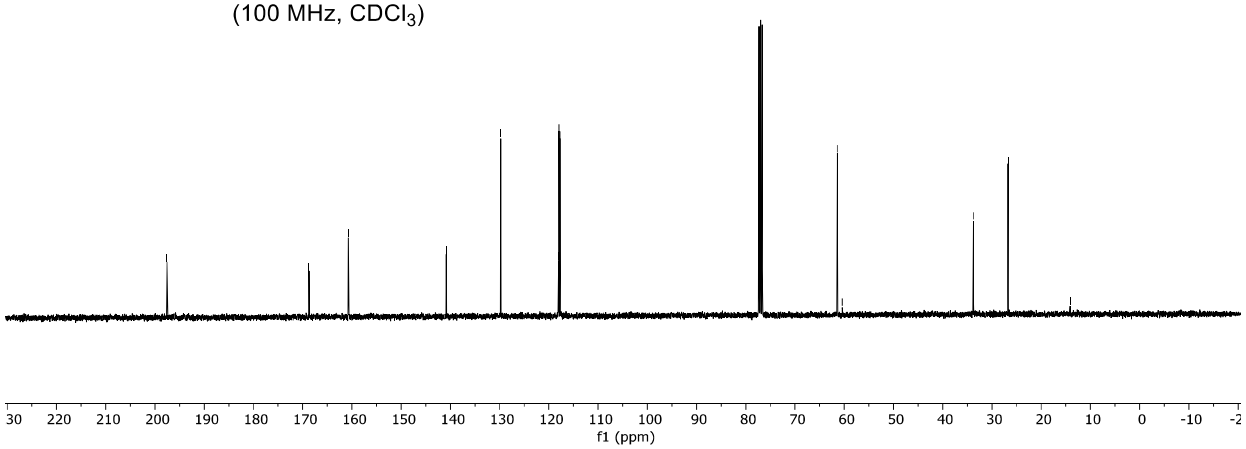

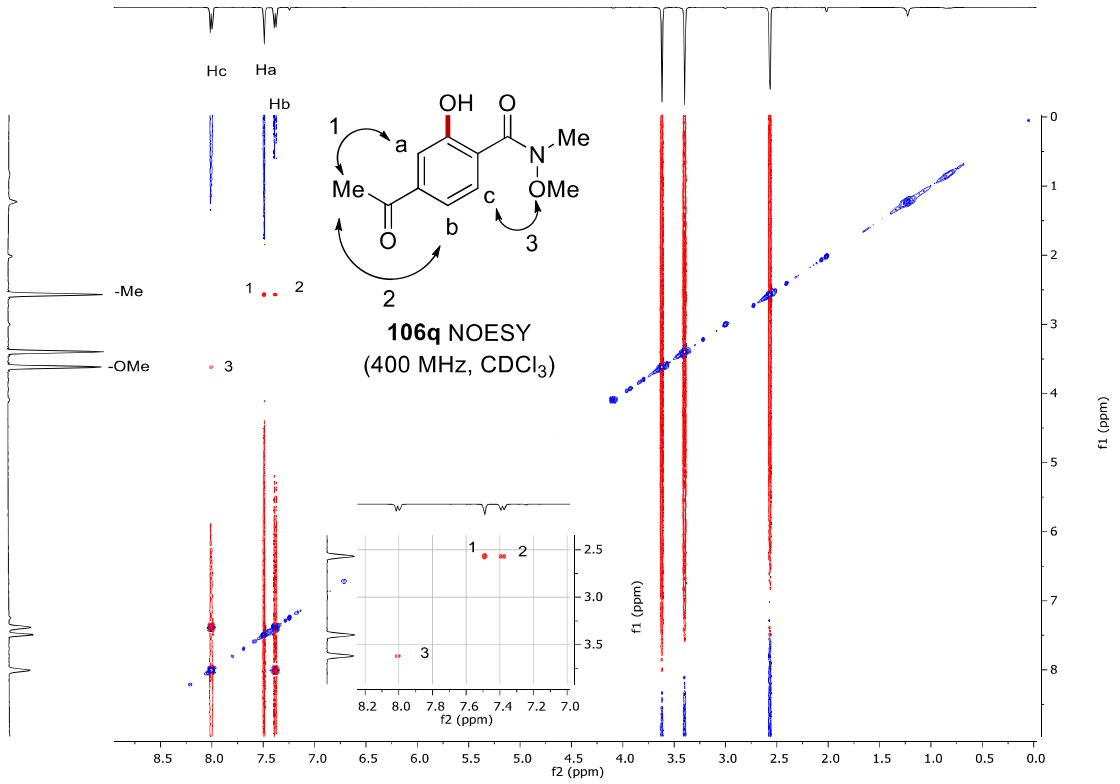

106q NOESY
(400 MHz, $CDCl_3$)

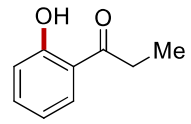

197b ^{1}H-NMR
(400 MHz, $CDCl_3$)

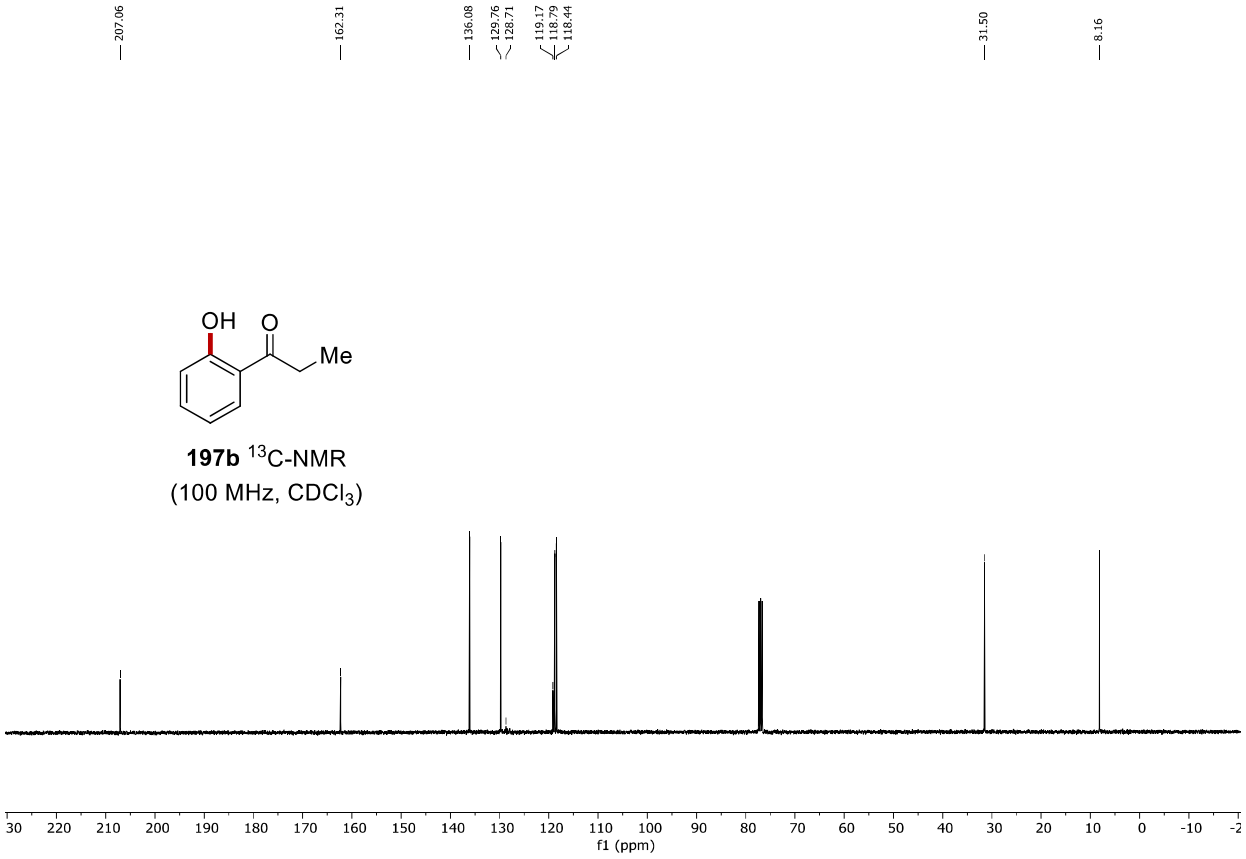

197b ^{13}C-NMR
(100 MHz, $CDCl_3$)

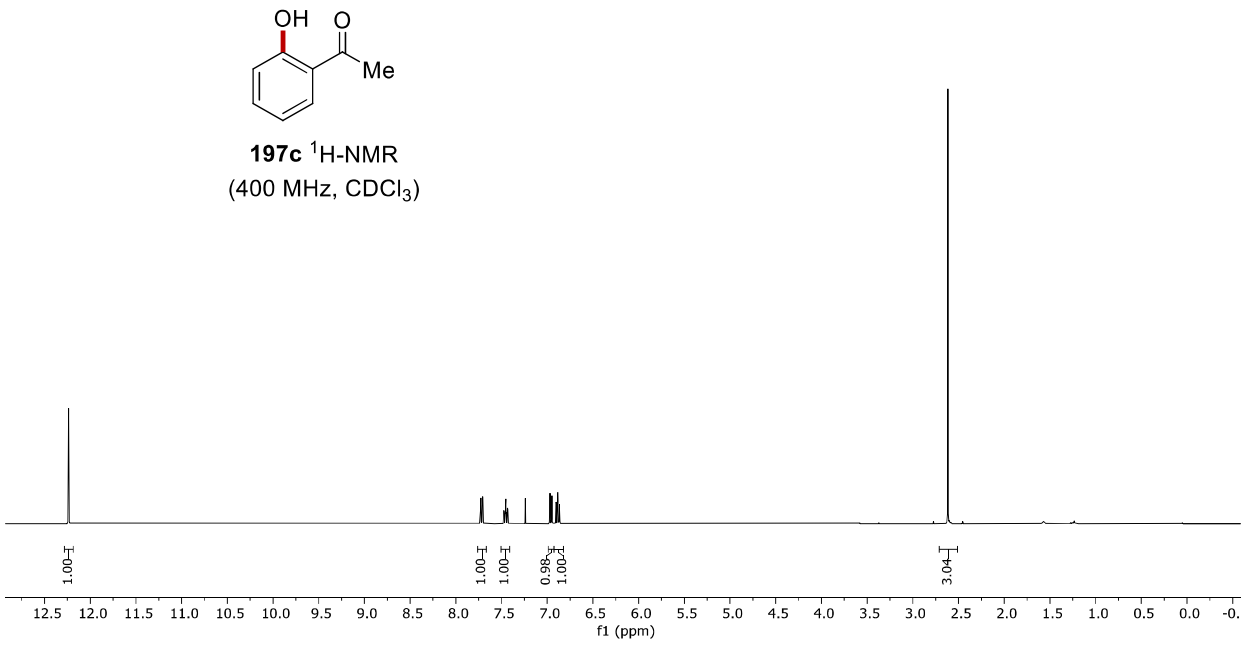

197c ^{1}H-NMR
(400 MHz, $CDCl_3$)

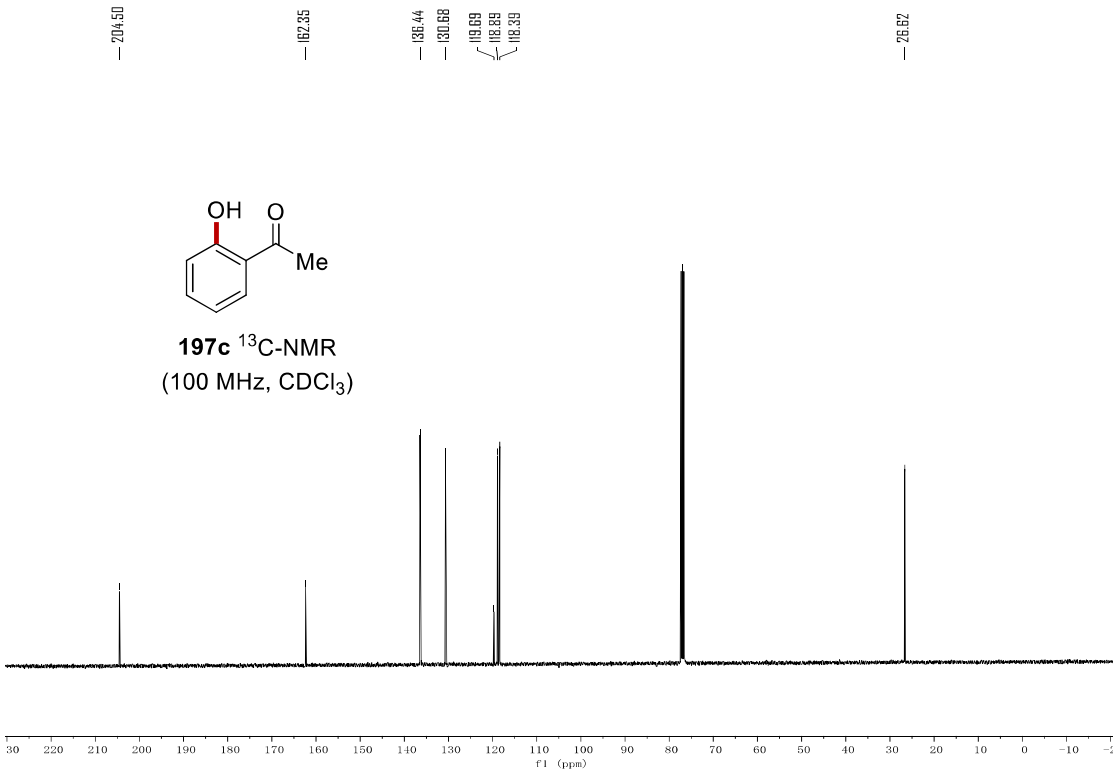

197c ^{13}C-NMR
(100 MHz, $CDCl_3$)

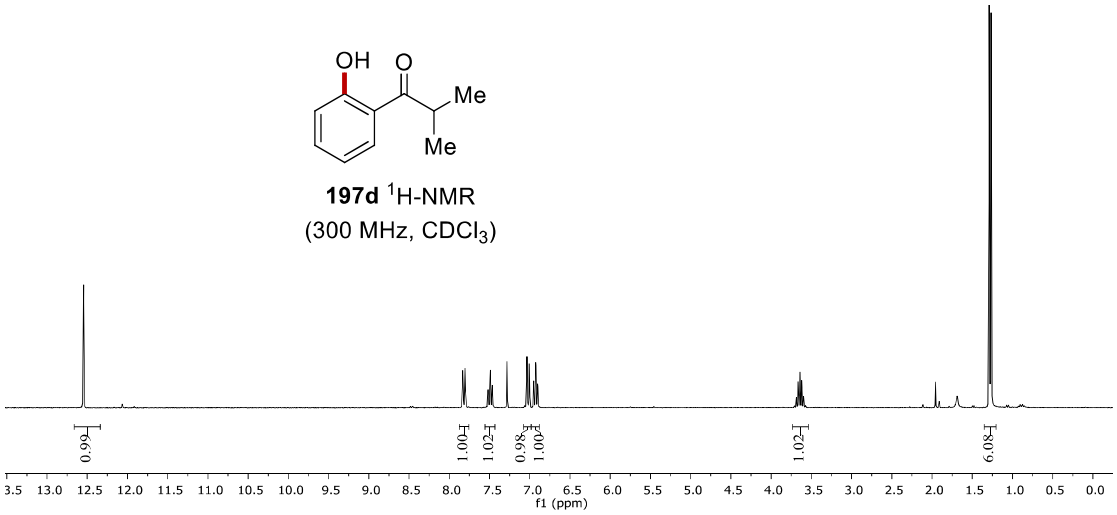

197d ^{1}H-NMR
(300 MHz, $CDCl_3$)

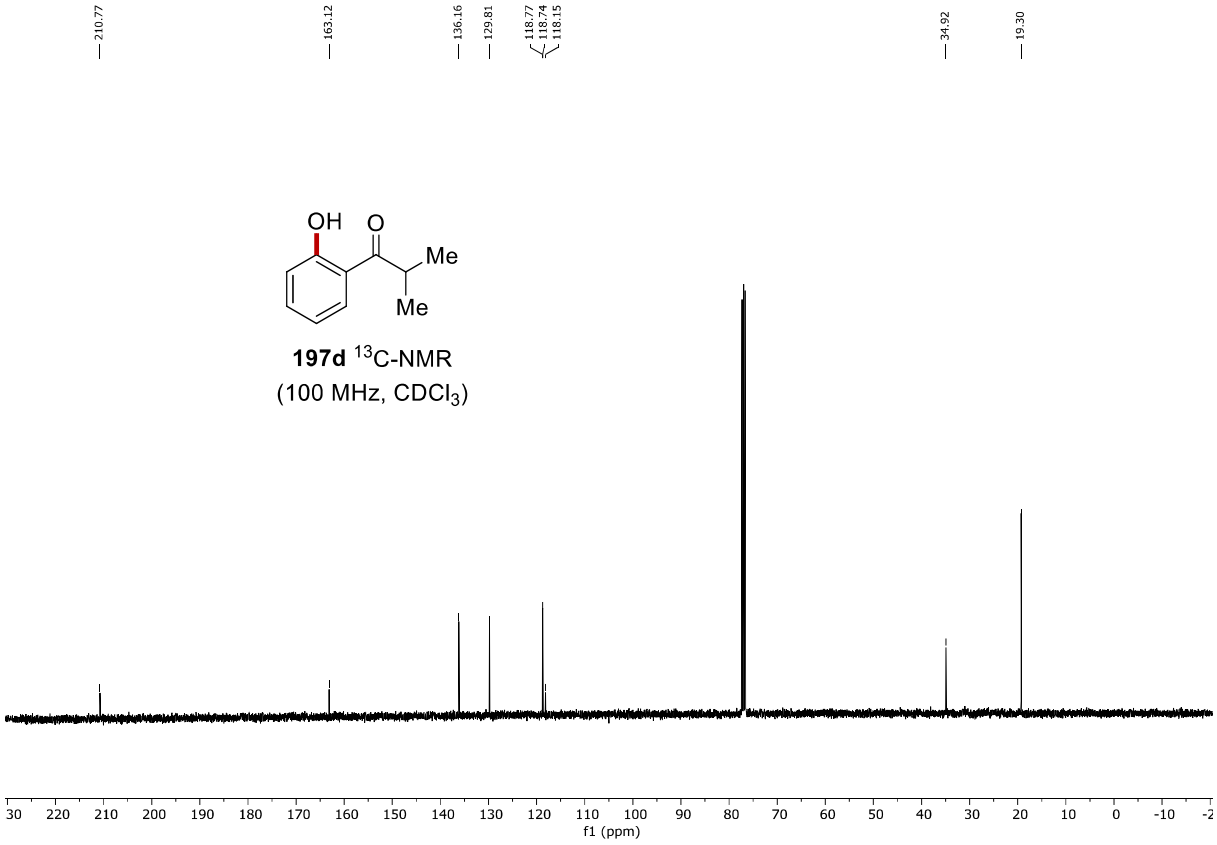

197d ^{13}C-NMR
(100 MHz, $CDCl_3$)

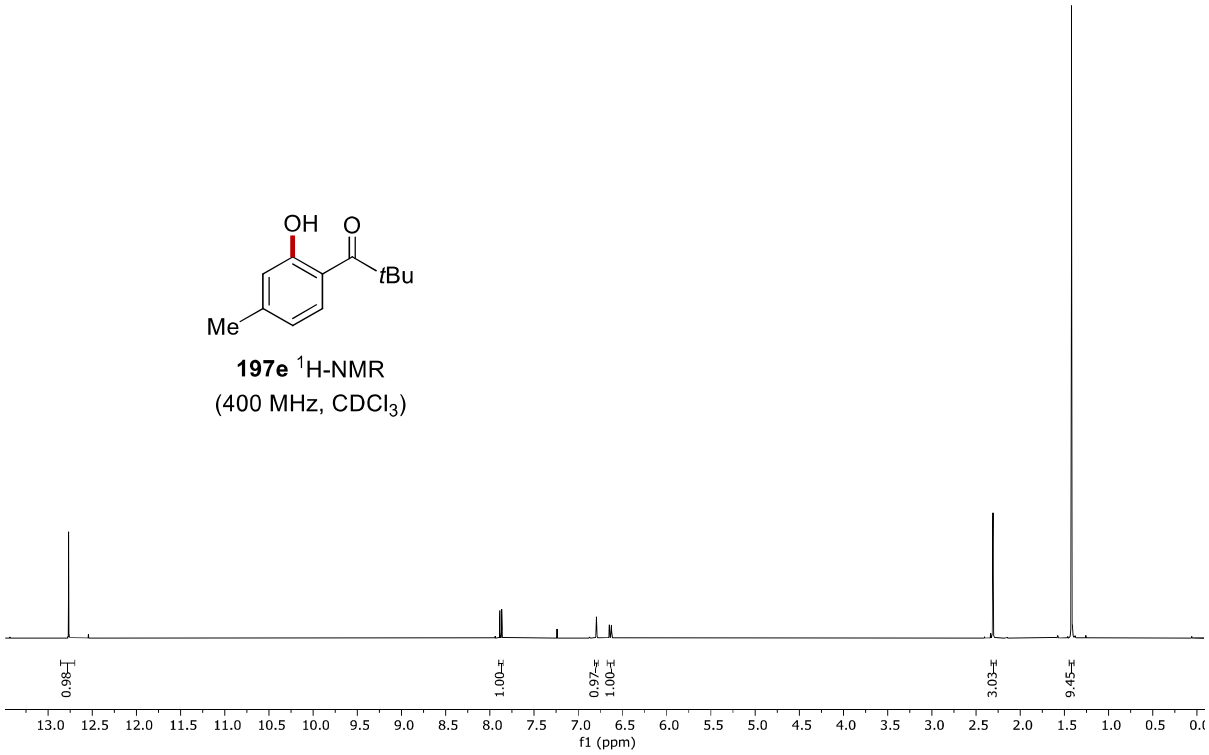

197e ^{1}H-NMR
(400 MHz, $CDCl_3$)

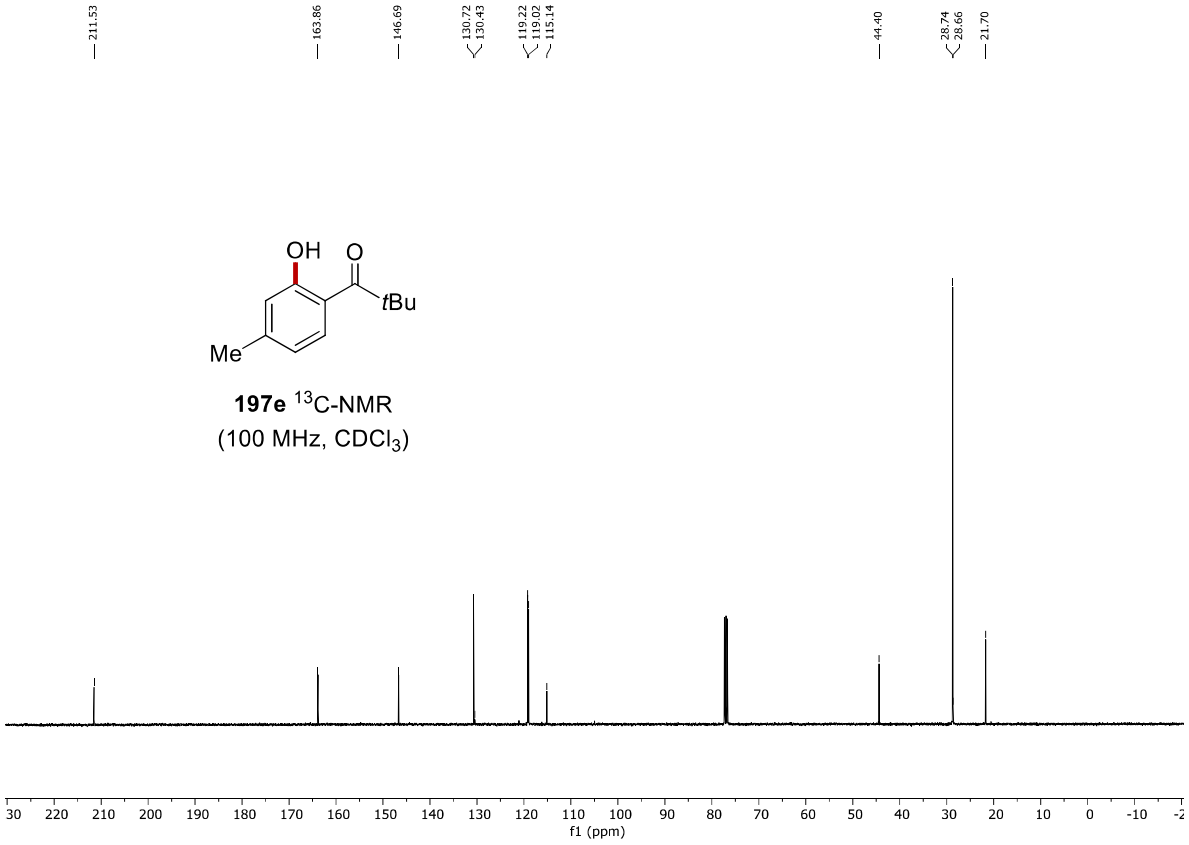

197e ^{13}C-NMR
(100 MHz, $CDCl_3$)

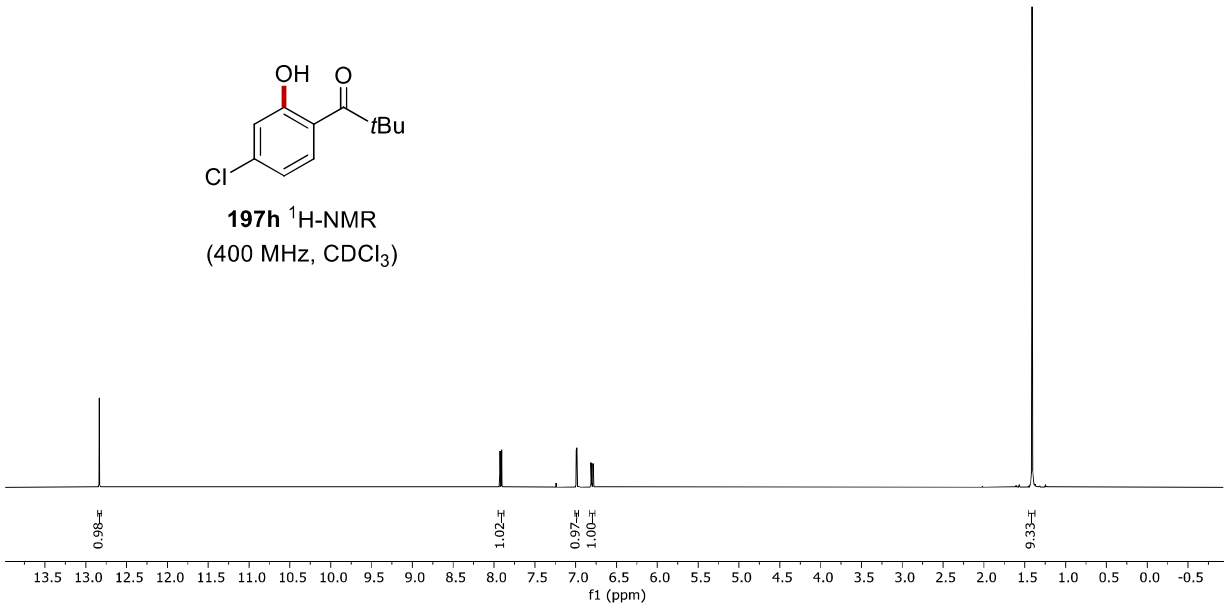

197h ^{1}H-NMR
(400 MHz, $CDCl_3$)

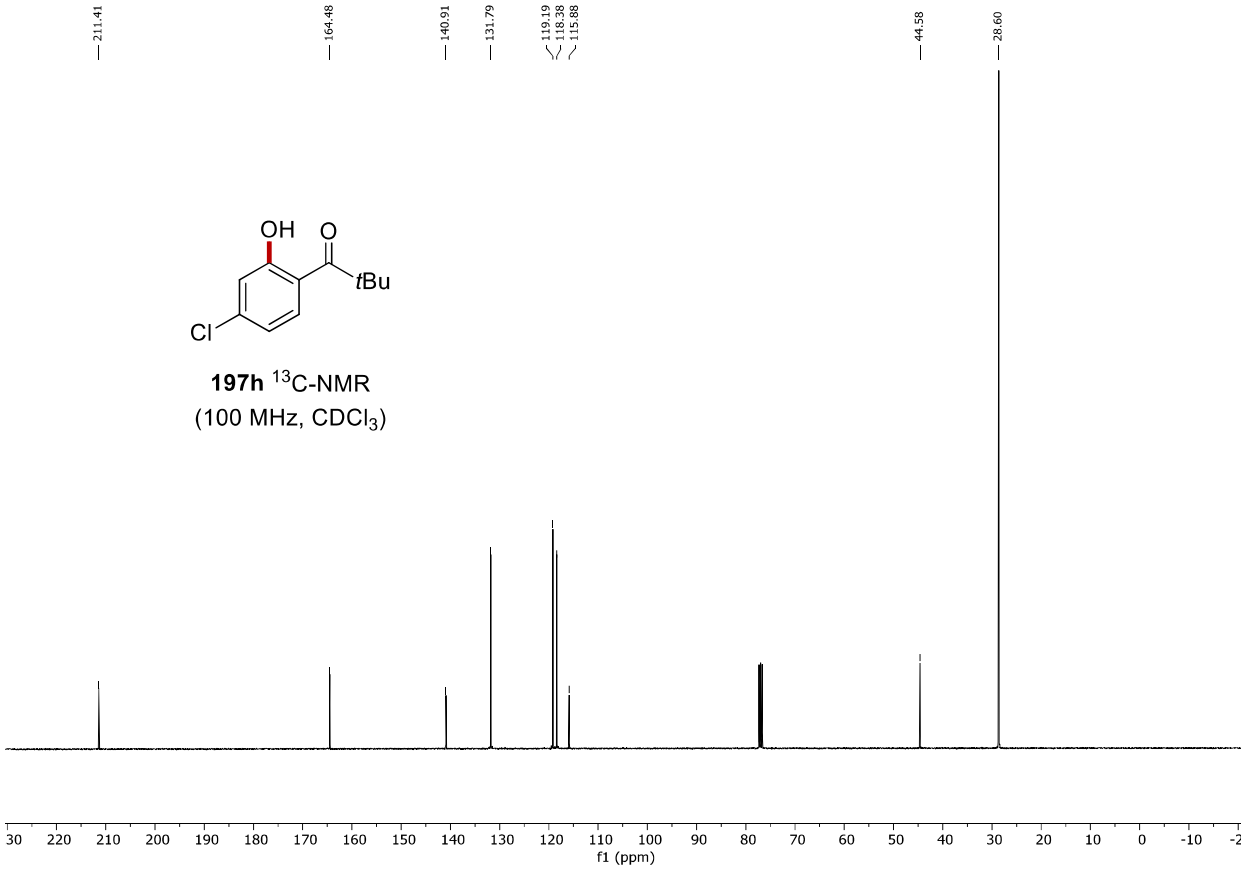

197h ^{13}C-NMR
(100 MHz, $CDCl_3$)

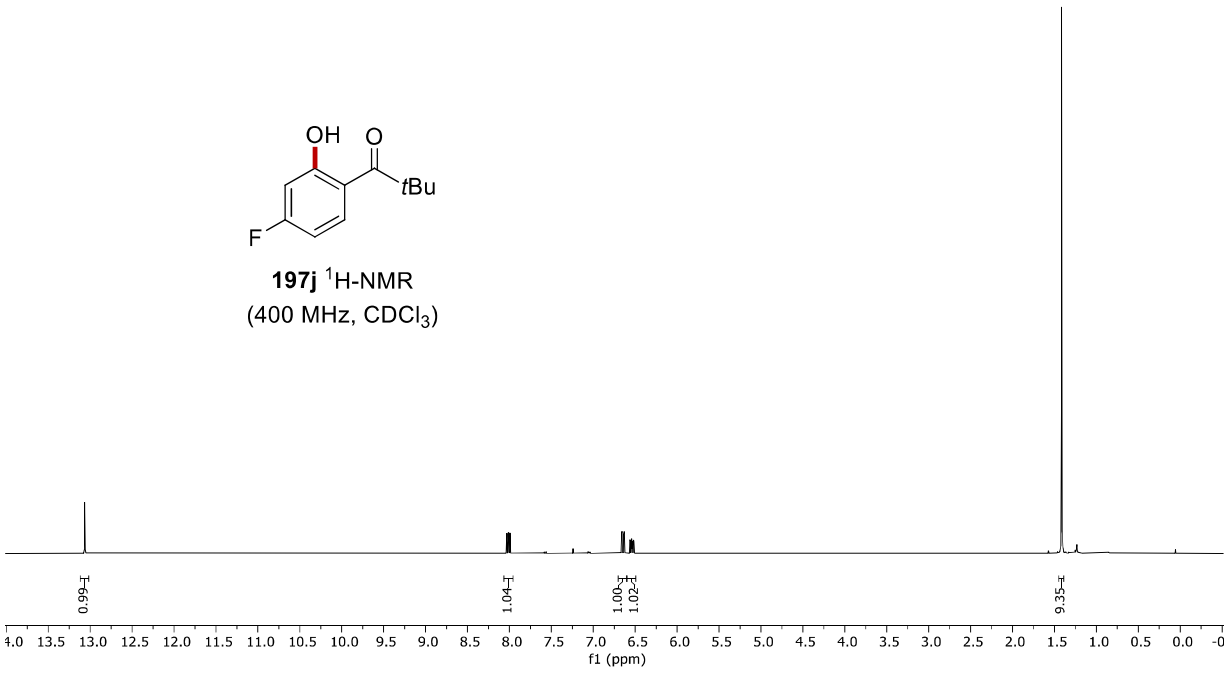

197j ^{1}H-NMR
(400 MHz, $CDCl_3$)

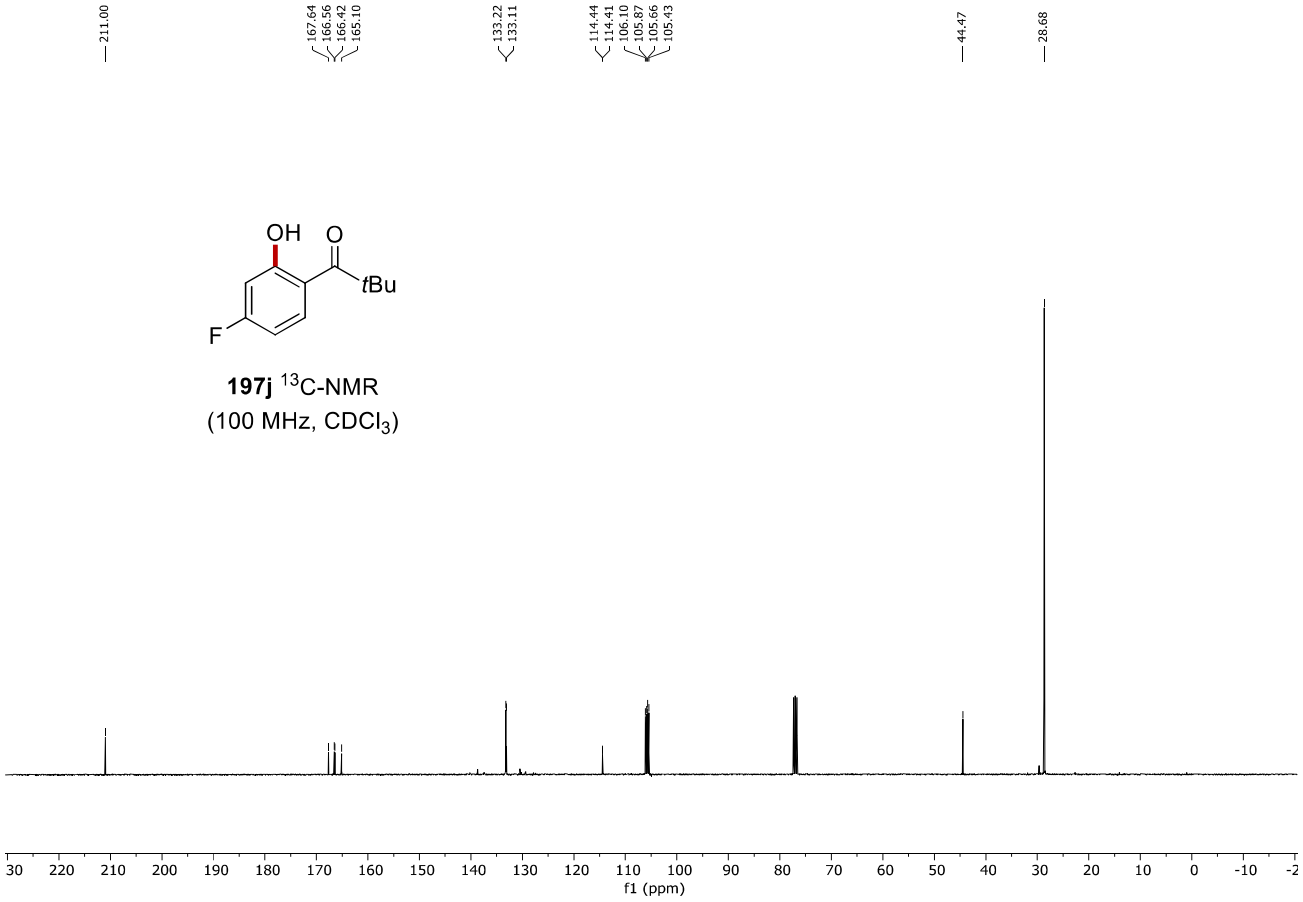

197j ^{13}C-NMR
(100 MHz, $CDCl_3$)

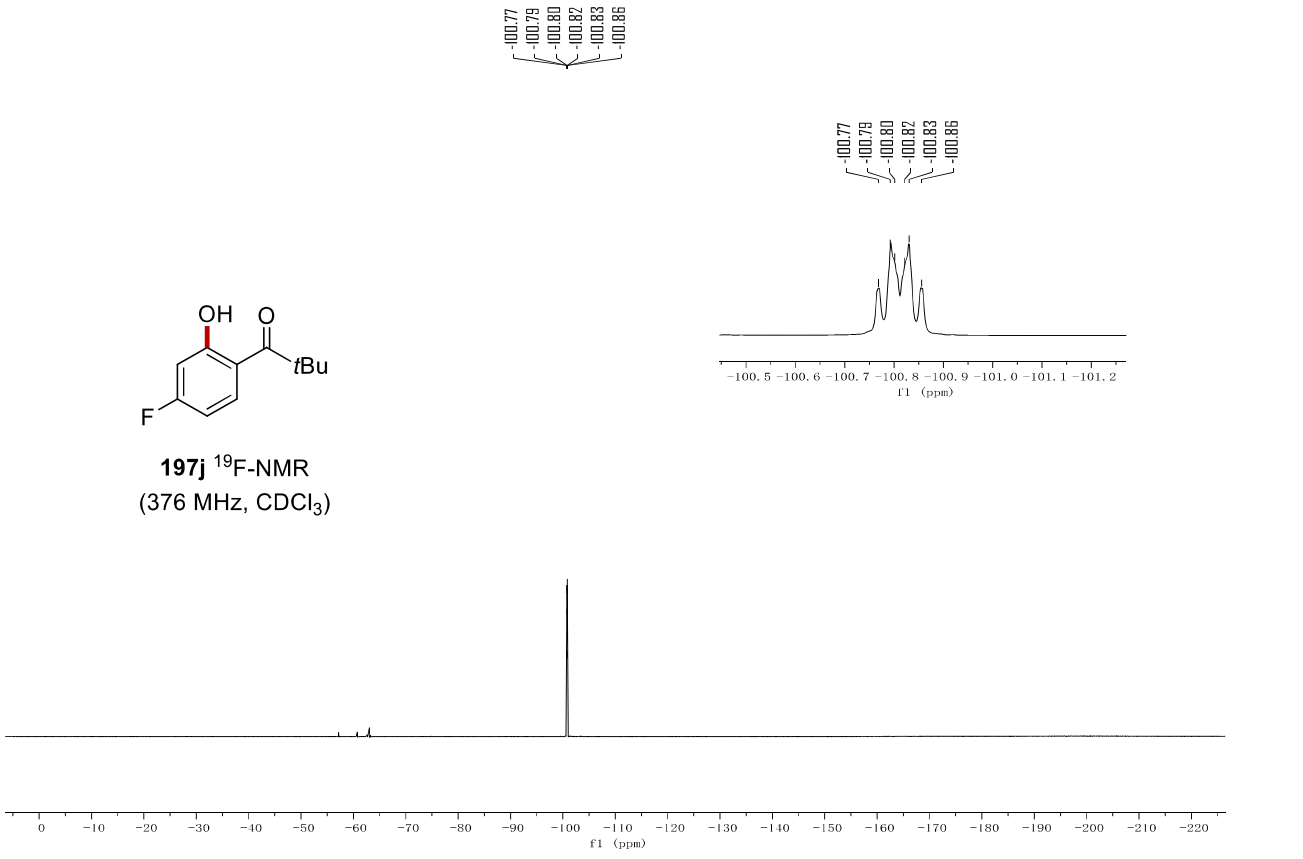

197j ^{19}F-NMR
(376 MHz, $CDCl_3$)

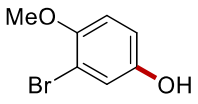

109a ^{1}H-NMR
(600 MHz, $CDCl_3$)

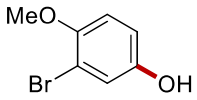

109a ^{13}C-NMR
(150 MHz, $CDCl_3$)

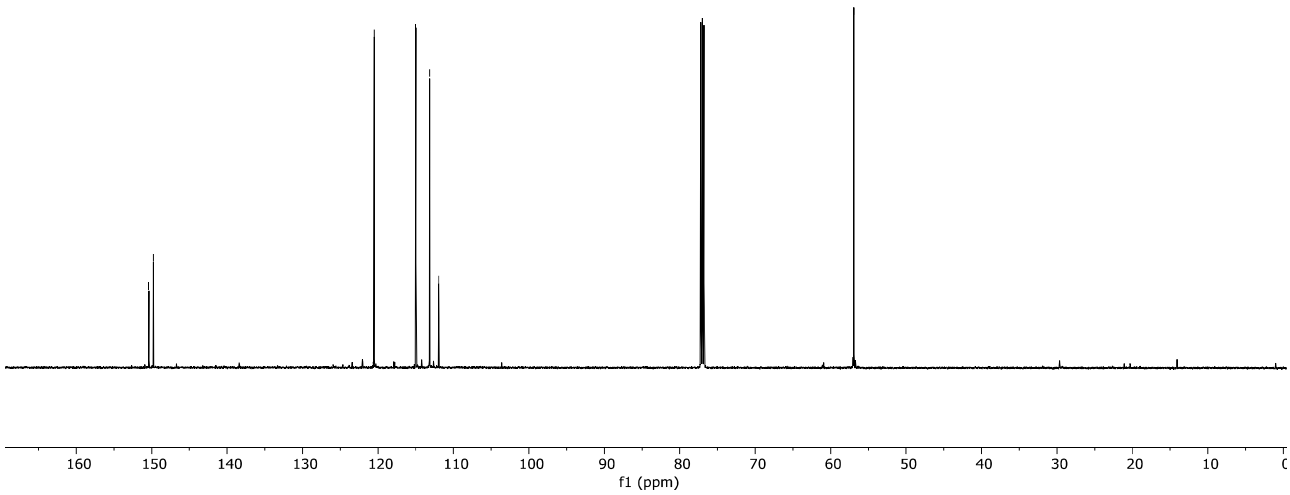

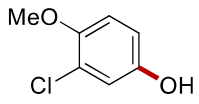

109b ^{1}H-NMR
(600 MHz, $CDCl_3$)

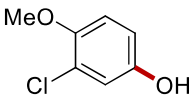

109b ^{13}C-NMR
(150 MHz, $CDCl_3$)

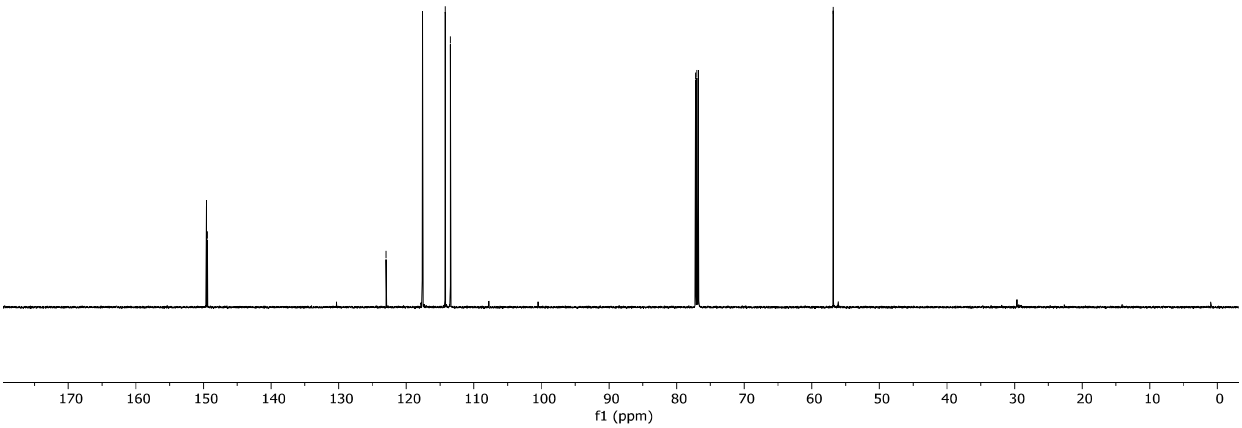

7.4 Rhoda-Electrocatalyzed Bimetallic C–H Oxygenation by Weak *O*-Coordination

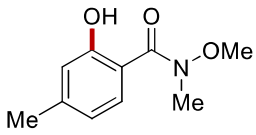

106b ^{1}H-NMR
(300 MHz, $CDCl_3$)

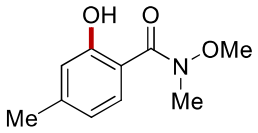

106b ^{13}C-NMR
(100 MHz, $CDCl_3$)

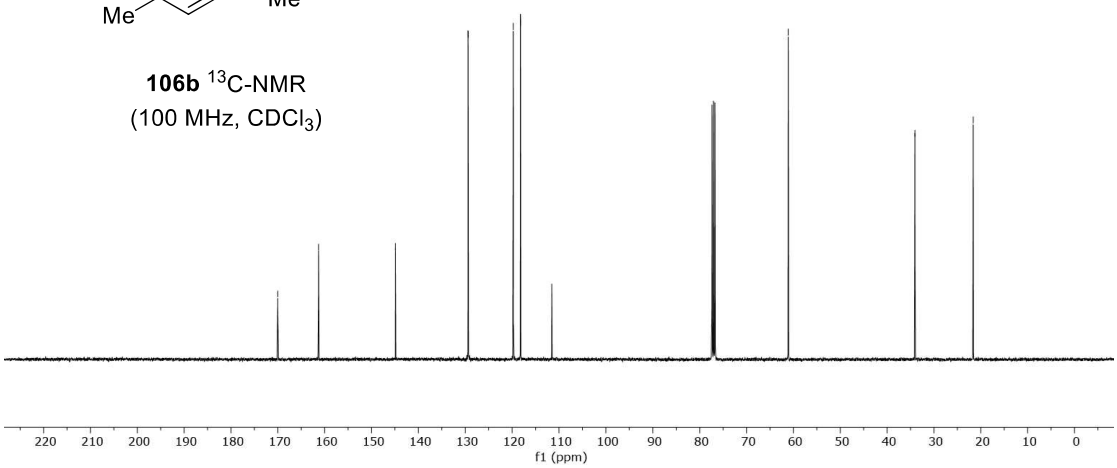

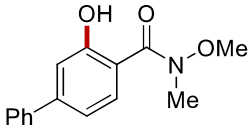

106t ^{1}H-NMR
(300 MHz, $CDCl_3$)

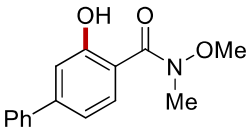

106t ^{13}C-NMR
(100 MHz, $CDCl_3$)

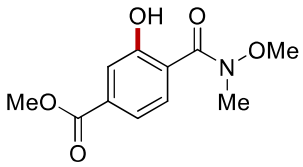

106u ^{1}H-NMR
(300 MHz, $CDCl_3$)

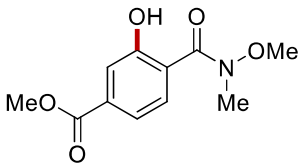

106u ^{13}C-NMR
(100 MHz, $CDCl_3$)

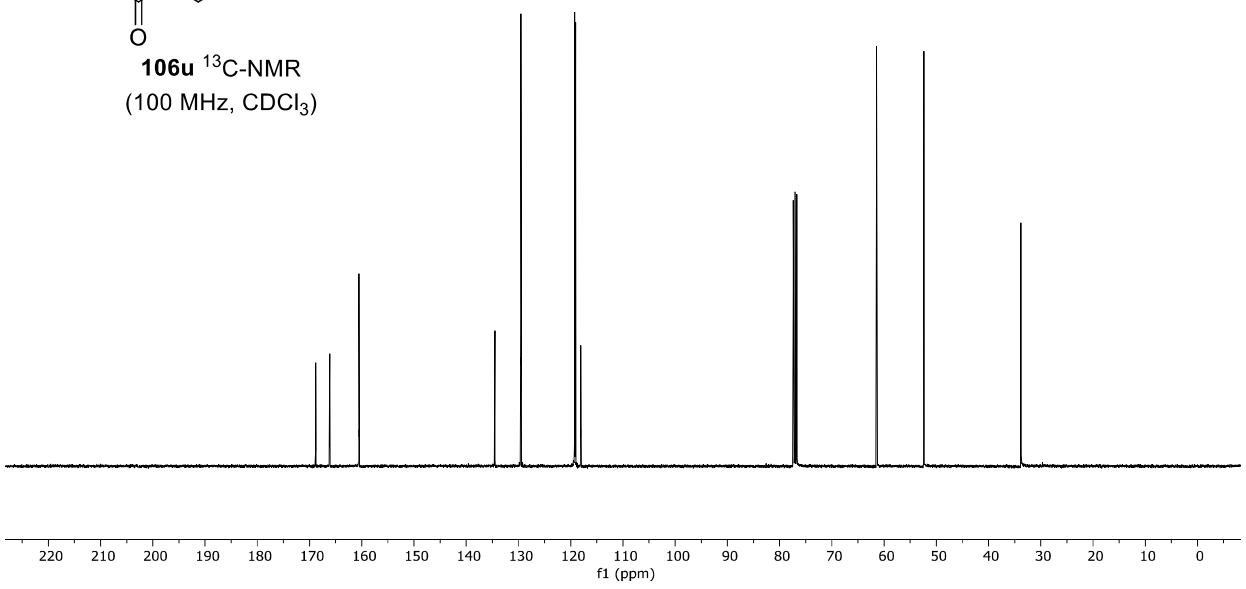

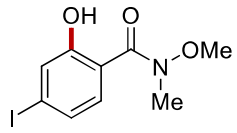

106o ^{1}H-NMR
(300 MHz, $CDCl_3$)

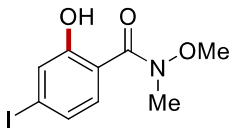

106o ^{13}C-NMR
(100 MHz, $CDCl_3$)

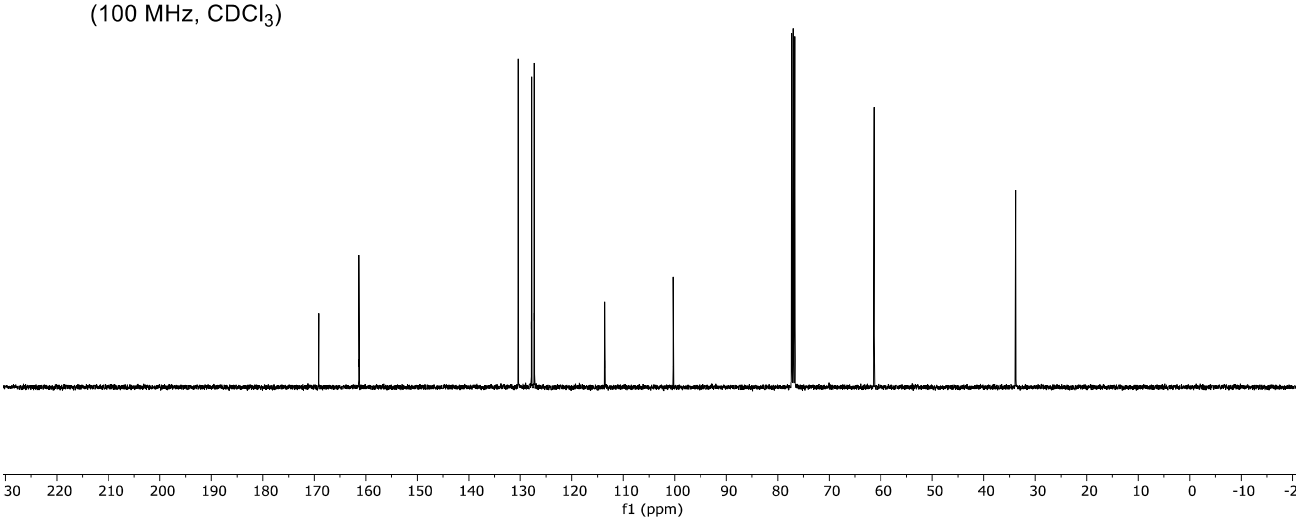

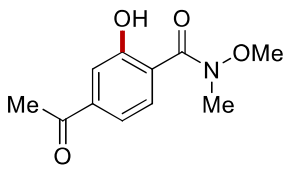

106q ^{1}H-NMR
(300 MHz, $CDCl_3$)

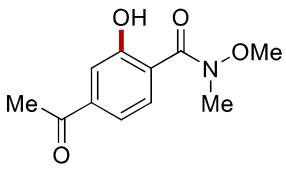

106q ^{13}C-NMR
(100 MHz, $CDCl_3$)

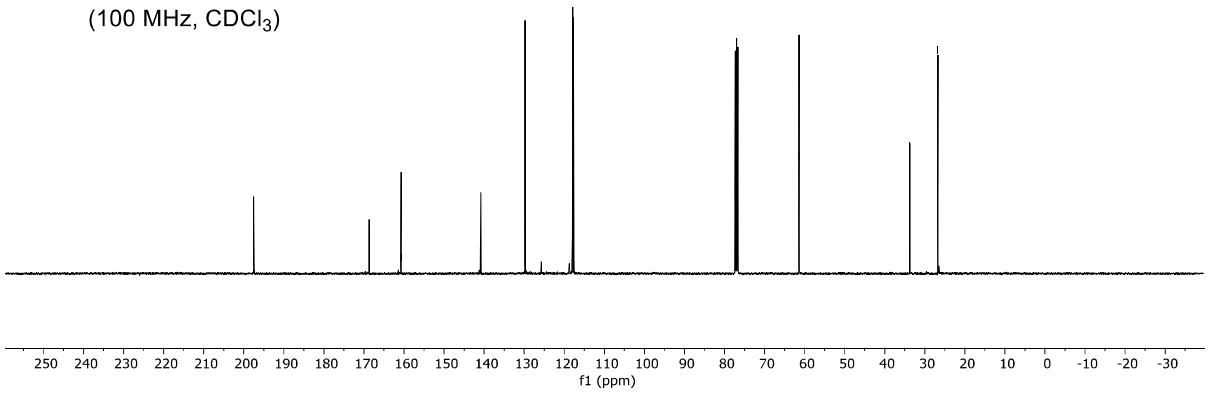

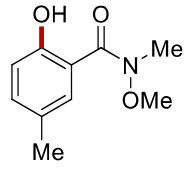

106j ^{1}H-NMR
(400 MHz, $CDCl_3$)

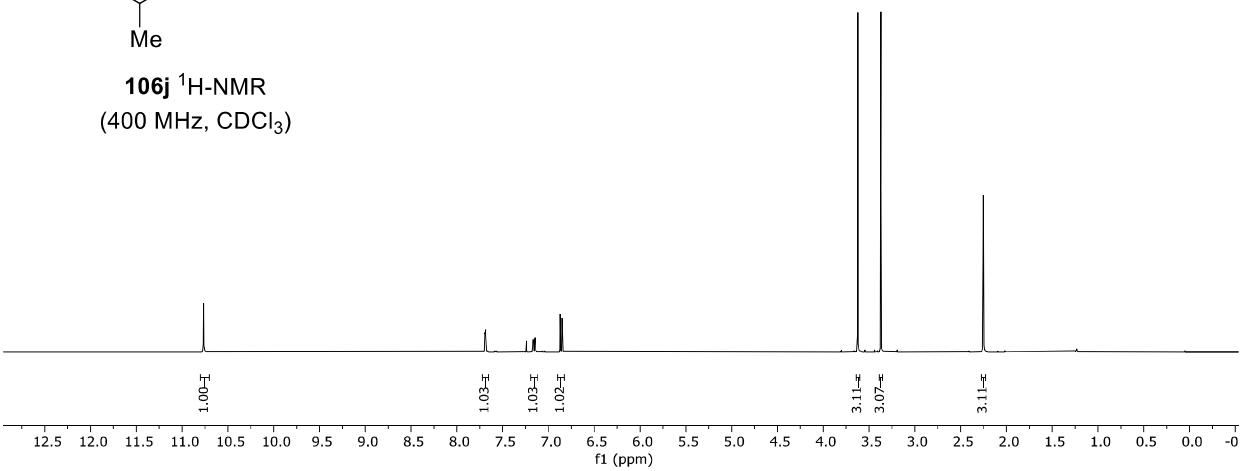

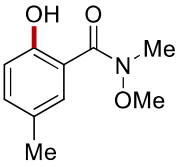

106j ^{13}C-NMR
(100 MHz, $CDCl_3$)

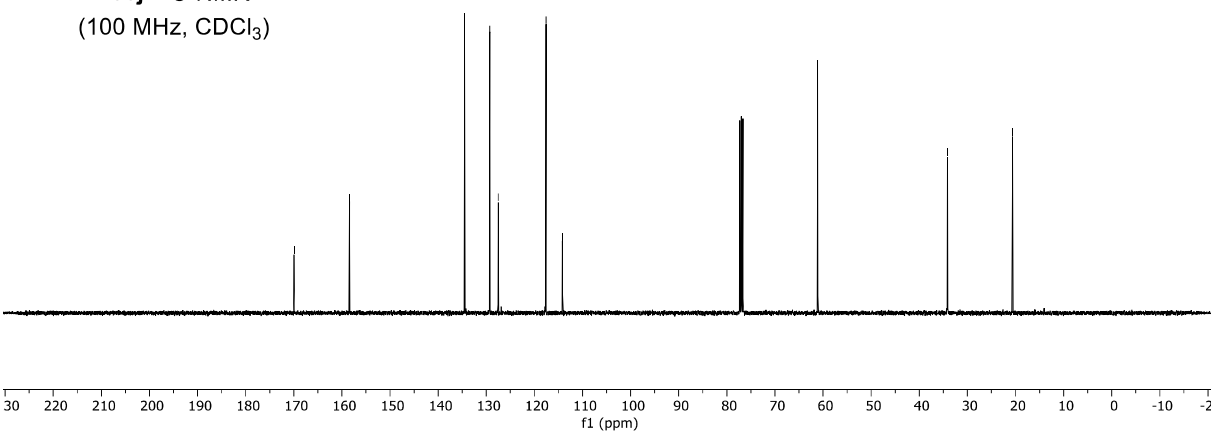

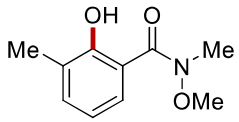

106j' ^{1}H-NMR
(400 MHz, $CDCl_3$)

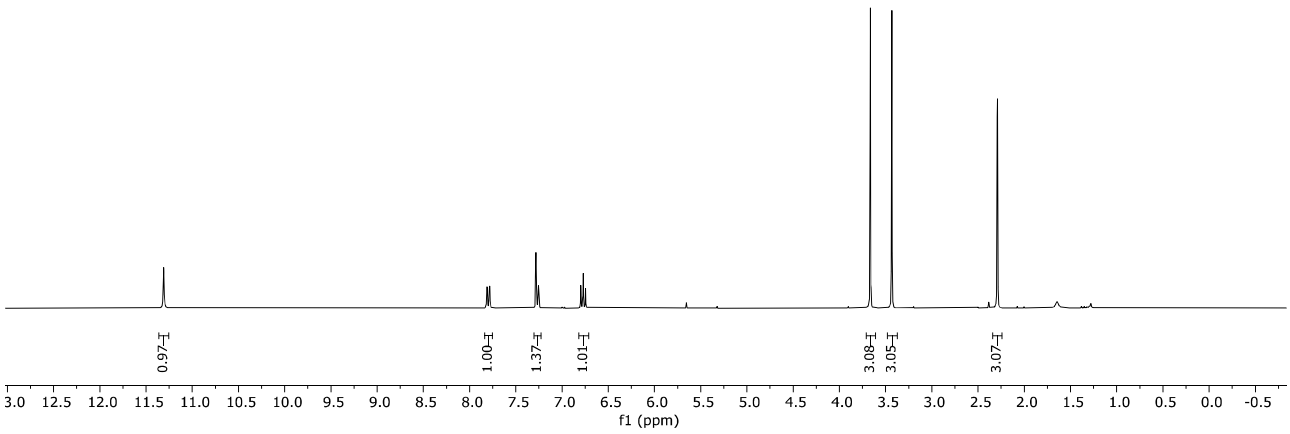

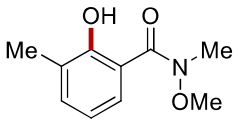

106j' ^{13}C-NMR
(100 MHz, $CDCl_3$)

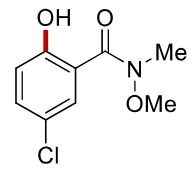

106m ^{1}H-NMR
(400 MHz, $CDCl_3$)

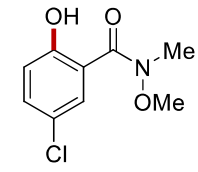

106m ^{13}H-NMR
(100 MHz, $CDCl_3$)

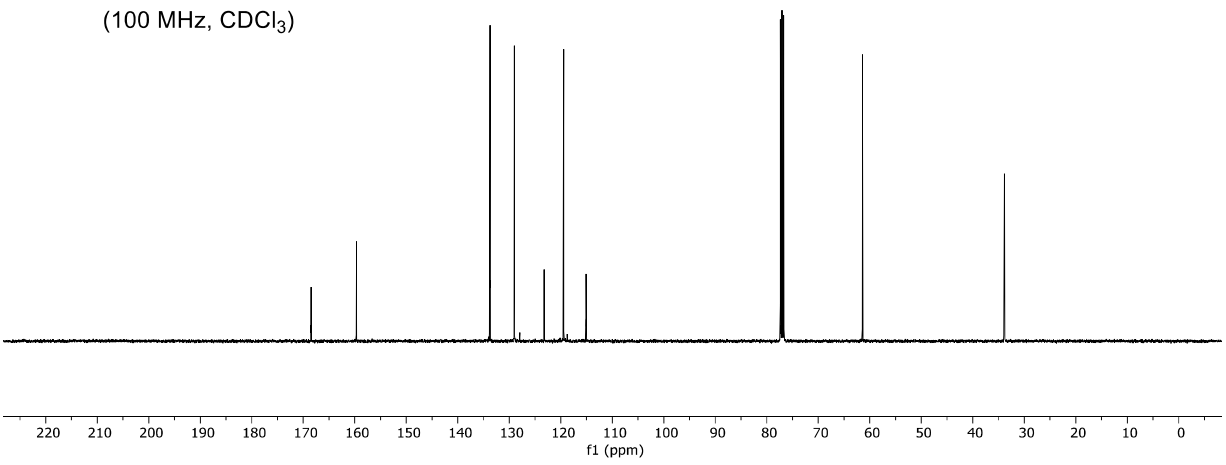

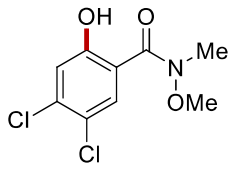

106f ^{1}H-NMR
(300 MHz, $CDCl_3$)

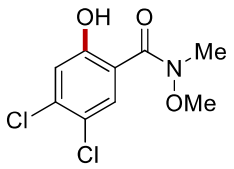

106f ^{13}C-NMR
(100 MHz, $CDCl_3$)

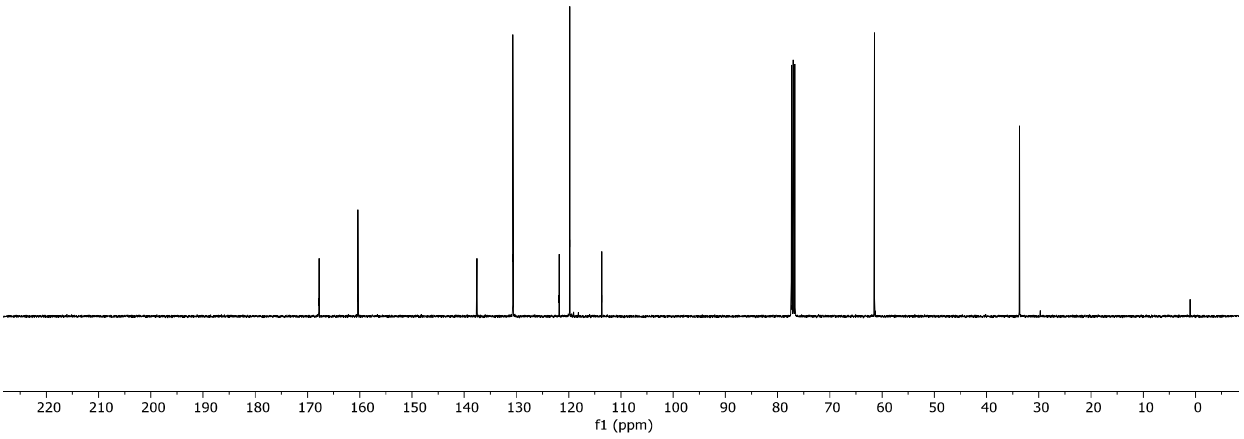

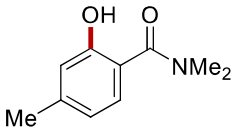

104b ^{1}H-NMR
(300 MHz, $CDCl_3$)

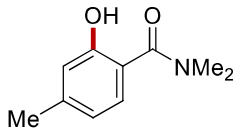

104b ^{13}C-NMR
(100 MHz, $CDCl_3$)

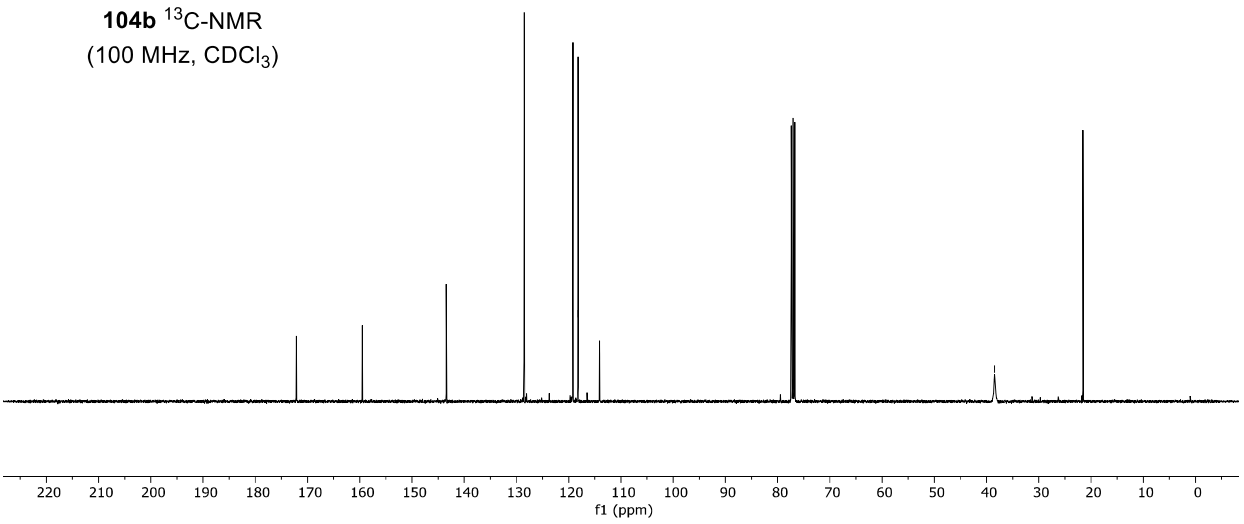

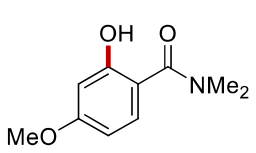

104h ^{1}H-NMR
(400 MHz, $CDCl_3$)

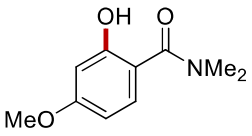

104h ^{13}C-NMR
(100 MHz, $CDCl_3$)

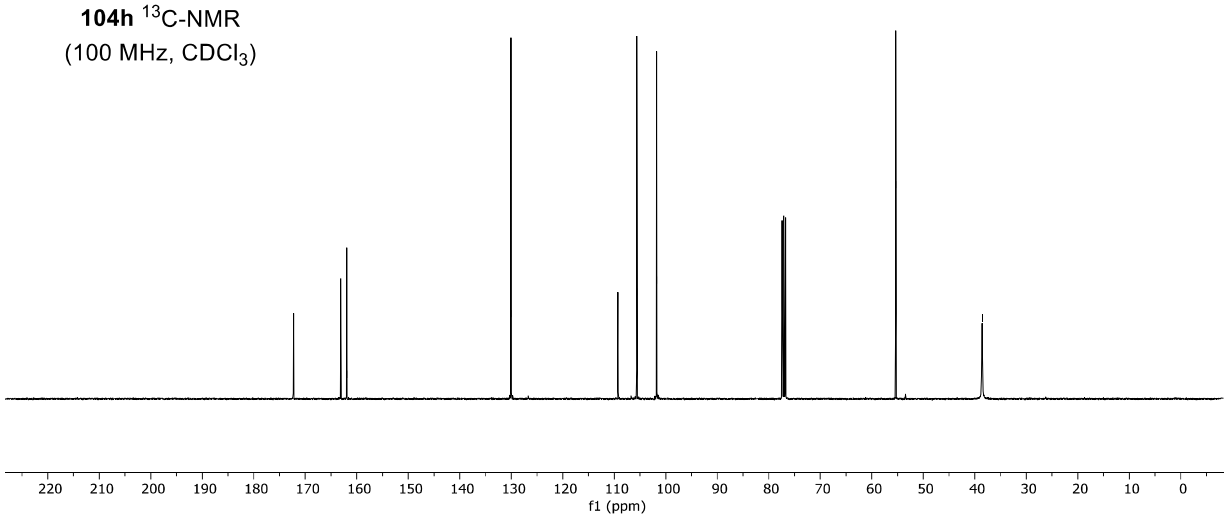

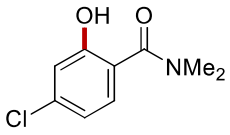

104i ^{1}H-NMR
(400 MHz, $CDCl_3$)

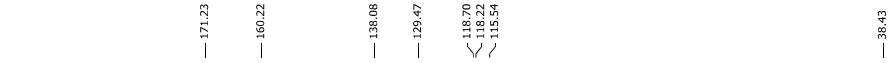

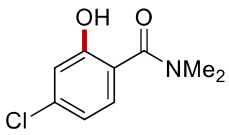

104i ^{13}C-NMR
(100 MHz, $CDCl_3$)

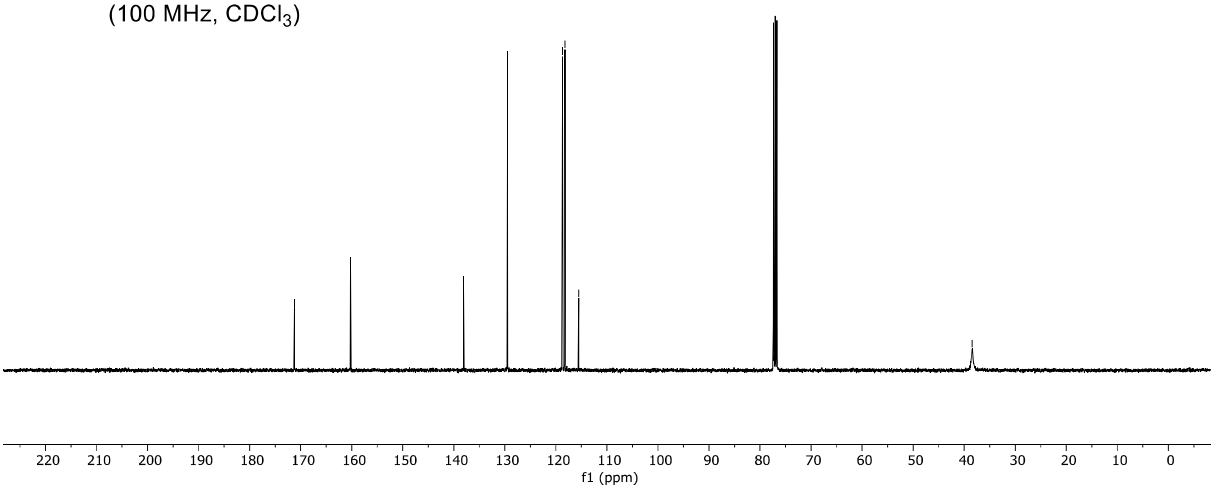

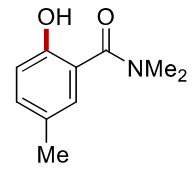

104k ^{1}H-NMR
(300 MHz, $CDCl_3$)

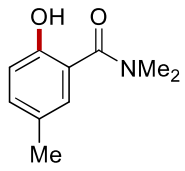

104k ^{13}C-NMR
(100 MHz, $CDCl_3$)

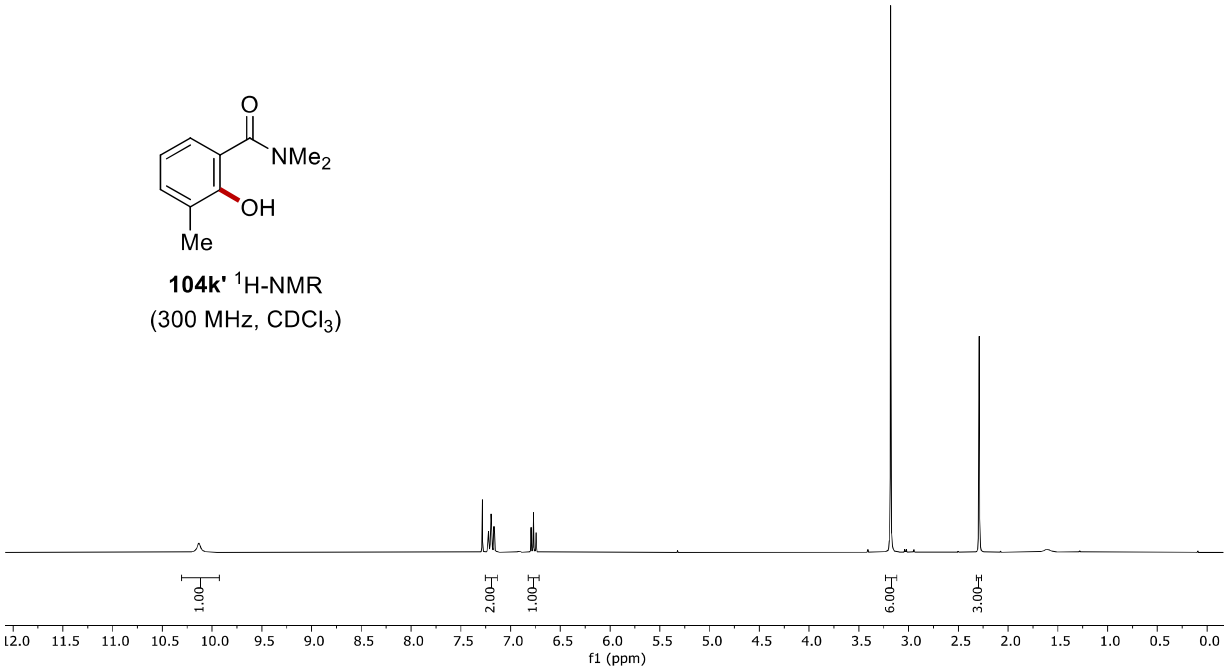

104k' ^{1}H-NMR
(300 MHz, $CDCl_3$)

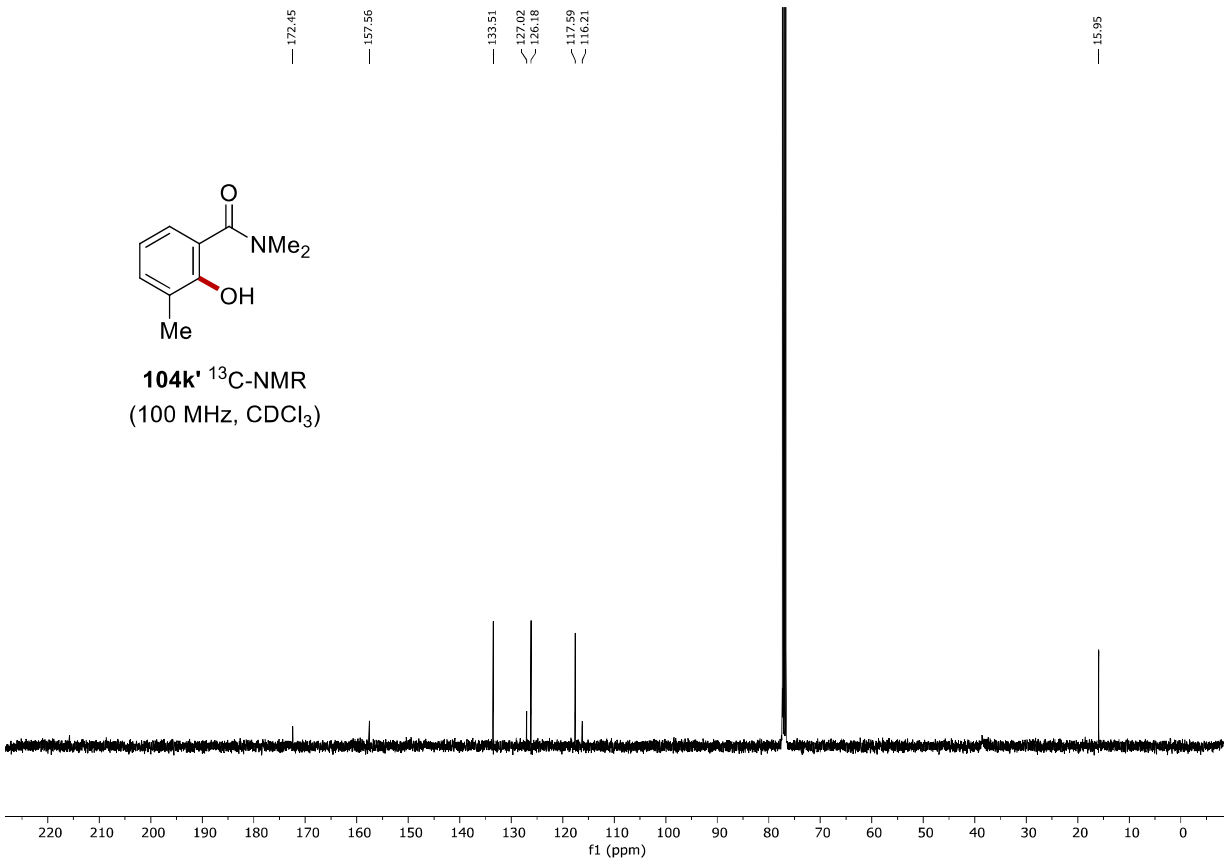

104k' ^{13}C-NMR
(100 MHz, $CDCl_3$)

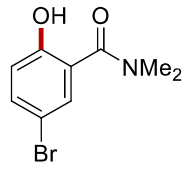

104n ^{1}H-NMR
(400 MHz, $CDCl_3$)

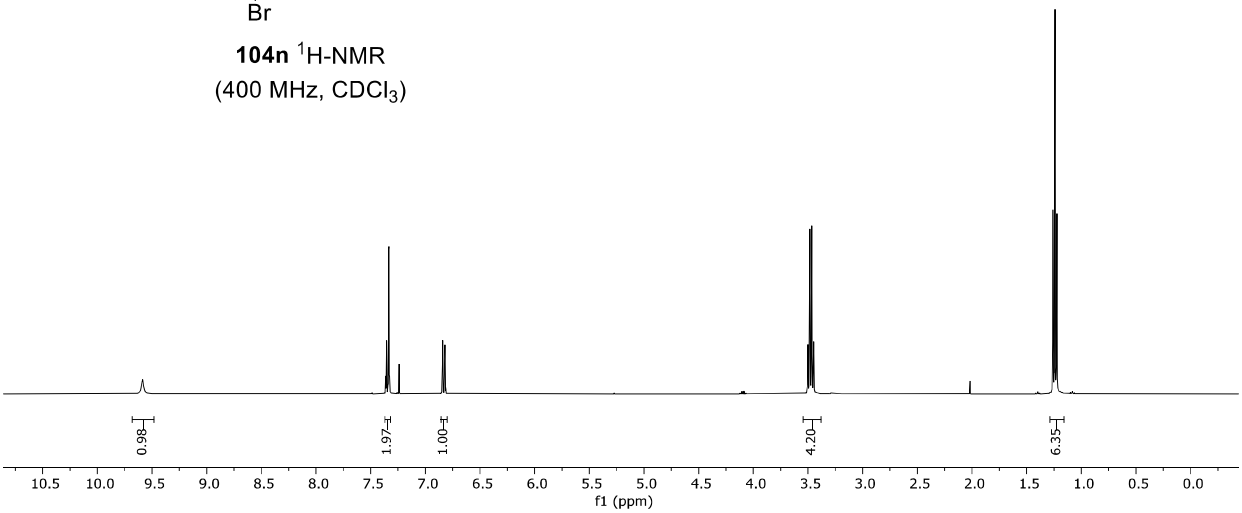

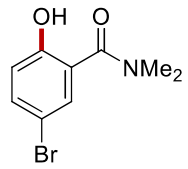

104n ^{13}C-NMR
(100 MHz, $CDCl_3$)

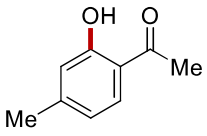

197n ^{1}H-NMR
(300 MHz, $CDCl_3$)

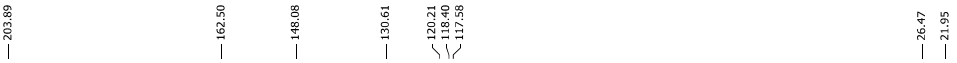

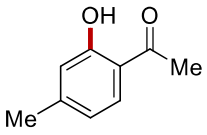

197n ^{13}C-NMR
(100 MHz, $CDCl_3$)

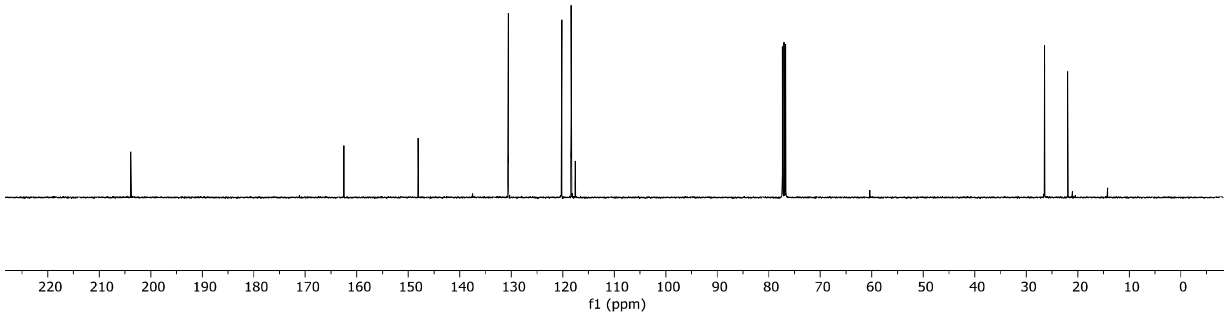

7.5 Manganaelectro-Catalyzed Azine C–H Arylations and C–H Alkylations by Assistance of Weakly-Coordinating Amides

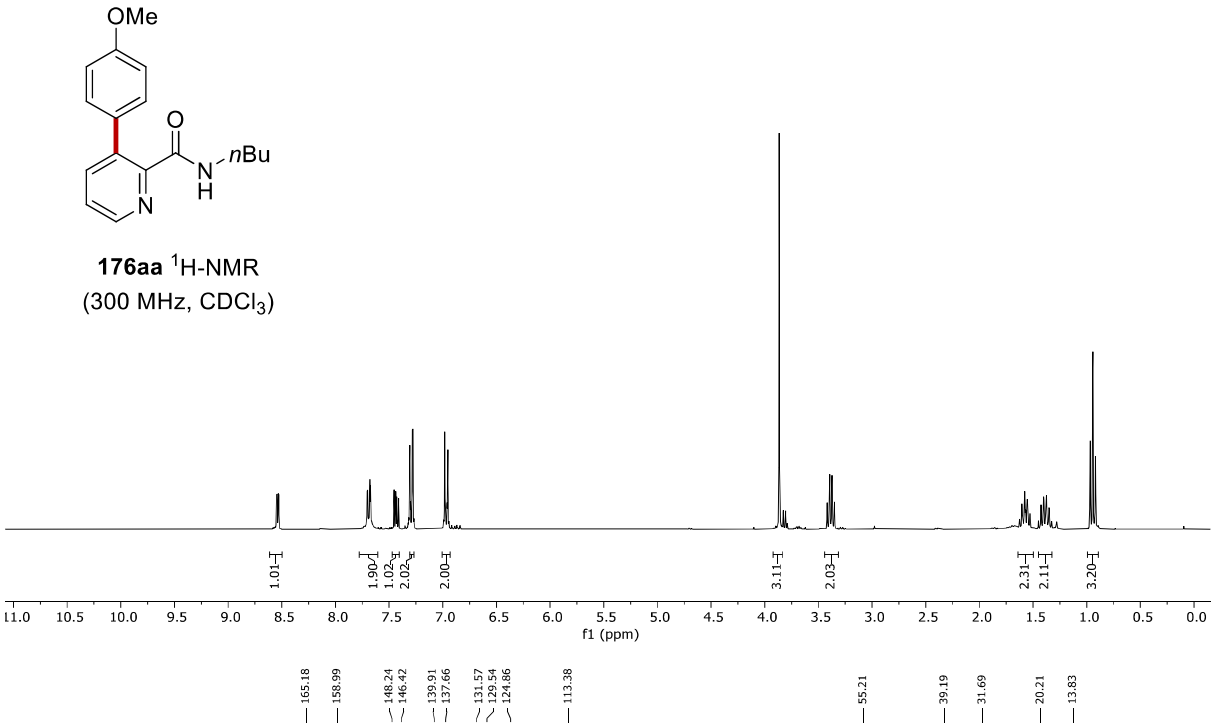

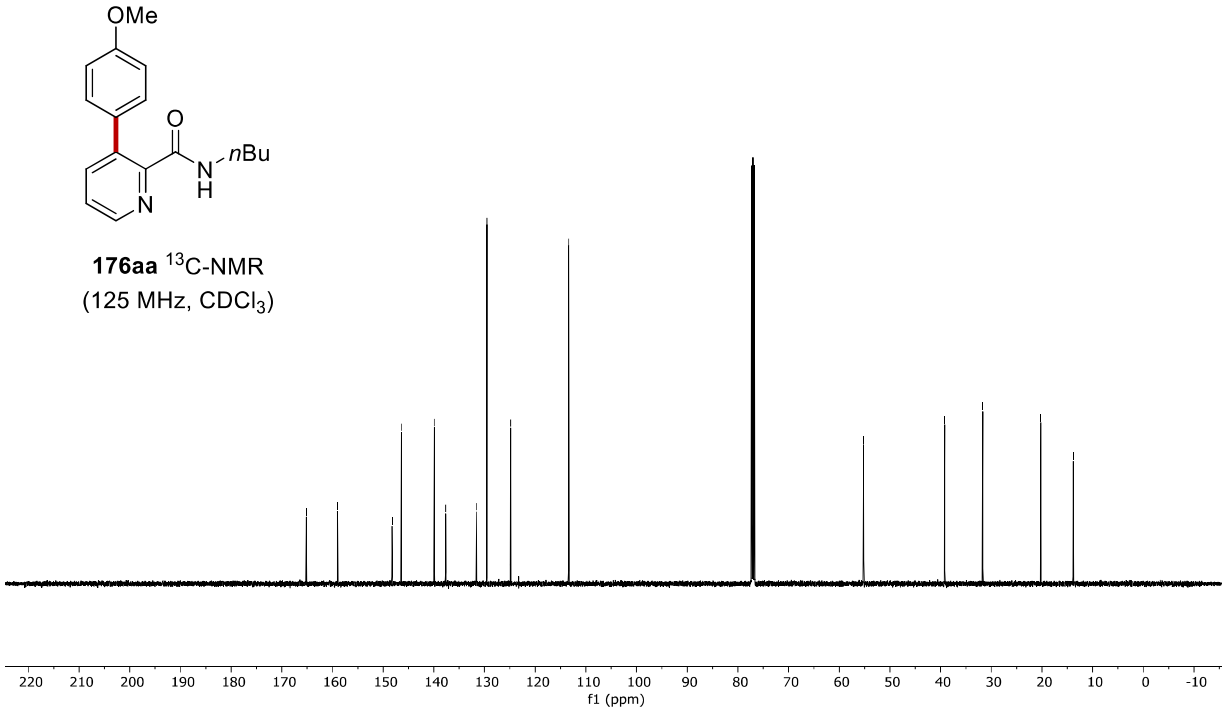

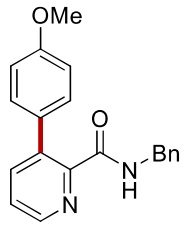

176ba ^{1}H-NMR
(300 MHz, $CDCl_3$)

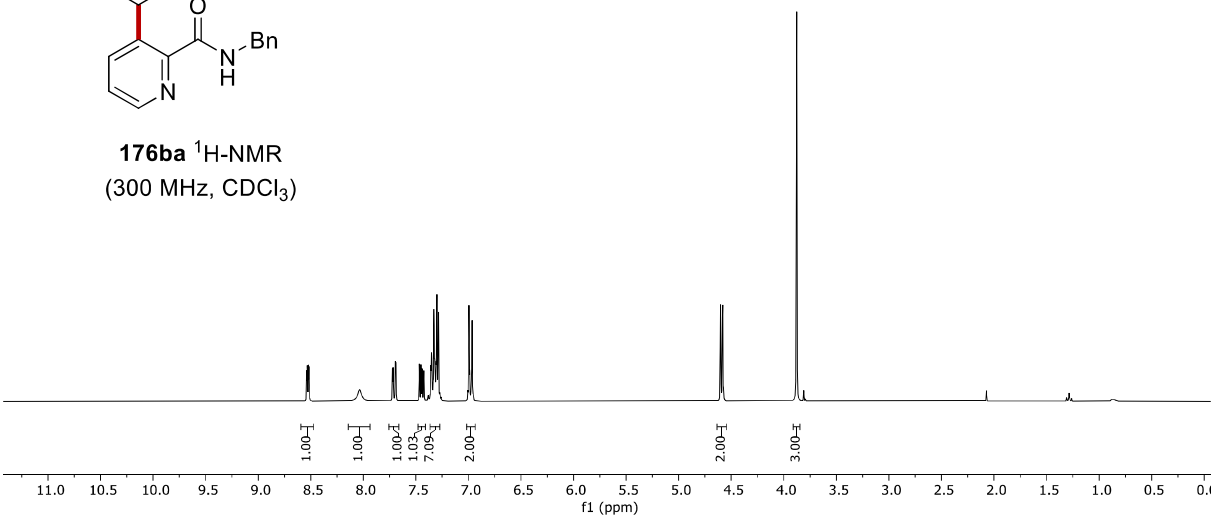

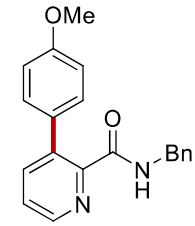

176ba ^{13}C-NMR
(100 MHz, $CDCl_3$)

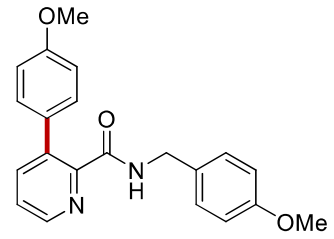

176da ^{1}H-NMR
(300 MHz, $CDCl_3$)

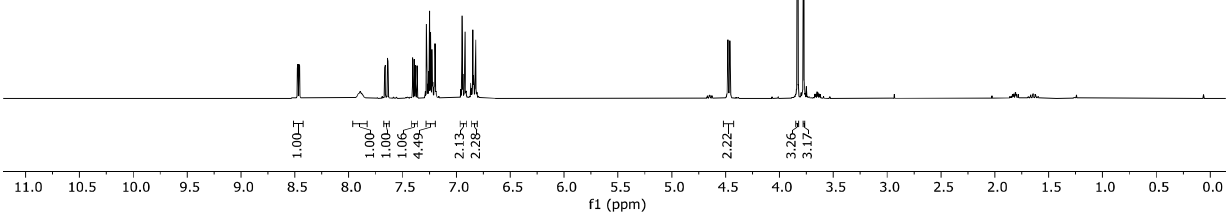

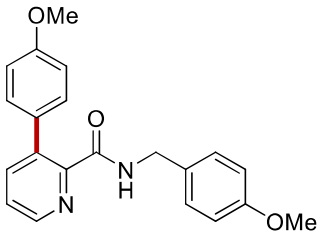

176da ^{13}C-NMR
(125 MHz, $CDCl_3$)

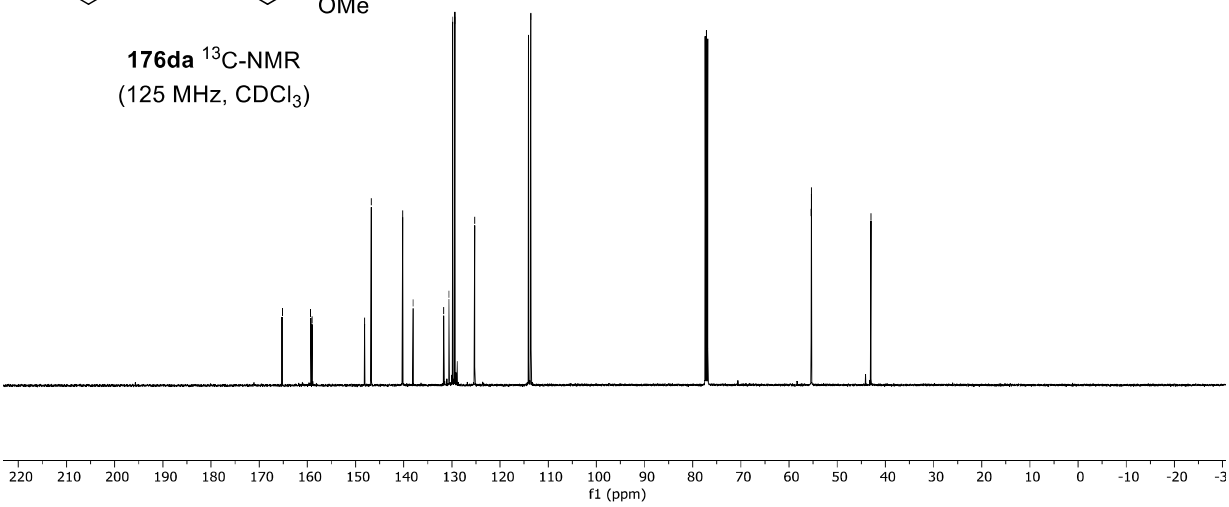

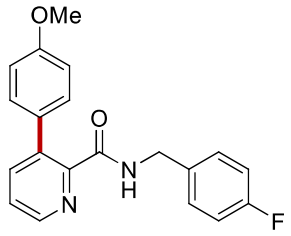

176ea ^{1}H-NMR
(300 MHz, $CDCl_3$)

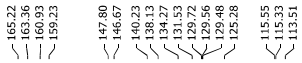

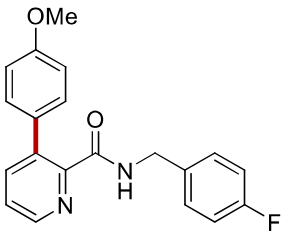

176ea ^{13}C-NMR
(100 MHz, $CDCl_3$)

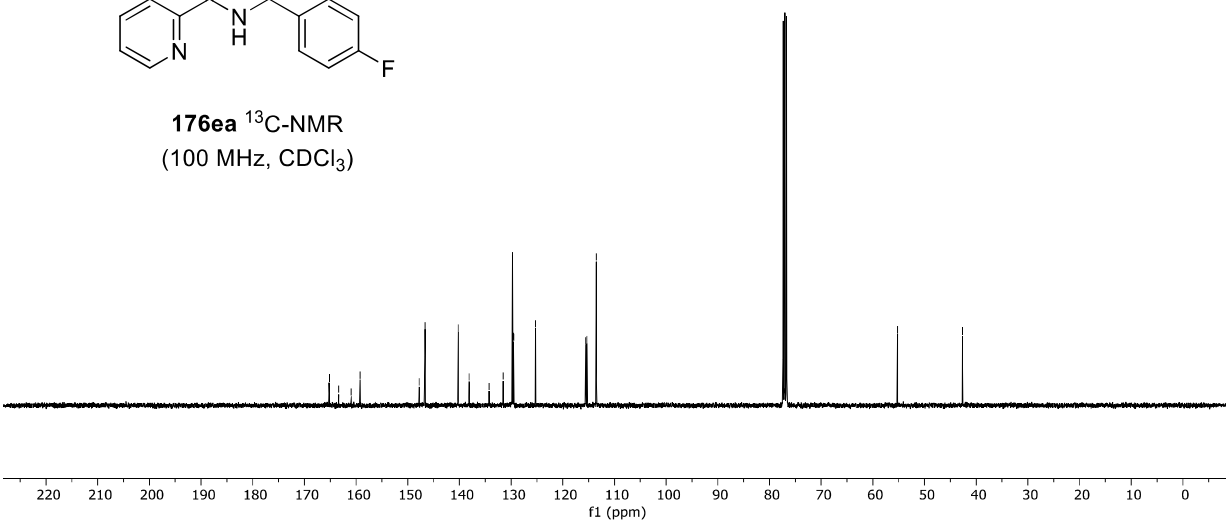

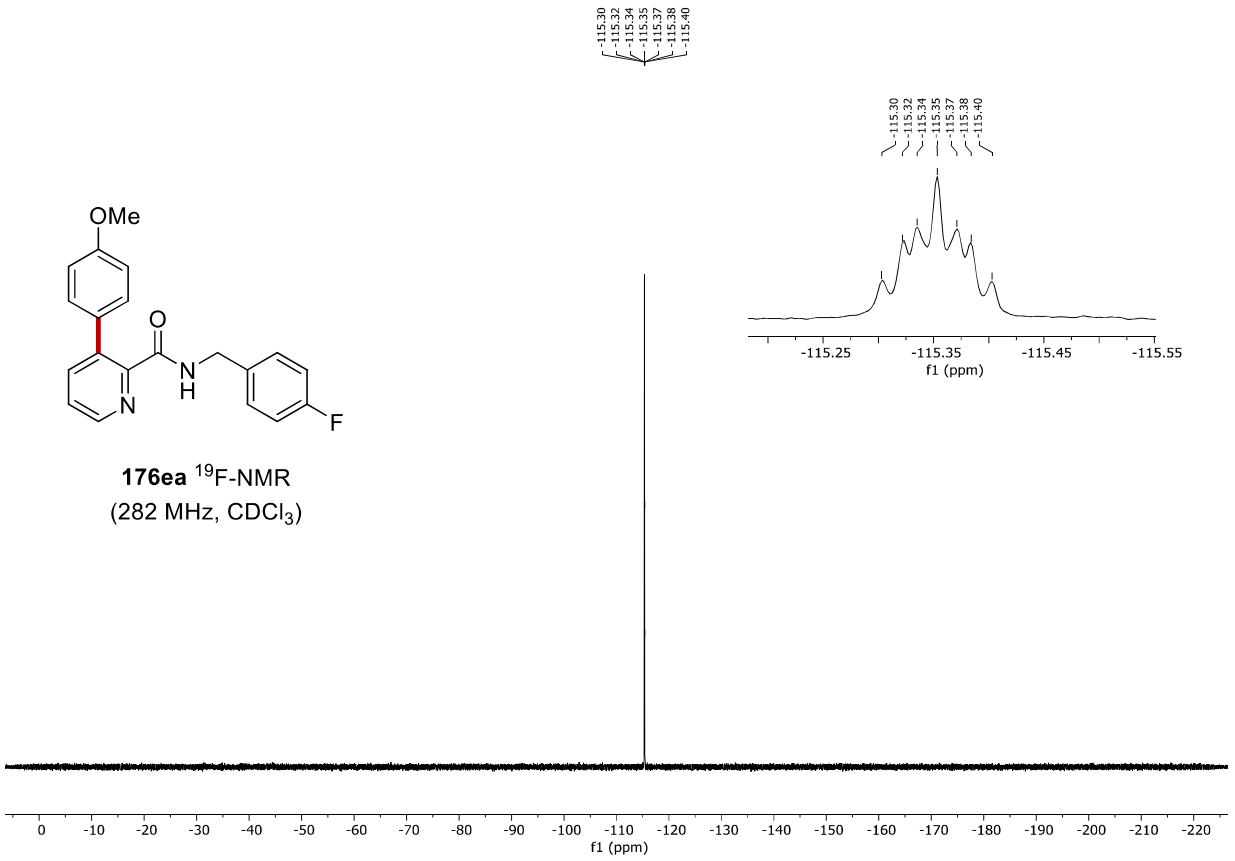

176ea ^{19}F-NMR
(282 MHz, $CDCl_3$)

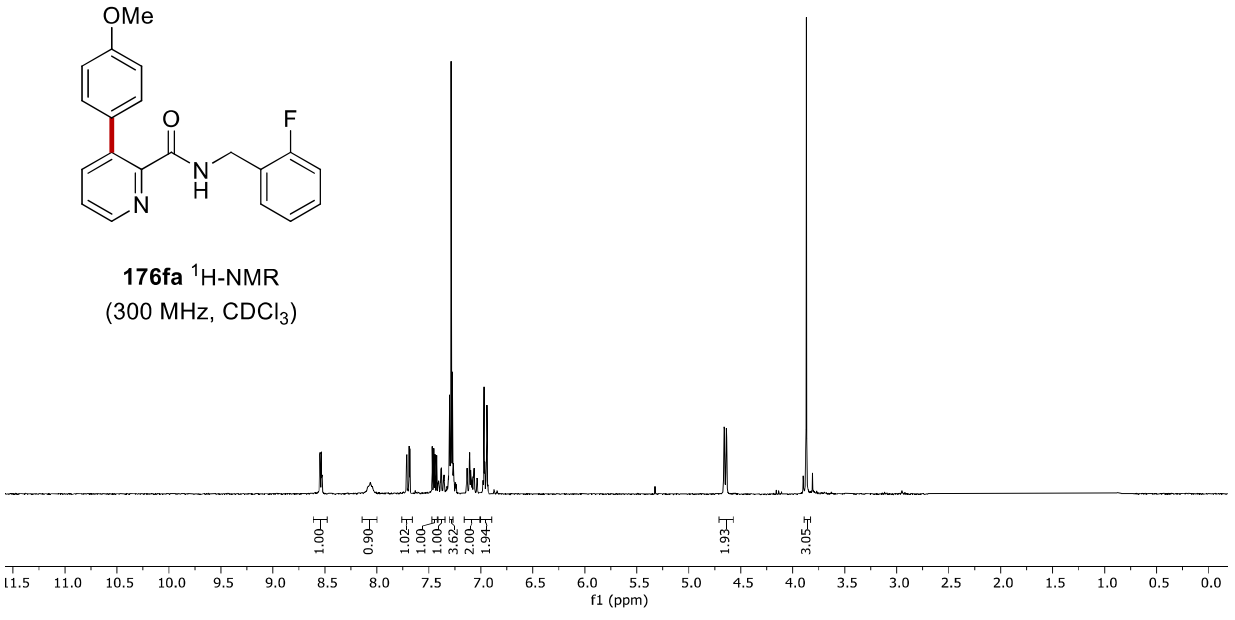

176fa ^{1}H-NMR
(300 MHz, $CDCl_3$)

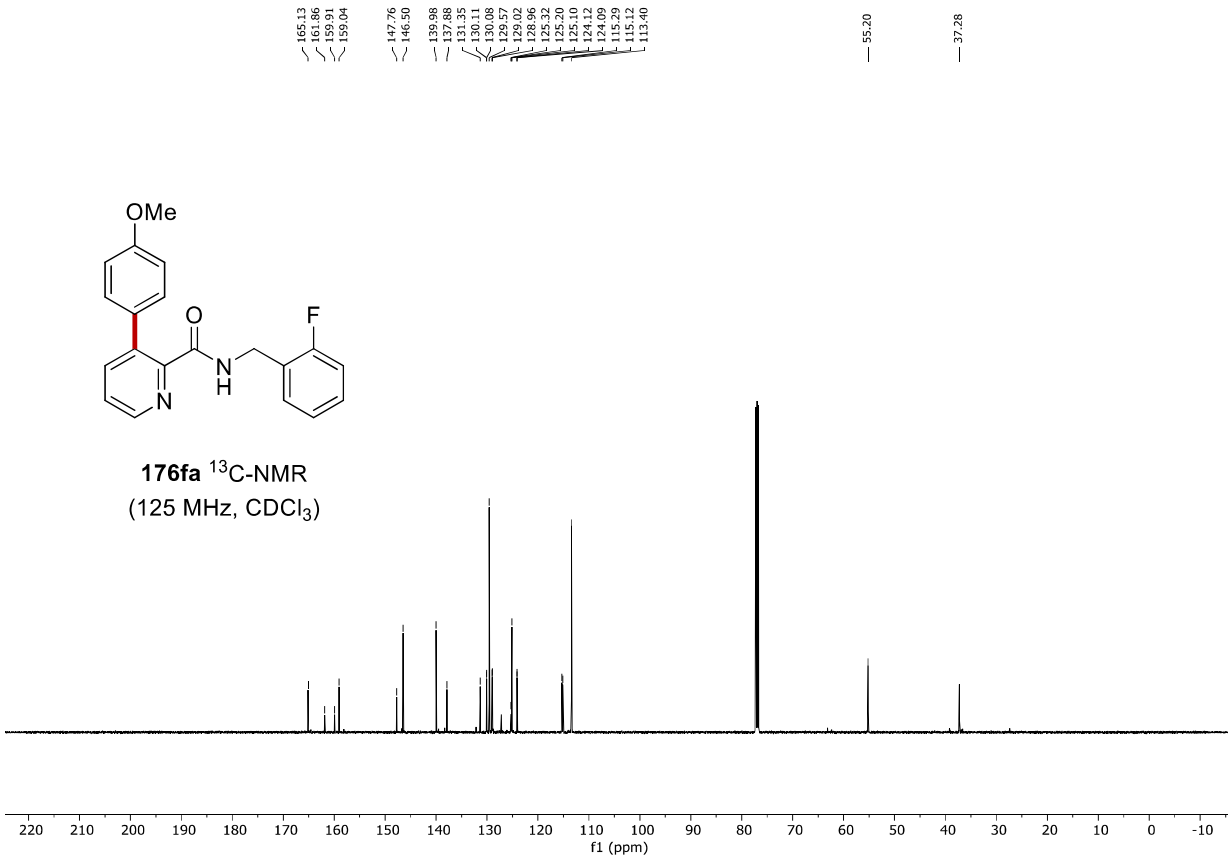
165.13
161.86
159.91
159.04
147.76
146.50
139.98
137.88
131.35
130.11
130.08
129.57
129.02
128.96
125.32
125.20
125.10
124.12
124.09
115.29
115.12
113.40
55.20
37.28
OMe
O
F
N
H
N
176fa 13C-NMR
(125 MHz, CDCl3)
220 210 200 190 180 170 160 150 140 130 120 110 100 90 80 70 60 50 40 30 20 10 0 -10
f1 (ppm)

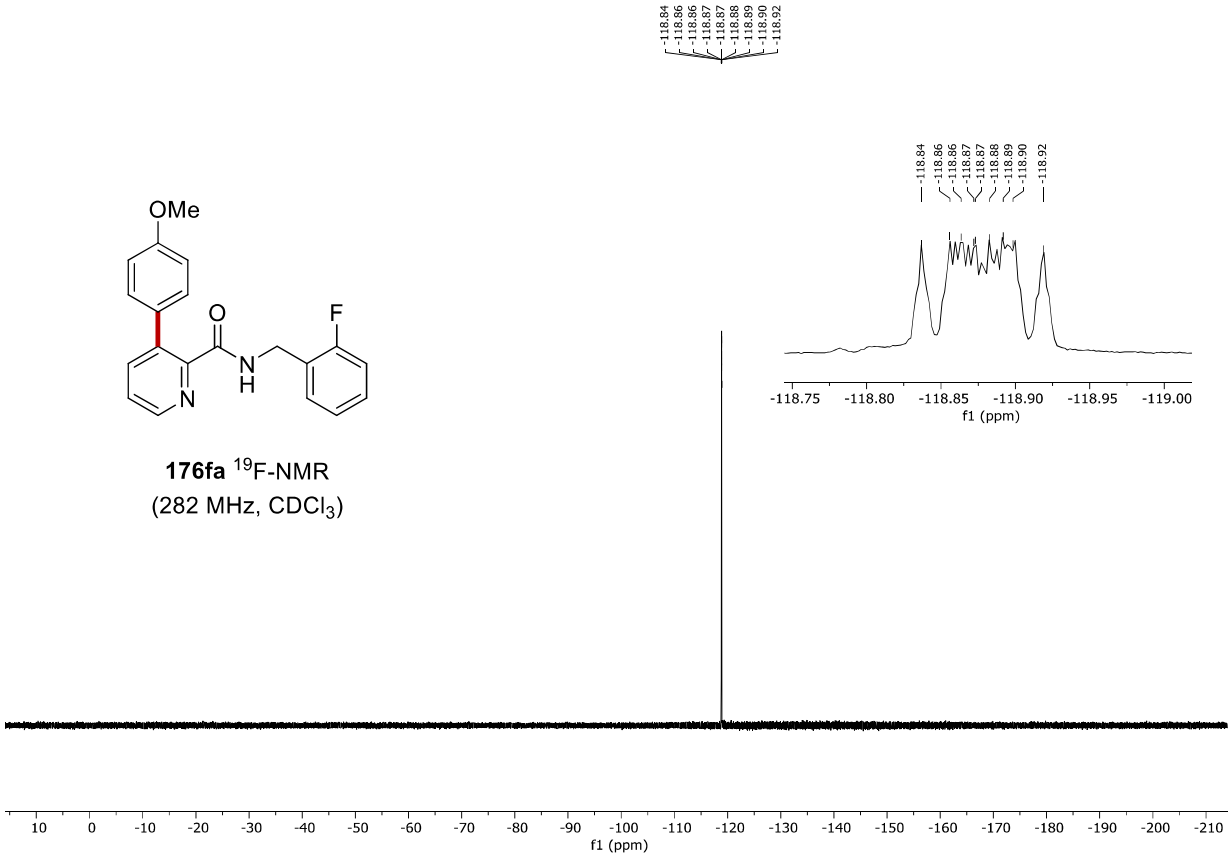
-118.84
-118.86
-118.86
-118.87
-118.87
-118.88
-118.89
-118.90
-118.92
OMe
O
F
N
H
N
176fa 19F-NMR
(282 MHz, CDCl3)
-118.75 -118.80 -118.85 -118.90 -118.95 -119.00
f1 (ppm)
10 0 -10 -20 -30 -40 -50 -60 -70 -80 -90 -100 -110 -120 -130 -140 -150 -160 -170 -180 -190 -200 -210
f1 (ppm)

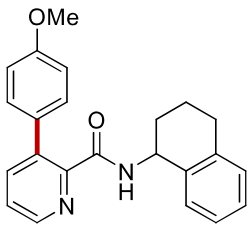

176ga ^{1}H-NMR
(400 MHz, $CDCl_3$)

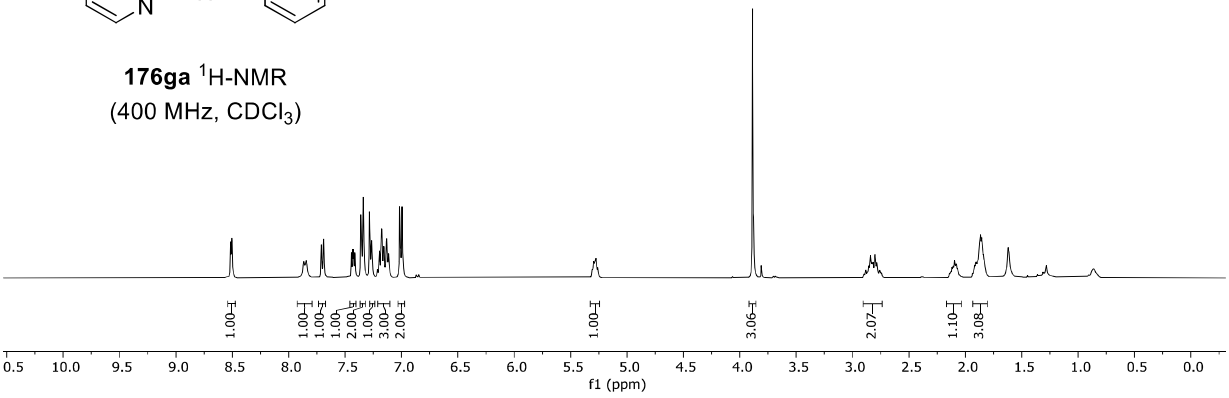

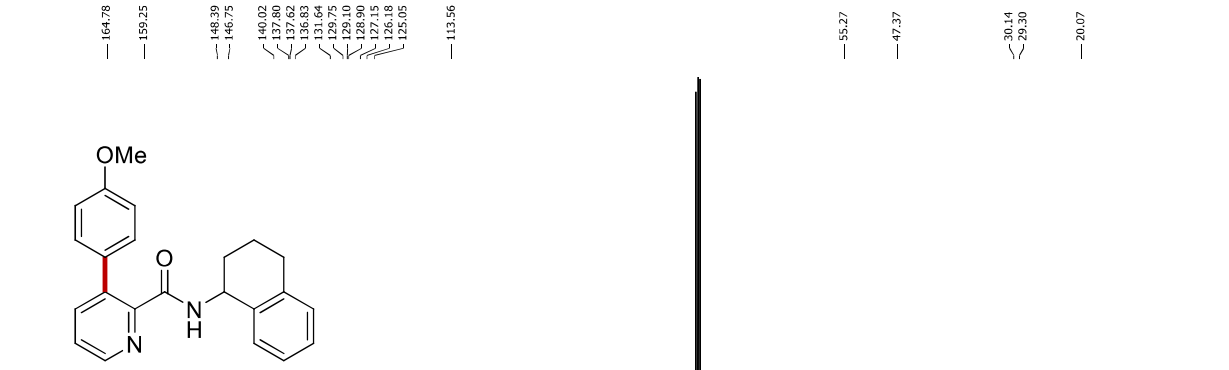

176ga ^{13}C-NMR
(100 MHz, $CDCl_3$)

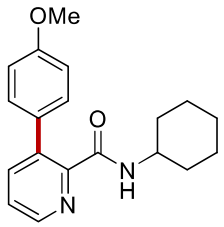

176ha ^{1}H-NMR
(300 MHz, $CDCl_3$)

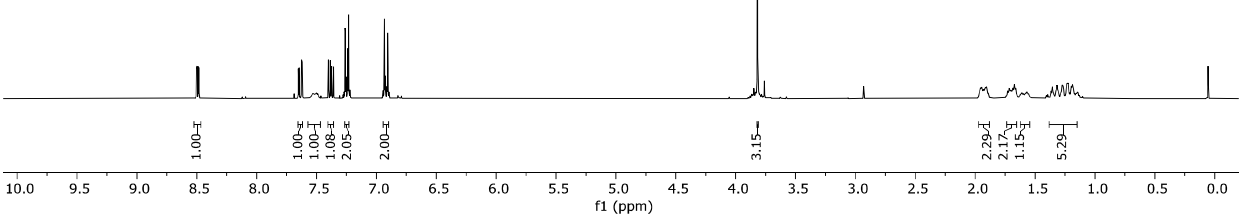

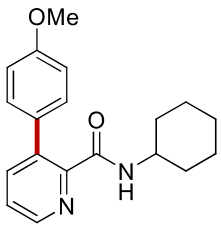

176ha ^{13}C-NMR
(125 MHz, $CDCl_3$)

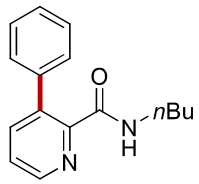

176ab ^{1}H-NMR
(400 MHz, $CDCl_3$)

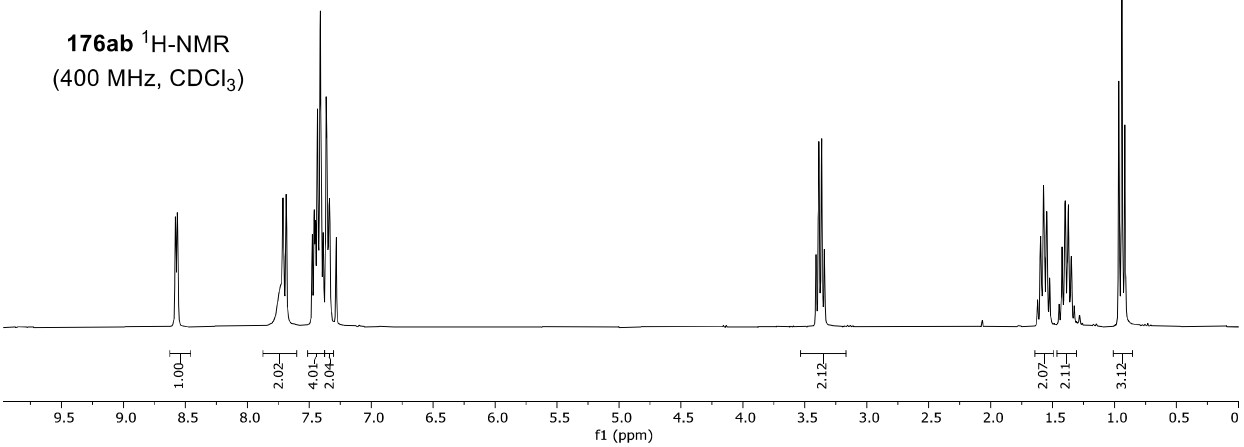

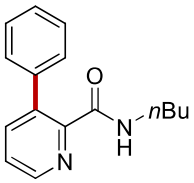

176ab ^{13}C-NMR
(100 MHz, $CDCl_3$)

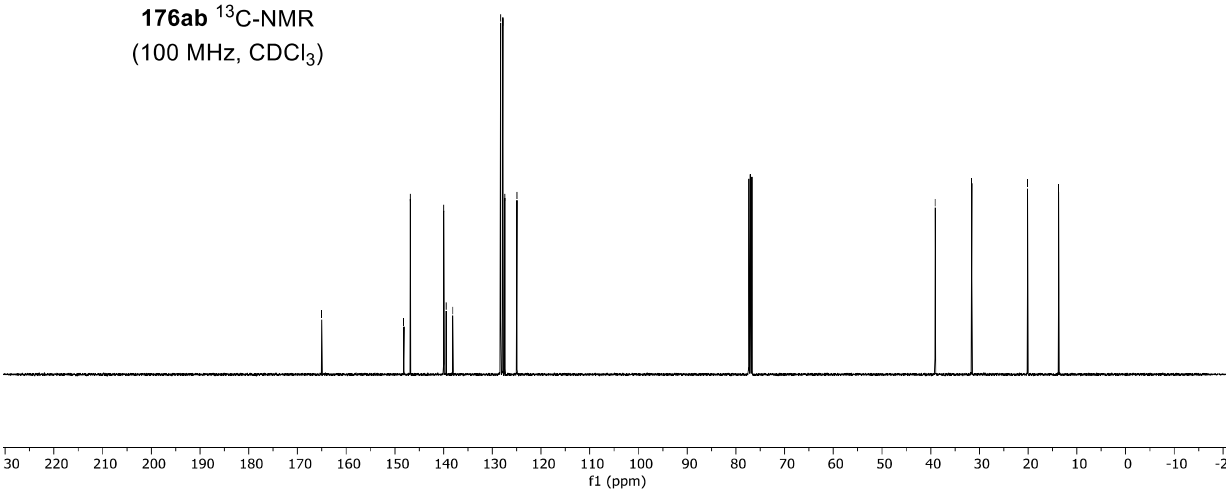

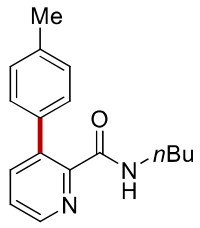

176ac ^{1}H-NMR
(400 MHz, $CDCl_3$)

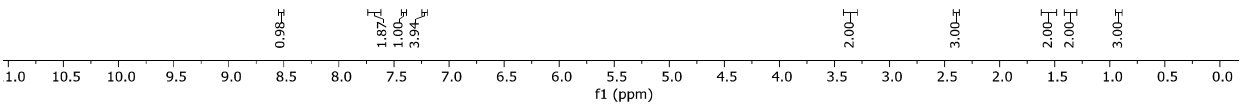

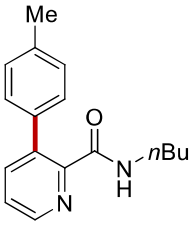

176ac ^{13}C-NMR
(100 MHz, $CDCl_3$)

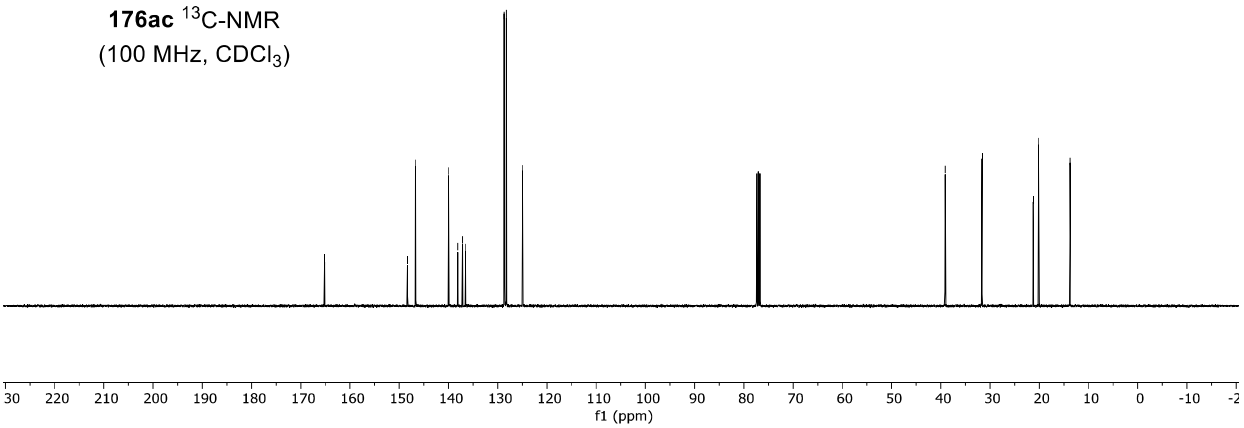

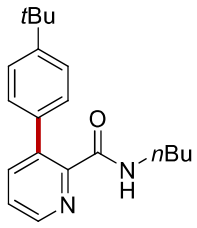

176ad ^{1}H-NMR
(400 MHz, $CDCl_3$)

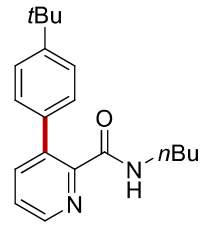

176ad ^{13}C-NMR
(100 MHz, $CDCl_3$)

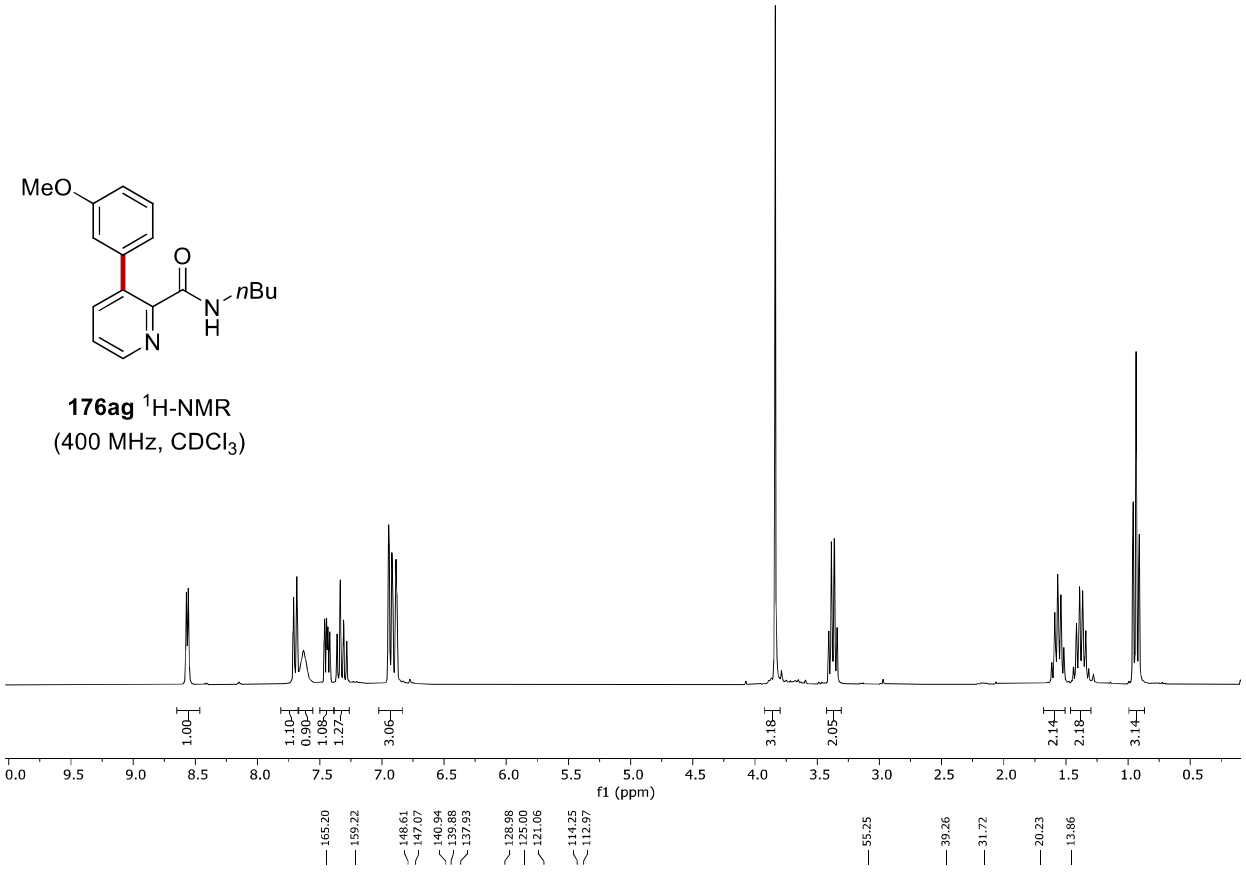
MeO
O
N
H
nBu
N
176ag 1H-NMR
(400 MHz, CDCl3)
1.00
1.10
0.90
1.08
1.27
3.06
3.18
2.05
2.14
2.18
3.14
f1 (ppm)
165.20
159.22
148.61
147.07
140.94
139.88
137.93
128.98
125.00
121.06
114.25
112.97
55.25
39.26
31.72
20.23
13.86

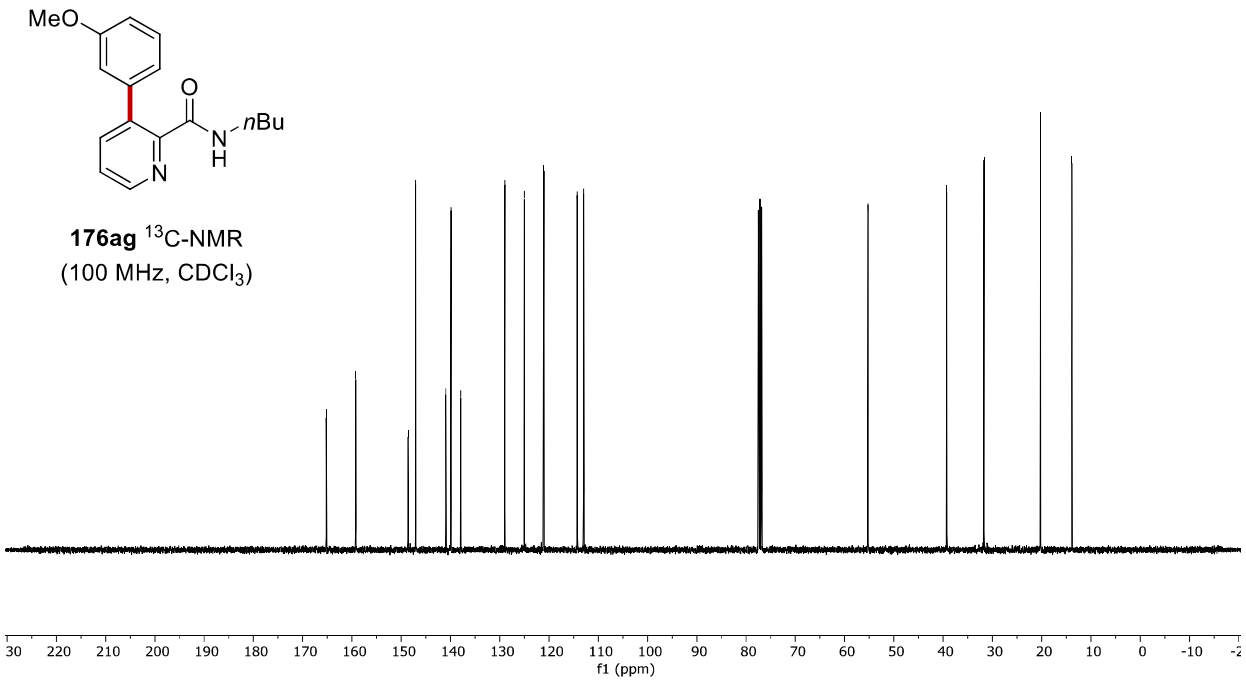
MeO
O
N
H
nBu
N
176ag 13C-NMR
(100 MHz, CDCl3)
f1 (ppm)

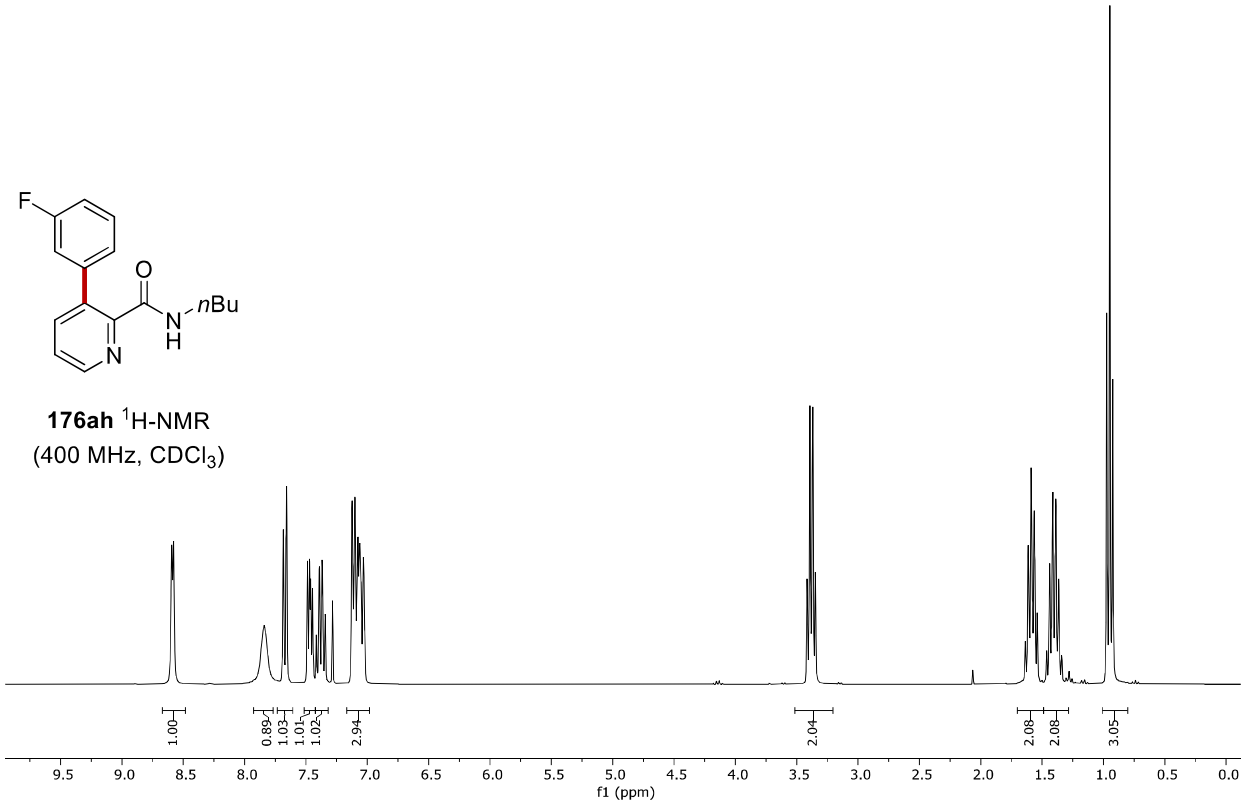
F
O
N
H
nBu
N
176ah 1H-NMR
(400 MHz, CDCl3)
1.00
0.89
1.03
1.01
1.02
2.94
2.04
2.08
2.08
3.05
f1 (ppm)

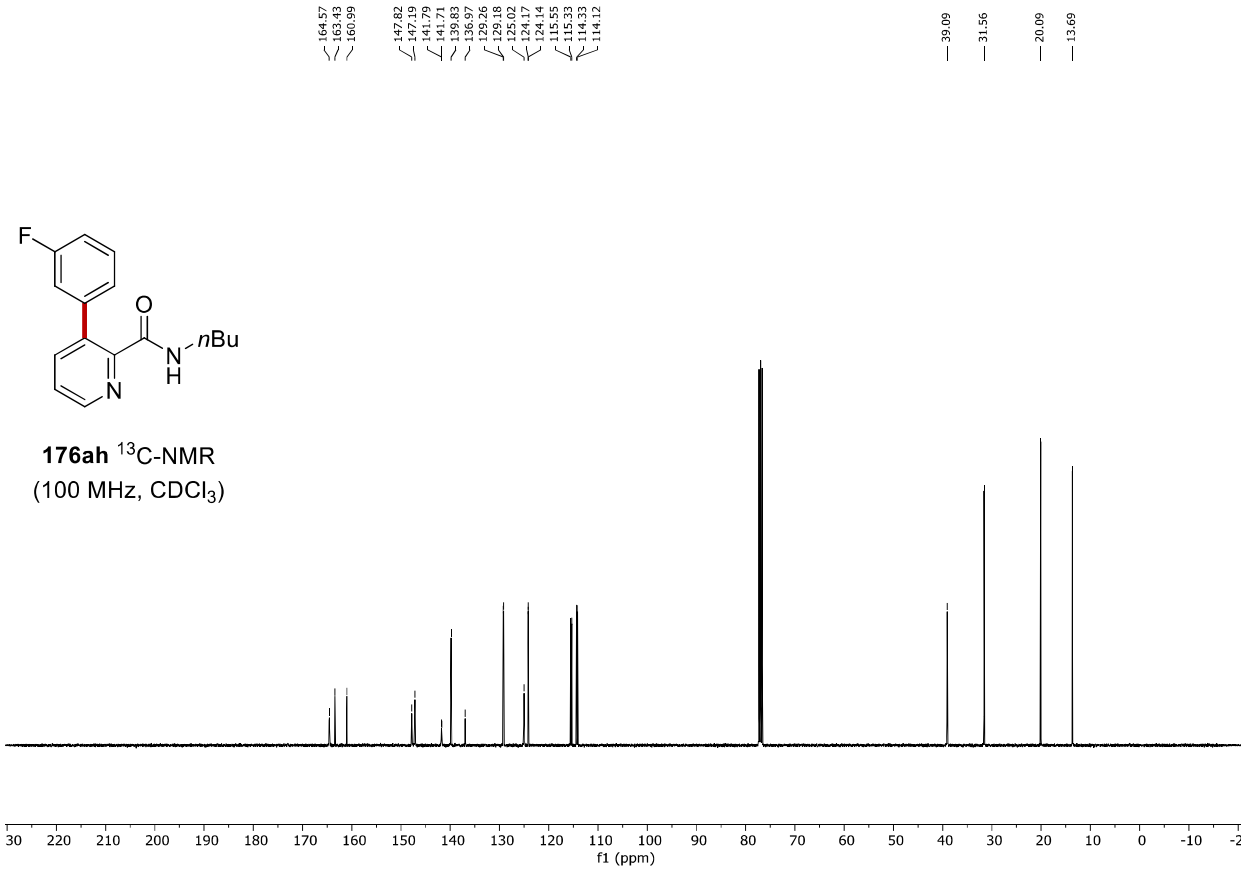
164.57
163.43
160.99
147.82
147.19
141.79
141.71
139.83
136.97
129.26
129.18
125.02
124.17
124.14
115.55
115.33
114.33
114.12
39.09
31.56
20.09
13.69
F
O
N
H
nBu
N
176ah 13C-NMR
(100 MHz, CDCl3)
f1 (ppm)

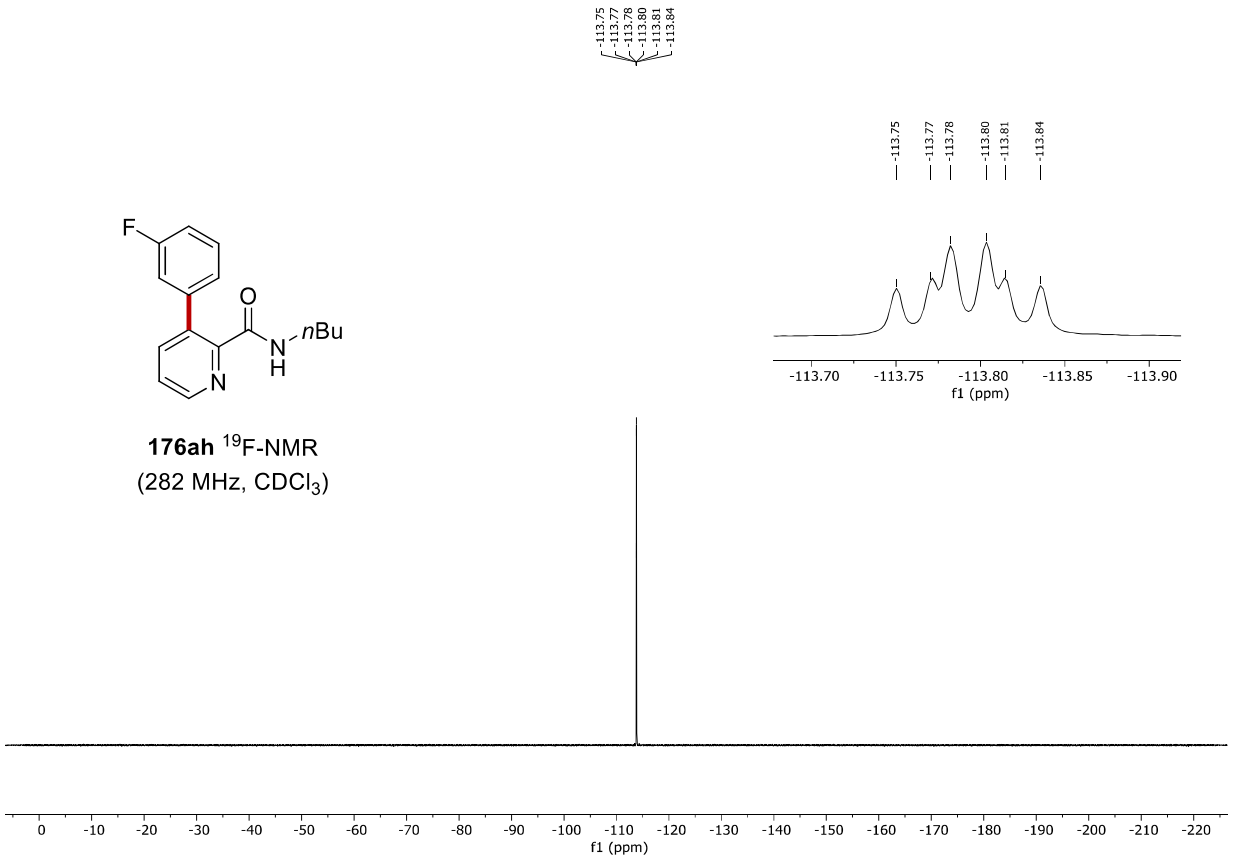

176ah ^{19}F-NMR
(282 MHz, $CDCl_3$)

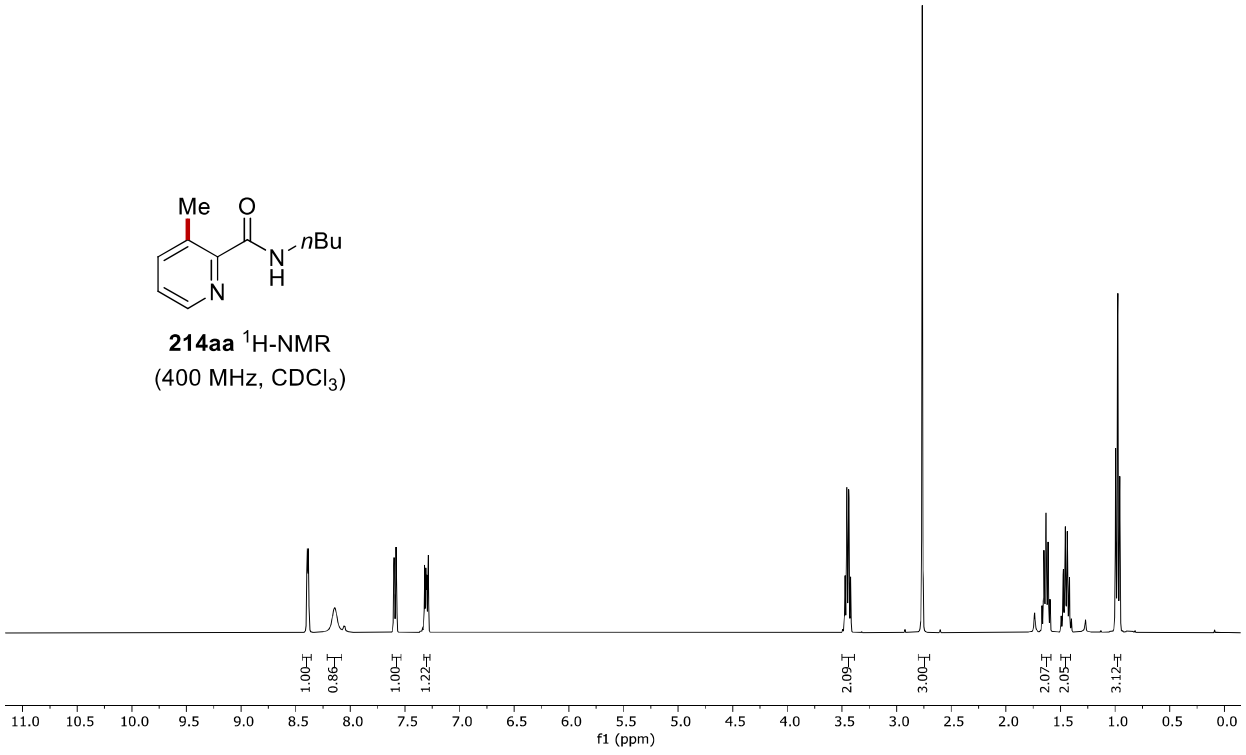

214aa ^{1}H-NMR
(400 MHz, $CDCl_3$)

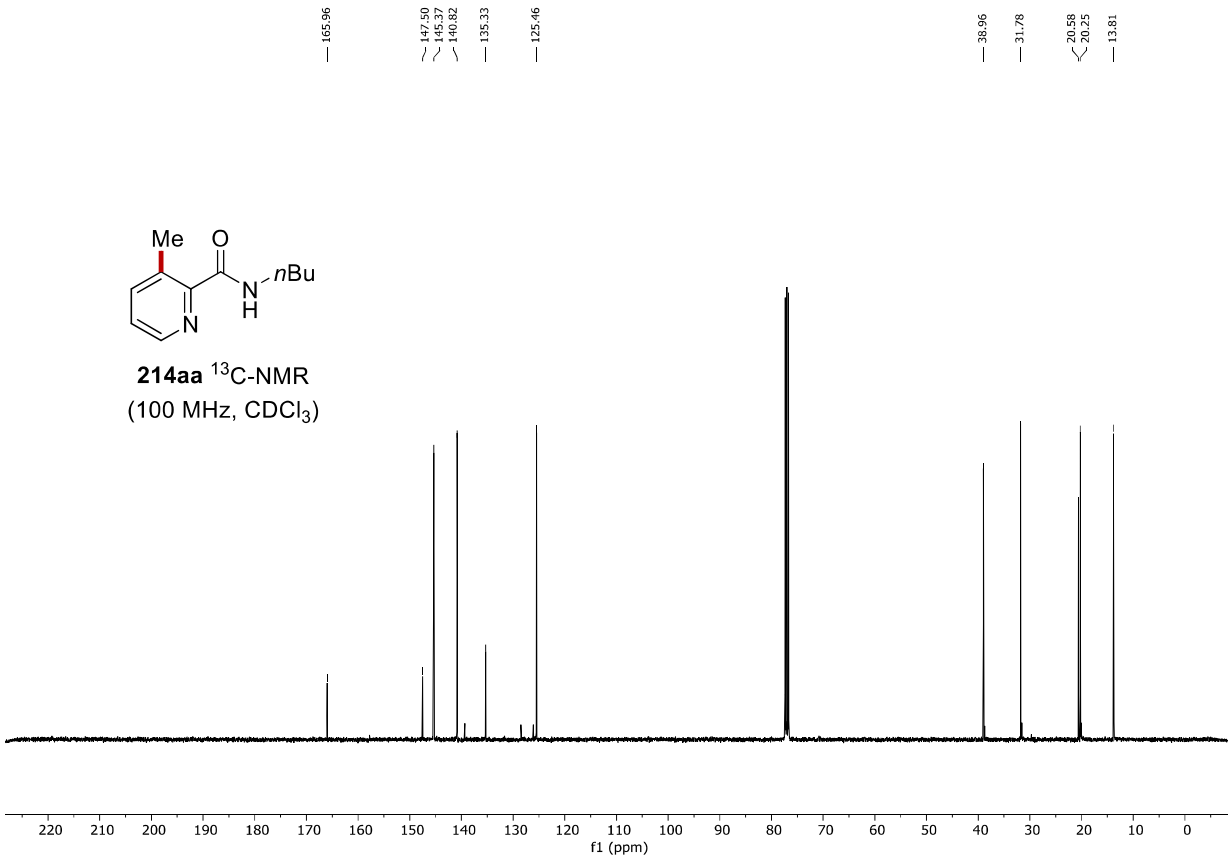

214aa ^{13}C-NMR
(100 MHz, $CDCl_3$)

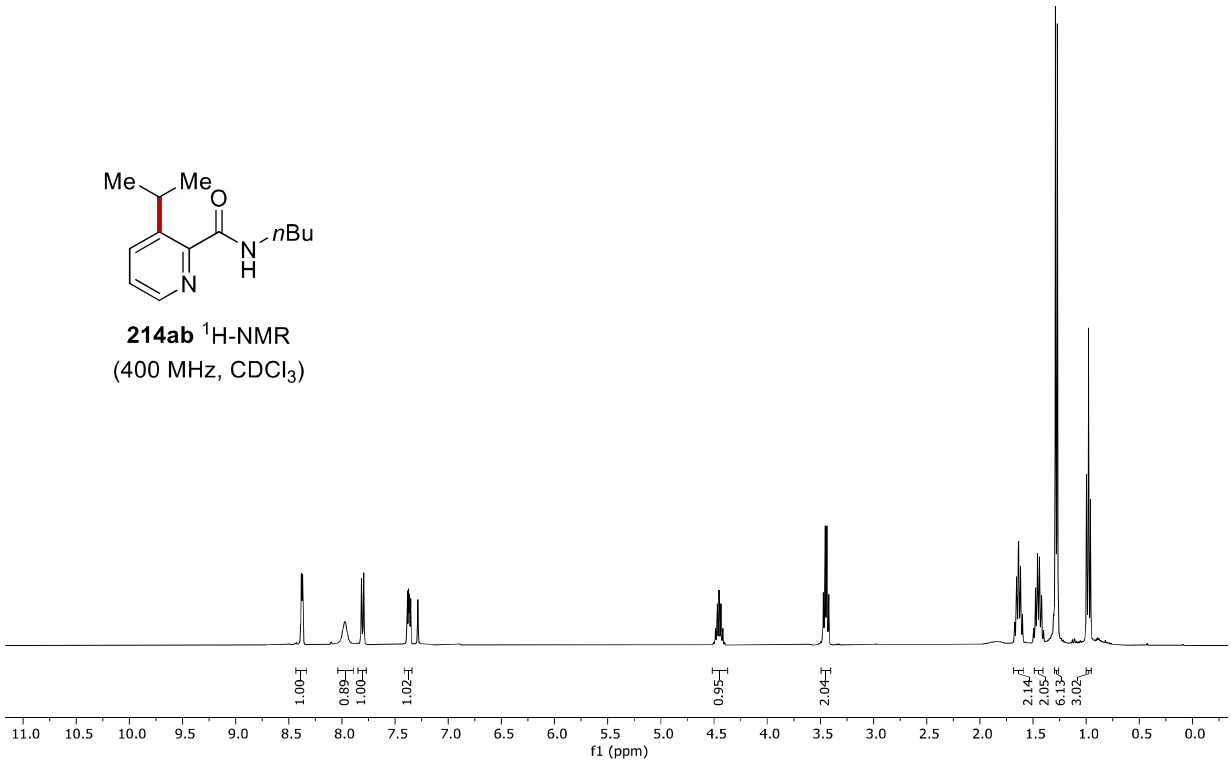

214ab ^{1}H-NMR
(400 MHz, $CDCl_3$)

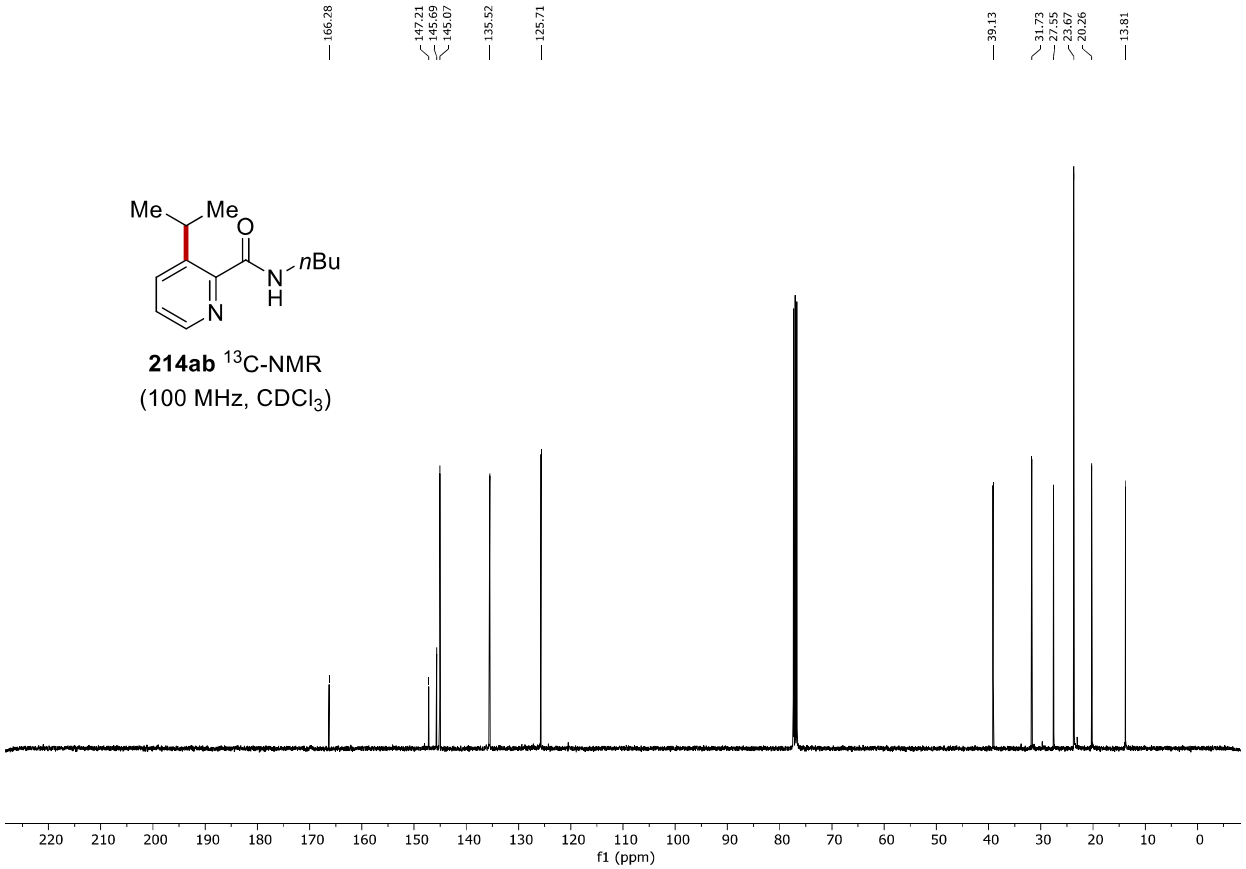

214ab ^{13}C-NMR
(100 MHz, $CDCl_3$)

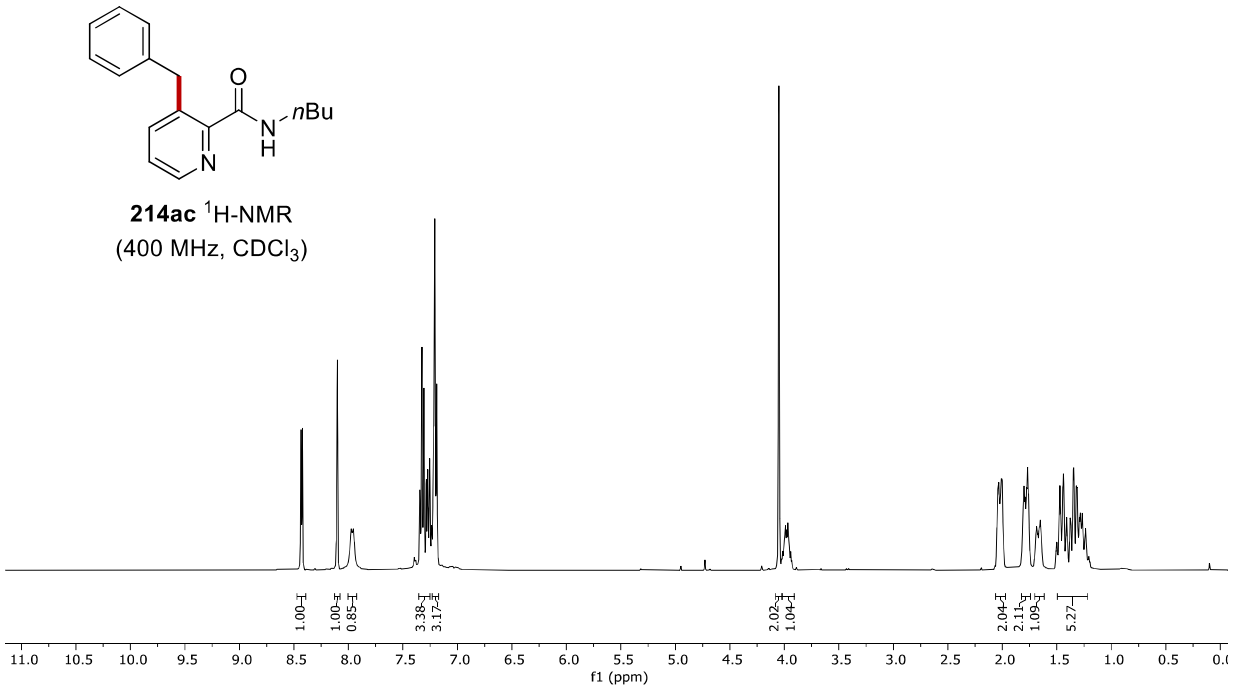

214ac ^{1}H-NMR
(400 MHz, $CDCl_3$)

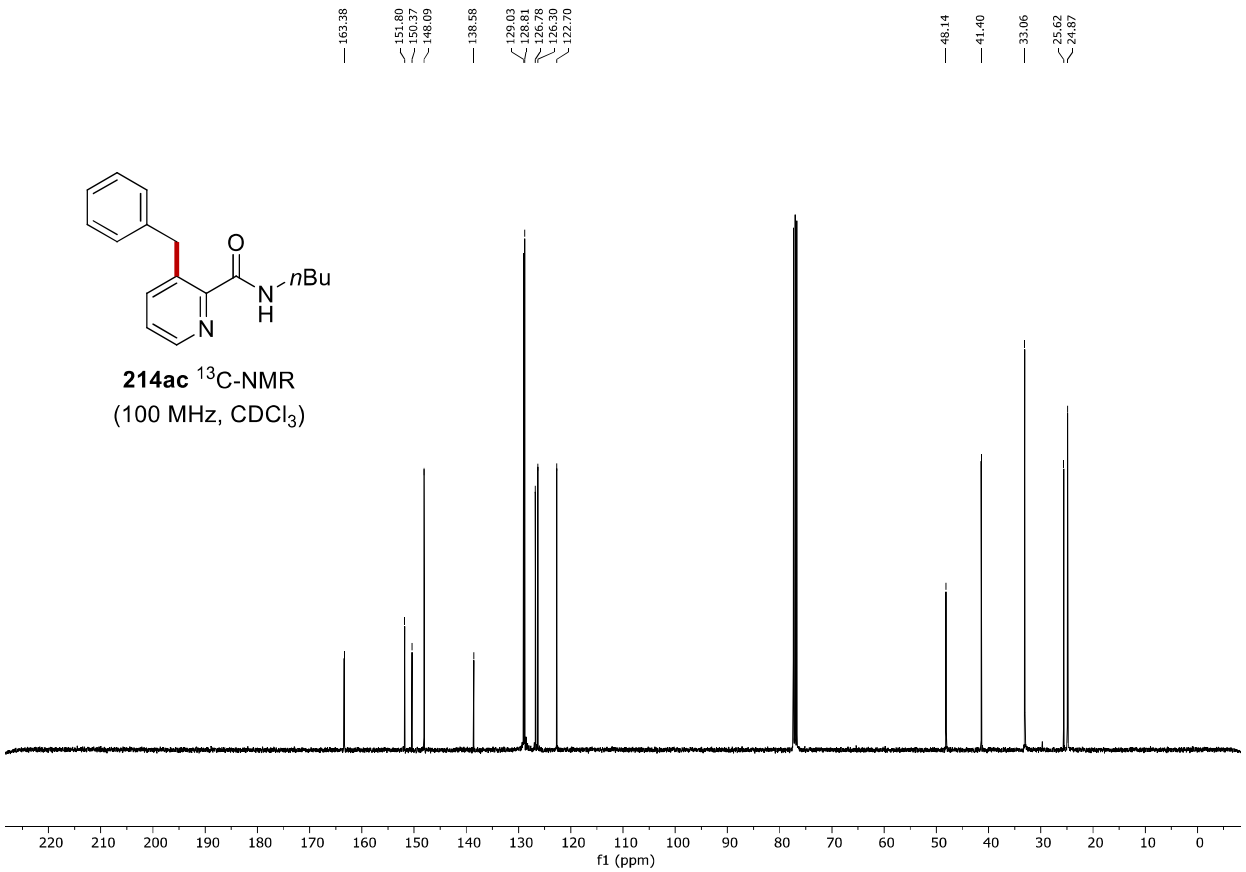

214ac ^{13}C-NMR
(100 MHz, $CDCl_3$)